

5 CRITERIA FOR EVALUATION OF GROUND MOTIONS FOR THE ANALYSIS OF NUCLEAR FACILITIES

5.1 Introduction

This section summarizes the recommended criteria for developing and evaluating artificial ground motions used to estimate the seismic response of nuclear power plants and other critical nuclear facilities.

The current version (NUREG-0800) of the USNRC Standard Review Plan (SRP) incorporates a specific requirement to consider the minimum Power Spectral Density (PSD) of ground motion records input to building, component, and soil models. Prior to this SRP, ground motion time histories used for such analyses were evaluated based solely upon comparison of their response spectra with the design response spectrum for the site. The response spectrum enveloping criteria was based upon the engineering judgment that if the response spectral input at a given frequency exceeds the corresponding design spectral criteria, the computed system response at that frequency will exceed the response from the criteria input.

However, it was recognized that a design response spectrum could be enveloped by the computed free-field response spectrum across a given frequency range, even though the PSD (or equivalently the Fourier amplitude spectrum) of the input ground motion could possess low levels (gaps) within the same frequency range. For this case, the computed system response may be underpredicted if, for example, the soil-structure interaction (SSI) frequencies fall within those gaps. In addition, the development of large structural response computer codes currently used for system evaluations has made the ability to perform simple checks of computed response more difficult for the reviewer.

Because of the ambiguities in the definition of a PSD as well as the effort involved in developing a minimum PSD requirement for an arbitrary target response spectrum, revised criteria are proposed herein that can be used to evaluate ground motion time histories to be used in the design or evaluation of critical facilities. These revised criteria eliminate the need for a separate PSD check but require that the target 5% damped response spectrum be closely matched both from above and below. The intent of the more stringent matching criteria is to ensure that the developed ground motion does not possess any significant gaps in frequency content. These revised criteria satisfy the general intent of the criteria contained in the SRP, which is currently defined in detail only for the spectral shape embodied by the R.G. 1.60 spectrum.

5.2 Current Regulatory Criteria

In the current regulatory environment, the minimum PSD requirement is included as an additional check on the developed ground motion along with the enveloping criteria of the design response spectra. The PSD criteria was included in the SRP as a result of the studies conducted as part of the resolution of the USI A-40 issues (NUREG/CR 5347, 1989). The detailed specification of the minimum PSD for motions associated with the R.G. 1.60 spectrum was added in an attempt to ensure that no gaps at critical frequencies would occur in the selection of free-field ground motion time histories used in the system response analyses. However, due to the difficulties encountered in

generating time histories that closely match both target response and PSD spectra, it was recommended that a minimum PSD requirement should be included to ensure that the ground motion record had no significant gaps in frequency content. The primary evaluation criteria remains the fit of the calculated response spectrum to the target response spectrum.

To satisfy these recommendations, the following procedure was included in Revision 2 to the SRP when the target response spectrum under consideration is the R.G. 1.60 spectrum:

- The average PSD should exceed 80% of the specified target over the frequency range from 0.3 Hz to 24 Hz.
- At any frequency, the average PSD is computed over a frequency band of $\pm 20\%$ centered on the frequency at which the PSD is being calculated.
- The duration of the ground motion used in the definition of the PSD is the strong motion duration for which the Fourier components of the ground motion are calculated.
- For the case where an ensemble of time histories is used for the generation of spectra, the PSD of the ensemble can be generated at the 84th percentile level and compared to the appropriate target PSD.

The frequency range specified, from 0.3 Hz to 24 Hz, is based on two relatively subjective considerations. First, the power in actual ground motion recordings above 24 Hz was considered negligible so that there is no need to consider spectral content above this value. Secondly, the check below 0.3 Hz was considered unnecessary since most nuclear facilities are relatively stiff and have response frequencies well above this lower bound cutoff. However, since those recommendations were promulgated, several issues have arisen which make these limits potentially problematic. First, at some deep soil sites, it was noted that site response fundamental frequencies extend to values well below 1 Hz. The details of the ground motion at these low frequencies could become important in evaluating site response, requiring more consideration of the frequency content at these lower frequencies of interest. Secondly, at some CEUS rock sites, rock outcrop motions may have significant energy at frequencies as high as 50 Hz (Silva and Darragh, 1995). Thus, even though these motions may not have a significant percentage of their total power at these high frequencies, the Fourier amplitudes of the high frequency components of the motion could become important when these rock outcrop motions are used as input to convolution calculations to determine surface motions at low frequency soil sites.

For design response spectral shapes other than the R.G. 1.60 shape, the SRP does not provide specific guidance but indicates that the procedures used to develop the minimum PSD associated with the R.G. 1.60 shape be used to develop PSD requirements for these other spectral shapes. This is not always a simple task, but generally can require the investment of some significant effort for a given target spectrum. For this study, where spectral shapes are being developed as continuous functions of distance and magnitude (Section 4), such an effort can prove daunting. As a result, guidelines are recommended here that can be used to ensure that artificial design ground motions developed for response analyses satisfy the intent of the SRP.

In addition to the minimum PSD requirement, other characteristics of the developed ground motions are important in judging their adequacy. The strong motion duration, peak velocity and displacement parameters, and correlation among the three component motions of an artificial record set are of interest to ensure that the records are sufficiently "earthquake-like" to satisfy the intent of the SRP. Part of criteria recommended here therefore involve the characteristics of the empirical WUS data base (Appendices A, B, and F).

5.3 Recommended Regulatory Criteria

Based on the results of numerical studies described in the following paragraphs, together with discussions with the project Peer Review Panel, a number of conclusions were reached on recommendations for artificial ground motion records. These artificial records must be generated to "match" or "envelop" given response spectral shapes associated with appropriate magnitude and distance bins (Section 3) and to satisfy other general characteristics associated with these bins. To evaluate the adequacy of artificial records, the following information should be made available with each record. This information can then be used for comparison with bin characteristics.

- Plots of time history and Arias Intensity function;
- Plots of Fourier amplitude and smoothed Fourier amplitude spectra, scaled by the factor FT as discussed in Section 5.4.3 to correlate with bin duration characteristics;
- Comparative plots of 5% damped target response spectrum and spectrum resulting from the ground motion;
- Total duration of the record, time increment, frequency window and Nyquist frequency;
- Strong motion duration of the record as defined by the 5%-75% Arias Intensity;
- Peak motion parameters PGA, PGV and PGD, and ratios PGV/PGA , PGD/PGA and $PGA \cdot PGD/PGV^2$.

Based upon this information the following general criteria are recommended to evaluate the adequacy of the artificially developed ground motions.

- (a) The general objective is to generate an artificial or synthetic accelerogram that achieves approximately a mean-based fit to the target spectrum. That is, the average ratio of the spectral acceleration calculated from the accelerogram to the target, where the ratio is calculated frequency by frequency, is only slightly greater than 1. The aim is to achieve an accelerogram that does not have significant gaps in the Fourier amplitude spectrum but that is not biased high with respect to the target. An accelerogram that exceeds the target may overdrive a site soil column or structure where nonlinear response is of interest.
- (b) Records should have a sufficiently small frequency window and sufficiently high maximum frequency (or alternatively time increment and maximum duration). The total duration of the

record can be increased by zero packing to satisfy these frequency criteria. It is recommended that records have a maximum frequency window of 0.05 Hz with a Nyquist frequency of at least 50 Hz, or a time increment of at most 0.010 seconds for a total duration of 20 seconds. If frequencies higher than 50 Hz are of interest, then the time increment of the record must be suitably reduced to provide a Nyquist frequency above the maximum frequency of interest. Such records can be easily generated with currently available computer power and software. This recommendation is similar to that presented in NUREG/CR-5347.

- (c) Spectral accelerations at 5% damping should be computed at a minimum of 100 points per frequency decade, uniformly spaced over the log frequency scale from 0.1 Hz to 50 Hz or the Nyquist frequency. This results in an increment in \log_{10} frequency of 0.01. If the target response spectrum is assumed to be defined in the frequency range from 0.2 Hz to 25 Hz, the comparison of the artificial motion response spectrum with the target spectrum should be made at each frequency computed above in this frequency range. The number of frequencies at which spectra are computed is therefore increased from 57 (Table 3.7.1-1 of the SRP) to well over 200 from 0.2 Hz to 25 Hz as recommended herein. Again, with current computer power generally available, this requirement should pose no hardship and should result in an accurate representation of the computed spectra.
- (d) The computed 5% damped response spectrum of the accelerogram (if one artificial motion is used for analysis) or of the average of all accelerograms (if a suite of motions is used for analysis) should not fall more than 10% below the target spectrum at any one frequency point. Since the objective is to achieve a mean based fit to the target spectrum, many more points will generally fall below the target spectrum than the 5 point limit mentioned in the current SRP. However, to prevent large frequency ranges falling below the target, no more than 9 adjacent spectral points may be allowed to fall below the target spectrum at any frequency. Using the frequency spacing mentioned above, this corresponds to a moving frequency window of $\pm 10\%$ centered on the frequency.
- (e) The computed 5% damped response spectrum of the artificial ground motion (if one motion is used for analysis) or the mean of the 5% damped response spectra (if a suite of motion is used for analysis) should not exceed the target spectrum at any frequency by more than 30% (a factor of 1.3) in the frequency range between 0.2 Hz and 25 Hz.
- (f) Because of the high variability in time domain characteristics and because few CEUS recordings are available to quantify these characteristics, strict time domain criteria are not recommended. In general, artificial motions should have durations (5%-75% Arias intensity), and ratios PGV/PGA and $PGA \cdot PGD/PGV^2$ that are generally consistent with bin average values. For WUS motions, strong motion durations should generally be within about $\pm 50\%$ of the bin median values (see Section 5.5.2) and PGV/PGA and $PGA \cdot PGD/PGV^2$ values should be within ± 1 sigma of the bin median values. It would be appropriate for CEUS acceleration time histories (excluding the 0 to 10 km distance bin) to have durations on average larger than WUS motions by 20 to 50% with this difference decreasing substantially for velocity and displacement time histories. This recommendation is particularly appropriate for rock outcrop motions.

- (g) Directional correlation coefficients between pairs of records are typically required to be relatively low to ensure that a structure or structural element cannot be oriented in an analysis in such a manner so as to minimize some important directional response quantity of interest. However, if the limiting value is made too low, a significant number of empirical recordings in any earthquake bin may unnecessarily be eliminated from further consideration as a seed for generating design ground motions. Since the response quantity is a function of the structural characteristics and not of the empirical bin data sets, it is recommended that the upper limit for the zero-log cross-correlation coefficient between any two design ground motions be 0.3. For correlation coefficients less than this limit, no significant reduction in response will be attained by orientation of the structure.

If these general criteria are followed, the matching requirements to the 5% damped response spectrum should be adequate to ensure that no gaps in the PSD or Fourier amplitude spectrum will occur over a significant frequency range. There is no special need to evaluate the PSD of the ground motion to compare with minimum PSD targets.

5.4 Description of Analyses

Empirical records appropriate for analyses have been catalogued into magnitude and distance bins (Section 3). These distance and magnitude bins are listed in Table 5.1. The four distance bins selected are labeled "D1" (0-10km), "D2" (10-50km), "D3" (50-100km) and "D4" (100-200km) and the three magnitude bins are labeled "M55" (M5-M6), "M65" (M6-M7) and "M75" (M7+). These magnitude and distance ranges for each bin were selected based upon the judgment of the investigators to arrive at ranges considered to be most significant. If a larger number of bins were selected, for example, the population within each bin would decrease, and this could lead to difficulties in developing average bin characteristics. If fewer bins were selected, then characteristic differences in recordings that were felt to be significant could be lost. The recordings contained within each bin listed in Table 5.1 represent the WUS database (Appendix A). Clearly some bins do not have sufficient empirical data with which to define average characteristics and must be supplemented as described in Section 3.

It should be mentioned that a number of approaches in the open literature are used to develop appropriate artificial time histories. These approaches are based on either time domain or Fourier domain methods that satisfy matching or enveloping criteria of a target response spectrum. It is not the objective of this project to either describe or evaluate these approaches, but rather to describe criteria that can be used to evaluate the appropriateness of given time histories developed by Applicants for use in various system response analyses. As mentioned previously, the primary criterion used to judge the adequacy of such time histories is to ensure that the computed response spectrum closely matches the target response spectrum and ensures that no significant gaps in frequency content exist.

From the outset of this effort, it was recognized that the use of a PSD criterion to evaluate the frequency gap issue has inherent problems with respect to application. First, several different expressions for computation of PSD are available in the open literature. These definitions may not be equivalent to one another. This was also noted in the comments provided by Kennedy (Appendix

A to NUREG/CR-5347), which was the study on which the revision to the current SRP was based. Secondly, it has been noted that there could be a disconnect encountered between the definition of time duration of the ground motion used in the development of the Fourier components of the ground motion and the duration used in computing the PSD as described in the SRP.

For example, in generating artificial time histories, it is usual to extend the initial trial record by zero packing to an integral power of two (2). The record duration used in the Fourier computation with the FFT procedures is then relatively long, consistent with the zero packed record length. In the computation of the PSD, as described in the SRP, the duration mentioned refers to the strong motion duration. Thus, unless one is careful during the review process, the duration used in the FFT and the PSD computations can be different, and can lead to an inconsistency in the computation of the power in the record.

In the work described in the following paragraphs, the average Fourier amplitude spectrum of the empirical records in each bin was computed. Examples of these bin averaged Fourier amplitude spectra are shown in Figures 5-1A and 5-1B and represent some typical results. In these and later figures, the following notation is used to represent a set of strong motion records:

D1RM65H

where D1 is the distance bin as defined above,
R means rock (or S means soil)
M65 is the magnitude bin as defined above,
H means horizontal (or V means vertical).

The Fourier amplitudes for each of the records in the bin, which were first scaled to 1g, were computed and then averaged over the bin without any weighting considered. The shapes plotted in Figure 5-1A compare the horizontal and vertical records in a particular bin (D1RM65) and indicate the general increase in high frequency content of the vertical records with respect to the horizontal records. Figure 5-1B presents a similar comparison of the bin results as a function of magnitude for a given distance bin. Again, the averages show the same general shape with an increase in Fourier amplitude with magnitude. The average Fourier amplitude spectra for all the bins are shown in Appendix E.

In the calculations performed to address the frequency gap issue, the general procedure consisted of (a) selecting target response spectral shapes with different characteristics, (b) generating artificial records that satisfy the enveloping criteria of the SRP, (c) introducing gaps into these artificial records at various frequencies, and (d) determining the influence of these frequency gaps on the recomputed 5% response spectra. In generating appropriate records, the ability to match a given target spectrum reasonably closely is controlled by two characteristics of the spectrum. First, if the target spectrum consists of a series of straight line segments (as plotted, say, on arithmetic spectral acceleration vs. log frequency scales), the discontinuities in the slope of the spectrum can cause difficulties in the iteration process used to generate the artificial time history. Secondly, if the shape of the spectrum is very peaked (relatively large amplification ratio over a narrow frequency band), the iteration

process may again have difficulties in convergence. A number of such spectral shapes were used and the results of some of these computations are presented in the following paragraphs.

5.4.1 Generation of Artificial Enveloping Time Histories, Segmented Target

In generating these trial time histories, a relatively peaked spectral shape of the acceleration spectrum was generated early in the study using the median shape computed for the D2RM55H bin (distance 10-50 km, rock site, magnitudes 5-6, horizontal direction) and shown in Figure 5-2. This spectral shape was computed from all the records (unweighted) in this particular bin and was not modified to match data in adjacent bins. It should be noted that this spectral shape is not necessarily the same as that shown in Section 4 for the given average magnitude and distance, although it is not too different. This smooth bin spectral shape was then enveloped with a series of closely matching straight-line segments. For general interest, a comparison of this segmental shape is made with the NUREG-0098 median rock spectral shape in Figure 5-2. The target spectrum is significantly narrower and more peaked than the generic spectrum.

Eight different time histories were then developed that generate response spectra that envelop this target segmental shape. The computer program CARES, which operates in the frequency domain, was used in these calculations (Costantino et al., 2000). A random phase spectrum was generally used in these computations, as this was simplest to perform and was as appropriate as any other assumption. The enveloping criteria used in each case satisfies the current SRP recommendations (no more than 5 spectral points falling below the target, with no one point falling more than 10% below the target spectrum) over the frequency range from 0.2 Hz to 34 Hz as recommended in Table 3.7.1-1 of the SRP.

The particular characteristics of these artificially generated time histories are listed in Table 5-2. Record 1 has a strong motion duration (Arias Intensity from 5%-75%) of 6.3 seconds. This duration characteristic is long for this particular bin as can be noted from Figure 5-14A, where the bin average is shown to be about 2.5 seconds, with the $\pm 50\%$ variations extending from about 1.6 seconds to about 3.8 seconds. A summary of these bin characteristics is presented in Appendix F. This artificial trial record used the most data points in the calculation by zero padding the record to achieve a total duration of 20 seconds. The frequency increment generated by the one-sided FFT routine is 0.05 Hz with a maximum frequency retained in the calculation of over 200 Hz. Records 2 through 4 have about the same duration as Record 1 but half the number of time steps of the previous record. Record 4S uses a longer zero padded length but with the same total number of time steps as Record 4, while Record 4L uses an increased strong motion duration of 8.4 seconds. Record 5 uses the fewest number of time steps and keeps a total padded duration of 20 seconds. Record 1S has characteristics similar to Record 1 except that the strong motion duration is reduced from 6.3 seconds to 3.4 seconds, which is more in keeping with the average bin characteristic.

Figures 5-3A through 5-3H plot the resulting 5% damped acceleration response spectrum for each generated motion, the segmented target spectrum and the computed error between the two spectra. It should be noted that in the CARES FFT computation, the frequency increment is selected as the inverse of the maximum total padded duration of the record while the maximum frequency is determined from the time increment of the record (defined through the Nyquist frequency). The

spectra computed and shown in the plots of Figure 5-3 are typically cutoff at either 50 Hz or at the Nyquist frequency of the generated motions. Thus for Records 4, 4S, 4L and 5, the cutoff frequency is as low as 12.8 Hz since the time increment selected is relatively large. It should be reiterated that the purpose of these calculations was not to develop closely enveloping records. Rather it was to ensure that records could be generated that yield spectra reasonably close to the target response spectra after only a few iterations, even for this target spectrum, which has relatively poor matching characteristics (segmented and relatively peaked).

The plots of Figures 5-3A through 5-3H indicate that the enveloping of such segmented response spectra can be easily achieved after only a few iterations with resulting errors in spectral amplitude less than 20% over the frequency range from 1 Hz to 25 Hz. This enveloping can be achieved provided that the record uses a sufficiently small frequency increment and sufficiently high cutoff frequency (or alternatively short time increment and long duration of the record). It has been our general experience that enveloping errors increase as frequency ranges approach the Nyquist frequency. The recommendations of NUREG/CR-5347 suggest a maximum frequency window of 0.05 Hz. With a Nyquist frequency of at least 50 Hz, the number of Fourier components computed in the one-sided Fourier computation is then 1024 and number of time steps in the record is 2048. The corresponding time increment of the record is then about 0.01 seconds for a record duration of 20 seconds. During the public comment period associated with the USI A-40 issues, some comments were received that recommended a large frequency window of 0.2 Hz. With today's available computational power on even the most ordinary desktop computer, such a recommendation does not have any real basis.

5.4.2 Generation of Artificial Enveloping Time Histories, Smooth Target

Figures 5-4A and 5-4B indicate similar results but using the smooth shape of the acceleration response spectrum rather than the segmented shape for the same bin (D2RM55H) discussed previously. As can be noted, the calculated artificial motions more closely envelop the smooth target spectrum as compared to the results of Figure 5-3, with errors between 1 Hz and 25 Hz on the order of 5%. This behavior confirms the general experience of the additional convergence difficulties introduced into the fitting process by the use of segmented target spectrum, which has been typical in the past. At low frequencies where the amplitudes of the target spectrum are low, the computed errors become larger although the closeness of the fit (on an absolute basis) is better than in the mid-frequency range. At the high frequency end of the spectrum, the errors in the fitting become larger as the Nyquist frequency is approached, as previously mentioned.

Artificial recordings were also developed using the smooth spectral shape for the same bin (D2RM55H) as used above, but this time using the recommended spectral shapes documented in Section 4. A comparison of the spectral shapes using the recommended WUS, CEUS 1-corner and CEUS 2-corner source models is shown in Figure 5-5 for the average magnitude and distance associated with the empirical bin data. In these calculations, artificial recordings were generated for four different assumed Fourier phase spectra; namely, a random phase and three phase spectra taken from three recordings contained in the empirical bin. Figures 5-6A through 5-6D show the developed spectral comparisons and corresponding error computations for the WUS bin spectral shape. Figures 5-7A through 5-7D show similar results using the CEUS 1-corner model, again using the random

phase spectrum and the phase spectra from the same three recordings used to generate matches to the WUS bin shape.

Figure 5-8A is a plot of the Arias Intensity ratio as a function of time for the four time histories developed to envelop the WUS acceleration spectrum of Figures 5-6A through 5-6D. In addition, the Arias Intensity ratios for the three empirical recordings from which the phase spectra were taken are included on this figure. Figure 5-8B presents the same data, but plotted with respect to the time ratio (T/T_{max}) for each record, since the artificial records were developed for a different duration than the records from which the source spectra were taken. The time characteristics of the Arias Intensity ratios for the artificial records show similar growth rates as those from which the phase spectra were obtained, while the random phase assumption shows a relatively uniform growth in intensity with time, as expected. Figures 5-9A and 5-9B show similar results for the time histories developed to fit the acceleration spectral shape associated with the CEUS 1-corner model used in Figures 5-7A through 5-7D.

5.4.3 Comparison of Fourier Amplitude Spectra with Bin Averages

Figure 5-10A compares the Fourier amplitude spectra for the various generated motions that were developed to envelop the segmented target spectrum (which itself envelops the median response spectrum computed for the bin, Figure 5-3). The Fourier spectra from the artificial records all envelop the bin average spectrum, with the exceedences increasing at the higher frequencies where the fits to the segmented target response spectrum showed high (positive) errors. Similar comparisons are shown Figures 5-10B and 5-10C for those artificial records enveloping the smooth target spectra of Figures 5-4 and 5-6. The same characteristic exceedences can be noted for these two example sets.

One cause of the exceedence of the Fourier amplitude spectra from the generated motions over the bin target amplitude spectrum relates to the response spectra being higher than the target bin response spectrum. However, an additional important cause of this exceedence is the strong motion duration (TT) of the artificial record as compared to the bin average duration (TBA). To correct for this effect in order to make an appropriate comparison of Fourier amplitude spectra with the target bin average Fourier spectrum, either the Fourier amplitude spectrum of the trial motion should be reduced by the factor FT or the target bin average Fourier amplitude spectrum increased by FT, where

$$FT = \sqrt{TT/TBA}$$

As an example, using trial 1 record, the value of TT is equal to 6.3 seconds while the bin average TBA is about 2.5 seconds. The factor FT is then about 1.59. Thus the Fourier amplitude spectrum of the trial motion should be decreased by 1.59 when comparing with the bin average Fourier amplitude spectrum.

To demonstrate this effect more clearly, the Fourier amplitude spectra from Trials 1 and 1S are compared with the bin average in Figure 5-10D. This comparison shows that the Fourier amplitudes for Trial 1S are closer to the bin average values. In addition, the ratio of the Fourier spectra from the two trials is plotted over the frequency range. The strong motion duration for trial 1S is 3.36 seconds

leading to a value of FT of 1.16. The ratio of the factors FT for the two records is then 1.59/1.16 or 1.37. This ratio is a reasonable approximation to the ratio of Fourier amplitudes for the two records. If a Fourier amplitude acceptance criteria is to be added in the future to these recommended criteria, such a scaling of the Fourier spectra is recommended.

5.4.4 Influence of Gaps in the Fourier Spectrum

Following the generation of the artificial ground motions that envelop the 5% target response spectrum for one of the bins, a series of gaps was placed in the Fourier amplitude spectra for the motions. We then determined the influence of these gaps on the 5% damped response spectra. Examples of this process are shown in Figures 5-11A through 5-11G for the record designated "trial03", which was generated to envelop the segmented target spectrum. Gaps in the Fourier spectrum were located at frequencies centered at 0.5 Hz, 1 Hz, 2.5 Hz, 6 Hz, 10 Hz, 15 Hz and 25 Hz, with the width of each gap chosen to be $\pm 20\%$ of the center frequency and the depth of the gap varied by 10%, 20% and 30% of the Fourier amplitude. The phase spectra for these gaps were unchanged. For each revised record, the corresponding smoothed Fourier spectrum and the 5% damped response spectrum were calculated. The smoothing was conducted as described in Appendix A to Section 3.7.1 of the SRP, by computing the average over the frequency band of $\pm 20\%$ of the frequency being evaluated.

The results of this computation indicated that the reduction in the damped response spectrum was similar in magnitude to the reduction in the Fourier spectrum amplitudes at frequencies of 1 Hz, 2.5 Hz, 6 Hz and 10 Hz. The gaps centered at 0.5 Hz and 15 Hz led to a reduction in the response spectrum amplitudes of about one-half the decrease in the Fourier spectrum amplitudes. The gap centered at 25 Hz led to a significantly smaller change in the recomputed response spectrum. Similar changes in response spectra were noted for the case of gaps placed in the "trial01" record described in Table 5-3.

In addition, a similar computation was performed for the case of a gap placed in the Fourier spectrum at 2.5 Hz, but this time using a width of only $\pm 10\%$ in the frequency band. The results of this computation are shown in Figure 5-11H. For this case the error in the computed 5% damped response spectra is of the same order as that in the Fourier spectra. However, the resulting gaps in the smoothed Fourier spectra are now much smaller, as would be expected since the smoothed Fourier spectra are computed using a band width of $\pm 20\%$. Therefore, comparison of smoothed Fourier spectra alone are in general not enough to determine the potential significance of gaps in the input motions. A summary comparison of the magnitudes of change in 5% damped response spectra for a given change in Fourier amplitudes is shown in Figure 5-12, using the results for the "trial03" record shown in Figures 5-11A through 5-11G.

5.4.5 Limitations on Exceedences of Response Spectra

It is well known that the computed 5% damped response spectrum for a time history composed of a single frequency can be made to exceed a given target spectrum if no limitations are placed on the amount of the spectral exceedences that can occur at any one frequency. As an example, a time history was generated using a single frequency sine wave at 5 Hz with a magnitude of 1g. The 5%

damped spectral amplification (SA/PGA) for this motion is shown in Figure 5-13A and is compared to the median spectrum shape obtained from the median empirical (WUS) data for bin D2RM55H. The sine wave record was then uniformly increased in magnitude to either totally envelop the bin target response spectrum or to minimally match at least 90% of the target. It is clear that if large exceedences of the target spectrum were allowed, such a severely gapped motion could satisfy the enveloping criterion alone. However, checking the corresponding Fourier spectrum, illustrated in Figure 5-13B, can uncover the gaps in frequency content in the record. The computed Fourier spectrum is very spiked in appearance although the amplitudes of the spikes depend on the specific details of the digitized record used in the FFT calculation.

Unfortunately, the smoothing process typically used to plot computed Fourier amplitude spectra could serve to severely change the character of even this extreme example, as noted in Figure 5-13B. Care must then be used when judging such smoothed plots. A similar computation was made using a time history generated from three frequencies of 2.5 Hz, 5 Hz and 10 Hz and scaled to a 1g amplitude. Again, the exceedences of the response spectrum are very large as shown in Figure 5-13C. Also, the computed Fourier spectrum shown in Figure 5-13D is very spiked although the smoothing process again tends to hide the spikes. This simple exercise serves to indicate that the acceptance criteria used to judge the adequacy of ground motions must also contain a maximum allowable spectral exceedence criteria as well as a recommendation on the appropriate frequency content of the generated record, as mentioned previously. In addition, reliance on the appearance of smoothed Fourier spectra alone are generally not adequate to judge frequency gaps in such motions.

5.5 Other Important Ground Motion Characteristics

In addition to the two primary acceptance criteria discussed above, other characteristics of artificial ground motions are considered significant when judging acceptability for use in design or evaluation of critical facilities. In Appendices E, F, and G, a number of parameters typically considered of interest in ground motion studies were computed for each record in the WUS empirical database and are summarized in scatter plots for each magnitude and distance bin.

5.5.1 Peak Velocity and Displacement Parameters

The velocity and displacement parameters of interest typically include the peak velocity ratio (PGV/PGA), the peak displacement ratio (PGD/PGA), and the parameter $PGA \cdot PGD / PGV^2$. From the plots in Appendix F, it is evident that the scatter in these data is extremely high, but the data clearly indicate that the parameters are functions of both distance and magnitude as well as site condition (rock vs. soil sites). Average values of these parameters for horizontal motions in each bin of the WUS empirical data are presented in Table 4-1. These bin averages and uncertainties reflect equal weighting for each earthquake within any single bin.

5.5.2 Duration Parameter

In addition to the average parameters of Table 4-1, the recommended duration parameter for each bin has also been defined by an empirical WUS duration model (Appendix I). The results are shown in Figures 5-14A, B and C for horizontal motions in the various magnitude and distance bins for rock

sites. The duration parameter is defined by the 5% - 75% Arias intensity, and is an important characteristic of the ground motion. As described by Kennedy (Appendix A to NUREG/CR-5347, 1989), when an excessively long strong motion duration is selected, the computed combined responses of multimodal systems can be either severely overestimated or underestimated depending upon the details of the Fourier phasing selected in generating the ground motion.

In addition, when using the generated ground motion to evaluate liquefaction potential of a particular soil site, the duration parameter becomes important when using either equivalent linear or nonlinear analyses to estimate soil site responses. It is therefore recommended that the duration of the artificial ground motion approximately satisfy the characteristics shown in Figure 5-14. The solid line in these figures indicates the median bin value, while the dashed limits indicate values 50% higher and lower than these median bin values. Dotted lines forming boxes indicate the \pm one sigma values for the bins. Scatter plots of the duration parameters from the WUS database are contained in Appendix I.

In addition to this duration parameter, the Arias intensity and Cumulative Absolute Velocity (CAV) properties of each record in the empirical bins were evaluated to see if any particular characteristic emerges to differentiate the motions between bins. Figures 5-15A, B and C present plots of the results for a particular bin (D1RM55H). The total Arias intensity was computed for each record, scaled to a total value of unity, and the times associated with the 5% through the 100% Arias intensity ratio were determined in 5% increments. These times were normalized to a value of 1 for the total duration and were ordered. The minimum, 15th, 50th and 85th percentile and maximum time were determined for each Arias intensity level. Figure 5-15A presents the results, with the time parameter for each record scaled by its maximum duration. Results from the majority of the records indicate energy growth at the beginning of the records. This results from the selection of the long time window over which the records in the bin were digitized.

Figure 5-15B shows similar results for the same bin but with the time for each record scaled to the time associated with the 95th percentile Arias intensity ratio (designated " T_{95} "). Figure 5-15C shows a similar comparison for the case where the times for each record are scaled to the time window for the 5% to 95% Arias intensity ratio (designated " $T_{5,95}$ "). The results shown in Figures 5-15B and 5-15C are typical of all bins analyzed. They indicate the large scatter in the data and the different rates of growth in Arias intensity for the records in any one bin. Figures 5-16A and B show the results of similar calculations for CAV. In this case, scatter in the computed data is much less than in the Arias intensity function, which may indicate that the CAV is a more stable indicator of the characteristics of the time details of a given record. Scatter plots of both total Arias Intensity and CAV for the WUS database are contained in Appendix G.

5.5.3 Component Correlation Characteristics

The characteristics of the lag-zero cross-correlation coefficients of the three component data sets in the WUS empirical database were computed and are tabulated in Tables 5-4 and 5-5, with summary plots presented in Appendix F. Table 5-4 summarizes the average component correlations for the rock site bins for acceleration, velocity and displacement. Table 5-5 contains correlations for the soil sites. A typical plot is shown in Figure 5-17A and indicates a relatively wide scatter in the average

values in each bin. In general, the correlation coefficient for acceleration records is somewhat smaller than for integrated velocity and displacement components.

A comparison of the component correlations computed from the vertical and horizontal record pairs is also summarized in Tables 5-4 and 5-5 and a sample plot shown in Figure 5-17B for rock sites. The correlation between the vertical and each horizontal record of the data set is similar. Again, the results indicate higher correlation coefficients for velocity and displacement than with acceleration.

The current NRC staff position limits the correlation between component pairs of artificial acceleration records of a three component enveloping set to a value of 0.16 or less. This is based on some early limited computational results generated by Chen (1975). More complete evaluations were generated by Hadjian (1978, 1981) who included the effect of recorder orientation to estimate maximum values of correlations for a somewhat larger data set. The results of this computation indicated maximum values of acceleration correlation coefficients of 0.32. The data summary of Tables 5-4 and 5-5 do not include the effect of recorder orientation. As mentioned in Section 5.3, a value of 0.3 is recommended for the acceptance criteria.

5.6 Example Application of Spectral Matching Criteria

A further expansion of these general recommendations is provided for the following case in which a typical Uniform Hazard Spectrum (UHS) is defined as the basic target spectrum for the site. The UHS is assumed to be based on studies using the latest ground motion information (source zones and attenuation models) appropriate for the site for which it is defined. The use of older hazard studies based on attenuation models no longer considered appropriate for the site could lead to the definition of target spectra that have deficiencies in certain frequency ranges. Generating appropriate ground motions for such deficient targets requires special considerations that are not incorporated into the following description.

A schematic example of an appropriate UHS is shown in Figure 5-18A. The UHS is defined by spectral ordinates over a given frequency range (shown to be 0.2 Hz to 25 Hz in the figure) and its PGA. To properly generate ground motions that envelop this UHS and satisfy the generic criteria listed above, the spectrum needs to be extrapolated at the low and high frequency ends as shown in Figure 5-18A. As mentioned above, the purpose of these extrapolations is to generate ground motions that have realistic low and high frequency characteristics.

In addition to the UHS, additional spectra are often generated from dominant earthquakes determined from the deaggregated hazard analysis. Such spectra are used to study nonlinear effects (liquefaction assessment, structural damage estimates, etc.). The use of ground motions generated from enveloping the very broad banded UHS spectrum could lead to overdriving systems and incorrectly predicting nonlinear responses. For such cases, ground motions are often generated for separate events that dominate the hazard at low frequency (1 Hz) and high frequency (10 Hz) to attempt to capture the nonlinear characteristics for these dominant events. The low frequency event is typically defined as a large magnitude, distant earthquake while the high frequency deaggregated event is a smaller, close-in earthquake.

The spectra from the deaggregated events are then typically scaled back to the UHS at their corresponding frequencies. It should be noted that an interface frequency, f_c , can then be defined at the intersection of the two deaggregated spectra. For frequencies below f_c , the low frequency deaggregated spectrum is higher than the high frequency spectrum. For frequencies above f_c , the high frequency spectrum governs. In addition, a PGA for each of these two deaggregated spectra is also defined by the scaling process back to the UHS.

Thus three spectra are often defined for a given site, namely the UHS and the two deaggregated scaled spectra. It should be noted that the maximum difference between the UHS and the deaggregated scaled spectra, particularly around the frequency f_c , is assumed to be less than 10%. If this gap between the UHS and the deaggregated spectra exceeds 10%, a third deaggregated spectrum should be defined and scaled back to some intermediate frequency so as to limit the maximum difference between the UHS spectrum and the other deaggregated spectra to less than 10%. Site and structural response analyses can then be performed for either or all of the UHS spectrum and the scaled deaggregated events.

In the following discussion, it is assumed that three such target spectra are defined, requiring that appropriate sets of time histories be generated to envelop each of these spectra. The following recommendations are provided to generate these three sets of time histories, each of which is intended to satisfy the general criteria listed above. If additional spectra are required to fill in areas where gaps exceed the 10% recommendation mentioned above, it should be obvious how to expand the recommendations below for the additional spectra.

If a time history is generated to envelop the UHS, the upper and lower bound enveloping criteria listed above are shown schematically in Figure 5-18B. The PGA of the digitized time history should be at least equal to the PGA defined for the UHS. It is recommended that the strong motion duration associated with this UHS be the longer duration defined for the low frequency deaggregated event. The time step and total zero-packed duration of the motion should satisfy the general criteria mentioned above.

If a time history is generated to envelop the low frequency deaggregated spectrum, the bounding process is similar to that described above, but becomes somewhat more complicated. As evident in Figure 5-18C, below the interface frequency f_c , the bounding criteria should be controlled by the UHS spectrum while above f_c , the bounding criteria should be controlled by the deaggregated spectrum; that is,

$$\begin{aligned} 0.9*UHS < RS < 1.3*UHS & \text{ for frequencies between } 0.2 \text{ Hz} < f < f_c, \text{ and} \\ 0.9*DES1 < RS < 1.3*DES1 & \text{ for frequencies between } f_c < f < 25 \text{ Hz.} \end{aligned}$$

Where RS stands for the Response Spectrum of the artificial record and DES1 is the deaggregated spectrum scaled to 1 Hz. The peak acceleration of the digitized record should equal or exceed the PGA of the low-frequency deaggregated spectrum. The strong-motion duration should be appropriate for the magnitude and distance of the low-frequency deaggregated event.

If a time history is generated to envelop the high-frequency deaggregated spectrum, the bounding process is opposite to that described above; that is, below the interface frequency f_c , the bounding criterion is the deaggregated spectrum while above the interface frequency f_c , the bounding criterion is the UHS. As shown in Figure 5-18D, the criteria

$$\begin{aligned} 0.9 \cdot \text{DES10} < \text{RS} < 1.3 \cdot \text{DES10} & \text{ for frequencies between } 0.2 \text{ Hz} < f < f_c, \text{ and} \\ 0.9 \cdot \text{UHS} < \text{RS} < 1.3 \cdot \text{UHS} & \text{ for frequencies between } f_c < f < 25 \text{ Hz.} \end{aligned}$$

The peak acceleration of the digitized record should equal or exceed the PGA of the high-frequency deaggregated spectrum. The strong motion duration should be appropriate for the magnitude and distance of the high frequency deaggregated event.

5.7 Conclusions

This study has led to recommendations that can be used to generate artificial records that envelop response spectra generated for a particular site and that have sufficient energy content at all frequencies of interest. The conclusions based on these studies are as follows.

1. In the frequency range from 1 Hz to 15 Hz, the 5% damped response spectrum is about as sensitive to gaps in the frequency content of an artificial time history as is the smoothed Fourier amplitude spectrum. There is no need to have additional checks of Fourier spectra or PSD to ensure that no significant gaps in frequency exist.
2. Artificial ground motions can be generated that envelop the target response spectra defined for the project. The artificial records must have small enough time increments and long enough zero packed durations to satisfy the requirements described in this section. These artificial motions should have peak motion characteristics and strong motion durations that are appropriate for the earthquake magnitudes and distances of interest.
3. In general, the artificial record should have a response spectrum that does not fall more than 10% below the target spectrum and does not exceed the target spectrum by more than 30%.

Additionally, time domain characteristics should be generally consistent with bin average values of durations, and the ratios PGV/PGA and $\text{PGA} \cdot \text{PGD}/\text{PGV}^2$. If these criteria are followed, artificial records can be developed that are considered appropriate for analysis of critical facilities.

References

- Chen, C. (1975), "The Definition of Statistically Independent Time Histories", *Journal of the Structures Division*, Amer. Soc. of Civil Engrs, February.
- Hadjian, A.H. (1978), "On the Correlation of the Components of Strong Ground Motion", *Proceedings*, 2nd International Conference on Microzonation, San Francisco.

- Hadjian, A.H. (1981), "On the Correlation of the Components of Strong Ground Motion - Part 2", *Bull. Seism. Soc. Am.*, 71(4), 1323-1331, August.
- Miller, C.A. and C.J. Costantino (2000), "CARES, (Computer Analysis for Rapid Evaluation of Structures)," Version 1.3, Costantino, Miller and Associates for Office of Nuclear Regulatory Research, U. S. Nuclear Regulatory Commission.
- NUREG-0800 (1989) "Standard Review Plan", Office of Nuclear Reactor Regulation, US Nuclear Regulatory Commission, Revision 2.
- NUREG/CR-3805, "Engineering Characterization of Ground Motion," R.P. Kennedy et al., for U.S. Nuclear Regulatory Commission, May 1994.
- Silva, W. J. and R. Darragh (1995), "Engineering Characterization of Earthquake Strong Ground Motion Recorded at Rock Sites", Elec. Power Res. Inst., Palo Alto, CA, Rept. TR-102261.

TABLE 5-1
MAGNITUDE AND DISTANCE BINS FOR RECORD LIBRARY
WUS EMPIRICAL MOTIONS

Magnitude Bins	Range:		Bin Center:	
	5 - 6	6 - 7	5.5	6.5
		7 +	7.5	
<u>Distance (km)</u>	<u>Site Type</u>	<u>Magnitude</u>	<u>Direction</u>	<u>No. of Records</u>
00 - 10	Rock	5.5	H	28
			V	13
		6.5	H	24
			V	10
		7.5	H	6
			V	3
	Soil	5.5	H	24
			V	11
		6.5	H	87
			V	42
		7.5	H	4
			V	2
10 - 50	Rock	5.5	H	184
			V	89
		6.5	H	200
			V	100
		7.5	H	6
			V	3
	Soil	5.5	H	370
			V	182
		6.5	H	504
			V	245
		7.5	H	56
			V	28
50 - 100	Rock	5.5	H	34
			V	15
		6.5	H	76
			V	39
		7.5	H	10
			V	5
	Soil	5.5	H	38
			V	17
		6.5	H	132
			V	61
		7.5	H	12
			V	6
100 - 200	Rock	5.5	H	2
			V	1
		6.5	H	12
			V	-
		7.5	H	16
			V	8
	Soil	5.5	H	2
			V	1
		6.5	H	28
			V	14
		7.5	H	84
			V	42

TABLE 5-2
CHARACTERISTICS OF GENERATED
ARTIFICIAL RECORDS

<u>TRIAL</u>	<u>1</u>	<u>2</u>	<u>3</u>	<u>4</u>	<u>4S</u>	<u>4L</u>	<u>5</u>	<u>1S</u>
Max Duration (secs)	20	20	20	20	40	40	20	20
Time Increment (msec)	2.44	4.88	9.76	19.53	39.06	39.06	39.06	2.44
Frequency Increment (Hz)	0.05	0.05	0.05	0.05	0.025	0.025	0.05	0.05
Max Frequency (Hz)	204.8	102.4	51.2	25.6	12.8	12.8	12.8	204.8
No. of Points in Record	8192	4096	2048	1024	1024	1024	512	8192
No. of Frequency Comps (one-sided FFT)	4096	2048	1024	512	512	512	256	4096
Duration 5%-75% (sec)	6.312	5.83	6.406	6.66	5.703	8.399	6.563	3.356
Duration 5%-95% (sec)	8.464	8.516	8.116	8.144	8.242	11.094	9.063	4.933

TABLE 5-3
PERCENT REDUCTION IN 5% DAMPED RESPONSE SPECTRUM

<u>Trial Time</u> <u>History</u>	<u>Gap Center</u> <u>Frequency (Hz)</u>	<u>% Reduction in Fourier Amplitude</u>		
		<u>10%</u>	<u>20%</u>	<u>30%</u>
Trial01	0.5	1.77	3.85	5.13
	1.0	8.4	16.73	25.03
	2.5	7.55	15.02	22.13
	6.0	7.52	15.04	22.38
	10.0	7.67	15.24	22.85
	15.0	7.73	15.48	22.67
	25.0	5.33	10.51	12.23
Trial03	0.5	4.32	8.7	13.02
	1.0	8.98	17.96	26.19
	2.5	9.22	18.42	27.17
	6.0	7.79	15.61	23.4
	10.0	9.25	18.49	27.14
	15.0	4.97	9.9	14.86
	25.0	1.88	3.77	5.65

TABLE 5-4

BIN CROSS CORRELATION STATISTICS FOR WUS ROCK SITE CONDITIONS*				
M 5 to 6 Distance (km)				
Component	0 - 10	10 - 50	50 - 100	100 - 200
H1 H2 (A)	0.24474	0.19976	0.09709	0.10252
	0.14561	0.16490	0.06540	--
H1 H2 (V)	0.23528	0.23007	0.13299	0.30565
	0.22155	0.17619	0.12378	--
H1 H2 (D)	0.26467	0.23792	0.16215	0.48630
	0.28185	0.18582	0.18043	--
V H1 (A)	0.14208	0.12349	0.11489	0.09163
	0.13028	0.10356	0.07688	--
V H1 (V)	0.20656	0.14220	0.13540	0.08181
	0.16548	0.11067	0.11873	--
V H1 (D)	0.24298	0.14093	0.21570	0.21314
	0.21375	0.13969	0.23893	--
V H2 (A)	0.13294	0.11819	0.12307	0.05975
	0.07192	0.09809	0.07898	--
V H2 (V)	0.13572	0.14827	0.22696	0.08052
	0.11772	0.11696	0.19476	--
V H2 (D)	0.22698	0.16942	0.33728	0.06636
	0.15993	0.15386	0.32475	--

* Averages of absolute cross correlation values

TABLE 5-4 (Cont'd)

BIN CROSS CORRELATION STATISTICS FOR WUS ROCK SITE CONDITIONS*				
M 6.01 to 7.00 Distance (km)				
Component	0 - 10	10 - 50	50 - 100	100 - 200
H1 H2 (A)	0.24003	0.16762	0.11364	0.16388
	0.15214	0.12874	0.10120	0.13329
H1 H2 (V)	0.33729	0.19778	0.21573	0.24105
	0.16690	0.14620	0.19764	0.16954
H1 H2 (D)	0.45990	0.28682	0.36527	0.34095
	0.24497	0.20133	0.26016	0.23319
V H1 (A)	0.11941	0.11436	0.14005	0.12966
	0.10825	0.10694	0.11210	0.08915
V H1 (V)	0.11435	0.16602	0.17746	0.17886
	0.20391	0.13839	0.12075	0.13957
V H1 (D)	0.27504	0.26410	0.26536	0.33865
	0.31230	0.21185	0.19269	0.26241
V H2 (A)	0.15335	0.10497	0.16704	0.11858
	0.13378	0.09000	0.13675	0.12004
V H2 (V)	0.24955	0.16984	0.18455	0.24106
	0.18884	0.13637	0.12658	0.12634
V H2 (D)	0.33334	0.23696	0.25052	0.27682
	0.26913	0.20953	0.19163	0.21686

* Averages of absolute cross correlation values

TABLE 5-4 (Cont'd)

BIN CROSS CORRELATION STATISTICS FOR WUS ROCK SITE CONDITIONS*				
M 7.01 to 9.00 Distance (km)				
Component	0 - 10	10 - 50	50 - 100	100 - 200
H1 H2 (A)	0.18850	0.05462	0.04872	0.12822
	0.12920	0.02904	0.03688	0.10639
H1 H2 (V)	0.14420	0.14262	0.29599	0.19985
	0.13480	0.17780	0.20285	0.08094
H1 H2 (D)	0.42750	0.31014	0.39377	0.20856
	0.48279	0.30137	0.09228	0.17709
V H1 (A)	0.15807	0.11610	0.05123	0.06826
	0.10115	0.10228	0.04747	0.08540
V H1 (V)	0.07071	0.13054	0.14465	0.09808
	0.05992	0.04417	0.12527	0.09805
V H1 (D)	0.30899	0.13038	0.24319	0.11781
	0.15030	0.07088	0.27172	0.07158
V H2 (A)	0.15152	0.07028	0.08265	0.10947
	0.12387	0.00809	0.04978	0.08325
V H2 (V)	0.09780	0.08613	0.14775	0.15762
	0.10510	0.07046	0.12636	0.12961
V H2 (D)	0.28972	0.13716	0.26869	0.18059
	0.10785	0.04979	0.14270	0.13162

*Averages of absolute cross correlation values

TABLE 5-5

BIN CROSS CORRELATION STATISTICS FOR WUS SOIL SITE CONDITIONS*				
M 5 to 6 Distance (km)				
<u>Component</u>	<u>0 - 10</u>	<u>10 - 50</u>	<u>50 - 100</u>	<u>100 - 200</u>
H1 H2 (A)	0.17342	0.15696	0.12166	0.04541
	0.13459	0.12548	0.12533	--
H1 H2 (V)	0.11912	0.20268	0.14745	0.08703
	0.07992	0.16194	0.11952	--
H1 H2 (D)	0.26516	0.22215	0.20062	0.34246
	0.15645	0.16740	0.15146	--
V H1 (A)	0.07054	0.09544	0.08626	0.21234
	0.07015	0.09584	0.08382	--
V H1 (V)	0.15751	0.13181	0.12122	0.07902
	0.10079	0.10267	0.07863	--
V H1 (D)	0.16078	0.15458	0.15456	0.03081
	0.10520	0.13357	0.13590	--
V H2 (A)	0.09258	0.09794	0.10937	0.05739
	0.09860	0.08555	0.09215	--
V H2 (V)	0.14943	0.13624	0.12658	0.12212
	0.13762	0.12026	0.07452	--
V H2 (D)	0.19849	0.15261	0.14552	0.05378
	0.16820	0.14123	0.11392	--

* Averages of absolute cross correlation values

TABLE 5-5 (Cont'd)

BIN CROSS CORRELATION STATISTICS FOR WUS SOIL SITE CONDITIONS*				
M 6.01 to 7.00 Distance (km)				
Component	0 - 10	10 - 50	50 - 100	100 - 200
H1 H2 (A)	0.15101	0.13212	0.12411	0.13606
	0.10475	0.10877	0.09097	0.09504
H1 H2 (V)	0.22037	0.19742	0.16072	0.15680
	0.20010	0.15411	0.13108	0.08728
H1 H2 (D)	0.34518	0.25817	0.20460	0.22099
	0.18472	0.21086	0.16757	0.20771
V H1 (A)	0.06658	0.09266	0.08217	0.08534
	0.04963	0.08532	0.08452	0.09121
V H1 (V)	0.16802	0.13399	0.11214	0.13228
	0.14589	0.11937	0.09121	0.09081
V H1 (D)	0.30871	0.18837	0.16510	0.17180
	0.17399	0.16174	0.17382	0.13845
V H2 (A)	0.10072	0.09171	0.09194	0.12848
	0.09775	0.08664	0.08619	0.09290
V H2 (V)	0.23739	0.14580	0.14041	0.12537
	0.15366	0.11026	0.12639	0.11255
V H2 (D)	0.31197	0.11847	0.19019	0.20311
	0.16903	0.15402	0.16104	0.15927

* Averages of absolute cross correlation values

TABLE 5-5 (Cont'd)

BIN CROSS CORRELATION STATISTICS FOR WUS SOIL SITE CONDITIONS*				
M 7.01 to 9.00 Distance (km)				
<u>Component</u>	<u>0 - 10</u>	<u>10 - 50</u>	<u>50 - 100</u>	<u>100 - 200</u>
H1 H2 (A)	0.11479	0.11722	0.08145	0.15557
	--	0.07127	0.07346	0.08992
H1 H2 (V)	0.29831	0.16527	0.17689	0.28864
	--	0.16624	0.15774	0.21156
H1 H2 (D)	0.12485	0.28326	0.33767	0.36374
	--	0.23762	0.22174	0.24434
V H1 (A)	0.12753	0.06408	0.04877	0.07670
	--	0.04024	0.03418	0.06024
V H1 (V)	0.14516	0.12108	0.16002	0.13618
	--	0.08480	0.11337	0.11040
V H1 (D)	0.75292	0.17739	0.29925	0.13846
	--	0.16239	0.23191	0.13786
V H2 (A)	0.21432	0.09004	0.07420	0.06756
	--	0.09686	0.03698	0.06532
V H2 (V)	0.23649	0.14661	0.13237	0.11420
	--	0.10674	0.15797	0.08882
V H2 (D)	0.2510	0.14113	0.20146	0.12856
	--	0.13691	0.16267	0.12542

* Averages of absolute cross correlation values

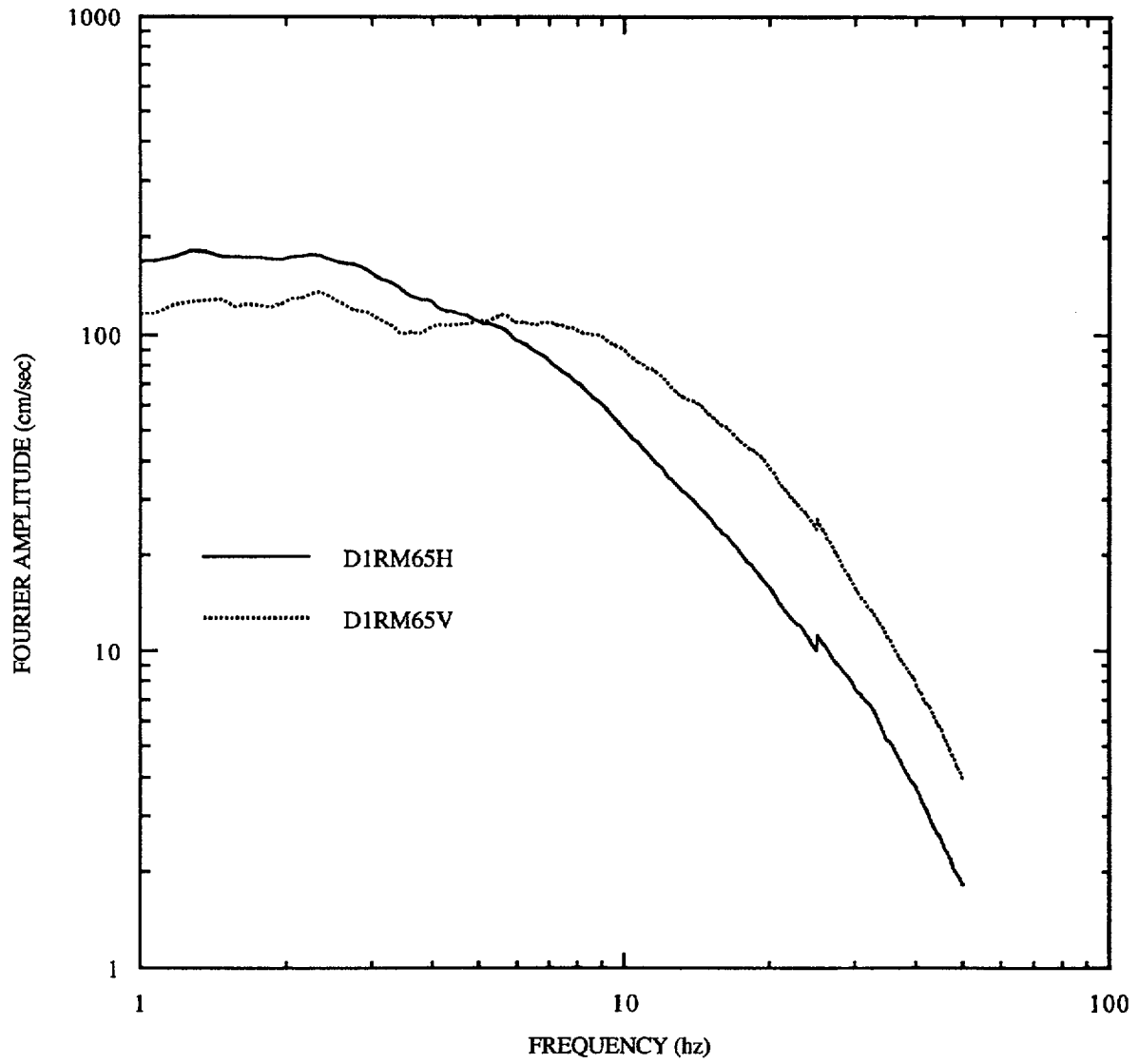


Figure 5-1A. Average smoothed Fourier amplitude spectra, distance 0-10 km, rock sites.

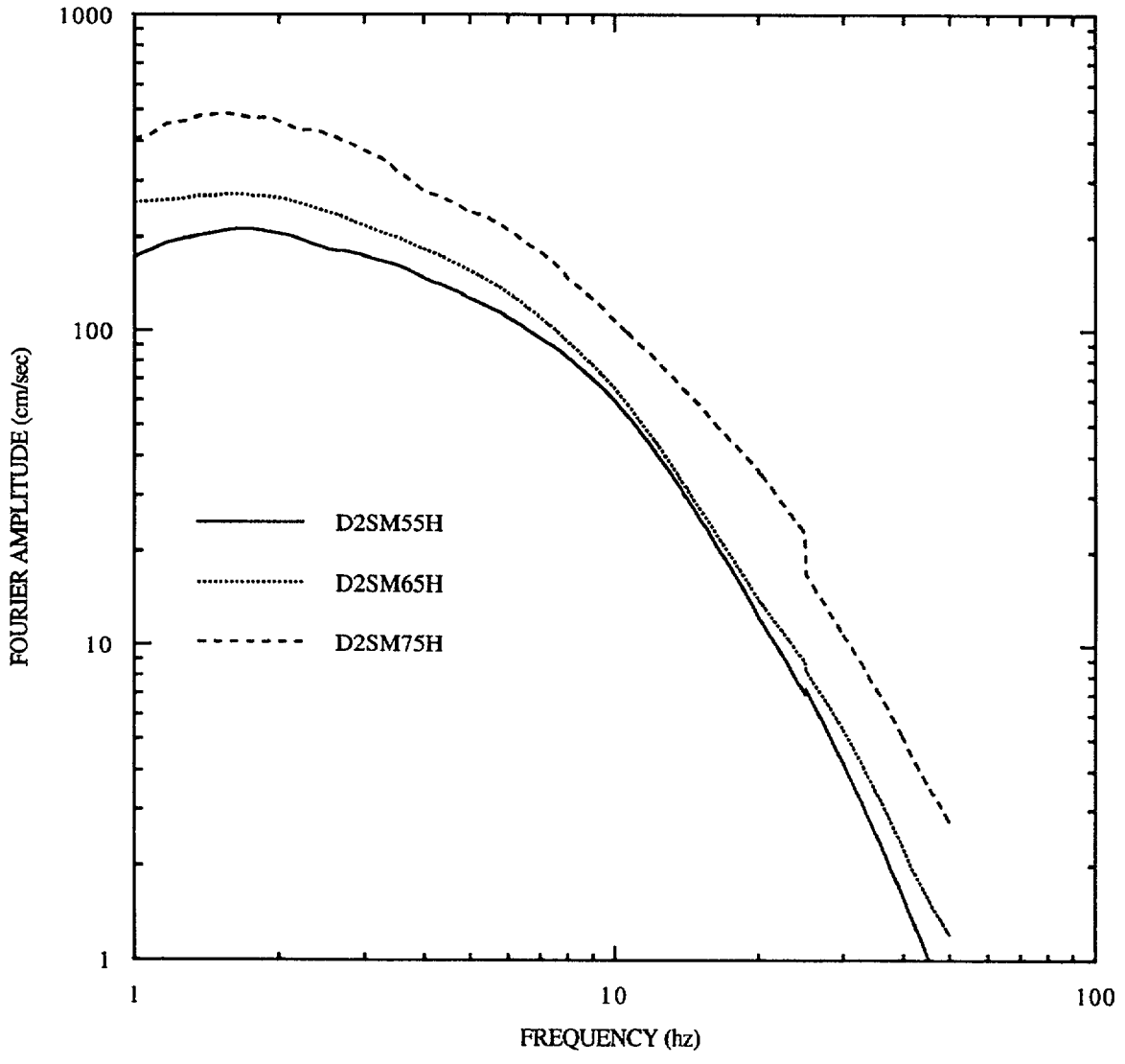


Figure 5-1B. Average smoothed Fourier amplitude spectra, horizontal motions, distance 10-50 km, soil sites.

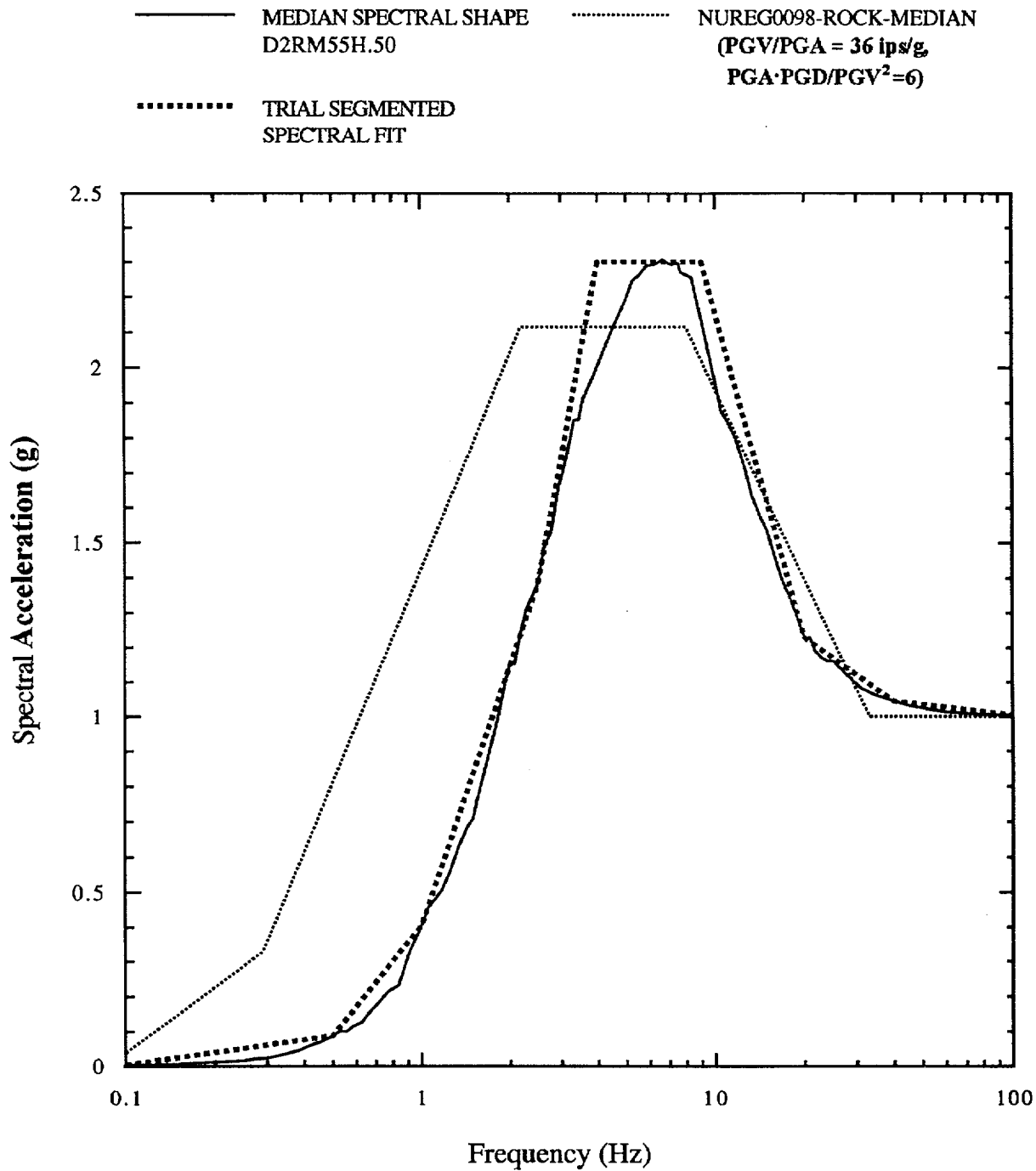


Figure 5-2. 5% damped spectrum for distance bin D2, rock sites, magnitude bin M55, horizontal motion.

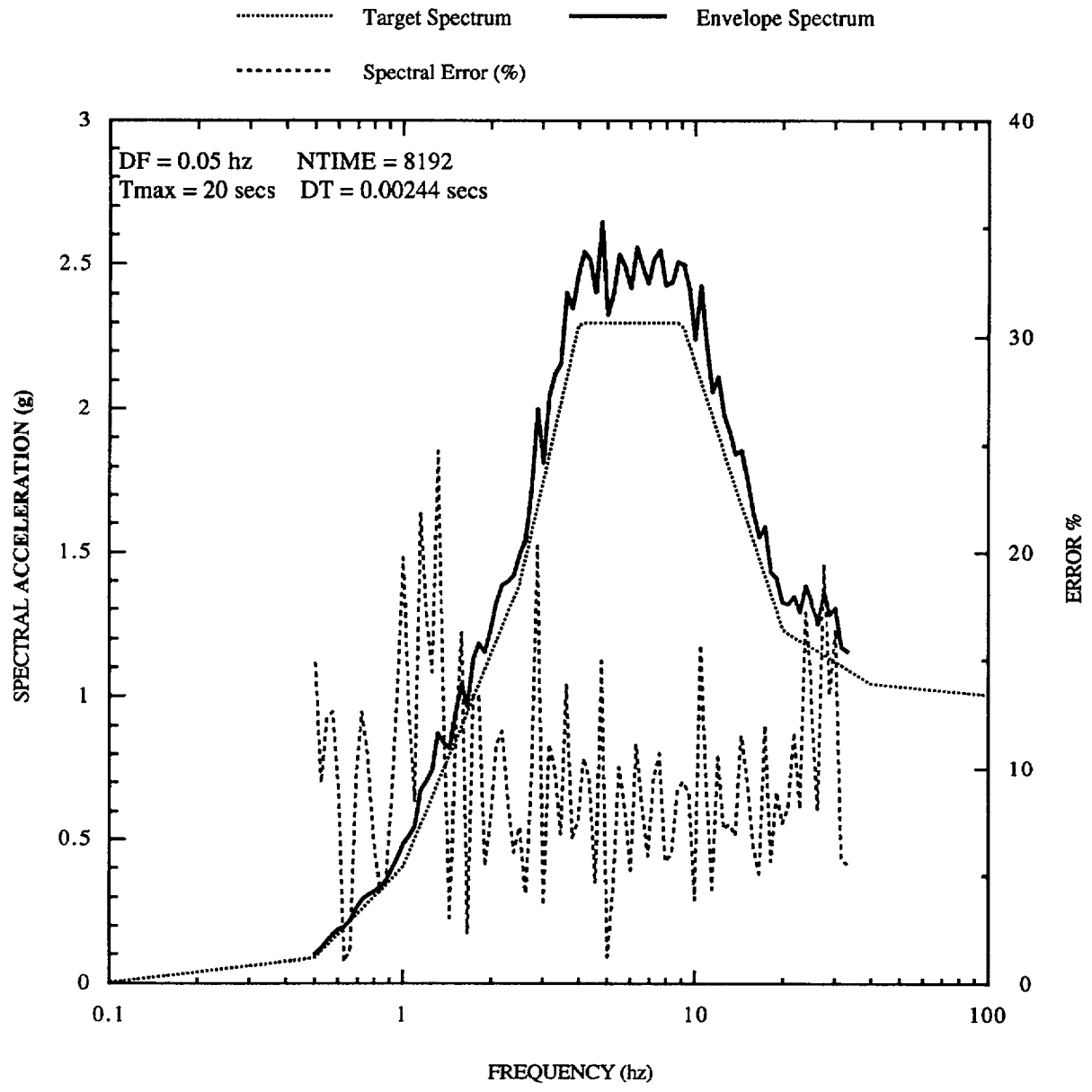


Figure 5-3A. 5% damped spectrum, trial 1

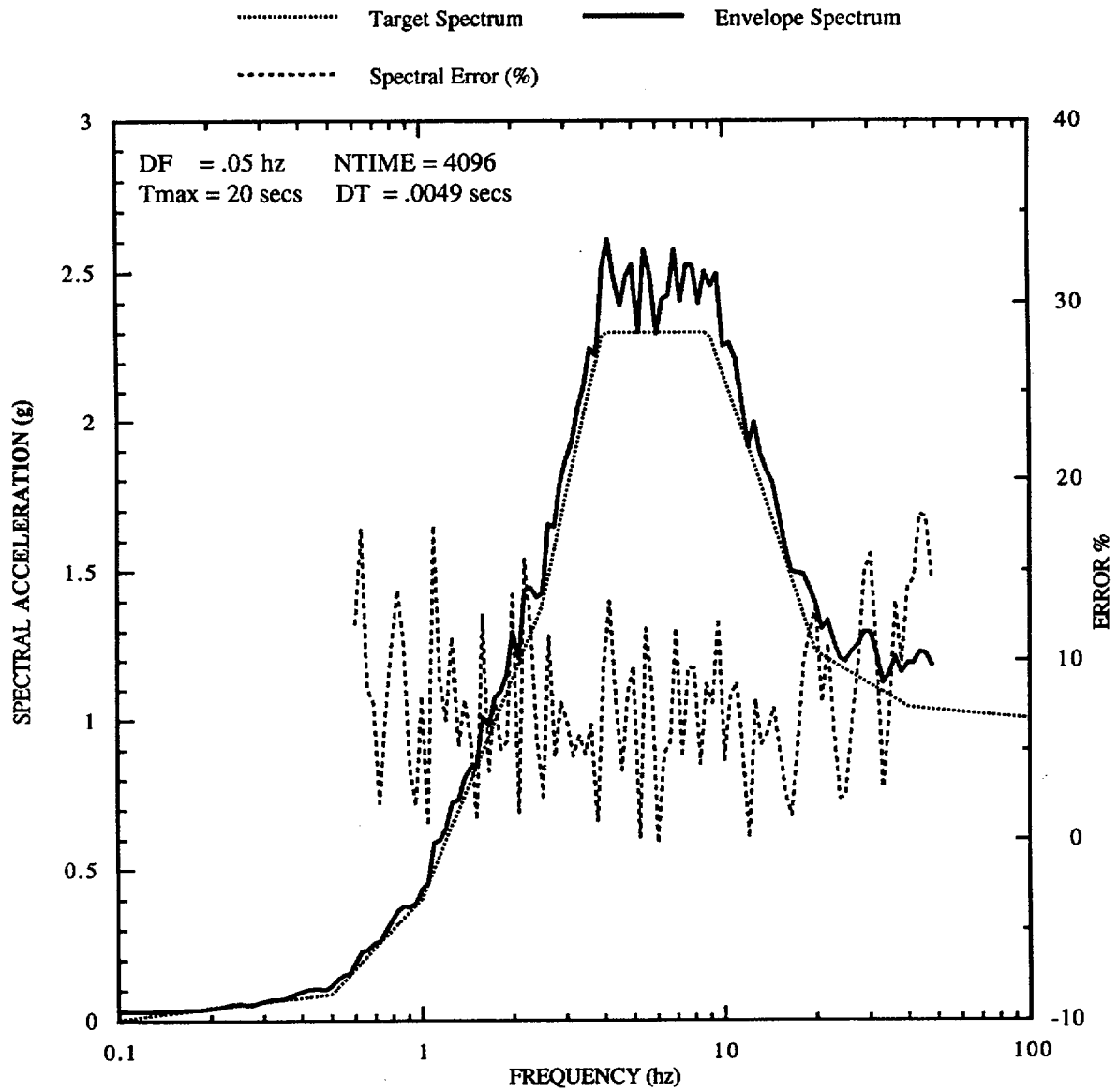


Figure 5-3B. 5% damped spectrum, trial 2

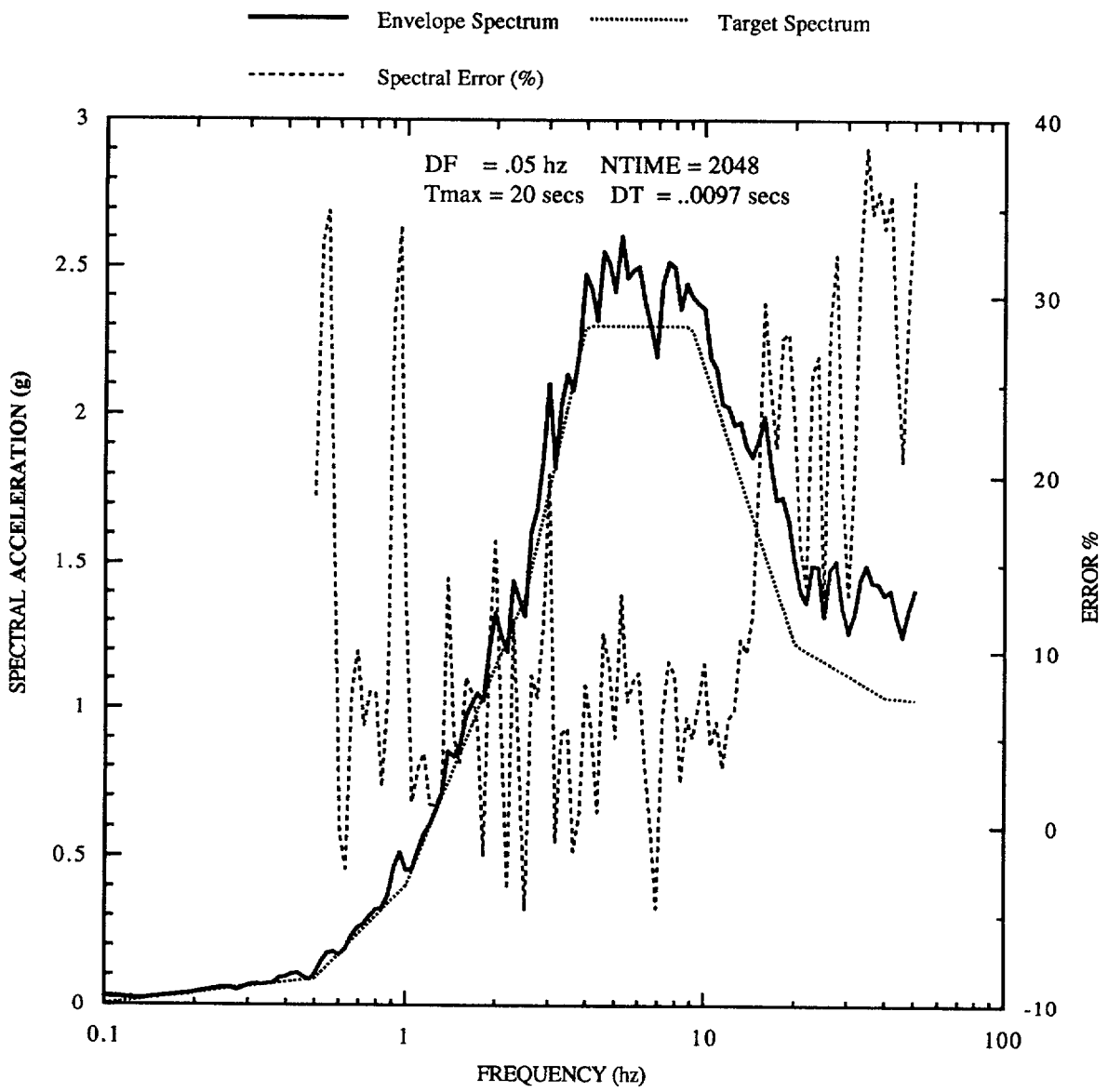


Figure 5-3C. 5% damped spectrum, trial 3

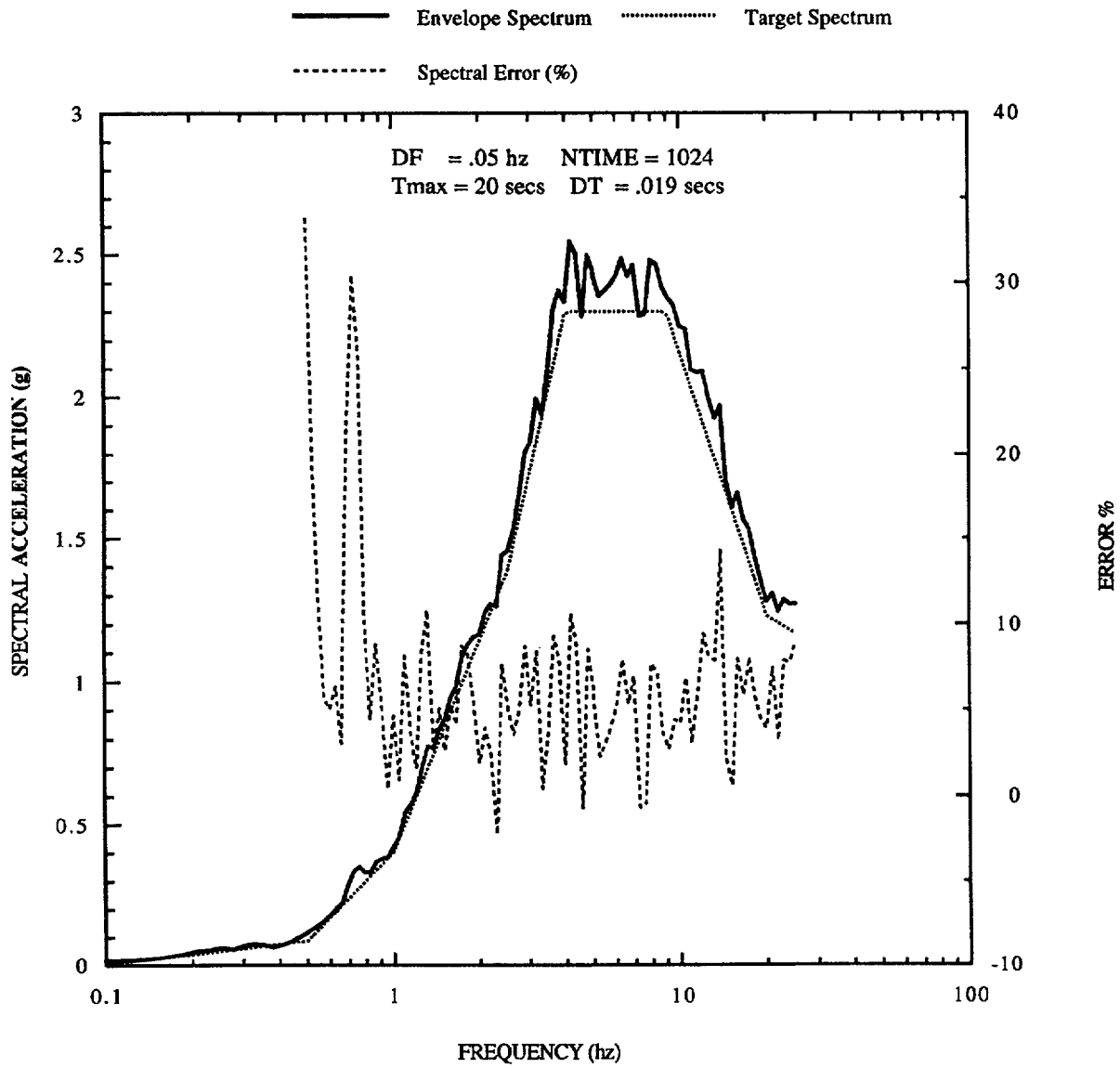


Figure 5-3D. 5% damped spectrum, trial 4

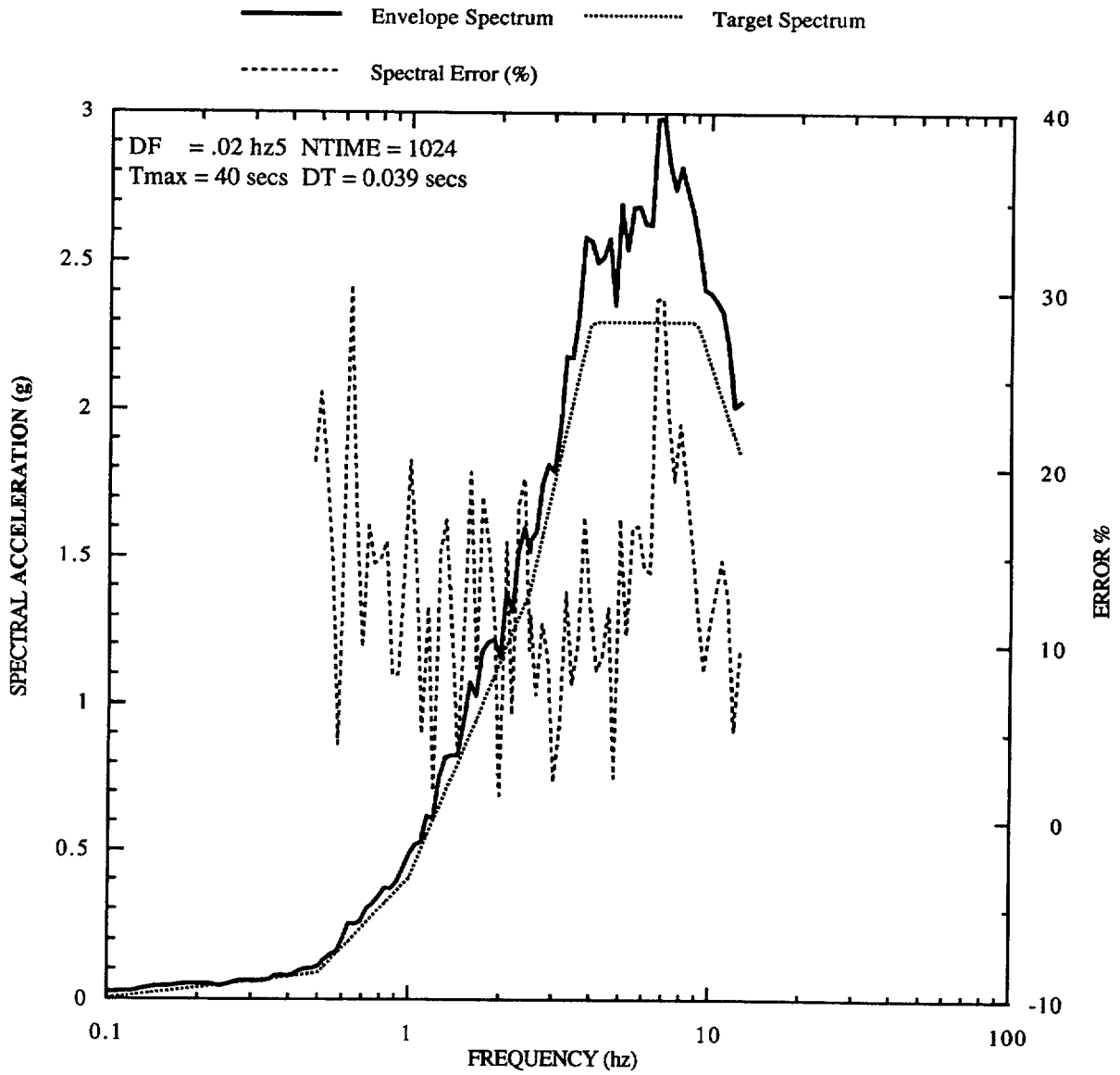


Figure 5-3E. 5% damped spectrum, trial 4S (shorter duration)

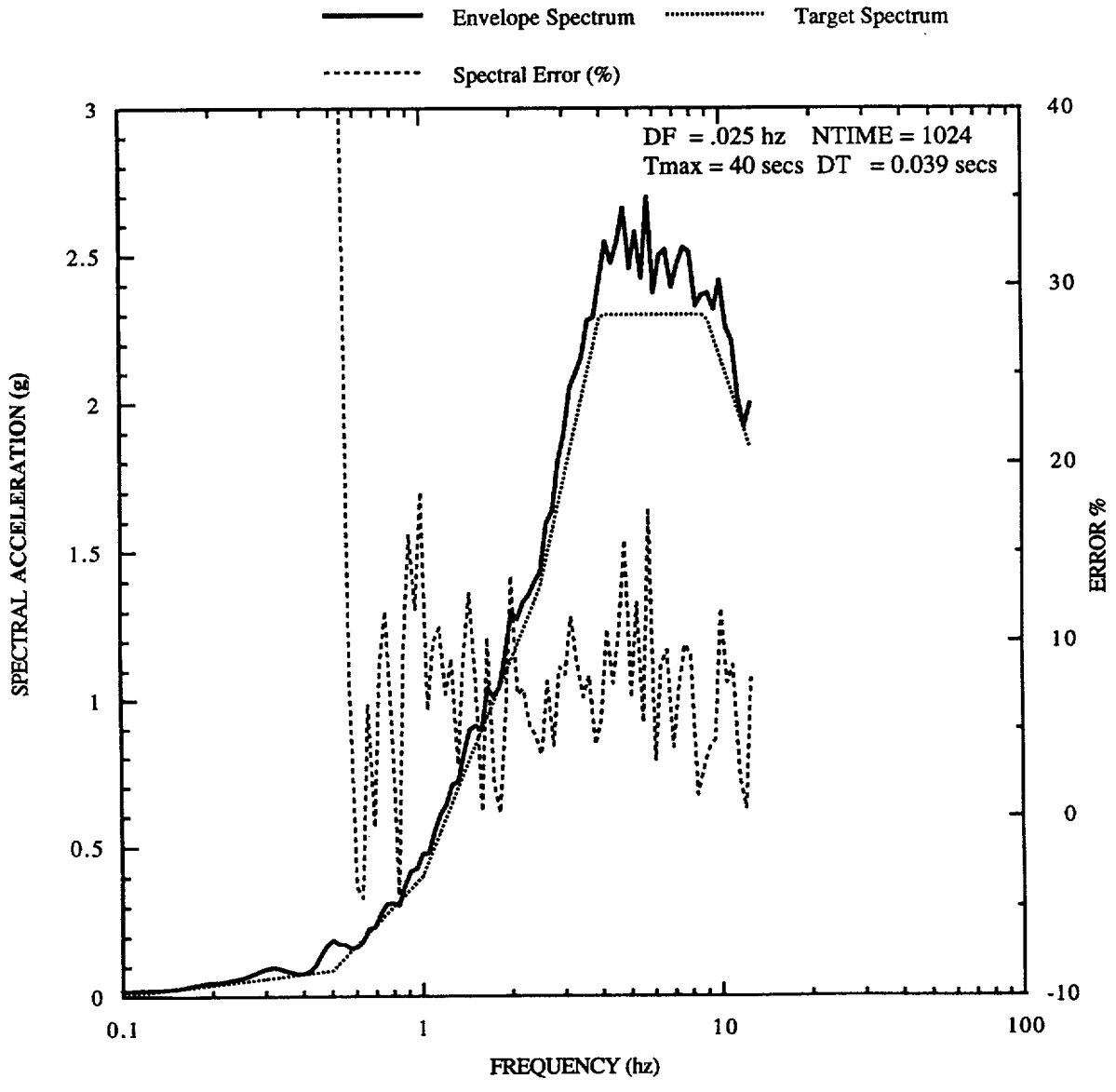


Figure 5-3F. 5% damped spectrum, trial 4L (longer duration)

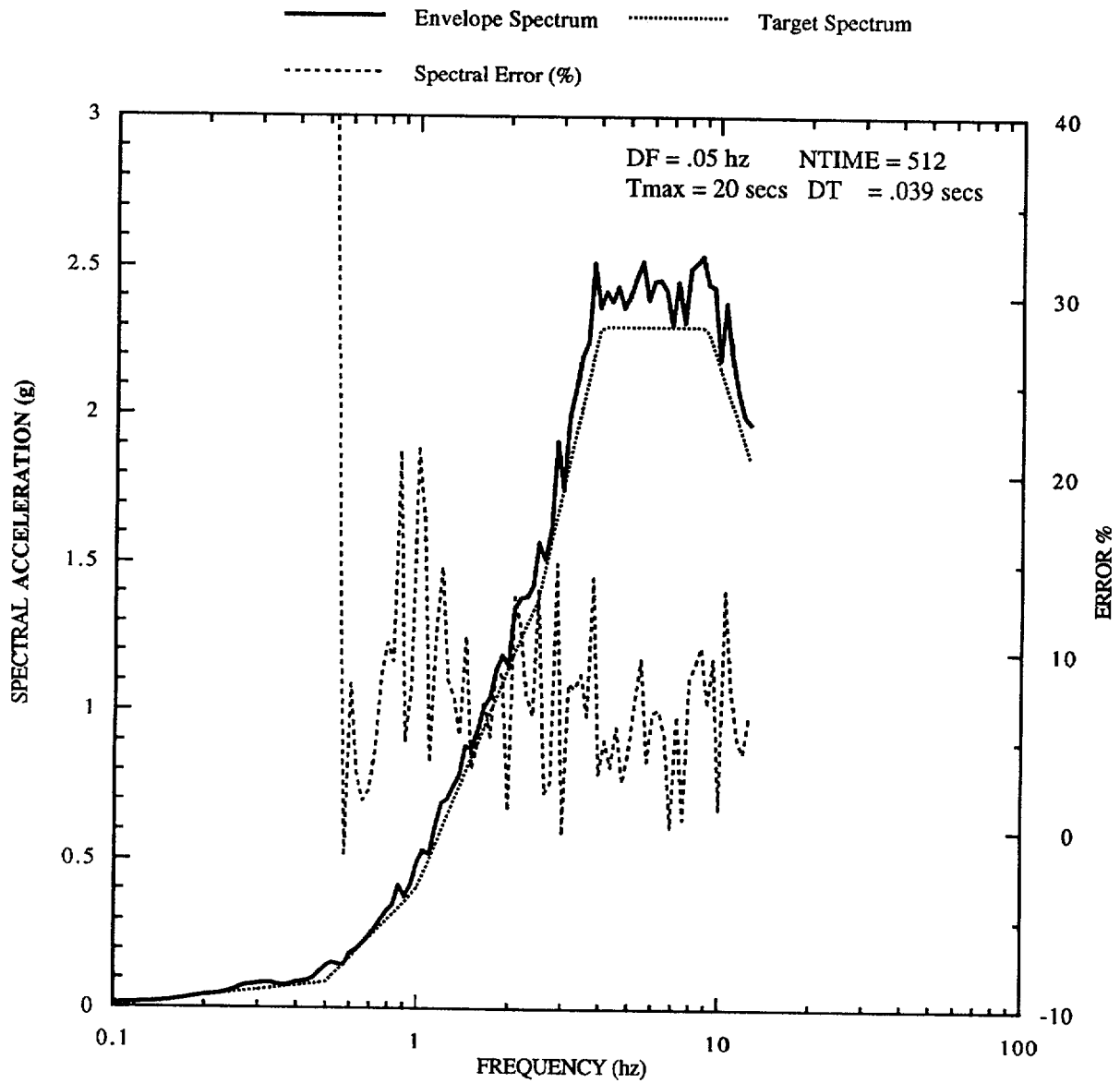


Figure 5-3G. 5% damped spectrum, trial 5

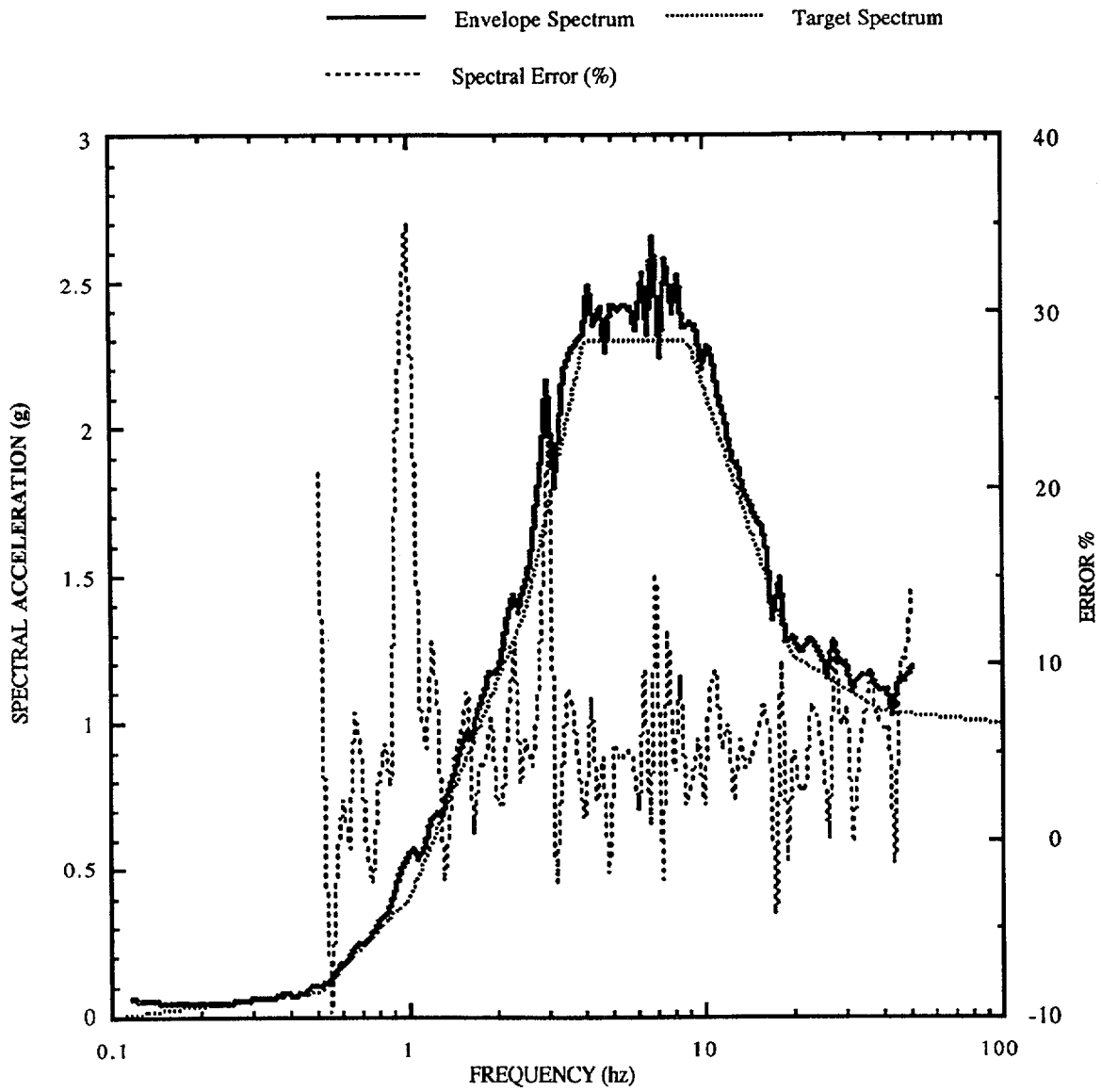


Figure 5-3H. 5% damped spectrum, trial 1S (shorter duration)

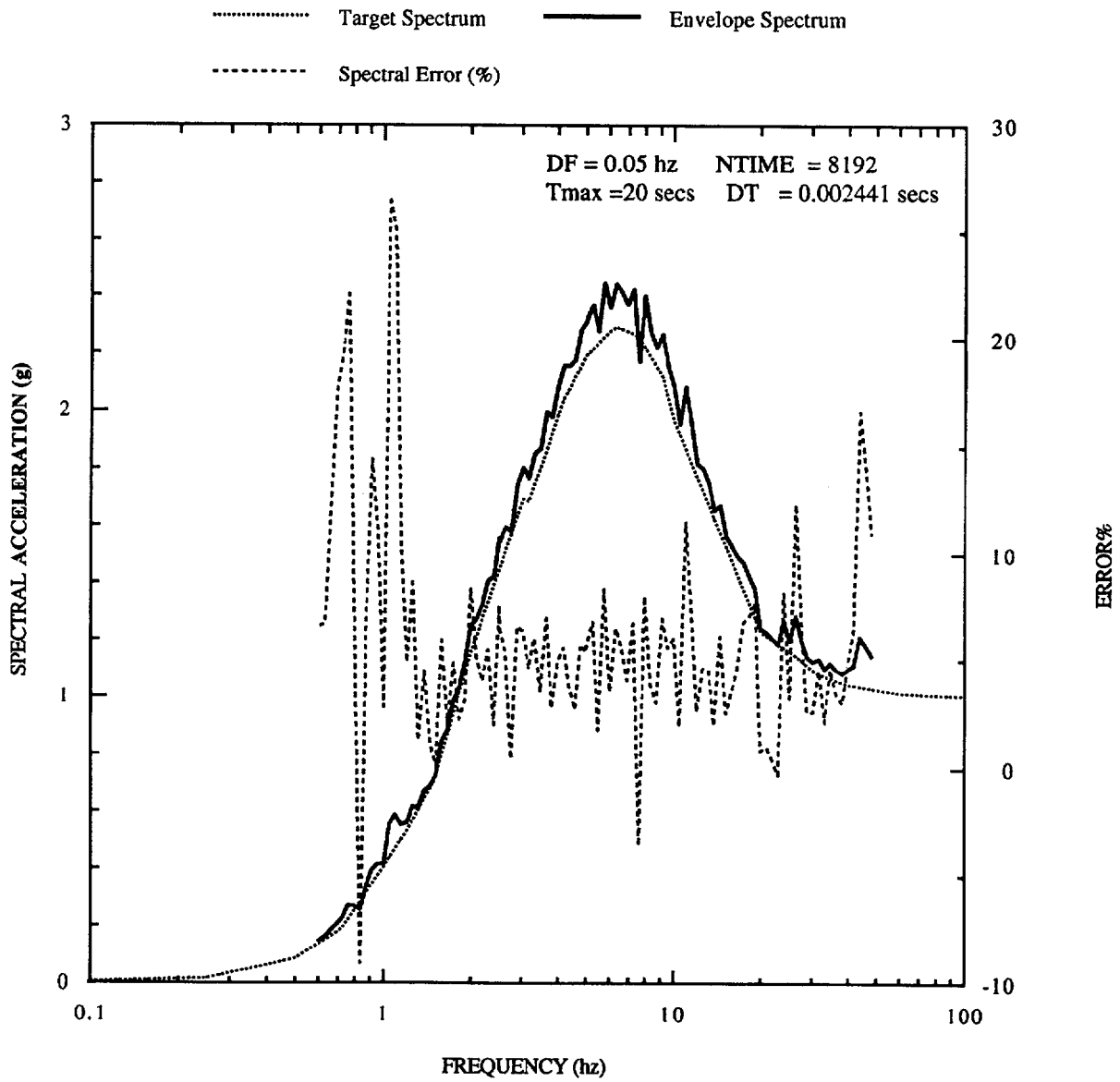


Figure 5-4A. 5% damped spectrum, trial SM01

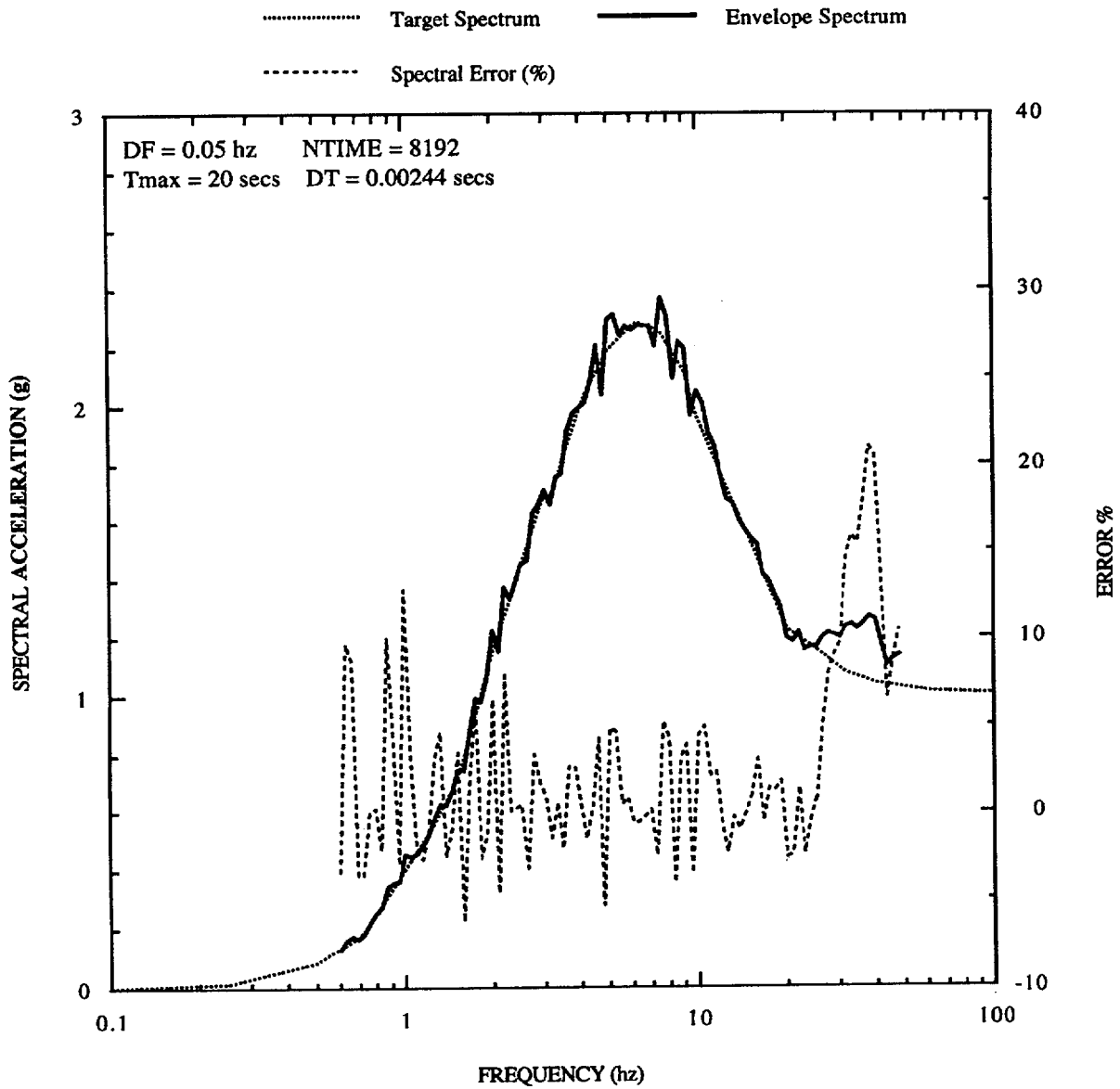


Figure 5-4B. 5% damped spectrum, trial SM02

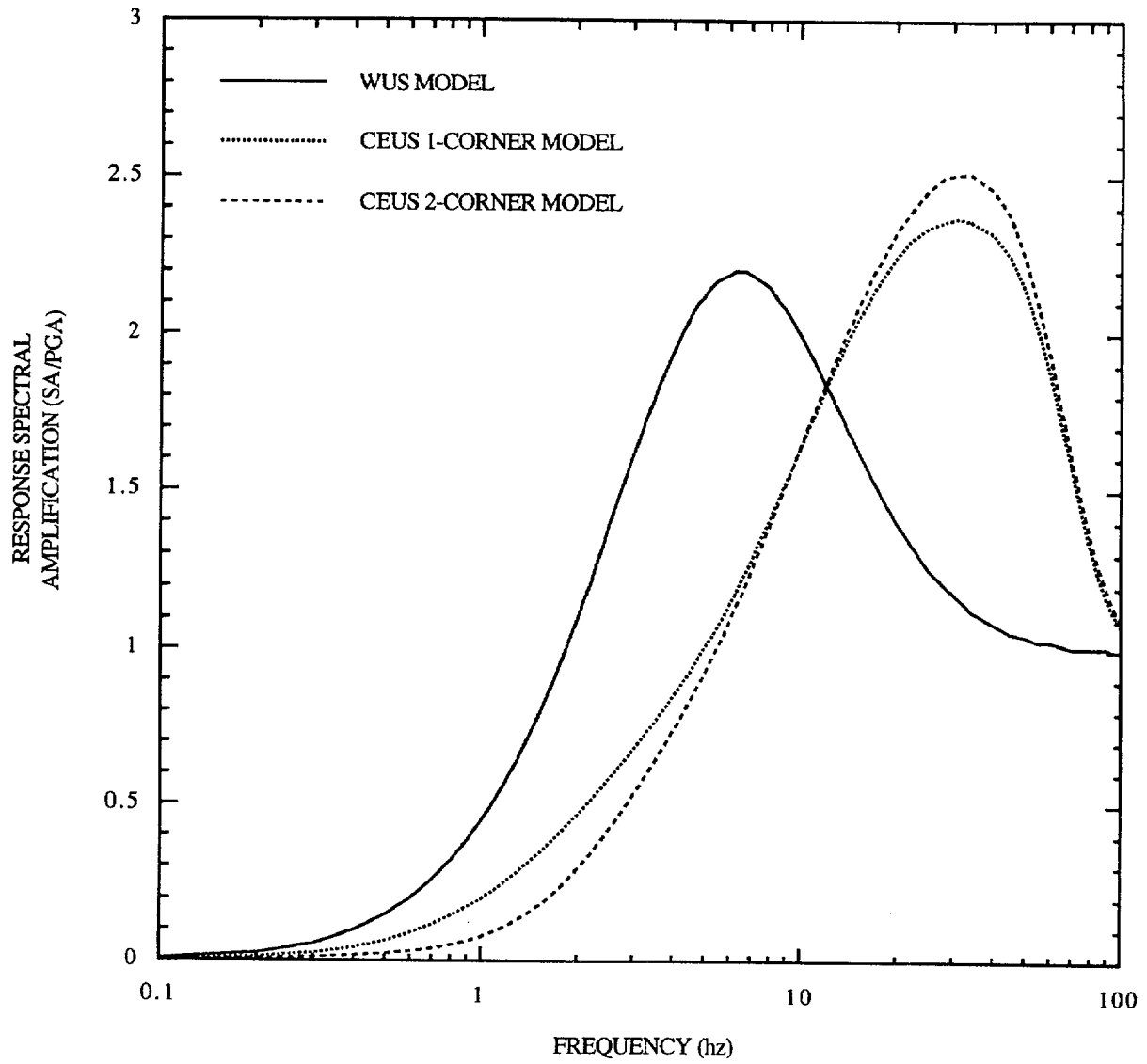


Figure 5-5. Spectral acceleration shapes for $\bar{M} = 5.57, \bar{R} = 21.8$ rock horizontal motion bin D2RM55H

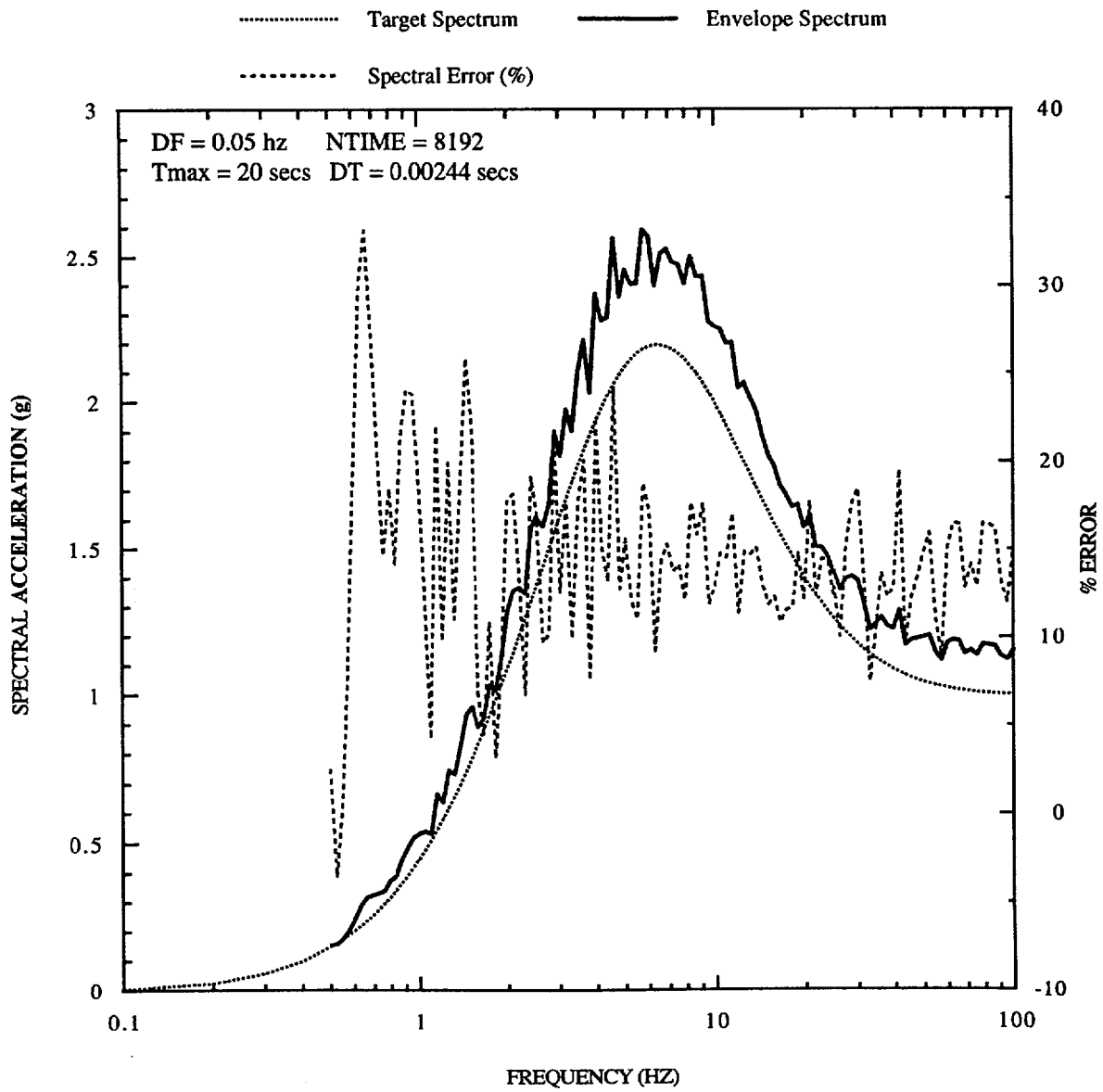


Figure 5-6A. 5% damped spectrum, trial SM01, WUS spectrum, $\bar{M} = 5.57$, $\bar{R} = 21.8$ km (random phase spectrum)

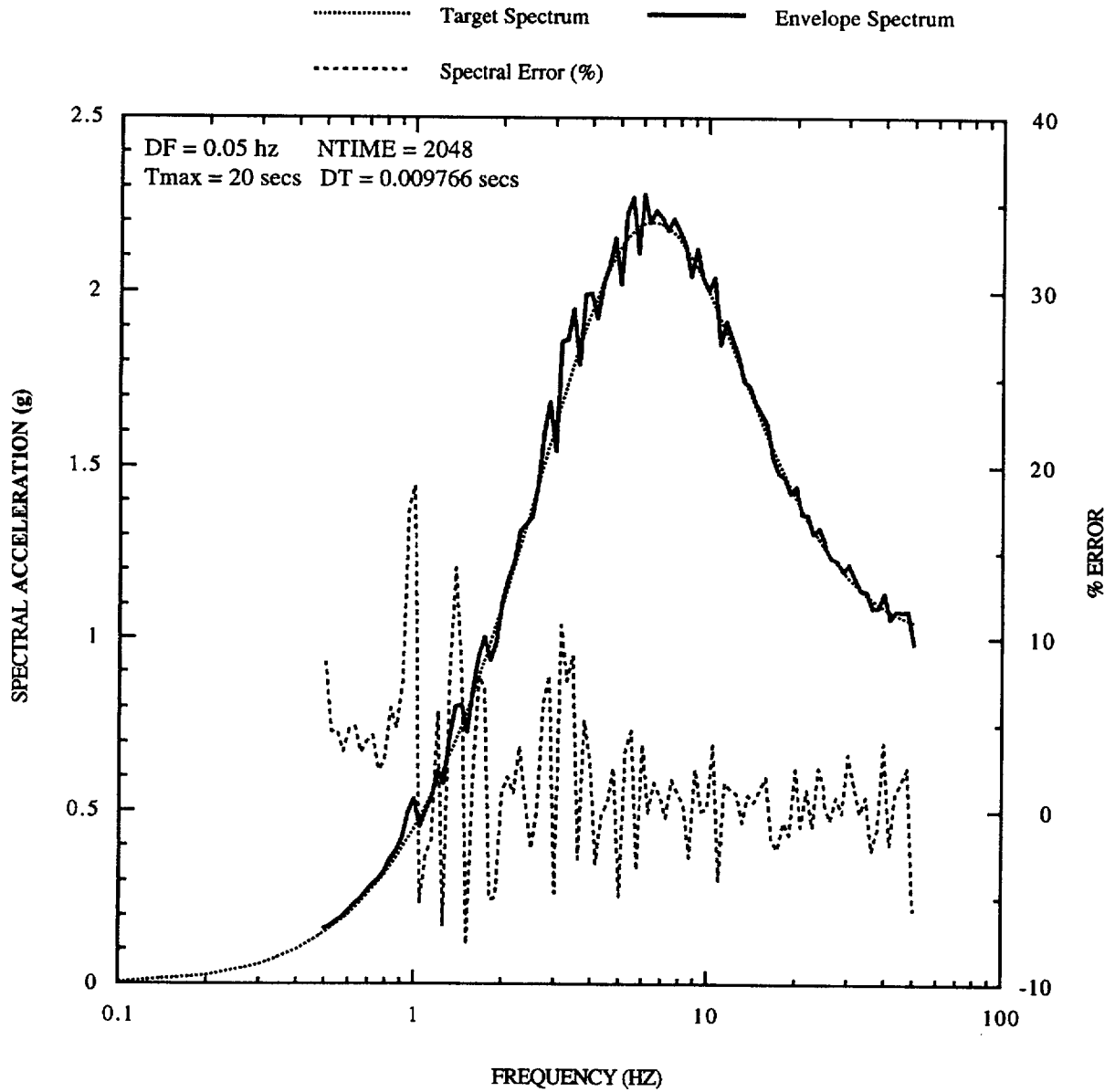


Figure 5-6B. 5% damped spectrum, trial SM02, WUS spectrum, $\bar{M} = 5.57$, $\bar{R} = 21.8$ km (record phase spectrum 1)

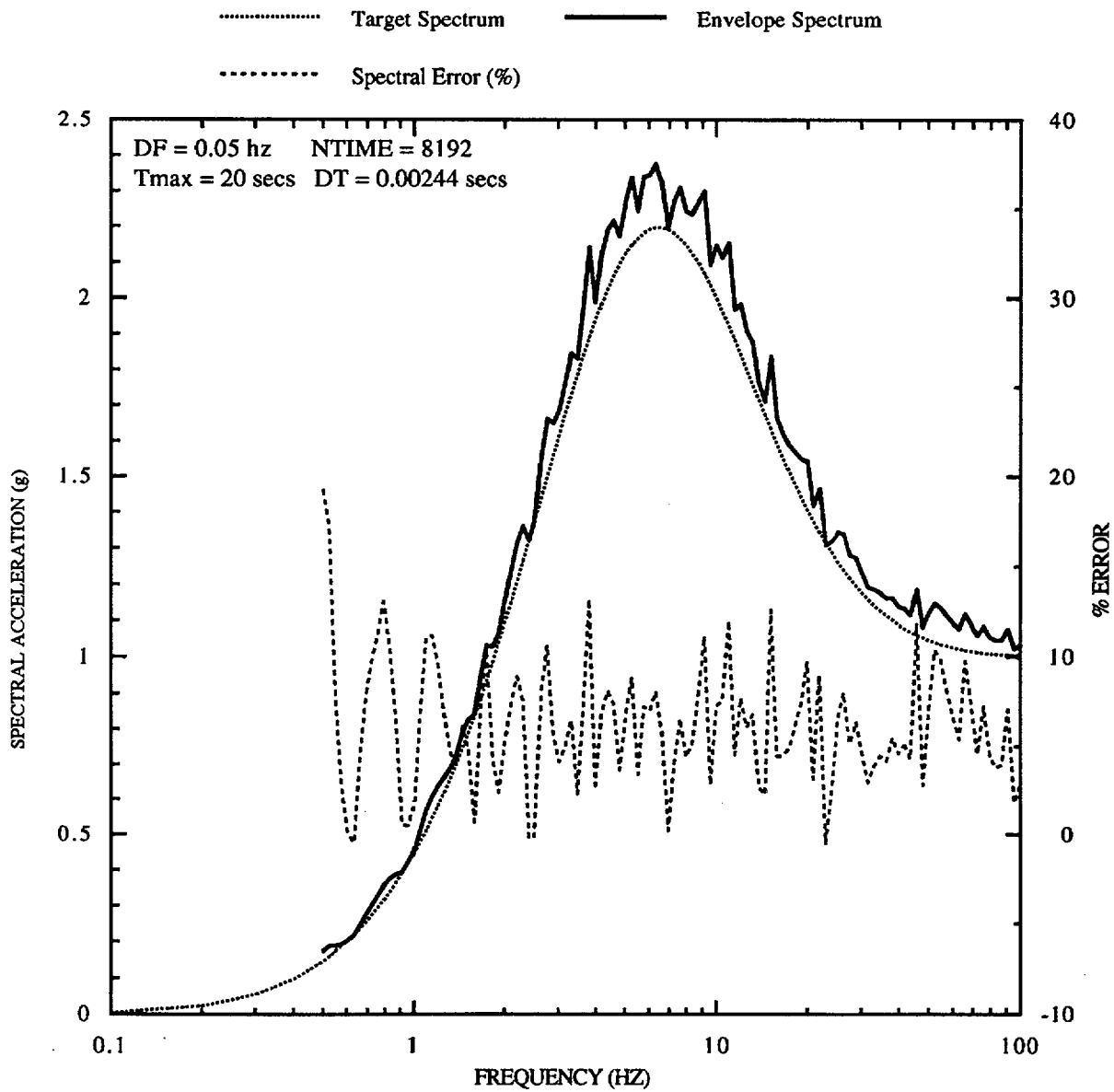


Figure 5-6C. 5% damped spectrum, trial SM03, WUS spectrum, $\bar{M} = 5.57$, $\bar{R} = 21.8$ km (record phase spectrum 2)

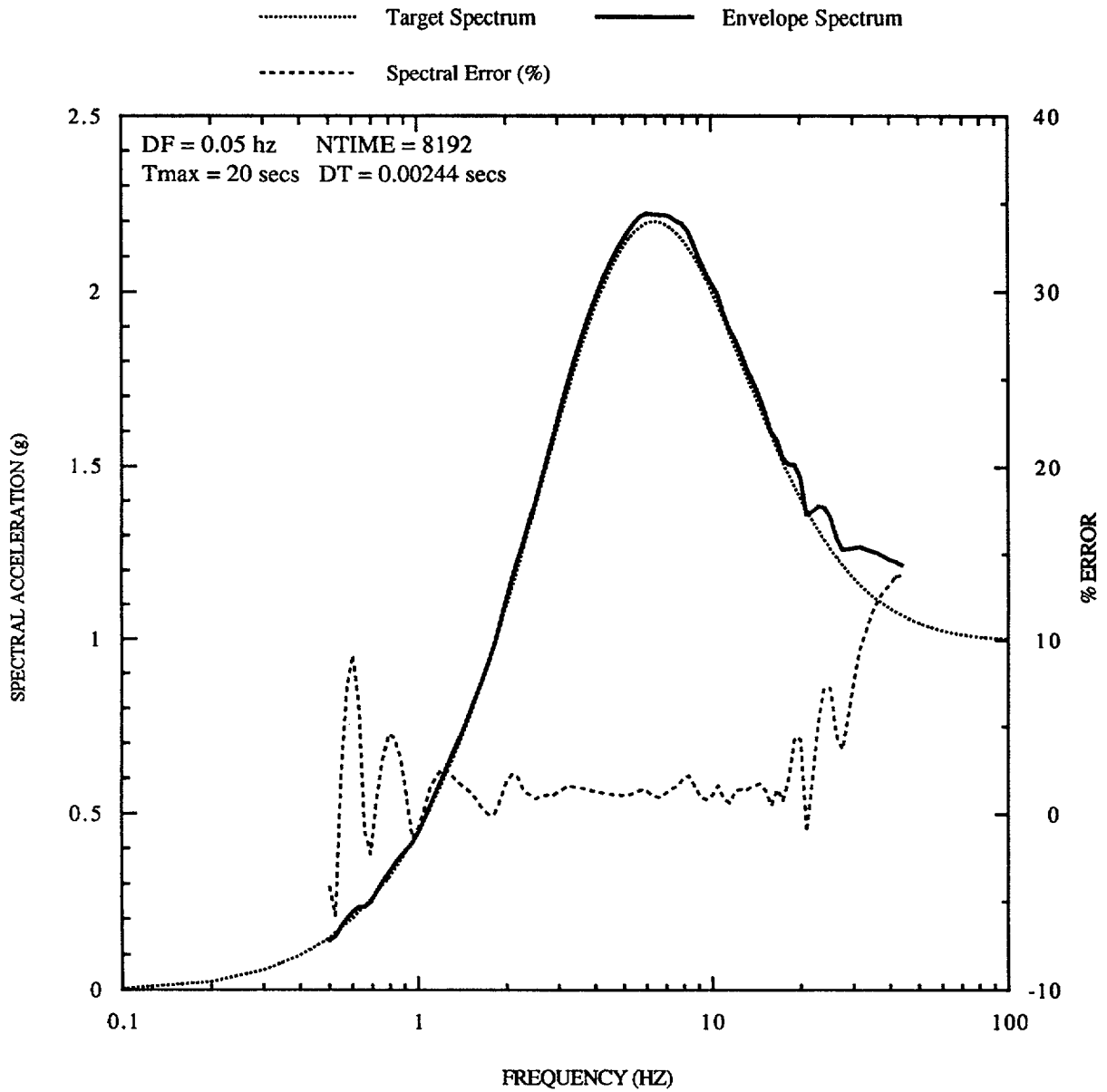


Figure 5-6D. 5% damped spectrum, trial SM04, WUS spectrum, $\bar{M} = 5.57$, $\bar{R} = 21.8$ km (record phase spectrum 3)

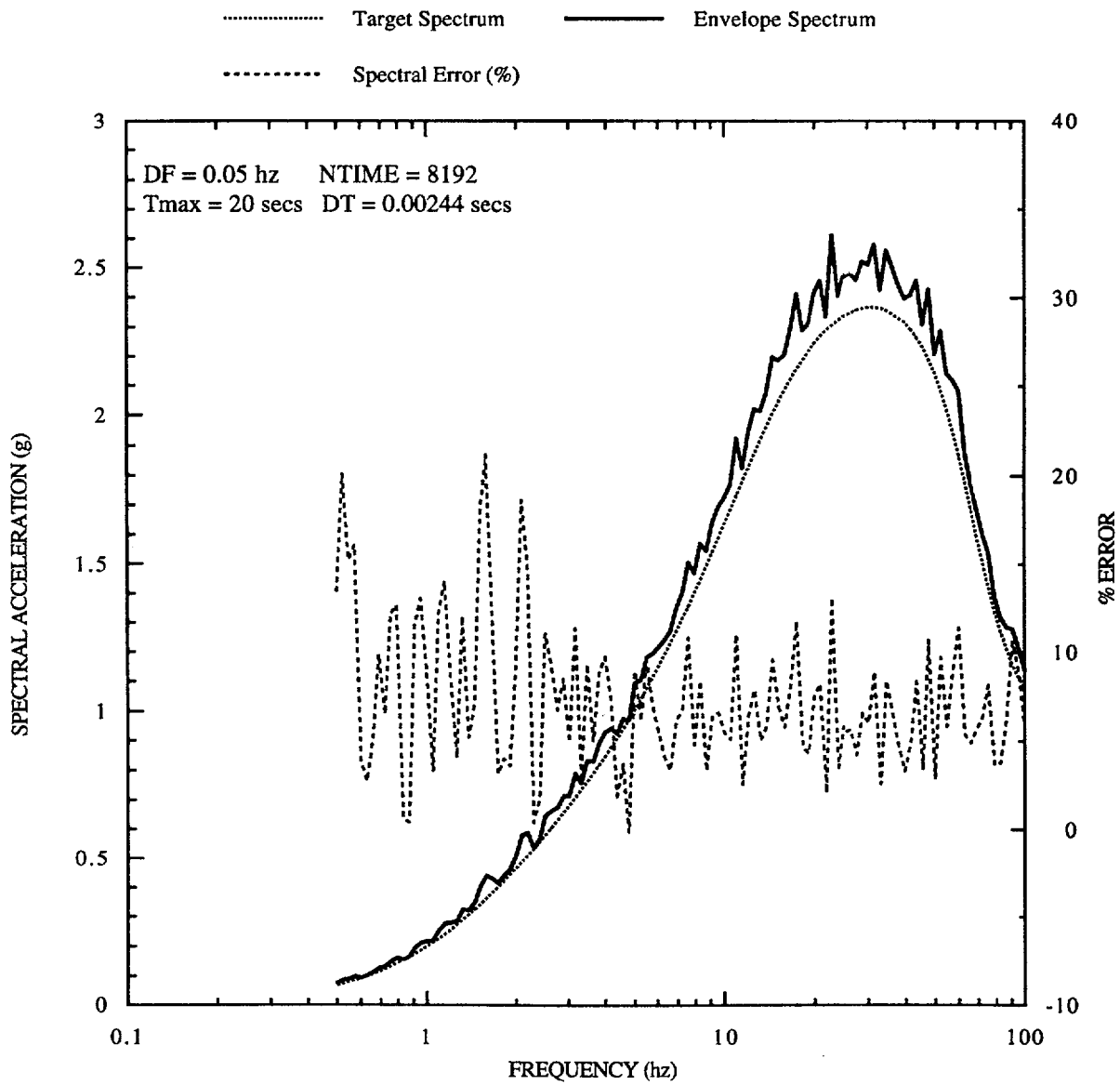


Figure 5-7A. 5% damped spectrum, trial SM01, CEUS 1-corner spectrum, $\bar{M} = 5.57$, $R = 21.8$ km (random phase spectrum)

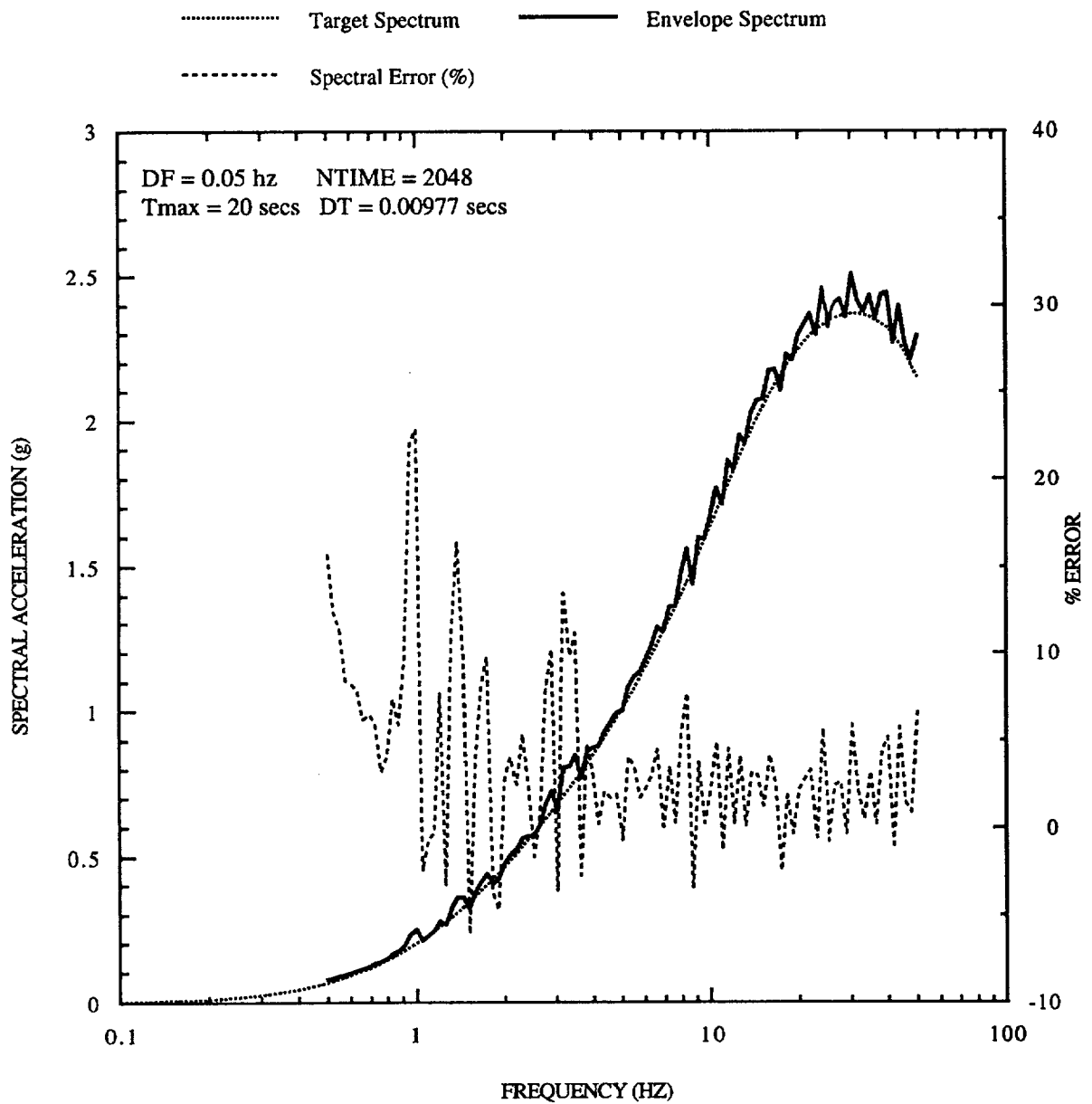


Figure 5-7B. 5% damped spectrum, trial SM02, CEUS 1-corner spectrum, $\bar{M} = 5.57$, $R = 21.8$ km (random phase spectrum 1)

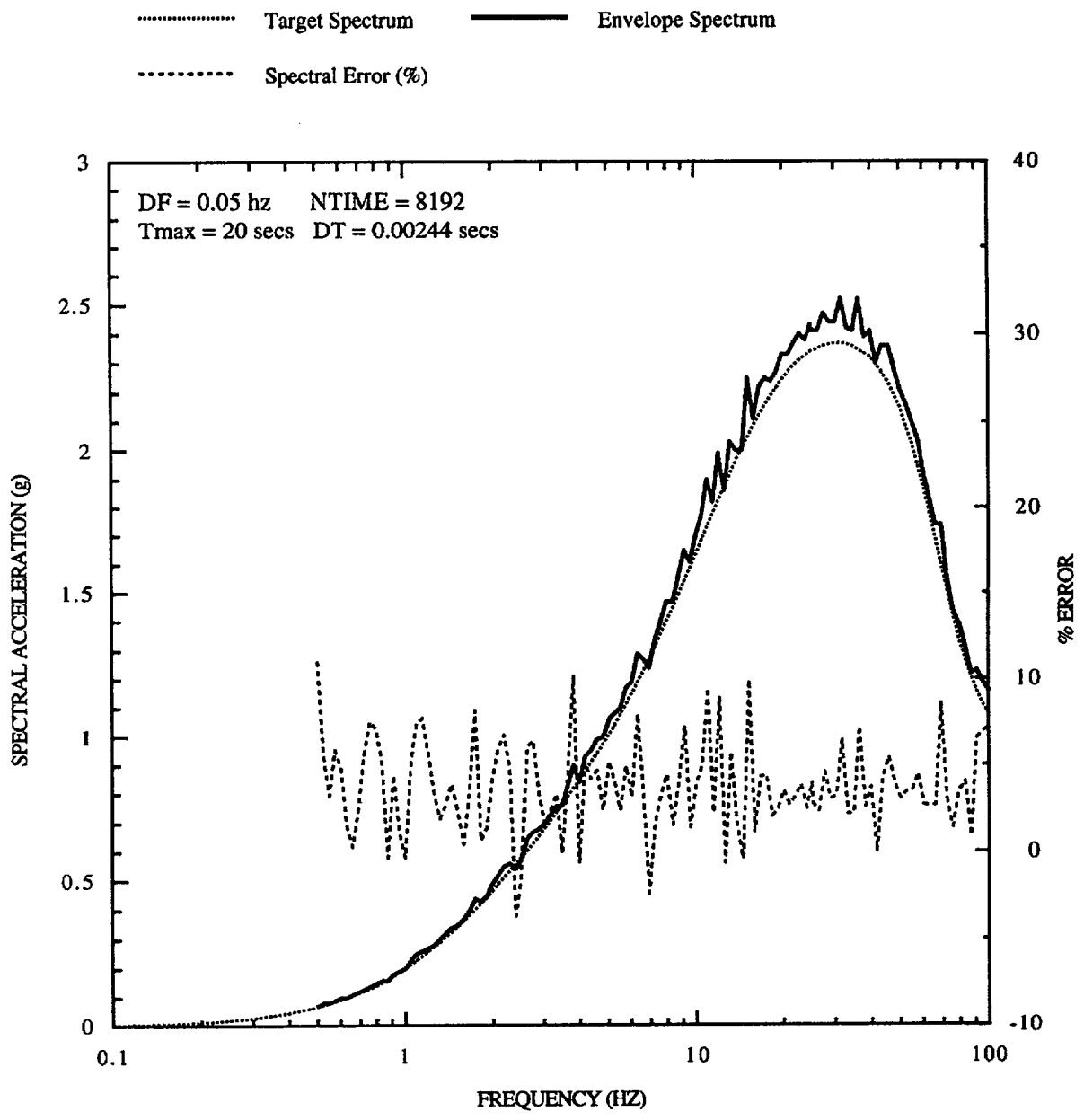


Figure 5-7C. 5% damped spectrum, trial SM03, CEUS 1-corner spectrum, $\bar{M} = 5.57$, $R = 21.8$ km (random phase spectrum 2)

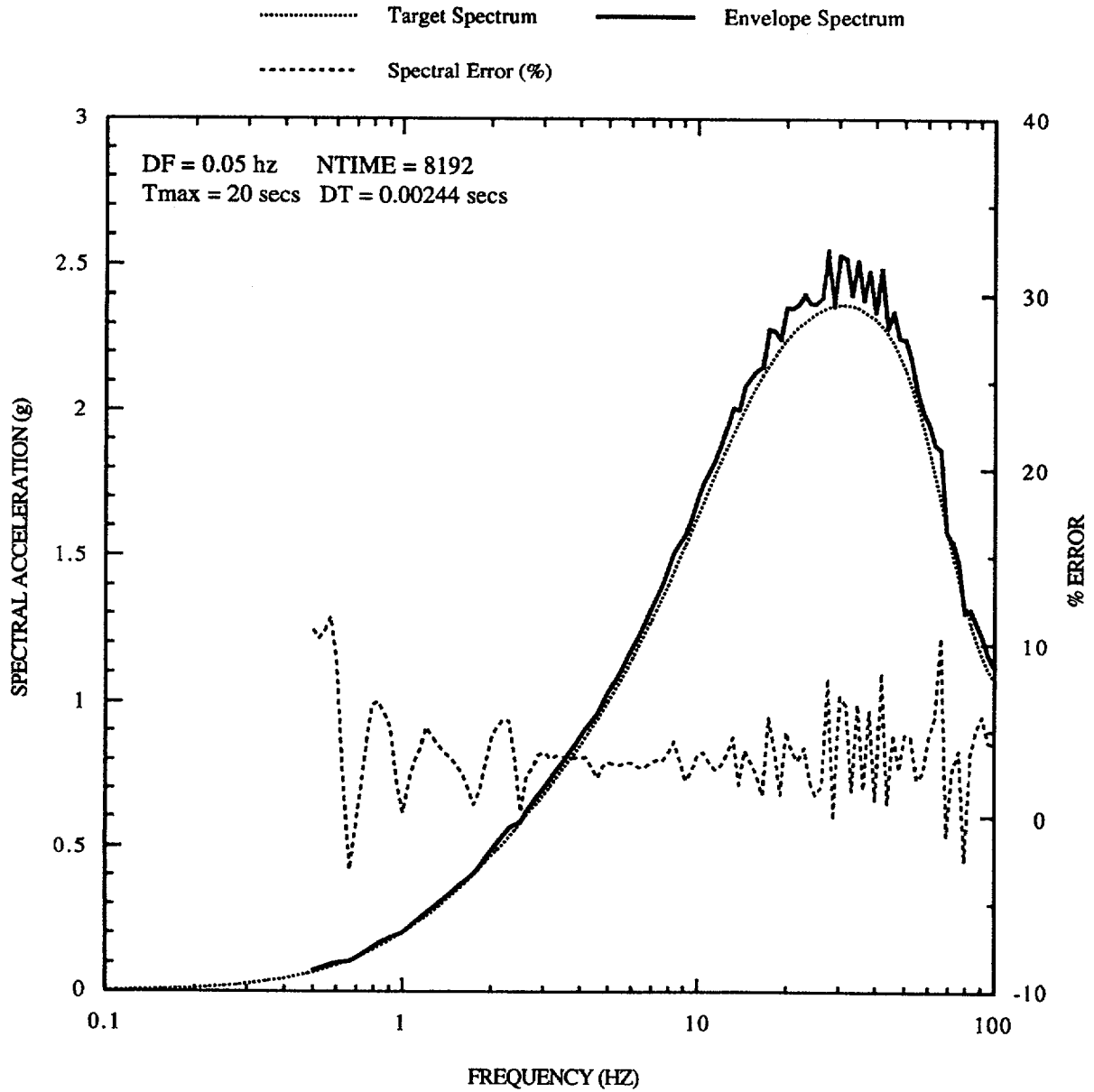


Figure 5-7D. 5% damped spectrum, trial SM04, CEUS 1-corner spectrum, $\bar{M} = 5.57$, $R = 21.8$ km (random phase spectrum 3)

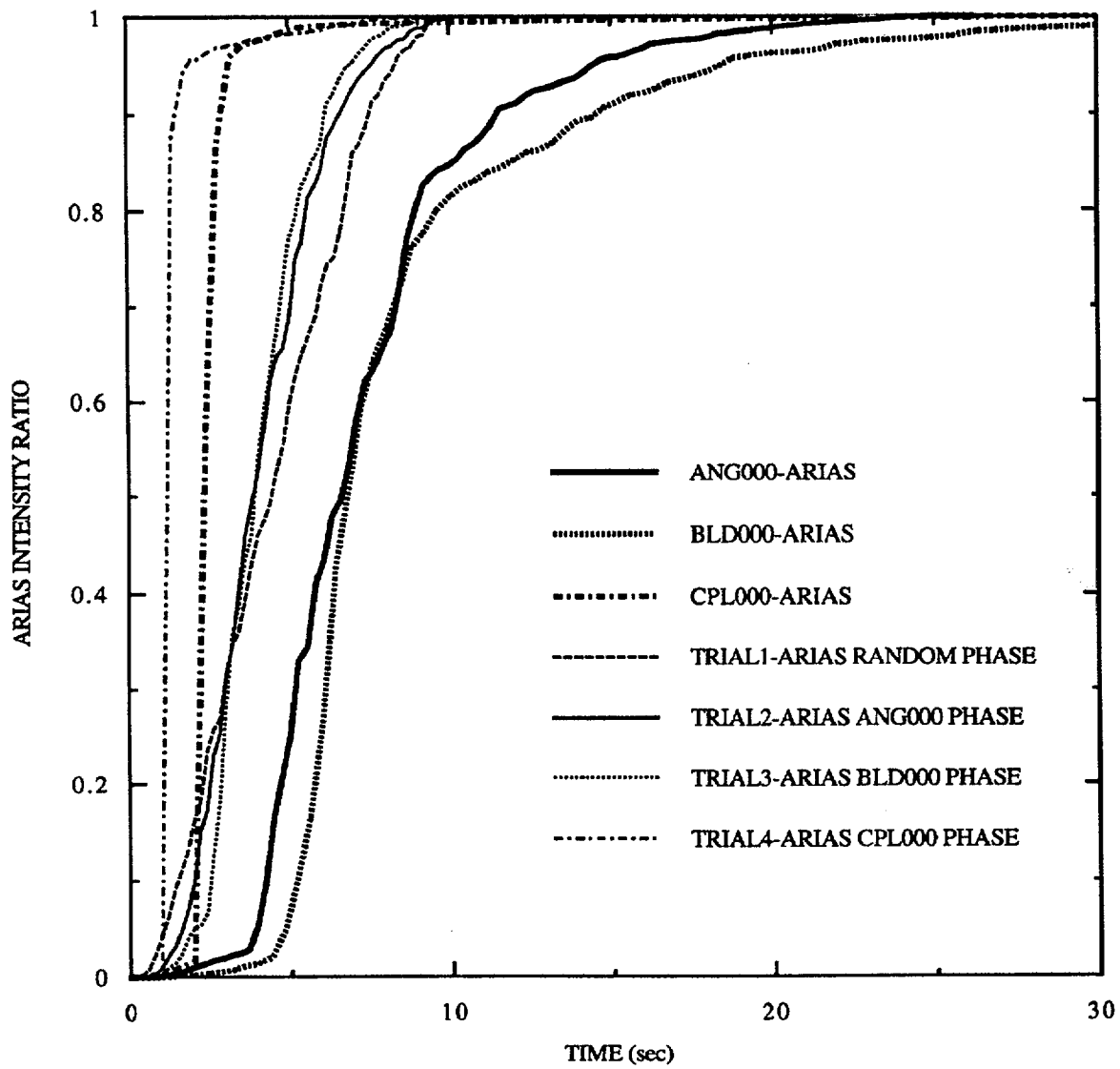


Figure 5-8A. Arias Intensity ratios for trial records used to envelop WUS bin spectrum of Figure 5-6.

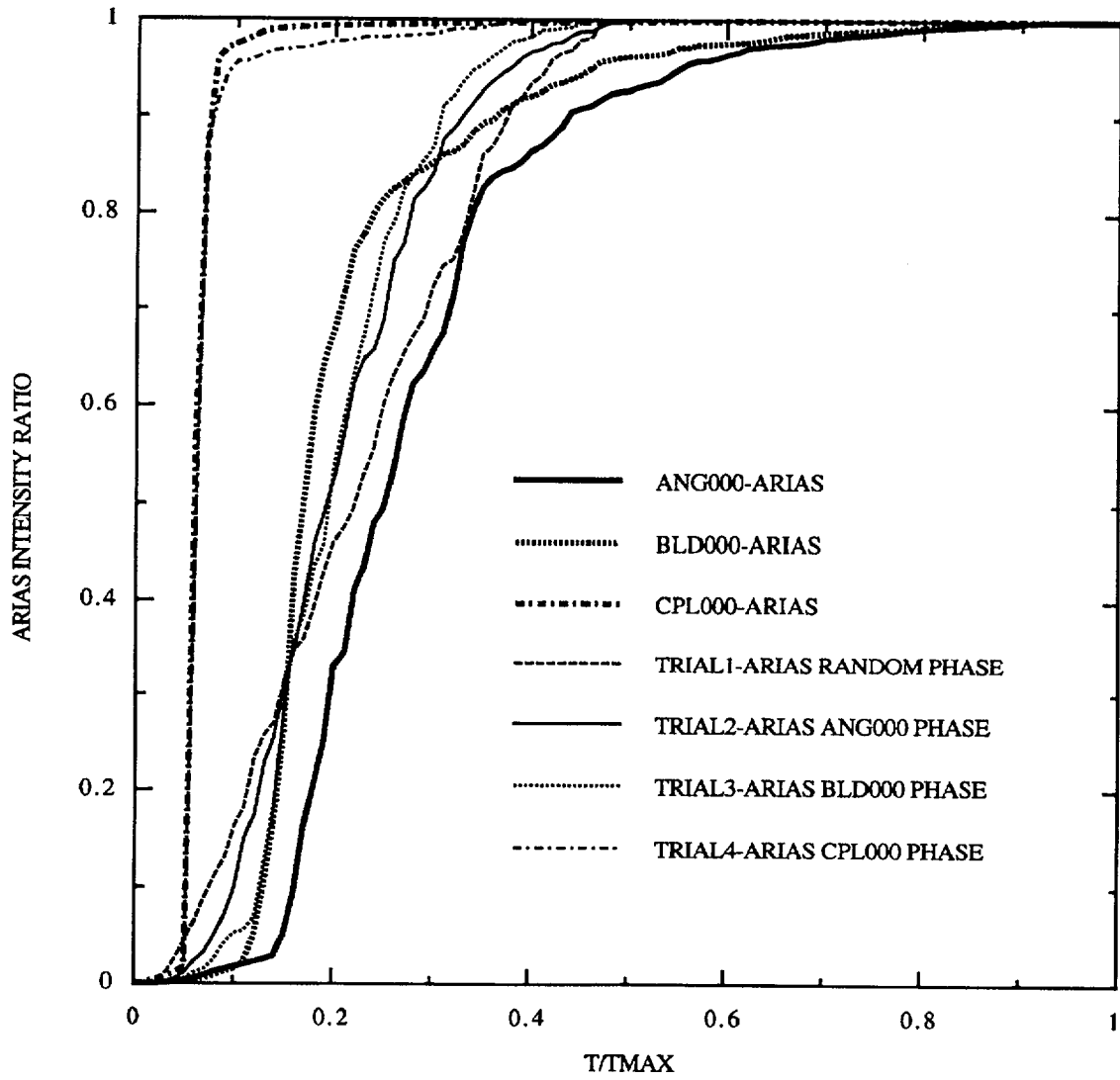


Figure 5-8B. Arias Intensity ratios for WUS records scaled to maximum time duration.

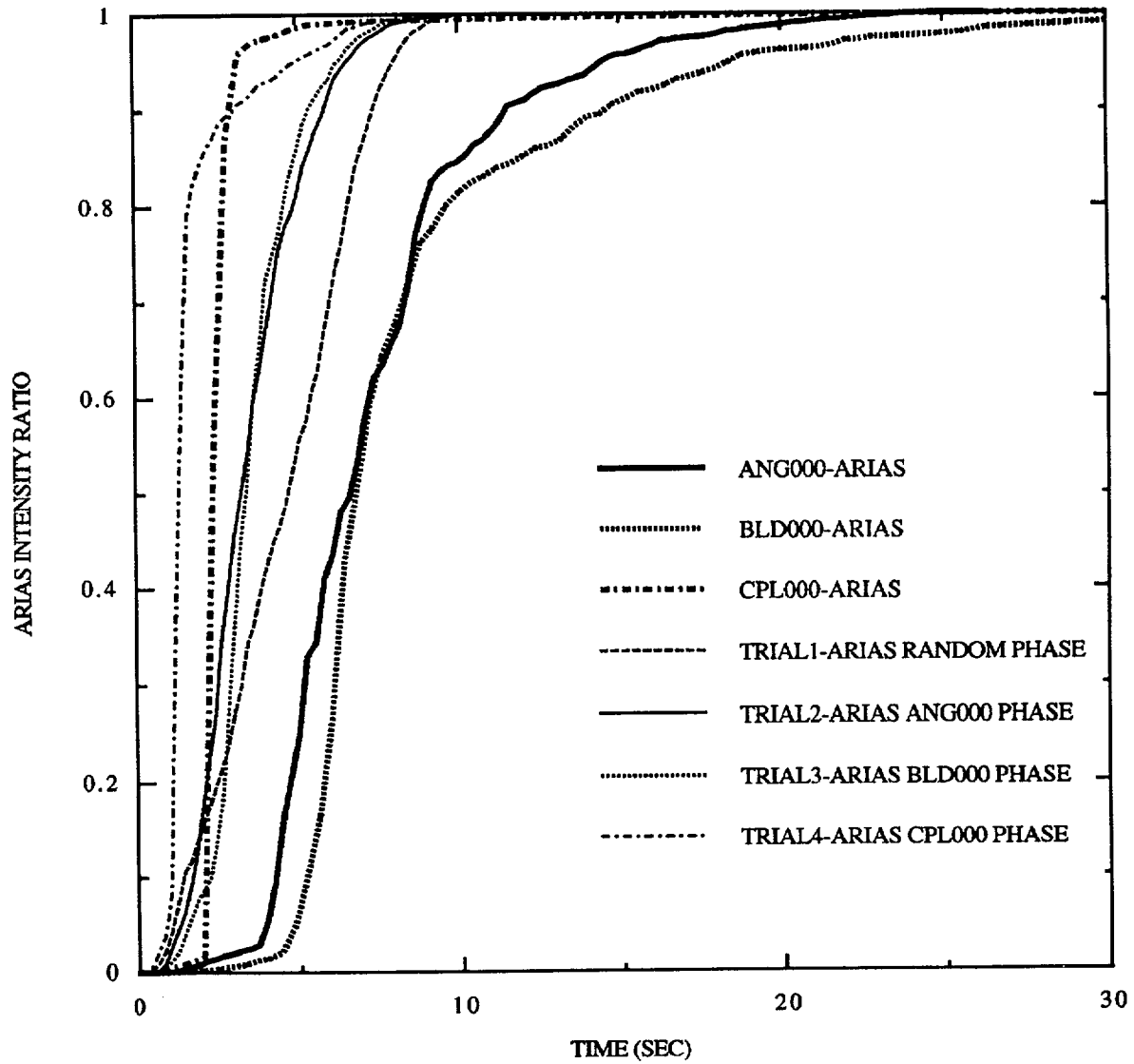


Figure 5-9A. Arias Intensity ratios for trial records used to envelop CEUS 1-corner spectrum of Figure 5-7.

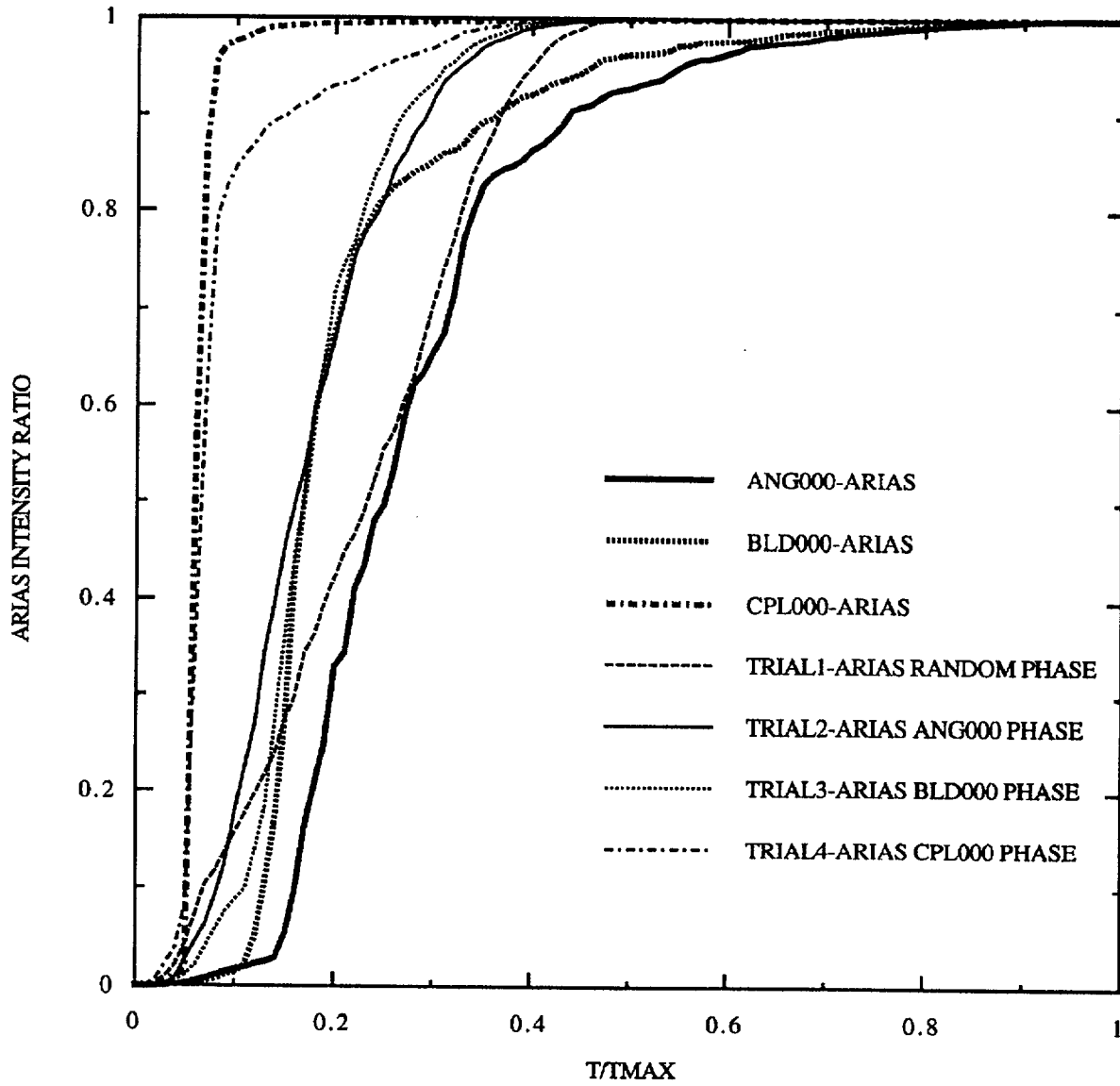


Figure 5-9B. Arias Intensity ratios for CEUS records scaled to maximum time duration.

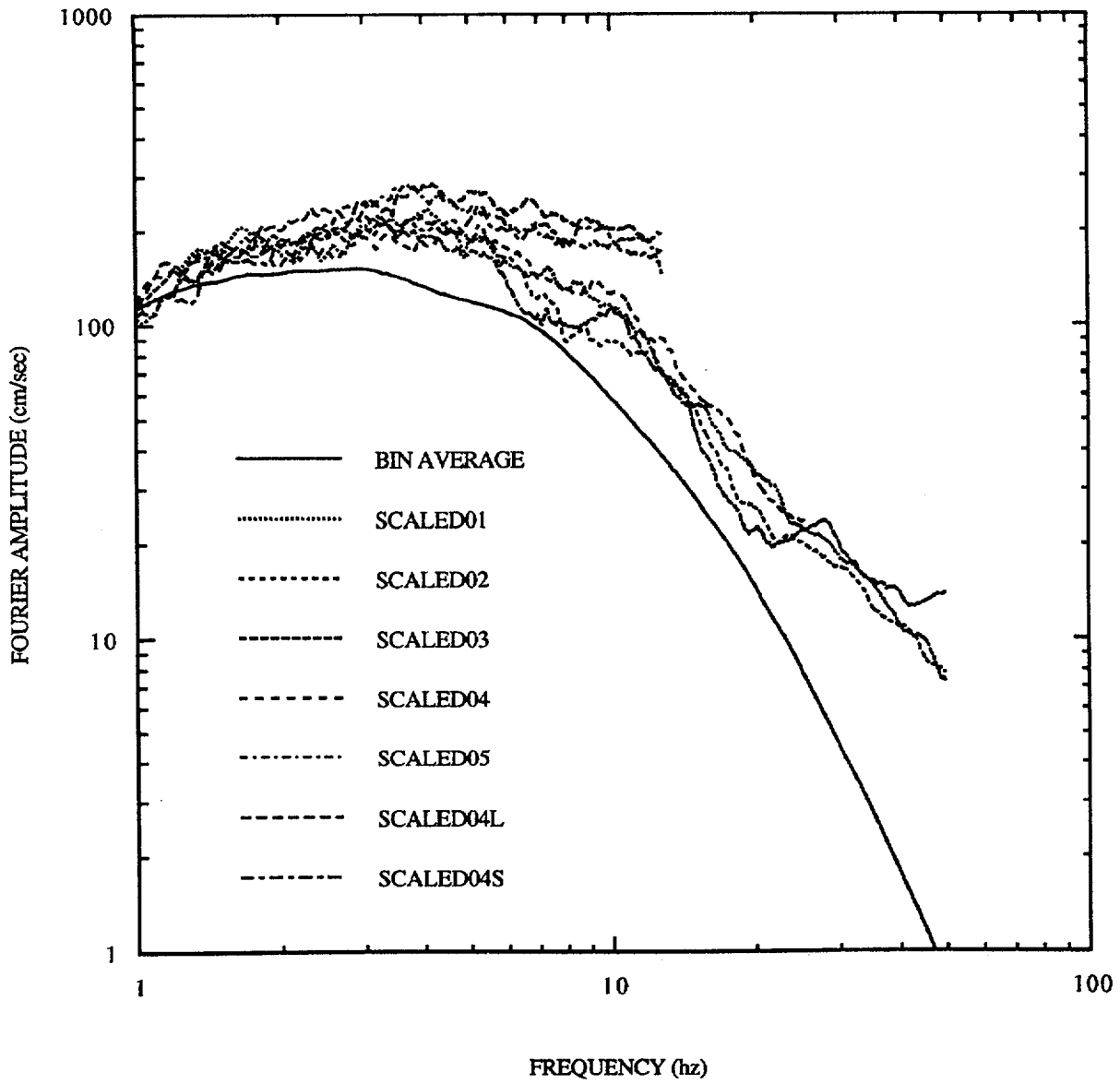


Figure 5-10A. Fourier amplitude spectra of envelope fits to 5% damped segmented target spectrum.

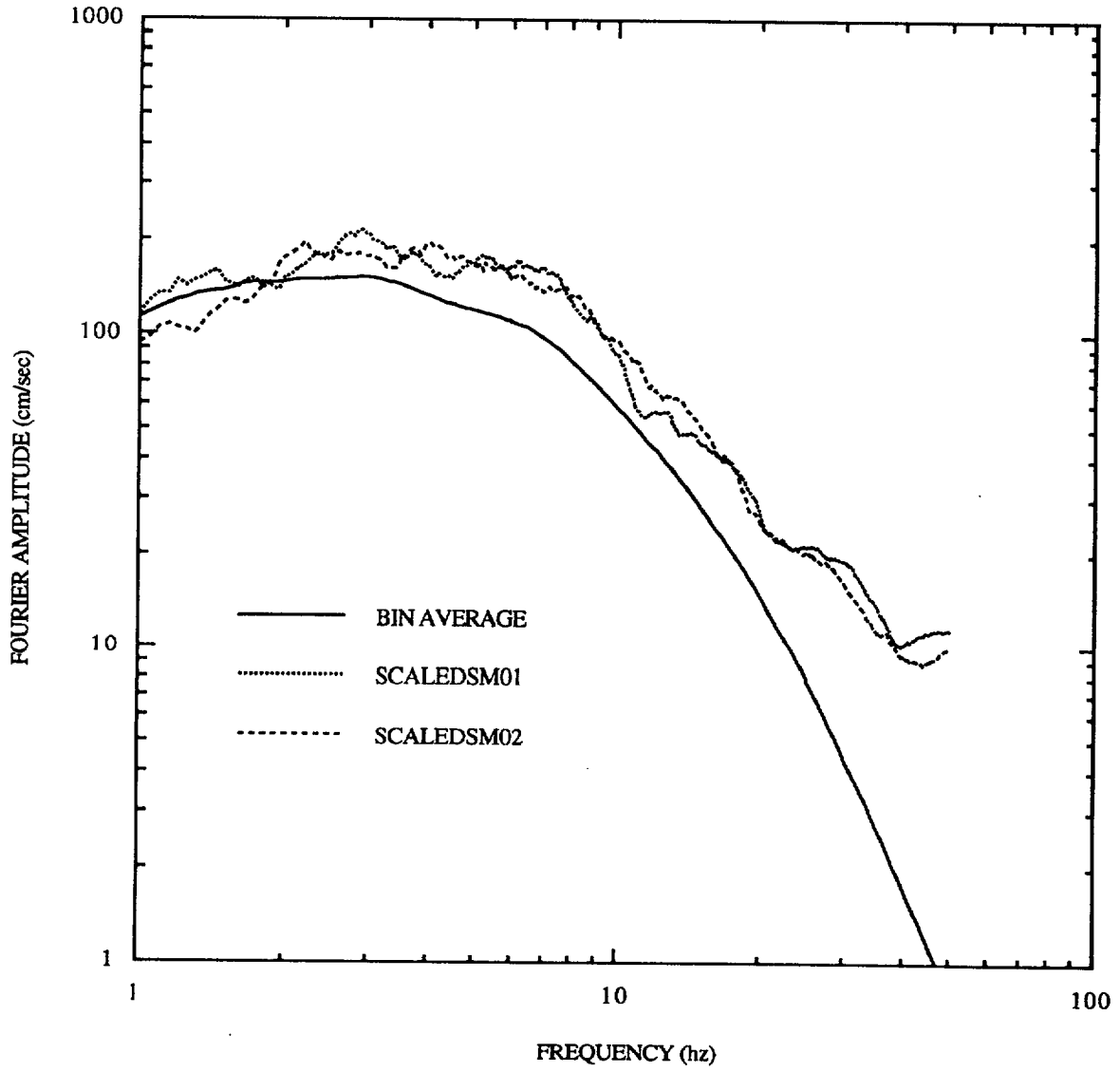


Figure 5-10B. Fourier amplitude spectra of envelope fits to 5% damped smooth target spectrum

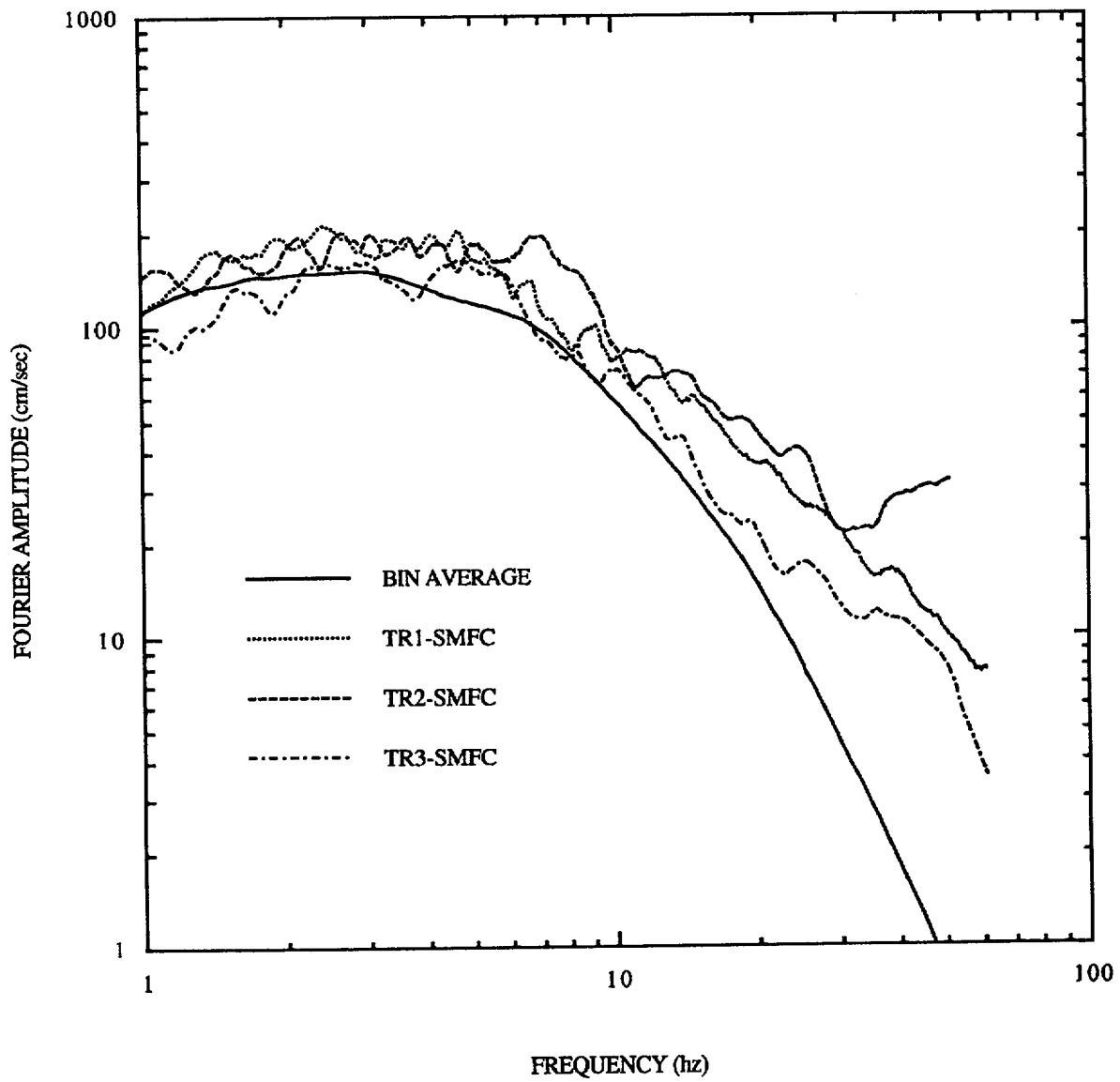


Figure 5-10C. Fourier amplitude spectra of envelope fits to 5% damped smooth WUS target spectrum

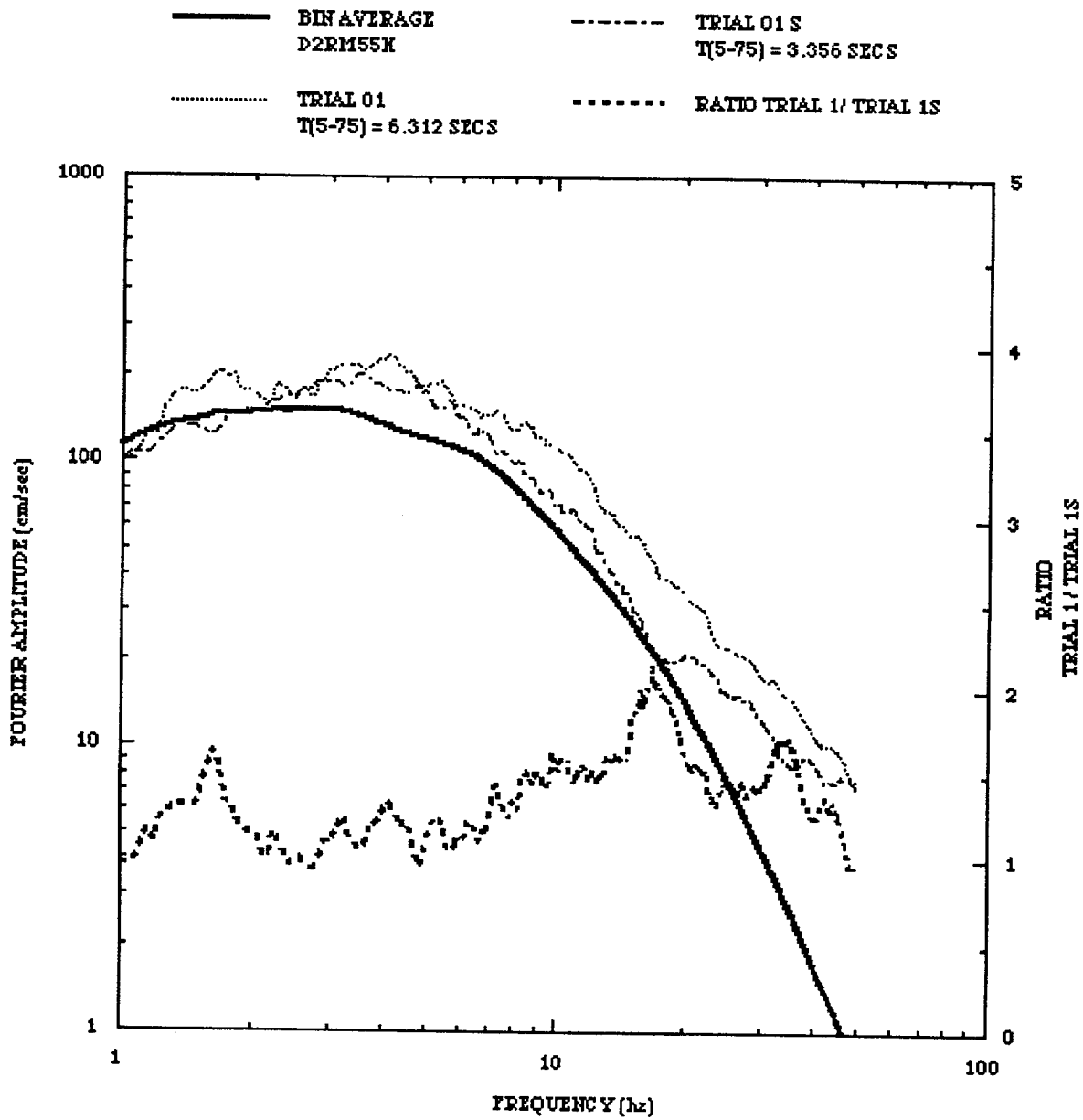


Figure 5-10D. Fourier amplitude spectra of enveloping fits to 5% damped segmented WUS target spectrum (bin D2RM55H)

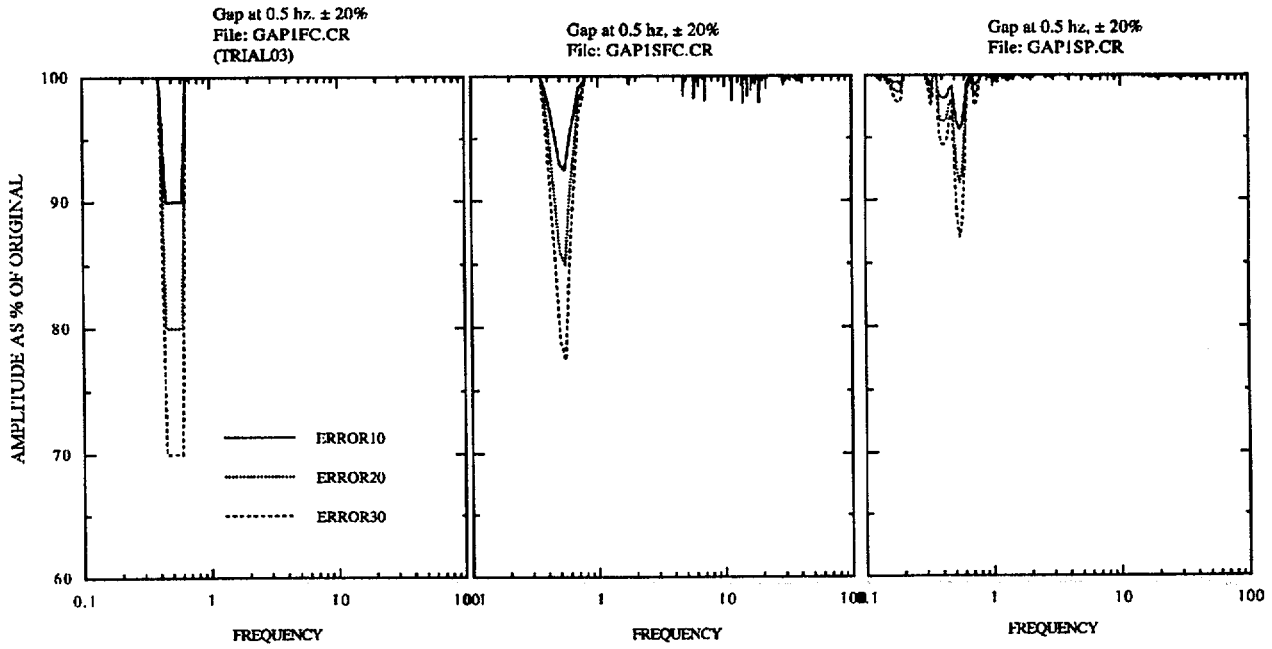


Figure 5-11A. Influence of gap in Fourier amplitudes at 0.5 Hz on 5% damped response spectra. Left: change in original Fourier amplitudes; center: change in smoothed Fourier amplitudes; right: change in 5% damped response spectrum

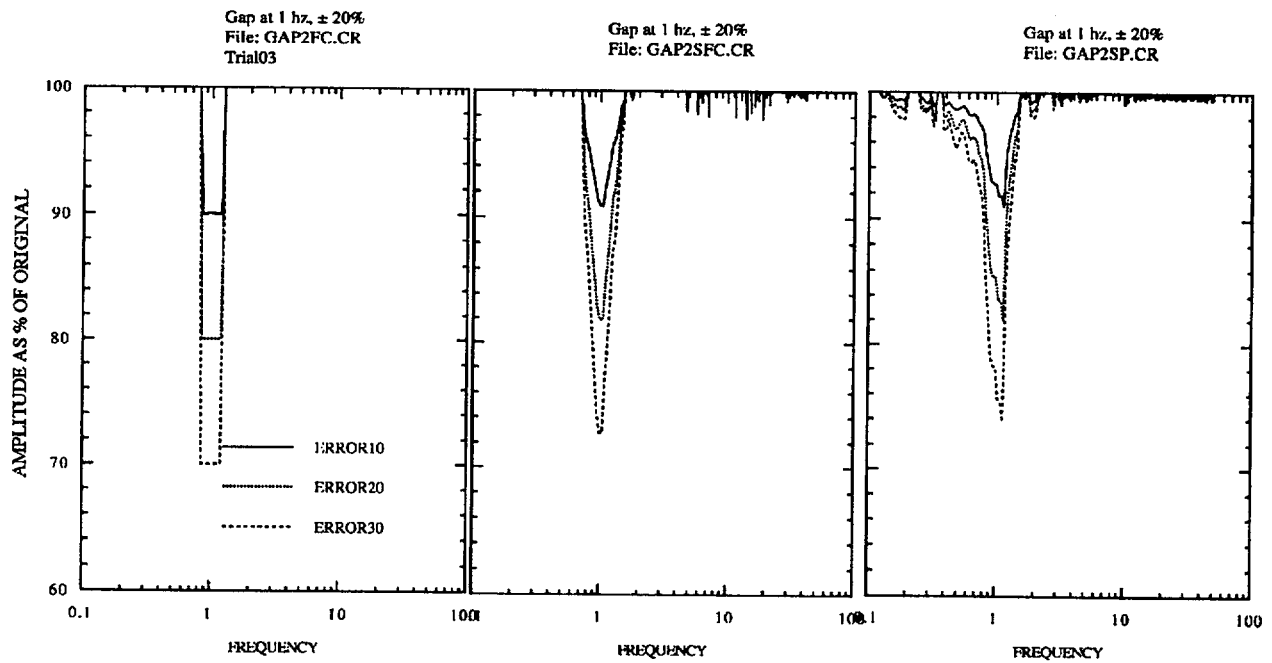


Figure 5-11B. Influence of gap in Fourier amplitude at 1 Hz on 5% damped response spectra. Left: change in original Fourier amplitudes; Center: change in smoothed Fourier amplitudes; Right: change in 5% damped response spectrum.

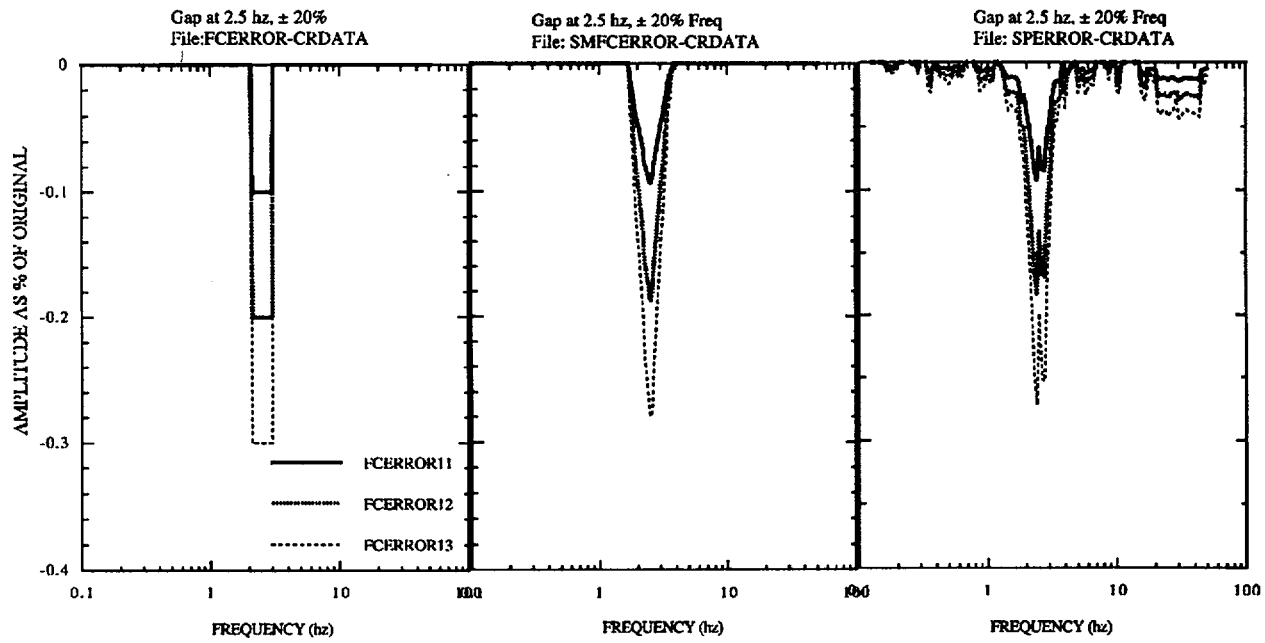


Figure 5-11C. Influence of gap in Fourier amplitudes at 2.5 Hz on 5% damped response spectra. Left: change in original Fourier amplitudes; Center: change in smoothed Fourier amplitudes; Right: change in 5% damped response spectrum.

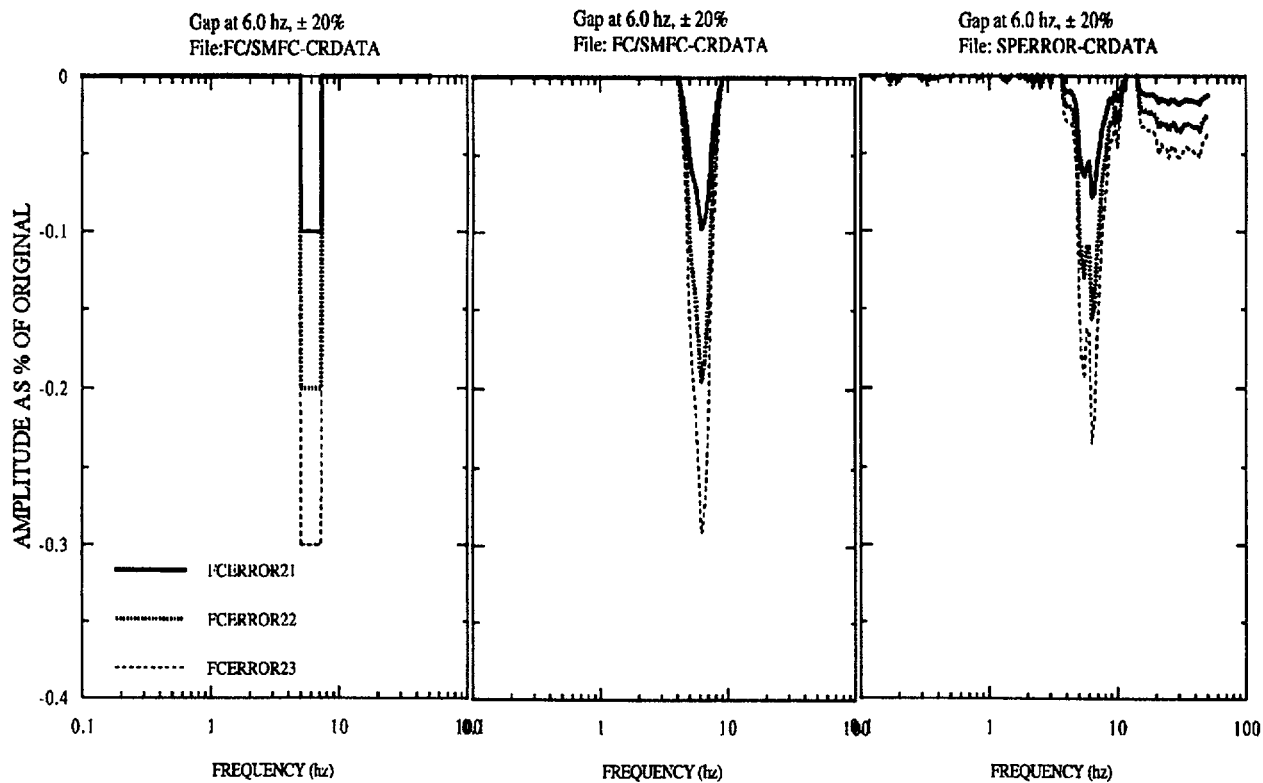


Figure 5-11D. Influence of gap in Fourier amplitudes at 6 Hz on 5% damped response spectra. Left: change in original Fourier amplitudes; Center: change in smoothed Fourier amplitudes; Right: change in 5% damped response spectrum.

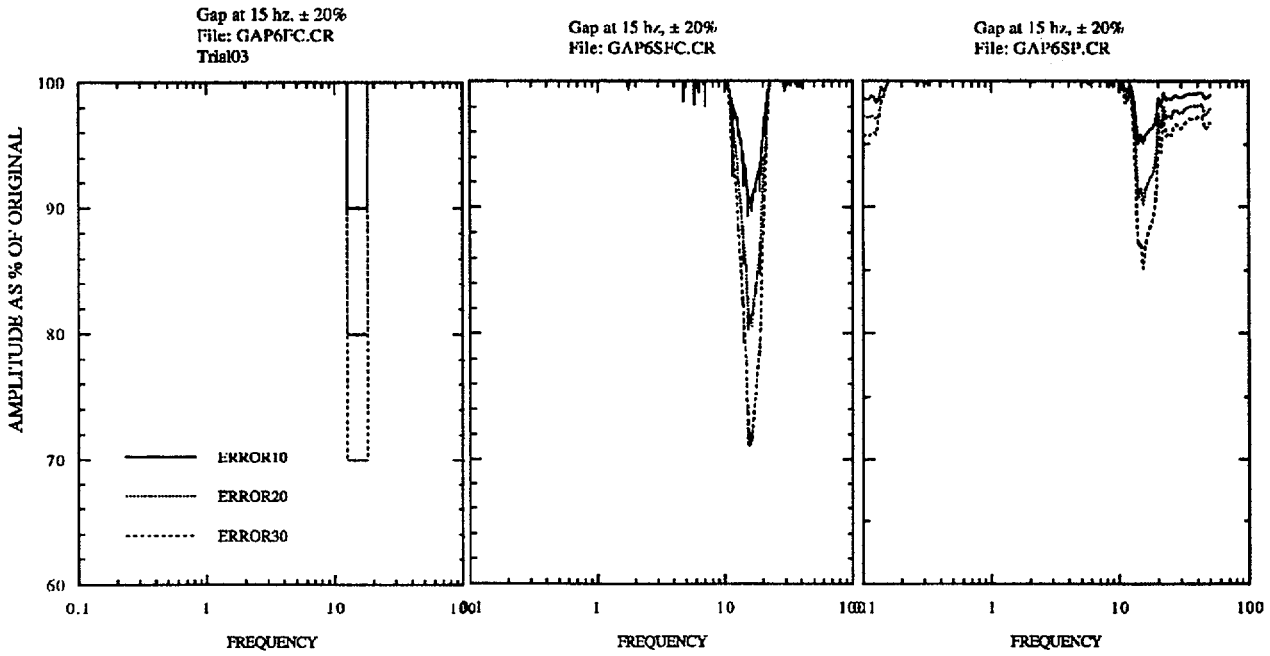


Figure 5-11F. Influence of gap in Fourier amplitudes at 15 Hz on 5% damped response spectra. Left: change in original Fourier amplitudes; Center: change in smoothed Fourier amplitudes; Right: change in 5% damped response spectrum.

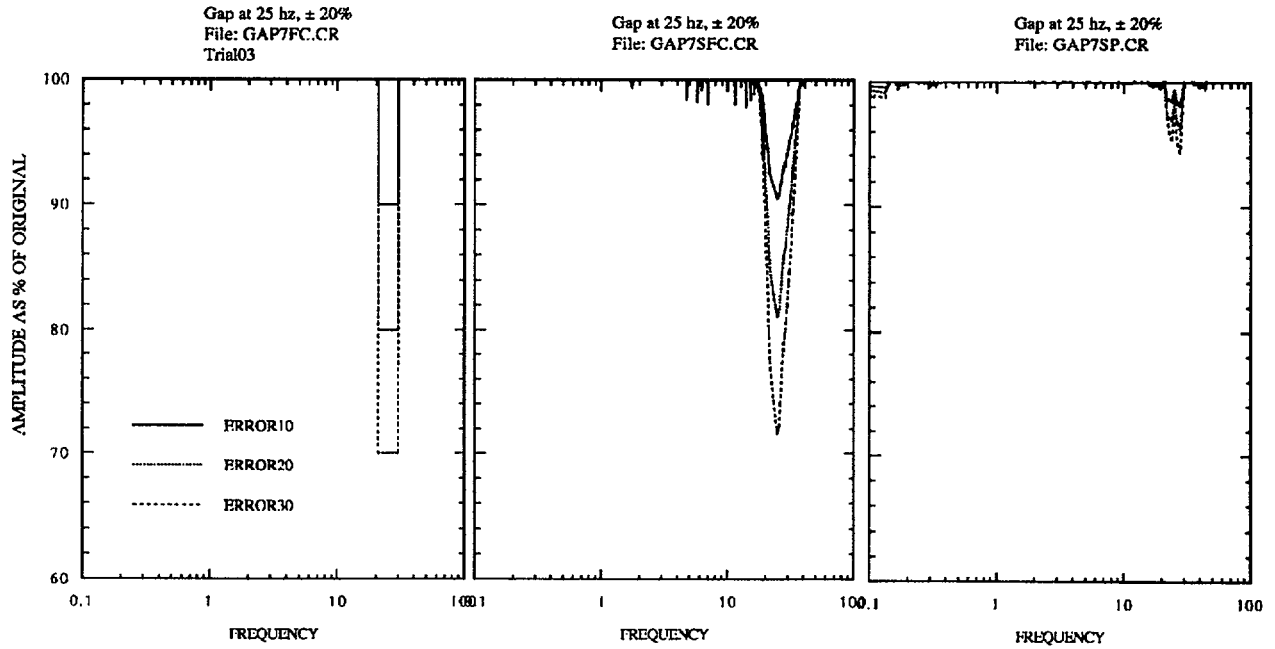


Figure 5-11G. Influence of gap in Fourier amplitudes at 25 Hz on 5% damped response spectra. Left: change in original Fourier amplitudes; Center: change in smoothed Fourier amplitudes; Right: change in 5% damped response spectrum.

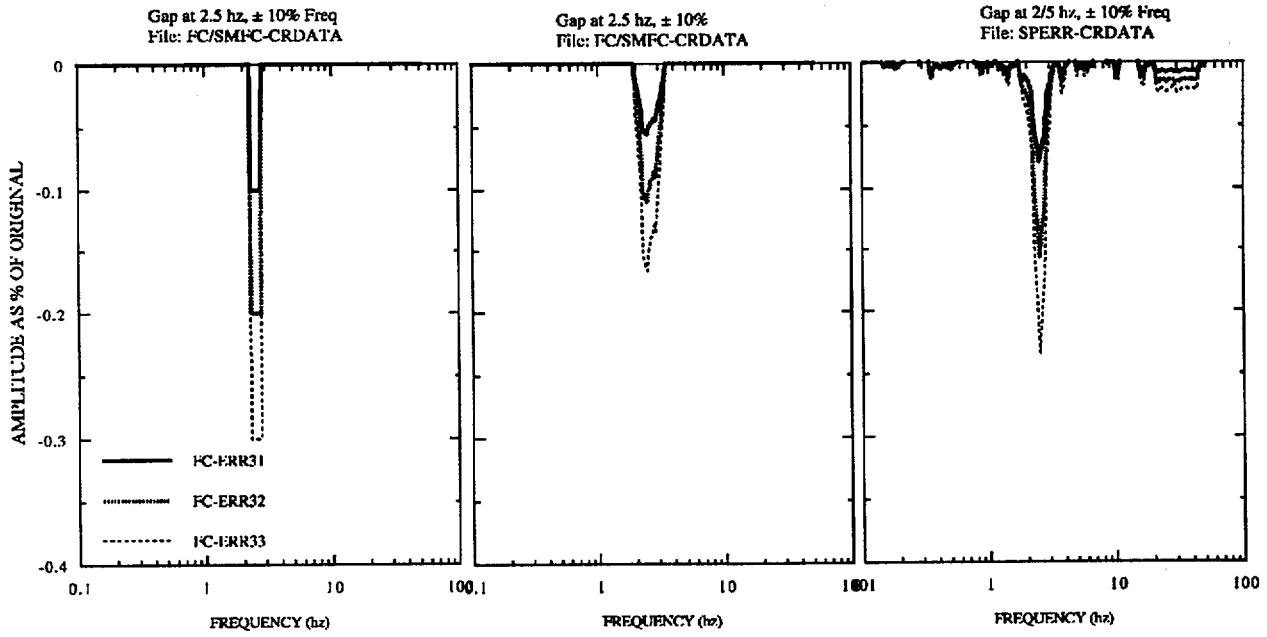


Figure 5-11H. Influence of narrower gap in Fourier amplitudes at 2.5 Hz on 5% damped response spectra. Left: change in original Fourier amplitudes; Center: change in smoothed Fourier amplitudes; Right: change in 5% damped response spectrum.

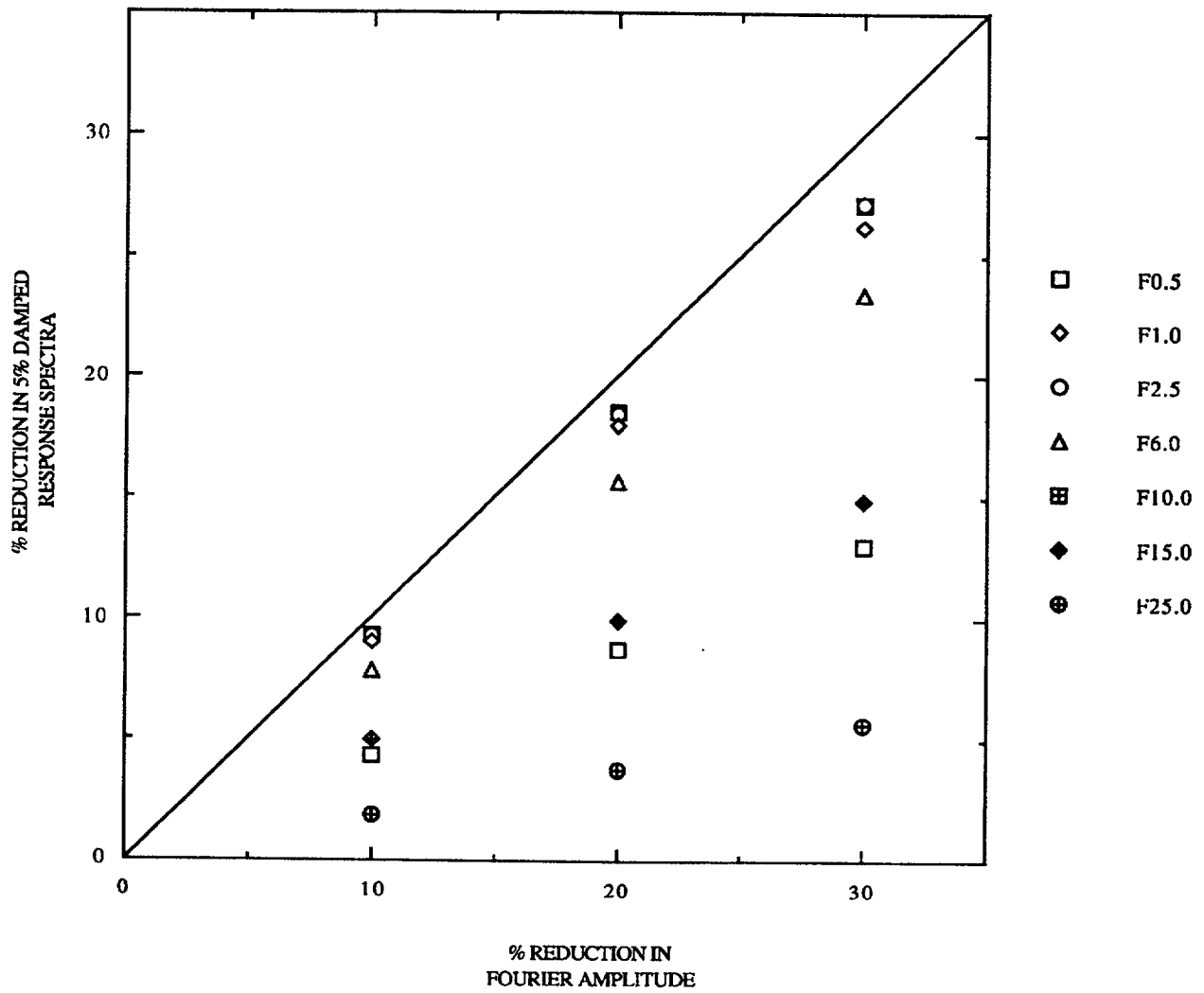


Figure 5-12. Influence of gaps in the Fourier amplitude spectrum on reduction of 5% damped response spectra, record "trial 03".

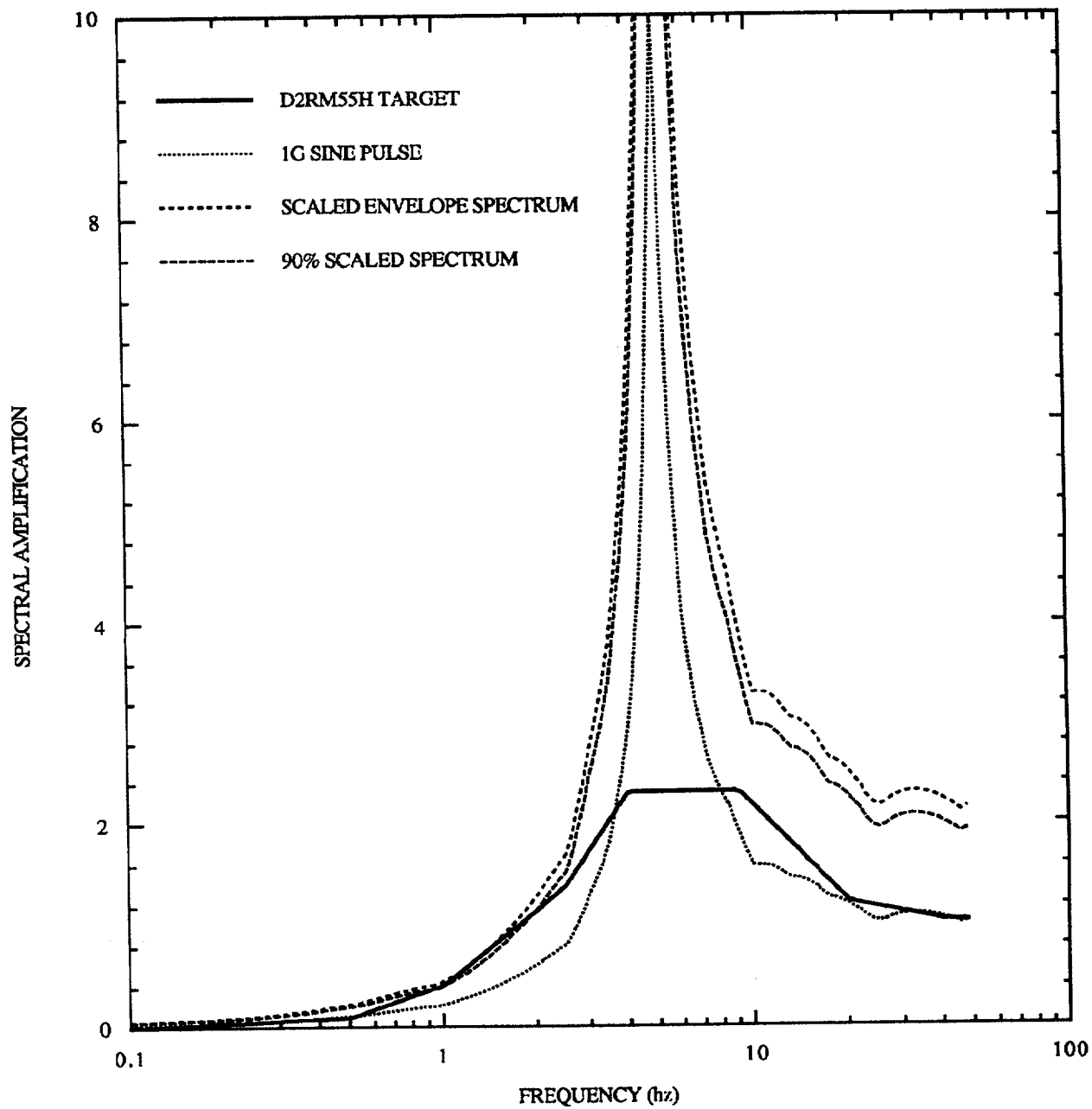


Figure 5-13A. 5% damped response spectra for 1g sine pulse at 5 Hz.

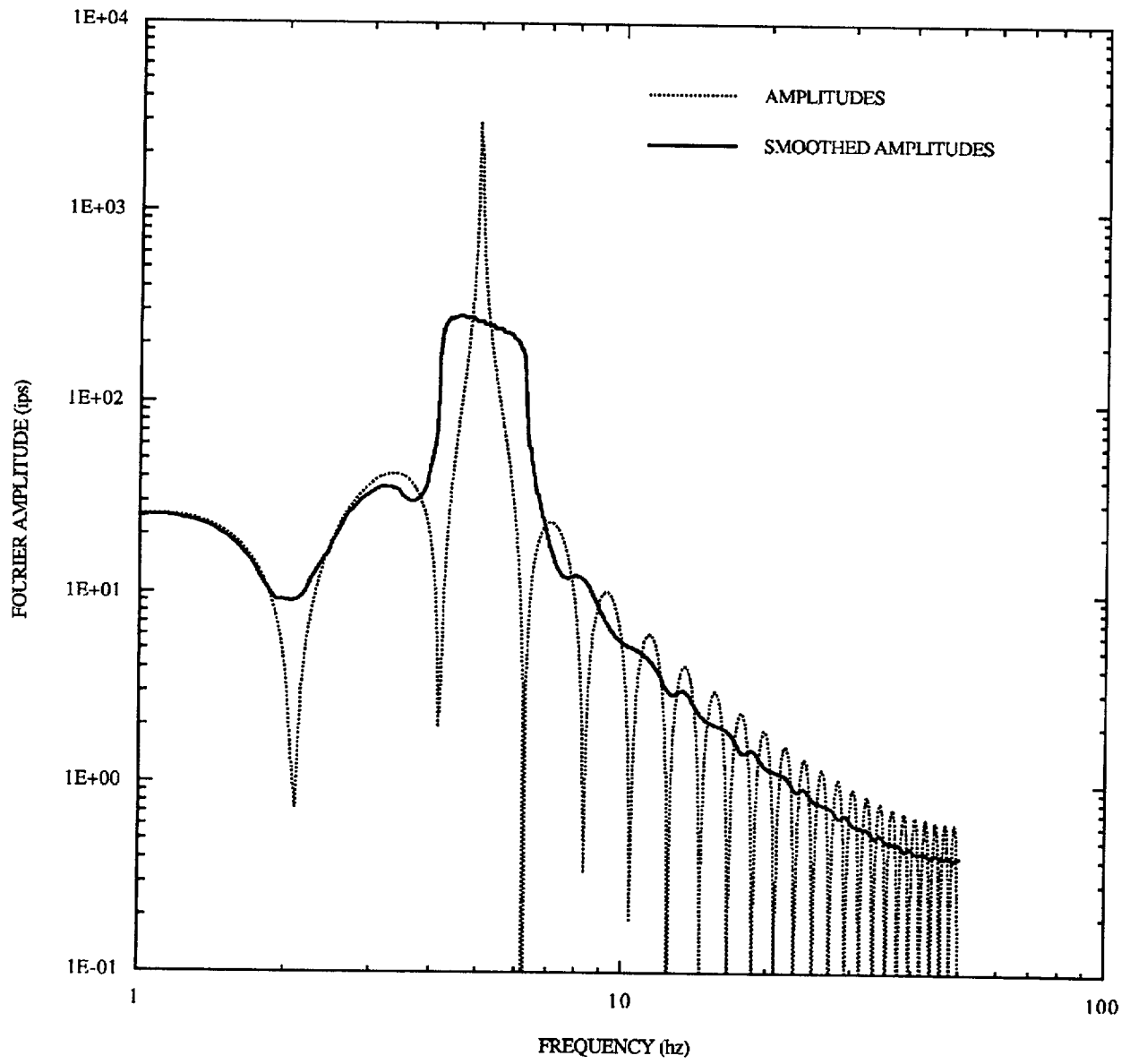


Figure 5-13B. Fourier spectra for 1g sine pulse with a frequency of 5 Hz.

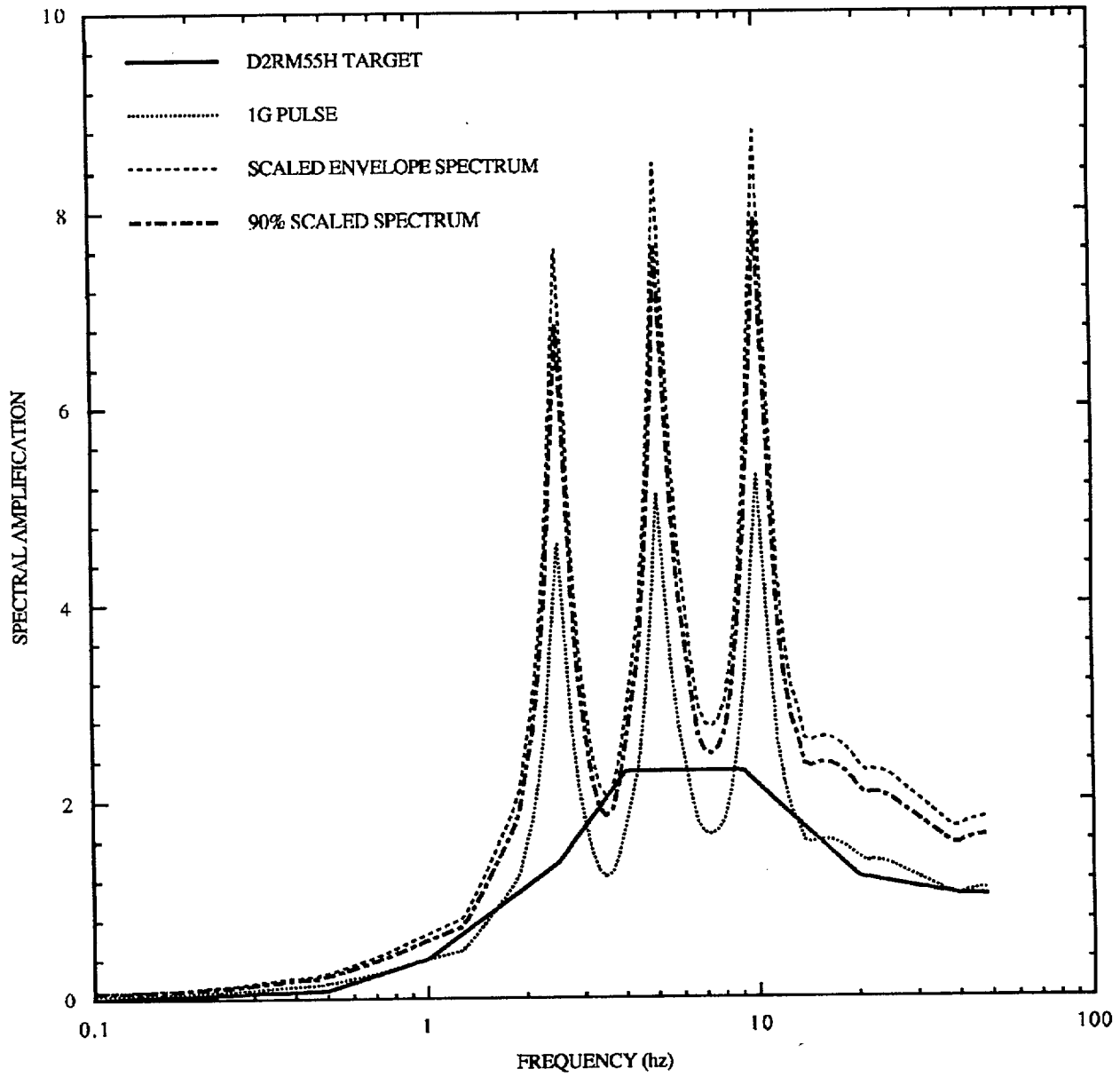


Figure 5-13C. 5% damped response spectra for 1g pulse consisting of three frequencies (2.5, 5, and 10 Hz).

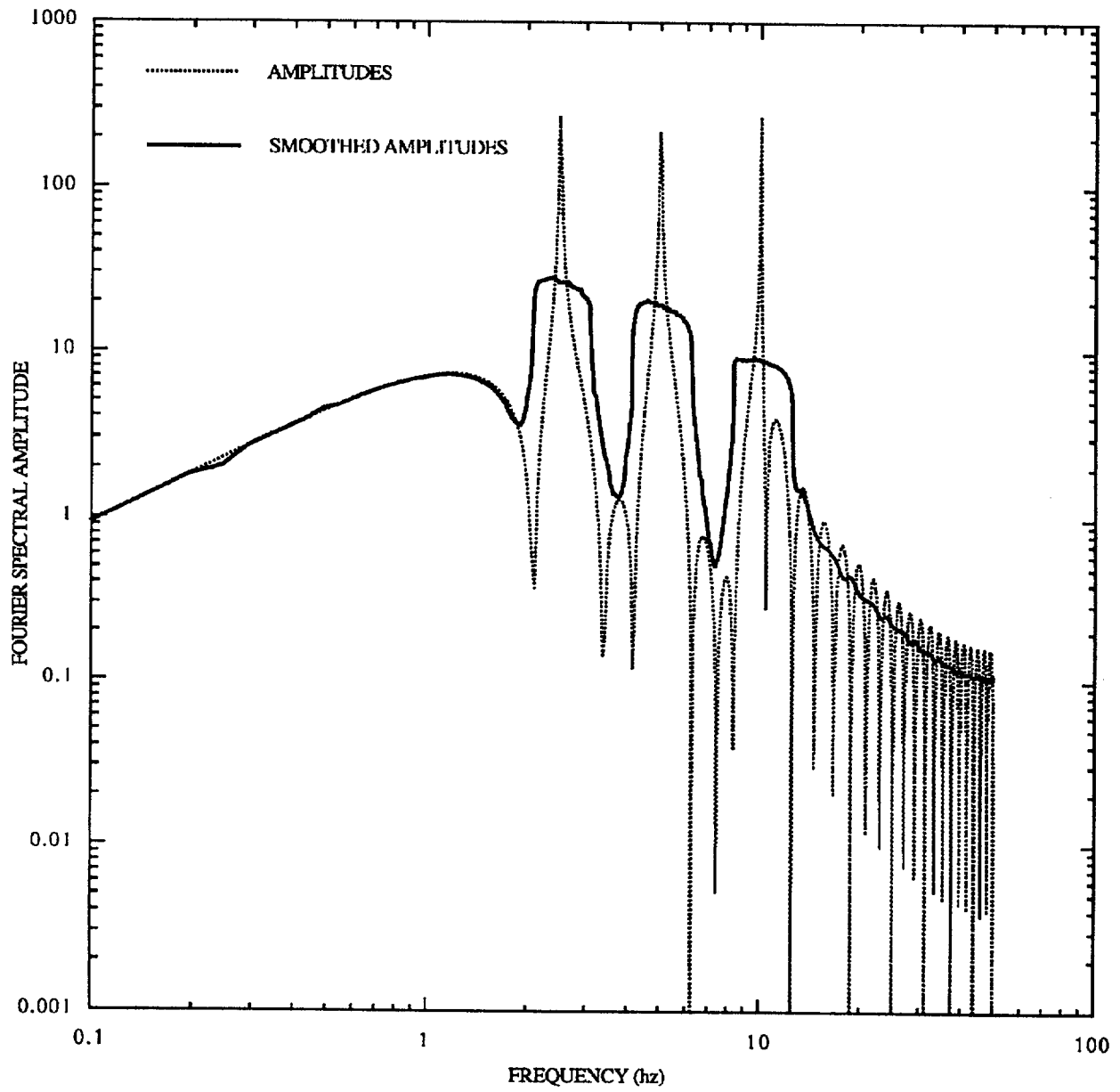


Figure 5-13D. Fourier spectra for 1g sine pulse consisting of three frequencies (2.5, 5, and 10 Hz).

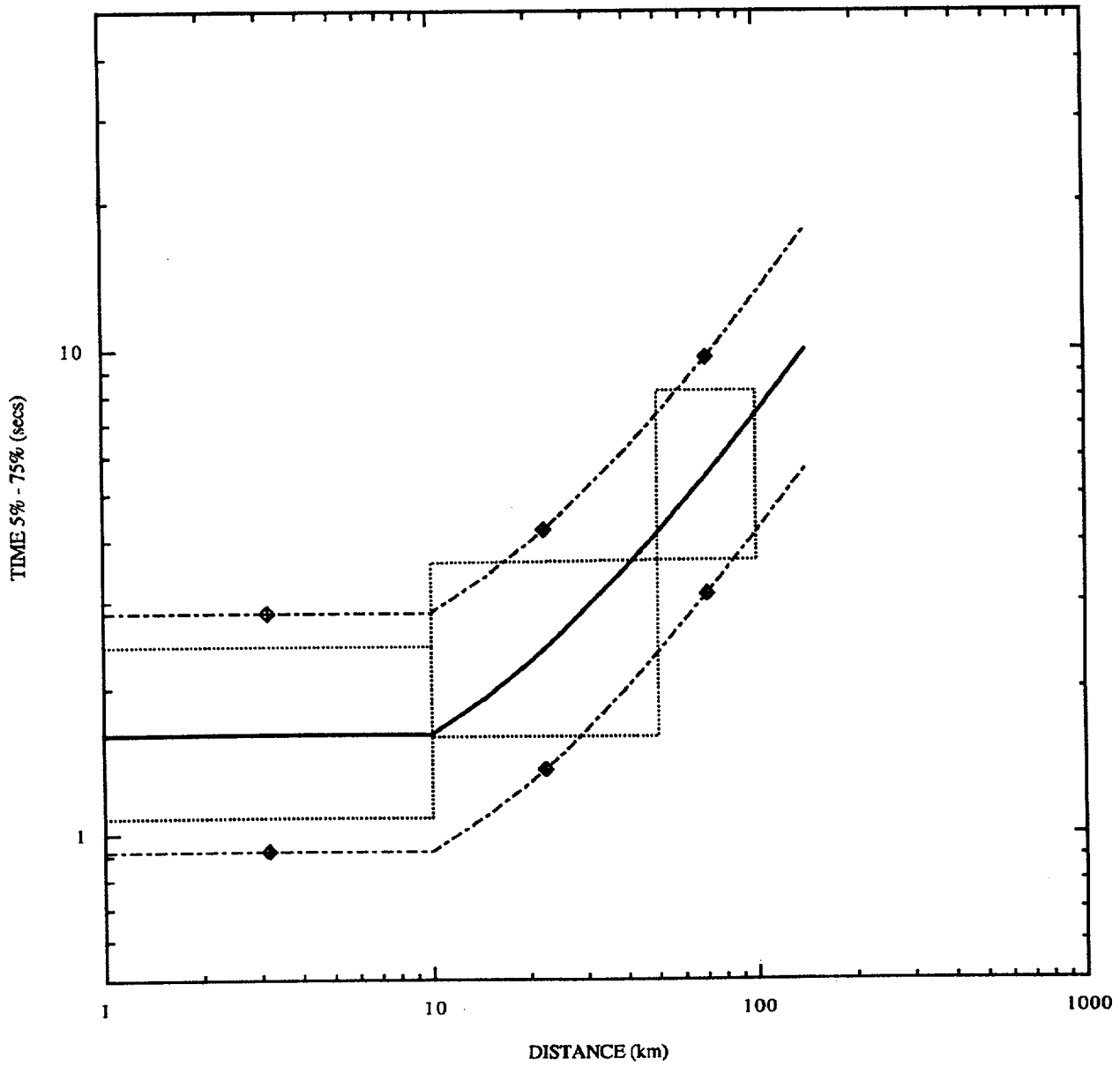


Figure 5-14A. Duration times from 5% - 75% Arias intensity, empirical WUS data for rock sites, M 5-6, horizontal motions.

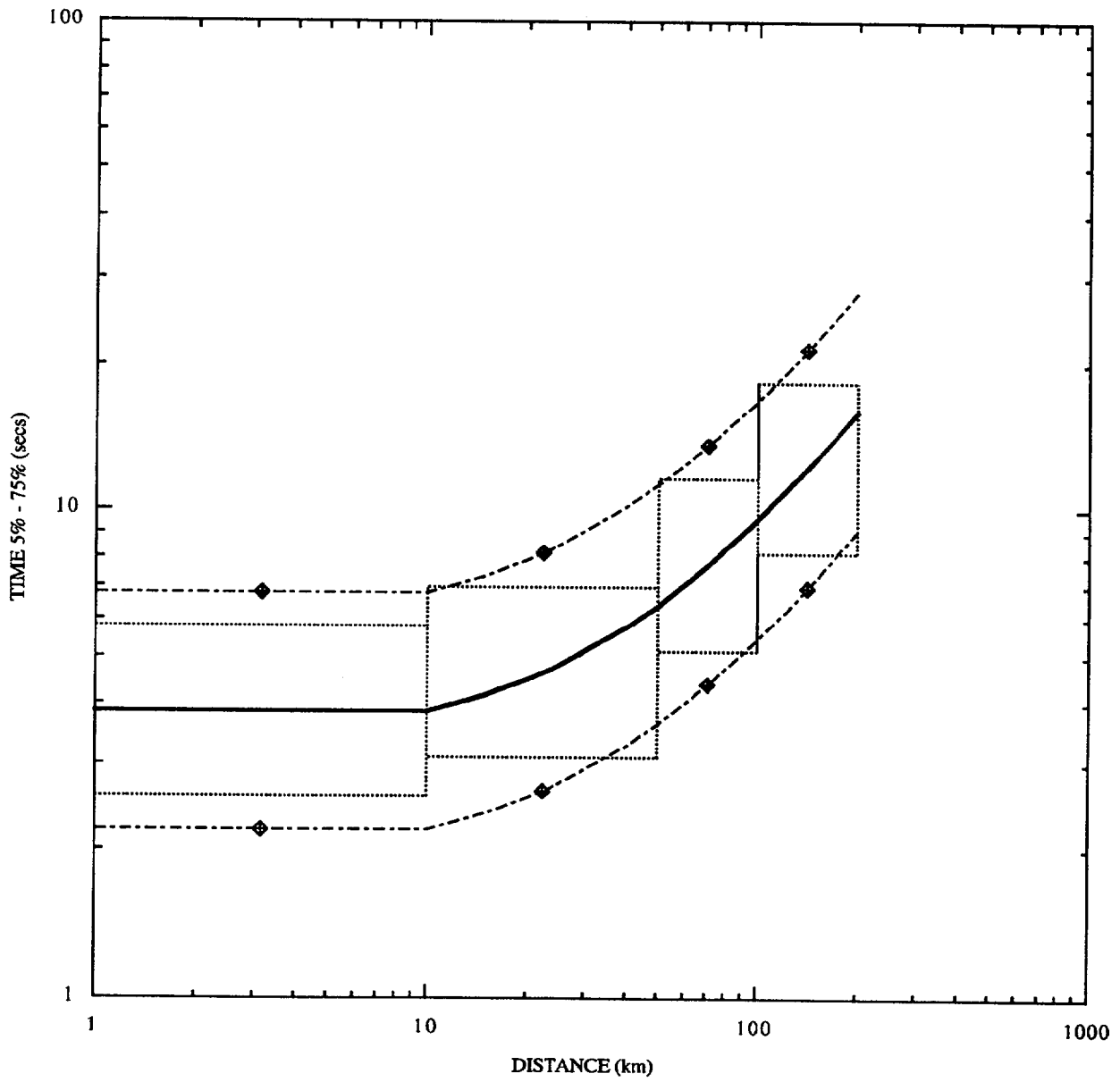


Figure 5-14B. Duration times from 5% - 75% Arias intensity, empirical WUS data for rock sites, M 6-7, horizontal motions.

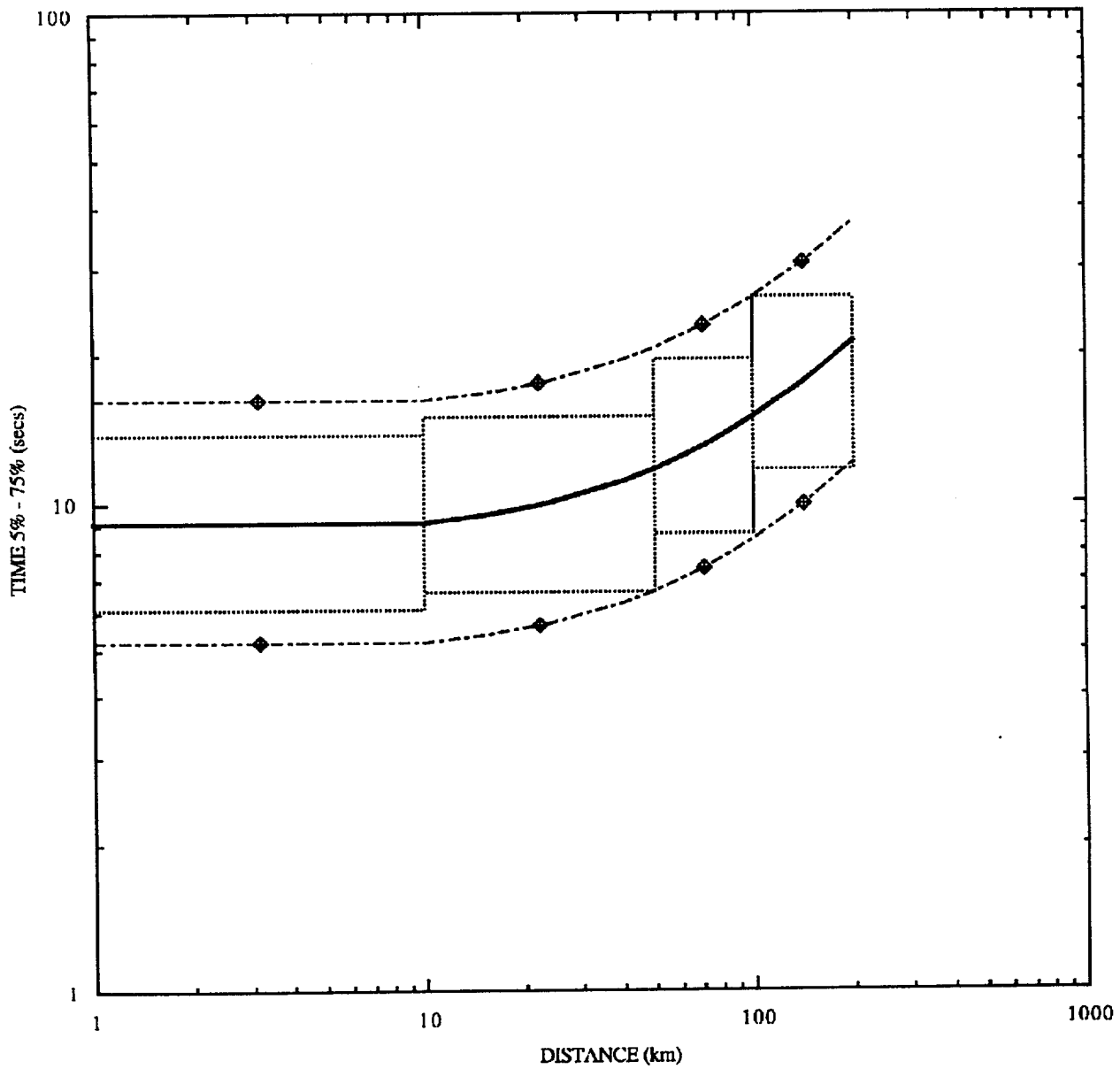


Figure 5-14C. Duration times from 5% - 75% Arias intensity, empirical WUS data for rock sites, M 7+, horizontal motions.

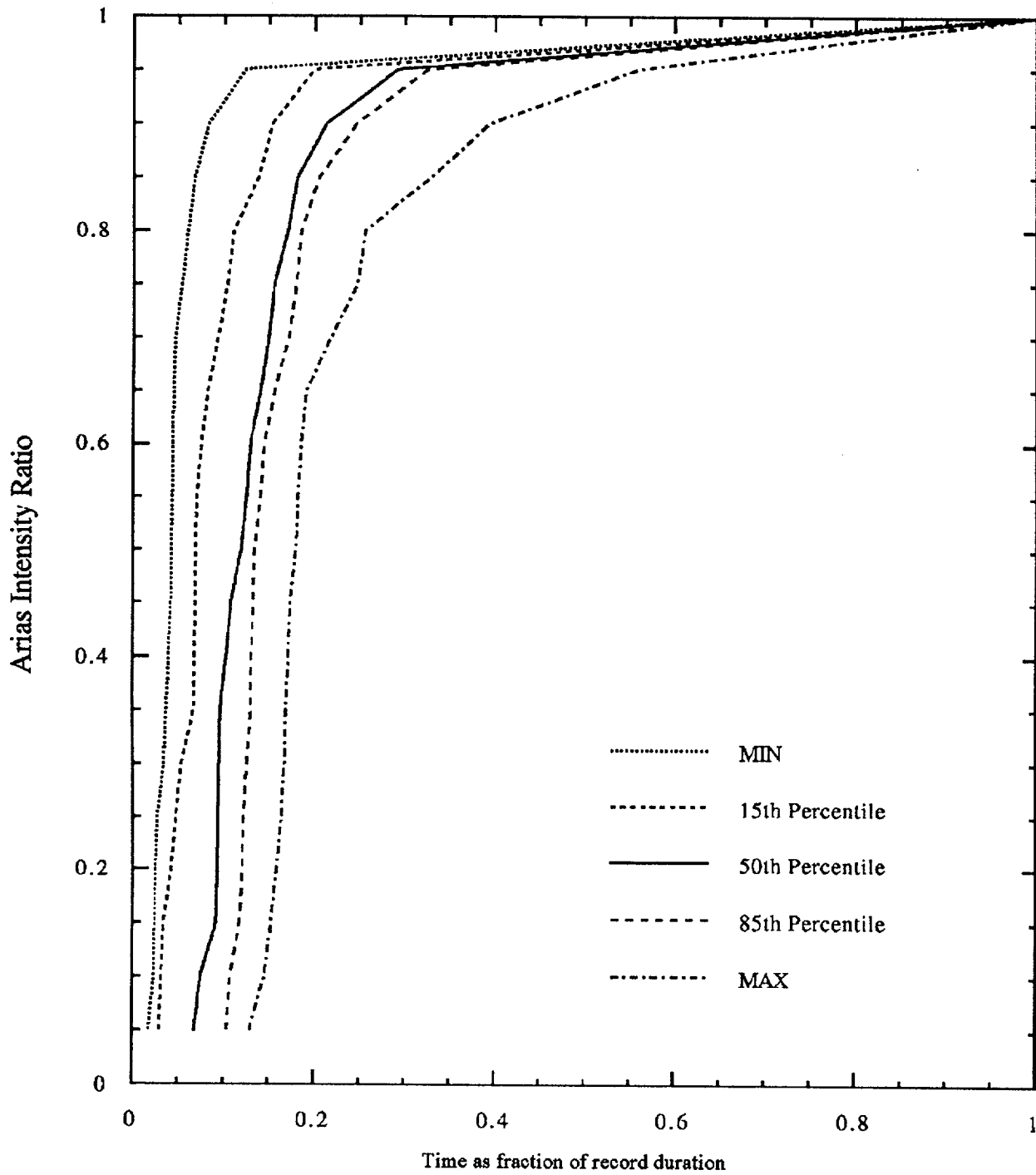


Figure 5-15A. Statistics of Arias intensity ratio vs. time scaled by record times for empirical WUS records in bin D1RM55H.

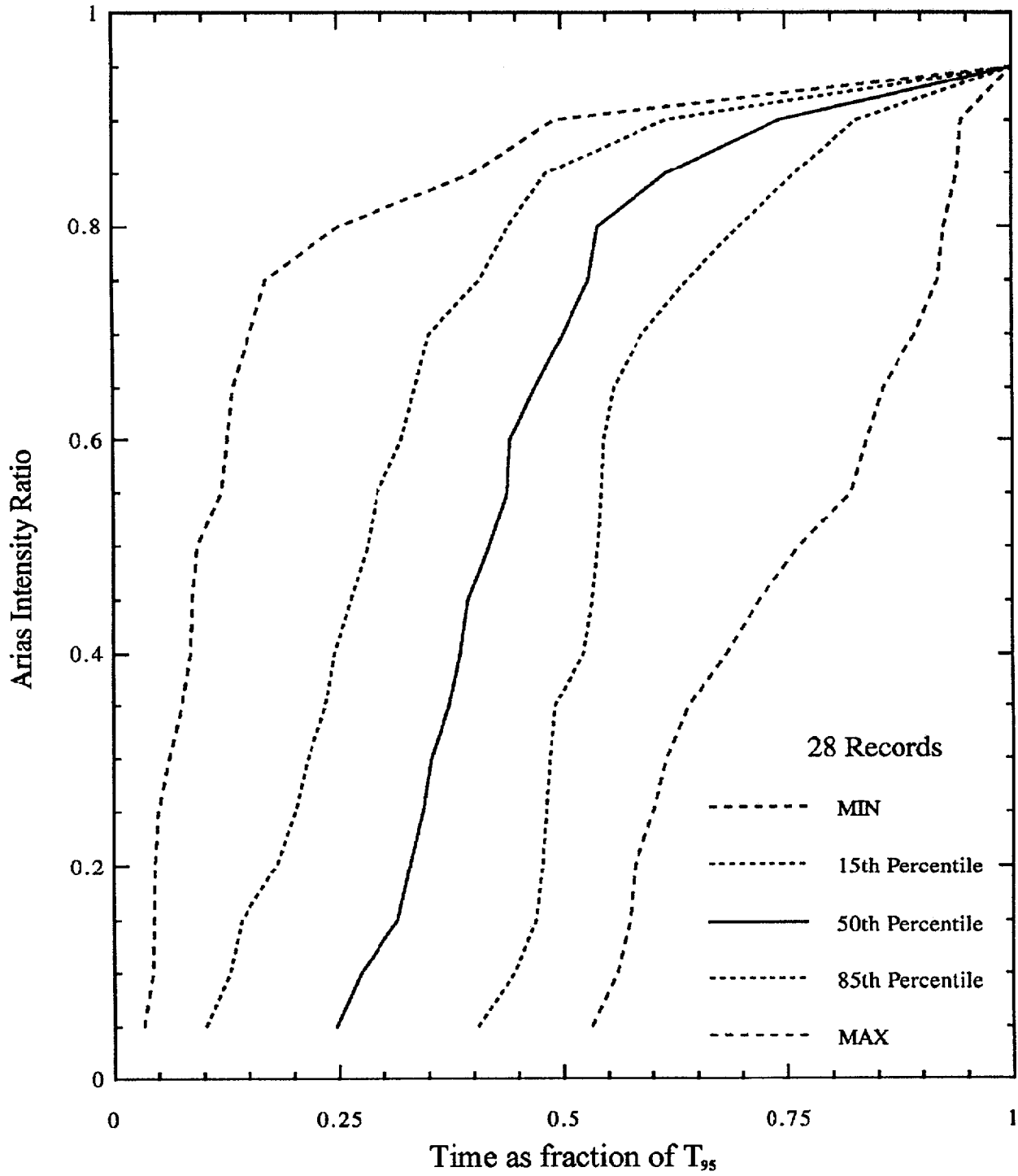


Figure 5-15B. Statistics of Arias intensity ratio vs. time scaled by Arias T_{95} for empirical WUS records in bin D1RM55H.

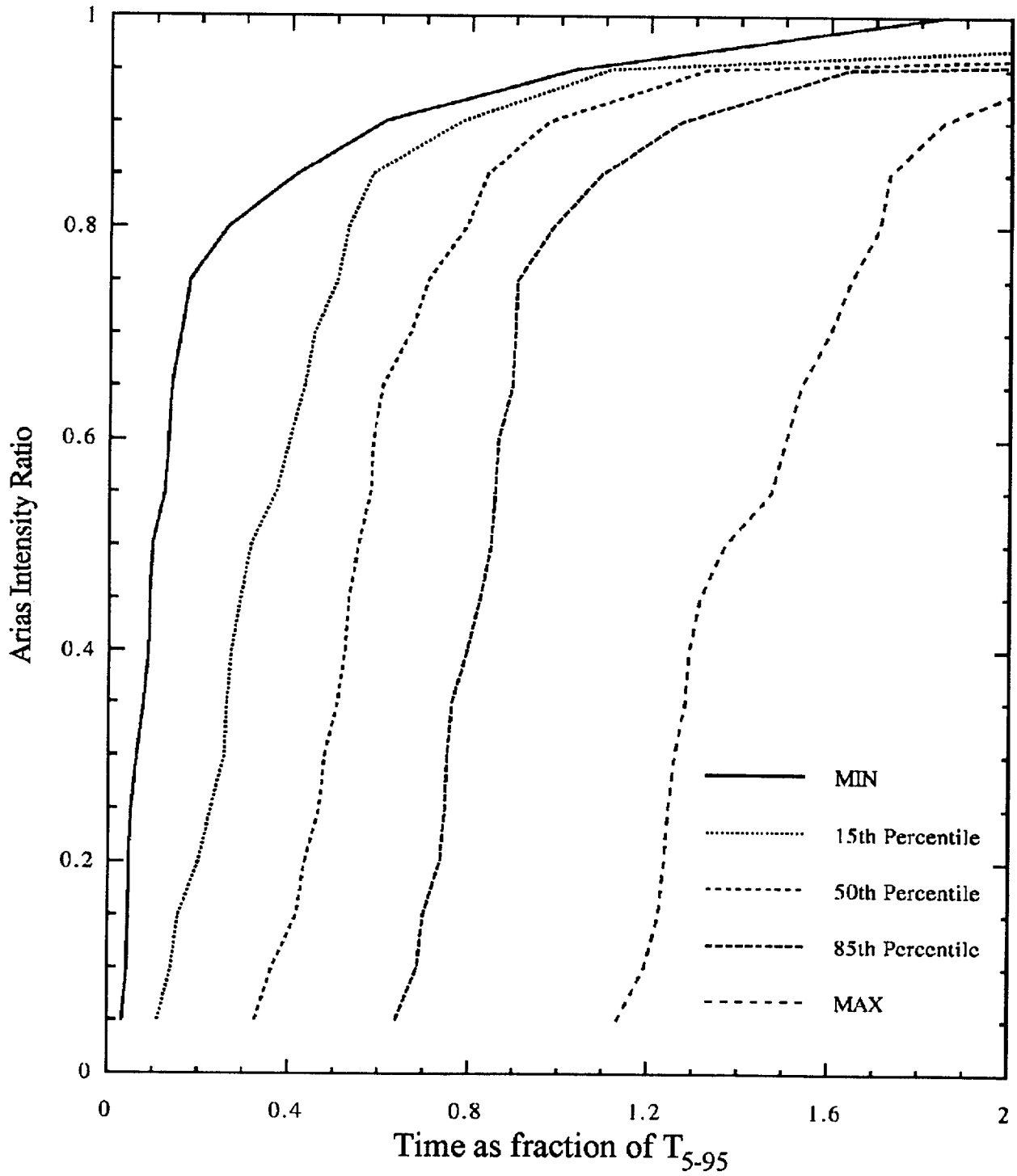


Figure 5-15C. Statistics of Arias intensity ratio vs. time scaled by Arias T_{5-95} for empirical WUS records in bin DIRM55H.

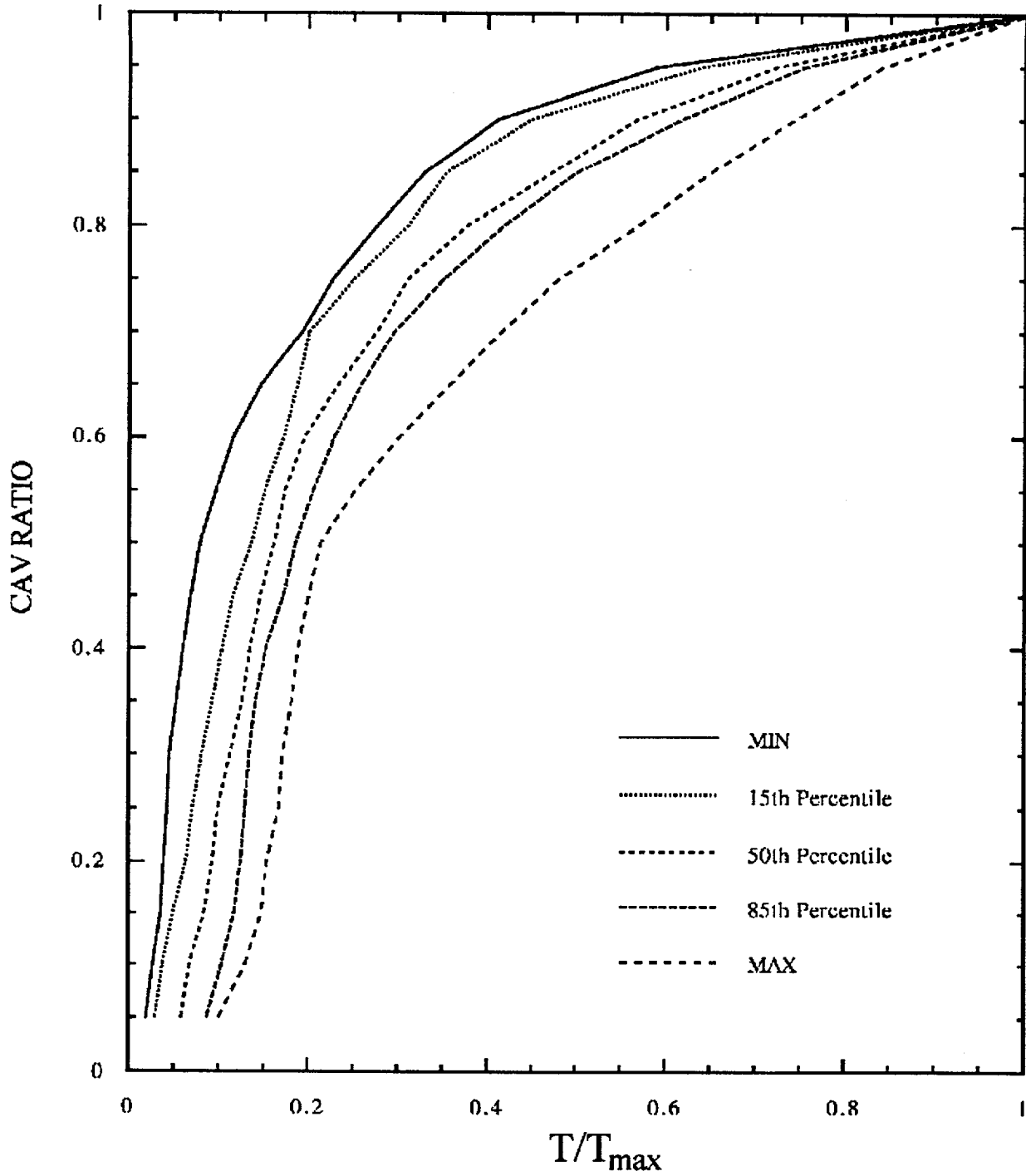


Figure 5-16A. Statistics for cumulative absolute velocity vs. time scaled by record times for empirical WUS records in bin D1RM55H.

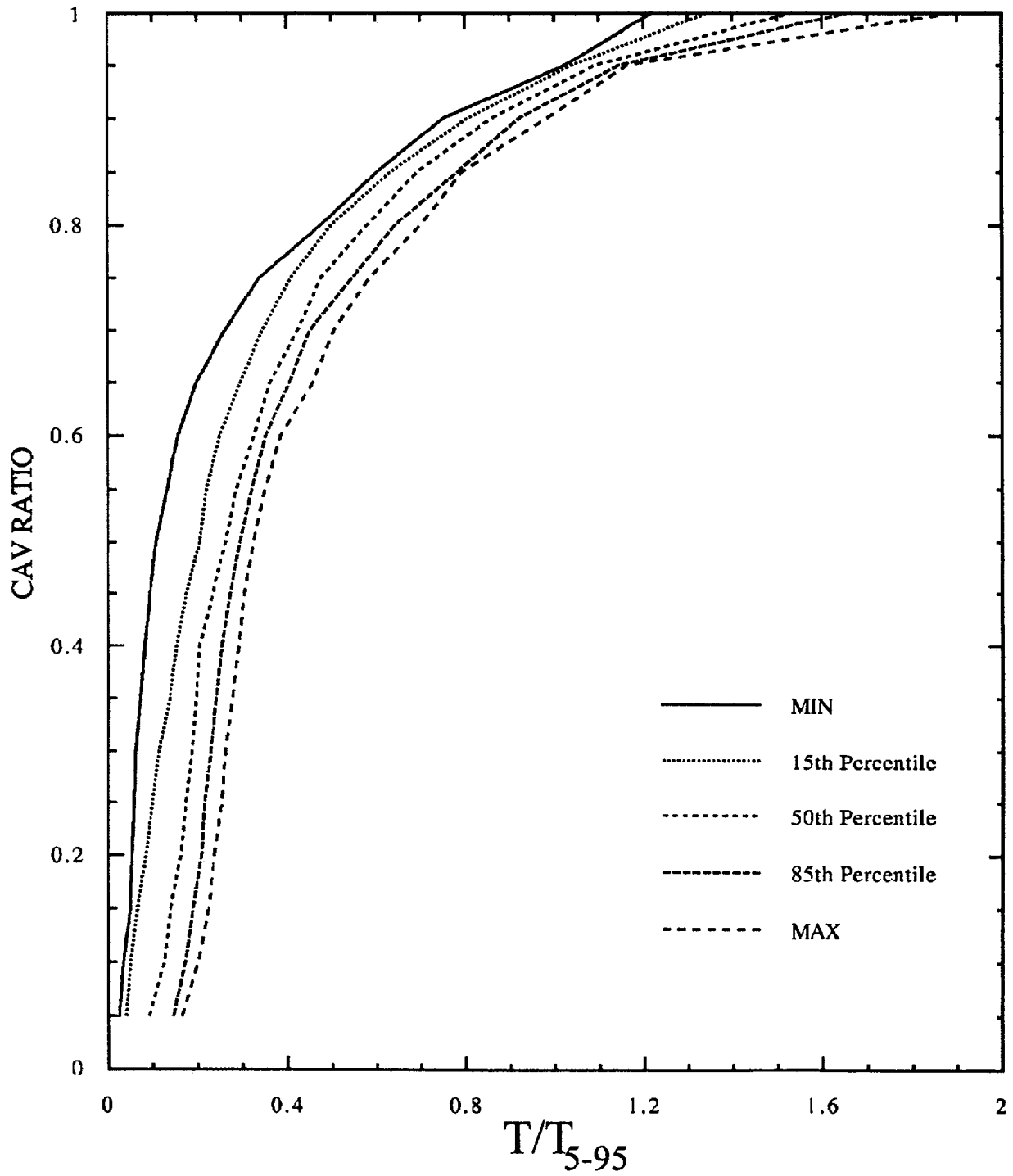


Figure 5-16B. Statistics of cumulative absolute velocity vs. time scaled by Arias T_{5-95} for empirical WUS records in bin D1RM55H.

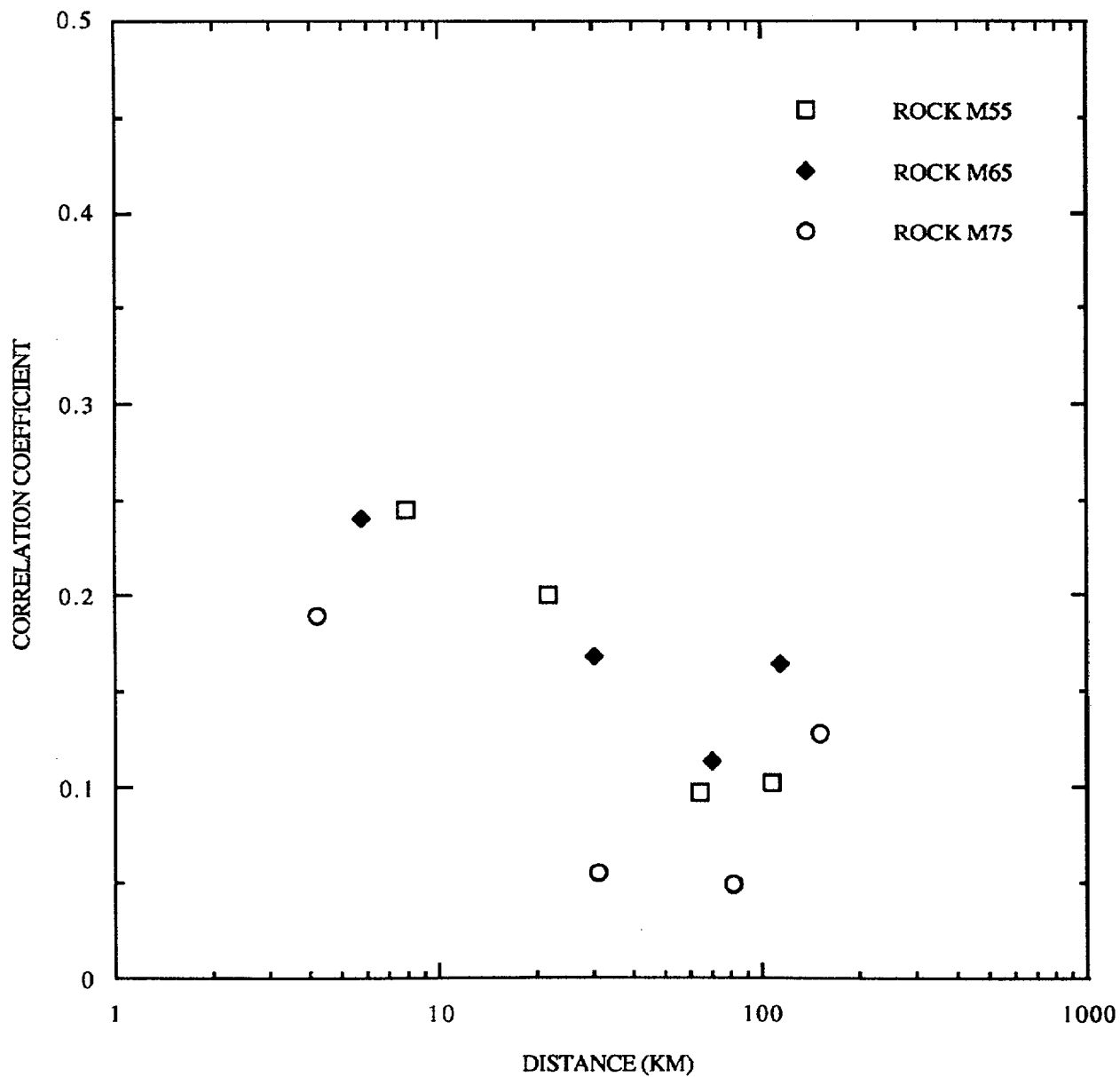


Figure 5-17A. Correlations of H1-H2 acceleration pairs, WUS rock sites.

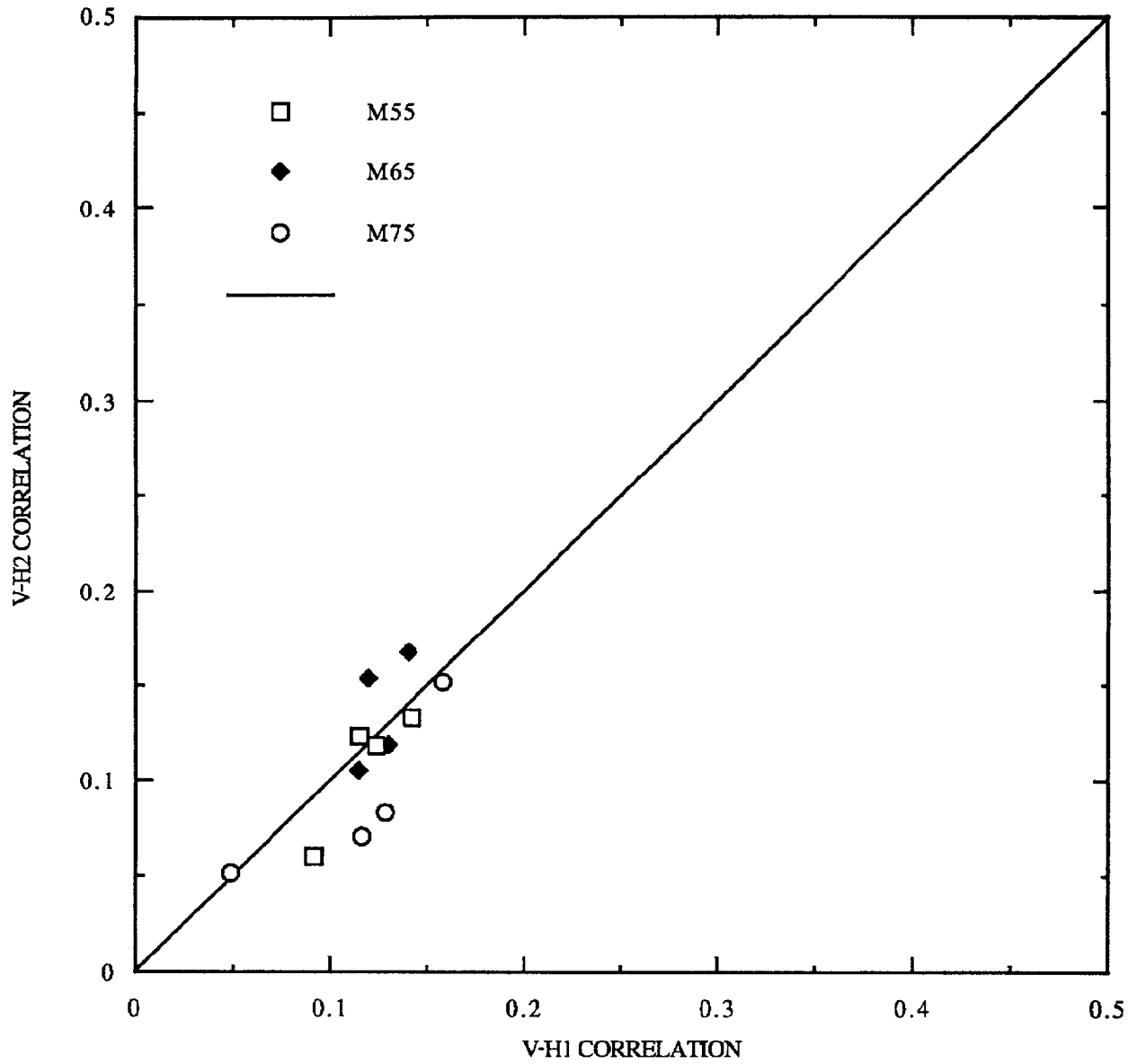


Figure 5-17B. Comparison of correlations of vertical-horizontal acceleration pairs at WUS rock sites.

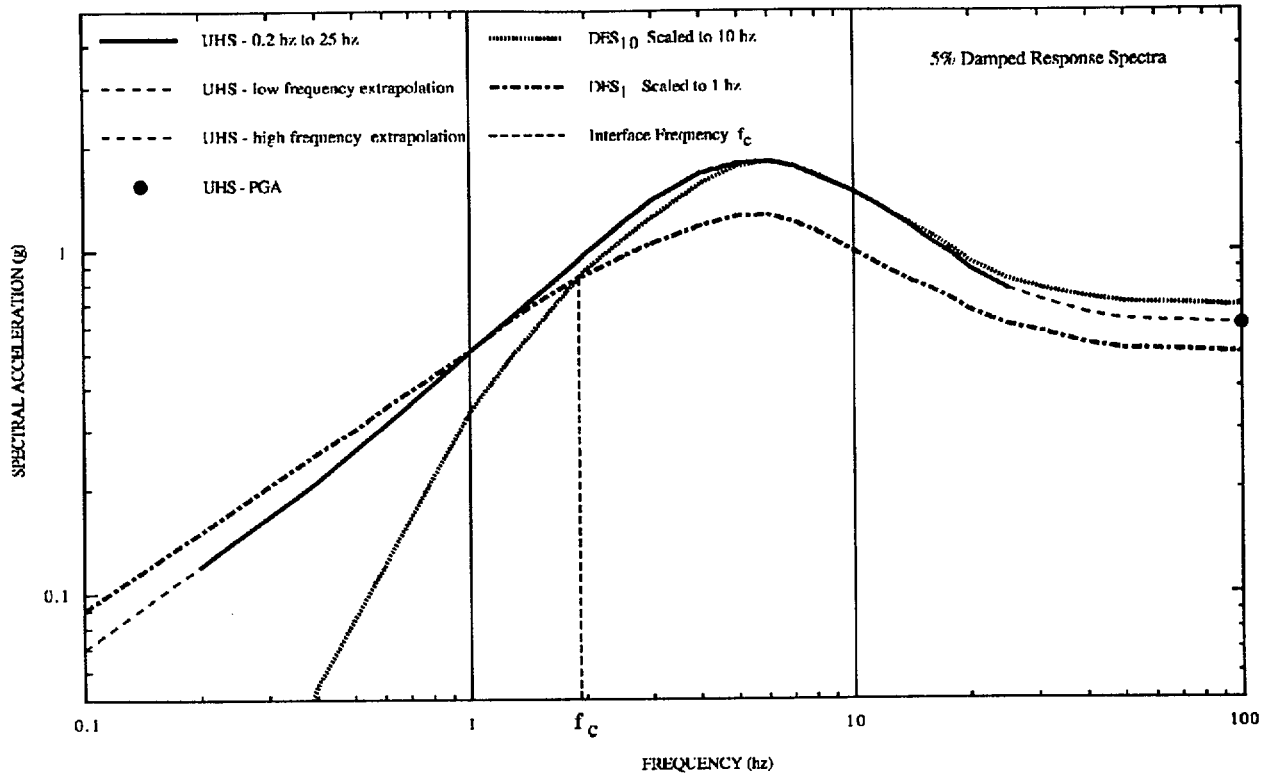


Figure 5-18A. Example of uniform hazard spectrum and scaled deaggregated spectra at low and high frequencies.

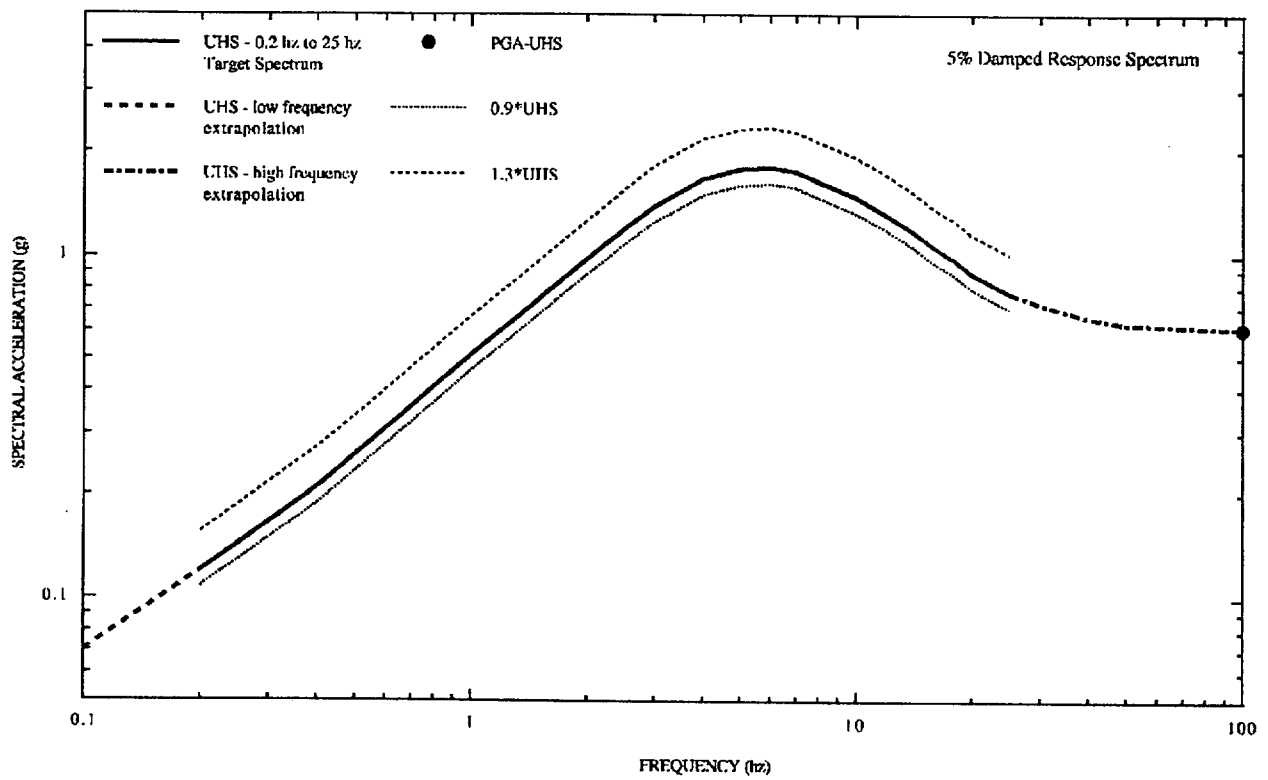


Figure 5-18B. Recommended upper- and lower-bound spectral limits to target UHS spectrum for time history designed to envelop UHS.

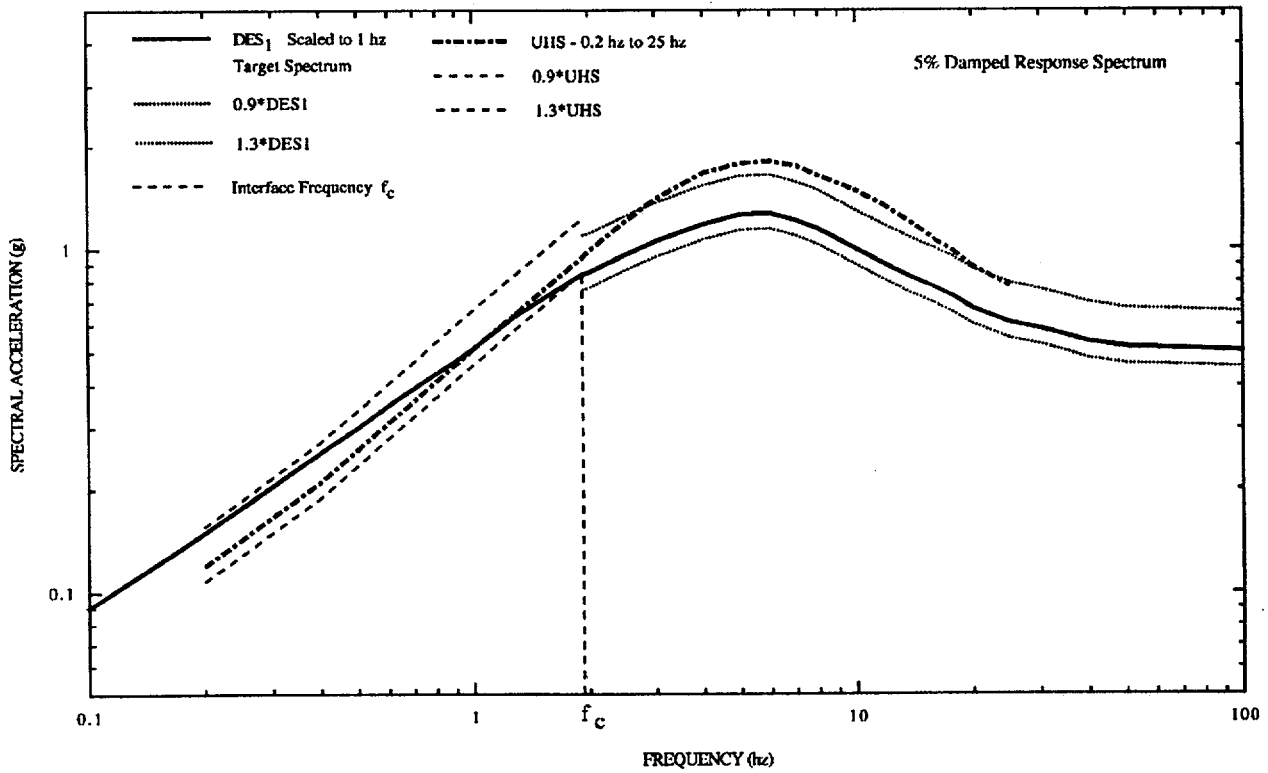


Figure 5-18C. Recommended upper- and lower-bound spectral limits to target low-frequency deaggregated spectrum.

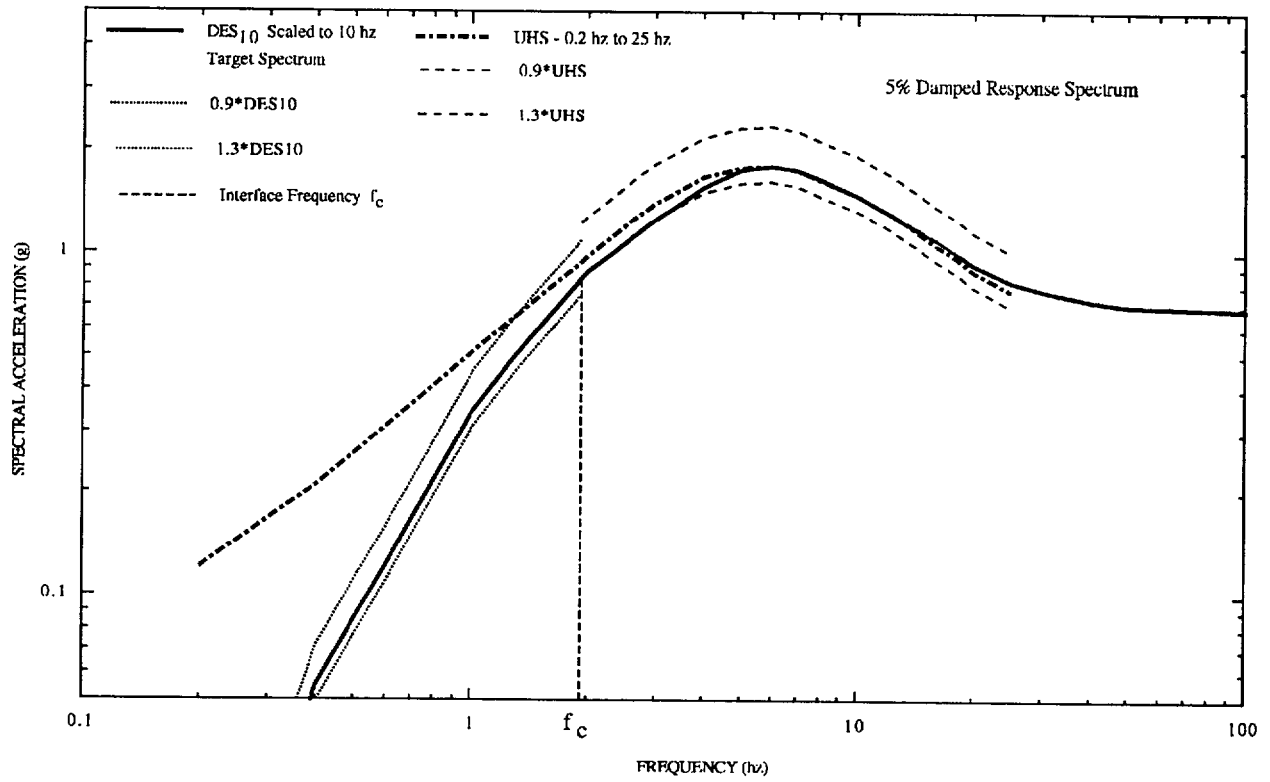


Figure 5-18D. Recommended upper- and lower-bound spectral limits to target high-frequency deaggregated spectrum.

6. PROCEDURES FOR DEVELOPING HAZARD-CONSISTENT SPECTRA ON SOIL

6.1 Approaches

Determining soil uniform hazard spectra (UHS) that are consistent with the underlying rock UHS is a challenging task. There are straightforward methods available, as described below, but they involve either performing a complete PSHA with soil attenuation equations, or extensive deaggregation of the rock hazard at multiple amplitudes and recalculation of soil hazard. For the latter approach the PSHA would not be repeated, per se, but there would be no simple, intuitive link between rock hazard results and soil hazard results. Such an intuitive link is desirable.

Available approaches to estimating soil UHS can be divided into two broad categories. First are those that integrate over multiple rock amplitudes to calculate soil hazard (probability of exceedence vs. amplitude), from which UHS on soil can be derived. Second are approaches that use the rock UHS at a given annual probability to derive a soil UHS at that same probability. Both approaches and their variants are described here, and in subsequent sections, we present examples of applications using soil data from actual sites. Table 6-1 lists these approaches, with a short description and an indication of whether the approach integrates over multiple earthquakes and multiple amplitudes. This table also indicates a label for each approach. The approaches labeled 1, 2A, 2B, and 4 are illustrated in Section 6.4 with quantitative calculations and comparisons for both eastern and western US seismic hazard conditions and multiple soil profiles. In developing these approaches we have benefitted from discussions with C.A. Cornell and P. Bazzurro, who have pursued similar work, most recently documented in Bazzurro (1998) and Bazzurro et al (1999). (Some of the notation below follows what is introduced in these references.)

Approaches Based on Integration. If we define the amplitude on soil at a certain natural frequency to be A^s , then the straightforward approach to calculate soil hazard is through a PSHA:

$$P[A^s > z] = \iint P[A^s > z | m, r] f_{m,r}(m, r) dm dr \quad (6-1)$$

which is the standard PSHA equation in which z is soil amplitude, m is magnitude and r is distance. (Equation (6-1) ignores, for simplicity, rates of occurrence on different faults and is therefore the probability of exceedence for one random earthquake. Rates of occurrence from multiple sources could be incorporated into this and subsequent equations, at the expense of more cumbersome equations.¹) We call this "Approach 4." It can lead to a defensible representation of soil hazard. The

¹The total frequency of exceedence from multiple faults can be written

$$v(A^s > z) = \sum_i v_i P_i[A^s > z]$$

where v_i is the occurrence rate on fault i and P_i is the probability in equation (6-1).

key to making this calculation defensible is to represent $P[A^s > z | m, r]$ accurately. This probability is related to the scatter observed from empirical data at soil sites when fitting an attenuation equation. The problem with this procedure is that empirical attenuation equations use observations at multiple sites, usually on similar soil conditions, whereas we are after the probability that $A^s > z$ for one specific site.

An approximation to Approach 4 can be made by recognizing that soil response can be determined from the level of input motion and the magnitude and distance of the causative earthquake. Thus we can modify equation (6-1) to the following:

$$P[A^s > z] = \iiint P[A^s > z | m, r, a] f_{M,RIA}(m, r; a) f_A(a) dm dr da \quad (6-2)$$

$$P[A^s > z] = \iiint P[AF > \frac{z}{a} | m, r, a] f_{M,RIA}(m, r; a) f_A(a) dm dr da \quad (6-3)$$

where a is the amplitude of shaking on rock, for example the spectral acceleration at the same frequency as A^s , and $f_A(a)$ is derived from the hazard curve. We call this "Approach 3." The first equation above calculates $P[A^s > z]$ from the deaggregated rock hazard, i.e. from $[a, m, r]$ sets. The second equation is equivalent except that it defines soil response by an amplification factor:

$$AF = A^s / a \quad (6-4)$$

where AF is a random variable with a distribution that can potentially be a function of m and r as well as a .

Equation (6-1) can be written slightly differently by conditioning the first factor on a , as well as m and r , and using the AF form:

$$P[A^s > z] = \iiint P[AF > \frac{z}{a} | m, r, a] f_{AIM,R}(a; m, r) f_{M,R}(m, r) dm dr da \quad (6-5)$$

This formulation recognizes AF as being dependent on m , r and a and integrates over all m and r to calculate $P[A^s > z]$. In effect it is doing the PSHA on a rock-modified-to-soil attenuation equation. Bazzurro (1998) found this method to be an accurate way to calculate soil hazard.

Approach 3 can be approximated by recognizing that soil response is governed primarily by the level of rock motion and the magnitude of the event; given these two variables, distance does not have a significant effect. Thus:

$$P[A^s > z] = \iint P[A^s > z | m, a] f_{MA}(m; a) f_A(a) dm da \quad (6-6)$$

$$P[A^s > z] = \iint P[AF > \frac{z}{a} | m, a] f_{MA}(m; a) f_A(a) dm da \quad (6-7)$$

This is a variant of Approach 3, and is labeled, "Approach 3A." For application of this method we would need only the conditional magnitude distribution for relevant amplitudes of a .

Figure 6-1 represents Approaches 4 and 3 in graphical form. Part A of the figure shows the rock PSHA curve, and part B indicates soil amplitude A^s as a function of rock amplitudes A^R , for a given magnitude earthquake and for a soil that responds non-linearly to rock motion.

For this soil, Figure 6-1 shows that scatter in rock amplitude (for a given M and a) translates to scatter in soil amplitude from aleatory uncertainties, as illustrated by the dashed distributions in Figure 6-1B. These distributions are $P[A^s > z / m, a]$ in equation 6-6. When rock variability is included, the solid distribution in Figure 6-1B results. This is $P[A^s > z / m, r]$ in equation 6-1. Often the uncertainty in soil response is smaller than for rock because the slope of soil A^s vs. rock A^R is less than unity. This effect is seen in observations: empirical attenuation equations often show less scatter for soil data than for rock data. The non-linear soil response means that the distribution of soil amplitudes will be negatively skewed relative to the rock amplitudes, as illustrated in part B. A possible resulting soil hazard curve is shown in Figure 6-1C.

The translation of rock σ (from scatter) to a soil σ (from scatter) would take place as illustrated in Figure 6-1B if soil parameters were known perfectly. Of course, they aren't: knowing rock motion, even from a specified magnitude event, does not allow us to predict soil motion perfectly even if multiple sets of dynamic soil properties are available. This is illustrated in Figure 6-2B. Part of the variability is random (aleatory), coming from random incidence angles, interference of waves, and source effects. The remainder is epistemic uncertainty, i.e. we do not know precisely the dynamic soil characteristics, particularly at high amplitude levels. This uncertainty is represented by alternative possible soil amplification curves.

These combined uncertainties will lead to a distribution of soil response that is larger (the dashed curve in Figure 6-2B). The combined distribution may have smaller or larger σ than the rock distribution, depending on the amount of soil uncertainty and the degree of non-linearity (the slope of soil vs. rock response).

The bottom graph, Figure 6-2C, shows the seismic hazard curve for the three sets of soil properties. Depending on the degree of uncertainty in soil properties and the amount of site-specific soil data available, the range in soil PSHA curves (Figure 6-2C) may be wide or narrow.

If we are concentrating on calculating soil hazard at a specific annual probability p^* , we can simplify the calculations further by focusing on a particular rock amplitude a' and associated magnitude m' . The soil amplification factor AF can be computed at a' and m' , so that:

$$AF(a, m) = AF(a', m') \quad (6-8)$$

This removes the magnitude dependence of equation (6-7), simplifying it to:

$$P[A^s > z] = \int P[AF(a', m') > \frac{z}{a} | a] f_a(a) da \quad (6-9)$$

where the notation $P[AF(a', m') > z/a | a]$ means that the distribution of AF is calculated for a' and m' , and a is used to calculate $P[AF > z/a]$. This approach is labeled “Approach 3B,” and was proposed by Bazzurro (1998).

It would of course be possible to devise an intermediate approach between 3A and 3B, where AF is made a function of either m and a . Bazzurro (1998), for example, found AF for two saturated soil sites to depend on a but not m given a . Modeling one of these dependencies would be advised if Equation (6-9) proves to be too inaccurate for practical use.

Figure 6-3 illustrates how Approach 3B works. Rock amplitude a' is determined from the rock seismic hazard curves (part A). Entering part B at rock amplitude a' gives for each of the three possible sets of soil characteristics, a distribution of soil response A^s (the solid distributions in Figure 6-3B) that reflects random aleatory variabilities. Recognizing that the soil characteristics themselves are uncertain, we combine the solid distributions in Figure 6-3B to obtain the overall (dotted) distribution of A^s given a' . This is transformed to a distribution of amplification factor AF by dividing A^s by a' . Then equation (6-9) is used to calculate the soil hazard curve (graph C). This will be most accurate at annual probabilities near p' , as that is where AF has been calibrated.

Approaches Based on UHS Scaling: Approach 3B above prompts the idea of simply scaling the rock UHS to calculate a soil UHS. If soil uncertainties are small, or if we can account for them explicitly, we can estimate the soil UHS accurately, for a given rock UHS. This would certainly be the most straightforward, intuitive approach. We label the simplest scaling “Approach 1.”

Figure 6-4 visually illustrates how this works. At a chosen annual probability p' , the corresponding rock amplitude a' is chosen. For this a' and for a central magnitude m_m (obtained from deaggregation) the distribution of soil response is obtained, accounting for soil uncertainties. (The soil distribution in Figure 6-4B corresponds to the dotted distribution in Figure 6-3B). The mean of

this distribution for frequency f is used to construct a UHS for soil (part C). Note that the mean of the distribution may be different from the value obtained with a “best estimate” set of parameters. Figure 6-4 illustrates this process for one frequency, but in its simplest form Approach 1 is applied to all frequencies simultaneously.

Consideration of Multiple Frequencies. The discussion of Approach 1 implies that a single, broadband motion representing the rock UHS will be used to drive the soil calculations. It has been recognized that a broadbanded motion may be inaccurate in many applications (e.g. USNRC, 1997) and may in fact be unconservative. As an alternative, two earthquakes can be used: one that dominates at high frequencies (10 Hz) and another that dominates at low frequencies (1 Hz). Approach 1 can be cast in terms of $A^R = a_{10}$ and $A^R = a_1$, for 10 and 1 Hz, respectively. The amplification factor AF can be defined for all frequencies as the ratio of $A^S(f) / a_{10}$ and $A^S(f) / a_1$.

Using the amplitudes of 10 Hz and 1 Hz will simplify the analysis since, where magnitude values are required, they will be available from the rock PSHA results. The resulting soil UHS can be plotted and enveloped to obtain an overall UHS for soil. If more than two frequencies are necessary on rock to define specific events whose envelope matches the UHS, then these same frequencies can (and should) be used to calculate soil UHS. The use of two frequencies in this way is labeled “Approach 2A.”

A variant of this approach recognizes that the magnitudes of earthquakes, for a given rock amplitude, may have a strong effect on non-linear soil behavior (through the duration of shaking and long period effects). Figure 6-5A shows the magnitude deaggregation at rock amplitude a' ; this distribution can be discretized into three magnitudes m_L , m_m , and m_H . Then the rock amplitude a' can be translated into soil distributions for each magnitude, Figure 6-5B. These can be weighted (using weights derived from the deaggregation) to produce an overall distribution, the mean of which becomes one value on the soil UHS (Figure 6-5C). This is labeled “Approach 2B.” The soil’s (nonlinear) response to changing magnitudes is itself nonlinear: a one-unit magnitude increase hurts soil response more (drives it more nonlinear) than a one-unit magnitude decrease helps soil response. The result is that the mean soil amplitude considering M variability may be higher than if M variability is ignored, as illustrated in Figure 6-5B.

Summary. This subsection has presented five approaches to defining UHS on soil. Subsequent sections will explore some of these approaches with specific, real soil columns to make comparisons and inferences on the best procedures to use for a proposed site. These example cases implicitly assume that site-specific shear-wave velocities are available, and that dynamic soil properties (damping and modulus) can be estimated.

6.2 Development of WUS and CEUS Attenuation Relations

Regional- and site-(soil column) specific attenuation relations are required to evaluate the suitability of various approaches for developing probabilistic soil spectra that are consistent with the probabilistic control motions (rock outcrop spectra). Soil-column-specific attenuation relations (median spectra and uncertainties) were used to generate uniform hazard spectra at the soil surface while regional-specific rock profiles were used to develop attenuation relations for outcropping rock.

The soil uniform hazard spectra were then compared to soil motions generated by Approaches 1 and 2 (involving soil response with rock input motion). This process was applied to four actual soil sites with measured properties: Savannah River, South Carolina, and California strong motion recording sites Gilroy Array No. 2, Meloland, and Rinaldi. Each soil site was assumed to be located in the CEUS and WUS (Section 6.3) necessitating the development of appropriate attenuation relations and their uncertainties.

The process of developing site and region specific attenuation relations involved exercising the point source model (Appendix D) for a suite of magnitudes and distances and then regressing on the predicted ground motions. Regional- and site-specific elements were introduced through the selection of appropriate model parameters and their uncertainties. Parametric uncertainty about the median ground motion regression (which includes regression uncertainty) was estimated through multiple ground motion estimates at each magnitude and distance based on random model parameters. Total uncertainty was then estimated by adding modeling uncertainty (Appendix D) to the parametric and regression uncertainties. This process resulted in a regression equation for median ground motions (5% damped response spectra) as a function of magnitude and distance as well as estimates of the total uncertainty, both of which are required by probabilistic seismic hazard analyses. This process has been applied to a number of Department of Energy sites as well as many other commercial projects and forms the basis for a number of CEUS attenuation relations. As a result, the process is both mature and stable, undergoing the scrutiny of widespread application to engineered structures.

6.2.1 Point Source Model Parameters

Dependent parameters for the point-source model included source depth, stress drop ($\Delta\sigma$), $Q(f)$ model (deep crustal damping), kappa (shallow crustal damping), a crustal model, and a shallow profile along with nonlinear dynamic material properties parameterized through G/G_{max} and hysteretic damping curves. Independent parameters were magnitude and distance, which were selected to cover the appropriate range in M and R in the hazard analyses. Three magnitudes were run (M 4.5 CEUS soil only, 5.5, 6.5, and 7.5) over the distance range of 1 to 400 km (Tables 6-2 and 6-3).

For the dependent parameters, base case (mean or median) values and their uncertainties are listed in Table 6-2 for the WUS and Table 6-3 for the CEUS. Source depth was based on region specific seismicity while $Q(f)$ [$Q(f) = Q_0 f^n$] models were based on inversions using the point-source model. WUS stress drops were based on inversions of the Abrahamson and Silva, 1997 empirical attenuation relation (Silva et al., 1997) and showed a magnitude dependency (EPRI, 1993; Atkinson and Silva, 1997). CEUS stress drops (Table 6-3) were assumed to follow the same magnitude scaling as WUS. The M 5.5 stress drop was set to 160 bars to correspond to Atkinson's (1993) value, which was based on high frequency spectral levels from CEUS earthquakes. In her database of CEUS earthquakes the mean magnitude was about 5.5. Interestingly, these stress drop values resulted in an average (over magnitude) difference of about a factor of two between CEUS (117 bars, Table 6-3) and WUS (65 bars, Table 6-2), in agreement with Hanks and Johnston's (1992) analyses of intensity data.

Kappa values were based on ground motion observations at hard rock sites in the CEUS (EPRI, 1993; Silva and Darragh, 1995) and soft rock sites in the WUS. The WUS kappa value of 0.03 sec

(Table 6-2) applied to the shallow portions of the Wald and Heaton (1994) crust (Table 6-4) and was adjusted to give a total kappa value of 0.04 sec for WUS rock (EPRI, 1993; Silva and Darragh, 1995; Silva et al., 1997; Boore and Joyner, 1997). The remaining kappa, 0.01 sec, was contributed by the shallow geotechnical portion of the profile, which had a shear-wave velocity of about 250 m/sec at the surface and increased roughly linearly to 1 km/sec at a depth of 30m, where it merged with the Wald and Heaton (1994) crustal model. The shallow geotechnical profile was based on shear-wave velocity measurements at strong motion sites classified as rock (Appendixes A and C; Silva et al., 1997). The profile was considered nonlinear to a depth of 150m (shear-wave velocity of 1 km/sec, Table 6-4) based on validations with recorded motions (Silva et al., 1997) and the damping for the shallow kappa contribution was taken from the rock damping curve at low strains. The crustal model is shown in Figure 6-6 along with the generic CEUS hard rock crustal model (Table 6-5).

The kappa value for the CEUS rock site was 0.006 sec (Table 6-3), significantly lower than the 0.04 sec value for the WUS rock site and was based on recordings (Section 2; EPRI, 1993). The variability in kappa $\sigma_n = 0.30$, was assumed to be the same in WUS and CEUS and was the observed variability in kappa values at rock sites in northern California that recorded the M 6.9 1989 Loma Prieta earthquake (EPRI, 1993). While this uncertainty of 0.3 for kappa may seem low to characterize both epistemic (uncertainty in the median value) and aleatory (uncertainty about the median value) variability in a site specific kappa value (Table 2-1), the point-source modeling uncertainty (Appendix D; Silva et al., 1997) already accommodates the effects of kappa variability. This arises because a fixed kappa value of 0.03 sec was used to characterize the linear rock damping at all rock sites in the validation exercises. As a result, site specific departures of kappa from the assumed value of 0.03 sec increased model deviations from recorded motions, and this resulted in larger estimates of model uncertainty. This also applied to shallow rock profiles (to a depth of a 300m [1,000 ft]) and soil profiles, both of which were randomized in developing the attenuation relations. While it is possible that the total variability in the attenuation relations was overestimated due to this probable double counting, validations are sparse for the CEUS (and are nonexistent for deep soil sites), and are sparse for M larger than about 7.0 in the WUS. As a result, assessment and partition of appropriate variability is not an unambiguous issue, particularly in the CEUS, and the approach taken here was to follow prudent design practice and not underestimate uncertainty.

The profile variability was taken over the top 300m to be as consistent as possible with the deepest soil profile (described in the next section), (Figure 6-6). Rock profile variability was incorporated using a profile randomization scheme that was based on an analysis of variance of over 500 measured profiles and has probabilistic models appropriate for WUS rock (both hard and soft) as well as soil conditions (EPRI, 1993; Silva et al., 1997). For WUS rock the soft rock model was used. For the CEUS profile, the WUS hard rock model was used, since there are few, if any, shallow geotechnical profiles with which to develop statistics on variability. Since the rock probabilistic model is only constrained to a depth of about 30m, only the top 30m of the rock profiles were randomized. To provide some consistency with the soil randomization, which included the entire soil column (typically 300m), a 270m thick layer was randomized in velocity using a σ_n of 0.3. This standard deviation is based on an analysis of variance of rock conditions beneath soil profiles. Figure 6-7 shows median and $\pm 1\sigma$ shear-wave velocity profiles for the WUS and CEUS rock sites. The profile variability models for rock were based on an analysis of variance of all rock profiles in the database and therefore are appropriate for generic applications. Site-specific applications would likely result in a

lower variability that reflects random (aleatory) variations over the dimensions of a foundation (or to a foundation dimension extending outside the footprint) as well as uncertainty in the mean or base case profile (epistemic). To develop these non-generic or small area models, multiple closely spaced holes are necessary. Such an analysis was undertaken at a deep soil site in the CEUS, and a footprint correlation model was developed by Gabriel Toro (Silva et al., 1997). However, similar data are not currently available for rock sites. The use of a generic statistical model for both WUS and CEUS rock sites therefore may also contribute to an overestimate of the variability in the rock outcrop attenuation relations.

To accommodate potential nonlinear response in the shallow portion (top 30m) of the soft rock profile (Table 6-4, Figures 6-6 and 6-7), the modulus reduction and hysteretic damping curves shown in Figure 6-8 were used. These curves were developed by modeling the rock site motions produced by a recently developed empirical attenuation relation (Abrahamson and Silva, 1997). The generic WUS rock profile (Figure 2-2) was used in developing the G/G_{max} and hysteretic damping curves and was validated by modeling the motions recorded at about 150 soft rock sites (Silva et al., 1997).

As with the soil material strain dependencies (Section 6.2.2), the rock G/G_{max} and hysteretic damping curves were randomized based on an analysis of variance of recent laboratory dynamic test results. To develop probabilistic models, multiple test results were analyzed and yielded standard errors (natural log) of 0.1 and 0.3 for G/G_{max} and hysteretic damping respectively, these values calculated at cyclic shear strains of 0.03%. These variabilities were appropriate for within-class (cohesionless or cohesive) uncertainties and were used to generate suites of random curves that follow the shapes of the base case G/G_{max} and hysteretic curves (EPRI, 1993). In the randomization process, upper and lower bounds of about $\pm 2 \sigma$ were used to prohibit physically implausible excursions (EPRI, 1993).

To model nonlinear response at the WUS rock site as well as the soil sites, RVT equivalent-linear analyses were performed (Appendix D). This process, the use of the simple point-source model coupled to RVT equivalent-linear site response, has been validated at about 500 sites for 17 earthquakes. This validation showed that the process results in an acceptably accurate characterization of strong ground motions for engineering design (Appendix D).

6.2.2 Soil Profiles And Nonlinear Properties

Four measured shear-wave velocity profiles (soil sites) were considered to be located at both the WUS and CEUS sites (Section 6.3). The soil profiles were placed on top of the rock crustal models (Wald and Heaton, 1994 for the WUS site; Table 6-4). The profiles selected include Savannah River (generic) South Carolina; Gilroy Arroyo site no. 2 in Northern California, which recorded the 1979 M 5.7 Coyote Lake, 1984 M 6.4 Morgan Hill, and 1989 M 6.9 Loma Prieta (and aftershocks) earthquakes; Meloland in the Imperial Valley, which recorded the 1979 M 6.5 Imperial Valley earthquake; and the Rinaldi substation in Southern California, which recorded the 1994 M 6.7 Northridge earthquake. All three California sites have recorded a maximum peak acceleration of at least 0.4g, with the Rinaldi site having a maximum peak horizontal acceleration of 0.84g (166.1 cm/sec peak velocity, Appendix A).

Base case shear-wave velocity profiles for the four sites are shown in Figure 6-9. The Rinaldi site, with a depth to 1 km/sec material of about 90m is comprised of cohesionless soils and is considered

a stiff site. Meloland is a “bottomless” soft profile consisting mainly of silty clays and silty sands with clay zones having a plasticity index (PI) less than about 20 but with some medium hard (MH) clays (PI \approx 40). The soil profile was truncated at a depth of 300m. The Savannah River generic site is a firm deep CEUS site modeled to a depth of about 300m (Figure 6-9). It is comprised of silty sands and low PI clays. To sample a site with gravelly soils, Gilroy was added. It is about 200m deep and consists of sands and silty sands with some thick gravelly zones. The low velocity zone at a depth of about 100m is comprised largely of gravels (EPRI, 1993).

As with the shallow (top 300m) rock profiles, the soil profiles were randomized using the same approach but with a soil statistical model appropriate for a footprint areal extent. The resulting median and $\pm 1 \sigma$ profiles are shown in Figure 6-10 for the Savannah River site. Compared to the rock site generic variability shown in Figure 6-7, the footprint soil site variability was significantly smaller. Part of the difference was caused by deep soil sites showing significantly smaller absolute variability than rock sites (EPRI, 1993; Silva et al., 1997). The remaining difference was attributed to variability over a limited area or similar depositional environment vs. generic conditions.

In addition to velocity and layer thickness variability, depth to basement material was also varied $\pm 5\%$ to accommodate changes that may occur over a site.

For the soil sites, three different sets of G/G_{max} and hysteretic damping curves were used. At the Gilroy site, validation exercises in modeling the Coyote Lake, Morgan Hill, and Loma Prieta earthquakes at a number of soil sites showed that the EPRI (1993) curves were appropriate for Bay Area soils (Figure 6-11). Similar modeling exercises at the Rinaldi (Northridge earthquake) and Meloland (Imperial Valley earthquake) sites, as well as other soil sites in the two areas, showed that the EPRI (1993) curves for cohesionless soils and the Vucetic and Dobry (1991) curves for cohesive soils resulted in too much nonlinearity (overdamping). As a result, revised sets of curves were developed for Southern California and Imperial Valley soils by modeling exercises at a number of soil sites (Silva et al., 1997). The revised sets of region specific curves are shown in Figure 6-12 for Southern California soils and Figure 6-13 for Imperial Valley soils. For reference, G/G_{max} and hysteretic damping curve recommendations from SHAKE (1992) and Vucetic and Dobry (1991) are shown in Figures 6-14 and 6-15. The revised curves generally reflect more linear response, particularly at depth. This may result from the maximum depth over which the profiles are considered nonlinear, which was taken to be 150m based on extensive validation exercises. The SHAKE (1992) and Vucetic and Dobry (1991) curves are independent of depth and may not have been intended to be implemented over such large depth ranges.

For the Savannah River generic site, the Rinaldi curves were used, as the soils at Savannah River are more similar in stiffness and grain size to southern California soils than to either northern California soils, more gravelly soils, or Imperial Valley soils. These soils are much softer (Figure 6-9) and contain more clays.

At the soil sites with depths exceeding 150m, profile damping was fixed at the low-strain value from the corresponding damping curves. The kappa values for the rock material was kept at 0.006 sec for CEUS sites and 0.03 sec for the WUS sites. For the WUS soil sites, the total kappa values were about 0.04 sec, similar to WUS rock and consistent with observations at low strains (Silva et al.,

1997). For the CEUS soil sites, this process resulted in total kappa values for the soil sites between about 0.01 and 0.02 sec, as the low strain kappa values for the soil columns was about 0.01 sec. This suggested different spectral shapes for the same soil profile located in the WUS and CEUS, particularly at low loading levels.

6.2.3 Attenuation Relations

The functional form used in the regression analyses accommodated both a magnitude saturation, due to both a magnitude-dependent stress drop and potential nonlinear response, and a magnitude-dependent, far-field attenuation (Tables 6-2 and 6-3):

$$\ln(y) = C_1 + C_2 M + (C_6 + C_7 M) \cdot \ln(R + e^{C_4}) + C_{10} (M - 6)^2 \quad (6-10),$$

where R is taken as the closest distance to the surface projection of the rupture (Boore et al., 1997). In arriving at this functional form, about 15 variations were used in regression analyses. This particular form resulted in an optimum combination of low sigma, accommodation of significant trends with M and R , stability over oscillator frequency (smoothness in spectral shape), and simplicity. The fictitious depth term, C_4 in Equation 6-10, appeared to be strongly related to nonlinear response, being nearly constant for CEUS rock (with a value near 3) and increasing strongly with frequency for WUS rock and for all four soil profiles from a value of about 2 at 0.2 Hz to about 3.5 at 10 Hz.

To illustrate the nature of the fits to the simulations (300 for each site) as well as the distribution about the regression lines, Figures 6-16 and 6-17 show peak accelerations M 7.5 for WUS and CEUS rock conditions. In general, the model captures the trends in the simulations for both rock site conditions. The variability about the regression for the CEUS (Figure 6-17) is larger than that for the WUS (Figure 6-16) reflecting the larger variability in stress drop and source depth (Tables 6-2 and 6-3) as well as shallow profile (Figure 6-7). The increase in variability at large distance for both WUS and CEUS resulted from the effects of variability in $Q(f)$ while the large variability at close distance for the CEUS resulted from the large range in source depth. The difference in the variability between WUS and CEUS rock site conditions for peak acceleration is significant, being about 0.64 for CEUS and 0.57 for WUS.

6.2.3.1 Attenuation Relations for WUS and CEUS Rock Site Conditions

Attenuation curves of peak acceleration for M 5.5, 6.5, and 7.5 for WUS and CEUS rock site conditions predicted by the regression equations are shown in Figures 6-18 and 6-19 respectively. Magnitude saturation at close distances is apparent in the jumps in peak acceleration as M increases. CEUS peak accelerations are close to the WUS at close distances and exceed the WUS at large distance. The WUS relation is generally consistent with empirical relations for comparable site conditions while the CEUS relation shows lower peak accelerations, particularly at large magnitude, than the (Toro et al., 1997; EPRI, 1993) relation. The difference results from the assumption of decreasing stress drop with increasing magnitude (Table 6-3). Toro et al. (1997) used a constant stress drop of 120 bars, perhaps resulting in motions that are too high at large magnitudes and somewhat low at small magnitudes.

To illustrate the resulting spectra for typical conditions, Figure 6-20 shows spectral accelerations (5% damping) at a distance of 10 km for magnitudes 5.5, 6.5, and 7.5 for WUS rock site conditions. Since the regression coefficients were not smoothed (Equation 6-10), some of the crustal resonances are present in the spectra. Shallow profile resonances were smoothed in the profile randomization, and the bump in the spectra near 0.5 Hz results from a deeper crustal velocity discontinuity (Figure 6-6). For M 6.5, Figure 6-21 shows median and $\pm 1 \sigma$ estimates of the WUS rock site spectra computed from the simulations. Comparison with M 6.5 spectra computed with the attenuation relations (Figure 6-20) shows the regression equations provide good estimates of median motions. Interestingly, the logarithmic standard deviation displayed in Figure 6-21 decreased at low frequency, which is opposite the trend in most empirical regressions (Abrahamson and Shedlock, 1997). The modeling uncertainty, however, increases with decreasing frequency (Appendix D) and, when combined with the parametric uncertainty, reverses the trend exhibited in Figure 6-21. Apparently neither the model nor regressions on recorded motions capture deterministic elements in the WUS strong ground motions at low frequency. Interesting, the empirical relation of Campbell (1997), when including depth to basement material ($V_s \approx 3$ km/sec) results in a largely frequency-independent sigma. Since the sigma is computed over all site conditions, the depth dependency suggests that the effects of deep sedimentary basins may not be fully captured in the other empirical relations, which neglect such a term.

For the CEUS rock site conditions, Figures 6-22 and 6-23 show corresponding plots. The CEUS spectra show the expected shift in peak to higher frequencies (near 30 Hz) as well as the result of larger uncertainty at high frequency (Figure 6-23).

Logarithmic uncertainties for both WUS and CEUS rock site conditions are shown in Figure 6-24. This sigma reflects variation about the median regression over the magnitude and distances listed in Tables 6-2 and 6-3. It includes only the variability in motions due to parametric variability as well as goodness-of-fit using the functional form shown in Equation 6-10. The difference between CEUS and WUS sigmas is about 30% at high frequency (PGA) but comparable at low frequency. As previously mentioned, the uncertainty for CEUS rock site conditions exceeds that for WUS because of the larger variability in stress drop and source depth (see Tables 6-2 and 6-3) and in the shallow (300m) part of the crustal models.

6.2.3.2 Attenuation Relations For WUS and CEUS Soil Site Conditions

This section illustrates the attenuation of peak accelerations and the magnitude dependence of response spectra at a distance of 10 km for the four soil profiles: Gilroy, Meloland, Rinaldi, and Savannah River Generic. For each profile results for both WUS and CEUS source and path conditions are presented.

Gilroy Profile

Figures 6-25 and 6-26 show peak acceleration attenuation and response spectra at 10 km, respectively, for profile Gilroy and for WUS conditions. For CEUS conditions, Figures 6-27 and 6-28 show corresponding plots. This site has the most nonlinear set of G/G_{max} and hysteretic damping curves (Figure 6-11), and these curves, contribute to the magnitude saturation shown at high frequency particularly for CEUS rock control motions. Nonlinearity in soil response also controls the large shift in the peak spectra to lower frequency as magnitude increases. The two low velocity

zones in the Gilroy profile at depths of about 30m and 100m (Figure 6-9) contribute to high strains as loading levels increase.

Meloland Profile

Figures 6-29 through 6-32 show the attenuation of peak acceleration and the magnitude dependence of spectra at 10 km for the Meloland profile. Although the G/G_{max} and hysteretic damping curves for the Imperial Valley (Figure 6-13) are more linear than the EPRI (1993) curves (Figure 6-11), the softer profile (Figure 6-9) results in saturation effects similar to Gilroy.

For the Meloland profile and both WUS and CEUS conditions, this saturation effect is very strong near 10 Hz (Figures 6-30 and 6-32). This trend indicates that the soils saturate in the levels of motions they can transmit as strains increase to high levels. This observation is not new, since soils are known to fail (lose shear strength) at very high loading levels and simply will not propagate waves with wavelengths shorter than about four times the width of the failed zone. However, early predictions on saturation of peak acceleration have routinely been exceeded, suggesting an incorrect assumption in the dynamic nonlinear properties of soils, particularly soft soils. The revised sets of G/G_{max} and hysteretic damping curves, based on modeling high levels of motions and recent laboratory testing (Figures 6-11 to 6-14), are believed to capture nonlinear properties reasonably well, suggesting that the degrees of saturation displayed in the spectra plots for profiles Gilroy and Meloland are appropriate for these sites. These results should be confirmed with nonlinear (effective stress) analyses with properties adjusted so that the nonlinear soil models produce the same G/G_{max} and hysteretic damping curves used in the equivalent-linear analyses. This is an important issue and may have significant impacts on probabilistic seismic hazard analyses since the uncertainties typically used in attenuation relations assume a lognormal distribution, symmetric about the median in log spectral ordinates. Saturation, on the other hand, suggests a lower probability for motions above the median than below (equivalent fractile levels) with the difference increasing with cyclic shear-strains.

Rinaldi Profile

The stiffest profile is Rinaldi (Figure 6-9). This site recorded a maximum peak acceleration of 0.84g during the M 6.7 Northridge earthquake. It is located at a rupture distance of 7.1 km updip from the Northridge earthquake rupture surface. These are high motions for a soil site, and model predictions result in high motions for both WUS and CEUS conditions (Figures 6-33 to 6-36). The WUS peak accelerations (Figure 6-33) agree reasonably well with the Northridge recordings (0.63g for average horizontal component (Appendix A). For the CEUS, the maximum predicted peak acceleration for M 7.5 exceeds 1g out to about 10 km (Figure 6-35), indicating that stiff soil profiles have the capacity to amplify high frequency ground motions in the CEUS.

Another feature of interest includes comparing the WUS and CEUS Rinaldi soil spectra (Figures 6-34 and 6-36 respectively). The WUS Rinaldi spectra have distinctly different shapes than the corresponding CEUS Rinaldi spectra, showing peak spectral amplification at considerably lower frequencies. For stiff soils, as well as soft soil at the lower loading levels (Figures 6-30 and 6-32), the soil spectra preserve a significant degree of the spectral shift between the WUS and CEUS rock motions (Figures 6-20 and 6-22). This is a significant issue and illustrates that care must be exercised in scaling WUS soil motions to CEUS conditions. For soft soils such as Meloland and for high loading conditions, e.g. M 7.5, Figures 6-30 and 6-32 suggest that this process may be acceptable,

as the spectral shapes are similar for WUS and CEUS conditions. For M 5.5 however, the same figures show significantly different spectral shapes. These observations also indicate the difficulty in developing spectral shapes for generic soil site conditions.

Savannah River Profile

The generic Savannah River profile and the Meloland profile are the two deepest profiles analyzed (300m, Figure 6-9). The Savannah River profile is considered a firm soil. It has the highest shear-wave velocity at the surface, 400m/sec, with a broad soft zone extending from the near surface to a depth of about 70m. The attenuation of peak acceleration shown in Figures 6-37 and 6-39 indicate that this site is capable of transmitting high levels of high frequency motions, due largely to the assumed G/G_{\max} and hysteretic damping curves (Figure 6-12). For M 7.5, at a distance of 10 km, the spectral shapes are similar for WUS and CEUS conditions but differ significantly for M 5.5, showing a pattern similar to Meloland.

6.2.3.3 Uncertainty Estimates For Soil Sites

The uncertainties about the regression equations over all magnitudes and distances (Table 6-2 and 6-3) are shown in Figure 6-41 for WUS conditions and Figure 6-42 for CEUS conditions with the CEUS variability generally exceeding that of the WUS. These uncertainties result from the regression analyses and reflect parametric variability as well as goodness-of-fit provided by the regression functional form (Equation 6-10). They average about 0.5 (natural log units), lower than the corresponding sigmas for rock site conditions for frequencies above about 1 to 2 Hz (Figure 6-24). This reduction is likely due to the reduced profile variability, (compare Figures 6-7 and 6-10), and the effects of nonlinear response, which dampens variability in the control or input motions (EPRI, 1993). These variabilities are used in the generic site hazard analyses. Modeling (or model) uncertainty, Appendix D, has not been added to the parametric plus regression sigma for the hazard study as it is the same for all rock and soil sites. Total uncertainty, which includes the addition of modeling uncertainty (Appendix D), would be the appropriate uncertainty to use in applications to assess probabilistic hazard at a site for design purposes.

6.3 Seismic Hazard at CEUS and WUS Example Sites

6.3.1 Introduction

The purpose of testing soil amplification calculations is to ensure that methods of accounting for uncertainty in soil properties work in a variety of seismic hazard environments. To this end, we selected sites in both the central and eastern US (CEUS) and in the western US (WUS) that have high frequencies dominated by local sources of seismicity, and low frequencies dominated by more distant sources. In the CEUS the site was Columbia, South Carolina, which is about 130 km from the Charleston seismic zone (represented here by a fault). In the WUS we selected a site in the Mojave desert located about 30 km east of the San Andreas fault. Both sites are a good test of the soil amplification methodology, which uses one or a few events (magnitudes and distances) to calculate the effects of soil amplification, in order to accurately estimate uniform hazard spectra (UHS) on soil given the UHS on rock. It should be understood that the over-riding purpose here is not to make a perfectly accurate estimate of hazard at any one site, but to create several reasonable

hazard representations that test the alternative soil amplification methodologies under extreme conditions.

The four soil profiles examined in these seismic hazard test cases have been described in previous sections. They consist of a profile (no. 1) representative of the Savannah River site, a profile (no. 2) for Gilroy, California, array station no. 2, a profile (no. 3) for the Meloland site in the Imperial Valley in California, and the profile for the Rinaldi substation site, California. In both the CEUS and WUS, attenuation curves for each region reflect the properties of crustal rocks in that region as well as the local soil properties.

6.3.2 Seismic Hazard Environment, CEUS Example Site

Columbia, South Carolina was the site chosen as the example site in the CEUS. Its seismic hazard is affected by a local source and by the Charleston earthquake zone, represented here by a fictitious fault (see Figure 6-43).

Seismicity parameters of the two earthquake sources affecting Columbia were as follows. The local source consisted of a box surrounding Columbia, 220 km on a side, with a minimum magnitude M_{\min} of 4.5 (corresponding to $m_{Lg} = 5$, which is standard for CEUS seismic hazard assessments) and a maximum magnitude M_x of 6.5. The seismicity in the local source was taken to be exponentially distributed and spatially homogeneous, with a rate $\nu_0 = 1.13E-2$ and a b-value = 0.9. Both values came from the US Geological Survey assessment of seismicity for the national hazard maps, the rate being calculated as an average over the spatially-varying rate for the southeastern US derived by the USGS.

For the fictitious Charleston fault, earthquakes between $M=6.5$ and 7.8 were considered equally likely, that is a characteristic magnitude model was used between these two magnitudes with a rate of occurrence $\nu=1.54E-3$, meaning a mean recurrence period of 650 years. This is the rate used by the USGS for the Charleston fault, although they used a single characteristic magnitude of 7.3. We assumed a range of magnitudes for this test example to make the task of choosing a single (or a few) analysis earthquakes more challenging.

Contributions to hazard at Columbia. The Columbia site was selected because different earthquakes dominate the high and low frequency seismic hazard. This is illustrated in Figures 6-44 and 6-45, which show the contributions to hazard at Columbia for 10 Hz and 1 Hz spectral acceleration (SA). The ground motion attenuation equation used for these calculations was the CEUS rock curve. For 10 Hz SA, the local background source dominated at all ground motions levels, as illustrated in Figure 6-44. For 1 Hz SA the Charleston fault was dominant for annual frequencies around 10^{-3} to 10^{-5} (see Figure 6-45), which is the level at which seismic design motions are selected. The background source dominated at very low ground motions (because the recurrence rate in the background is higher than for the Charleston fault) and at high ground motions (because background earthquakes can occur very close to Columbia, generating high levels of shaking).

Figures 6-46 through 6-49 show the deaggregation of seismic hazard by magnitude, distance, and attenuation equation epsilon for 10 Hz and 1 Hz SA, respectively. This deaggregation was performed for 0.38g SA at 10 Hz, and 0.067g SA at 1 Hz, which are the levels corresponding to 10^{-4}

hazard. For 10 Hz (Figures 6-46 and 6-47), the large contribution of small local earthquakes ($M=4.5$ to 6.5 , $R \approx 20$ km) is evident. For 1 Hz (Figures 6-48 and 6-49), the dominance of large events from the Charleston fault ($M \approx 7.5$, $R \approx 130$ km) is clear. For both natural frequencies the ϵ values contributing to hazard are predominantly positive (see the bottom frame of Figures 6-46 and 6-48), mostly from 0 to 1.5 for 10 Hz and 1.0 to 1.7 for 1 Hz. This means that ground motions *higher* than the median dominate the hazard, which is typical at 10^{-4} ground motion levels.

Choices of deaggregation events. With these contributions to seismic hazard, the choices for deaggregation seismic events for Approach 2B were made as follows. The general approach was to use three magnitudes, one at the mean deaggregation event, one higher or lower representing the non-dominant source, and a third value representing the dominant source. Weights on the magnitudes were assigned so that the non-dominant source received its appropriate weight, and weights for the mean magnitude and dominant source were assigned so the mean of the three magnitudes equaled the mean magnitude calculated from deaggregation of the hazard.

For 10 Hz this worked as follows. The mean deaggregation magnitude was 5.6, a value of $M=7.7$ was chosen to represent the contribution from the Charleston fault (this is the most likely magnitude of that contribution—see the top plot of Figure 6-46), and a value of $M=4.6$ was chosen as the mode of the contributions from local magnitudes. The $M=7.7$ value received a weight of 0.12 (obtained from the deaggregation), and the other two values received weights of 0.25 and 0.63, assigned to give the correct mean of 5.6. In summary, the three seismic events and their weights were:

$M = 4.6$, $R=8$ km, weight=0.25,
 $M = 5.6$, $R=8$ km, weight=0.63,
 $M = 7.7$, $R=130$ km, weight=0.12,

where the distances were picked from Figure 6-47 to correspond to the magnitudes being represented.

For 1 Hz the choices were different. The mean deaggregation earthquake was 7.0 and a value of 7.6 was chosen to represent the Charleston earthquakes (see the top plot of Figure 6-48). The total contribution from the Charleston fault to the 10^{-4} hazard is 0.70. A third magnitude representing local earthquakes was assigned the remaining weight of 0.3, and the value of this magnitude was selected to be 5.8, which was calculated so that the mean magnitude of the distribution (5.8) was preserved. To summarize,

$M = 5.7$, $R=20$ km, weight=0.3,
 $M = 7.0$, $R=100$ km, weight=0.0,
 $M = 7.6$, $R=130$ km, weight=0.7.

This then represents the case of a bi-modal magnitude distribution where the mean magnitude has a low probability of contributing to exceedences of the 10^{-4} UHS.

For both of these derivations the single "design earthquake" was designated to be the central value, for use in Approach 2A.

6.3.3 Calculated spectra, CEUS

Rock motions. The seismic hazard calculations led to uniform hazard spectra (UHS) for rock conditions, for the Columbia site. In addition, the six deaggregation seismic events were used to calculate spectra. In this calculation the M and R value of each 10 Hz seismic event was used with the CEUS rock attenuation equation to calculate a spectrum; this spectrum was then scaled to the 10^{-4} UHS value at 10 Hz (0.38g) to create 3 deaggregation event spectra. This process was repeated for 1 Hz, except that the spectra were scaled to the 10^{-4} UHS value at 1 Hz (0.067g). This process created 6 spectra, and these are plotted in Figure 6-50 along with the UHS. This plot illustrates the range of spectral shapes used in the deaggregation events.

Soil motions. To calculate soil UHS, four alternative representations of the residual distribution for the four soil attenuation equations were investigated, as follows:

- Constant sigma, no truncation of residual distribution,
- Variable sigma, no truncation of residual distribution,
- Variable sigma, truncation of residual distribution at 1σ ,
- Variable sigma, truncation of residual distribution at $1.5 \times$ median.

The 1st alternative above is a standard assumption, particular for the CEUS. The 2nd alternative recognizes that the scatter around median predicted values of ground motion decreases with increasing amplitude, reflecting perhaps more homogeneous, repetitive characteristics of motion for large magnitude earthquakes. A variable sigma has been calculated for rock conditions in California from empirical data (Abrahamson and Silva, 1997; Campbell, 1997; Idriss, 1993; Sadigh et al, 1997) and the variation of sigma has generally been dependent only on magnitude. (Campbell, 1997, reports one equation where sigma varies with peak ground acceleration.) The 3rd and 4th alternatives recognize that the amplitudes of motion on soil will saturate because of non-linear response, thereby creating a ceiling on the soil amplitudes that can occur, even for large input rock motions. These last two alternatives investigate the effects on hazard of recognizing this saturation of soil response.

The values of sigma calculated for the four soil profiles (Savannah, Gilroy, Meloland and Rinaldi) are shown in Figures 6-51 through 6-54. Separate plots are shown for the soil profiles in the CEUS (top of each figure) and WUS (bottom of each figure). The standard deviation was calculated as a function of M and R , and curves are shown for six values of M and R as well as for a constant sigma (the first assumption listed above). Note that these standard deviations represent parametric variability and goodness-of-fit errors only, not modeling uncertainty.

The choice of constant or variable σ in the residual distribution does not make a large difference in the UHS for the CEUS rock site. This is illustrated in Figure 6-55. Rock motions remain largely linear, so there was no justification for truncation of the residual distribution. As a result, further comparisons with rock UHS are made with the variable σ spectrum.

The four alternatives for the soil residual distribution were used to calculate UHS for the Columbia site. These are shown in Figures 6-56 through 6-59, along with the rock UHS for comparison. The general observation from these figures is that the variable sigma UHS (alternative 2) indicates UHS similar to the constant sigma alternative (no. 1). The largest decrease in the UHS occurs when truncation is added (alternatives 3 and 4). Figures 6-56 through 6-59 show that truncating the residual distribution of soil response really limits the large amplitudes that can occur and reduces the calculated UHS.

6.3.4 Seismic Hazard Environment, WUS Example Site

A site in the Mojave desert of California was chosen as the example site for the WUS. This site, the nearby faults, and background seismicity points are illustrated in Figure 6-60.

Seismicity parameters for the faults and background points were selected following the USGS/CDMG interpretation for California. In this interpretation, major earthquakes ($M > 6.5$) are ascribed to faults and lower-level seismicity is ascribed to background points. The rate of activity of these background points, spaced at 0.1° longitude and latitude, is calculated based on a smoothed interpretation of historical seismicity. An exponential magnitude distribution with a $b=0.9$ is assigned to these points.

The seismicity model for the faults was taken to be that used by the USGS/CDMG in deriving seismic hazard maps for California. That is, each fault is assumed to produce a single characteristic magnitude with a specified annual frequency of occurrence. The characteristic magnitudes and associated frequencies were taken from the USGS/CDMG work.

Contributions to hazard at Mojave site. The Mojave site was selected because different sources of earthquakes dominate different natural frequency ranges of the ground motion spectrum. Figures 6-61 and 6-62 show the contribution of background sources and faults to the seismic hazard on rock at 10 Hz and 1 Hz, respectively. For 10 Hz the background sources dominate the hazard; for 1 Hz the San Andreas fault gives the largest contribution to hazard.

Figures 6-63 through 6-66 show the deaggregation of seismic hazard by magnitude, distance, and attenuation equation epsilon for 10 Hz and 1 Hz SA. This deaggregation was performed at 1.92g SA for 10 Hz and at 0.65g SA for 1 Hz, which are the levels corresponding to 10^{-4} hazard. For 10 Hz (Figures 6-63 and 6-64), the large contribution of the small background earthquakes ($M=5$ to 6.5 , $R \sim 20$ km) is evident. For 1 Hz (Figures 6-65 and 6-66), the large events on distant faults produced most of the hazard.

Choices of deaggregation events. With the contributions to hazard shown in Figures 6-63 through 6-66, choices for the deaggregation seismic events were made in a manner identical to that for the CEUS. For 10 Hz the mean deaggregation magnitude was 6.1, and the resulting three seismic events and weights were as follows:

$M = 5.1, R=10$ km, weight=0.05,
 $M = 6.1, R=14$ km, weight=0.90,

$M = 7.8, R = 40 \text{ km}, \text{weight} = 0.05,$

where the distances were picked from Figure 6-64 to correspond to the magnitudes being represented.

For 1 Hz the choices for the three deaggregation seismic events were:

$M = 5.4, R = 10 \text{ km}, \text{weight} = 0.15,$

$M = 6.7, R = 18 \text{ km}, \text{weight} = 0.67,$

$M = 7.8, R = 30 \text{ km}, \text{weight} = 0.18.$

For both of these derivations the single "design earthquake" was designated to be the central value.

6.3.5 Calculated Spectra, WUS

Rock motions. The seismic hazard at the Mojave site led to UHS for rock conditions, and in addition six deaggregation seismic events were used to calculate spectra. Following the same procedure as for the Columbia site, the deaggregation spectra were scaled to the 10^{-4} UHS amplitude at 10 Hz and 1 Hz, as appropriate. These six spectra are shown in Figure 6-67, along with the 10^{-4} UHS spectrum.

The constant σ and variable σ attenuation residual distributions were examined for the Mojave site, as they were for the Columbia site. Again, little difference between the two assumptions was calculated, as shown in Figure 6-68, except between frequencies of 5 to 20 Hz, where the variable σ spectrum is up to 20% below the constant σ spectrum. The variable σ assumption was used for comparison purposes in the plots with soil UHS.

Soil motions. For soil hazard calculations, four soil attenuation equations were investigated, and for each, four alternatives on the residual distribution were examined (these are the same four alternatives used for CEUS soil calculations):

- Constant sigma, no truncation of residual distribution,
- Variable sigma, no truncation of residual distribution,
- Variable sigma, truncation of residual distribution at 1 sigma,
- Variable sigma, truncation of residual distribution at 1.5 x median.

This resulted in 16 different soil characteristics (four soils times four residual distribution alternatives). The 10^{-4} UHS for these 16 different characteristics are shown in Figures 6-69 through 6-72. As for the CEUS soils, the largest change in UHS occurs when truncation of the residual distribution is included.

6.4 Evaluation of Procedures to Develop Site-specific Soil Hazard Spectra

Section 6.1 presented a number of approaches to estimating site-specific soil spectra that are consistent with a specified hazard level and that accommodate uncertainties in soil properties. In

this section, comparisons are made among several of these approaches, and site-specific soil UHS are computed for the four soil profiles located in the WUS and CEUS (Section 6.3). The site-specific soil UHS presented in Section 6.3 reflect the desired hazard level with which to evaluate the various degrees of approximations using rock outcrop UHS and site response analyses. However, an issue exists in the soil UHS calculated with Approach 4 involving long return periods where the hazard may result from motions that significantly exceed the median ground shaking during earthquakes contributing to the hazard (see the epsilon distributions in Figures 6-46, 6-48, 6-63, and 6-65). Under these conditions the site-specific UHS may overestimate the hazard at high frequency, as the residual dispersion does not reflect the soils limited capacity to transmit high levels of motion (i.e. its non-linearity). This issue is discussed in the next Section.

6.4.1 Site-specific Soil UHS

The site-specific UHS were considered to represent “truth” in the context of the analyses of Section 6.1, as these spectra consist of amplitudes computed for the same probability of exceedence across structural frequency. However, as previously mentioned in Section 6.2, at high strains soil profiles tend to saturate, transmitting proportionally less high-frequency motion as loading levels increase. While this is reflected in the convolution analyses used to develop both the site-specific soil motions and the soil attenuation relations, the residual dispersion computed in a conventional (homoscedastic) regression analysis is a combination over all event (causative) conditions (all magnitudes and distances). As a consequence, for long return periods, much of the contribution to the soil UHS results from motions that significantly exceed median estimates for the magnitudes and distances dominating the hazard. These contributions are reflected in the deaggregation ϵ values (McGuire, 1995). This process can conceivably result in soil motions that imply control motions sufficiently high enough to fail the soil column. This apparent paradox, alluded to in Section 6.3, suggests that in the context of probabilistic seismic hazard analyses involving nonlinear site response, a magnitude- and distance-independent residual distribution may be inappropriate and can result in overly conservative soil motions. The “truth” or benchmark site-specific hazard level should then accommodate the appropriate (site-specific) amplitude dependencies in the residual dispersion as well as a distribution that accommodates negative skewness as depicted in Figure 6-2. Ongoing analyses of variance are intended to address this issue. These consist of developing an appropriate distribution for the residual dispersion about the regression as well as including potential amplitude or magnitude and distance dependencies in the standard error. Incorporating a residual dispersion in the development of the UHS that reflects an appropriate distribution of limiting values (perhaps a type II extreme value model) as well as conditional dependencies in the context of nonlinear response would provide a more appropriate benchmark or “truth” with which to evaluate the various approaches to developing hazard consistent soil spectra. While our current benchmark is limited in this respect because it uses a standard model of residual dispersion, it is consistent with current practice in the CEUS. WUS attenuation models do typically include a magnitude dependency in their standard errors (Abrahamson and Shedlock, 1997) resulting in a large decrease as magnitude increases for $M \geq 6.5$. However, the high frequency motions (≥ 5 Hz) are affected most by nonlinear saturation because of the contribution of low-magnitude ($M < 6.5$) close-in earthquakes. The magnitude dependency currently incorporated in WUS attenuation relations is not likely to resolve this issue, particularly since it is site independent, being applied at both rock and soil sites. As a result, we compare site-specific soil UHS with soil spectra computed using rock outcrop UHS and various approaches to conventional site

response analyses for a variety of profiles as well as different hazard environments. These comparisons provide valuable insights into potential degrees of conservatism implicit in soil site UHS computed using standard models of residual dispersion. These analyses will indicate the strain levels (degree of nonlinearity) that may require more sophisticated dispersion models.

6.4.2 Approaches To Developing Hazard-Consistent Site-specific Soil Motions Incorporating Profile Uncertainties

The conventional approach to developing site-specific soil motions involves convolutional analysis, either equivalent-linear or fully nonlinear, using rock outcrop control motions at the soil/rock transition zone. For “bottomless” profiles the “rock” control motions may be input at a sufficiently deep location such that soil amplification extends to the lowest frequency of interest, generally about 0.5 Hz. In the convolutional analyses, uncertainty in dynamic material properties is generally accommodated through parametric variations, either deterministically with upper-, mid-, and lower-range moduli or through a Monte Carlo approach using randomly generated properties with statistically based distributions. Uncertainties in soil properties and in model deficiencies (in the convolutional formulation) are accommodated by either smoothly enveloping the deterministic variations or selecting a fractile level, generally the mean, for the Monte Carlo approach. Both of these procedures appear to result in conservative spectral estimates since site variability is already accommodated in the variability associated with the attenuation relations used in developing the control (rock) motions. The approach using randomized material properties is preferred since the conservatism is quantified, provided the parameter distributions reflect a realistic assessment of how well the base case profile and nonlinear properties are known (epistemic uncertainty) and the variability over the site or footprint (aleatory uncertainty). A motivation for using the more conservative mean rather than median estimates, which acknowledges double counting site variability, is to accommodate a degree of model uncertainty in the convolutional formulation. Since this component of model uncertainty is currently unquantified, it is not possible to add it explicitly. It is, however, thought to be relatively small, based on validation exercises of the entire model (source, path and site, Appendix D). As a result, the possible double counting of site variability may be largely offset by neglecting the deficiencies in the convolutional formulation. For attenuation relations based solely on the validated stochastic point- or finite-source models (Appendix D; Silva et al., 1997) the inclusion of model uncertainty, accommodates the site model deficiencies for the vertically propagating shear-wave model using the equivalent-linear approximation.

The various approaches to developing hazard-consistent site-specific soil spectra include the following, in increasing order of accuracy (these approaches were described and illustrated in Section 6.1):

Approach 1: rock UHS used as control motions,

Approach 2A: develop transfer function for 1 Hz and 10 Hz design earthquakes, using a single magnitude for each frequency,

Approach 2B: develop transfer functions for 1 Hz and 10 Hz design earthquakes accommodating magnitude distributions,

Approach 3: approximations to UHS integrations (see Section 6.1 and Appendix J),

Approach 4: UHS computed using site-specific soil attenuation relations.

Approaches 1, 2A, 2B, and 4 are compared in the following sections, while Appendix J describes an evaluation of Approach 3 using different soil profiles and hazard environment. Approach 1 involves driving the soil column with the broad rock UHS spectrum and may result in unconservative high frequency motions, particularly in the context of equivalent-linear site response analyses. Additionally, the appropriate magnitude and time history duration are ambiguous using Approach 1 for hazard environments that do not result in strongly unimodal M and R deaggregation. Approach 2A recognizes that different earthquakes may dominate the high and low frequencies, and uses separate transfer functions for these events. This is the approach recommended by Regulatory Guide 1.165 (USNRC, 1997). Approach 2B requires some elucidation. In this approach, mean, high and low percentile magnitudes from deaggregation for each design earthquake (e.g., 1 Hz and 10 Hz, Section 6.3) are used to scale spectral shapes to the 1 Hz and 10 Hz rock UHS, and the resulting control motions are used to develop weighted mean transfer functions for each design earthquake. The transfer functions are then used to scale each design earthquake or are combined to scale the rock UHS. The use of a three-point magnitude distribution for each design earthquake accounts for non-linear effects caused by a wide range of magnitudes contributing to the hazard.

6.4.3 Control Motions

Figure 6-73 shows a comparison of the WUS and CEUS rock outcrop UHS. The effects of both the hazard environment (Section 6.3) and attenuations relations (Section 6.2) are evident, with the WUS motions generally exceeding the CEUS motions by a factor of five or more for frequencies below about 10 Hz. The scaled design earthquakes were presented earlier in Figures 6-50 and 6-67 for the CEUS and WUS respectively. The difference in the hazard environments between the WUS and CEUS is evident in the large differences in the 1 Hz and 10 Hz magnitude distributions (Section 6.3). The difference in magnitudes for the 1 Hz and 10 Hz design earthquakes is 1.3 units for the CEUS (Figure 6-72) and only 0.4 units for the WUS (Figure 6-73). The effects of magnitude distribution in the rock UHS on nonlinear soil response are much less an issue for WUS conditions than CEUS, at least for the example sites, which were chosen to maximize the differences at 1 and 10 Hz.

In the site response analyses, two additional issues are important: the degree of fit to the control motions (rock UHS and scaled design earthquake spectra computed using attenuation relations, Section 6.2) and the effect of control motion variability on median soil spectra. The first issue involves developing appropriate Fourier amplitude spectra for use in the RVT equivalent-linear soil analyses (Appendix D) that are consistent with target response spectra. To illustrate the RVT spectral matching process (Silva and Lee, 1987), Figure 6-74 compares a response spectrum computed using the CEUS attenuation relation (Section 6.2) for $M = 7.5$ and $R = 1$ km (target spectrum) to a spectrum resulting from spectral matching. The difference is less than a few percent over the entire frequency range.

The second issue involving the effect of control motion variability is of potential significance since the convolutional process uses a fixed or constant control motion while varying site properties. This

is not the process used in developing the attenuation relations where source, path, and site parameters were varied simultaneously. The implicit assumption involved in comparing results from these two different processes is that soil response is either independent or weakly dependent on control motion variability. To demonstrate any dependence, Figure 6-75 shows median and $\pm 1 \sigma$ spectral estimates for CEUS conditions at $M = 7.5$ and $R = 1$ km varying only site properties while Figure 6-76 shows results for varying source, path, and site parameters simultaneously (Section 6-2). Although the variability is significantly larger when source and path parameters variations are added ($\sigma_{ln PGA}$ increases from 0.17 to 0.44, a factor of about 2.6), the median spectra are nearly identical as illustrated in Figure 6-77.

In the following sections, the profiles are discussed in order of decreasing overall stiffness as reflected in Figure 6-9. Each section presents results for CEUS conditions followed by WUS conditions, contrasting relatively low and high loading conditions (Figure 6-71). Approaches 1, 2A, 2B, and 4 are compared along with the effects of truncating the deep profiles at depths of about 150m (500 ft) and 90m (300 ft). This comparison assesses the profile depth required in the site response analyses (as well as site characterization) to properly accommodate low frequency (0.5 Hz) soil motions.

There are a number of competing effects operating in the following analyses. The degree and extent of these analyses are intended to provide useful insights into issues that are significant in developing site-specific soil motions.

6.4.4 Example Case 1: Intermediate Depth Very Stiff Profile, Rinaldi

The Rinaldi profile is about 80m deep, is considered a very stiff soil, and has a column resonance near 2 Hz (Figure 6-9). All site properties, soil profile, depth to basement, and G/G_{max} and hysteretic damping curves, as well as their variabilities are the same (same probabilistic models) in these analyses as those used in the development of the site-specific attenuation relations (Section 6.2, Figures 6-9 and 6-12). This procedure was followed for all the profiles analyzed.

6.4.4.1 CEUS Conditions

To begin the approach comparisons, Figure 6-78 shows soil UHS computed using Approaches 1, 2B, and 4 for CEUS conditions. Approach 4 provides estimates of the UHS at the soil surface directly using the site-specific attenuation relation (Section 6.2) while Approach 1 simply uses the rock UHS as control motions. Approach 2B computes mean transfer functions for each design earthquake (based on 1 Hz and 10 Hz deaggregation) using the appropriate magnitude distribution for each earthquake. The two transfer functions are combined to scale the rock UHS or are used independently to scale the rock outcrop 1 Hz and 10 Hz design earthquakes to produce soil design earthquakes for cases where it may be desirable to perform two sets of design analyses. Figure 6-78 shows nearly the same motions for both Approaches 1 and 2B, both being conservative compared to the soil UHS. For a linear system, Approaches 1 and 2B should produce identical results and for the loading levels (Figure 6-71), profile stiffness (Figure 6-9), and nonlinear properties (Figure 6-12) used, this is nearly the case.

The median and $\pm 1 \sigma$ effective strains resulting from Approach 1 are shown in Figure 6-79. With median values generally less than about $10^{-2} \%$, little change in shear-wave velocity and hysteretic damping is expected (Figure 6-12) suggesting a nearly linear system. The apparent conservatism in Approaches 1 and 2B at frequencies exceeding 10 Hz shown in Figure 6-78 is about 20%. Near the fundamental column resonance at about 2 Hz and at low frequency (< 1 Hz) Approach 4 exceeds Approaches 1 and 2B by about 10%. Exceedence near a resonance is expected since there is a smoothing inherent to the regression process but the slight low-frequency underprediction and high-frequency exceedence are puzzling since the mean-to-median ratio resulting from profile variability is about 5% and the regression equations appear to provide a reasonable fit to the model predictions (Figures 6-16 and 6-17). Additionally, the RVT spectral matching process also appears to provide a good match to the target spectra, as Figure 6-74 suggests. While the degree of conservatism is larger than expected at high-frequency and requires further investigation along with the slight low-frequency underprediction, these results suggests that Approaches 1 and 2B are not likely to lead to unconservative spectral estimates for very stiff profiles under moderate loading conditions (peak rock outcrop acceleration of about 0.3g, Figure 6-73).

The transfer functions used to scale the rock outcrop spectra are shown in Figures 6-80 through 6-82. Figure 6-80 shows the ratio computed for the 1 Hz scaled design earthquake and Figure 6-81 the corresponding ratios for the 10 Hz design earthquake. Figure 6-82 compares the two (1 Hz and 10 Hz) mean ratios, the average of which is used to scale the rock outcrop UHS (Approach 2B). As expected, due to the largely linear response, little difference is seen between the ratios for frequencies below about 30 Hz, with about a 15% difference at peak acceleration (100 Hz). Approaches 1 and 2B are equivalent under these conditions (strain ranges and nonlinear properties).

For cases where multiple soil spectra are desired, Figure 6-83 compares 1 Hz and 10 Hz design earthquake soil motions (Approach 2A) with Approach 2B applied to the UHS along with Approach 1 results since they both reflect the use of rock UHS spectra. The 1 Hz and 10 Hz soil spectra are very close to the scaled rock UHS over the frequency ranges of the bounding criteria discussed in Section 5. At peak acceleration (near 100 Hz) Approach 2B applied to the rock UHS exceeds the 10 Hz soil motions by about 20%.

Figures 6-84 and 6-85 compare Approaches 1 and 2B using conventional deterministic profile variations. The deterministic variations reflect changes in the base case shear modulus of a factor of 2 and are shown in Figure 6-84. The mean and $\pm 1 \sigma$ spectra taken over the three spectra, reflecting base case and upper-and-lower-range profiles, are shown in Figure 6-85. The comparison in Figure 6-84 between the spectrum computed using the base case profile and the mean Approach 2B spectrum illustrates the effects of profile randomization, generally smoothing through the base case resonance peaks. With the exception of the fundamental resonance peak, Figure 6-84 suggests that an average of the three spectra (base case and upper- and lower-range profiles) may provide an acceptable soil spectrum. Figure 6-85 shows this comparison and confirms that a smoothed average of the three provides a reasonable estimate of design levels.

6.4.4.2 WUS Conditions

For the Rinaldi profile, Figures 6-86 to 6-93 show corresponding plots for WUS conditions. For this case, changes in the loading conditions (Figure 6-73) determined by the WUS hazard environment

as well as crustal structure resulted in distinctly different soil motions in both level and spectral shape. Figure 6-86 compares Approaches 1, 2B, and 4 and shows soil spectral shapes with peaks near 3 Hz compared to about 15 Hz for the same profile located in the CEUS (Figure 6-78). This difference results mainly from the difference in control motions, with a higher degree of nonlinearity for the WUS case contributing to the shift in peak spectral amplification to lower frequencies. For a deeper profile and a higher CEUS loading condition, the difference in spectral shapes between WUS and CEUS soil motions would diminish. However, a sufficient difference persists to conclude that the use of scaled broadband WUS deep soil motions is not appropriate for CEUS conditions.

At these higher loading levels in the WUS the high-frequency exceedence extends to about 0.5 Hz and neither Approaches 1 nor 2B are below the Approach 4 UHS. The effective strains for Approach 1 are shown in Figure 6-87 with a maximum in the median estimates of about $0.1 \pm 0.2\%$. This reflects a substantial change in dynamic material properties with material damping increasing to about 15% in the top 15m or so (Figure 6-12).

Exceedences of Approaches 1 and 2B over the soil UHS (Approach 4) spectra may actually not be as large as those depicted in Figure 6-86. The rock outcrop spectra are used as control motions for Approaches 1 and 2B and these contain amplification in the shallow portion of the soft rock profile (Figure 6-6). The very shallow portion of the WUS rock profile, with shear-wave velocities less than 1 km/sec, is not present in the soil motions used to develop the WUS soil attenuation relations (Section 6.2). In these cases, the soil profiles are placed on top of the Wald and Heaton (1994) crustal model. This crustal model has a surface shear-wave velocity of 1 km/sec (Table 6-4) and reflects baserock or base-of-soil conditions. The potential differences in soft rock outcropping and baserock outcropping motions are not accommodated in the WUS approach comparisons. These differences are quantified in Section 6.10 and result in about a 5% to 15% reduction in soil motions when using baserock outcropping, as opposed to surface, control motions. These results apply to all WUS approach comparisons, decreasing the difference between soil UHS (Approach 4) and Approaches 1 and 2B analyses.

For the WUS Rinaldi analyses, the accompanying transfer functions are shown in Figure 6-88 to 6-90 and show smaller resonances than the corresponding CEUS ratios (Figures 6-80 to 6-82). This is related to the differences in impedance contrast at the soil/rock boundary caused by the differences in shear-wave velocity between the top layers of the WUS and CEUS crustal models. For the CEUS, the shear-wave velocity is 2.83 km/sec while it is only 1 km/sec for WUS (Table 6-4 and 6-5). These values, along with the different densities, reflect a 84% larger impedance contrast for CEUS conditions giving rise to more energy trapped in the soil column, all other factors being the same. This effect naturally competes with the higher loading levels for WUS conditions in terms of inducing strains in the soil column. As with the CEUS ratios, little difference is seen in the 1 Hz and 10 Hz WUS ratios, suggesting largely linear response. However, in this case, the similarity in 1 Hz and 10 Hz ratios is driven largely by the similarity in 1 Hz and 10 Hz design earthquake scaled rock outcrop spectra (Figure 6-67). The similarity in the 1 Hz and 10 Hz control motions is reflected in Figure 6-91, which compares corresponding soil motions to Approaches 1 and 2B spectra. As with the CEUS, the 10 Hz spectrum controls at high-frequency (above about 3 Hz here) while the 1 Hz spectrum controls the low-frequencies.

Figures 6-92 and 6-93 compare deterministic profile variations and show that either the base case or mean (over deterministic profile variations) spectra provide motions comparable to those of Approach 2B. For very stiff profiles, these results and those of the previous section indicate that enveloping spectra based on conventional profile variations of twice and one half the base case shear moduli result in excessively conservative design motions. The implied velocity variation exceeds that typically associated with variability over a footprint or site area (Figure 6-10).

6.4.5 Example Case 2: Deep Stiff Profile, Gilroy 2

The Gilroy 2 profile is a deep stiff sandy to gravelly profile with a depth of about 180m (Figure 6-9) with a column resonance at about 1 Hz. Material nonlinearity for this site is modeled using the EPRI (1993) G/G_{max} and hysteretic damping curves (Figure 6-11). Gilroy 2 is located at a closest rupture distance of about 15 km from the 1989 M 6.9 Loma Prieta earthquake, and the site recorded an average horizontal component peak acceleration of about 35%g (Appendix A). The nearby hard California rock site Gilroy 1, about 2 km closer to the rupture, had a corresponding peak acceleration of about 50%g. Conversely, for the M 5.8 Coyote Lake earthquake, the Gilroy 2 site peak acceleration exceeded that of Gilroy 1 by about 100% (about 20% g and 10% g respectively). These two sites, with low level aftershocks recorded as well, provide compelling evidence for nonlinear response as well as validation of the nonlinear material strain dependencies (EPRI, 1993).

6.4.5.1 CEUS Conditions

As with the previous analyses, Figures 6-94 to 6-105 show approach comparisons, effective strains, and transfer functions. In this case and for subsequent profiles, the comparisons are augmented with additional comparisons for profiles truncated at about 150m (500 ft) and 90m (300 ft) to assess the extent of profile depth required to capture potential amplification effects at low frequency (0.5 Hz).

The comparisons of Approaches 1, 2B, and 4 shown in Figure 6-94 share features in common with the Rinaldi CEUS results (Figure 6-78) but with a smaller difference between the soil UHS and the spectra of Approaches 1 and 2B. A larger difference, however, exists between Approaches 1 and 2B at high frequency (> 10 Hz). This is the expected consequence of potential unconservatism at high frequencies resulting from driving the profile with a broad UHS (Approach 1). The larger difference in Approaches 1 and 2B for this site than for the Rinaldi profile is related to the more nonlinear material strain dependencies and softer profile. The effective strains are still relatively low, however, with median values less than about 0.05% (Figure 6-95).

The transfer functions, Figures 6-96 to 6-98, show larger effects than for Rinaldi, particularly for the 10 Hz design spectrum. The differences in the mean ratios, 1 Hz and 10 Hz shown in Figure 6-98, are still only significant at very high frequency, beyond about 30 Hz where they are up to about 30%. The difference between Approach 2B and the 10 Hz design soil spectrum (from Approach 2A) shown in Figure 6-99 is large above about 20 Hz, reflecting the tendency of Approach 1 to overdrive the soil column.

Comparisons of Approach 2B with deterministic profile variations are shown in Figures 6-100 and 6-101. As with the Rinaldi profile, enveloping is overly conservative. The mean spectrum from

Approach 1 (Figure 6-101) is lower than Approach 2B at the fundamental resonance near 1 Hz and at high frequency, above about 10 Hz.

To illustrate the effects of soil column truncation, Figures 6-102 to 6-105, show corresponding plots for column depths of 150m (500 ft) and 90m (300 ft) (Approach 2B reflects full column depth). For the profile truncated at 150m (full depth is about 180m), Figure 6-103 shows mean spectra (over deterministic profile variations) comparable to those in Figure 6-101 with the full profile, about 180m. Truncating to a depth of 90m (Figure 6-105), which is about half the original profile depth, results in slightly larger high frequency motion and lower motions at frequencies below the strain compatible fundamental resonance near 1 Hz (Figure 6-100). These results, strictly valid only for this profile, assumed material nonlinearity, and loading conditions suggest that at least 150m of profile is necessary to accommodate amplification effects frequencies of 0.5 Hz and above.

6.4.5.2 WUS Conditions

Figures 6-106 to 6-117 show the corresponding plots for the Gilroy 2 profile considering WUS conditions. For this case, the Gilroy 2 soil UHS (Approach 4) exceeds Approaches 1 and 2B but in this case by a larger amount (Figure 6-106). As discussed in Section 6.41, this feature likely results from the sigma or residual variability in the soil attenuation relations, which neglects the diminishing capacity of a soil column to transmit high frequency motions as the degree of nonlinearity (loading level) increases. As a result, the UHS computed for long return periods reflects sources generating rare, large earthquakes at close distances. High motions are then generated by sampling higher fractile levels. For these conditions, Approach 2B provides more reliable spectral estimates since it directly accommodates the soils amplification capacity. Additional verification will involve more accurately representing these site-specific soil capacities in models of the residual dispersion. The accompanying effective strains shown in Figure 6-107 are significantly larger as well, with shallow median values near 0.4%. For cases with effective strains larger than 1% over a depth range exceeding 10 to 20 feet, equivalent-linear results should be verified with corresponding nonlinear analyses. Sufficient care must be exercised with the nonlinear properties to ensure the nonlinear model matches the G/G_{max} and hysteretic damping curves. The transfer functions illustrated in Figures 6-108 to 6-110 show a stronger magnitude dependency than for the Rinaldi profile, a consequence of larger nonlinear effects (softer profile and more nonlinear material strain dependencies). The difference in the mean ratios for the 1 Hz and 10 Hz design earthquakes is only about 10% for frequencies 1 to 10 Hz range. As with the WUS Rinaldi results, Figure 6-111 shows that both the 1 Hz or 10 Hz soil design motions from Approach 2A closely reflect the Approach 2B spectrum.

For this case, the system is significantly nonlinear, (particularly for depths less than about 50m, see Figure 6-107), so the deterministic variation of two times the shear modulus (0.4 on shear-wave velocity) has a dramatic effect. Figure 6-112 shows shifts in the fundamental resonance of nearly a factor of ten (from about 3 Hz to 0.4 Hz) with a maximum range in spectral ordinates of nearly a factor of 8 around 3 Hz. These changes occur with a factor of 2 shift in overall stiffness (shear-wave velocity).

For systems well into nonlinear response, the range in conventional deterministic profile variations can result in dramatic differences in ground motions. Enveloping the deterministic range is generally quite conservative but, as with the Rinaldi profile and the CEUS Gilroy 2 results, leads to varying

degrees of conservatism with oscillator frequency. The mean spectrum over the three deterministic profile variations (Figure 6-113) shows some unconservatism near 1 Hz and may be inappropriate for both WUS and CEUS conditions near the column fundamental resonance. The trough in the -1σ (16th percentile) spectrum near 3 Hz is due to the large variability in the spectra from the three deterministic profile variations at 3 Hz (Figure 6-112) resulting in a sigma (normal) that is near the mean value of about 1g. The $+1 \sigma$ value is then near 3g and the -1σ spectrum then is about 0.05g. Truncating the profile at 150m (500 ft) and 90m (300 ft) show results (see Figures 6-114 through 6-117) similar to the full profile with some unconservatism in the 0.5 to 1.0 Hz range (Figures 6-116 and 6-117). These results suggest that fixed rules regarding required profile depths are going to be both elusive and conservative.

6.4.6 Example Case 3: Deep Firm Profile, Savannah River Generic

The Savannah River Generic profile (Figure 6-9) is very stiff near the surface, with a shear-wave velocity of about 400m/sec. It has a deep soft zone just below the surface extending to a depth of about 70m. Below that, the shear-wave velocity gradient is fairly steep and merges with the CEUS and WUS crustal models at about 300m (1,000 ft). The low-strain column resonance is at about 0.8 Hz. Nonlinearity is modeled through equivalent-linear G/G_{max} and hysteretic damping curves that are based on modeling strong ground motions in southern California at sites comprised of predominantly cohesionless soils. These are the same sets of curves that were used for the Rinaldi profile analyses (Figure 6-12).

6.4.6.1 CEUS Conditions

Following the patterns of the previous analyses, Figures 6-118 to 6-129 show comparisons of Approaches 1, 2B, and 4, effective strains, transfer functions, and the effects of profile truncation for the Savannah River Generic profile. For the relatively low strain CEUS motions, Figure 6-118 shows Approach 4 soil UHS comparable to the spectra of Approaches 1 and 2B. As with the Rinaldi and Gilroy 2 profiles, the Approach 1 spectrum falls below that of Approach 2B as well as Approach 4 for frequencies above about 10 Hz due to increased damping associated with the broadband control motions (rock outcrop UHS).

The effective strains shown in Figure 6-119 are relatively low, with median values below about 0.02 to 0.03%. The largest strains occur throughout the soft zone (Figure 6-9). With these strain values, modulus reduction is only about 0.8 to 0.9 and hysteretic damping ranges from about 2% to 4% (Figure 6-12). The combination of a firm profile and relatively linear G/G_{max} and hysteretic damping curves results in nearly linear response but with an increase in damping of about 50% in the soft zone.

The transfer functions shown in Figures 6-120 to 6-121 reflect the small degree of nonlinearity, showing small changes (about 20%) with earthquake magnitude. Differences in the mean ratios (Figure 6-122) are largest above 30 Hz (100 Hz reflects PGA scaling) and are about 20%. As with the previous CEUS cases, the 10 Hz design earthquake soil motion from Approach 2A compares favorably with Approach 2B for frequencies below about 20 Hz (Figure 6-123) but falls below at higher frequencies.

Comparisons of Approach 2B to deterministic soil variations shown in Figures 6-124 and 6-125 suggest that enveloping spectra for shear modulus variations of a factor of 2 will overestimate the effect of actual footprint variability (Figure 6-10), while a mean spectrum is unconservative, especially near the column resonance at about 0.5 Hz.

Profile truncation to 150m, Figures 6-126 and 6-127, shows results very similar to the original profile of about 300m depth. However, truncation at about 90m (300 ft) results in motions that are too low for frequencies below about 0.8 Hz (Figures 6-128 and 6-129). These results are similar to those of Gilroy 2 for CEUS conditions (Figures 6-112 to 6-117).

6.4.6.2 WUS Conditions

Figures 6-130 to 6-141 contain the results for the Savannah River Generic profile considering WUS hazard and rock conditions. In this case, even with the WUS higher loading conditions, Figure 6-130 shows that the Approach 4 soil UHS lies below those of Approaches 1 and 2B. Soil column saturation effects are insufficient to bring Approaches 1 and 2B spectra below the soil UHS at high frequency. A contributing factor may be related to the WUS Savannah River residual dispersion about the attenuation relation. It is among the lowest soil site sigmas overall (Figure 6-41) and is the lowest for frequencies exceeding about 1 Hz. A larger sigma would result in higher high frequency soil UHS.

The effective strains shown in Figure 6-131 show median values around 0.1 to nearly 0.2% throughout much of the profile with +1 σ values reaching 0.2%.

The transfer functions (Figures 6-132 to 6-134) show about the same magnitude dependency as the CEUS but extending to lower frequency. The difference in the mean ratios is generally less than about 5%. This latter similarity is again driven by the similarity in control motions (Figure 6-67).

Figure 6-135 shows the comparison of 1 and 10 Hz design events (Approach 2A) with Approaches 1 and 2B. In this application the envelope of spectra developed for Approach 2A would be below Approaches 1 and 2B, over much of the frequency range.

The effects of deterministic profile variations (Figures 6-136 and 6-137) show some exceedence of the base case profile spectrum for frequencies near 5 Hz, similar to the Rinaldi and Gilroy 2 profiles, again illustrating the effects of smooth (base case) vs. rough (randomized) profiles. In the context of nonlinear analyses, the median or mean spectrum computed with variation in soil properties is lower at high frequency than the spectrum computed from a mean or median profile. While the envelope of the deterministic profile variation spectra is overly conservative, Figure 6-137 suggests that the mean from Approach 1 may be unconservative at low frequency. Profile truncation to about 150m (500 ft) in Figures 6-138 and 6-139 shows results very similar to the full profile (305m, 1,000 ft) while truncation at 90m (300 ft), Figures 6-140 and 6-141, results in low motions at low frequency (below about 1 Hz). These results are similar to the CEUS conditions and to Gilroy 2 WUS and CEUS results as well. A tentative conclusion is that 150m of profile is adequate to reflect potential amplification for frequencies as low as about 1 Hz.

6.4.7 Example Case 4: Deep Soft Profile; Meloland

The Meloland Profile, located in the Imperial Valley of Southern California and Northern Mexico is the softest profile analyzed (Figure 6-9) and has a column frequency of about 0.5 Hz. While it is considered “bottomless” and extends kilometers in depth, it was truncated at a depth of 304m (1,000 ft) for these analyses. It is the location of a recently installed (Caltrans) vertical strong motion array and the nearby CDMG strong motion site recorded the M 6.5 1979 Imperial Valley earthquake at a rupture distance of 0.5 km (average horizontal component peak acceleration of about 0.3g). The modulus reduction and damping curves used are shown in Figure 6-13. They are based on modeling strong motions from the 1979 Imperial Valley earthquake recorded at Meloland and nearby sites (Silva et al., 1997) and reflect relatively weak strain dependencies.

6.4.7.1 CEUS Conditions

For the Meloland profile, the standard suite of comparisons are shown in Figures 6-142 to 6-153. For this soft profile, the soil UHS (Approach 4) exceeds spectra computed with Approach 1 for CEUS conditions (Figure 6-142). As explained previously in regard to Figures 6-83, 6-94, and 6-124, the Approach 2B spectrum exceeds the Approach 1 spectrum at high frequency (≥ 10 Hz). The effective strains are relatively small, as shown in Figure 6-143 yet the soil UHS exceeds Approach 1 motions. For this soft soil, magnitude differences in the transfer functions shown in Figure 6-145 for the 10 Hz design earthquake are large, reaching nearly a factor of 2 in total range near 10 Hz. The difference in mean ratios for the 1 Hz and 10 Hz design earthquake remains very small for frequencies below about 30 Hz but is important at peak acceleration (100 Hz), similar to the other profiles for CEUS conditions.

The comparison between Approaches 1 and 2B and the 1 Hz and 10 Hz design earthquake soil spectra (Approach 2A) is illustrated in Figure 6-147. As with the other profiles, Approach 1 and the 10 Hz soil Approach 2A design spectra fall below the Approach 2B spectra for frequencies above about 10 Hz. In this case, Approach 1, using the broad UHS rock spectrum, overdrives the soil column and is lower than the 10 Hz soil motion, which uses a rock shape reflecting a single magnitude. At lower frequencies, Approach 1 and the Approach 2A 1 Hz soil design spectrum are equivalent to the Approach 2B spectrum.

Deterministic profile variations shown in Figures 6-148 and 6-149 reflect the same results as the other profiles. Enveloping reflects overly conservative motions for footprint profile variations while the average is too low at some frequencies. Profile truncation to ~150m (~500 ft) adequately captures amplification at low frequency (to about 0.5 Hz) but the mean is low at high frequency ($\geq 8-10$ Hz) (Figures 6-150 and 6-151) relative to Approach 2B. Truncation at 90m (300 ft) does not adequately portray the profile amplification at low frequency (0.5 Hz), (this observation is similar to the other profiles) and is a bit low at higher frequencies as well.

6.4.7.2 WUS Conditions

Figures 6-154 to 6-165 show results for the Meloland profile considering WUS conditions. The comparison of Approaches 1, 2B, and 4 is illustrated in Figure 6-154 and shows the expected exceedence of the soil UHS (Approach 4) over the spectra of Approaches 1 and slightly for 2B as

well. The effective strains are large, with values significantly greater than for CEUS conditions. The median values are near 0.4% in the intermediate portion of the profile (compare Figures 6-107 and 6-155).

Magnitude dependencies in the transfer functions, Figures 6-156 and 6-157, are weak for the 1 Hz scaled design outcrop spectrum and strong for the corresponding 10 Hz spectrum, as they were for the Gilroy 2 and Savannah River Generic profiles (Figure 6-109 and 6-133). Because of the similarity in the 1 Hz and 10 Hz scaled rock outcrop spectra (Figure 6-173), the corresponding mean transfer functions are similar (Figure 6-158).

Comparisons of the 1 Hz and 10 Hz design earthquake soil spectra (Approach 2A) with those of Approaches 1 and 2B are shown in Figure 6-159. These results are similar to those of the other profiles and show expected similarity. With 0.6 magnitude difference between 1 Hz and 10 Hz contributions and at similar distances, the distinction between the shapes is not significant in site response.

The effects of deterministic profile variations are shown in Figure 6-160 and 6-161 and show results very similar to those of Gilroy 2 (Figures 6-112 and 6-113). There is a large variation in motions, a range of about a factor of 6 near 3 Hz for a factor of 2 range in shear-wave velocity. This is a strongly nonlinear system, due principally to the high loading level and low initial stiffness (its dynamic material strain dependencies are considered relatively linear). The combination of either a soft profile with relatively linear curves, as here, or a stiff profile and more nonlinear curves, such as Gilroy 2, results in a similar strong dependence on initial stiffness (variations in shear-moduli) under high loading conditions. The mean spectrum (over deterministic variations) is conservative for all frequencies (see Figure 6-161).

Truncating the profile to 150m (500 ft) also produces a mean spectrum that is very close to the full profile (304m) and compares favorably with that of Approach 2B for frequencies down to about 0.5 Hz (see Figures 6-162 and 6-163). It is, however, a bit high above the 2 Hz to 3 Hz frequency range (Figure 6-163). Truncation at 90m (300 ft) however, shows serious deficiencies at 1.0 Hz and below and larger motions above 2 to 3 Hz (see Figures 6-164 and 6-165).

6.4.8 Baserock Motions

Soft rock (WUS) shear-wave velocity profiles are characterized by steep shallow gradients (Figure 2-2) with median surface velocities in the 200 to 300m/sec range. Median and 1σ shear-wave velocity profiles based on measurements made at WUS strong motion recording sites classified as rock are shown in Figure 6-166. This strong velocity gradient results in large amplifications (source region to surface) at high frequency (Figure 2-3). At the base of soil profiles, due to more limited weathering, basement rock generally does not show such characteristics. Most boreholes that penetrate soil and into competent rock do not extend deep enough to fully characterize shear-wave velocities 15 to 30m into basement material. Nonetheless, most existing profiles suggest a large jump in velocity over a short depth range into baserock material. For WUS conditions, this jump or very steep gradient typically reflects a baserock shear-wave velocity ranging from about 1 to 2 km/sec over a depth range of several to tens of meters. The very shallow (top 30m or so) gradient shown in

Figure 6-166 is not typically present beneath soil profiles. As a result, the accompanying amplification present in motions recorded at soft rock sites may not be present in baserock motions that drive the soil column. Additionally, the variability of baserock motions, particularly for very deep profiles (> 150m), may also be significantly lower than rock outcrop motions due to a smaller variability in velocities, being less subject to weathering. While the issue of variability is currently not resolvable, the effects of the shallow soft rock velocity gradient on response spectra may be easily estimated.

6.4.8.1 Development of Outcrop-to-Basement Spectral Correction Factors

Two approaches are available to develop correction factors for conditioning soft rock (surface) motions to be more appropriate as base of soil control motions. An empirical approach that involves deconvolving strong motion recordings at soft rock sites with measured shear-wave velocities to base of soil velocities (1 to 2 km/sec) is currently underway as part of a PEER project (I.M. Idriss, personal communication, 1999). Another approach, implemented here, is analytical and involves point-source simulations (Appendix D) of motions at the surface of the soft rock profile (Figure 6-166) and progresses deeper (into higher velocities) in the profile by stripping off overlying materials. Taking ratios of motion at depth to surface motion results in depth- (velocity-) dependent correction factors. To provide statistical stability to the transfer functions or correction factors and to estimate their uncertainties, multiple simulations are run using the profile randomization scheme. The correction factors are then taken as ratios of median motions: depth as outcropping over surface. Potential nonlinearity is accommodated with equivalent-linear analyses using the rock G/G_{max} and hysteretic damping curves (Figure 6-8) and these parameters are also randomized.

An example of the motions (5% damped spectral acceleration) computed for $M = 6.5$ at a distance of 25 km is shown in Figure 6-167. The suite of spectra reflect median motions computed at the surface and at increasing depths in the soft rock profile, from 1.5m (5 ft) with a surface velocity of 305m/sec (1,000 ft/sec), to 386m (1,268 ft) with a corresponding "surface" velocity of 1,828m/sec (6,000 ft/sec). The decrease in spectral amplitudes begins below a depth of about 2m and progressively decreases in level and over a wider frequency range as more of the profile is stripped off. The resulting transfer functions are shown in Figure 6-168. These represent correction factors to be applied to surface motions to remove the effects of the shallow soft rock gradient to the same shear-wave velocity as that underlying a soil column. The factors range as low as about 0.5 near 3 Hz for a shear-wave velocity of about 1.9 km/sec (6,000 ft/sec), showing the large effects of the shallow gradient (Figure 6-166).

To assess the effects of potential nonlinearity on the correction factors, similar analyses were done for distances of 10 km (surface PGA \approx 0.3g) and 1 km (surface PGA \approx 0.5g). The resulting correction factors are shown in Figures 6-169 and 6-170 for distances of 10 km and 1 km respectively. The ratios actually increase, particularly at high frequency, because the surface (and shallow) motions decrease as the loading levels increase.

6.4.8.2 Effects Of Baserock Motions On The WUS Soil Motions

In developing the WUS soil attenuation relations (Section 6.2) the soil profiles were placed on top of the Wald and Heaton (1994) crustal model. This model has a surface shear-wave velocity of 1.0 km/sec implying a jump in velocity at the soil/rock interface (Figure 6-9). The attenuation relations

for WUS rock motions are appropriate for surface motions at an average soft rock site (Figure 6-6) and incorporate the shallow steep gradient shown in Figure 6-166. Since control motions for the WUS site response analyses are based on the soft rock attenuation relations, they incorporate near-surface amplification for velocities lower than 1 km/sec, not included in the simulations for the WUS soil attenuation relations. To assess the effects of using surface as opposed to baserock outcropping control motions, comparisons are made to the soil motions computed using Approach 1 with both sets of rock control motions.

The modified WUS rock outcrop UHS for baserock conditions is shown in Figure 6-171 compared to the original spectrum. The modified spectrum is appropriate for outcropping rock with a shear-wave velocity of about 1 km/sec (300 ft/sec) and is considered to reflect a much closer representation of control motions used in developing the soil attenuation relations. It was produced by multiplying the rock surface UHS (solid line in Figure 6-171) by the ratio computed for the velocity of 914m/sec and 0.5g surface peak acceleration (Figure 6-170). It shows a maximum reduction of about 20% in the 2 to 3 Hz range and 15% at peak acceleration. This corrected motion is then used as an outcropping control motion for an Approach 1 analysis.

For the Rinaldi profile, the results of using the modified motion as input to the soil column are shown in Figure 6-172. The solid line reflects Approach 1 soil spectra computed using the WUS UHS rock spectrum, and the dashed line shows the results using the modified control motion. The difference in soil spectra is about 10 to 15% over much of the bandwidth (11% at peak acceleration), nearly the same as the difference in control motions (Figure 6-171).

The Gilroy 2 profile is softer with more nonlinear dynamic material properties and shows less of a difference (10% at peak acceleration, Figure 6-173). The Savannah River Generic profile is softer still, but with more linear dynamic material properties than Gilroy 2. It has the same G/G_{max} and hysteretic damping curves as those used for the Rinaldi profile. Figure 6-174 shows nearly the same difference as Rinaldi (Figure 6-172), about 10 to 15% over much of the frequency range and 13% at peak acceleration. The softest profile, Meloland, also has the most linear dynamic material strain dependencies and shows a 10 to 15% reduction (Figure 6-175), 12% at peak acceleration.

In general, the soil motions computed using the more appropriate baserock motions in place of rock outcrop motions showed broadband reductions ranging from about 5 to 15%. The reductions depended upon initial profile stiffness as well as dynamic nonlinear properties and are generally somewhat less than the differences in control motions, rock outcrop vs. base rock or base of soil conditions. The correction factors have uncertainties associated with them, based on profile uncertainties (Figure 6-7), so fractiles other than the median may be used. As with the V/H ratios (Section 4.7), the correction factors may be implemented for ranges in rock outcrop peak acceleration values.

6.5 Conclusions and Recommendations

In the proceeding analyses three major issues were addressed in developing site-specific soil motions based on a rock outcrop UHS: (1) evaluation of procedures to develop hazard consistent soil spectra,

(2) assess minimum profile depth required to characterize soil motions in the frequency range of 0.2 to 5.0 Hz, and (3) assess the effects of baserock vs. rock outcrop control motions on soil spectra.

To address these issues, four deep profiles were analyzed reflecting a wide range in both overall stiffness (range in column frequency of 0.5 Hz to 2.0 Hz) and nonlinear dynamic material properties. To capture ranges in loading conditions of amplitude levels and spectral content, the four profiles were considered to be located in both the WUS (high hazard) and CEUS (moderate hazard) tectonic regions. Analyses consisted of comparisons of UHS computed directly for the soil sites using region- and site-specific soil attenuation relations with approaches that start from region-specific rock UHS and use traditional convolution analyses to produce site-specific soil motions.

Results of the analyses indicate that a conventional soil UHS can result in large high frequency motions. This is likely due to a combination of a symmetric (in log) uncertainty about median attenuation estimates, including the effects of profile saturation. However, the larger more significant effect is the inclusion of combinations of both high and low rock motions with large soil amplification. Such combinations are captured in the soil UHS by its very nature (aggregation of motions that exceed a given level) and are ignored in Approaches 1 and 2. As a result, at some exceedence level, Approaches 1 and 2 will become unconservative. Unfortunately, the exceedence level above which this occurs depends on the nonlinear properties of the soil column, range in loading levels, initial stiffness, and nonlinear dynamic material properties. Results presented herein suggest that for hazard levels up to 10^{-4} , Approach 2B results in adequately conservative soil motions, however, more work is clearly needed.

Further analyses showed that the conventional deterministic site property variation of a factor of 2 on shear modulus is too large for footprint variability. This variation results in overly conservative envelope motions and mean values that are unconservative at low-frequencies, near the column frequency of deep profiles. Profile truncation to about 150m (500 ft) provides soil motions that largely capture site amplifications for frequencies down to about 0.5 Hz. Truncation to about 90m (300 ft) will likely produce unconservative soil motions for frequencies below about 1 Hz.

The use of soft rock surface recordings as base-of-soil (baserock) control motions produces about 5% to 15% larger soil motions compared to correcting these rock motions to rock-soil interface motions. The degree of conservatism depends on frequency, shear-wave velocity at the base of the soil column, and level of rock motion. The effect is broadband, extending from about 0.3 Hz to 100 Hz (peak acceleration).

References

- Abrahamson, N.A and K.M. Shedlock (1997). "Overview." *Seis. Research Lett.*, 68(1), 9-23.
- Abrahamson, N.A. and W.J. Silva (1997). "Empirical response spectral attenuation relations for shallow crustal earthquakes." *Seism. Soc. Am.*, 68(1), 94-127.
- Atkinson, G.M and W.J. Silva (1997). "An empirical study of earthquake source spectra for California earthquakes." *Bull. Seism. Soc. Am.* 87(1), 97-113.

- Atkinson, G.M. (1993). "Source spectra for earthquakes in eastern North America." *Bull. Seism. Soc. Am.*, 83(6), 1778-1798.
- Bazzurro, Paolo (1998). Probabilistic Seismic Demand Analysis, Ph.D. Thesis, Supervised by C.A. Cornell, Stanford University, Palo Alto, CA.
- Bazzurro, P., C.A. Cornell and F. Pelli (1999). "Site- and soil-specific PSHA for nonlinear soil sites," Proc., 4th Earthq. Resist. Design Structures Conf. (ERES99), Catania, Italy, June 15-17.
- Boore, D.M, and W.B. Joyner (1997). "Site amplifications for generic rock sites." *Bull. Seism. Soc. Am.*, 87(2), 327-341.
- Boore, D.M., W.B. Joyner and T.E. Fumal (1997). "Equations for estimating horizontal response spectra and peak acceleration from Western North American earthquakes: A summary of recent work." *Seism. Res. Lett.* 68(1), 128-153.
- Campbell, K W. (1997). "Empirical near-source attenuation relationships for horizontal and vertical components of peak ground acceleration, peak ground velocity, and pseudo-absolute acceleration response spectra." *Seism. Soc. Am.*, 68(1), 154-176.
- Electric Power Research Institute (1993). "Guidelines for determining design basis ground motions." Electric Power Research Institute, Palo Alto, CA, Rept. EPRI TR-102293, vol. 1-5:
 vol. 1: Methodology and guidelines for estimating earthquake ground motion in eastern NA.
 vol. 2: Appendices for ground motion estimation.
 vol. 3: Appendices for field investigations.
 vol. 4: Appendices for laboratory investigations.
 vol. 5: Quantification of seismic source effects.
- Hanks, T.C. and A.C. Johnston (1992). "Common features of the excitation and propagation of strong ground motion for north American earthquakes." *Bull. Seism. Soc. Am.*, 82(1), 1-23.
- Idriss, I.M. (1993). "Procedures for selecting earthquake ground motions at rock sites," Nat. Inst. Of Stan. And Techn., Rept. NIST GCR 93-625.
- McGuire, R.K. (1995) "Probabilistic Seismic Hazard Analysis and Design Earthquakes: Closing the Loop," *Bulletin of the Seismological Society of America*, Vol. 85, No. 5, pp. 1275-1284, October.
- Sadigh, K., C-Y. Chang, J.A. Egan, F. Makdisi, and R.R. Youngs (1997). "Attenuation relationships for shallow crustal earthquakes based on California strong motion data." *Seism. Soc. Am.*, 68(1), 180-189.

- SHAKE (1992). "A computer program for conducting equivalent linear seismic response analyses of horizontally layered soil deposits." Sponsored by Structures Building and Fire Research Lab., Nat'l Institute of Standards and Technology, Gaithersburg, Maryland. Modifications by I. Idriss and J. Sun.
- Silva, W.J. and Lee, K. (1987). "WES RASCAL code for synthesizing earthquake ground motions." State-of-the-Art for Assessing Earthquake Hazards in the United States, Report 24, U.S. Army Engineers Waterways Experiment Station, Miscellaneous Paper S-73-1.
- Silva, W.J. and R. Darragh (1995). "Engineering characterization of earthquake strong ground motion recorded at rock sites." Palo Alto, Calif: Electric Power Research Institute, TR-102261.
- Silva, W.J., N.A. Abrahamson, G.R. Toro, and C.J. Costantino (1997). "Description and validation of the stochastic ground motion model." Report to Brookhaven National Laboratory, Associated Universities, Inc. Upton, New York, Contract 770573.
- Toro, G.R., N.A. Abrahamson, and J.F. Schneider (1997). "Model of strong ground motions from earthquakes in Central and Eastern North America: Best estimates and uncertainties." *Seismological Research Let.*, 68(1), 41-57.
- USNRC (1997). *Identification and characterization of seismic sources and determination of safe shutdown earthquake ground motion*, US Nuclear Regulatory Commission, Regulatory Guide 1.165, March.
- Vucetic, M. and R. Dobry (1991). "Effects of Soil Plasticity on Cyclic Response," *Journal of Geotechnical Engineering*, ASCE, 117(1), 89-107.
- Wald, D.J. and T.H. Heaton (1994). "A dislocation model of the 1994 Northridge, California, earthquake determined from strong ground motions." *U.S. Geological Survey*, Open-File Rpt. 94-278.

Table 6-1
Approaches for Developing Soil UHS

<u>Description</u>	<u>Frequencies Used</u>	<u>Integration</u>	<u>Label</u>
PSHA using site-specific soil attenuation	multiple	over m and r	Approach 4
Calculate soil hazard from rock hazard and m and r deaggregation	several	over a , and over m and r given a	Approach 3
Calculate soil hazard from rock hazard and m deaggregation	several	over a , and over m given a	Approach 3A
Calculate soil hazard using soil amplification for input amplitude a^* and magnitude m^*	one, e.g. PGA	over a only	Approach 3B
Scale rock UHS to soil UHS accounting for soil parameter uncertainty	two, e.g. 10 and 1 Hz	none	Approach 2A
Scale rock UHS to soil UHS accounting for soil parameter uncertainty and m deaggregation	two, e.g. 10 and 1 Hz	none	Approach 2B
Scale rock UHS to soil UHS using broadbanded input motion	none	none	Approach 1

Table 6-2
Parameters for WUS Rock Outcrop Simulations

M	5.5, 6.5, 7.5		
D(km)	1, 5, 10, 20, 50, 75, 100, 200, 400		
30 simulations for each M, R pair = 810 runs			
Randomly vary source depth, $\Delta\sigma$, kappa, Q_o , profile			
<u>Depth</u> , $\sigma_{\ln H} = 0.6$, \bar{H} ($M > 5$) = 8 km; Source, California Seismicity			
M	Lower Bound (km)	\bar{H} (km)	Upper Bound (km)
5.5	2	6	25
6.5	4	8	20
7.5	5	8	15
<u>$\Delta\sigma$</u> , $\sigma_{\ln \Delta\sigma} = 0.5$, Based on California earthquake inversions (Silva et al., 1997)			
M	$\Delta\sigma$ (bars)	AVG. $\Delta\sigma$ (bars) = 65	
5.5	85	Based on inversions of the A&S 97 relation (BNL, 1997)	
6.5	64		
7.5	50		
<p><u>$Q(s)$</u>, $\bar{Q}_o = 275$, <i>Southern California inversions</i>; $\sigma_{\ln Q_o} = 0.4$, (Silva et al., 1997)</p> <p style="padding-left: 40px;">$\eta = 0.60$, <i>Southern California inversions</i>; $\sigma_\eta = 0$, (Silva et al., 1997)</p> <p>Varying Q_o only is sufficient, since $\pm 1 \sigma$ covers range of Southern California inversions from 1 to 20 Hz</p>			
<u>Kappa</u> , $\bar{\kappa} = 0.03$ sec, $\sigma_{\ln \kappa} = 0.3$ (EPRI, 1997): linear zone ($V_s \geq 1$ km/sec)			
<u>Profile</u> , California soft rock: GEOMATRIX A + B over Wald and Heaton (1994) Los Angeles Crust, randomize to 30m ft			
<p>Geometrical attenuation $R^{-(a+bM)}$, $a = 1.0296$, $b = -0.0422$</p> <p style="padding-left: 100px;">$R^{-(a+bM)/2}$, $R > 65$ km</p>			
Based on inversions of the Abrahamson and Silva (1997) relation			

Table 6-3
Parameters for CEUS Rock Outcrop Simulations

M 5.5, 6.5, 7.5			
D(km) 1, 5, 10, 20, 50, 75, 100, 200, 400			
30 simulations = 810 runs			
Randomly vary source depth, $\Delta\sigma$, kappa, Q_0 , η , profile			
<u>Depth</u> , $\sigma_{\ln H} = 0.6$, \bar{H} ($M > 5$) = 10 km; Intraplate Seismicity (EPRI, 1993)			
M	Lower Bound (km)	\bar{H} (km)	Upper Bound (km)
5.5	3	8	30
6.5	4	10	30
7.5	5	12	30
<u>$\Delta\sigma$</u> , $\sigma_{\ln\Delta\sigma} = 0.7$ (EPRI, 1993)			
M	$\Delta\sigma$ (bars)	AVG. $\Delta\sigma$ (bars) = 122, Assumes M 5.5 = 160 bars (Atkinson, 1993) with magnitude scaling taken from WUS (Table 6- 2)	
5.5	160		
6.5	120		
7.5	95		
<p>$Q(s)$, $\bar{Q}_0 = 351$, <i>Saguenay inversions</i>; $\sigma_{\ln Q_0} = 0.4$, (Silva et al., 1997)</p> <p>$\eta = 0.84$, <i>Saguenay inversions</i>; $\sigma_\eta = 0$, (Silva et al., 1997)</p> <p>Varying Q_0 only is sufficient, since $\pm 1 \sigma$ covers range of CEUS inversions from 1 to 20 Hz</p>			
<u>Kappa</u> , $\bar{\kappa} = 0.006$ sec $\sigma_{\ln \kappa} = 0.3$, (EPRI, 1993)			
<u>Profile</u> , Midcontinent Crust (EPRI, 1993), randomize to 30m			
Geometrical attenuation $R^{-(a+bM)}$, $a = 1.0296$, $b = -0.0422$ $R^{-(a+bM)/2}$, $R > 100$ km			
Based on inversions of the Abrahamson and Silva (1997) relation			

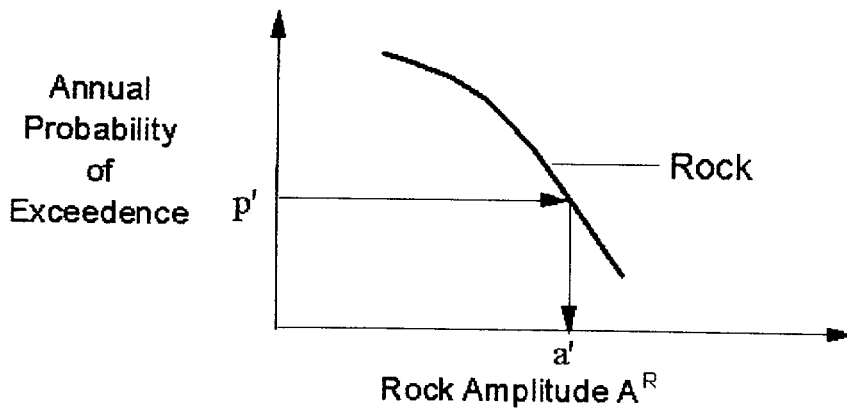
Table 6-4
Southern California Crustal Model**

Thickness (km)	V_s (km/sec)	Density (cgs)
0.0015239	0.24383	2.0
0.0024383	0.30478	2.0
0.0030479	0.42670	2.0
0.0042670	0.53337	2.0
0.0033526	0.63091	2.0
0.0042670	0.71624	2.0
0.0057909	0.83016	2.0
0.0067503	0.96617	2.0
0.5	1.0	2.1
1.5	2.0	2.3
2.5	3.2	2.5
23.0	3.6	2.6
5.0	3.9	2.9
	4.5	3.0

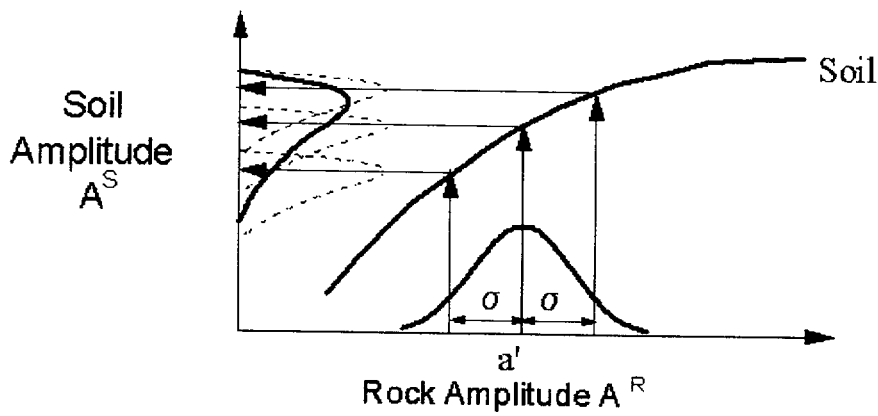
Table 6-5
CEUS Crustal Model (EPRI, 1993 Midcontinent)

Thickness (km)	V_s (km/sec)	Density (cgs)
1.0	2.830	2.52
11.0	3.520	2.71
28.0	3.750	2.78
	4.620	3.35

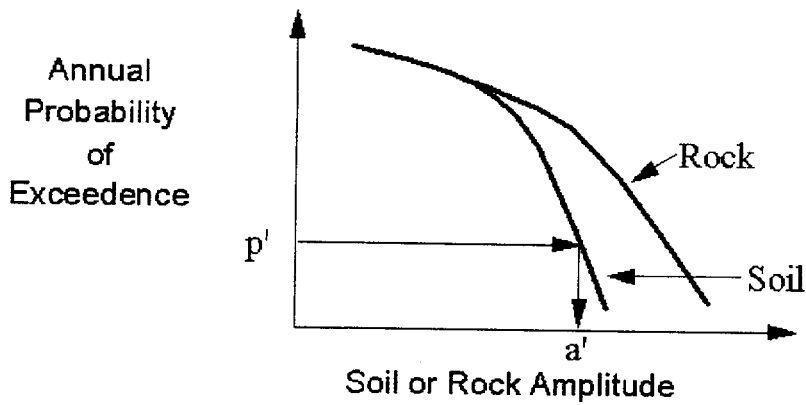
**Wald and Heaton, 1994 begins at $V_s = 1$ km/sec



A. Rock Seismic Hazard Curve

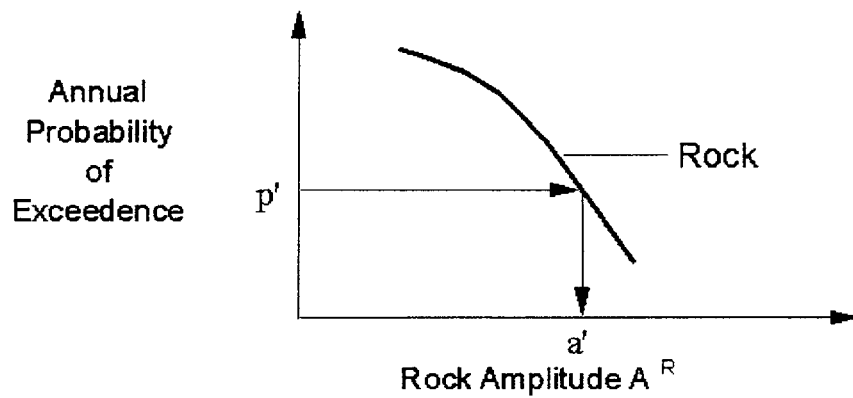


B. Soil Amplitude vs. Rock Amplitude, given M

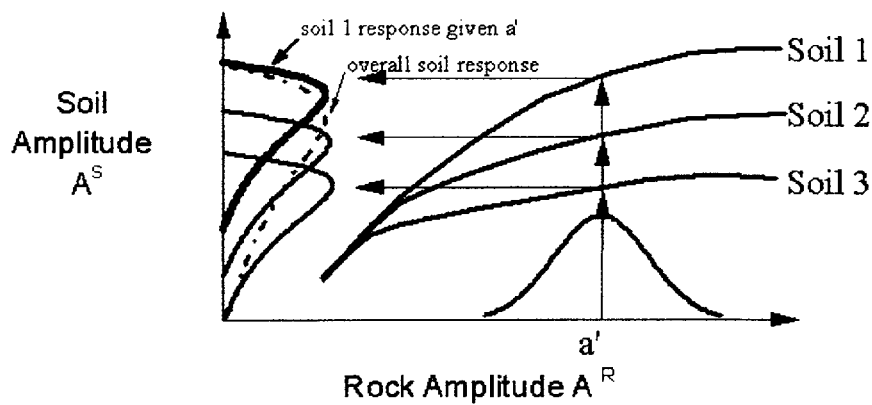


C. Soil Seismic Hazard Curves

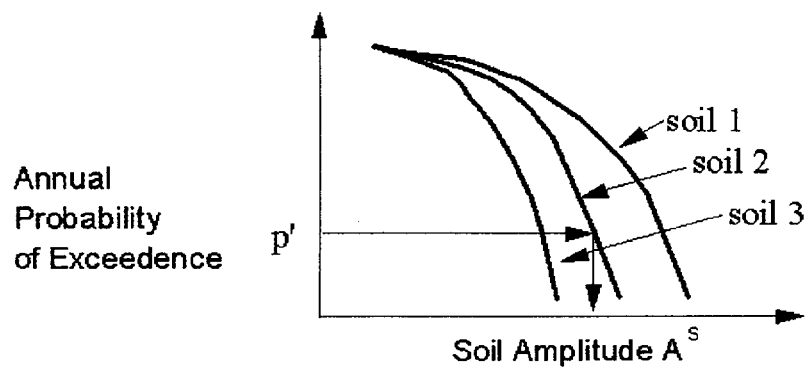
Figure 6-1. Integrations to calculate soil hazard, for known soil properties and aleatory variability on soil response.



A. Rock seismic hazard curve

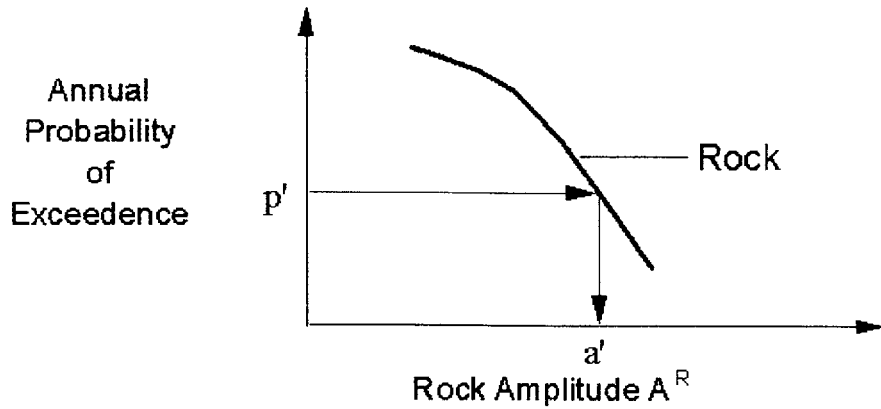


B. Soil amplitudes vs. rock for three sets of soil characteristics.

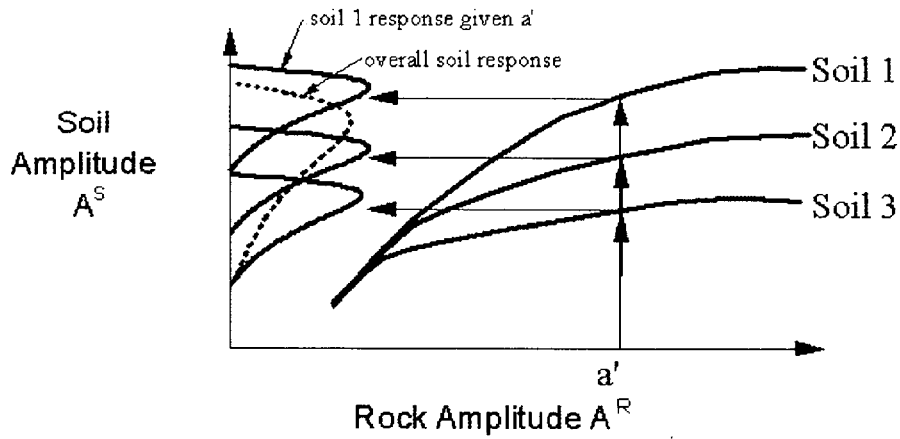


C. Soil seismic hazard curves

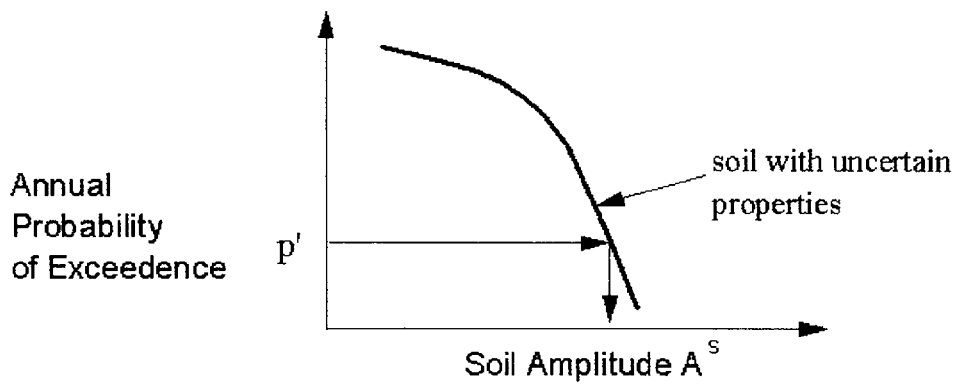
Figure 6-2: Integration to calculate soil hazard with uncertain soil properties.



A. Rock seismic hazard curve

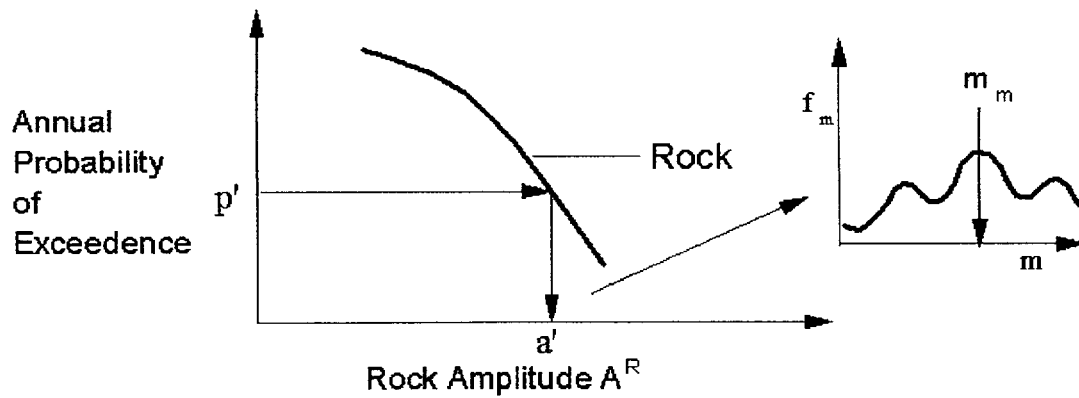


B. Soil amplitudes vs. rock for three sets of soil characteristics.

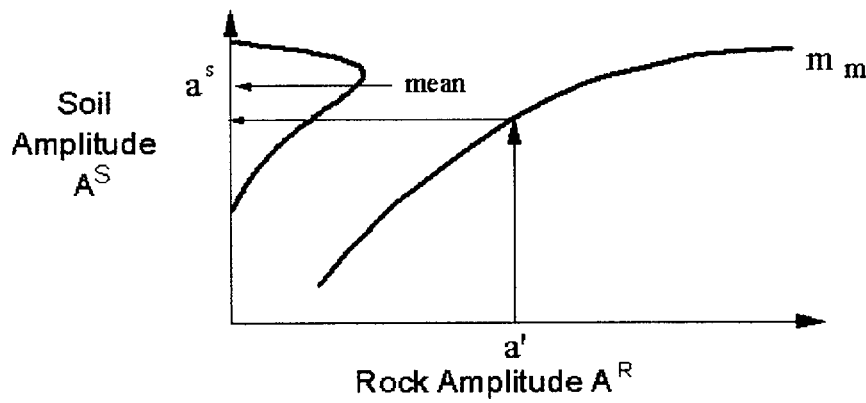


C. Soil seismic hazard curves

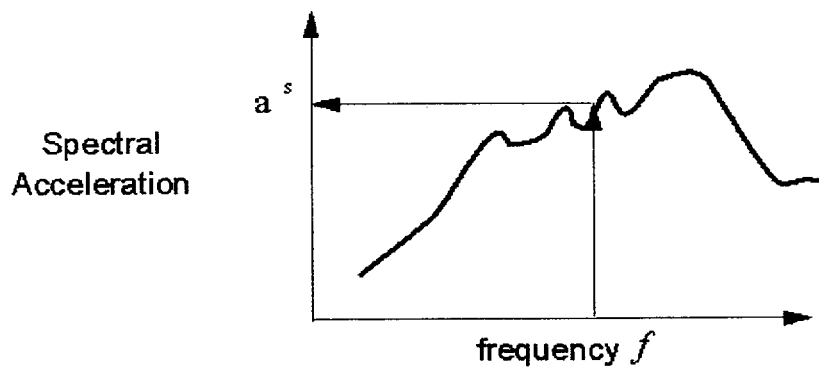
Figure 6-3: Integration to calculate soil hazard using distribution of AF at a' .



A. Rock Seismic Hazard Curve

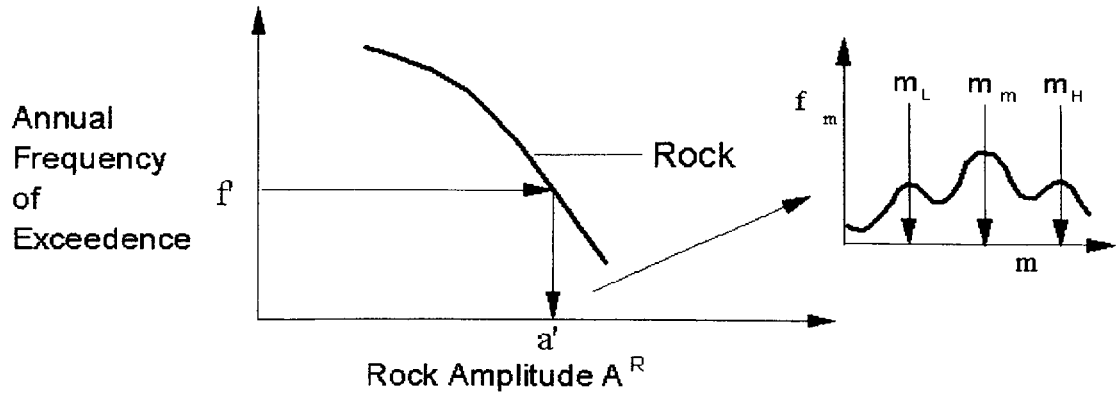


B. Soil Amplitude vs. Rock Amplitude, given a'

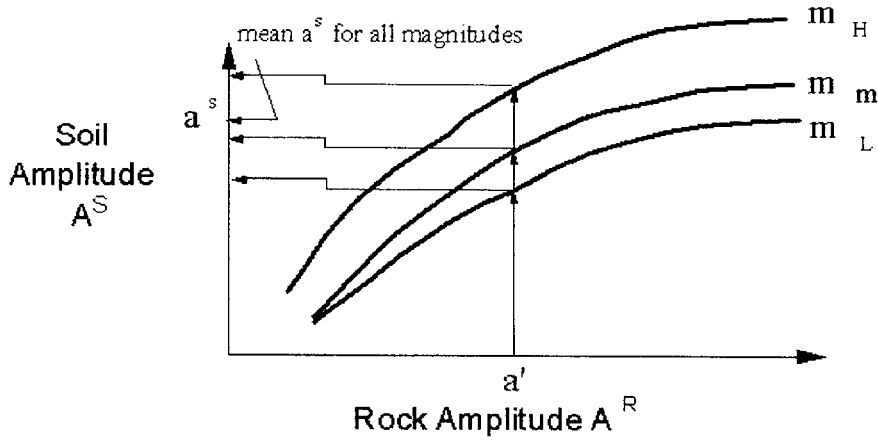


C. UHS on Soil

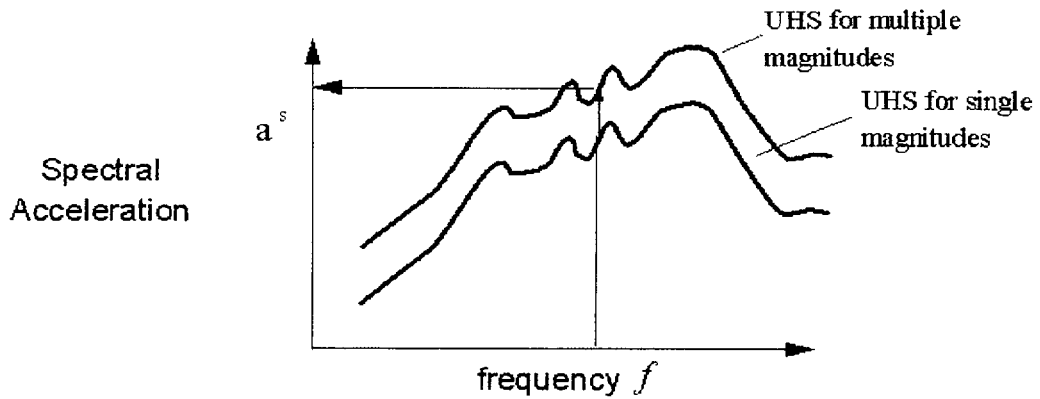
Figure 6-4: Scaling soil UHS from rock UHS, single magnitude.



A. Rock Seismic Hazard Curve

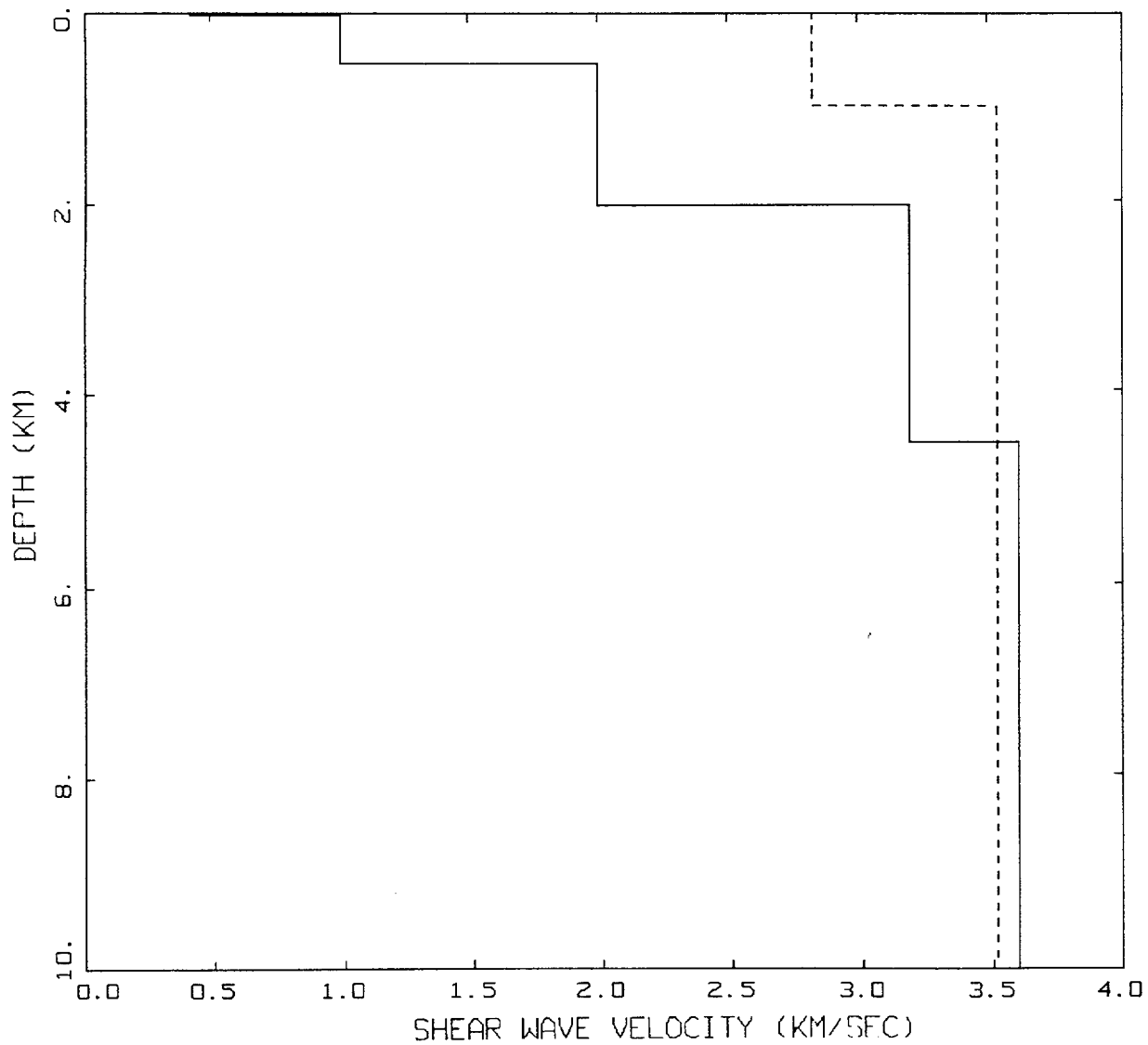


B. Soil Amplitude vs. Rock Amplitude, given a' , multiple magnitudes



C. UHS on Soil

Figure 6-5: Scaling soil UHS from rock UHS with magnitude dependence.



GENERIC WUS AND CEUS
CRUSTAL MODELS

LEGEND
 — WUS
 - - - CEUS

Figure 6-6. Comparison of generic shear-wave velocity profiles for WUS (Los Angeles) and CEUS crustal conditions.

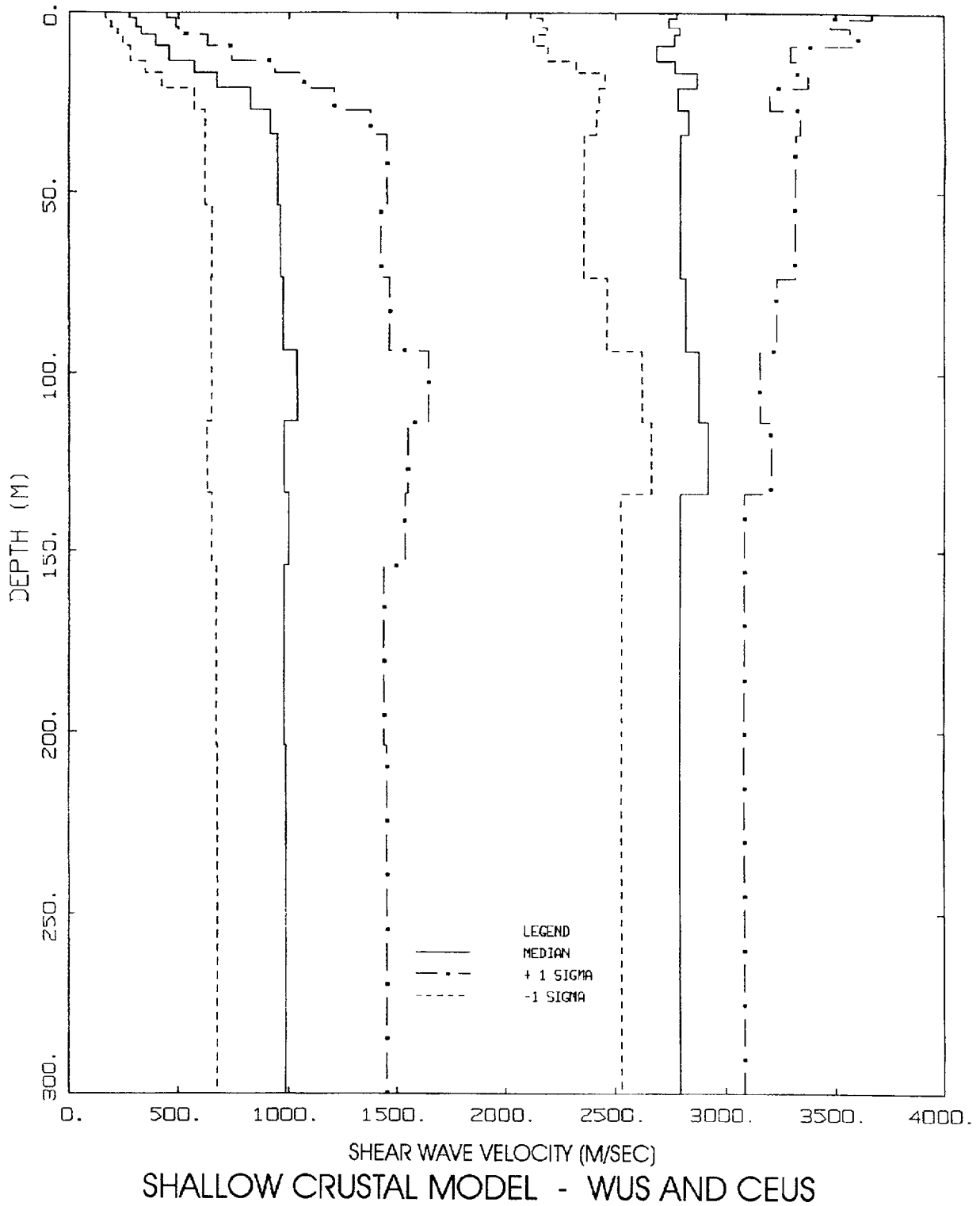
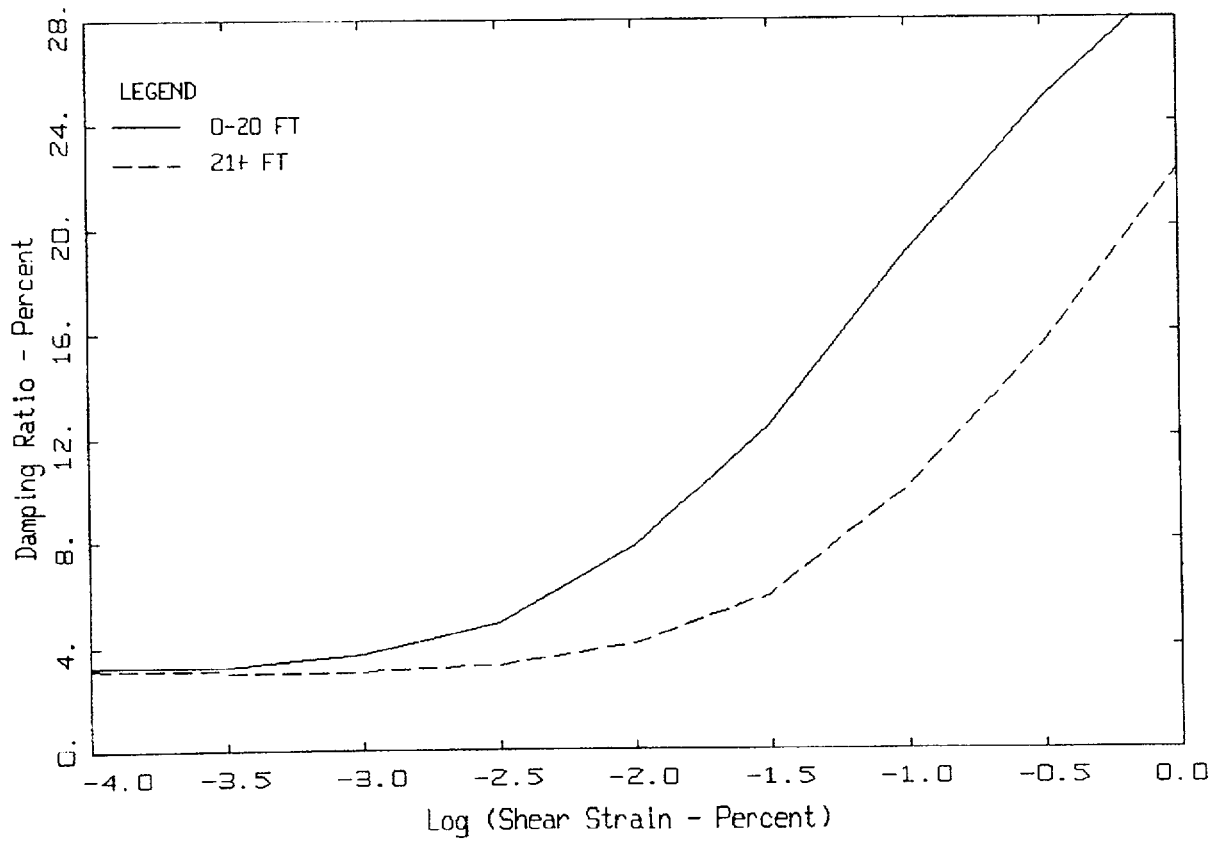
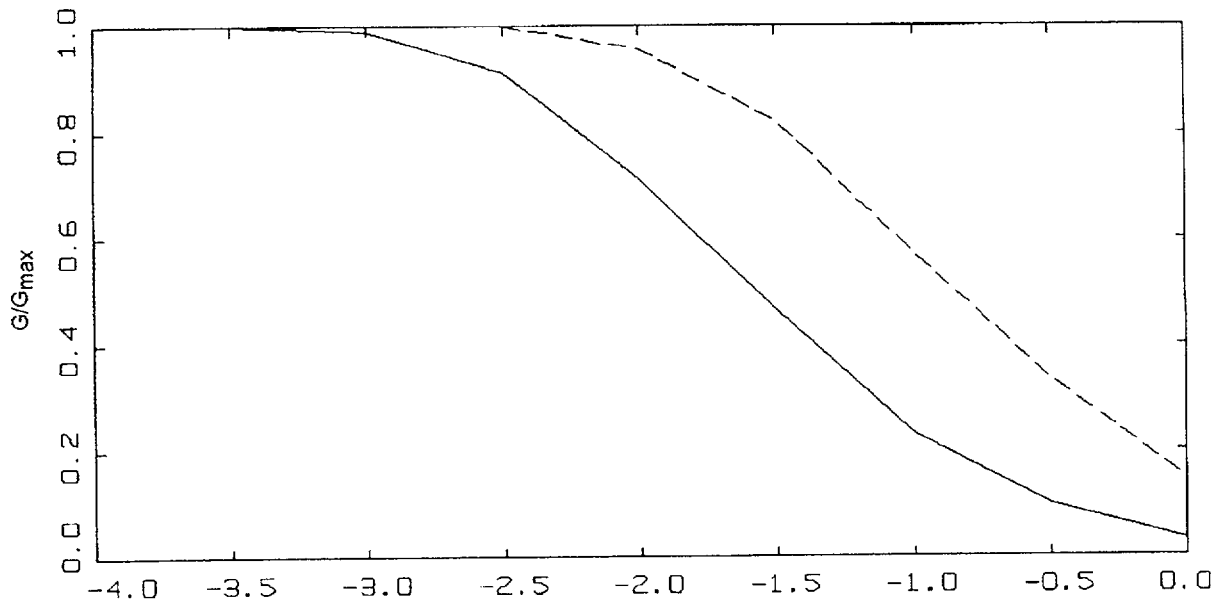
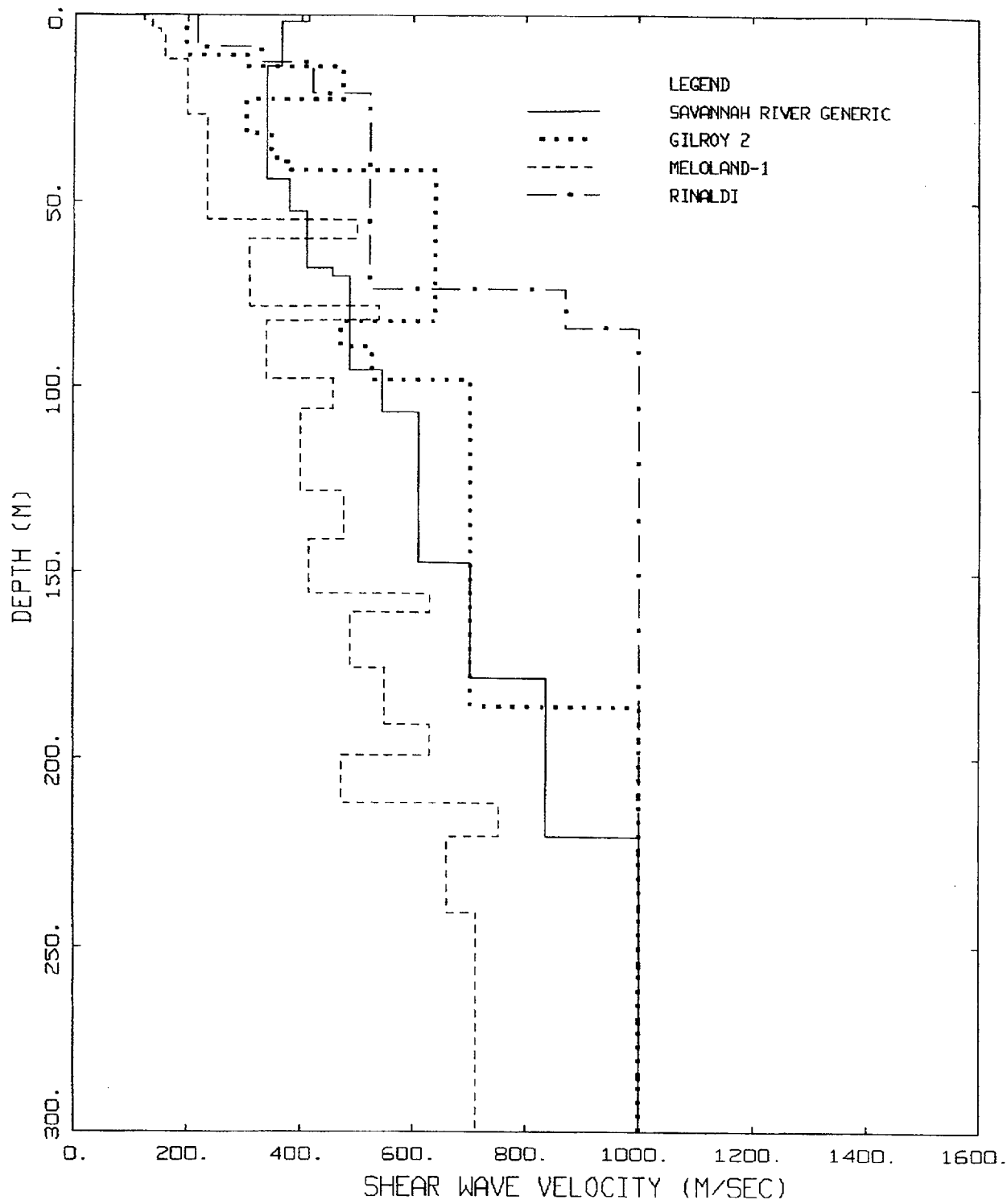


Figure 6-7. Variations in base case shallow crustal velocities. Solid lines are median estimates from a suite of randomly generated profiles (30) using base-case profiles (Figure 6-6) as input. Ranges reflect $\pm 1\sigma$ estimates.



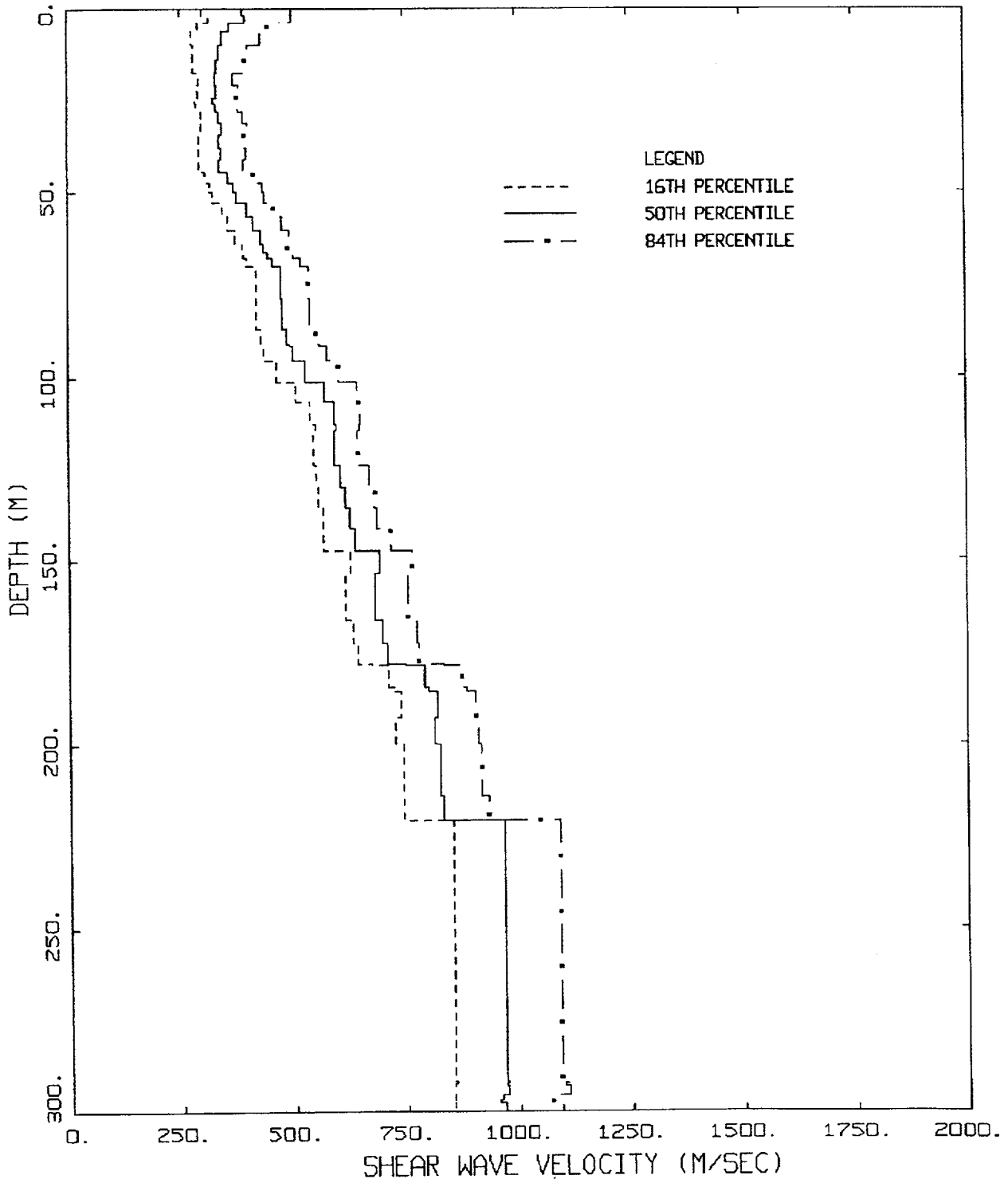
MODULUS REDUCTION AND DAMPING CURVES FOR ROCK

Figure 6-8. Generic G/G_{max} and hysteretic damping curves for soft rock.



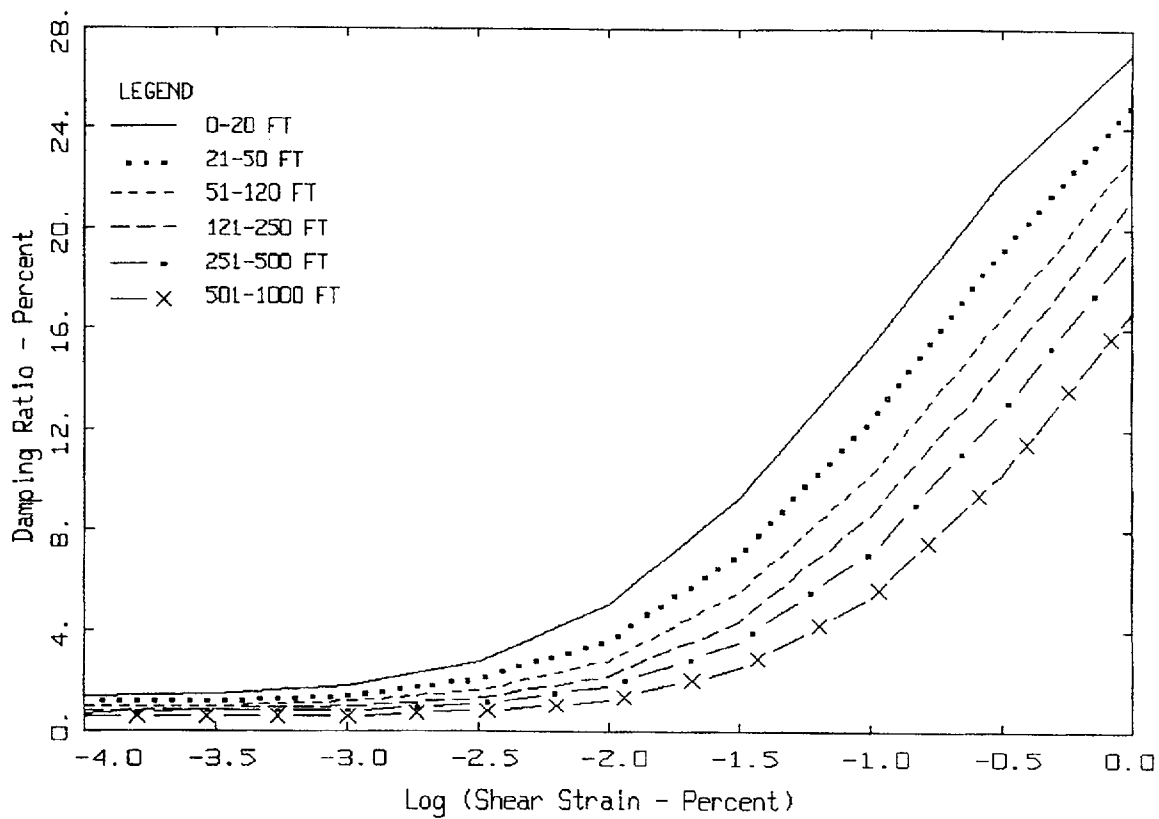
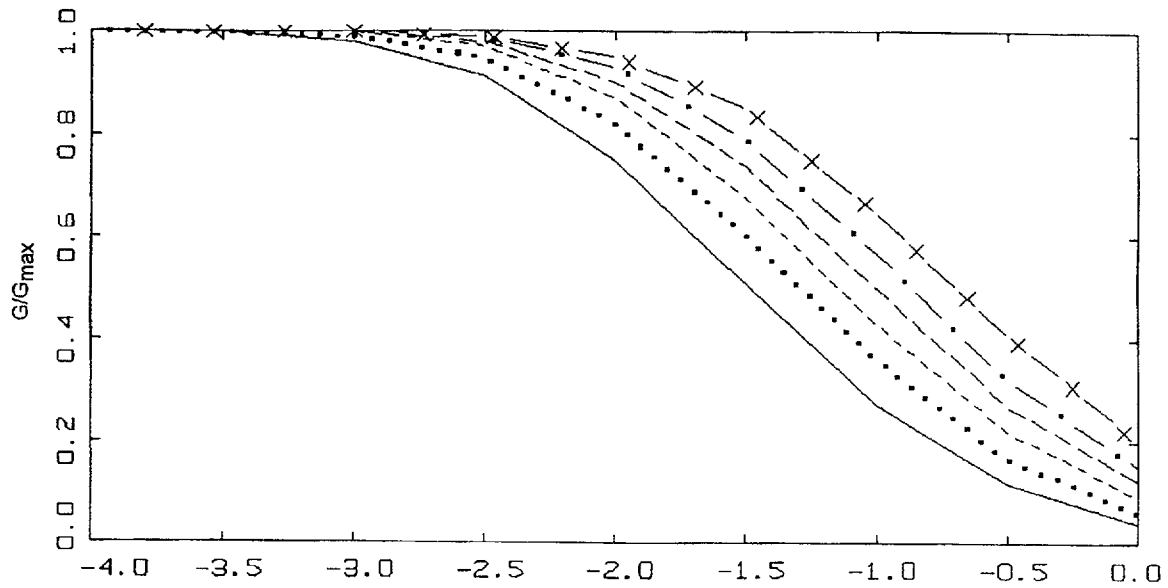
NRC, H_CON PROFILES

Figure 6-9. Base case shear-wave velocity profiles based on suspension logging measurements. Placed on top of Wald and Heaton (1994) crustal model (Table 6-4).



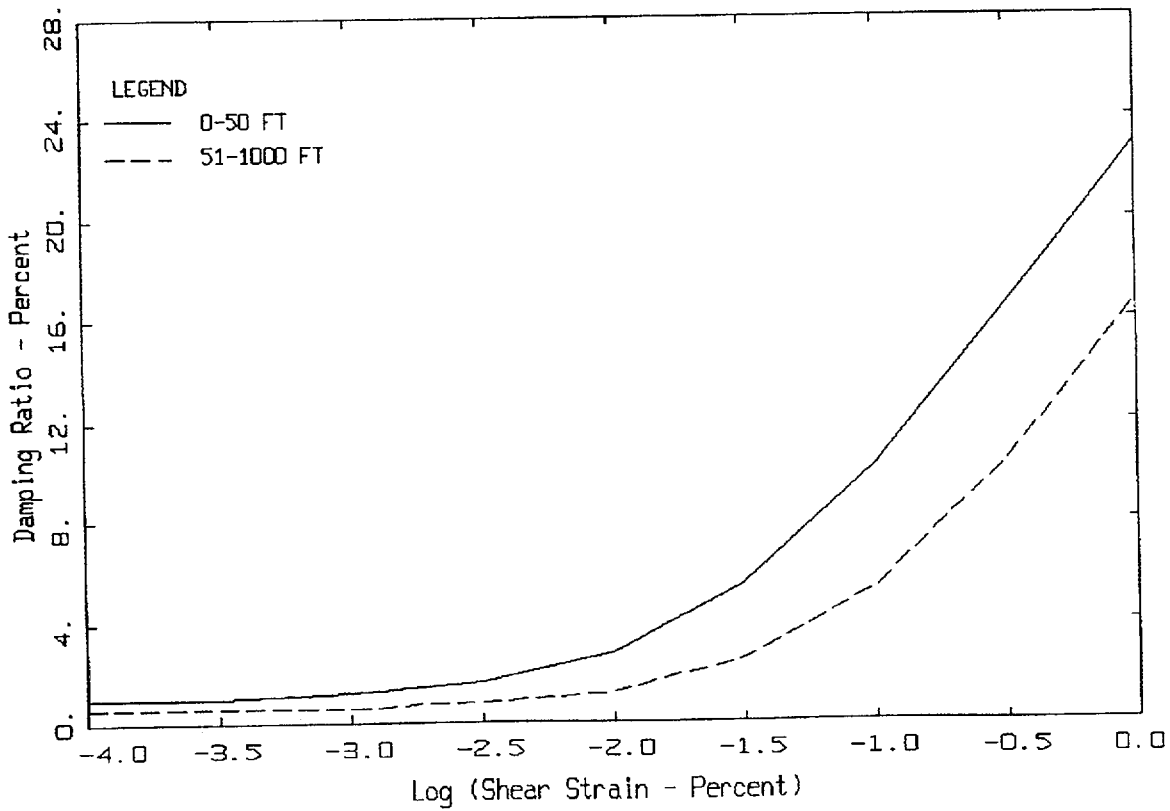
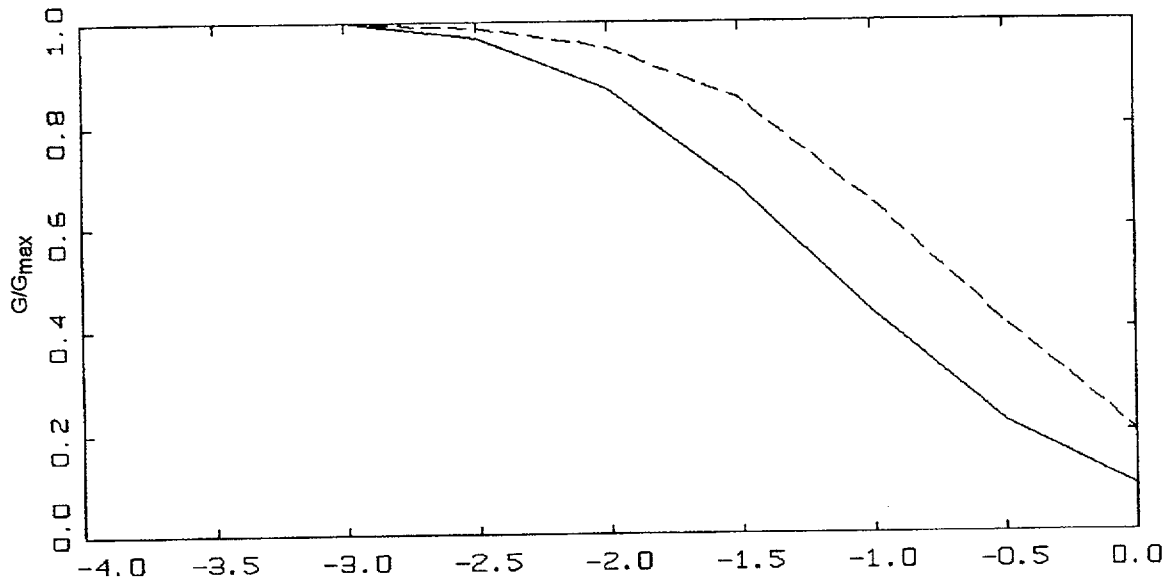
SAVANNAH RIVER GENERIC PROFILE

Figure 6-10. Variation in base case shear-wave velocity, generic Savannah River profile (Figure 6-9) based on thirty realizations. Median estimate along with $\pm\sigma$ values.



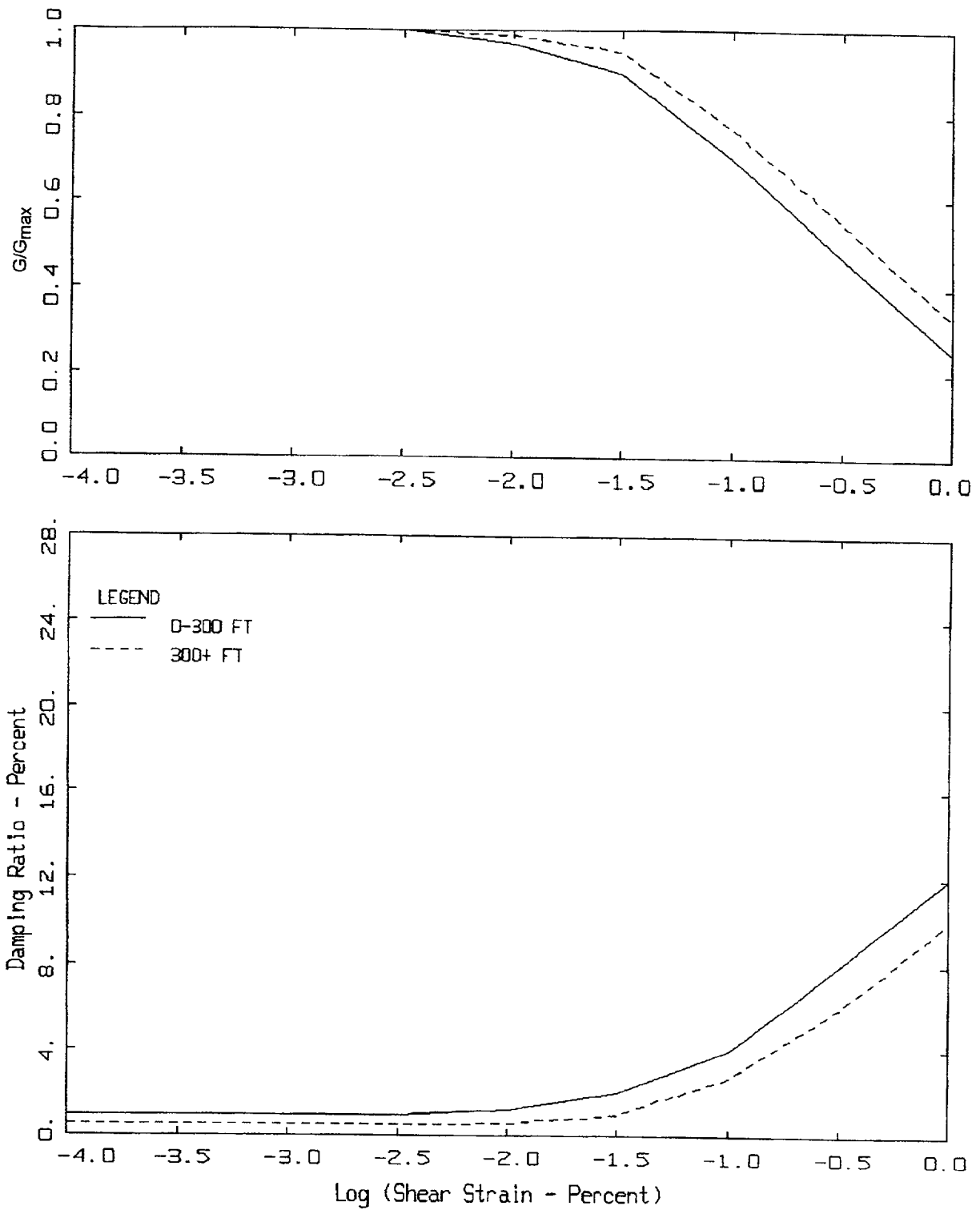
MODULUS REDUCTION AND DAMPING CURVES FOR COHESIONLESS SOILS

Figure 6-11. Generic G/G_{max} and hysteretic damping curves used for Northern California cohesionless soil site Gilroy 2 (EPRI, 1993).



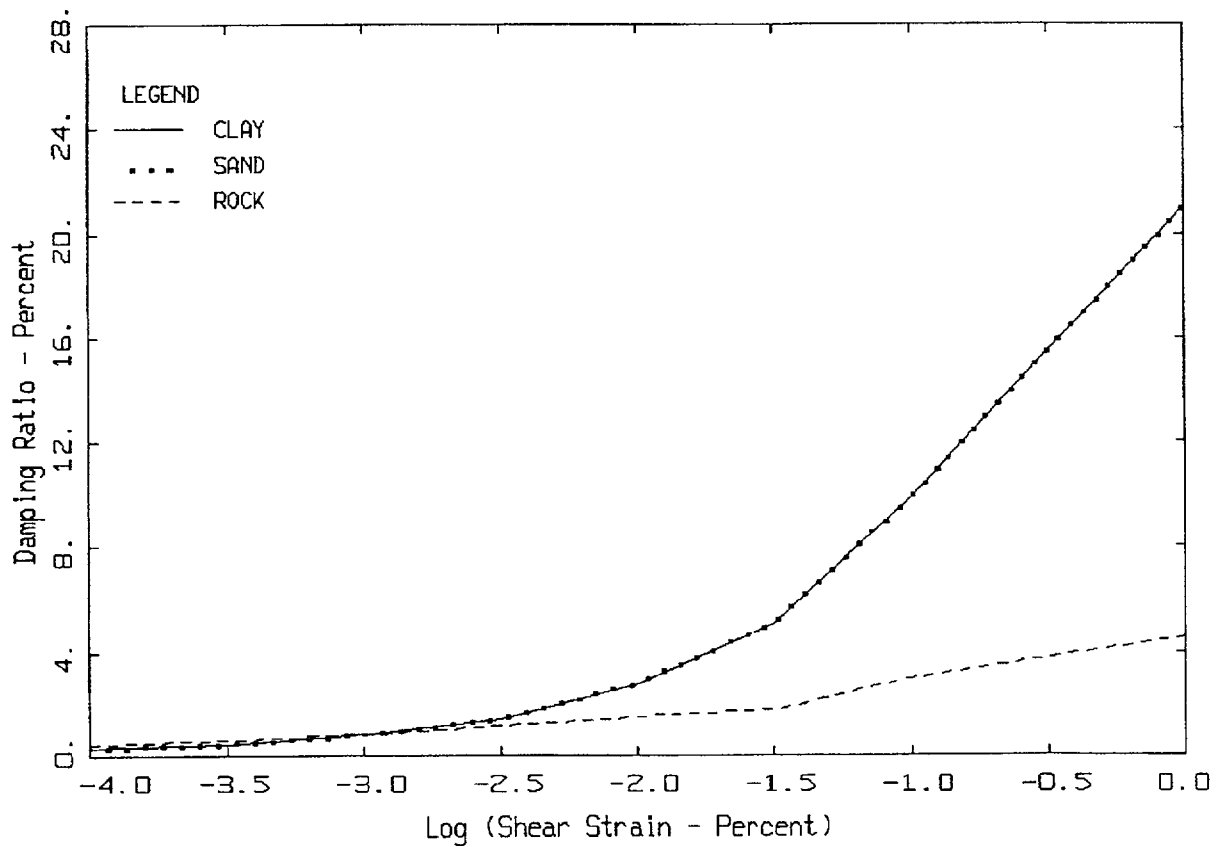
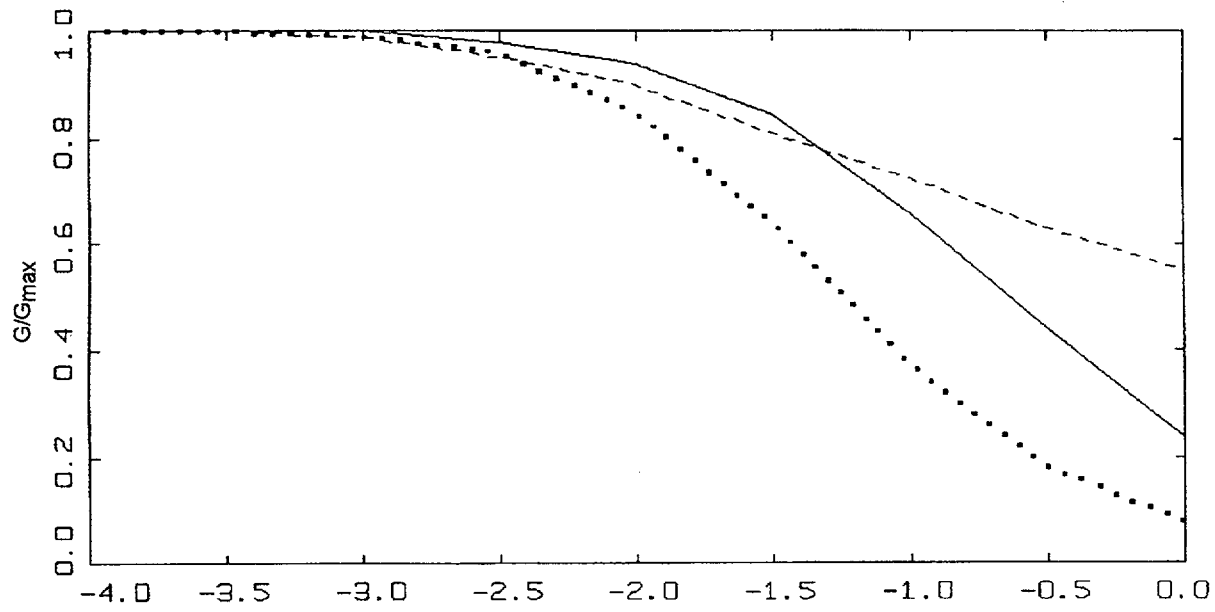
MODULUS REDUCTION AND DAMPING CURVES FOR COHESIONLESS SOILS

Figure 6-12. Generic G/G_{max} and hysteretic damping curves for Peninsular Range deep cohesionless soils. Used for soil sites Rinaldi and Savannah River Generic.



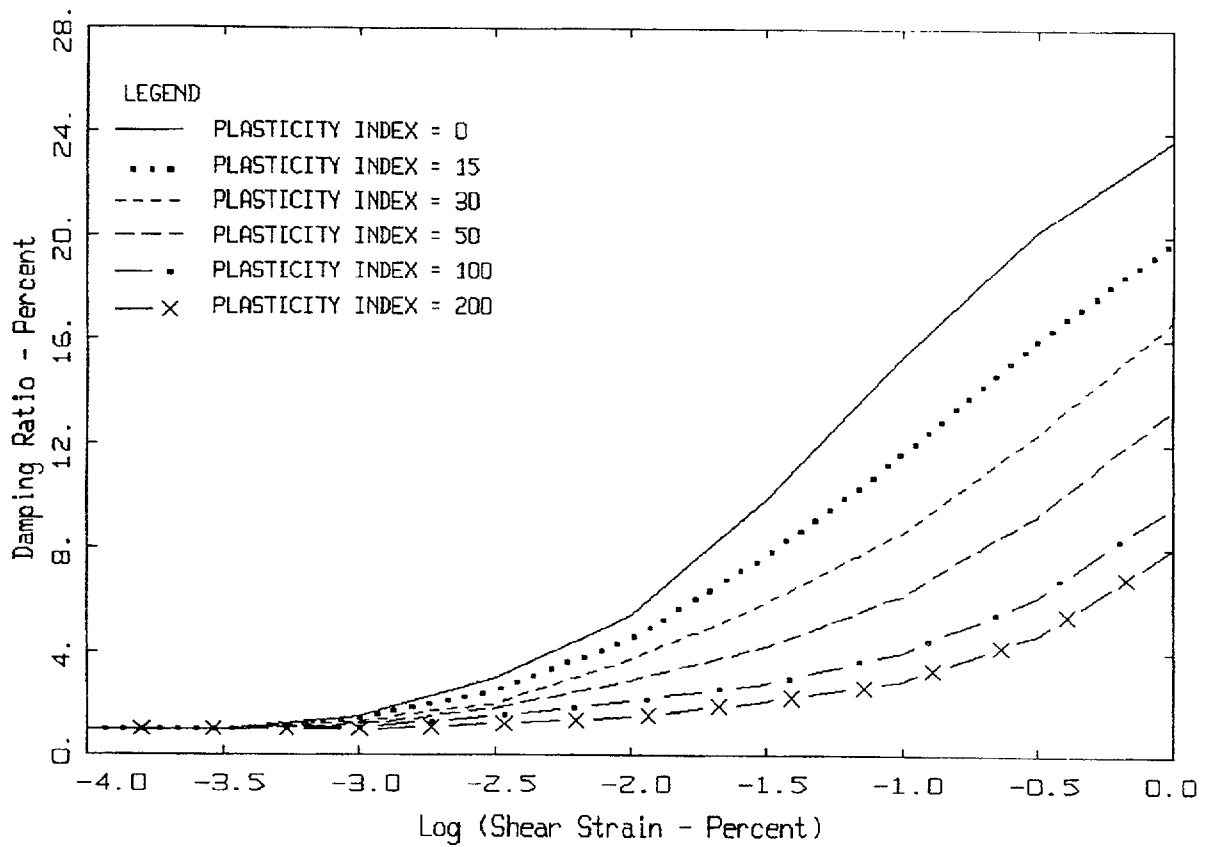
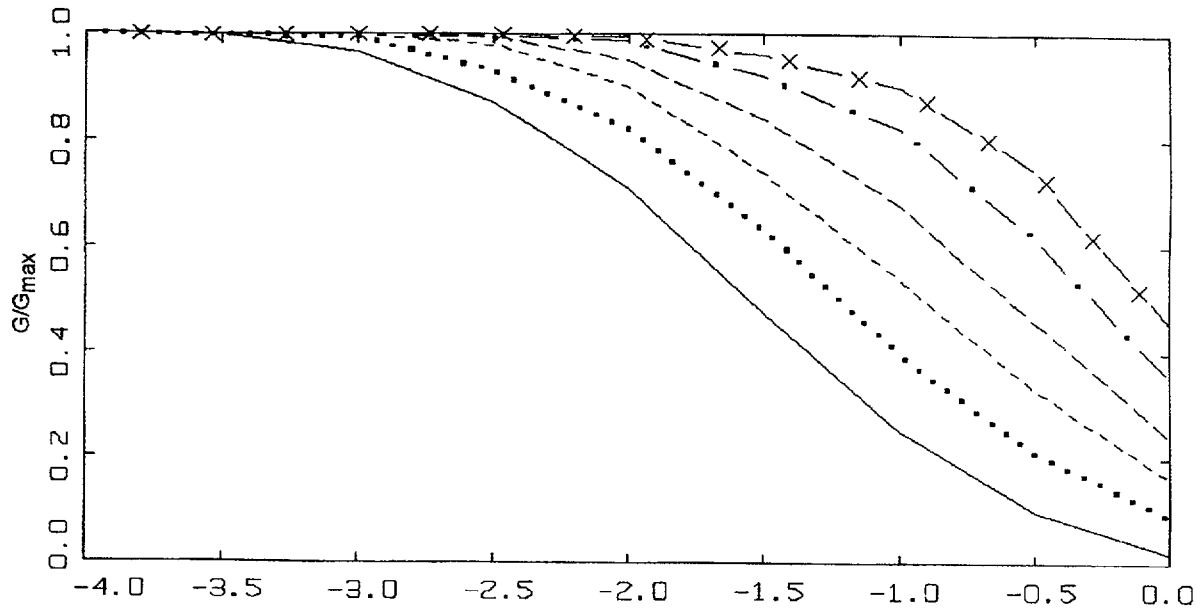
MODULUS REDUCTION AND DAMPING CURVES FOR EL CENTRO

Figure 6-13. Generic G/G_{max} and hysteretic damping curves for Imperial Valley soils. Used for soil site Meloland.



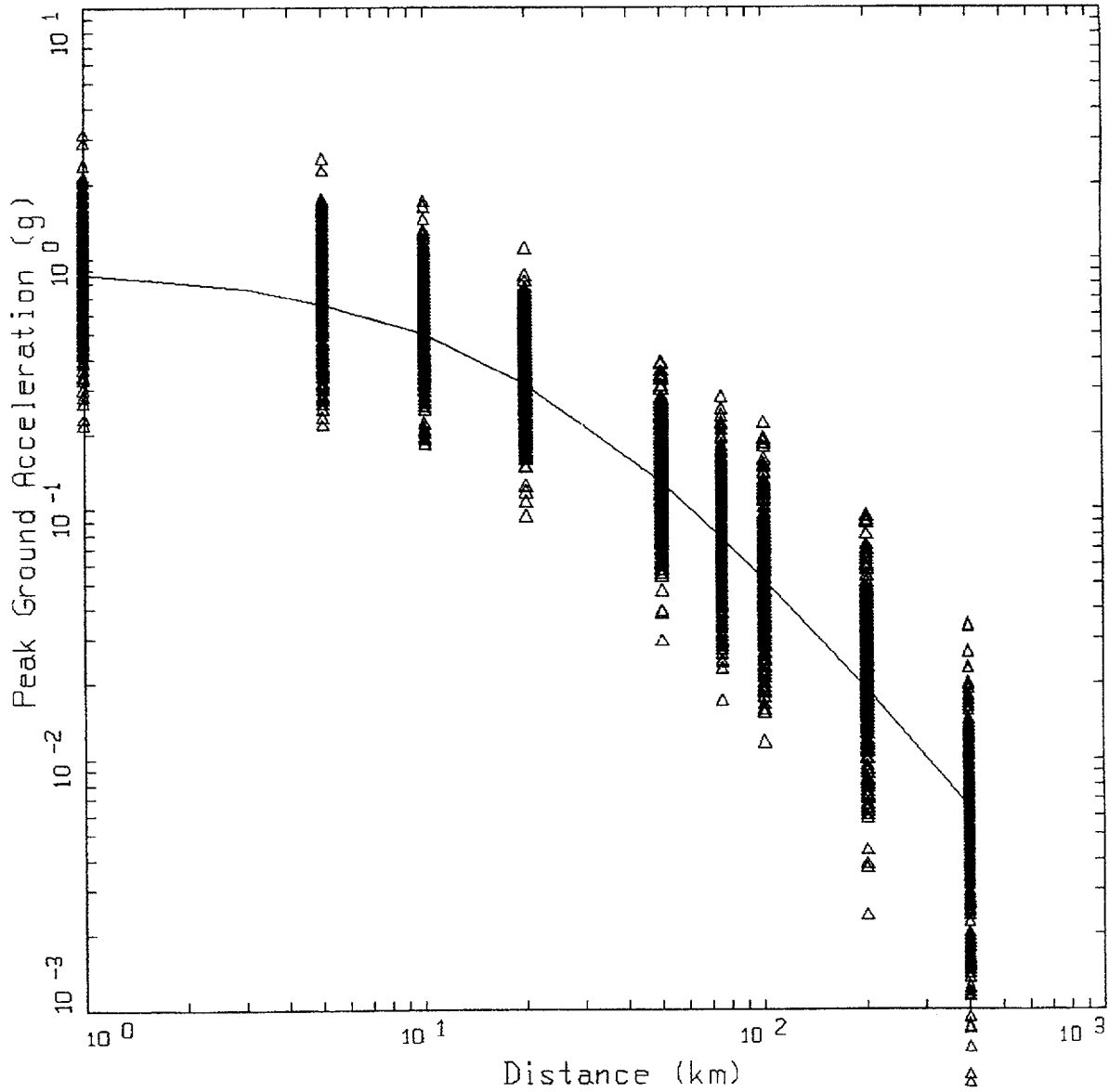
MODULUS REDUCTION AND DAMPING CURVES FROM SHAKE MANUAL

Figure 6-14. Generic G/G_{max} and hysteretic damping curves from SHAKE (Idriss and Sun, 1992).



VUCETIC/DOBRY MODULUS REDUCTION AND DAMPING CURVES

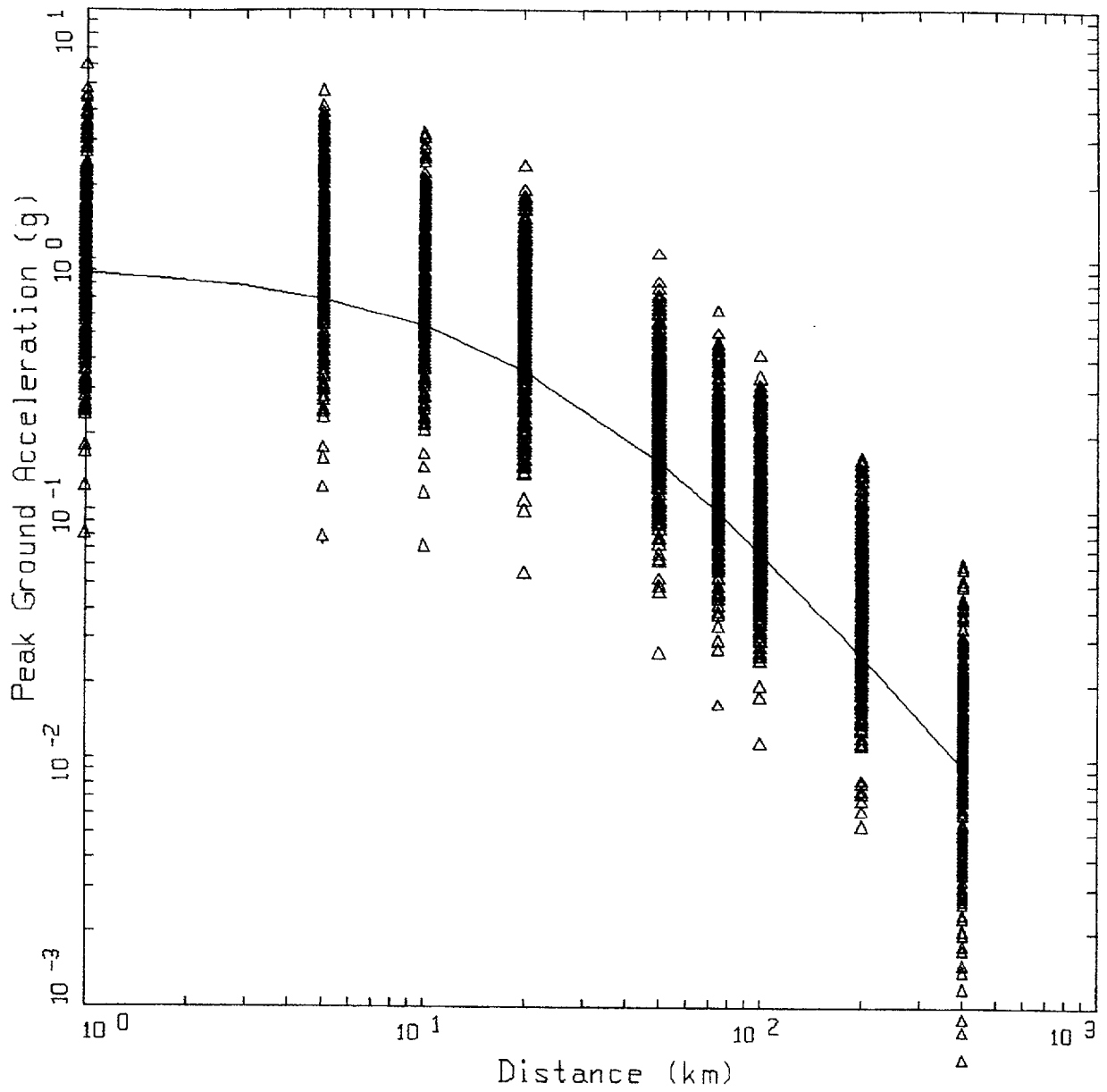
Figure 6-15. Generic G/G_{max} and hysteretic damping curves for cohesive soils (Vucetic and Dobry, 1991).



WUS ROCK
 M = 7.5

LEGEND
 Δ DATA: PGA
 — M=7.5, SIGMA=0.5655

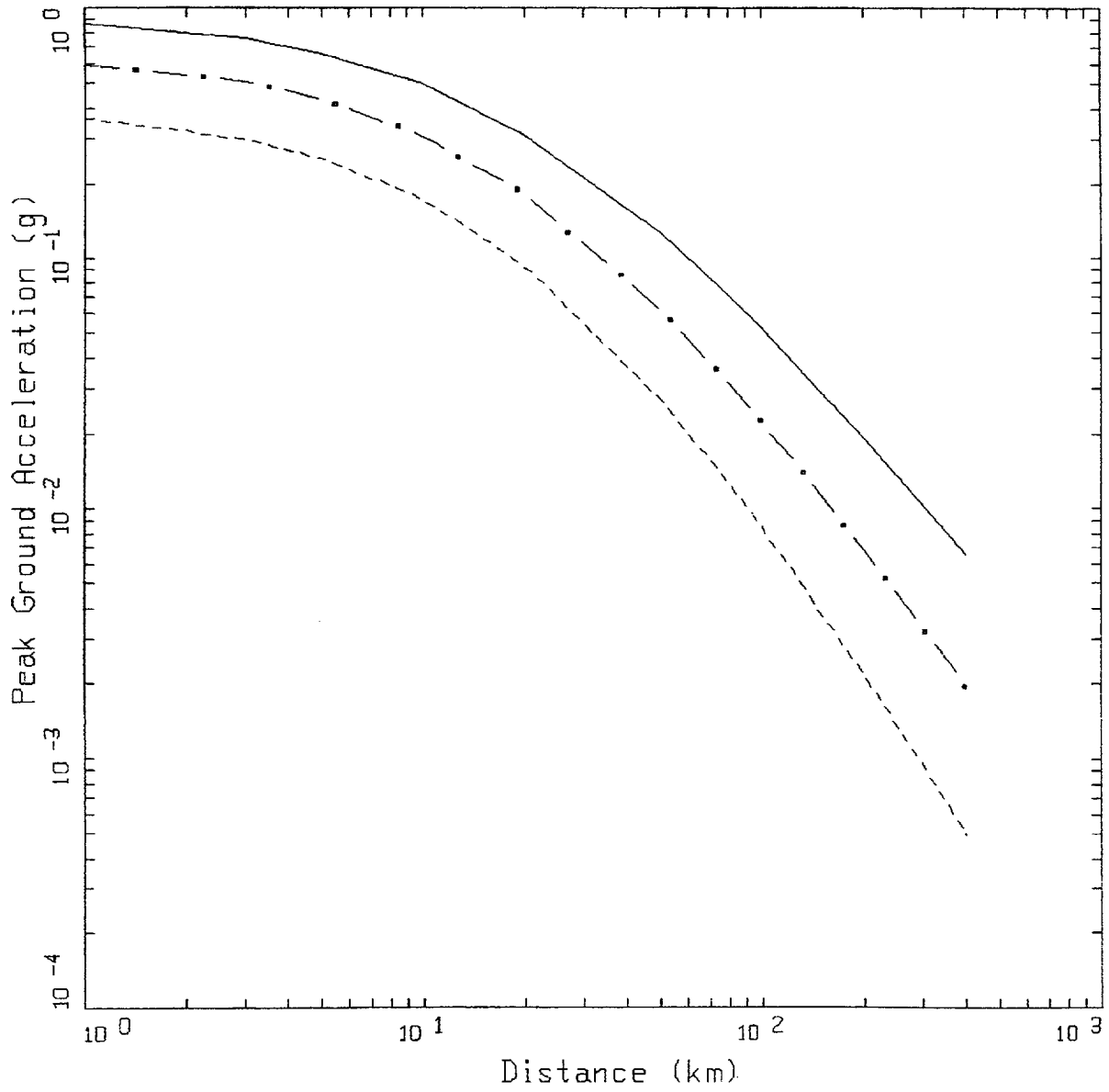
Figure 6-16. Peak acceleration estimates and regression fit at M 7.5 for WUS rock site conditions.



CEUS ROCK
 $M = 7.5$

LEGEND
 Δ DATA: PGA
 — $M=7.5, \text{SIGMA}=0.6387$

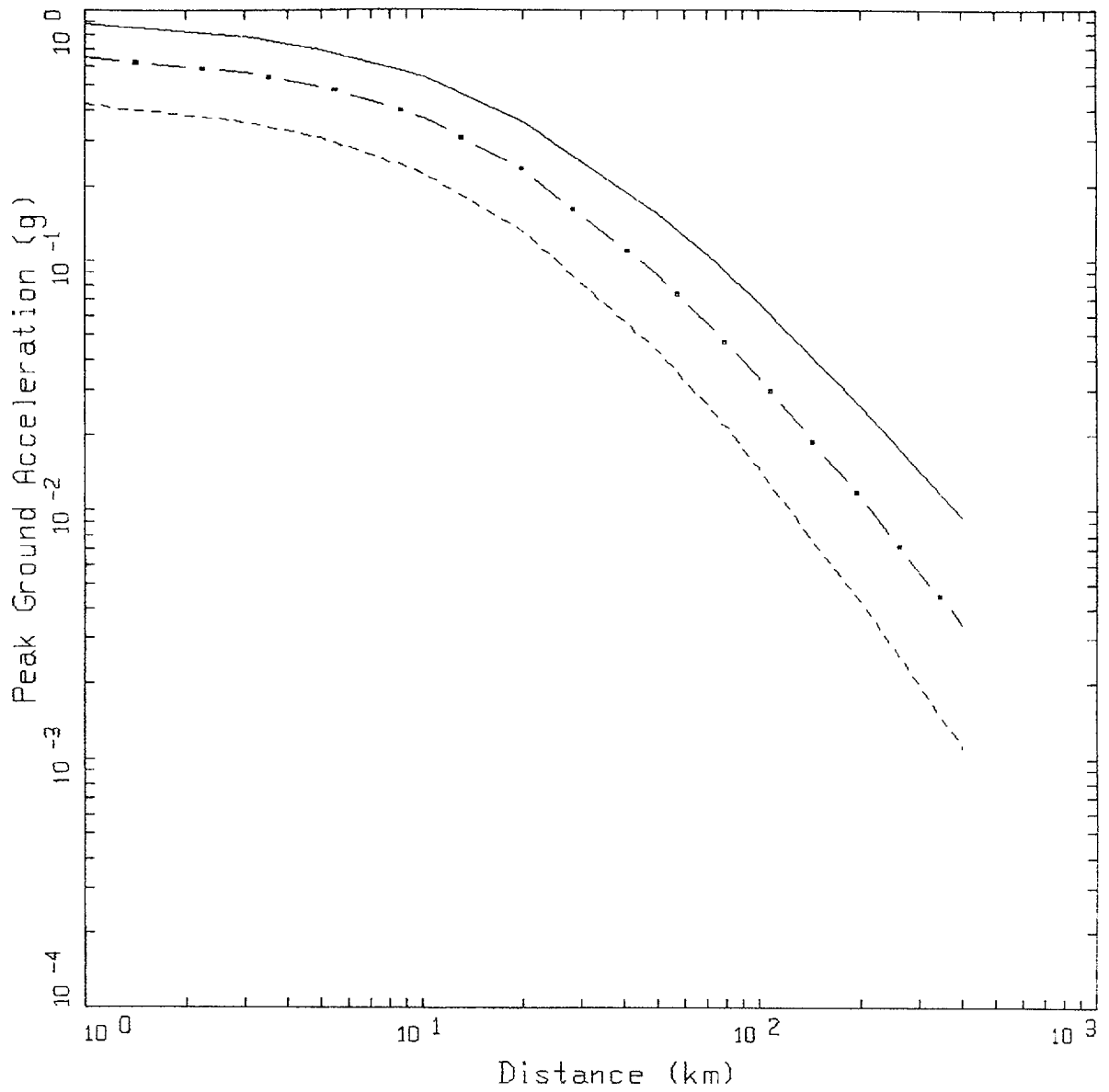
Figure 6-17. Peak acceleration estimates and regression fit at M7.5 for CEUS rock site conditions.



WUS ROCK

LEGEND
 ——— M=7.5, SIGMA=0.5655
 - · - M=6.5, SIGMA=0.5655
 - - - M=5.5, SIGMA=0.5655

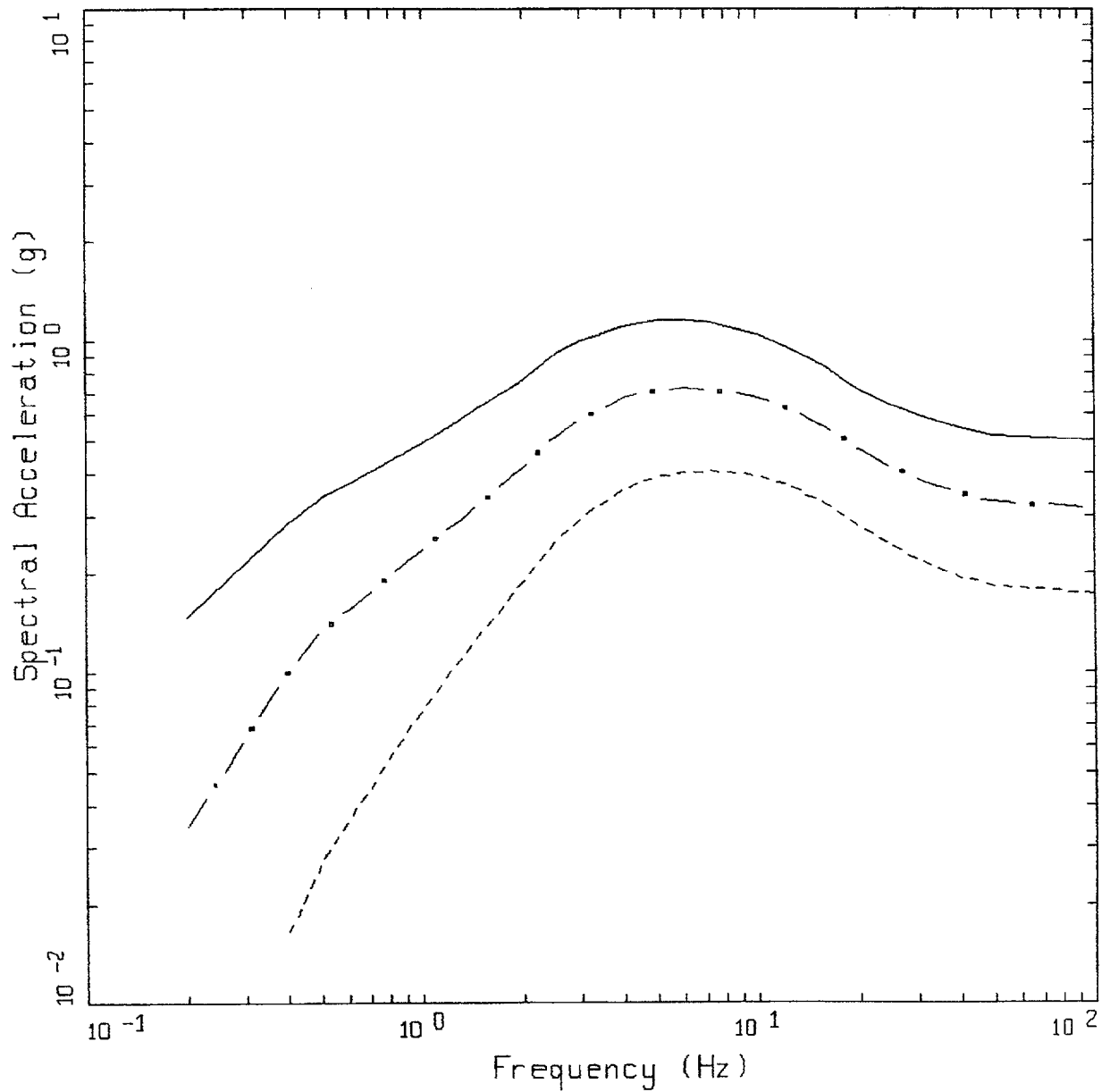
Figure 6-18. Attenuation of median peak horizontal acceleration at M 5.5, 6.5, and 7.5 for WUS rock site conditions.



CEUS ROCK

- LEGEND
- M=7.5, SIGMA=0.6387
 - ■ - M=6.5, SIGMA=0.6387
 - - - M=5.5, SIGMA=0.6387

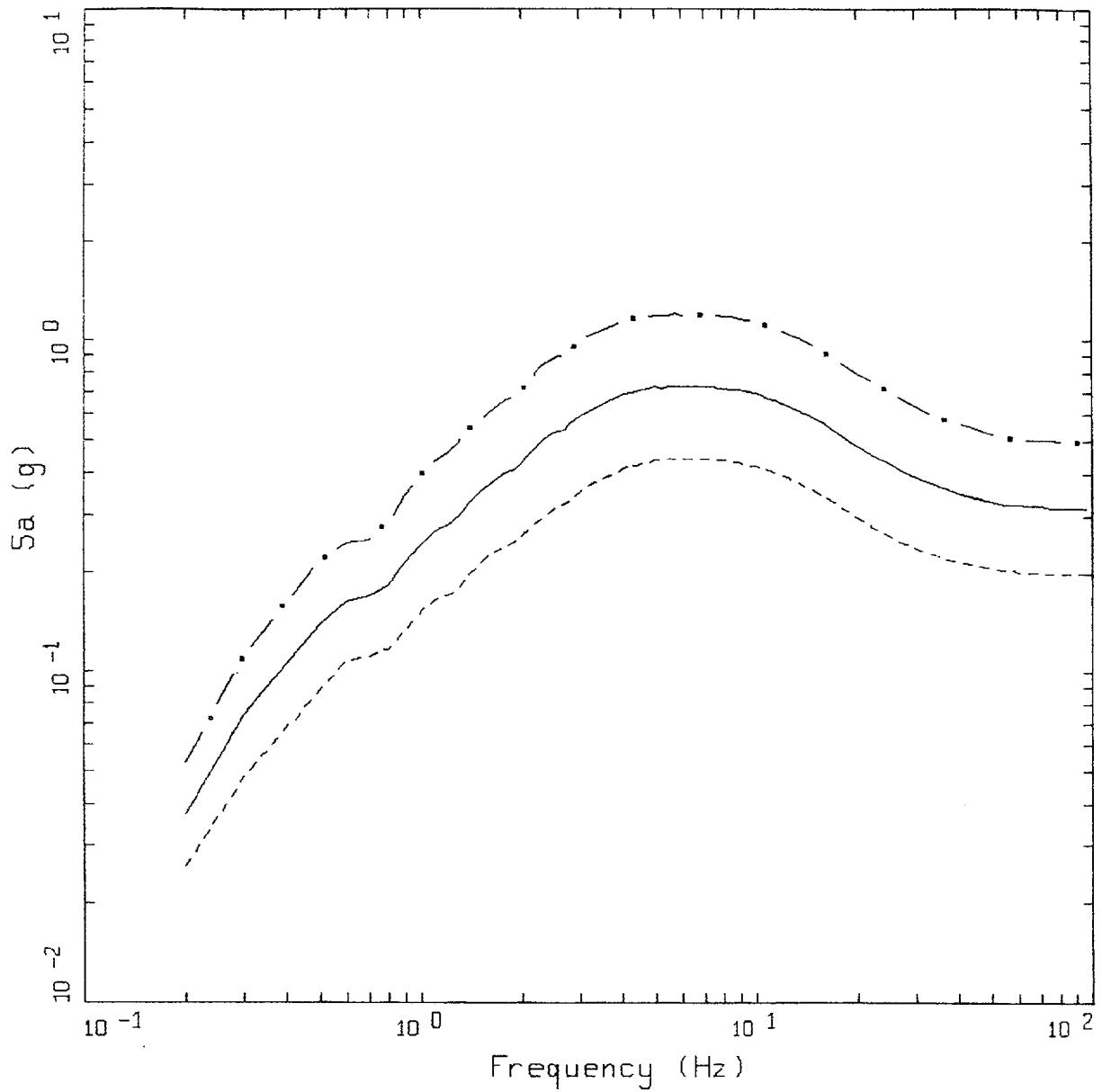
Figure 6-19. Attenuation of median peak horizontal acceleration at M 5.5, 6.5, and 7.5 for CEUS rock site conditions.



WUS ROCK
 DISTANCE=10 KM

LEGEND
 ————— M=7.5
 - · - · - M=6.5
 - - - - M=5.5

Figure 6-20. Median response spectra (5% damping) at a distance of 10 km for magnitudes M 5.5, 6.5, and 7.5: WUS rock site.

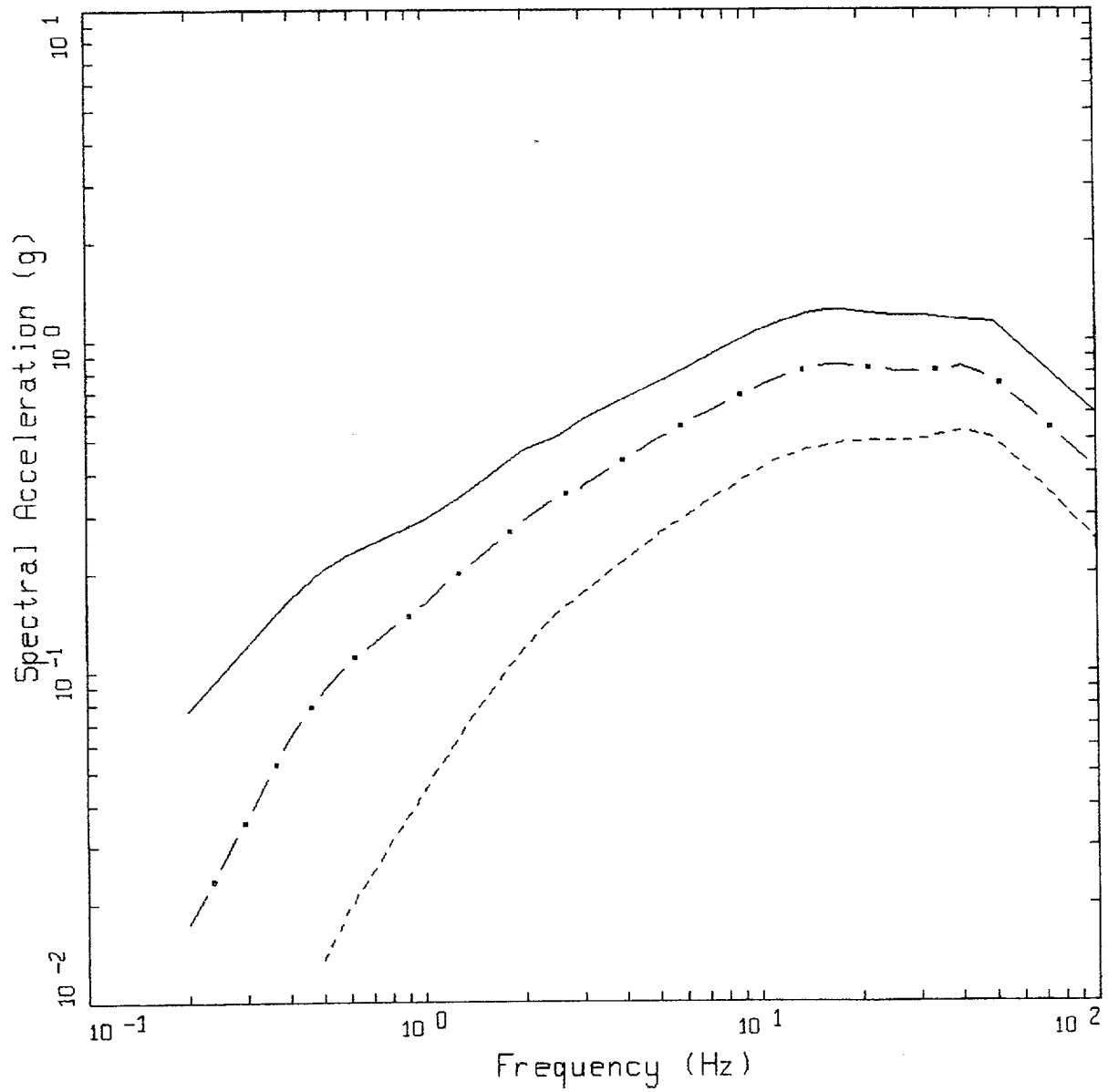


WUS ROCK
 M=6.5, DISTANCE=10 KM

LEGEND

- • — 84TH PERCENTILE, PGA = 0.500 G
- 50TH PERCENTILE, PGA = 0.315 G
- - - 16TH PERCENTILE, PGA = 0.199 G

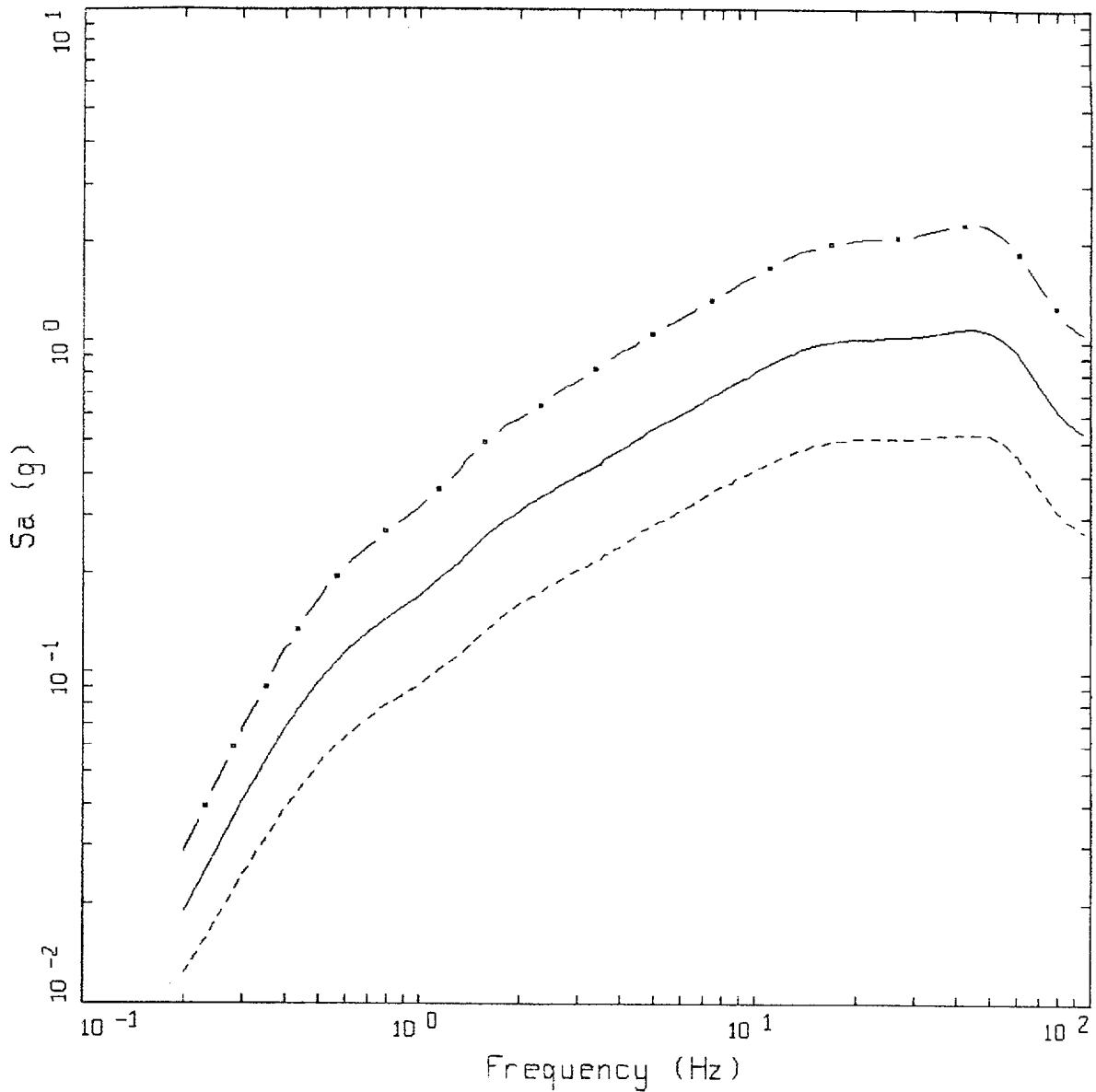
Figure 6-21. Response spectra (5% damping) at a distance of 10 km for M 6.5 showing median and $\pm 1\sigma$ estimates (parametric and regression uncertainty): WUS rock site.



CEUS ROCK
 DISTANCE = 10 KM

LEGEND
 — M=7.5
 - • - M=6.5
 - - - M=5.5

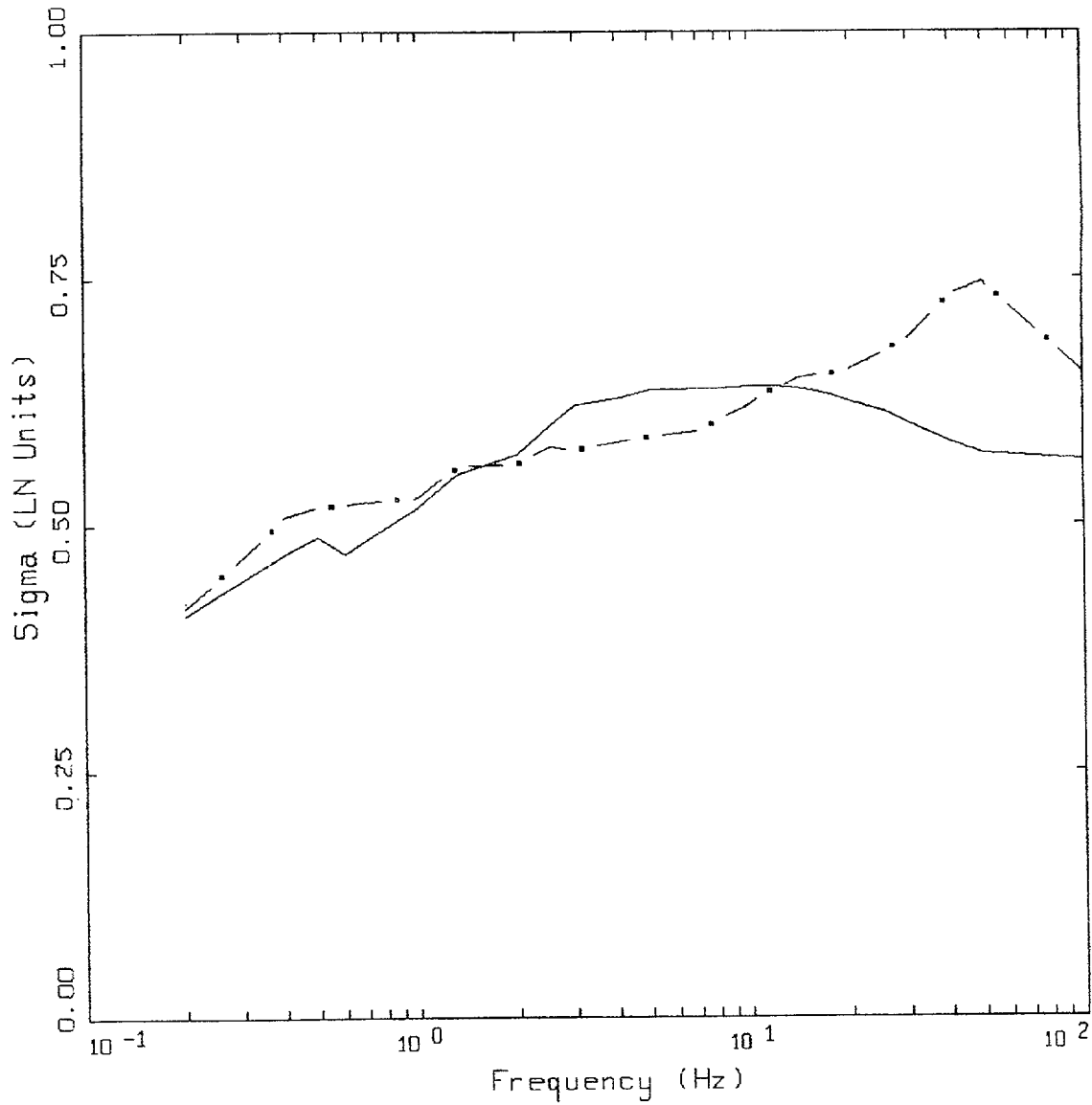
Figure 6-22. Median response spectra (5% damping) at a distance of 10 km for magnitudes M 5.5, 6.5, and 7.6: CEUS rock site.



CEUS ROCK
 M=6.5, DISTANCE=10 KM

- LEGEND
- · - 84TH PERCENTILE, PGA = 1.033 G
 - 50TH PERCENTILE, PGA = 0.520 G
 - - - 16TH PERCENTILE, PGA = 0.262 G

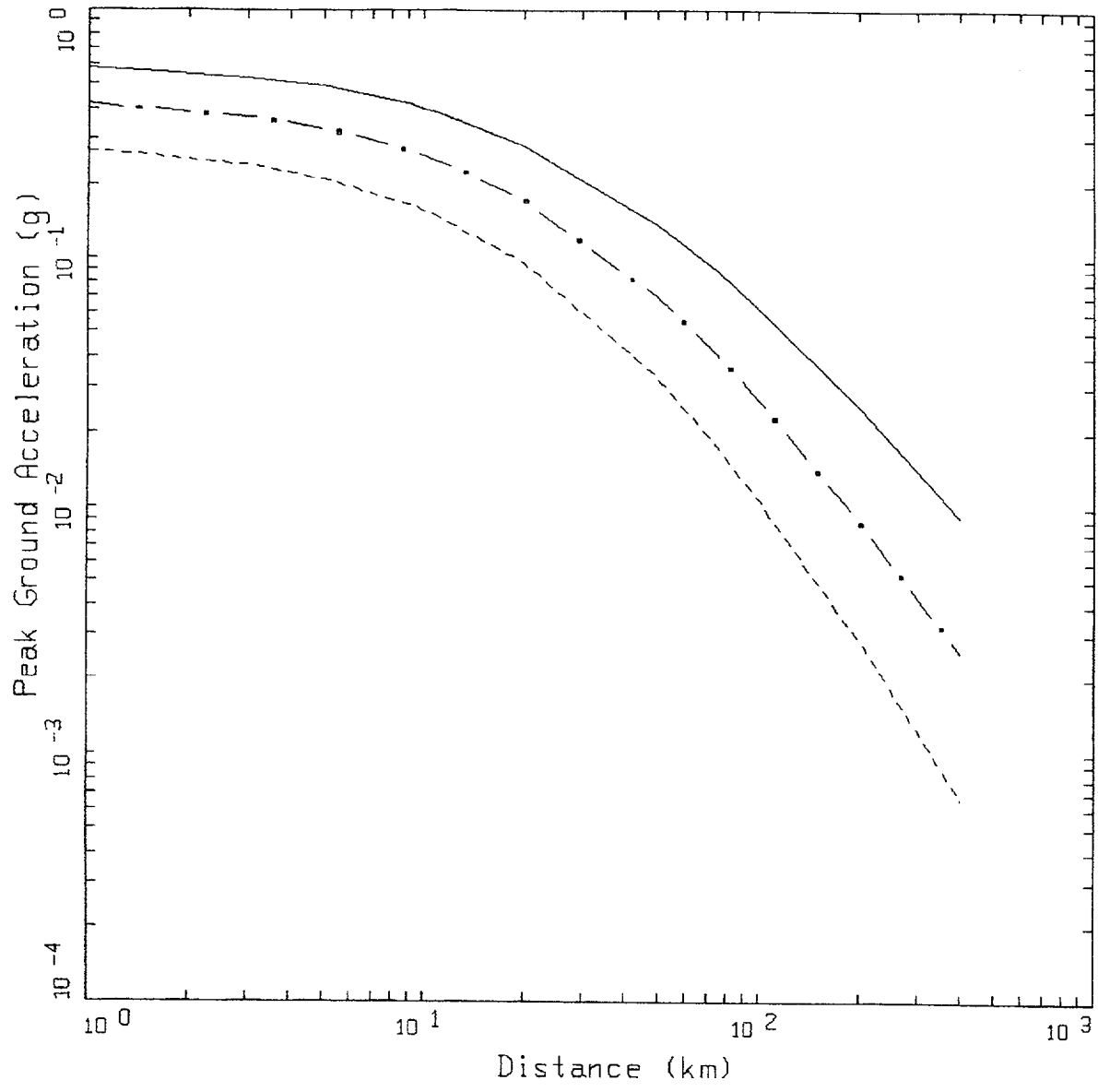
Figure 6-23. Response spectra (5% damping) at a distance of 10 km for M 6.5 showing median and $\pm 1\sigma$ estimates (parametric and regression uncertainty): CEUS rock site.



ROCK SITE VARIABILITY

——— WUS
 - . - CEUS

Figure 6-24. Variability in response spectral ordinates at WUS and CEUS rock sites resulting from parametric variability and regression fit over all magnitudes and distances (Tables 6-2 and 6-3).



NRC PT SOURCE WUS SOIL, GILROY2

- LEGEND
- M=7.5, SIGMA=0.4928
 - · - M=6.5, SIGMA=0.4928
 - - - M=5.5, SIGMA=0.4928

Figure 6-25. Attenuation of median peak horizontal acceleration at M 5.5, 6.5, and 7.5 for soil profile Gilroy 2 and WUS conditions.

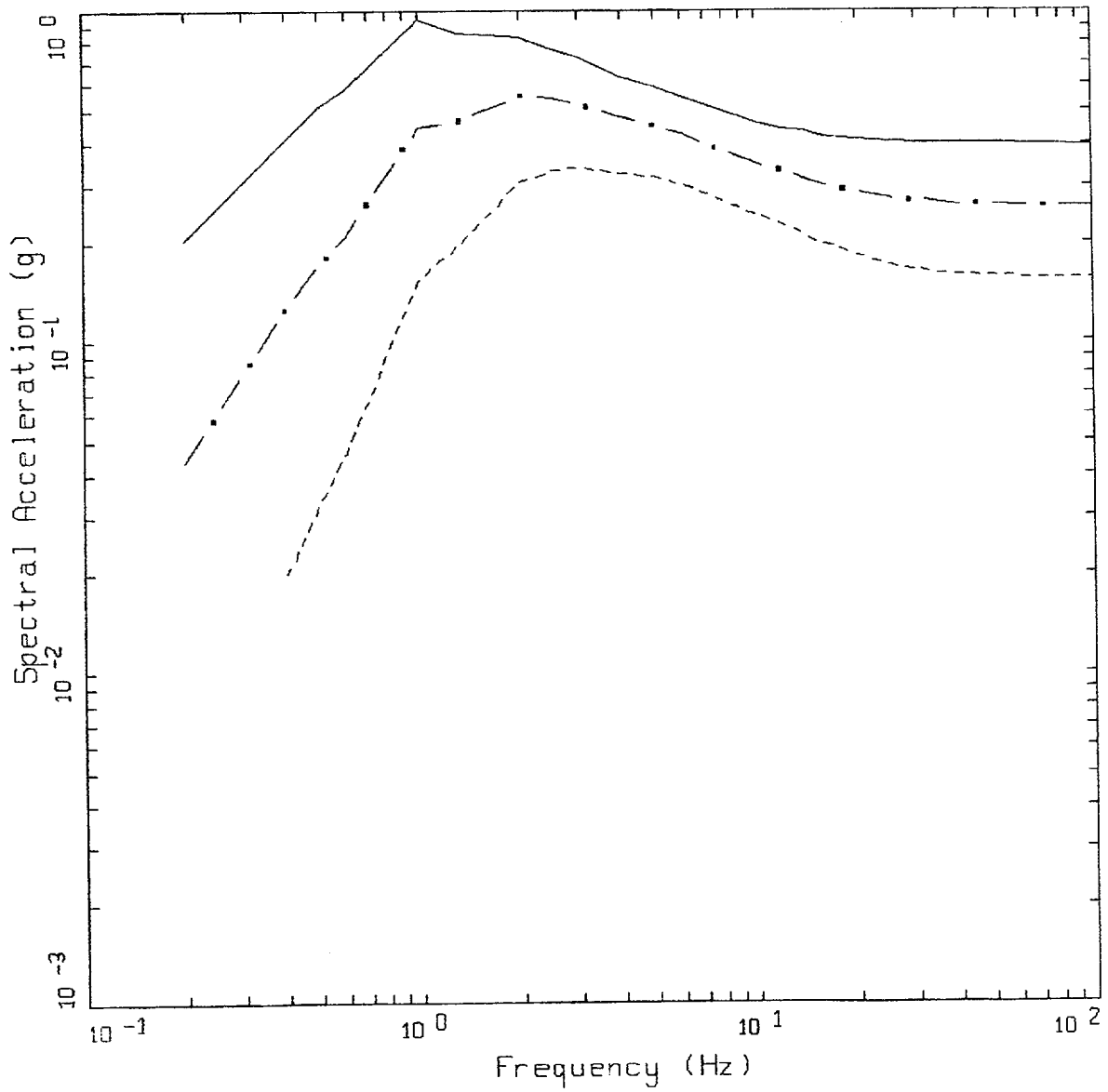
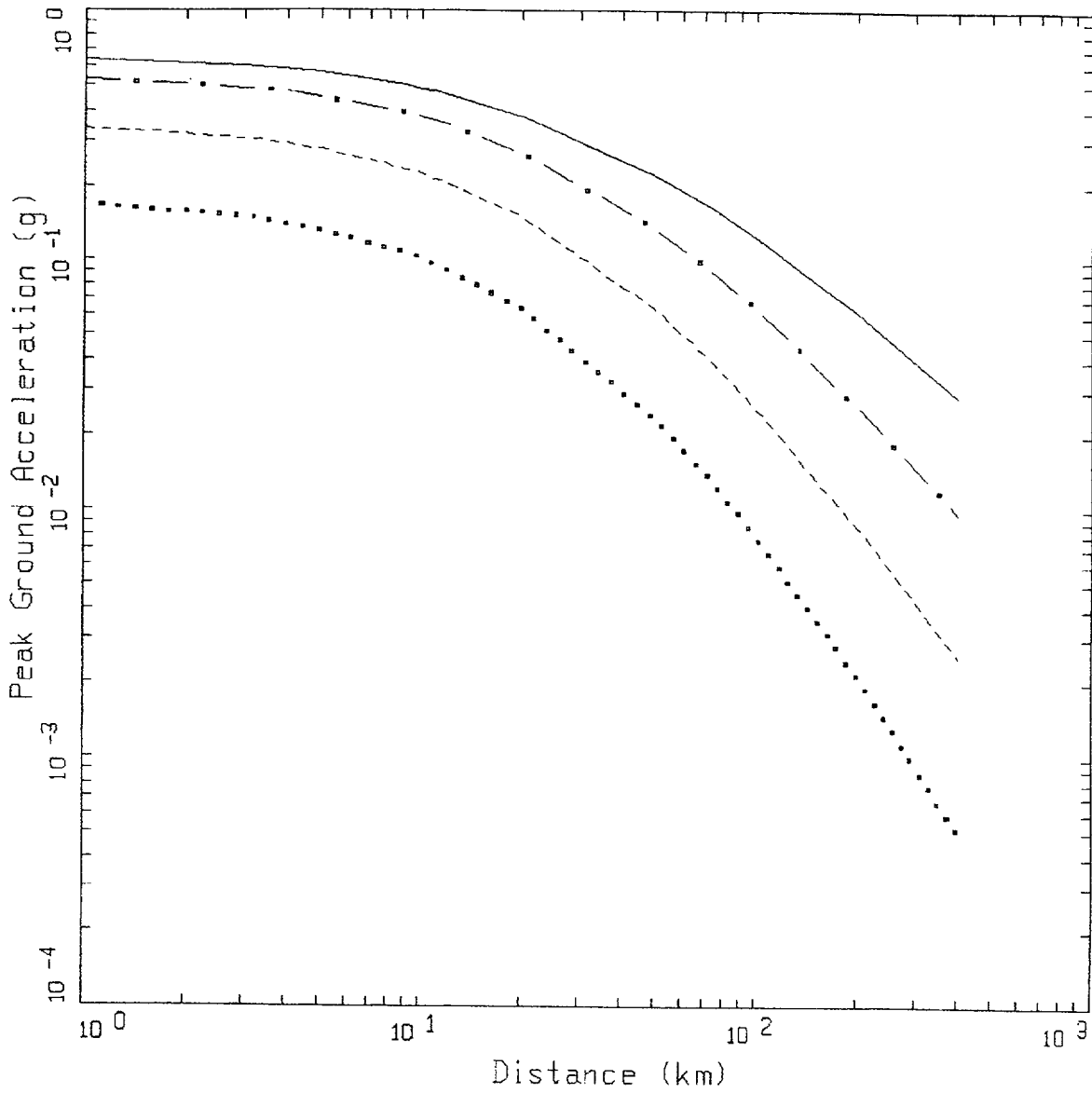


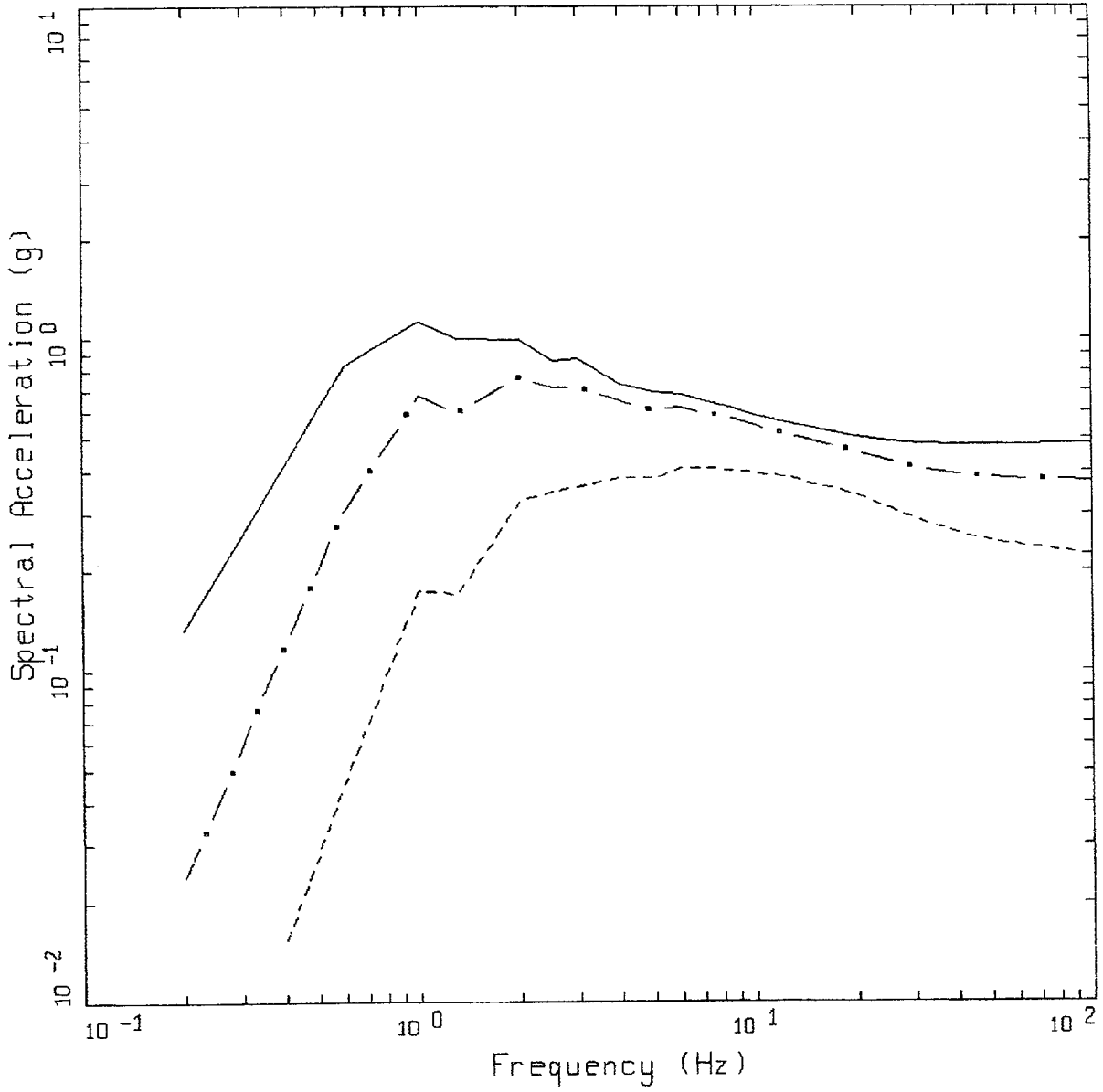
Figure 6-26. Median response spectra (5% damping) at a distance of 10 km for **M** 5.5, 6.5, and 7.5 for soil profile Gilroy 2 and WUS conditions.



CEUS SOIL, GILROY 2

- LEGEND
- M=7.5, SIGMA=0.4978
 - . - M=6.5, SIGMA=0.4978
 - - - M=5.5, SIGMA=0.4978
 - M=4.5, SIGMA=0.4978

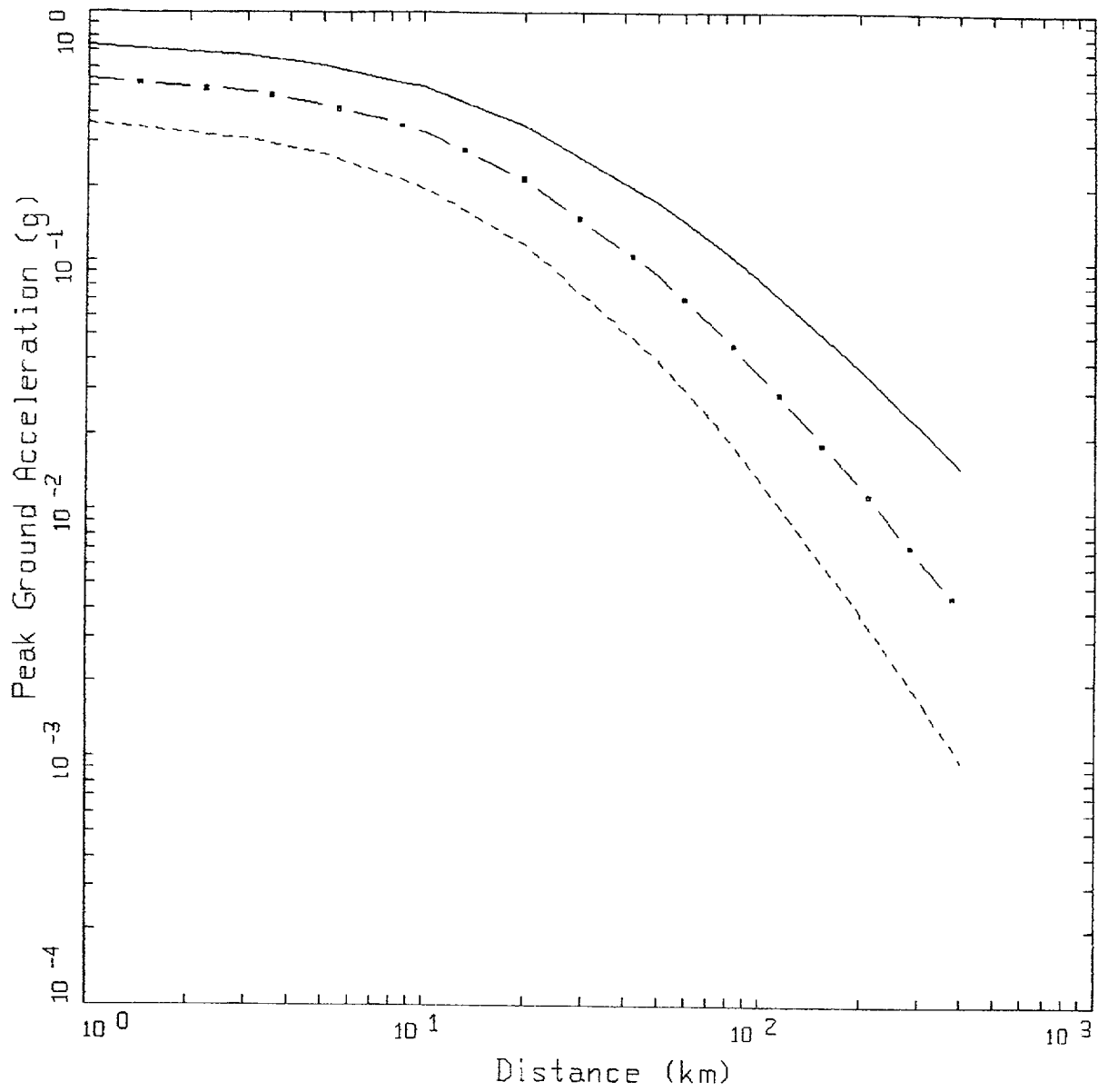
Figure 6-27. Attenuation of median peak horizontal acceleration at M 5.5, 6.5, and 7.5 for soil profile Gilroy 2 and CEUS conditions.



CEUS SOIL, GILROY 2
 DISTANCE=10 KM

LEGEND
 ————— M=7.5
 - . - . - . M=6.5
 - - - - - M=5.5

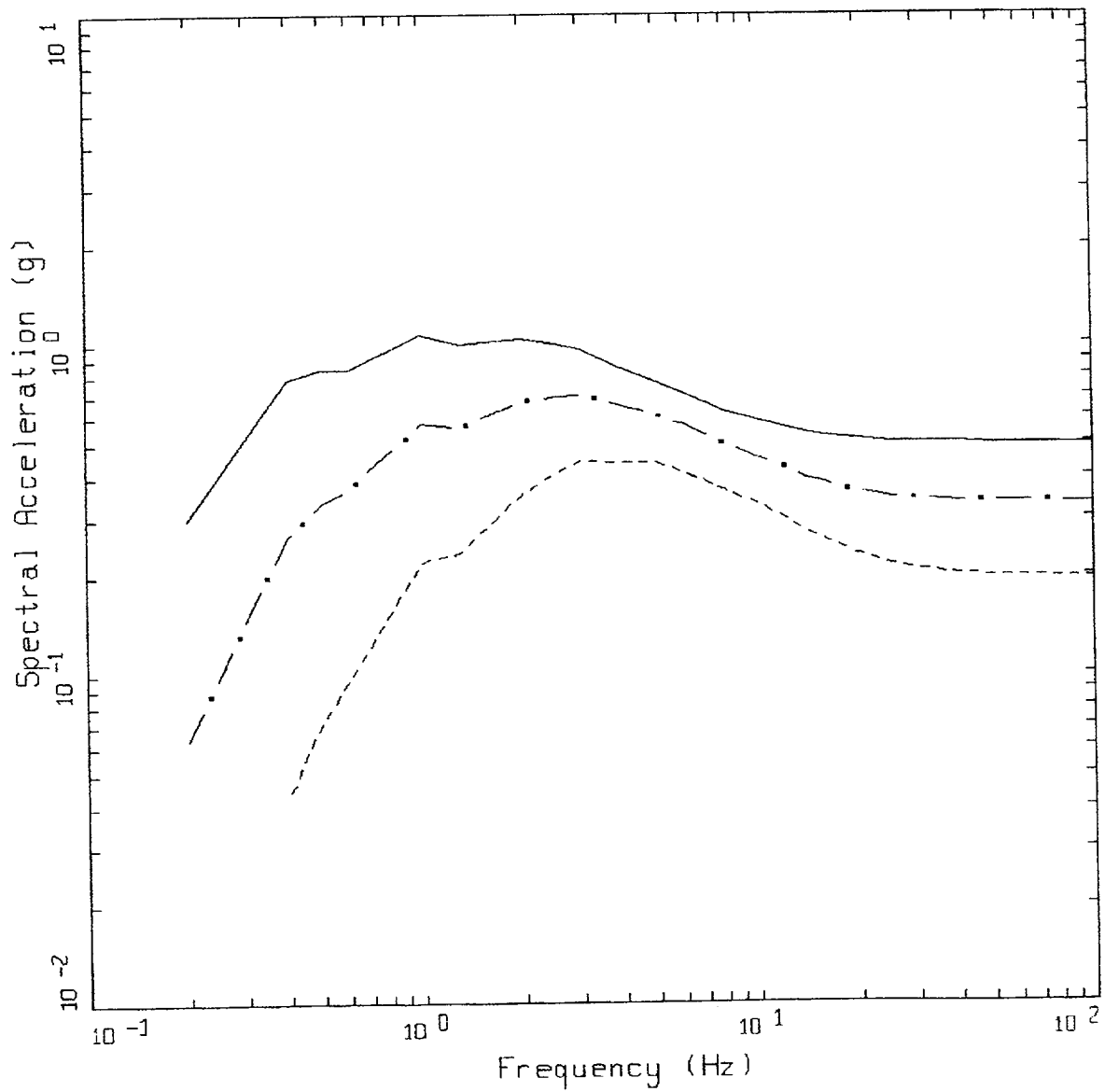
Figure 6-28. Median response spectra (5% damping) at a distance of 10 km for M 5.5, 6.5, and 7.5 for soil profile Gilroy 2 and CEUS conditions.



WUS SOIL, MELOLAND

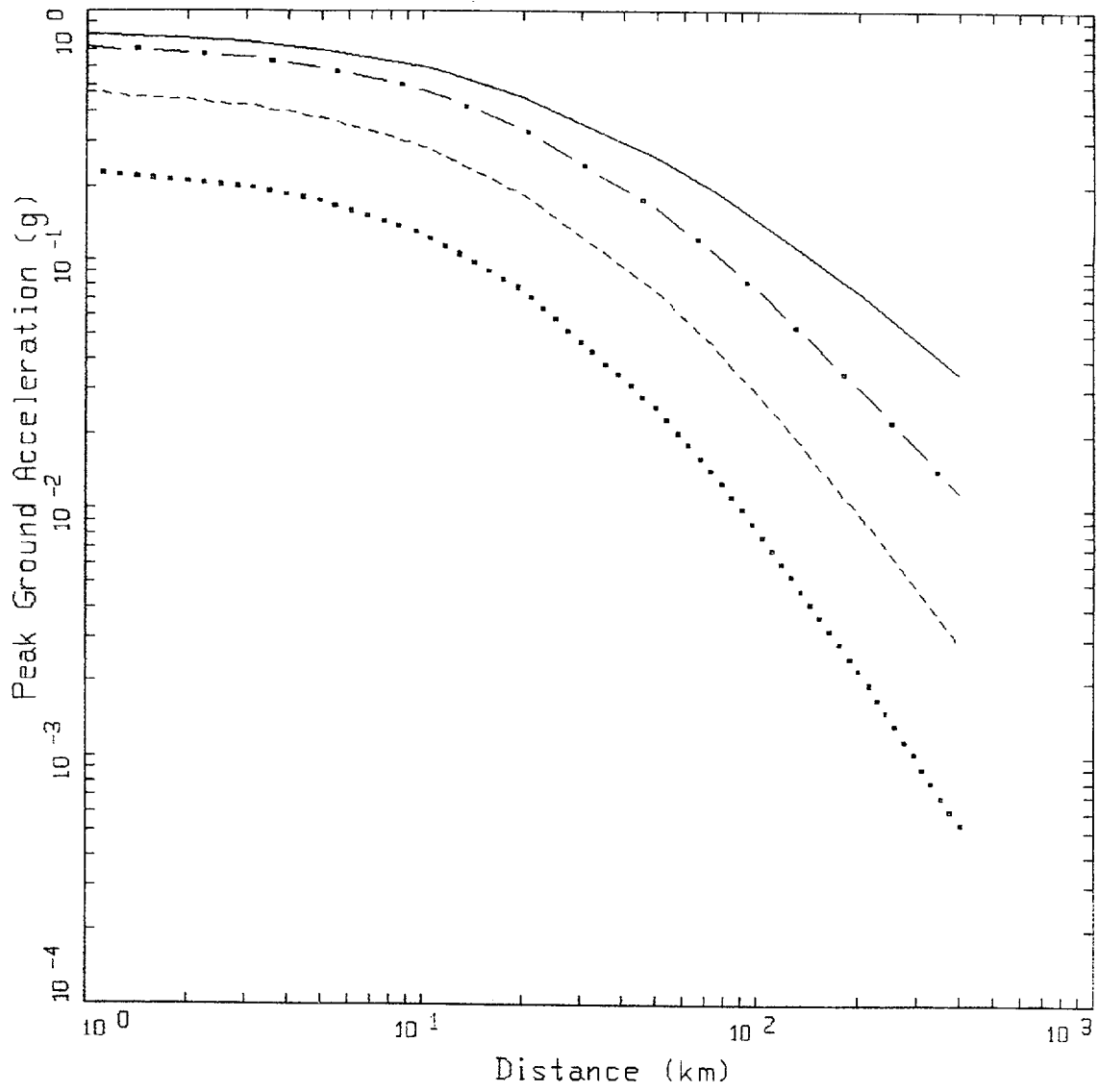
- LEGEND
- M=7.5, SIGMA=0.4774
 - · - M=6.5, SIGMA=0.4774
 - - - M=5.5, SIGMA=0.4774

Figure 6-29. Attenuation of median peak horizontal acceleration at M 5.5, 6.5, and 7.5 for soil profile Meloland and WUS conditions.



————— M=7.5
 - . - M=6.5
 - - - M=5.5

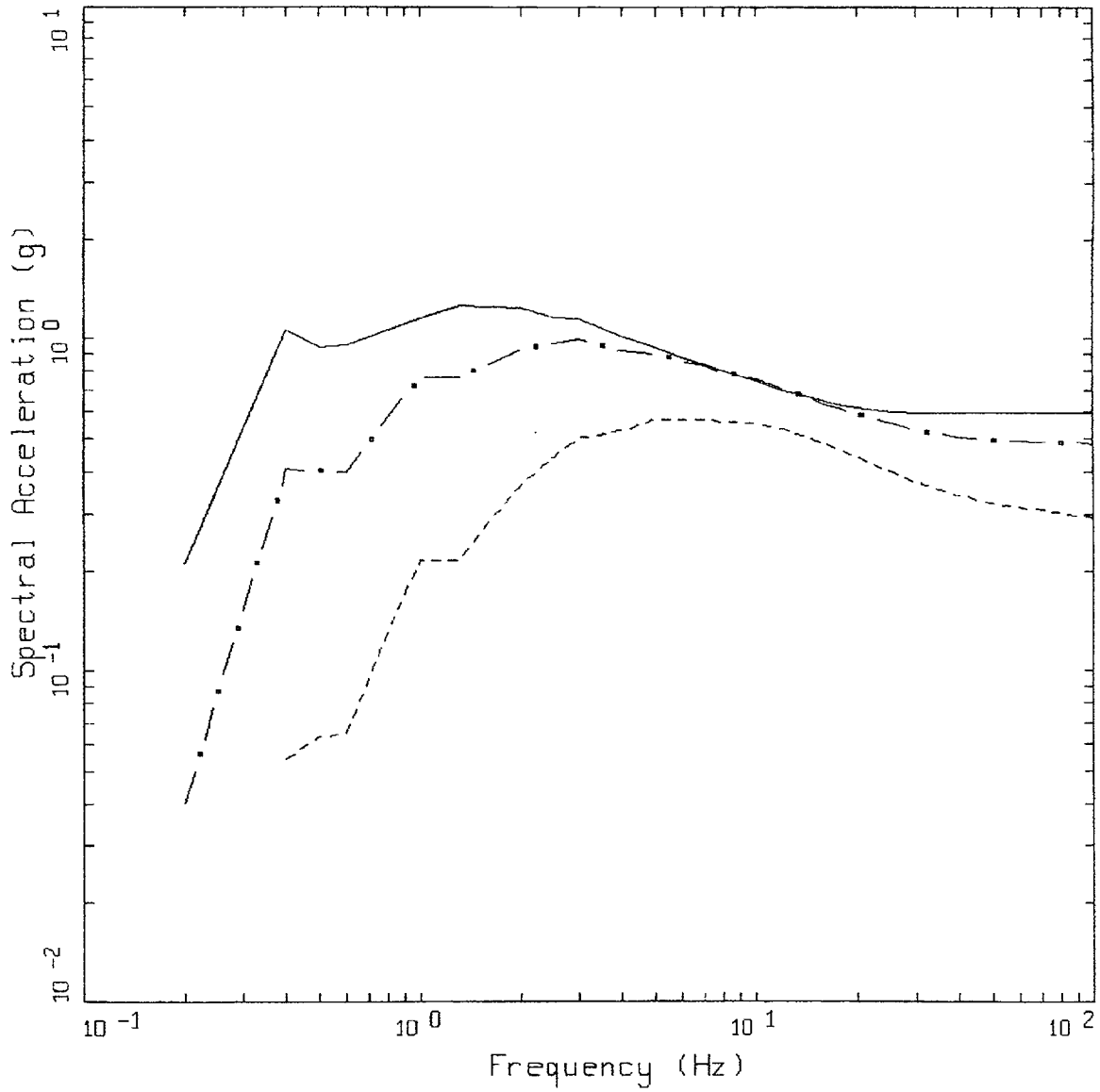
Figure 6-30. Median response spectra (5% damping) at a distance of 10 km for M 5.5, 6.5, and 7.5 for soil profile Meloland and WUS conditions.



CEUS SOIL, MELOLAND

- LEGEND
- $M=7.5, \text{SIGMA}=0.5046$
 - · - $M=6.5, \text{SIGMA}=0.5046$
 - - - $M=5.5, \text{SIGMA}=0.5046$
 - · · $M=4.5, \text{SIGMA}=0.5046$

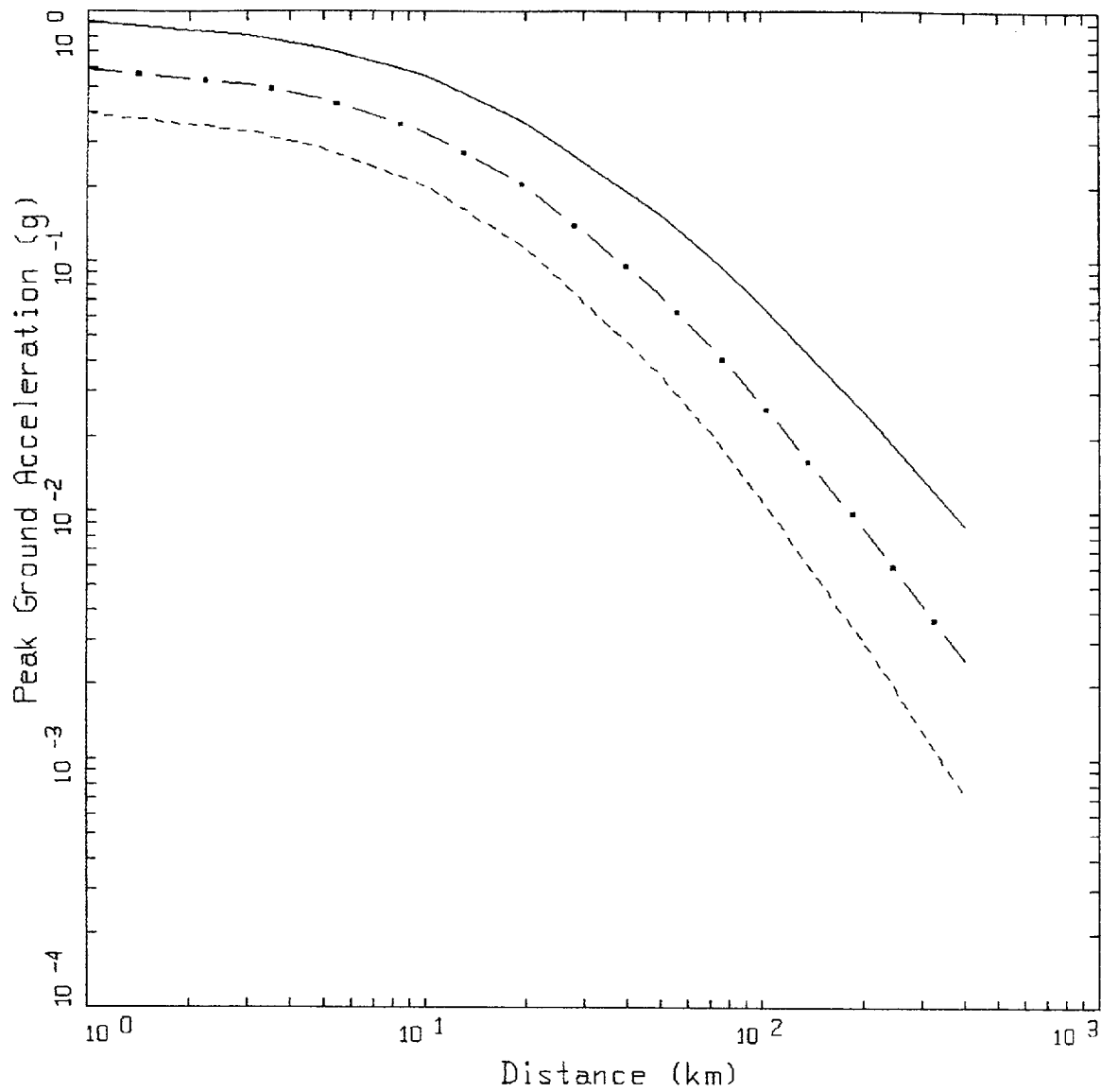
Figure 6-31. Attenuation of median peak horizontal acceleration at M 5.5, 6.5, and 7.5 for soil profile Meloland and CEUS conditions.



CEUS SOIL, MELOLAND
 DISTANCE = 10 KM

LEGEND
 — M=7.5
 - · - M=6.5
 - - - M=5.5

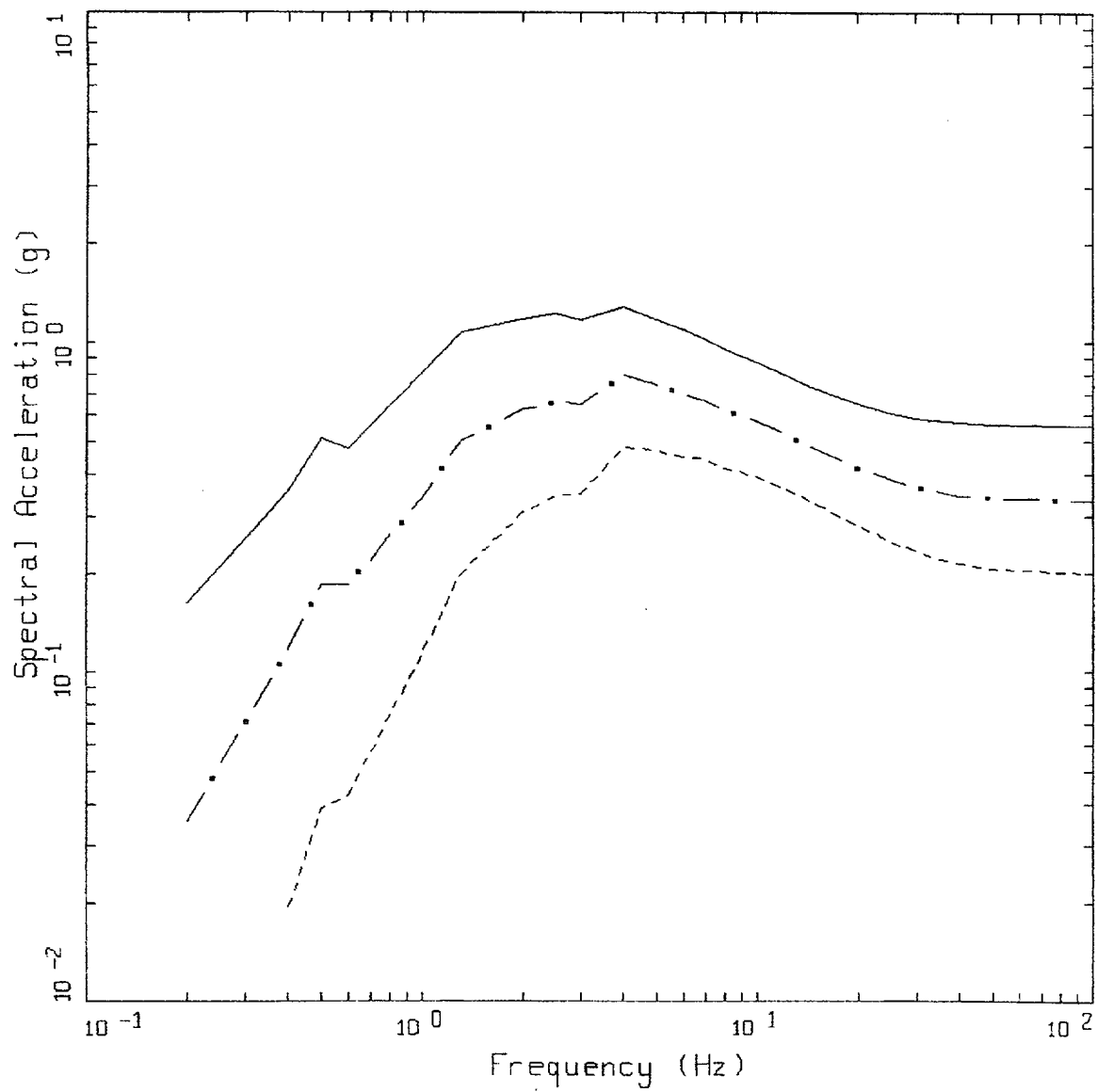
Figure 6-32. Median response spectra (5% damping) at a distance of 10 km for M 5.5, 6.5, and 7.5 for soil profile Meloland and CEUS conditions.



WUS SOIL, RINALDI

- LEGEND
- M=7.5, SIGMA=0.5320
 - · - M=6.5, SIGMA=0.5320
 - - - M=5.5, SIGMA=0.5320

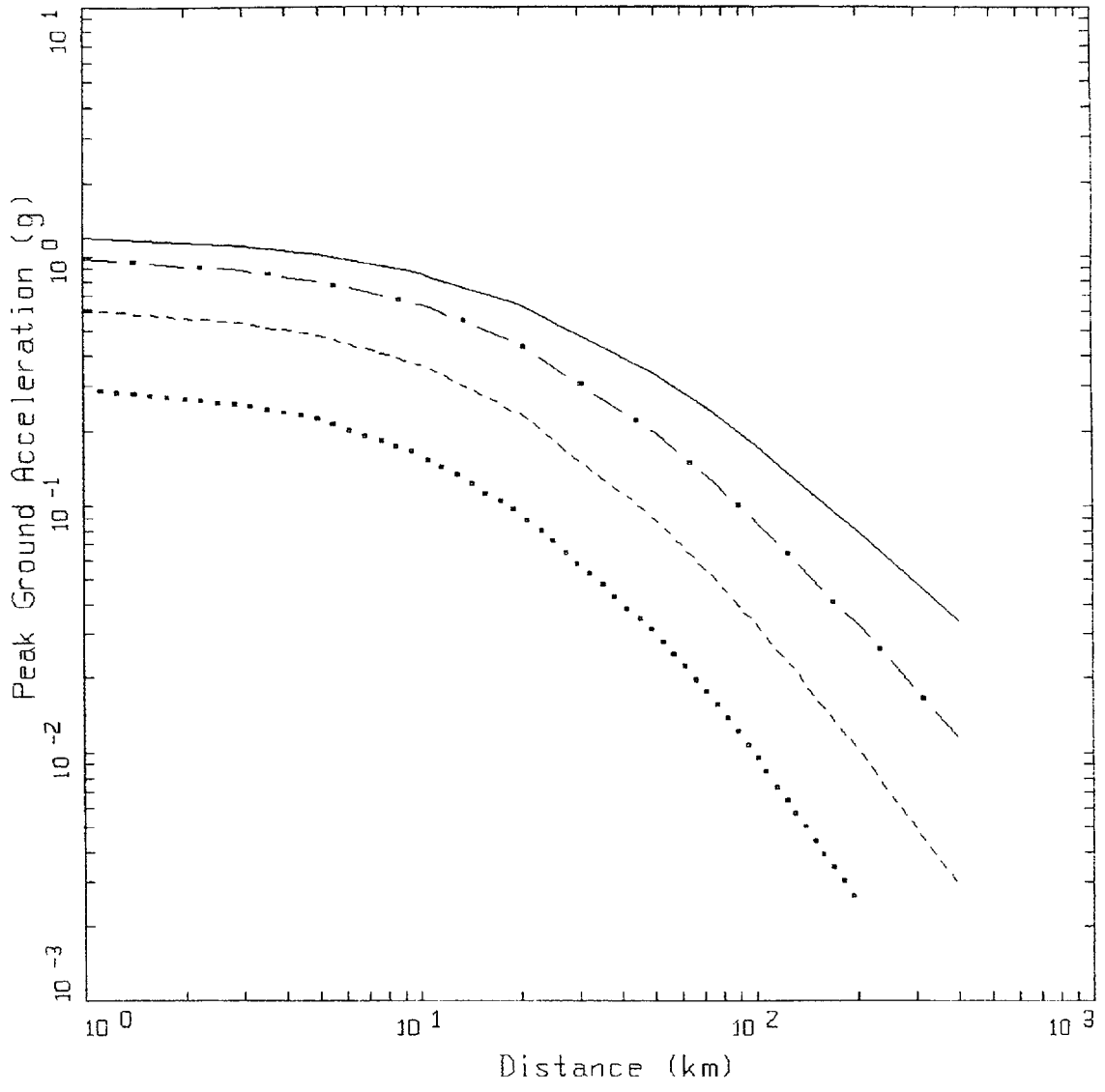
Figure 6-33. Attenuation of median peak horizontal acceleration at M 5.5, 6.5, and 7.5 for soil profile Rinaldi and WUS conditions.



WUS SOIL, RINALDI
 DISTANCE=10 KM

LEGEND
 — M=7.5
 - · - M=6.5
 - - - M=5.5

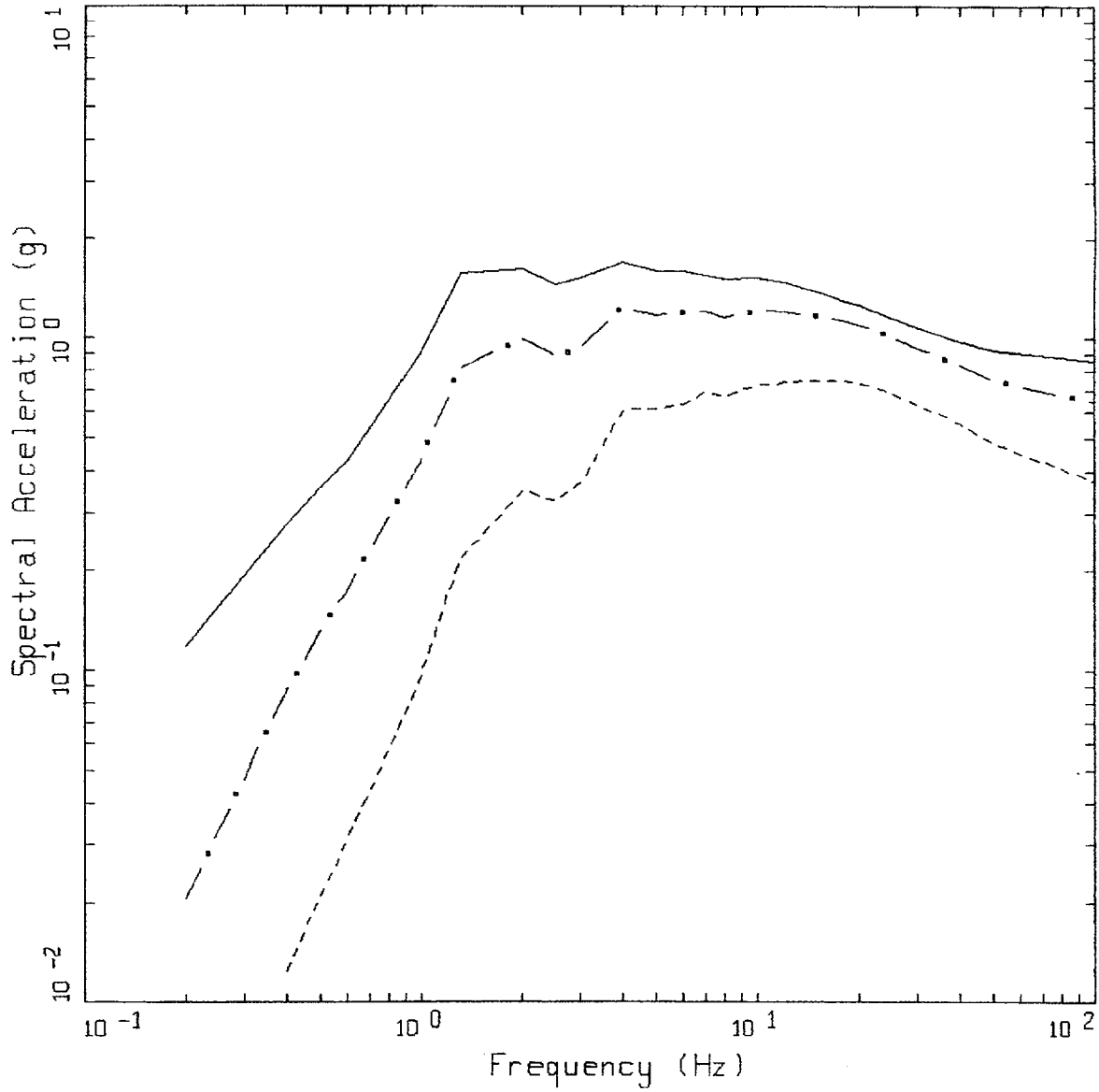
Figure 6-34. Median response spectra (5% damping) at a distance of 10 km for M 5.5, 6.5, and 7.5 for soil response Rinaldi and WUS conditions.



CEUS SOIL, RINALDI

- LEGEND
- M=7.5, SIGMA=0.5461
 - . - M=6.5, SIGMA=0.5461
 - - - M=5.5, SIGMA=0.5461
 - M=4.5, SIGMA=0.5461

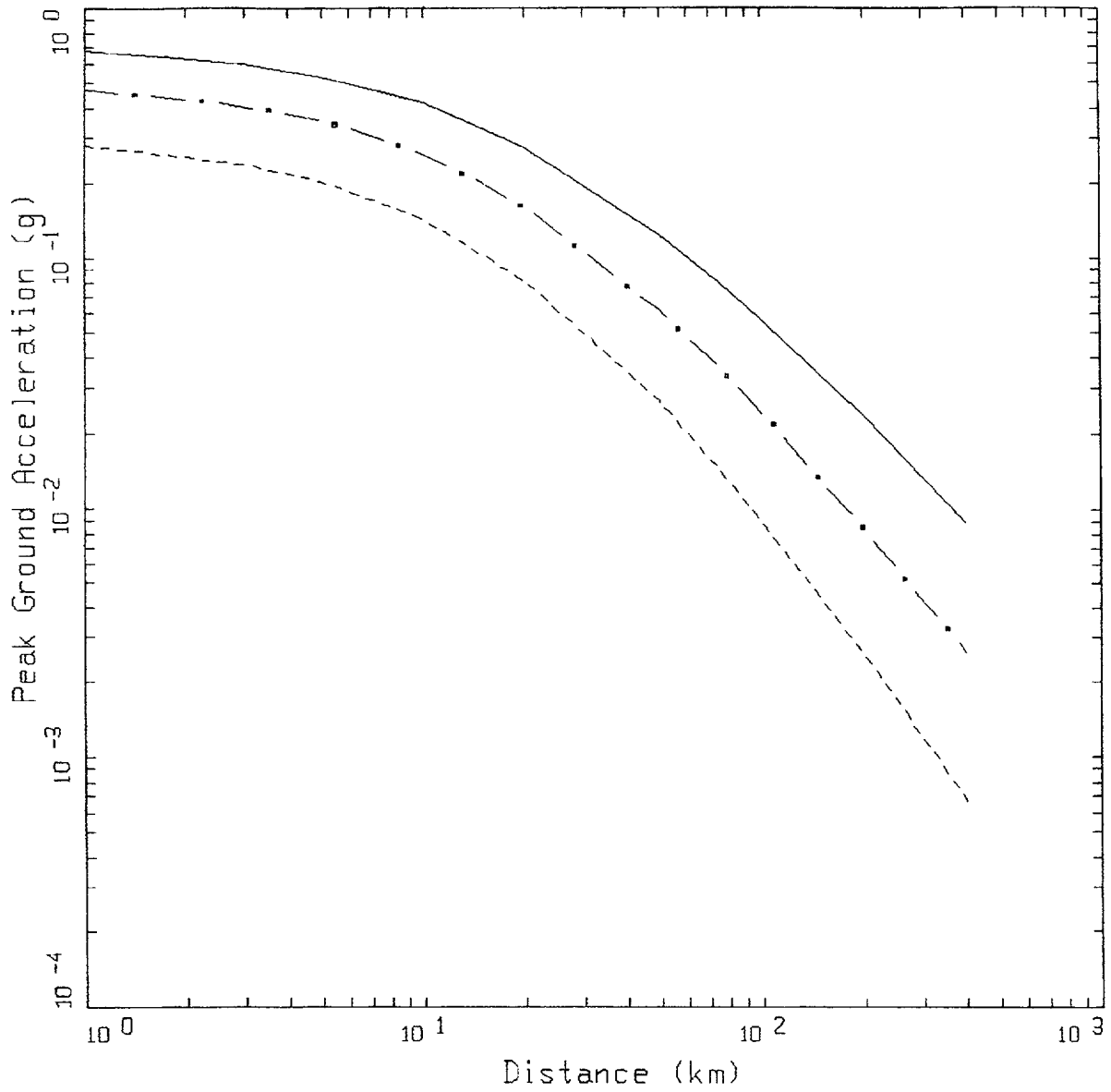
Figure 6-35. Attenuation of median peak horizontal acceleration at M 5.5, 6.5, and 7.5 for soil profile Rinaldi and CEUS conditions.



CEUS SOIL, RINALDI
DISTANCE=10 KM

LEGEND
 — M=7.5
 - · - M=6.5
 - - - M=5.5

Figure 6-36. Median response spectra (5% damping) at a distance of 10 km for M 5.5, 6.5, and 7.5 for soil profile Rinaldi and CEUS conditions.



WUS SOIL, GENERIC SRS

- LEGEND
- M=7.5, SIGMA=0.4732
 - ■ - M=6.5, SIGMA=0.4732
 - - - M=5.5, SIGMA=0.4732

Figure 6-37. Attenuation of median peak horizontal acceleration at M 5.5, 6.5, and 7.5 for soil profile Savannah River Generic and WUS conditions.

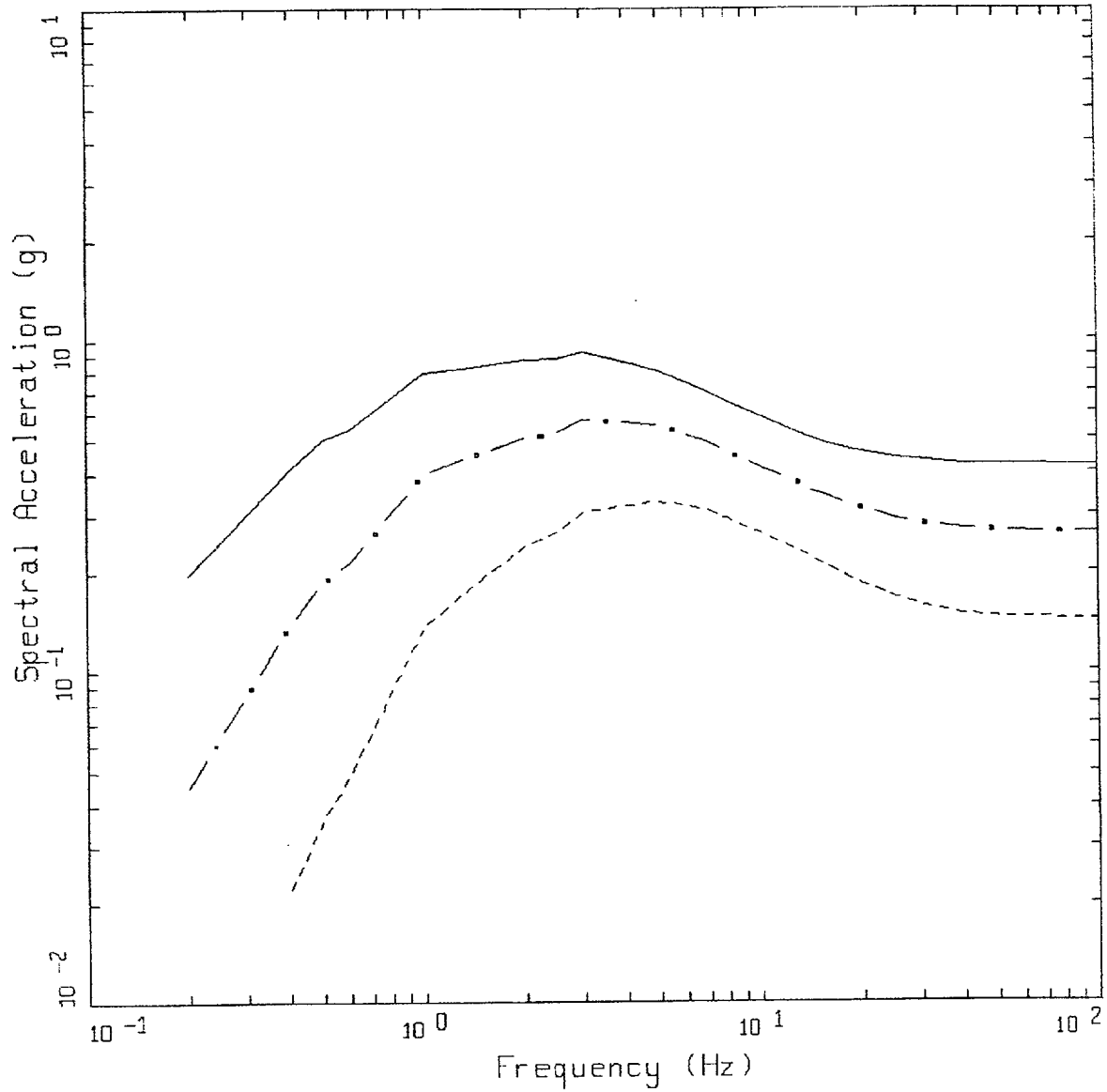
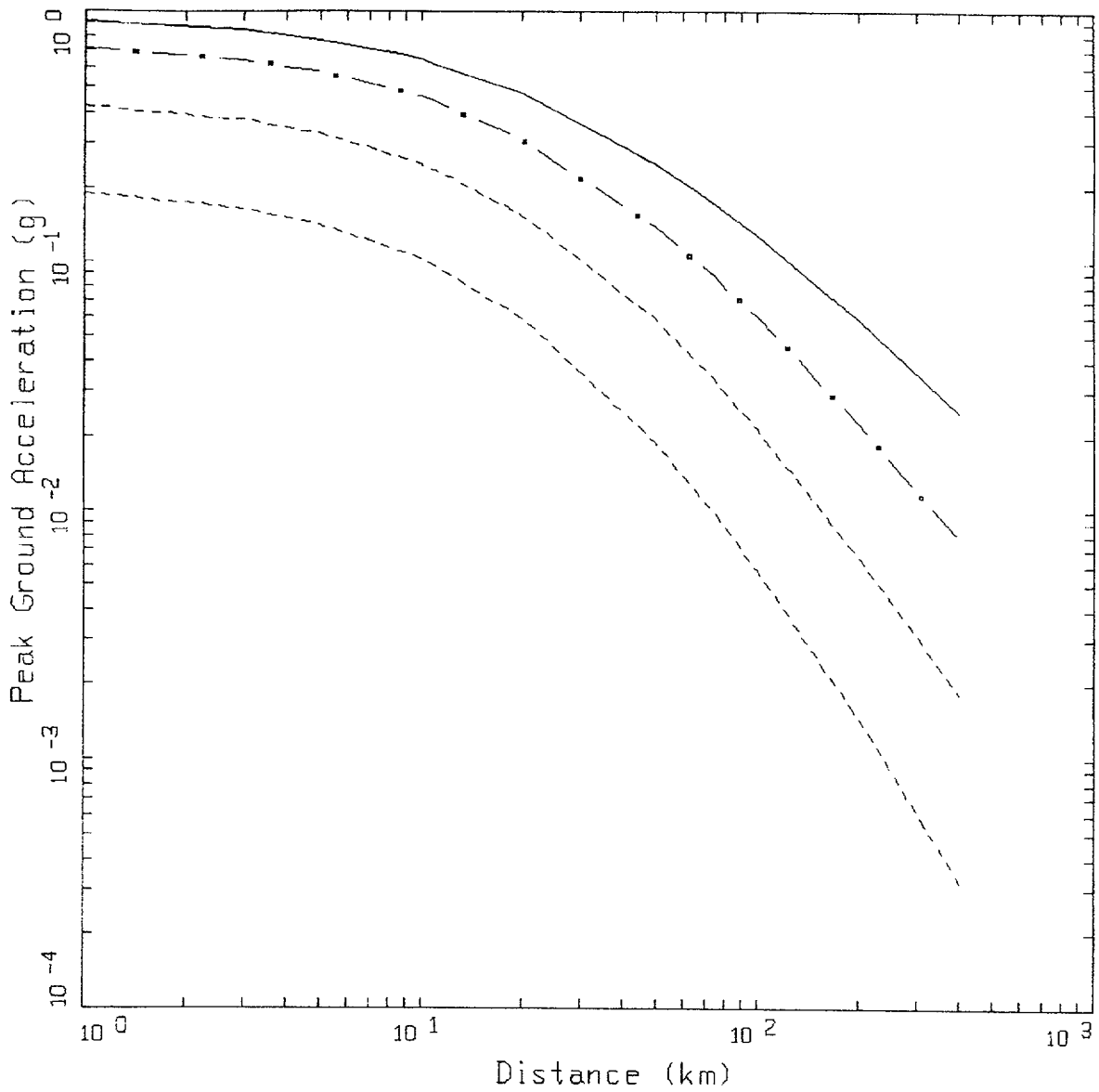


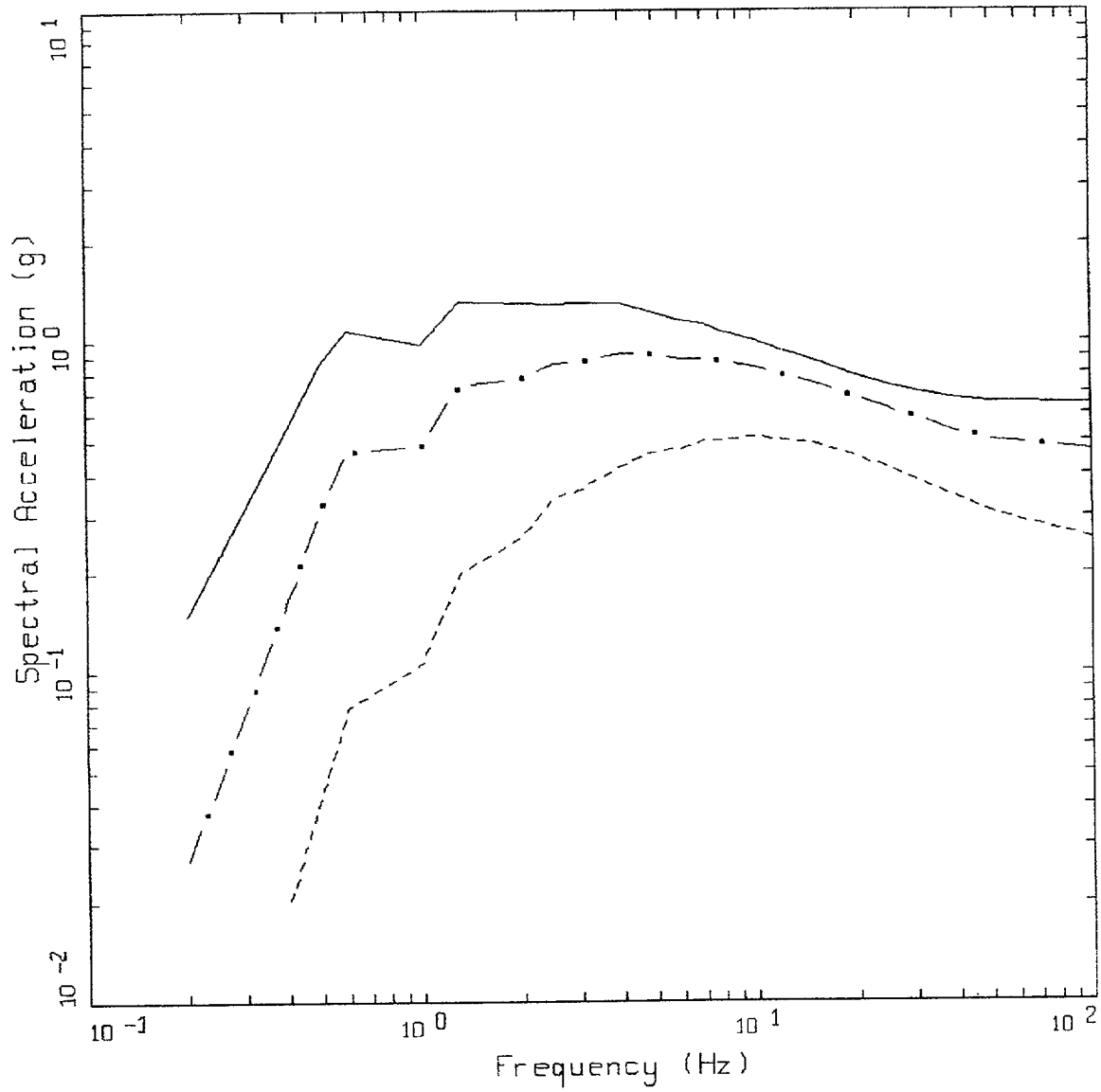
Figure 6-38. Median response spectra (5% damping) at a distance of 10 km for **M** 5.5, 6.5, and 7.5 for soil profile Savannah River Generic and WUS conditions.



CEUS SOIL, GENERIC SRS

- LEGEND
- M=7.5, SIGMA=0.5706
 - · — M=6.5, SIGMA=0.5706
 - M=5.5, SIGMA=0.5706
 - M=4.5, SIGMA=0.5706

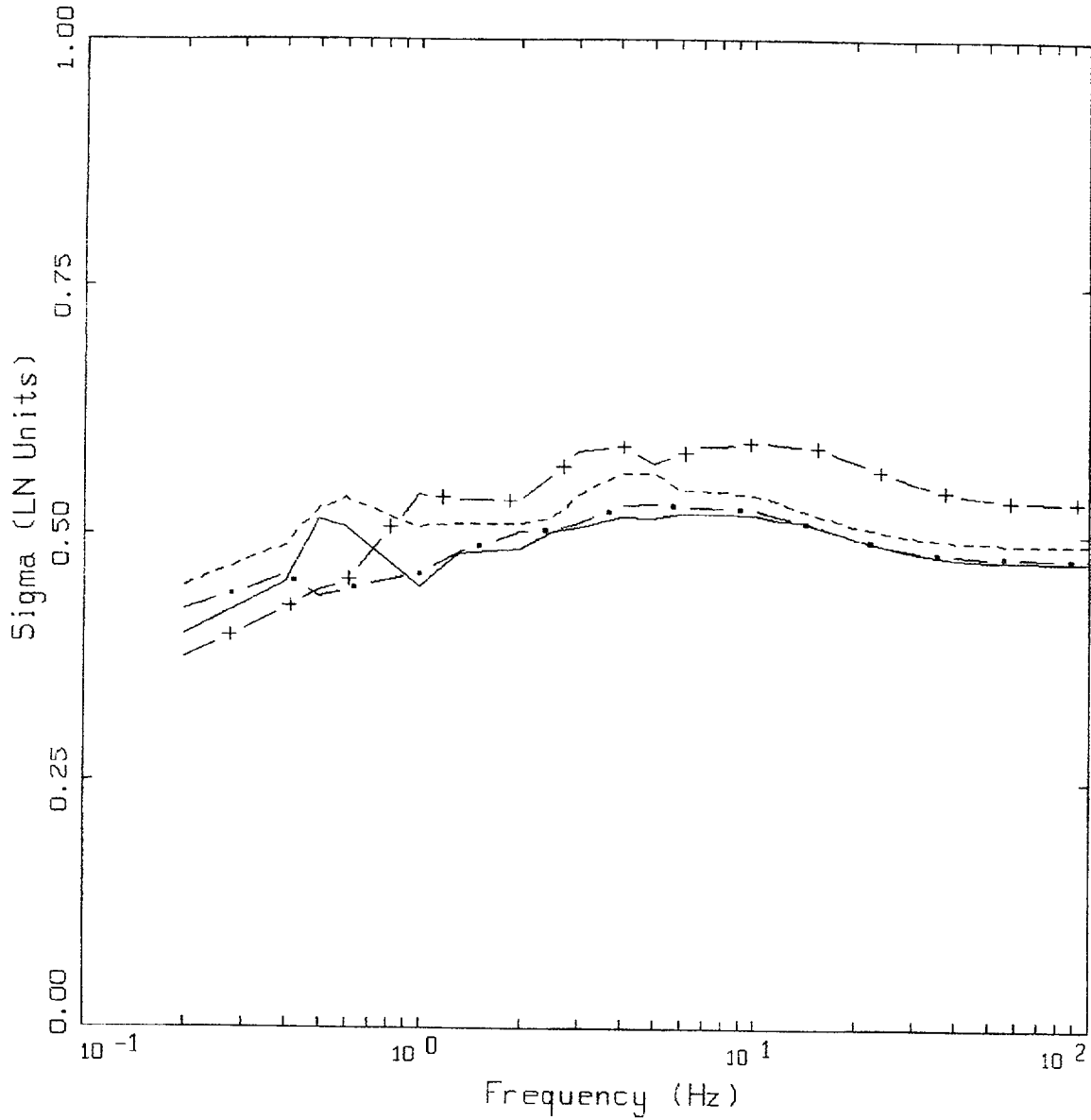
Figure 6-39. Attenuation of median peak horizontal acceleration at M 5.5, 6.5, and 7.5 for soil profile Savannah River Generic and CEUS conditions.



CEUS SOIL, GENERIC SRS
 DISTANCE=10 KM

LEGEND
 ————— M=7.5
 - · - · - M=6.5
 - - - - - M=5.5

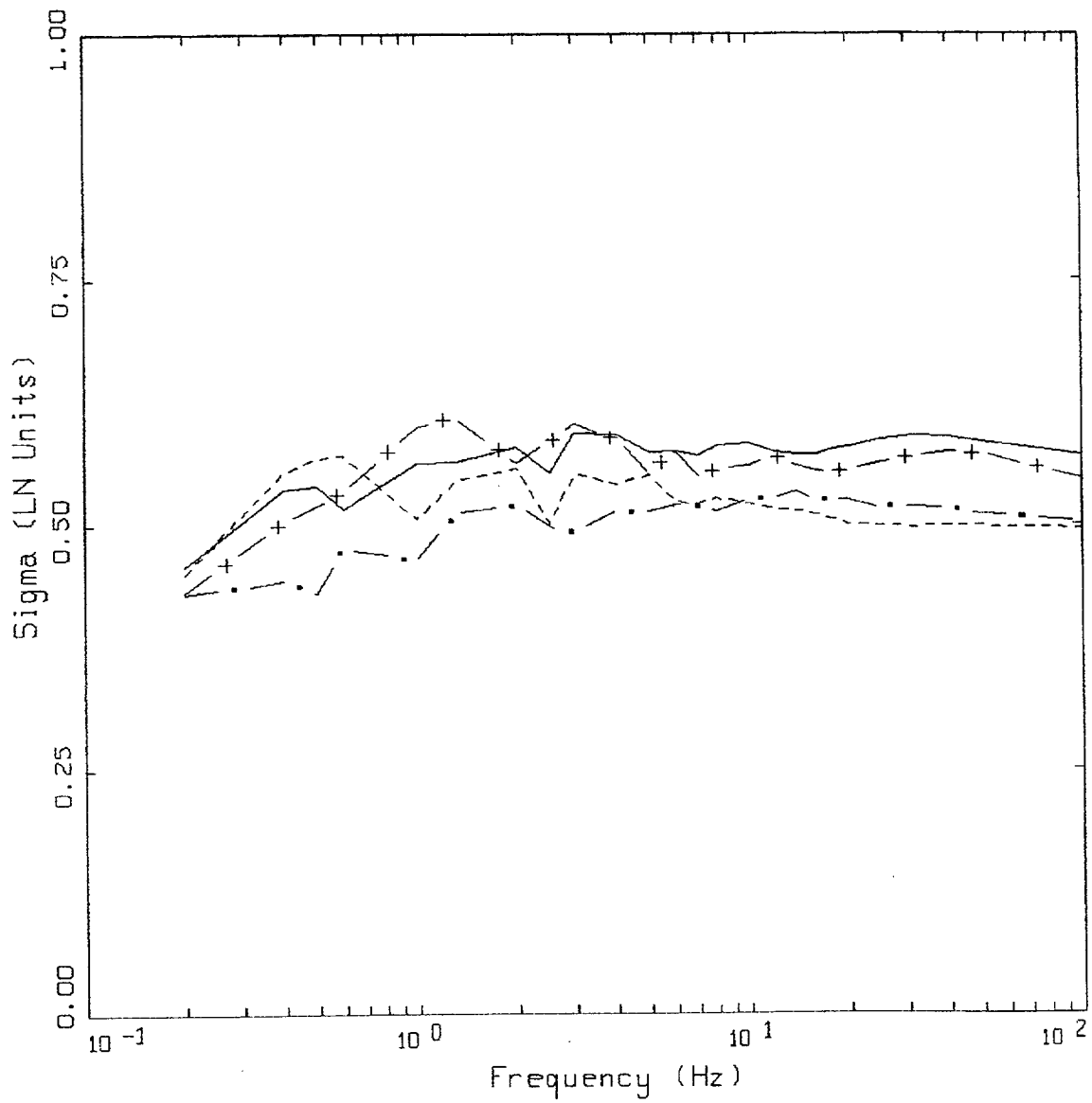
Figure 6-40. Median response spectra (5% damping) at a distance of 10 km for M 5.5, 6.5, and 7.5 for soil profile Savannah River Generic and CEUS conditions.



VARIABILITY, WUS SOIL

- LEGEND
- WUS SOIL (GILROY#2) SIGMA
 - . - WUS SOIL (MELOLAND) SIGMA
 - + - WUS SOIL (RINALDI) SIGMA
 - WUS SOIL (GENERIC SRS) SIGMA

Figure 6-41. Variability in response spectral ordinates for WUS soil sites resulting from parametric variability and regression fit over all magnitudes and distances (Table 6-2 and 6-3).



VARIABILITY, CEUS SOIL

- LEGEND
- CEUS SOIL (GILROY#2) SIGMA
 - . - CEUS SOIL (MELOLAND) SIGMA
 - + - CEUS SOIL (RINALDI) SIGMA
 - CEUS SOIL (GENERIC SRS) SIGMA

Figure 6-42. Variability in response spectral ordinates for CEUS soil sites resulting from parametric variability and regression fit over all magnitudes and distances (Tables 6-2 and 6-3).

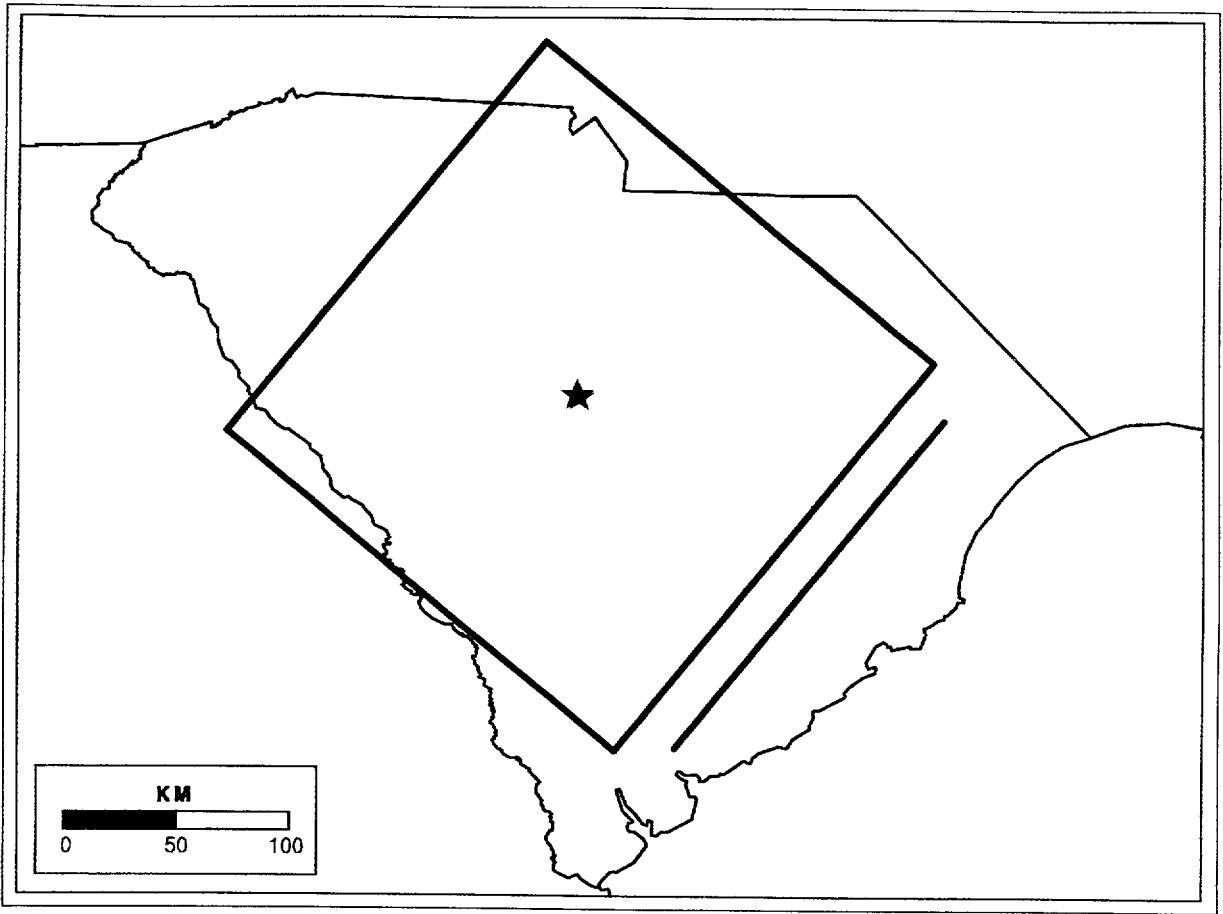


Figure 6-43. Configuration of background source and Charleston fault affecting CEUS example site (Columbia, South Carolina).

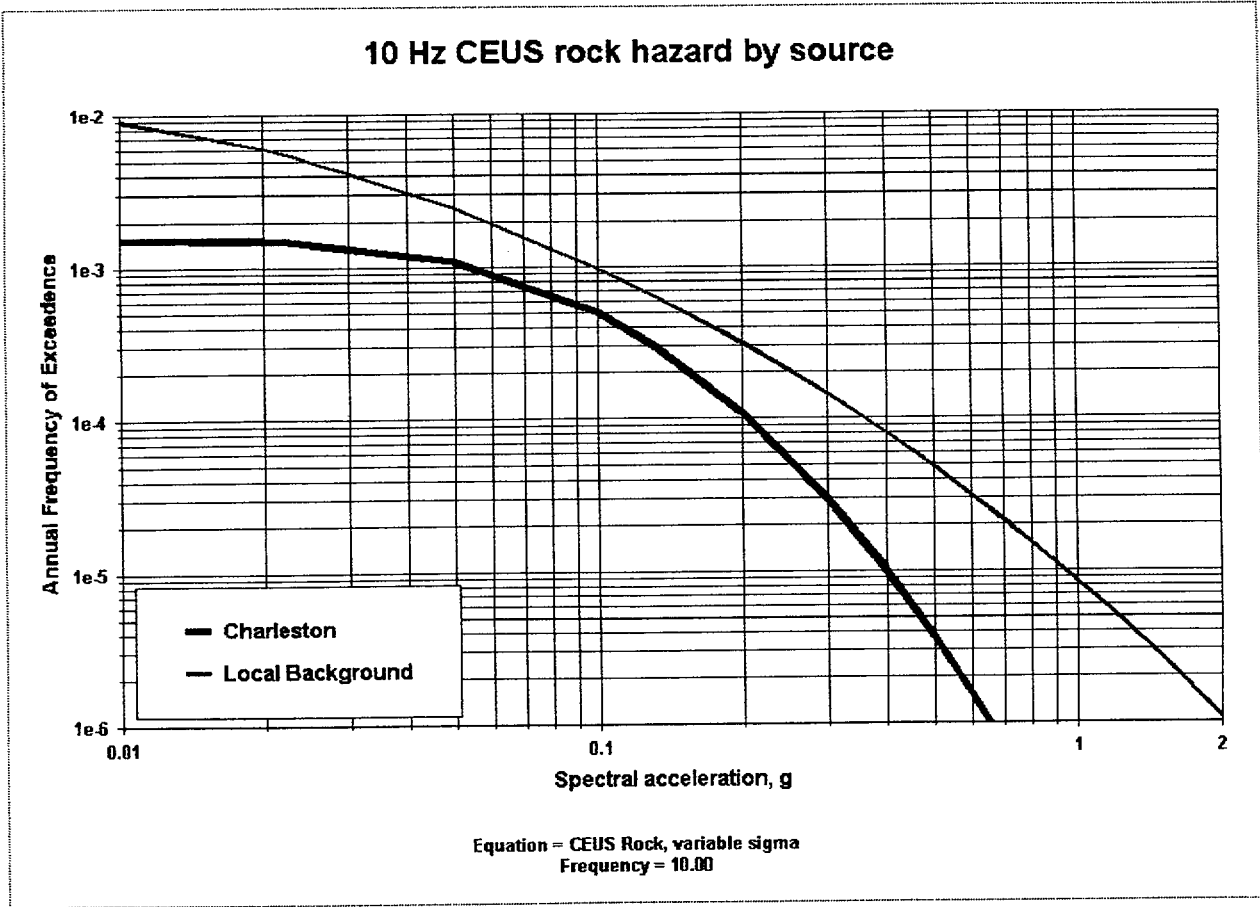


Figure 6-44. Contribution to seismic hazard by source for 10 Hz spectral acceleration, Columbia site.

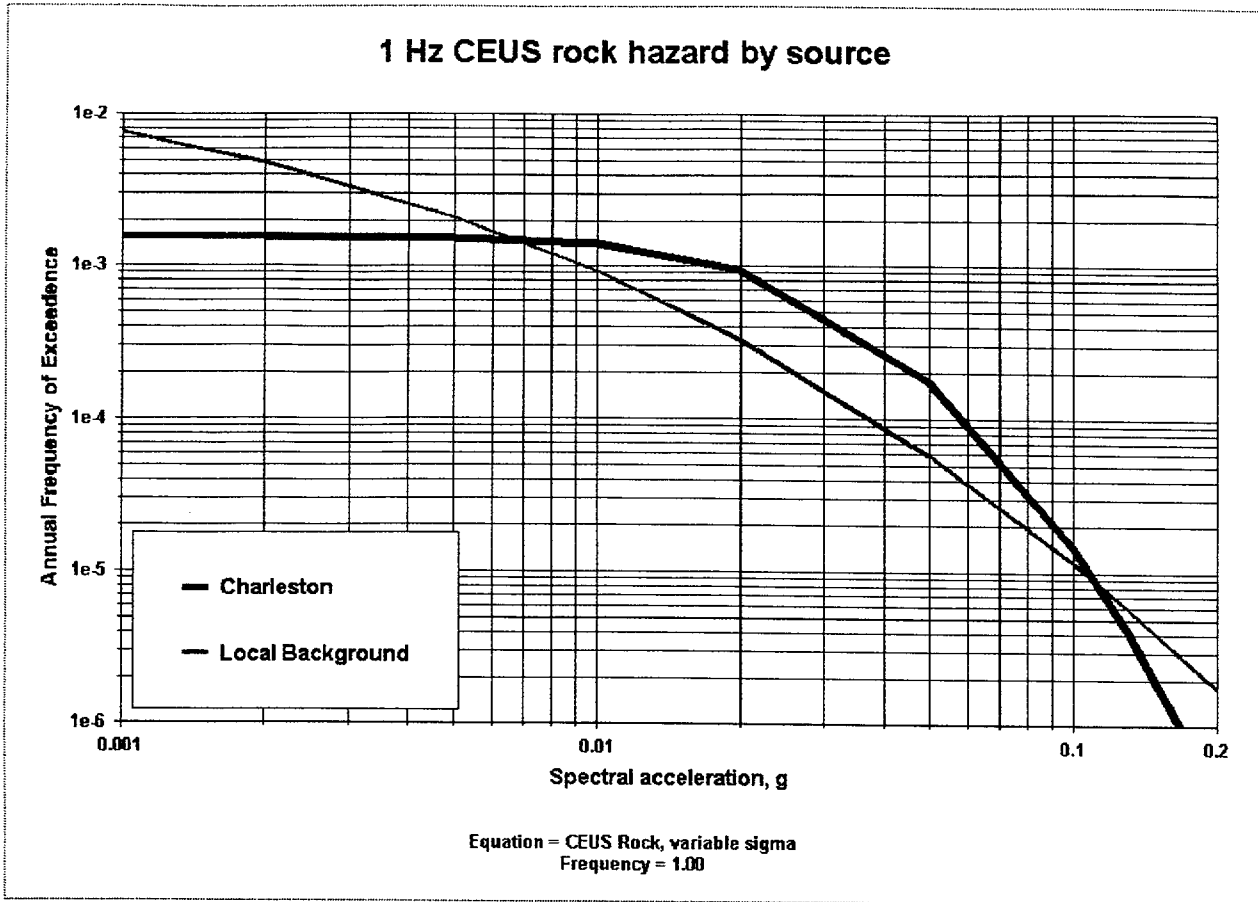


Figure 6-45. Contribution to seismic hazard by source for 1 Hz spectral acceleration, Columbia site.

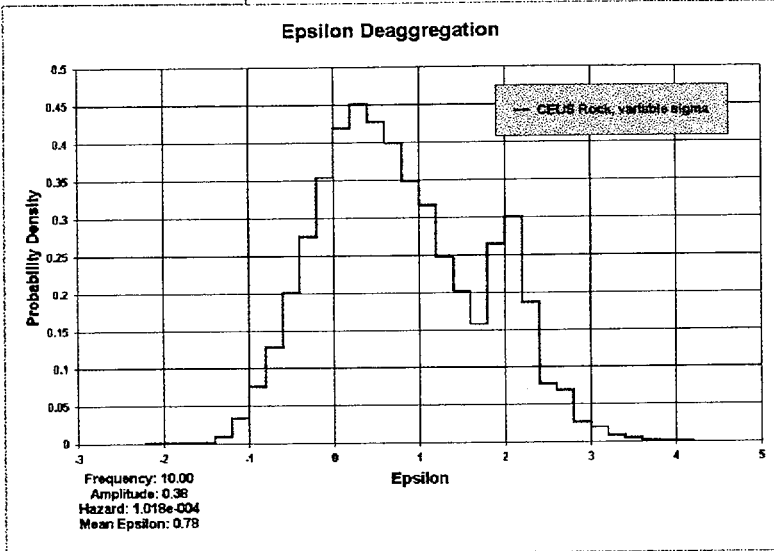
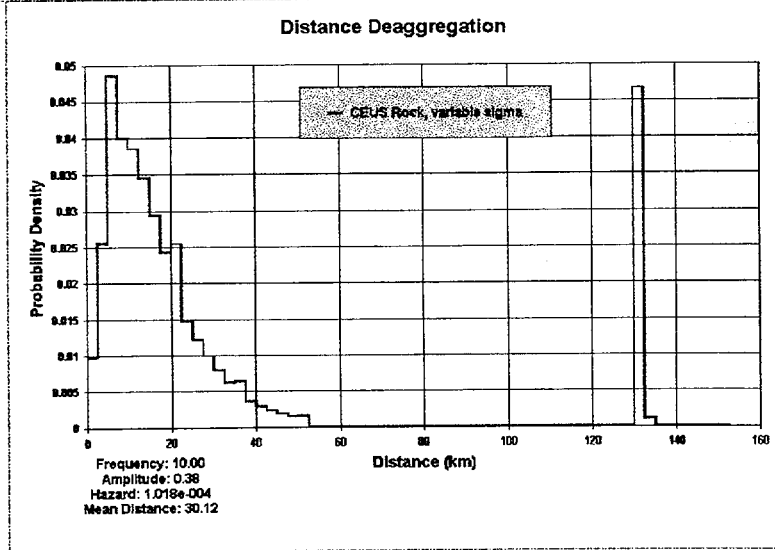
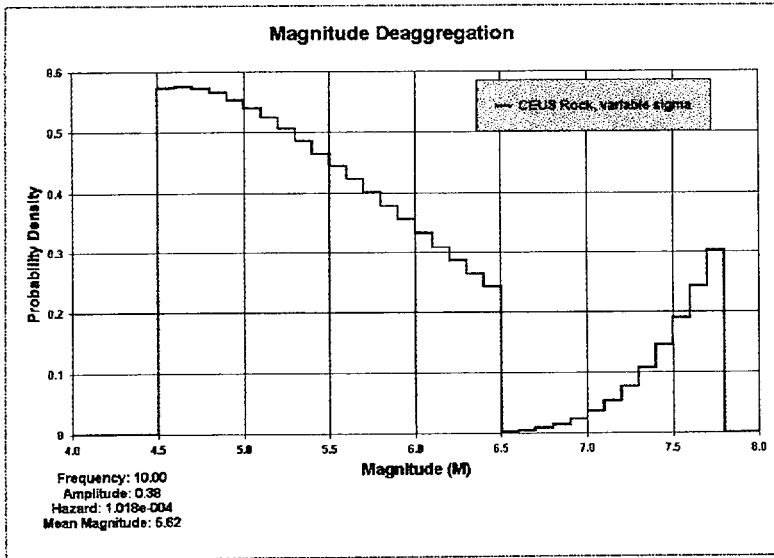


Figure 6-46. Deaggregation of seismic hazard by M, R, and a for 10 Hz SA at 0.38g, Columbia site.

CEUS 10 Hz magnitude-distance deaggregation

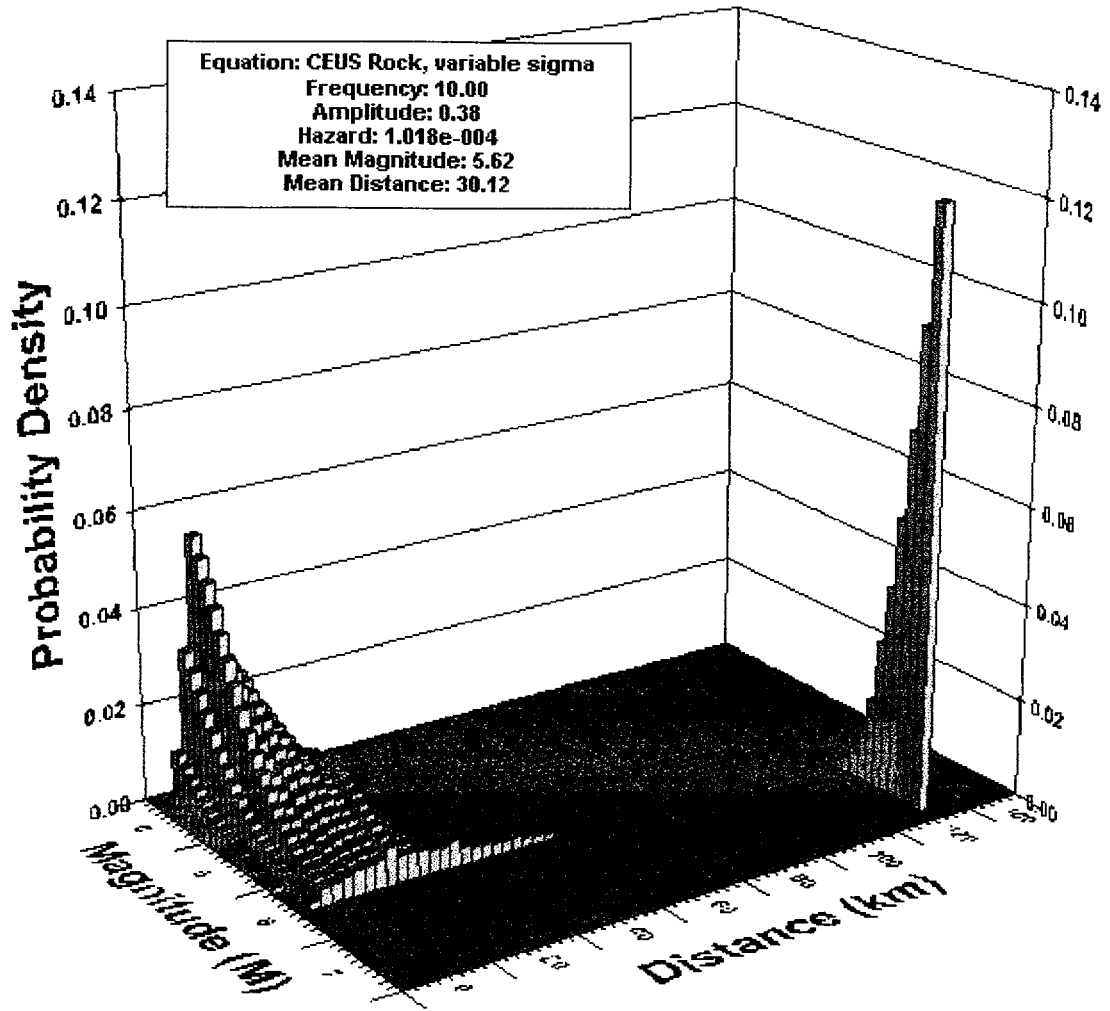


Figure 6-47. Deaggregation of seismic hazard by M and R for 10 Hz SA at 0.38g, Columbia site.

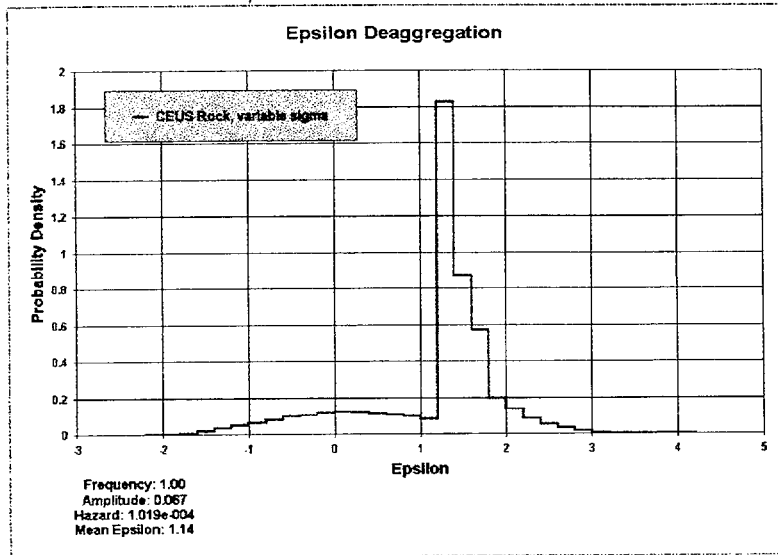
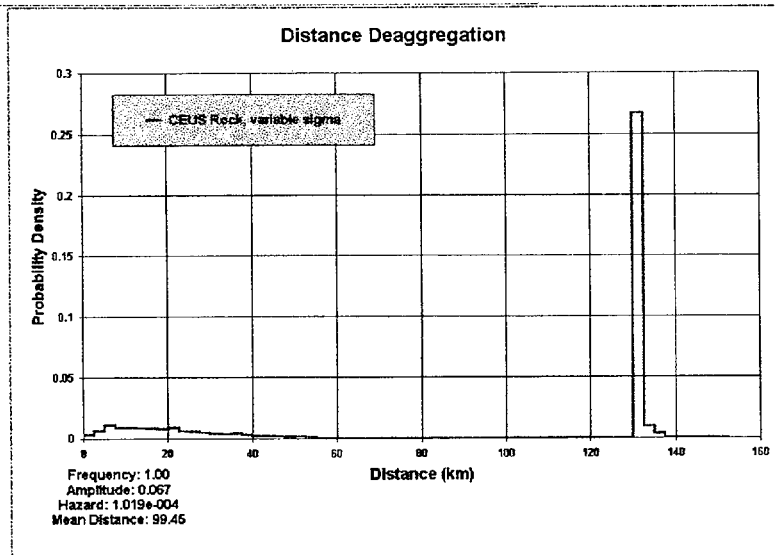
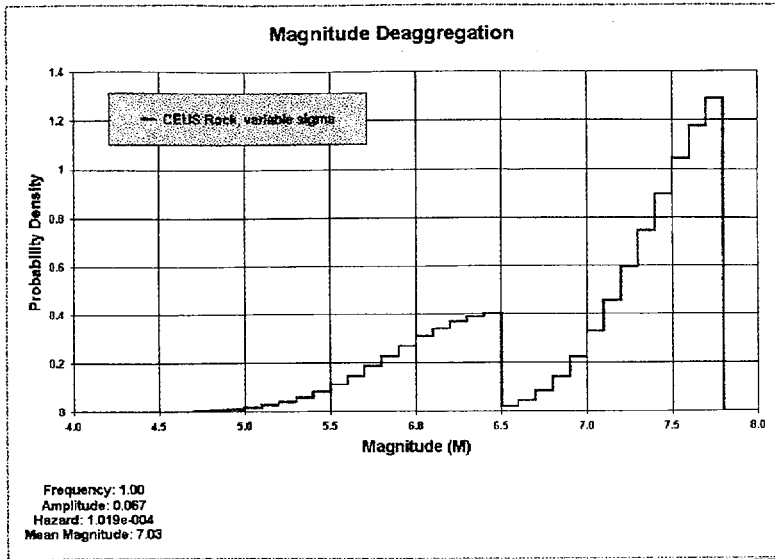


Figure 6-48: Deaggregation of seismic hazard by M, R, and a for 1 Hz SA at 0.067g, Columbia site.

CEUS 1 Hz magnitude-distance deaggregation

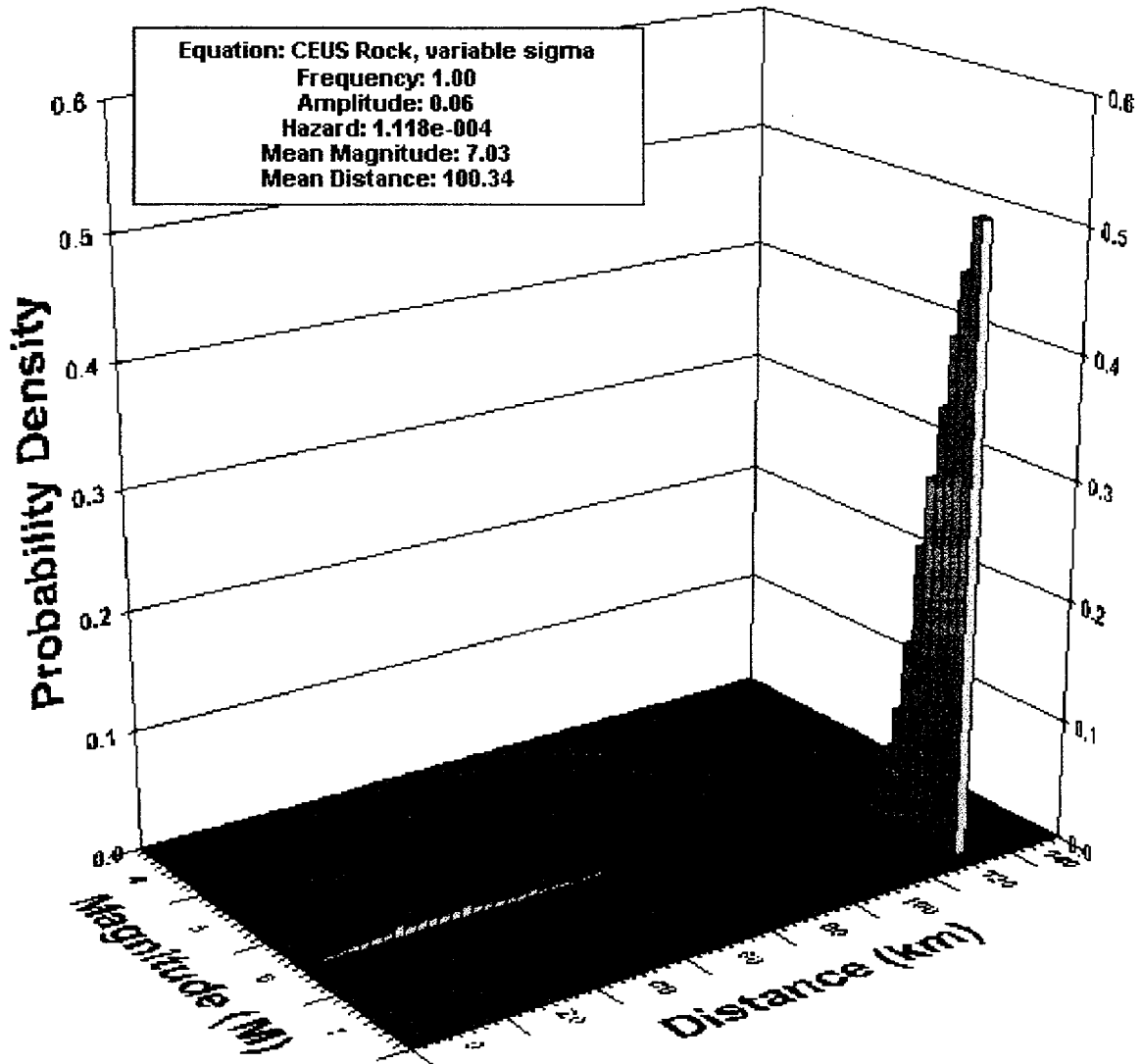


Figure 6-49. Deaggregation of seismic hazard by M and R for 1 Hz SA at 0.067g, Columbia site.

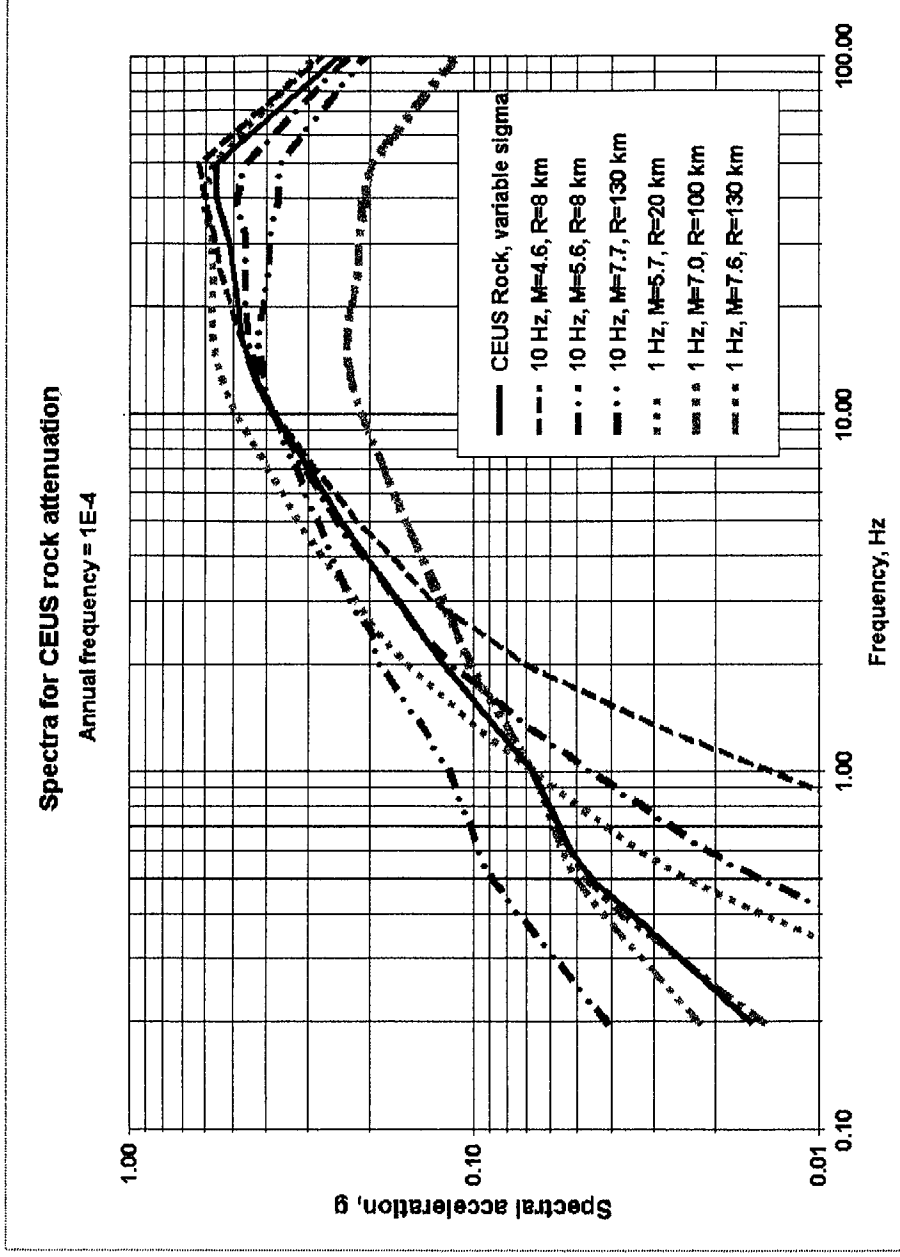
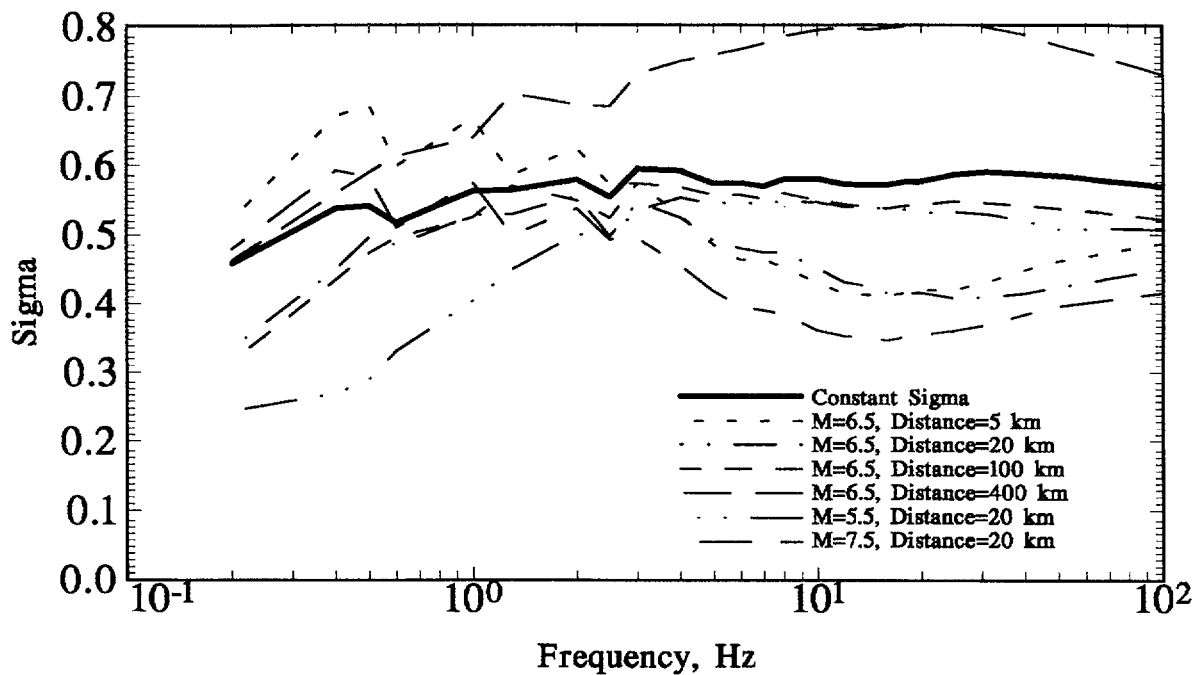


Figure 6-50. 10^{-4} UHS for rock, Columbia site, with spectra from deaggregation earthquakes.

Standard deviation of $\ln(SA)$, Savannah profile in CEUS



Standard deviation of $\ln(SA)$, Savannah profile in WUS

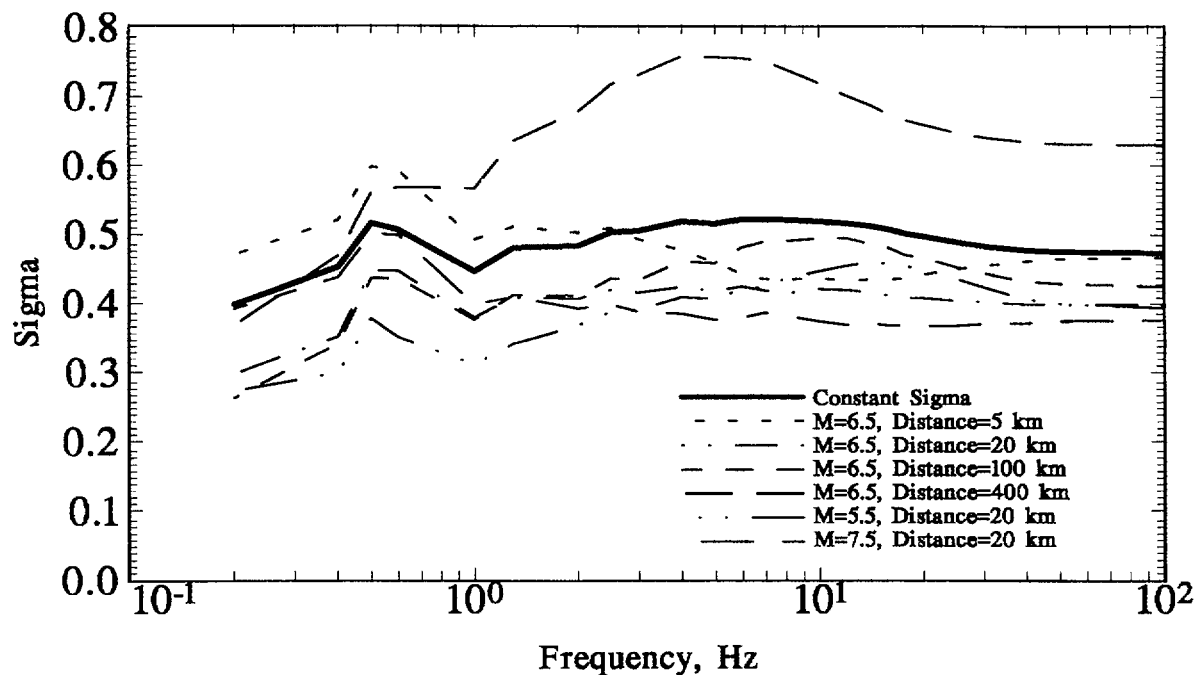


Figure 6-51. Variable σ and constant σ vs. frequency for Savannah profile.

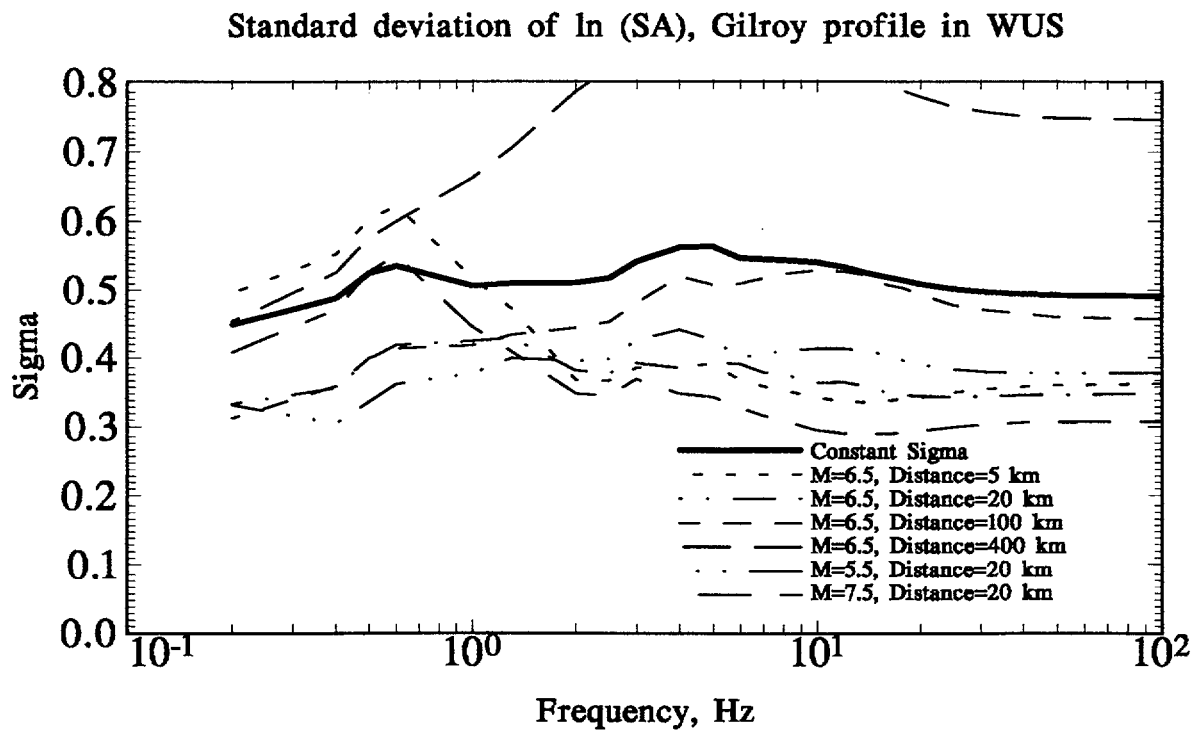
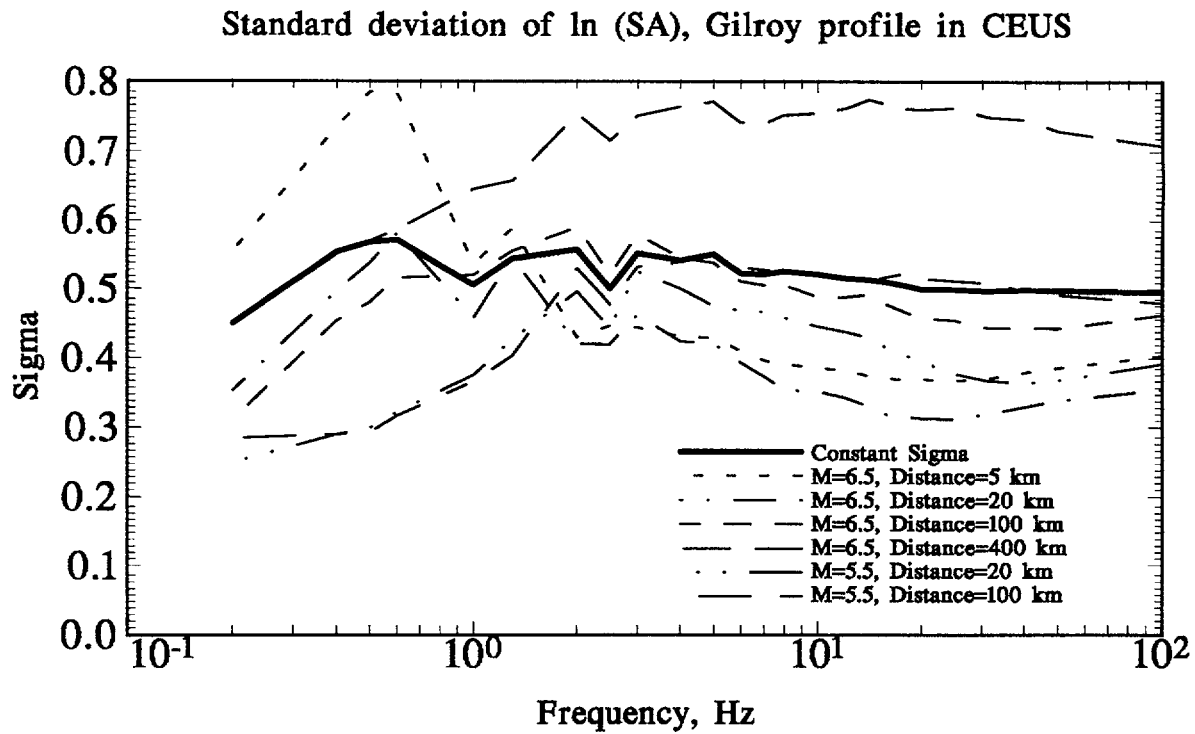
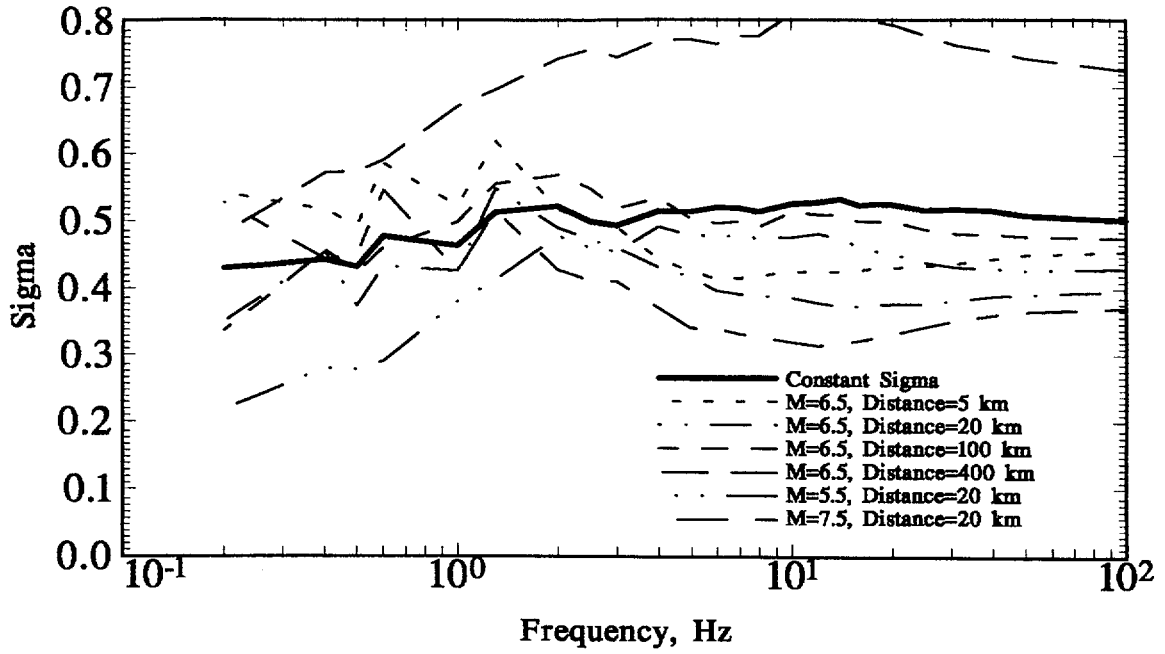


Figure 6-52. Variable σ and constant σ vs. frequency for Gilroy profile.

Standard deviation of $\ln(SA)$, Meloland profile in CEUS



Standard deviation of $\ln(SA)$, Meloland profile in WUS

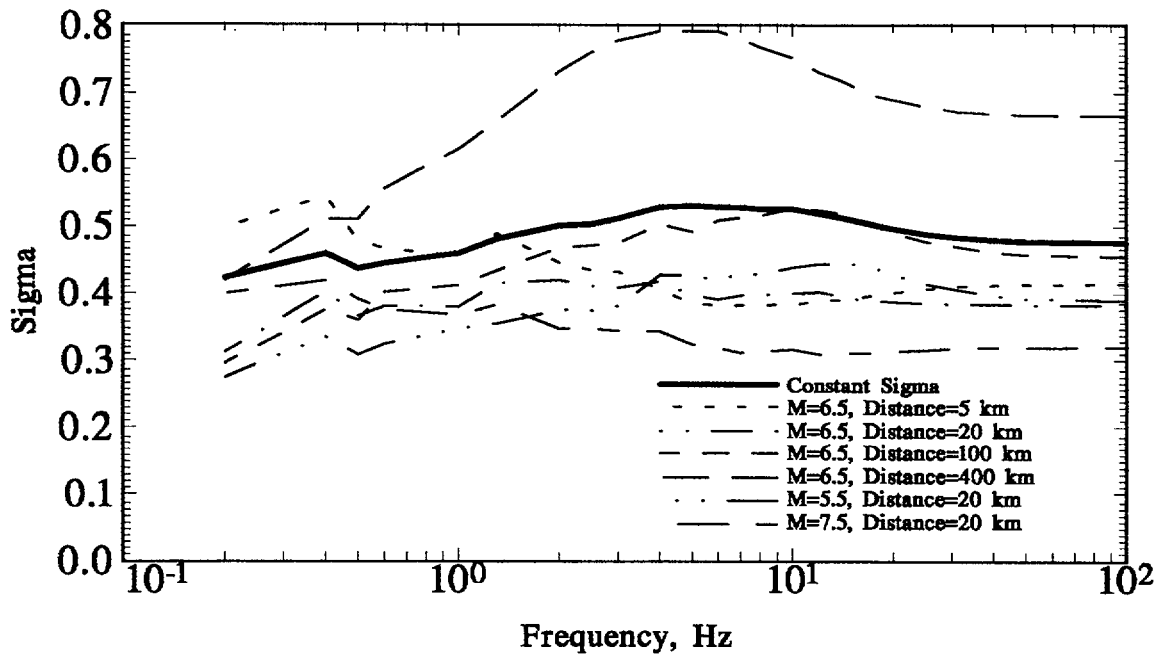
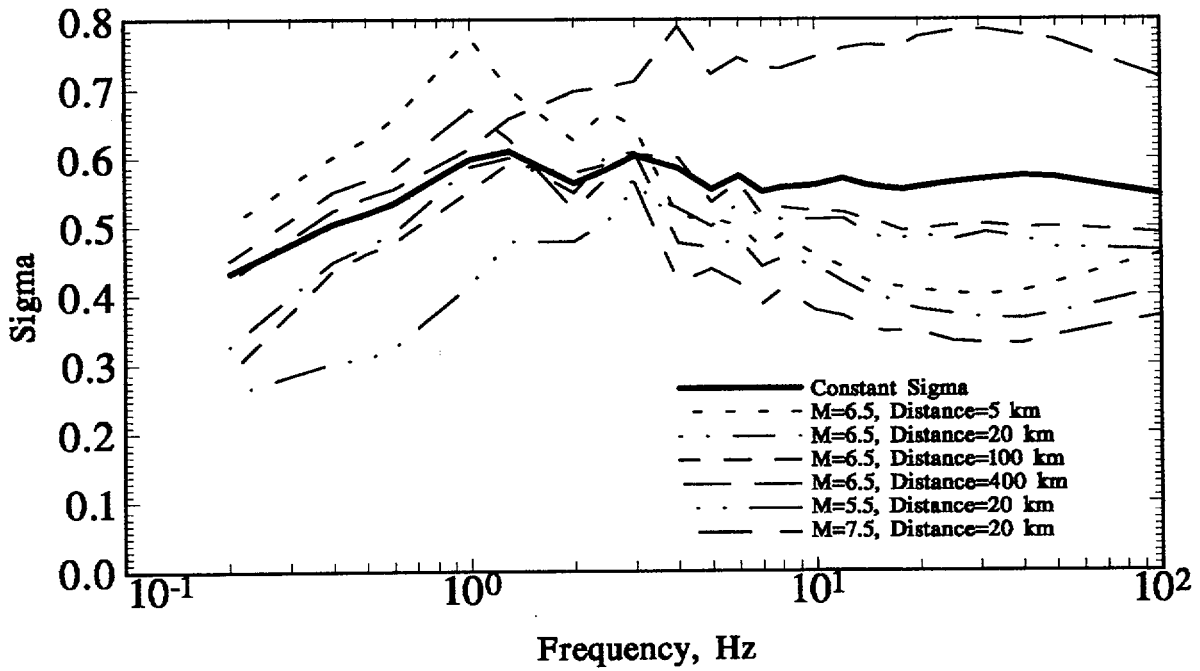


Figure 6-53. Variable σ and constant σ vs. frequency for Meloland profile.

Standard deviation of $\ln(SA)$, Rinaldi profile in CEUS



Standard deviation of $\ln(SA)$, Rinaldi profile in WUS

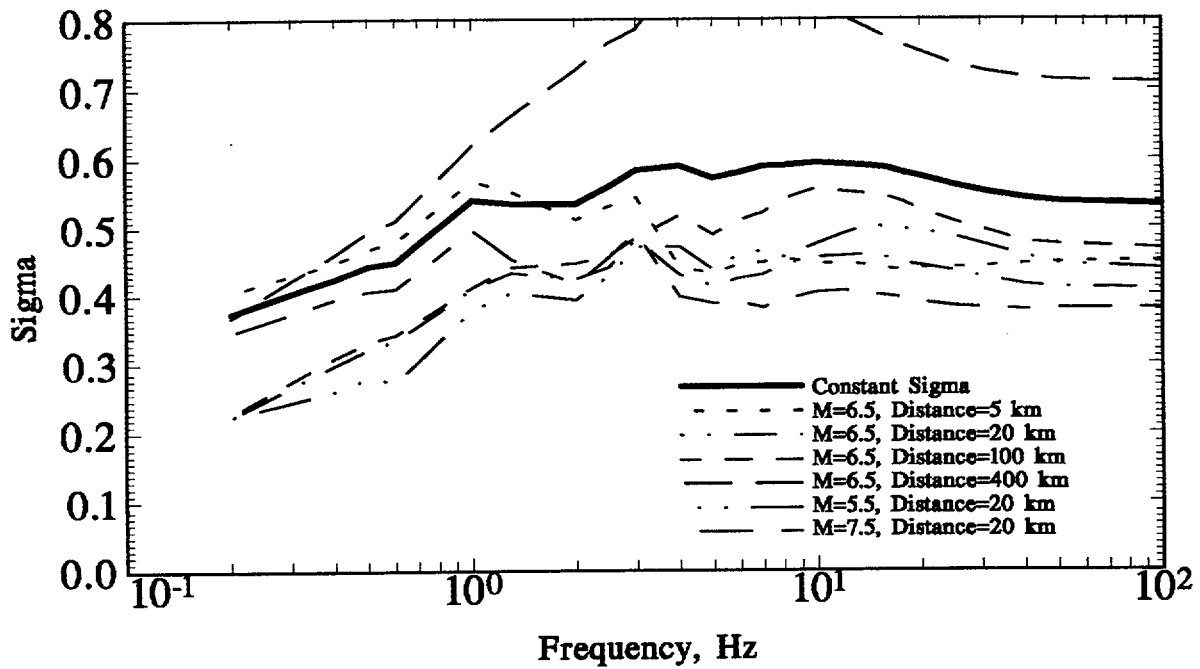


Figure 6-54. Variable σ and constant σ vs. frequency for Rinaldi profile.

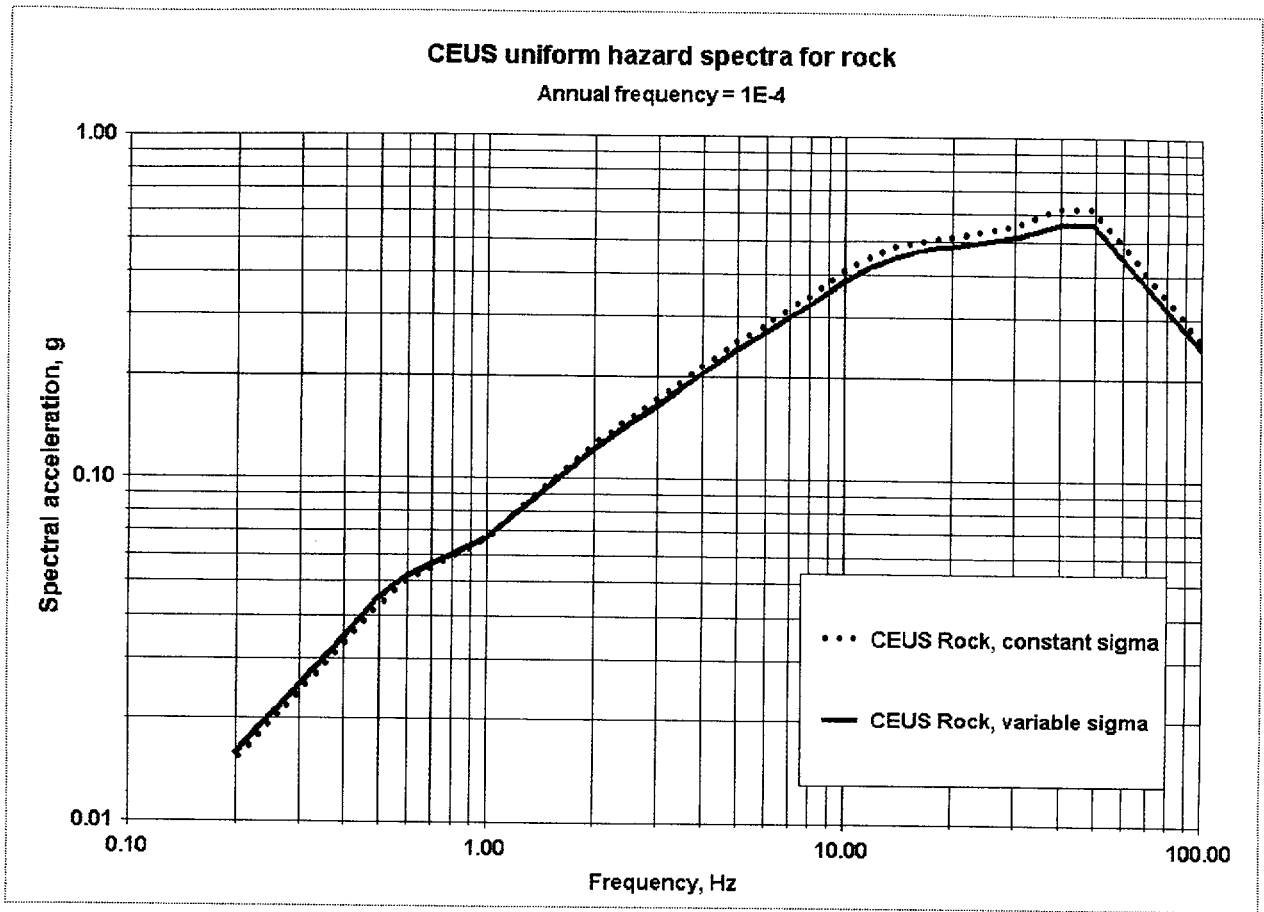


Figure 6-55: 10^{-4} UHS for rock, Columbia site, for constant σ and variable σ assumptions.

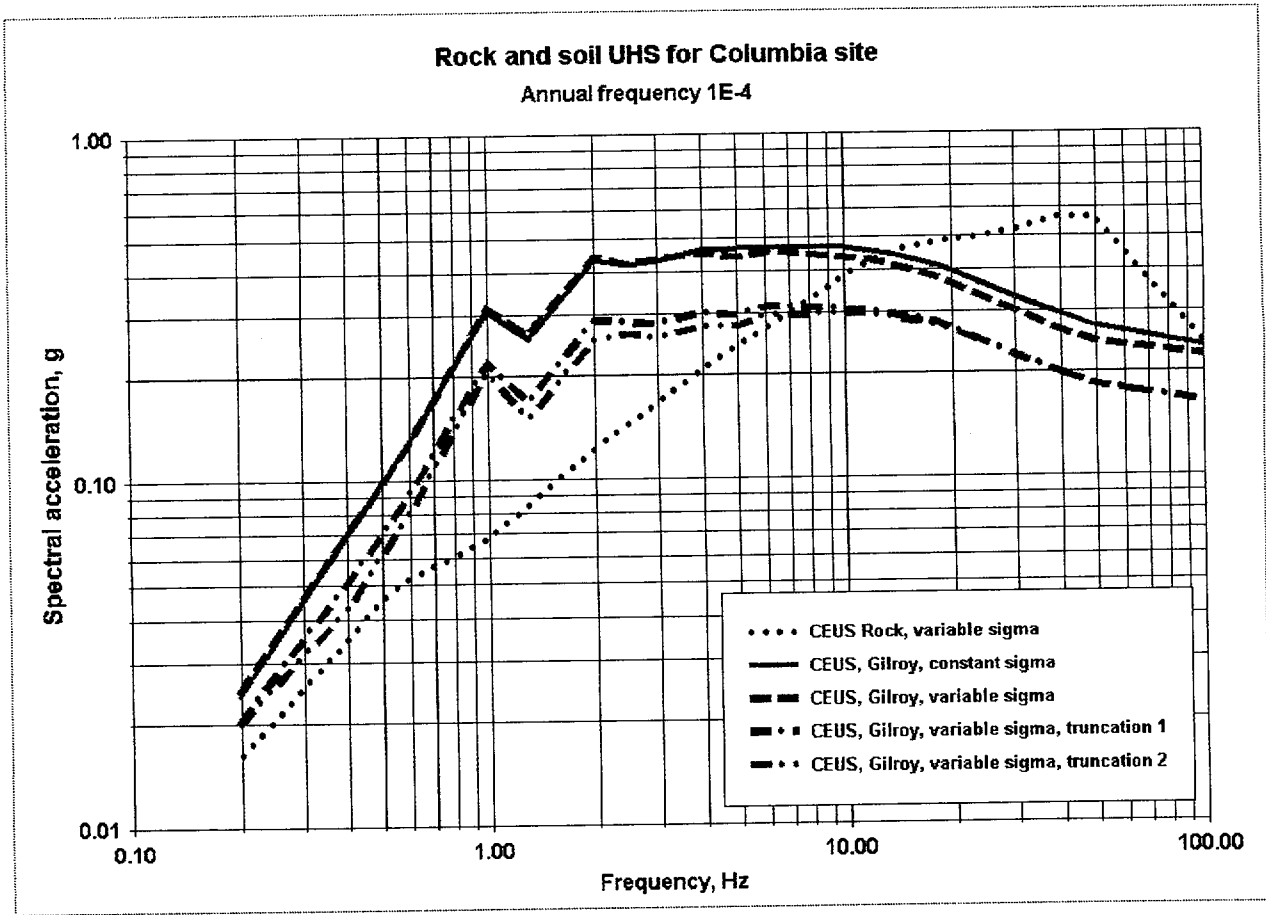


Figure 6-56. 10^{-4} UHS for CEUS rock and four soils, Gilroy profile.

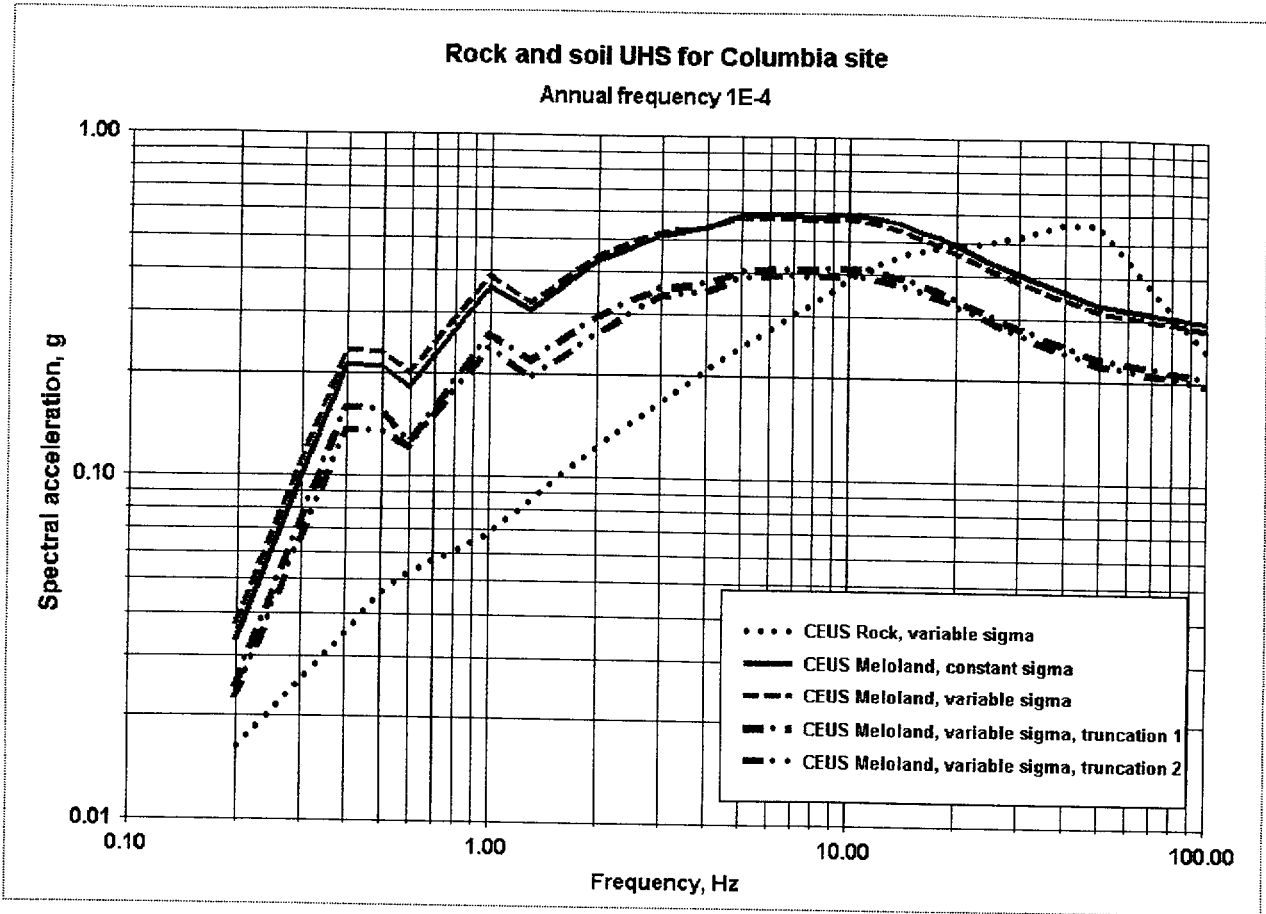


Figure 6-57. 10^{-4} UHS for CEUS rock and Meloland profile.

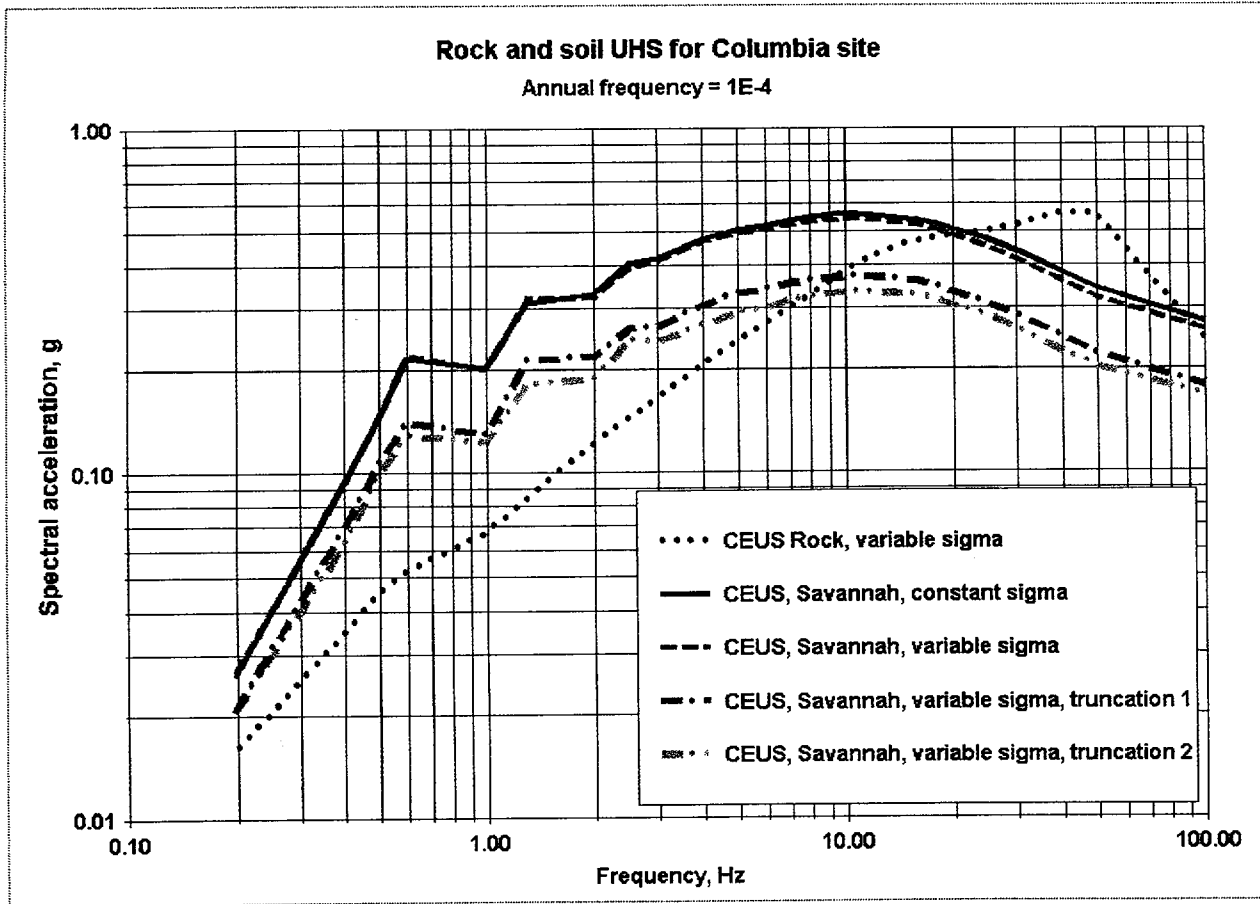


Figure 6-58. 10^{-4} UHS for CEUS rock and Savannah profile.

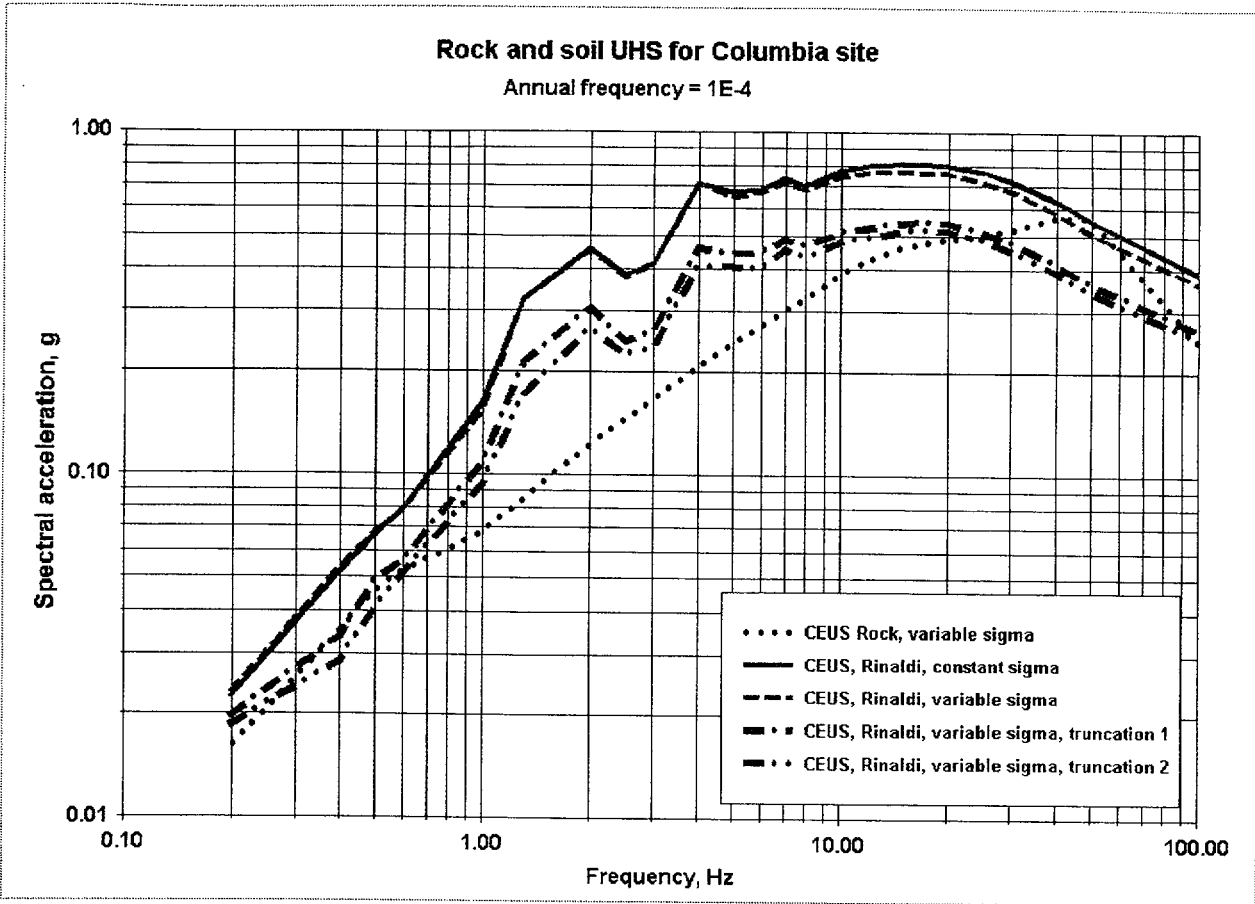


Figure 6-59. 10^{-4} UHS for CEUS rock and Rinaldi profile.

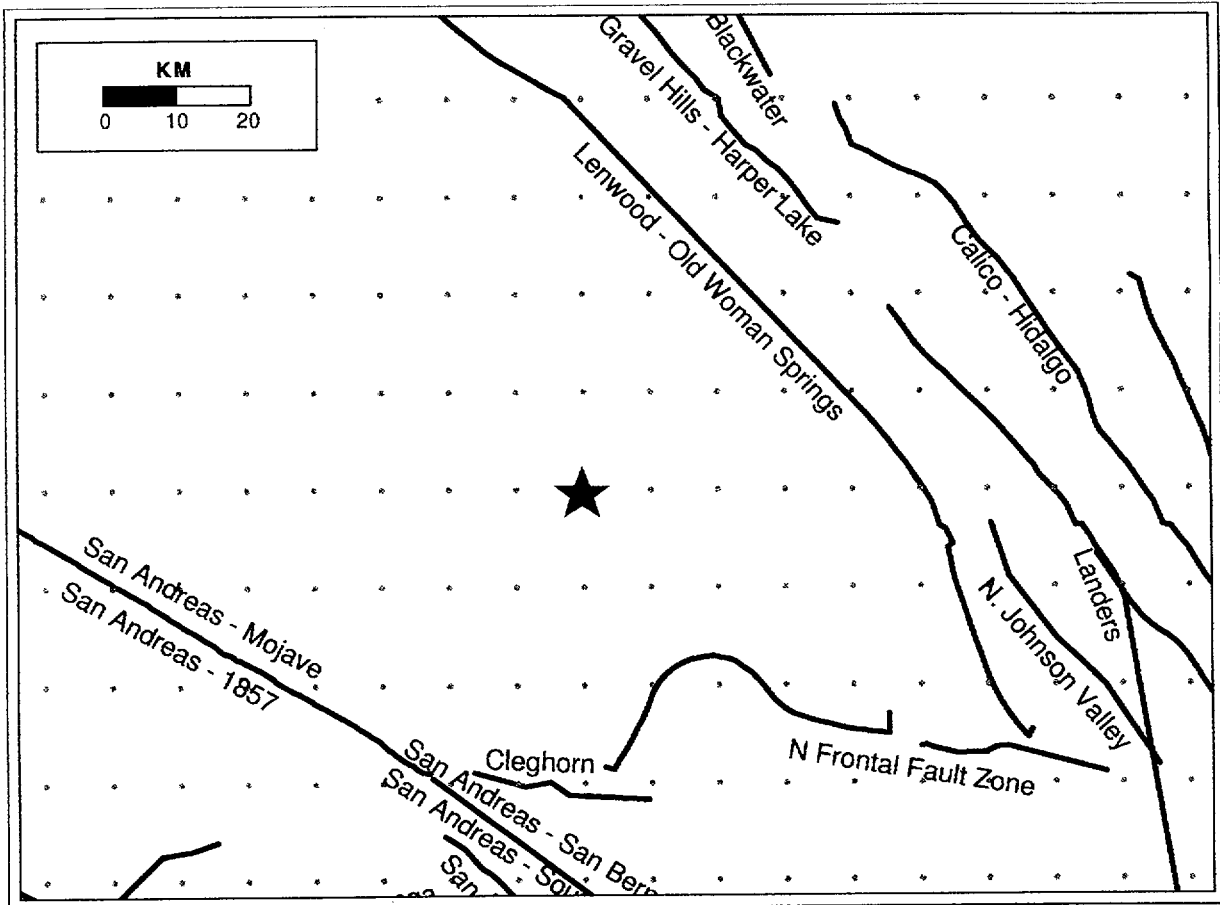


Figure 6-60. Configuration of background source and Mojave fault affecting WUS example site (Mojave, California).

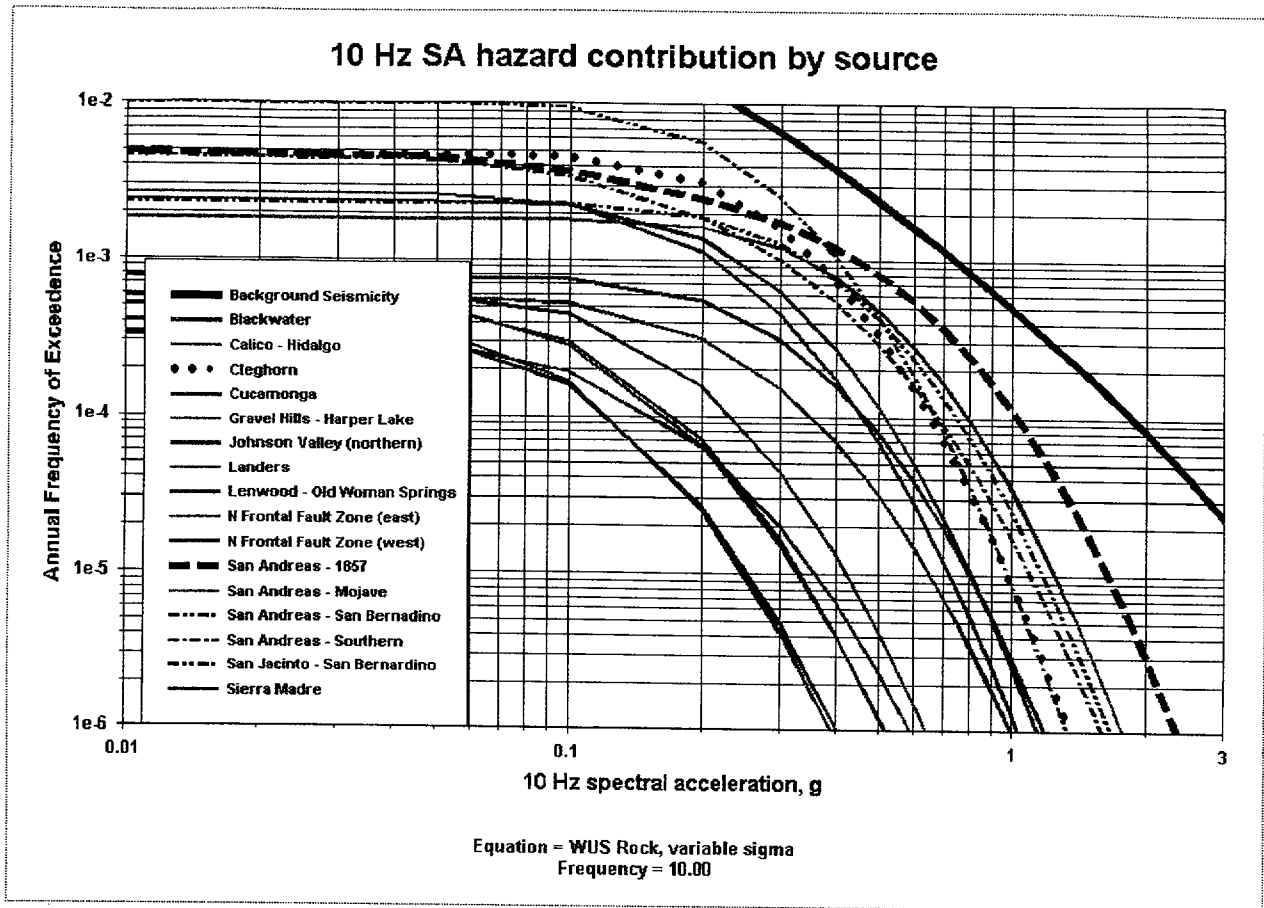


Figure 6-61. Contribution to seismic hazard by source for 10 Hz spectral acceleration, Mojave site.

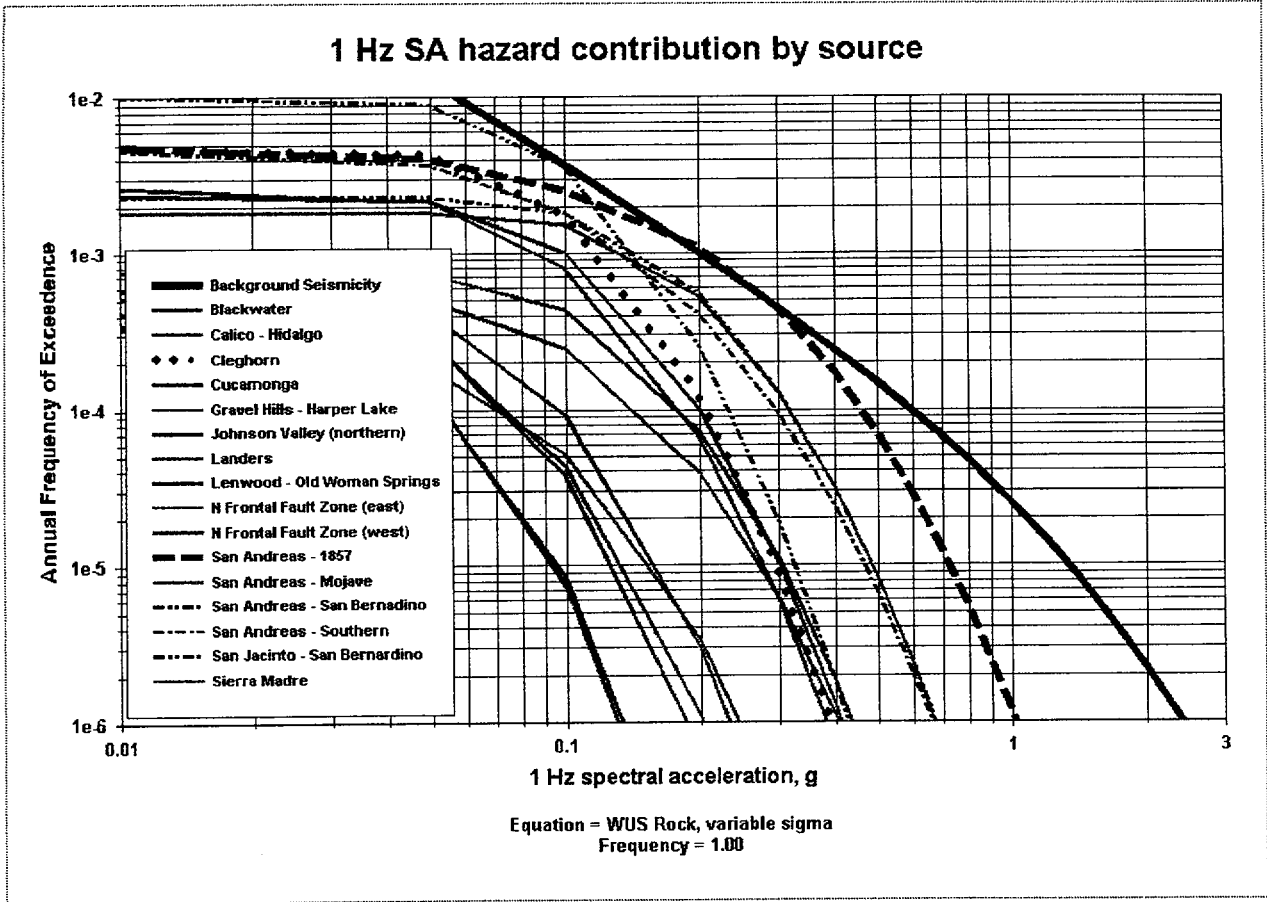


Figure 6-62. Contribution to seismic hazard by source for 1 Hz spectral acceleration, Mojave site.

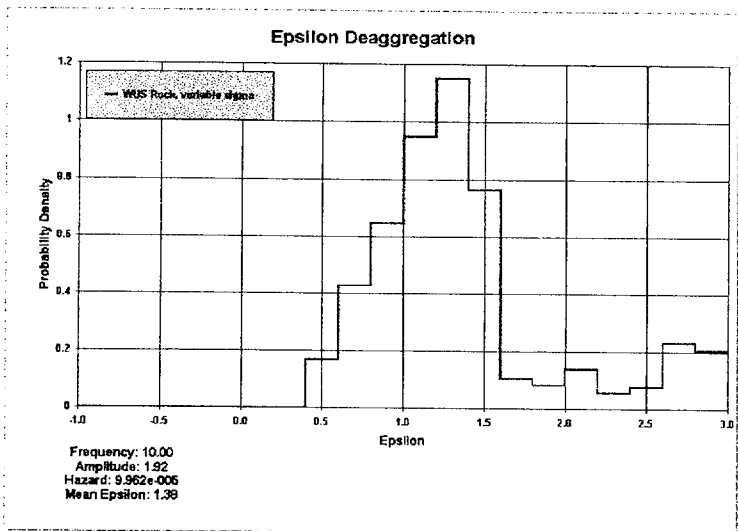
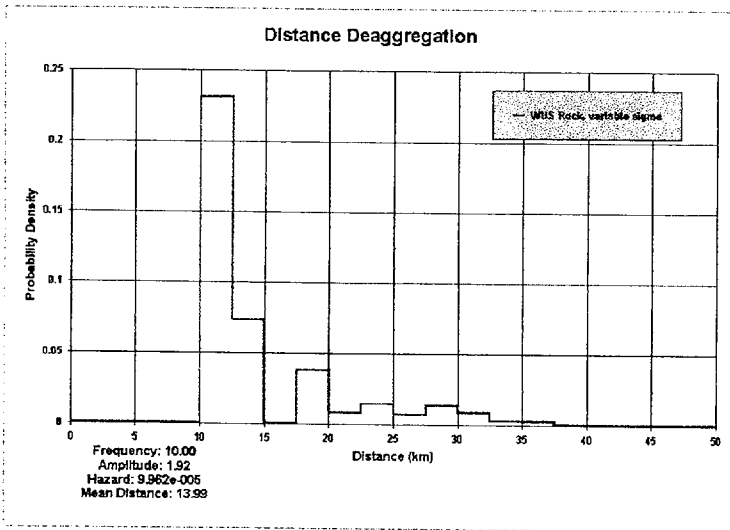
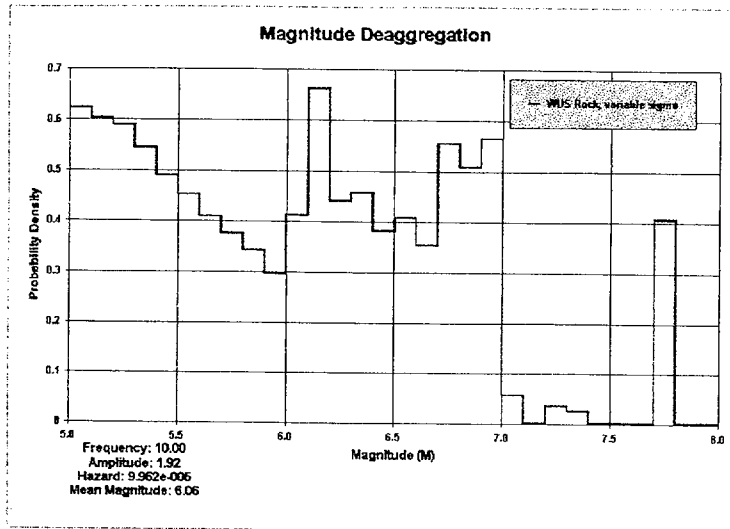


Figure 6-63. Deaggregation of seismicity hazard by M, R and ϵ for 10 Hz SA at 1.92g, Mojave site.

Magnitude-Distance Deaggregation

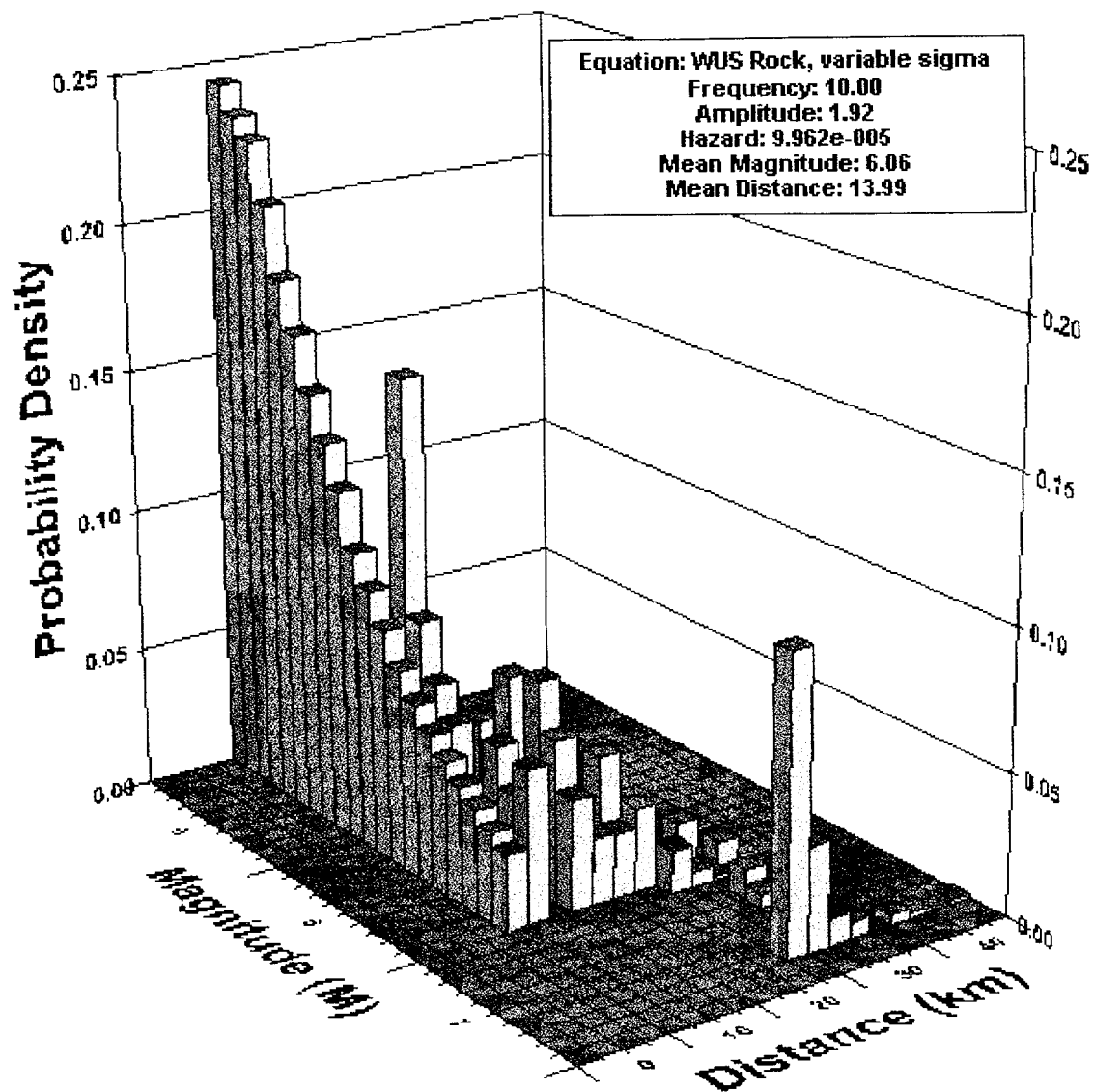


Figure 6-64. Deaggregation of seismic hazard by **M** and **R** for 10 Hz SA at 1.92g, Mojave site.

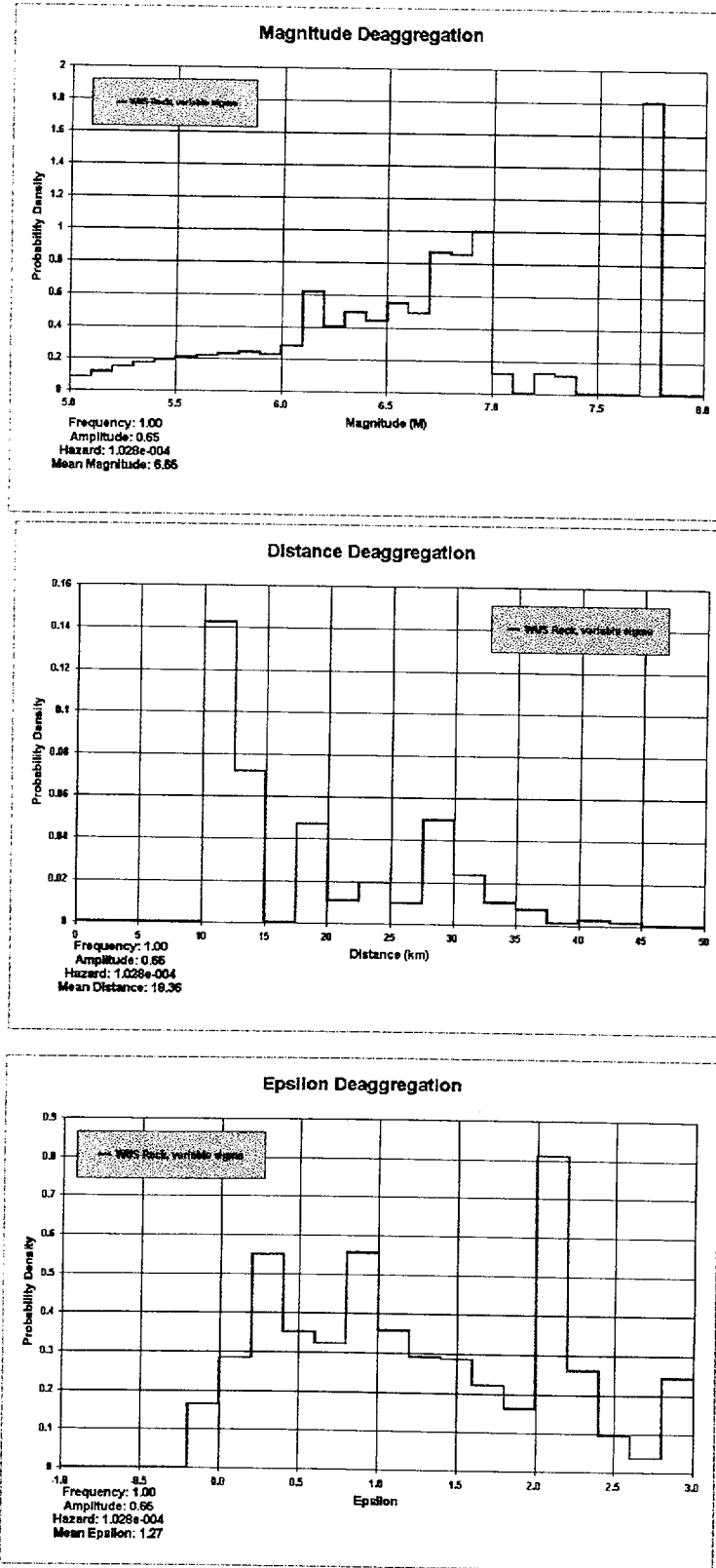


Figure 6-65. Deaggregation of seismic hazard by M , R and ϵ for 1 Hz SA at 0.65g, Mojave site.

Magnitude-Distance Deaggregation

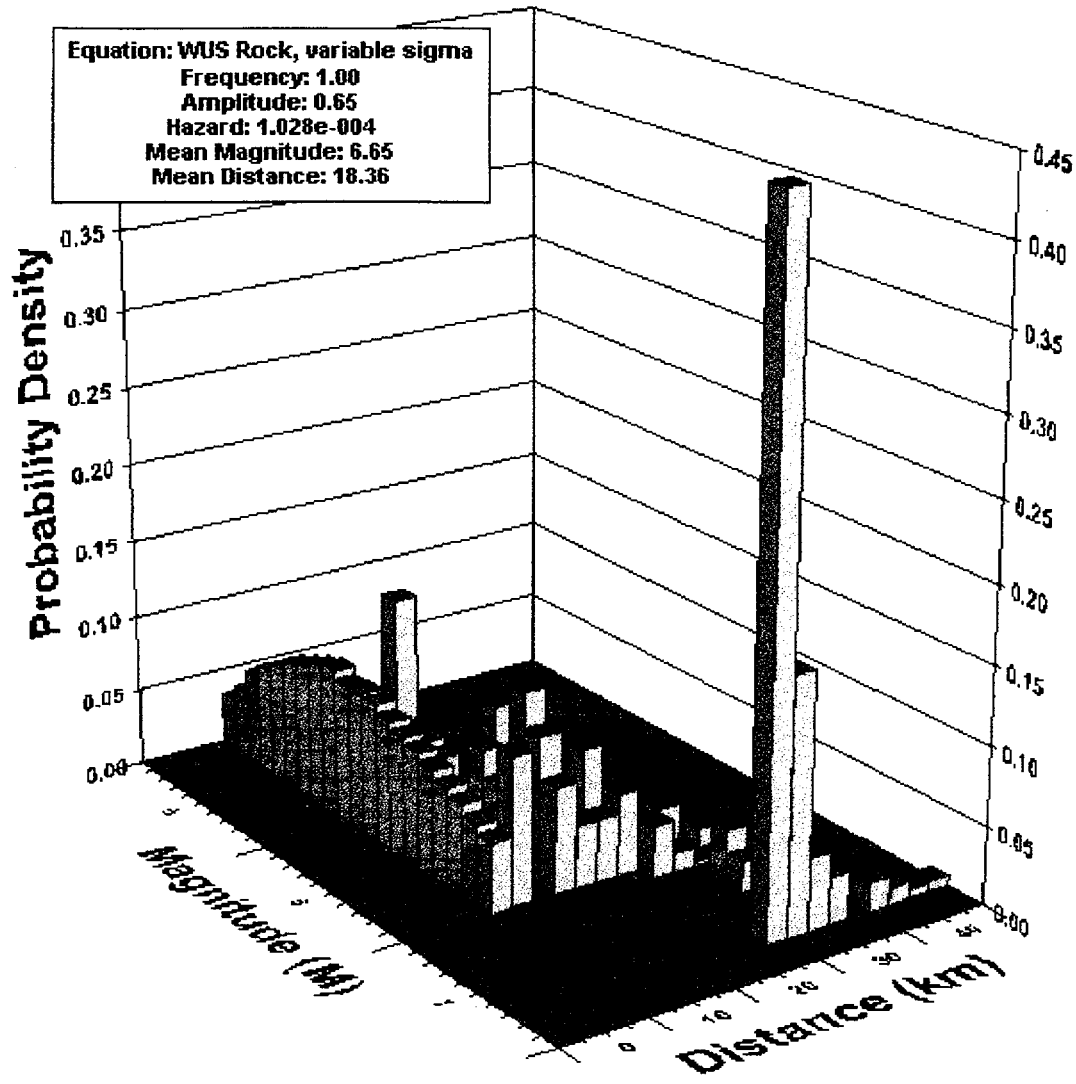


Figure 6-66: Deaggregation of seismic hazard by M and R for 1 Hz SA at 0.65g, Mojave site.

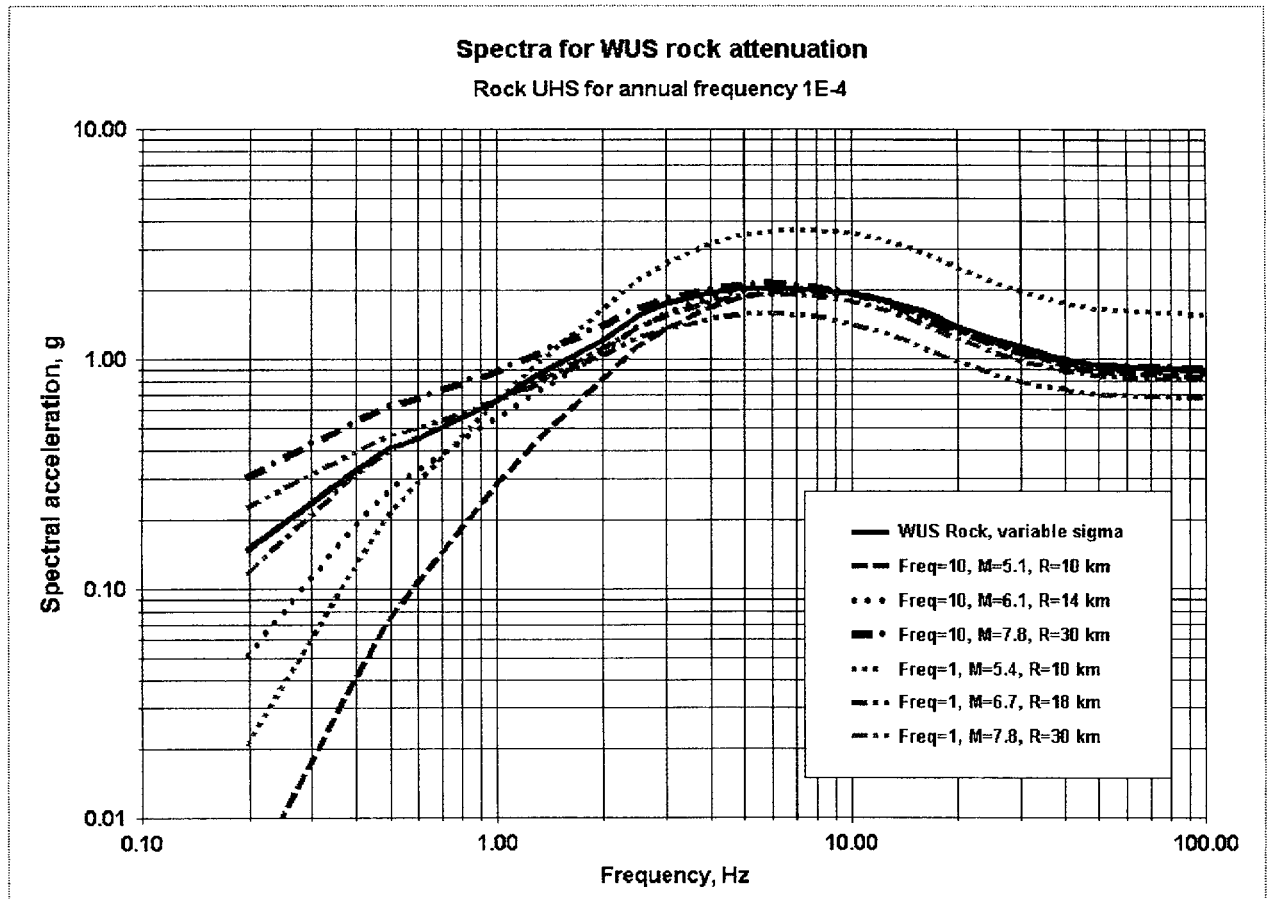


Figure 6-67: 10^{-4} UHS for rock, Columbia site, with spectra from deaggregation earthquakes.

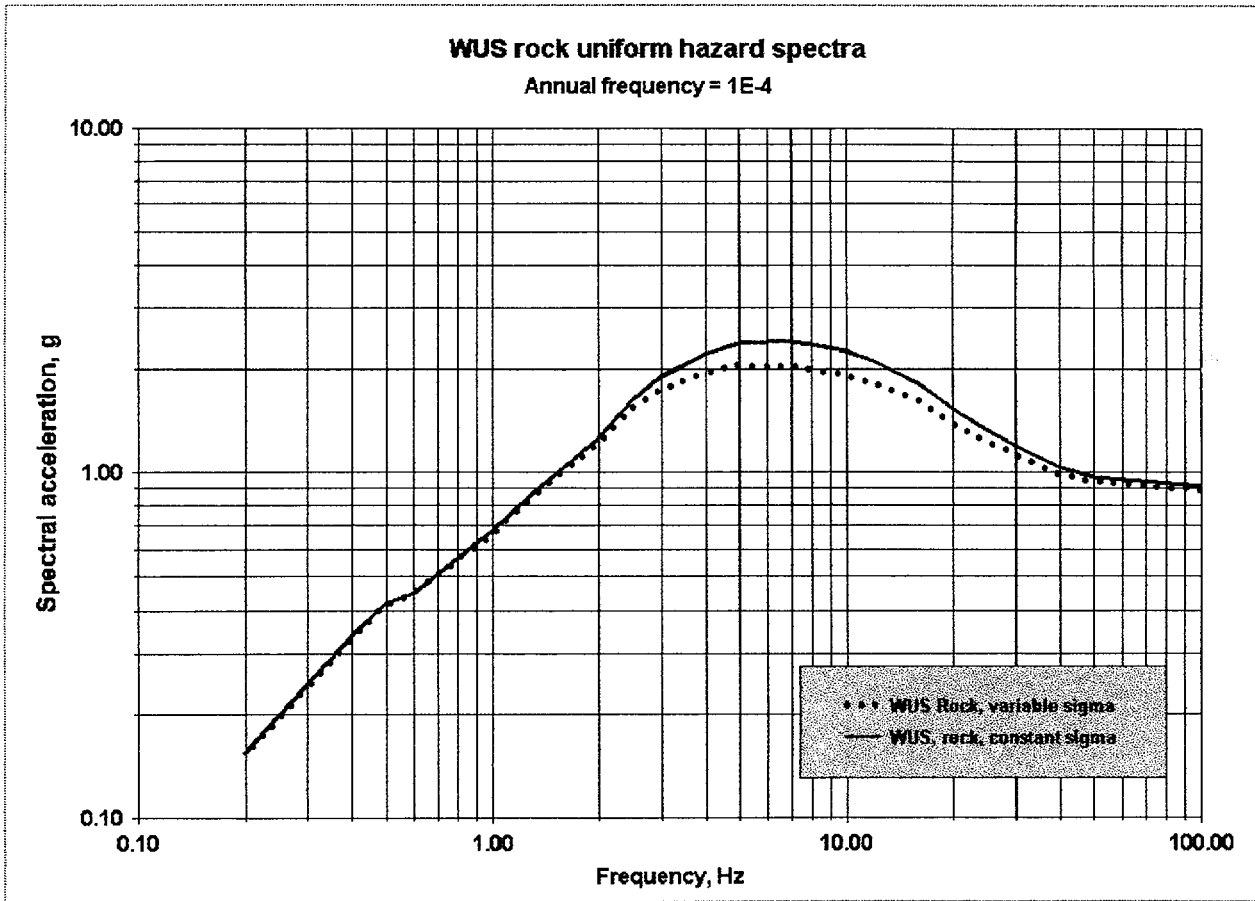


Figure 6-68: 10^{-4} UHS for rock, Mojave site, for constant σ and variable σ assumptions.

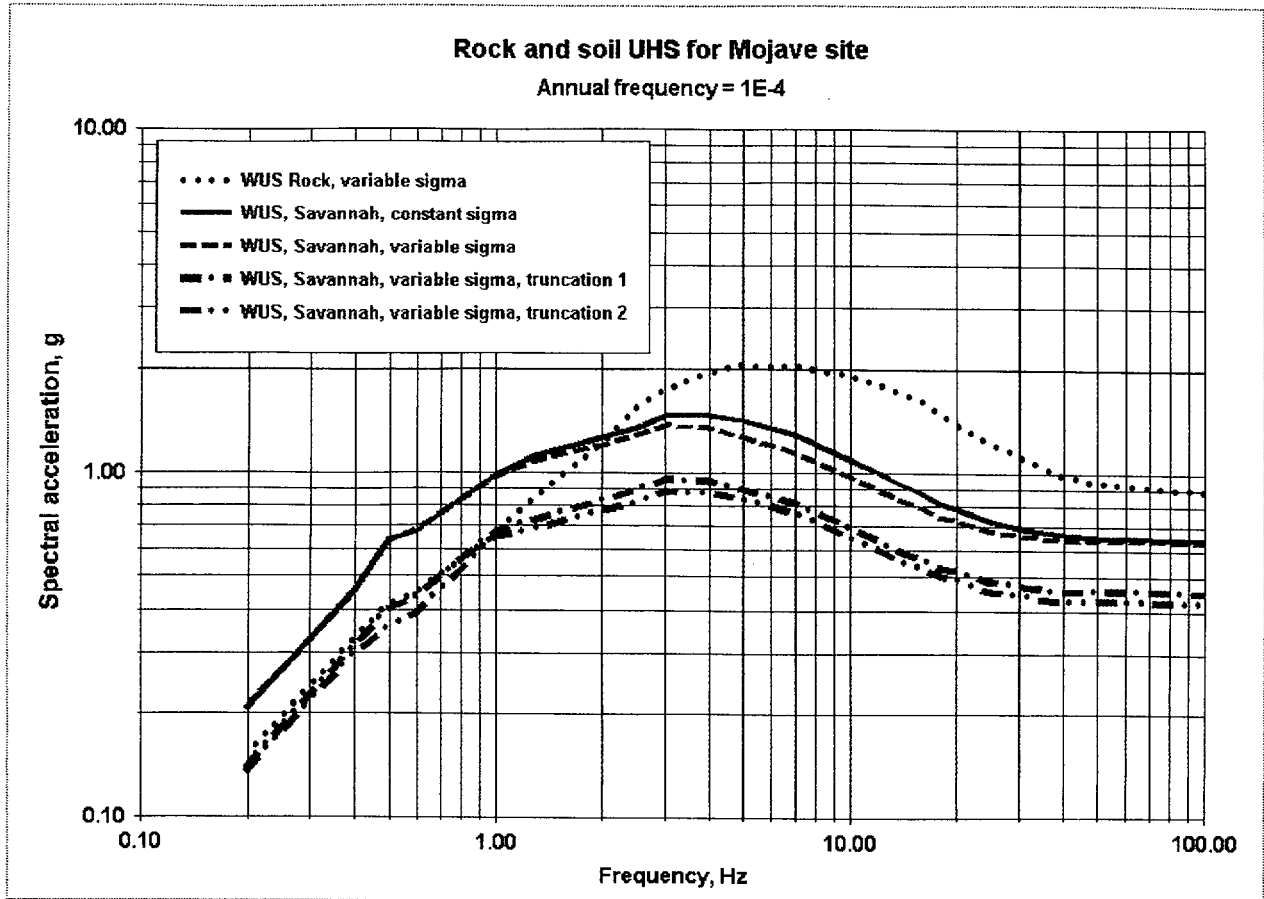


Figure 6-69: 10^{-4} UHS for WUS rock and Savannah site.

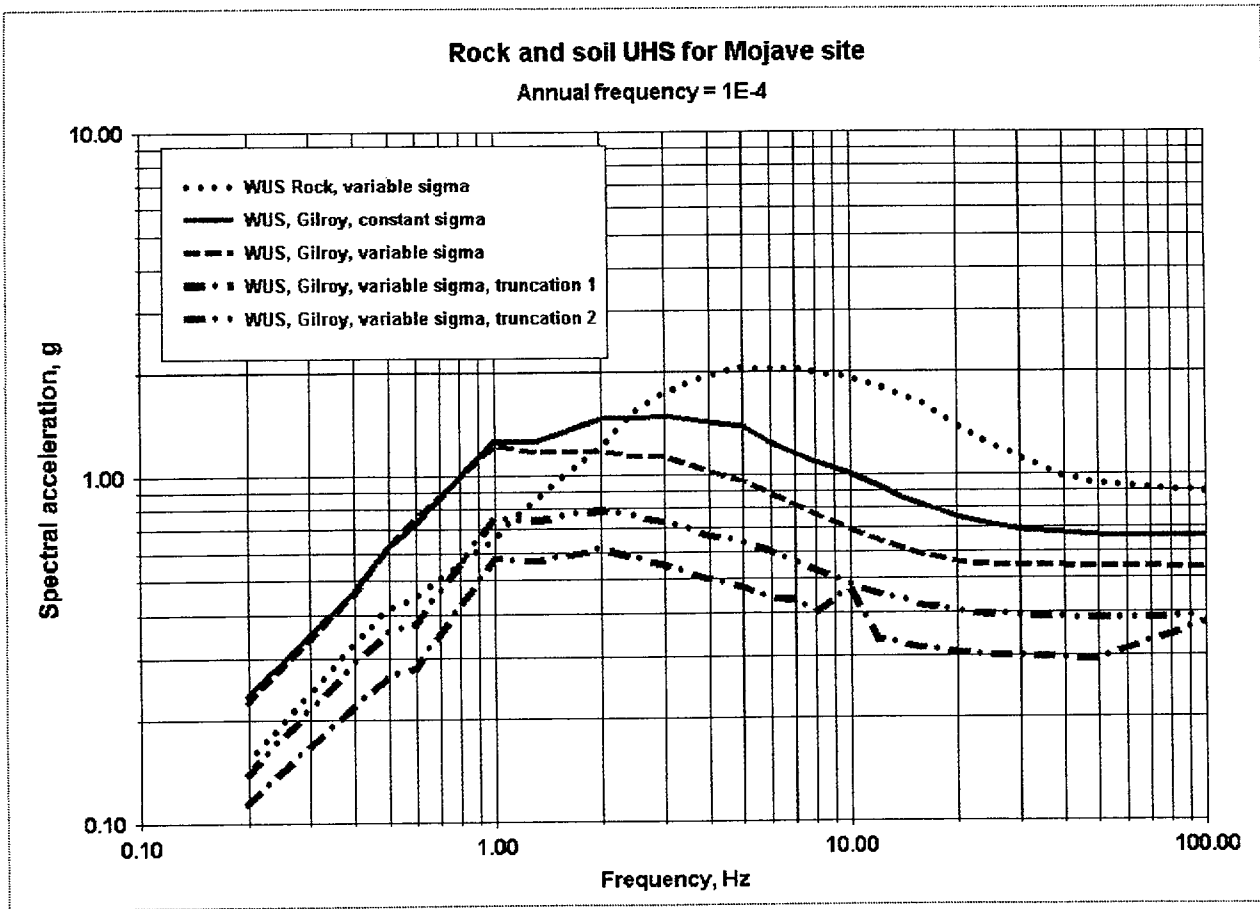


Figure 6-70: 10^{-4} UHS for WUS rock and Gilroy profile.

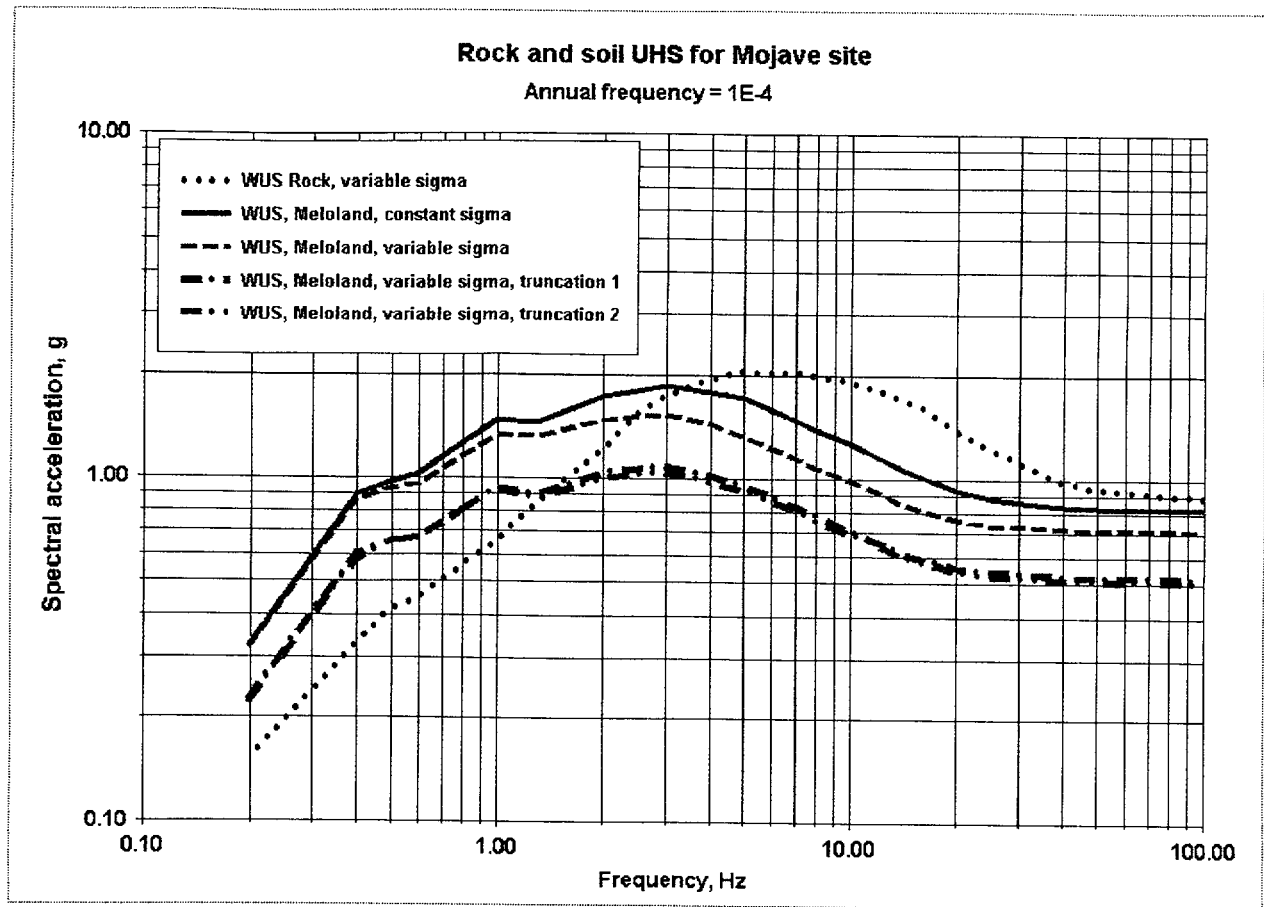


Figure 6-71: 10^{-4} UHS for WUS rock and Meloland profile.

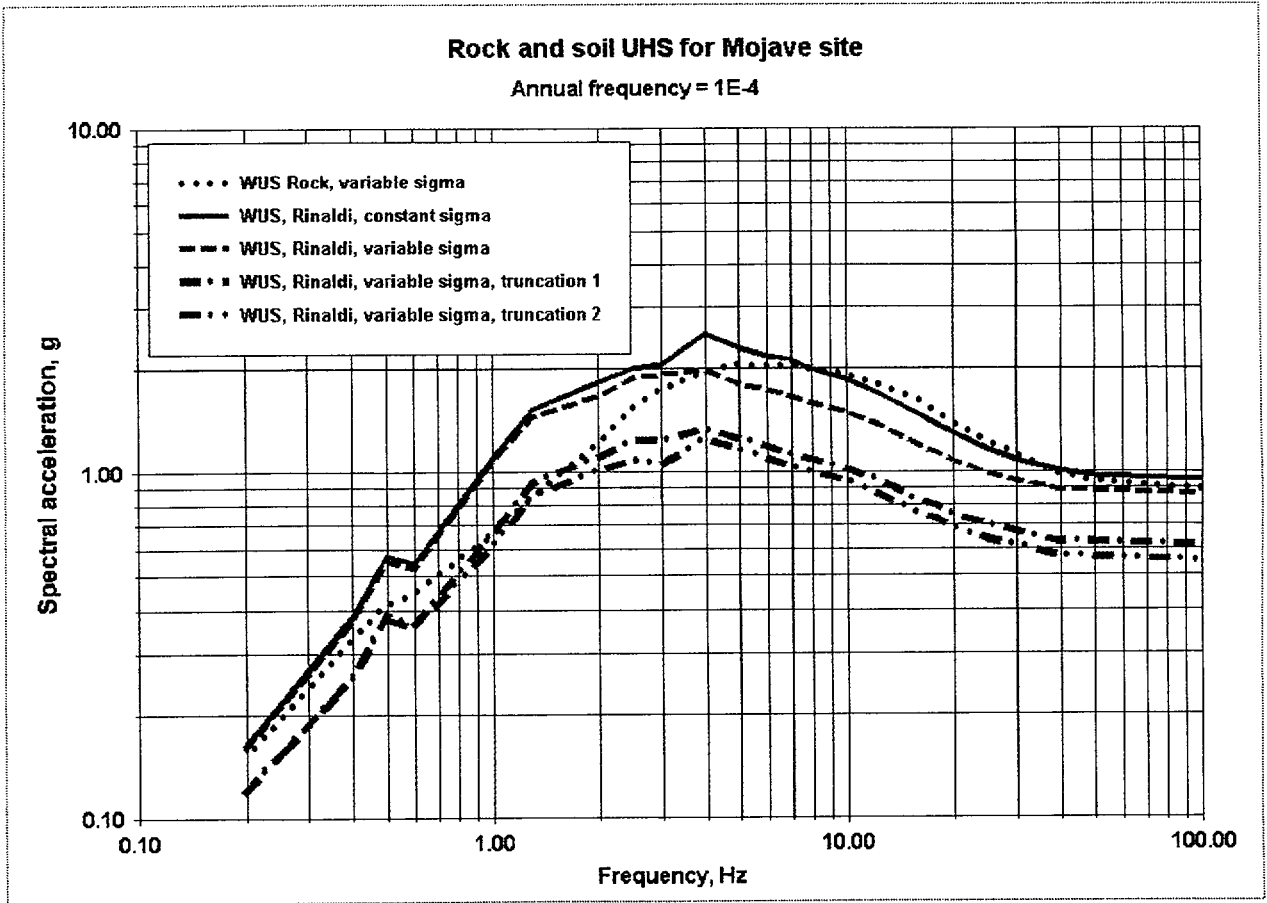


Figure 6-72: 10^{-4} UHS for WUS rock and Rinaldi profile.

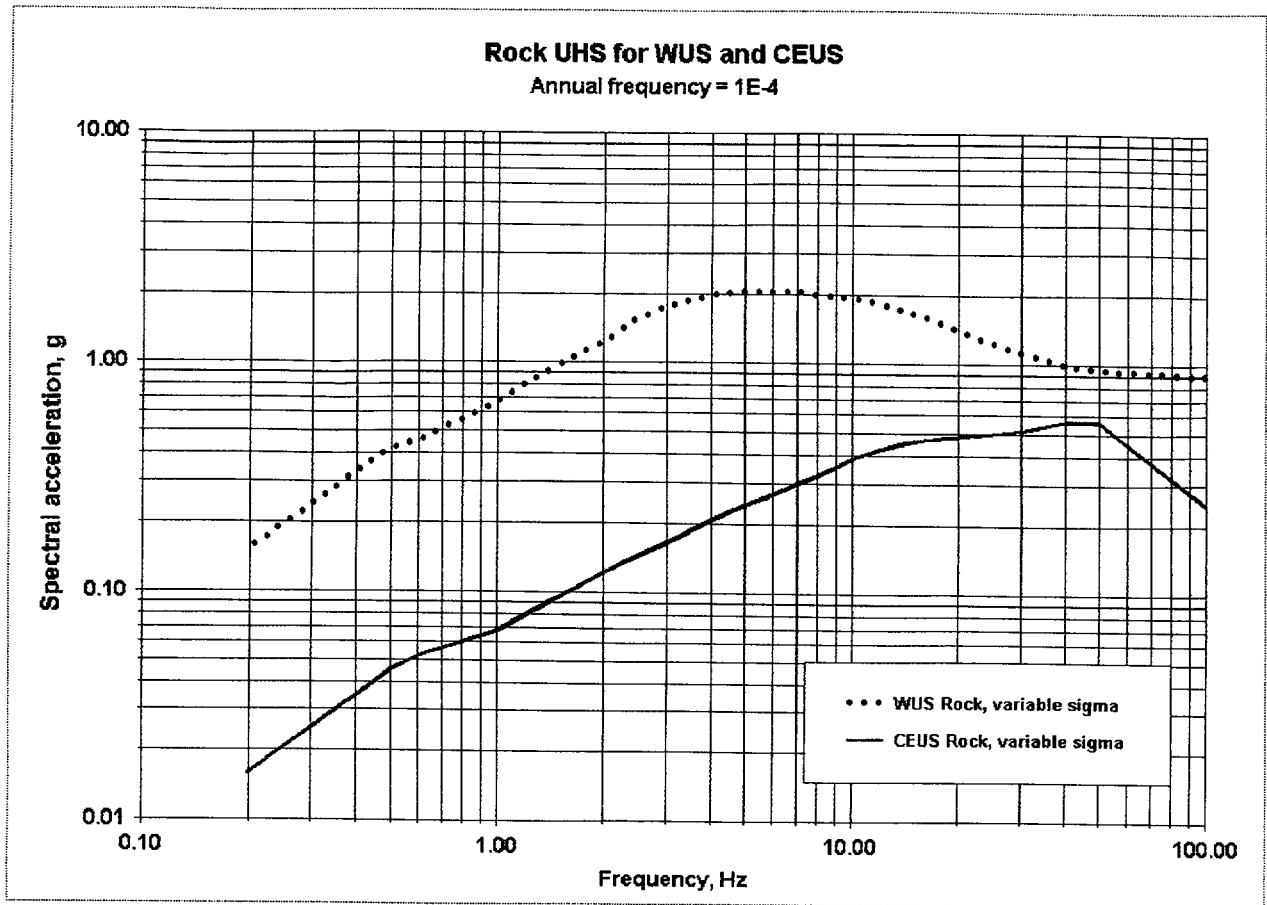
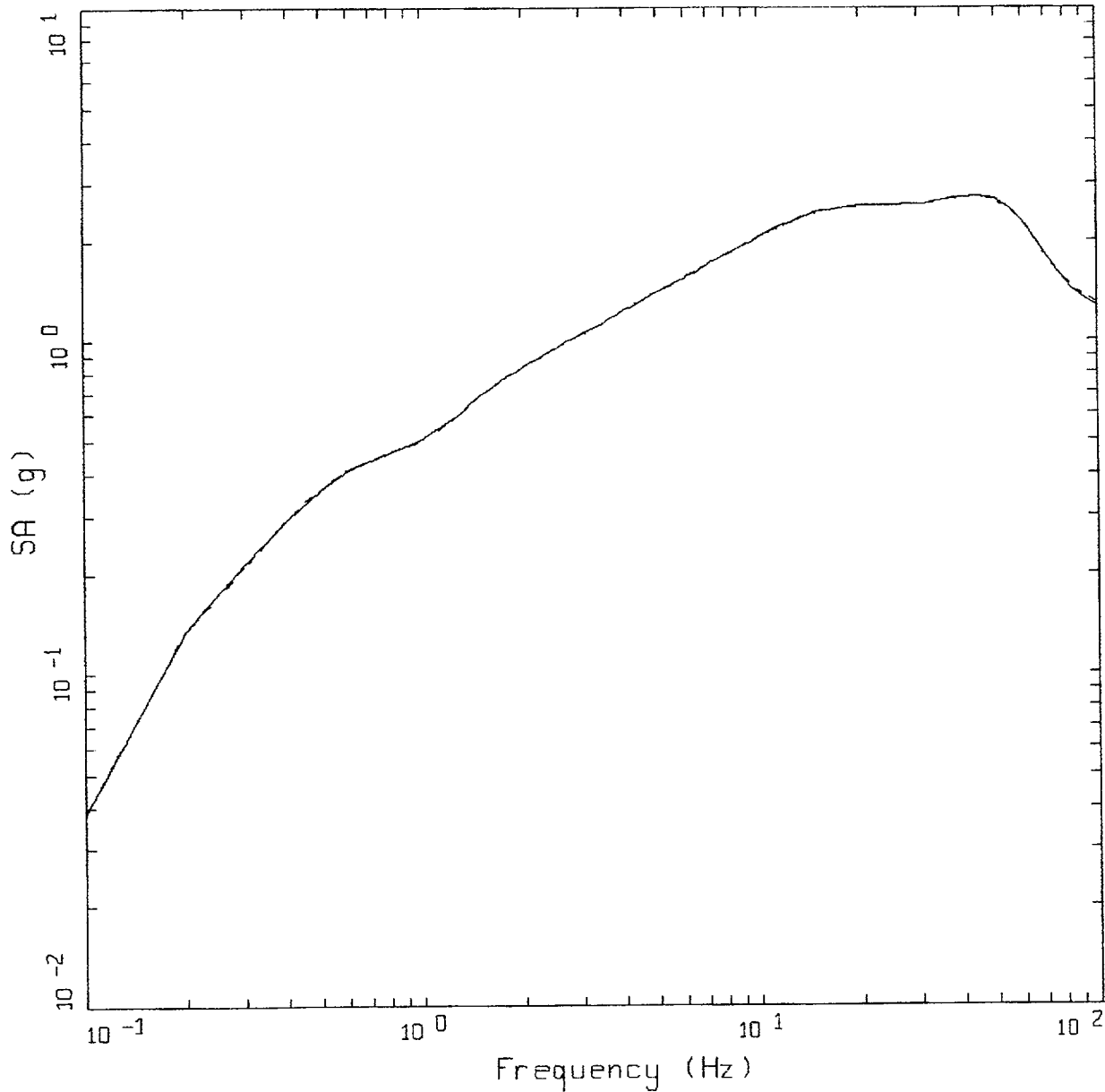


Figure 6-73. 10^{-4} UHS for CEUS site (Columbia) and WUS site (Mojave).

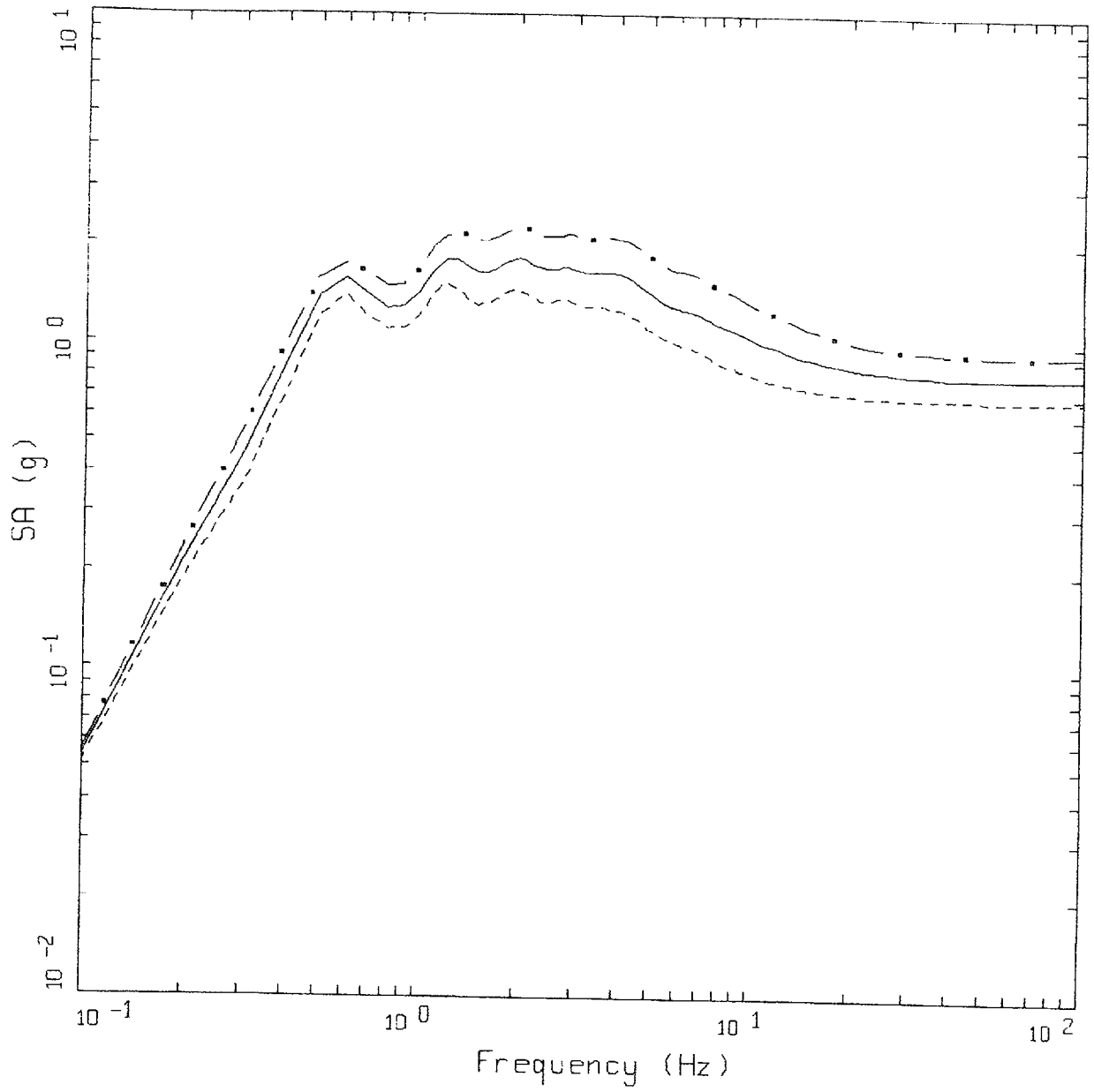


M = 7.5, D = 001 KM
 MATCH TO CEUS ROCK

LEGEND

- 5 %, TARGET; PGA = 1.271 G
- 5 %, SPECTRAL MATCH; PGA = 1.283 G

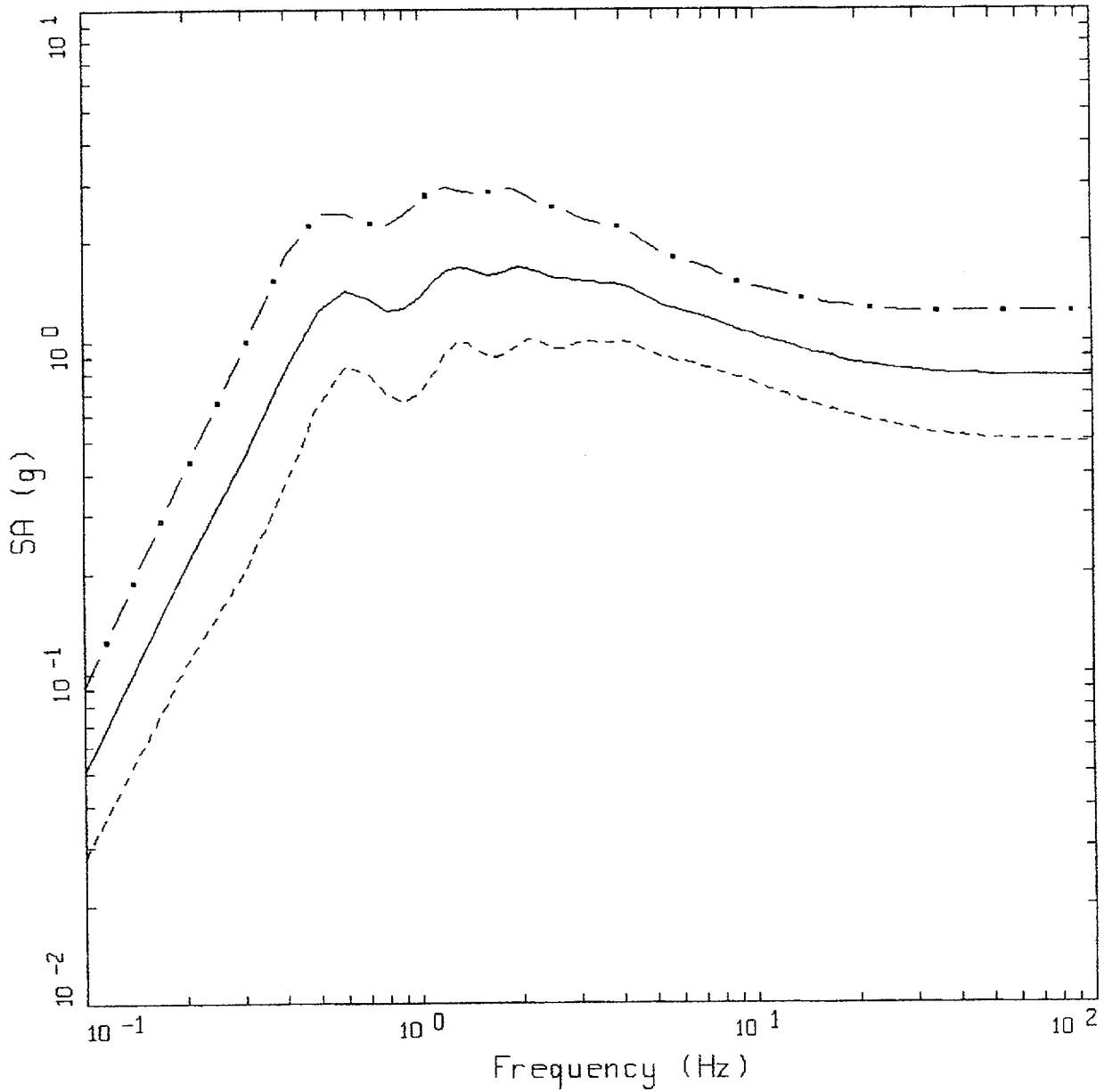
Figure 6-74. Comparison of spectral match (dotted line) to median spectrum computed for $M = 7.5$ at a distance of 1 km (solid line): CEUS rock outcrop.



CEUS, M = 7.5, D = 001 KM, H = 12 KM
 SD = 95 BARS, SAVANNAH GENERIC, SITE

- LEGEND
- · - 84TH PERCENTILE, PGA = 0.934 G
 - 50TH PERCENTILE, PGA = 0.801 G
 - - - 16TH PERCENTILE, PGA = 0.687 G

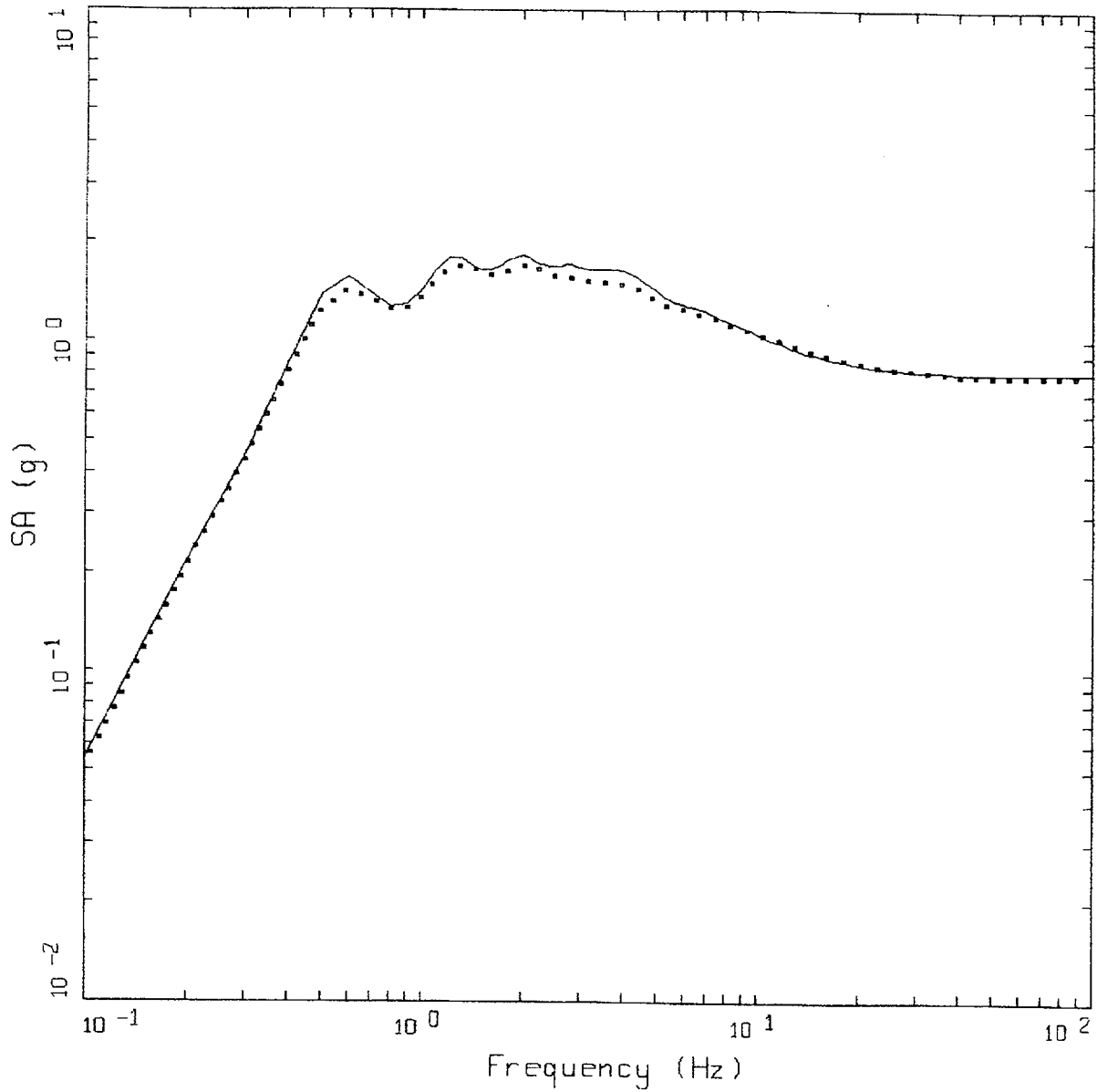
Figure 6-75. Median and $\pm\sigma$ spectra computed for $M = 7.5$ at a distance of 1 km using the Savannah River generic profile with site variations only (profile, G/G_{max} , and hysteretic damping): CEUS conditions.



CEUS, M = 7.5, D = 001 KM, H = 12 KM
 SD = 95 BARS, SAVANNAH GENERIC, SITE

- LEGEND
- · — 84TH PERCENTILE, PGA = 1.230 G
 - 50TH PERCENTILE, PGA = 0.782 G
 - - - 16TH PERCENTILE, PGA = 0.497 G

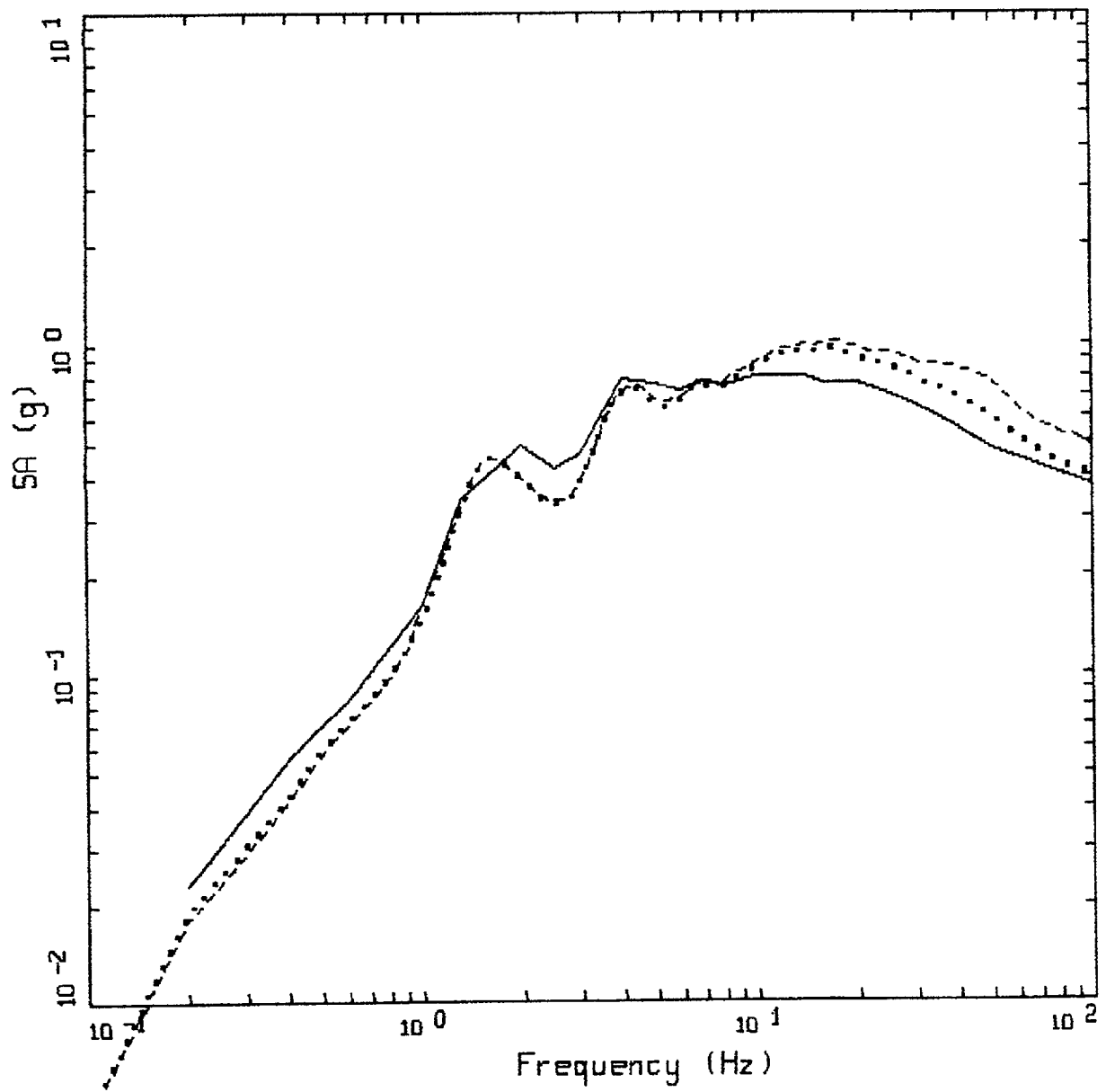
Figure 6-76. Median and $\pm\sigma$ spectra computed for $M=7.5$ at an epicentral distance of 12 km using the Savannah River Generic profile with source, path and site variations: CEUS conditions.



CEUS, M = 7.5, D = 001 KM, H = 12 KM
 SD = 95 BARS, SAVANNAH GENERIC

LEGEND
 — SITE; 50TH PERCENTILE, PGA = 0.801 G
 - - - S,P,S; 50TH PERCENTILE, PGA = 0.782 G

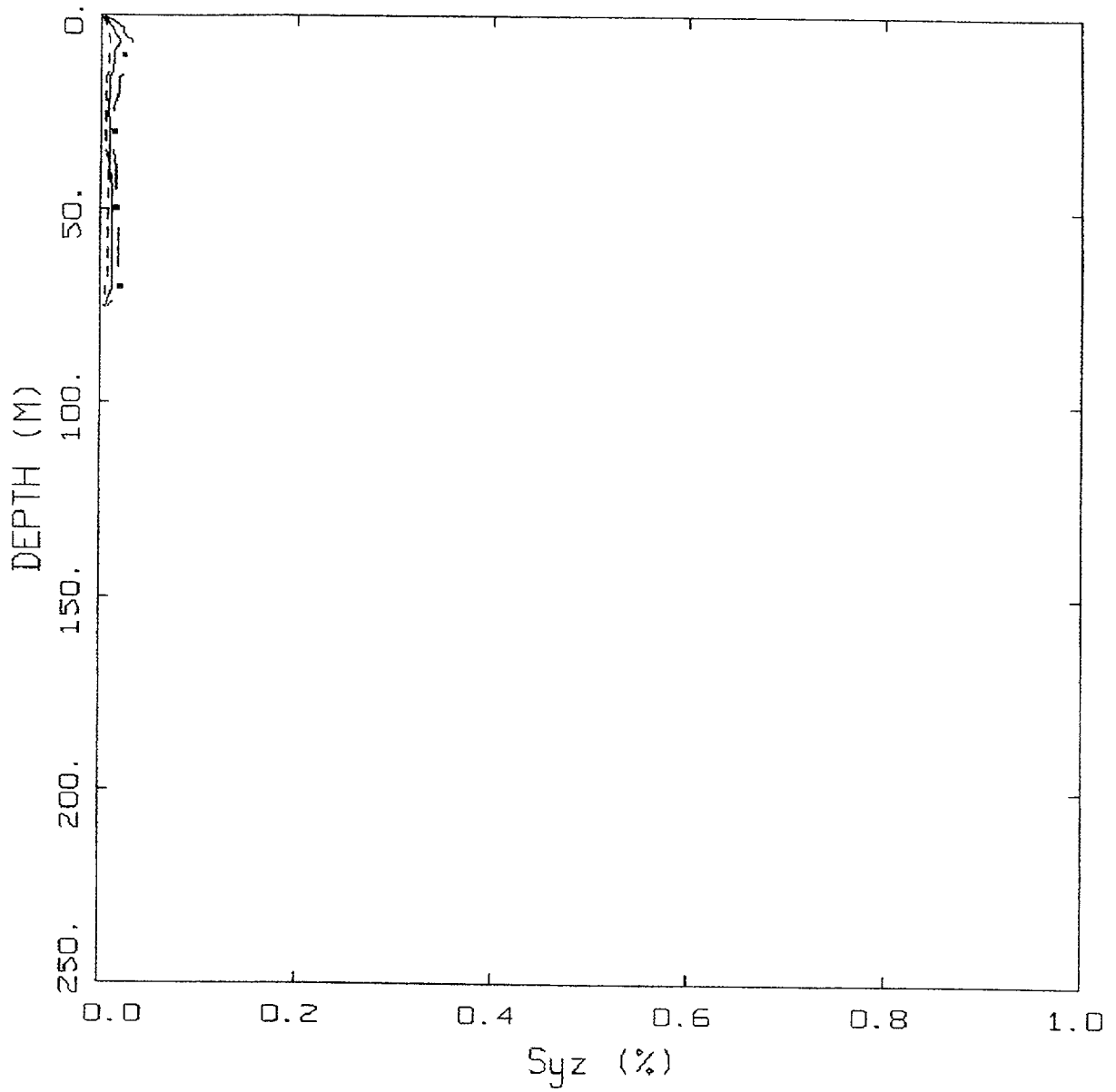
Figure 6-77. Comparison of median spectral estimates computed for $M=7.5$ at an epicentral distance of 1 km using the Savannah River Generic profile: varying site properties only (solid line) and varying source, path, and site properties (dashed line); CEUS conditions.



CEUS 10E-4 APPROACH COMPARISON, RI

- LEGEND
- APPROACH 4, 10⁻⁴ SOIL UNIFORM HAZARD SPECTRUM; PGA = 0.370 G
 - APPROACH 1, 10⁻⁴ ROCK CONTROL MOTION, MEAN PGA = 0.406 G
 - - - - APPROACH 2, 1 HZ AND 10 HZ DEAGGREGATION EQKS, MEAN PGA = 0.487 G

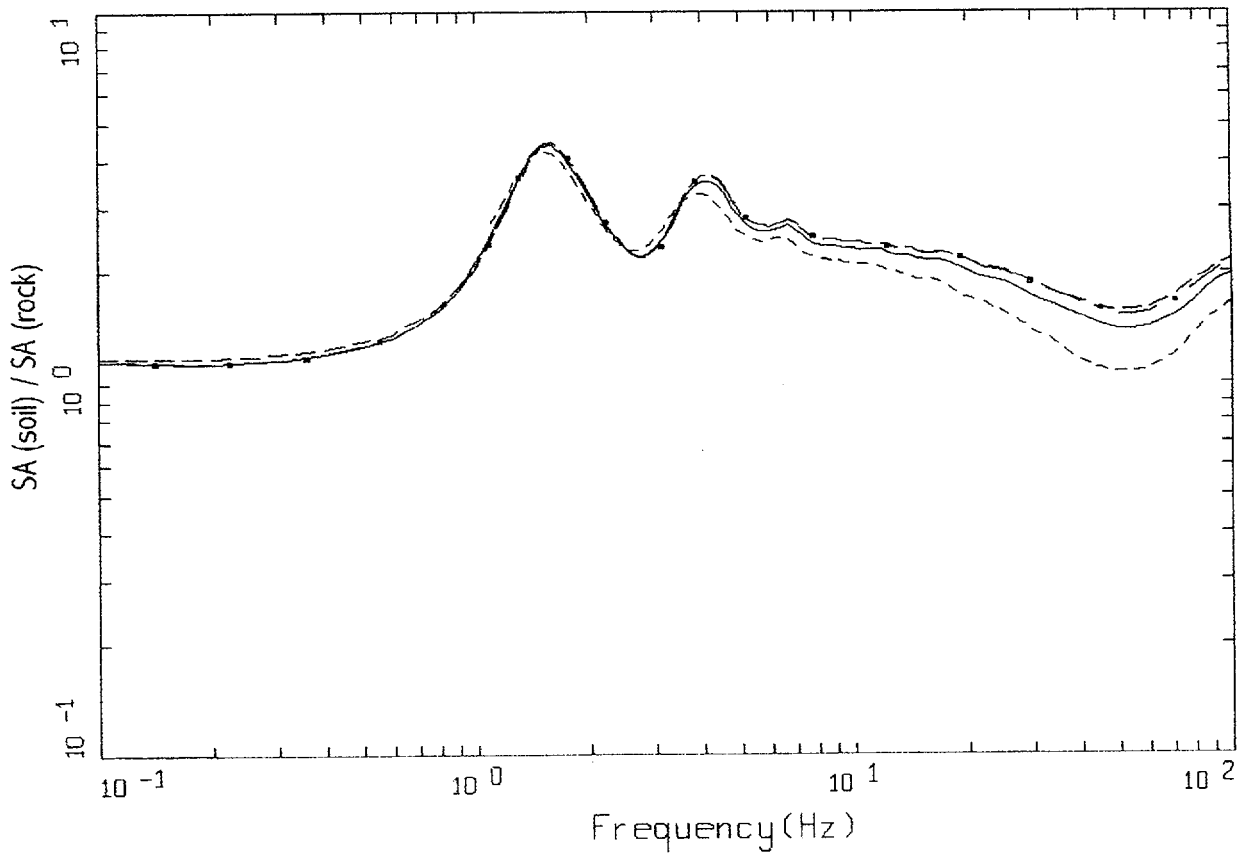
Figure 6-78. Comparison of Approaches 1, 2B, and 4 10⁻⁴ UHS on soil for profile Rinaldi: CEUS conditions.



CEUS, 10-4, RI
EFFECTIVE STRAINS (SYZ)

LEGEND
 - . - 84TH PERCENTILE
 — 50TH PERCENTILE
 - - - 16TH PERCENTILE

Figure 6-79. Median and $\pm\sigma$ effective strains for soil profile Rinaldi using Approach 1: CEUS conditions.

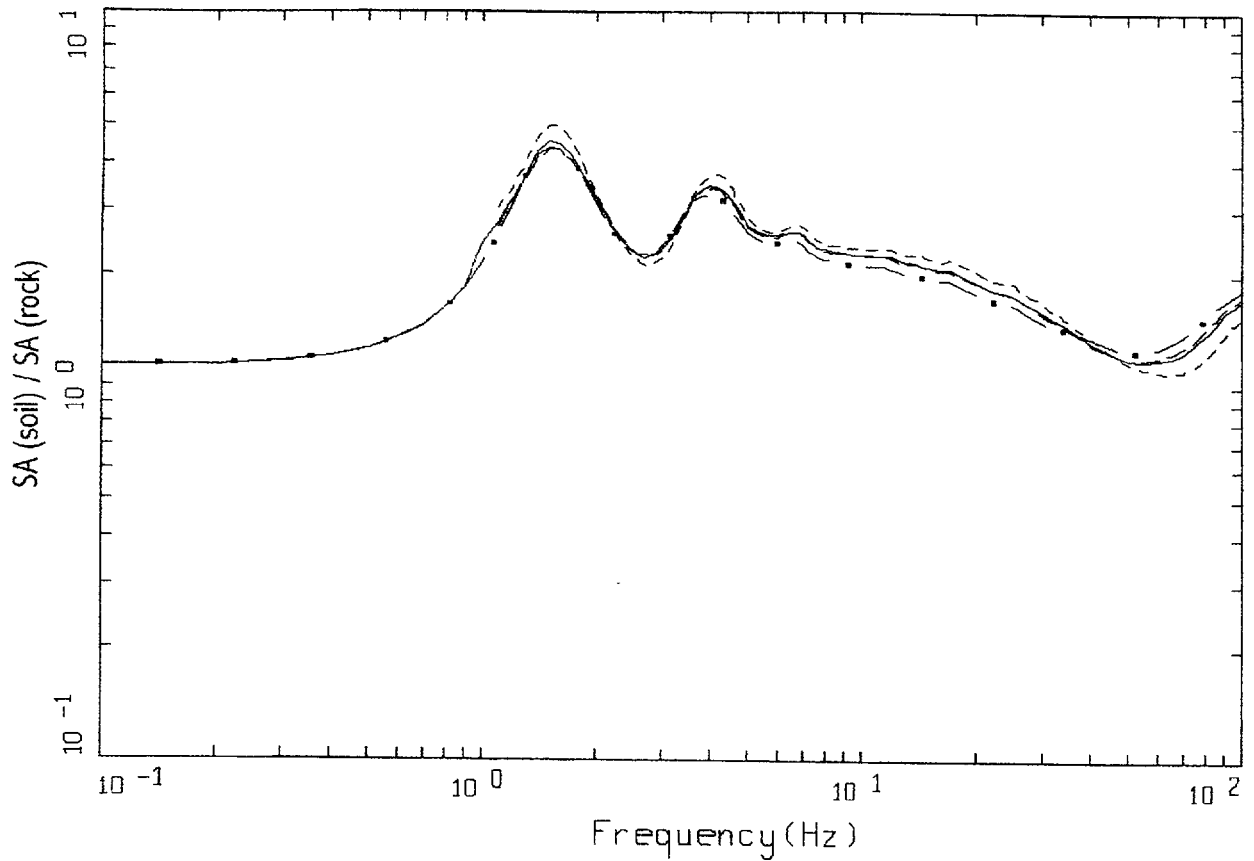


CEUS, 10E-4, 1HZ DESIGN, RI
 SURFACE MOTION, 1HZ TRANSFER FUNCTION
 WEIGHTS: ML=0.30, MM=0.00, MH=0.70

LEGEND

- ML = 5.7, D = 20 KM MEAN RATIO
- · - · - MM = 7.0, D = 100 KM, DESIGN MEAN RATIO
- · — MH = 7.6, D = 130 KM MEAN RATIO
- WEIGHTED MEAN RATIO

Figure 6-80. Comparison of transfer functions computed for the scaled 1 Hz design earthquake; soil profile Rinaldi, CEUS conditions.

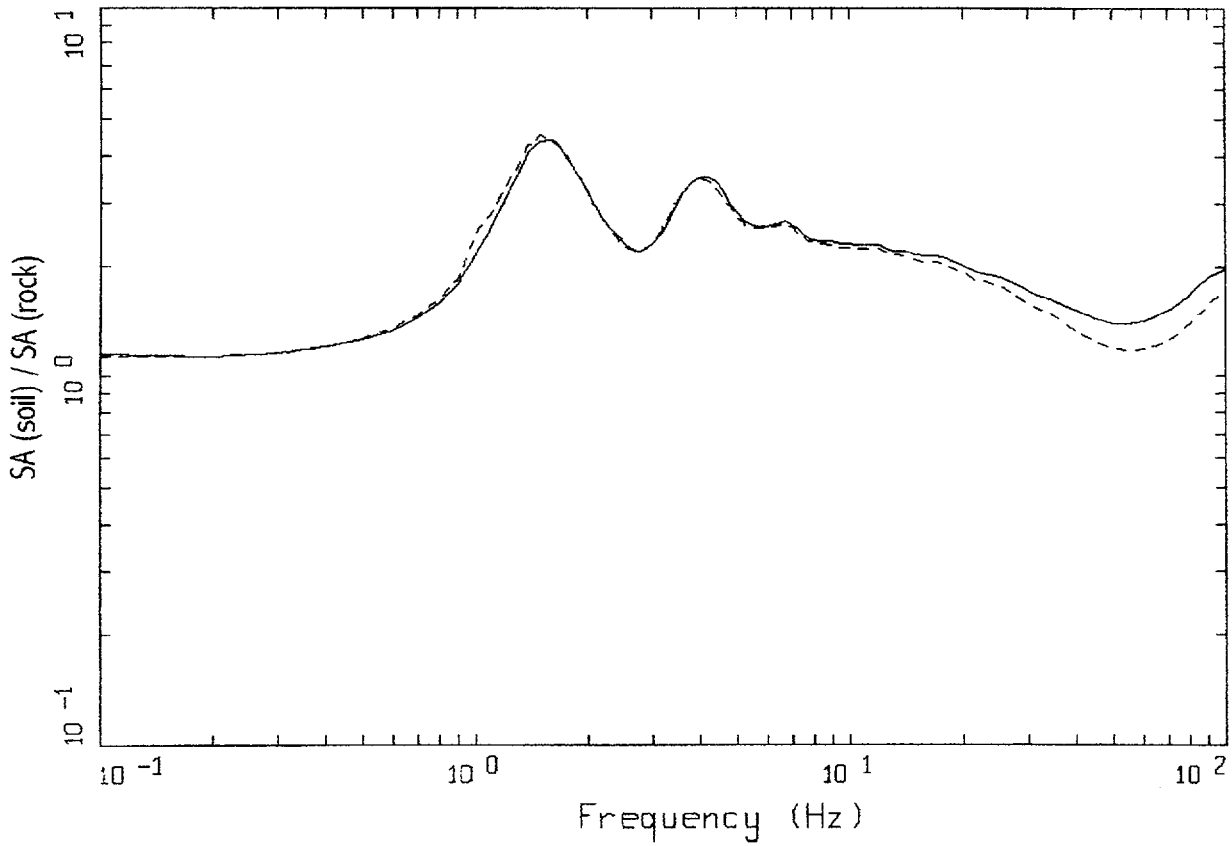


CEUS, 10E-4, 10HZ DESIGN, RI
 SURFACE MOTION, 10HZ TRANSFER FUNCTION
 WEIGHTS: ML=0.25, MM=0.53, MH=0.12

LEGEND

- ML = 4.6, D = 8 KM MEAN RATIO
- · - · - MM = 5.6, D = 8 KM, DESIGN MEAN RATIO
- · — MH = 7.7, D = 130 KM MEAN RATIO
- WEIGHTED MEAN RATIO

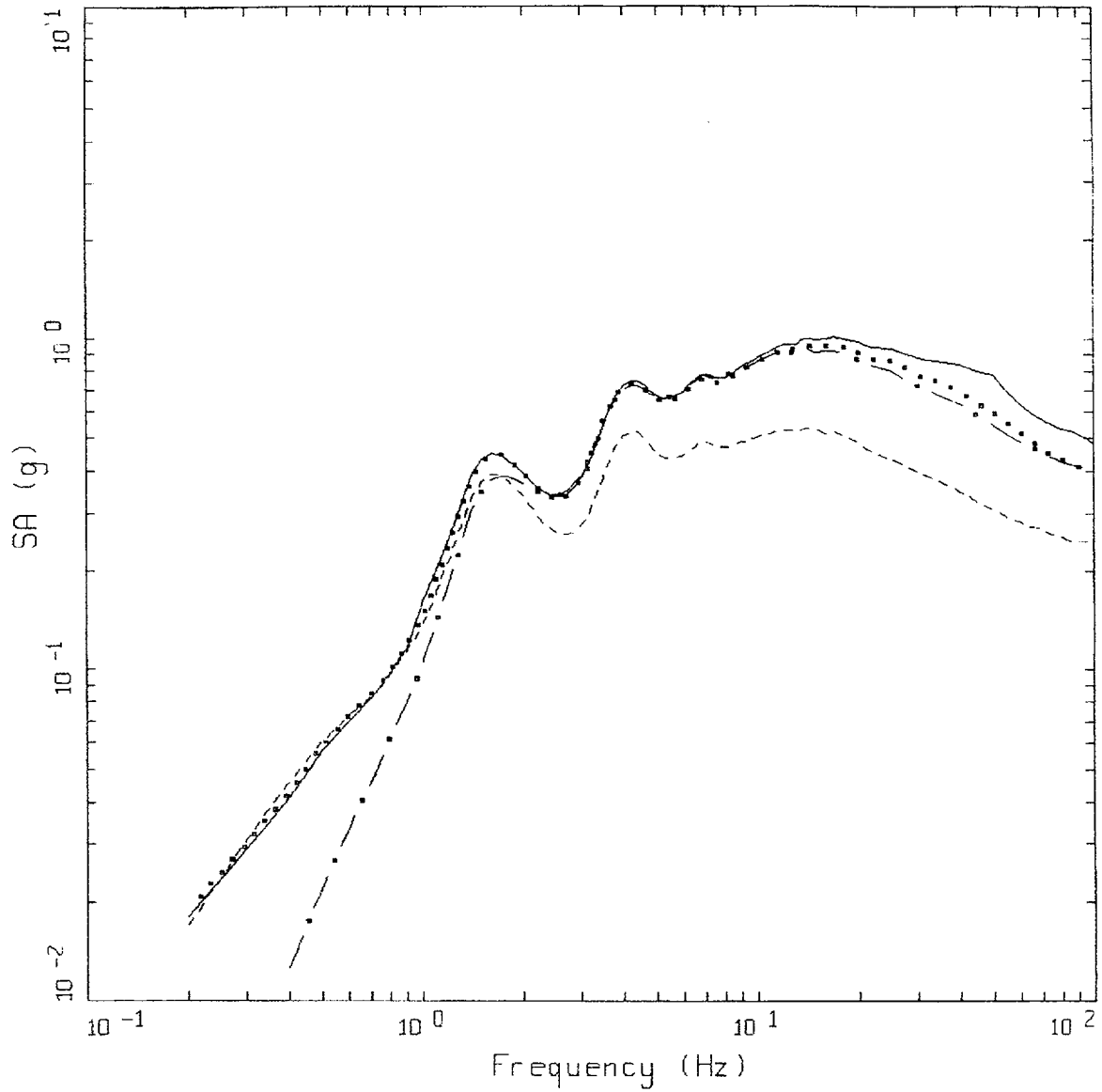
Figure 6-81. Comparison of transfer functions computed for the scaled 10 Hz design earthquake, soil profile Rinaldi, CEUS conditions.



CEUS, 10E-4, RI
TRANSFER FUNCTION

- LEGEND
- 1 HZ WEIGHTED MEAN RATIO; WEIGHTS:ML=0.30,MM=0.00,MH=0.70
 - 10 HZ WEIGHTED MEAN RATIO; WEIGHTS:ML=0.25,MM=0.63,MH=0.12

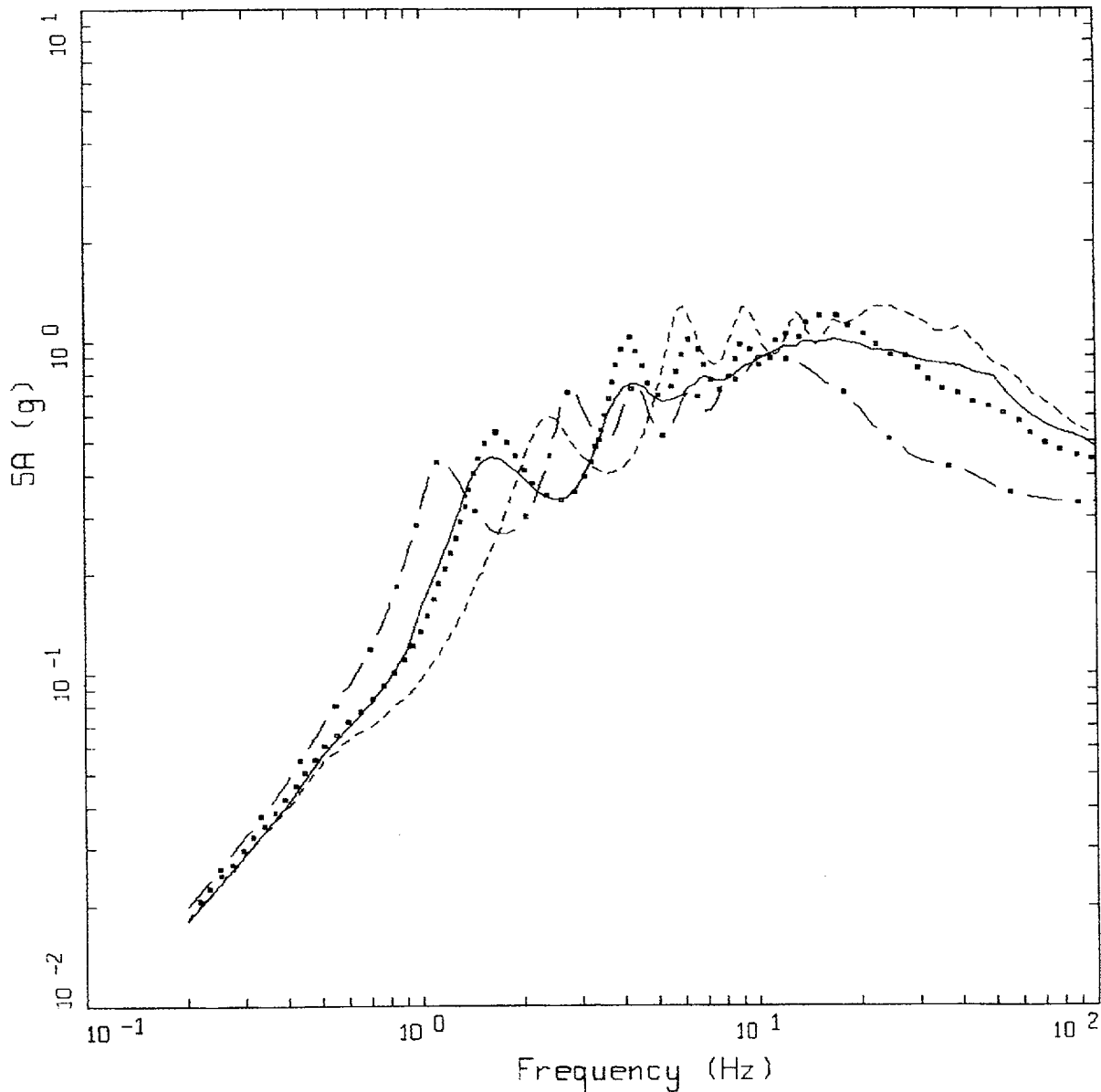
Figure 6-82. Comparison of mean transfer functions computed for the scaled 1 Hz and 10 Hz design earthquakes; soil profile Rinaldi, CEUS conditions.



CEUS, 10E-4 DESIGN SPECTRA, RI

- LEGEND
- APPROACH 2, 1 HZ AND 10 HZ DEAGGREGATION EQKS, MEAN PGA = 0.487 G
 - APPROACH 1, 10-4 ROCK CONTROL MOTION, MEAN PGA = 0.406 G
 - - - - 1 HZ MEAN; PGA = 0.243 G
 - • - • 10 HZ MEAN; PGA = 0.406 G

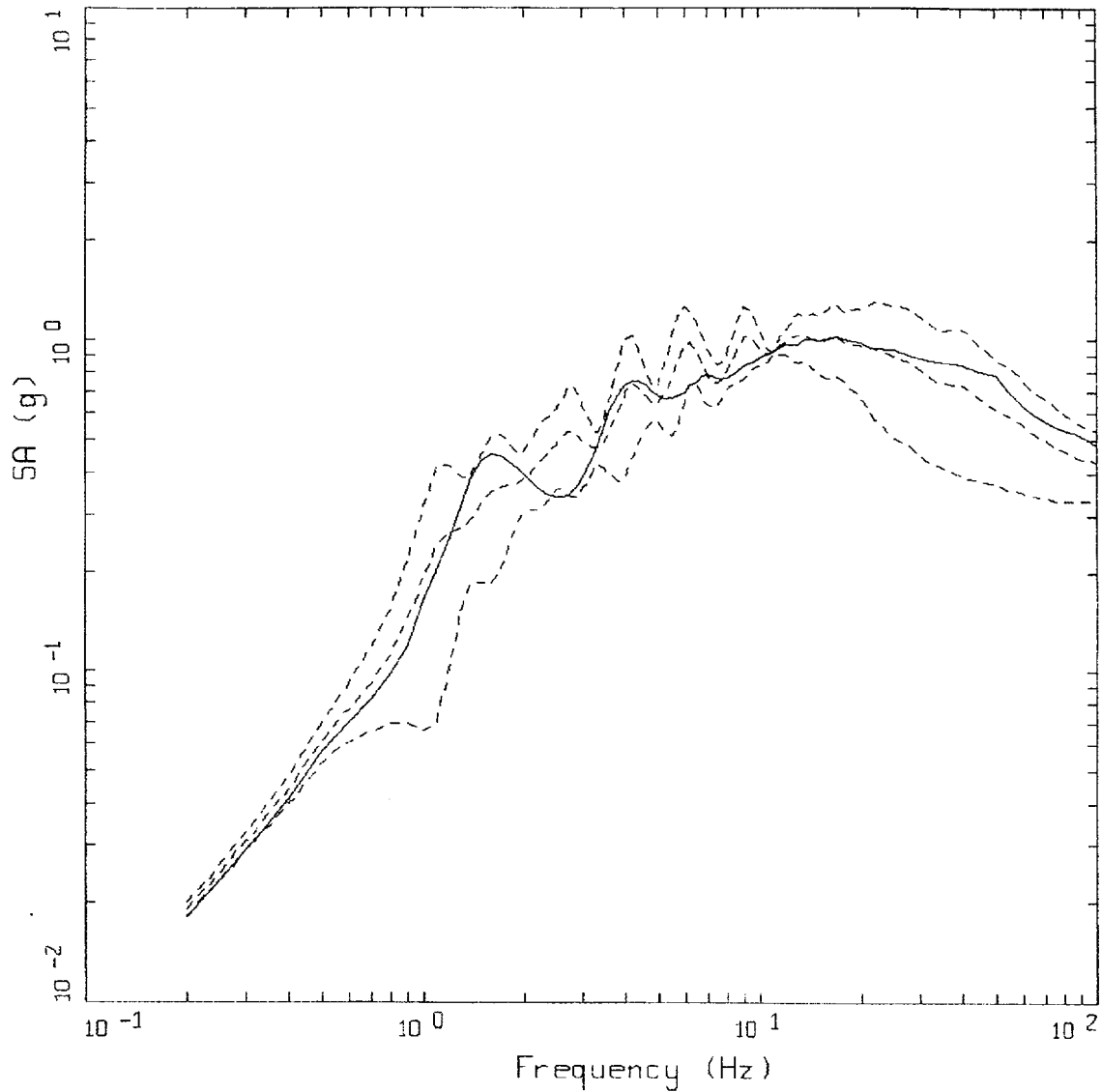
Figure 6-83. Comparison of soil spectra for Approaches 1, 2A, and 2B; soil profile Rinaldi, CEUS conditions.



CEUS 10E-4 APPROACH COMPARISON, RI

- LEGEND
- APPROACH 2, 1 HZ AND 10 HZ DEAGGREGATION EQKS, MEAN PGA = 0.487 G
 - APPROACH 1, 10-4 ROCK CONTROL MOTION, BASE CASE PGA = 0.445 G
 - APPROACH 1, 10-4 ROCK CONTROL MOTION, BASE CASE (UPPER) PGA = 0.528 G
 - . - - APPROACH 1, 10-4 ROCK CONTROL MOTION, BASE CASE (LOWER) PGA = 0.325 G

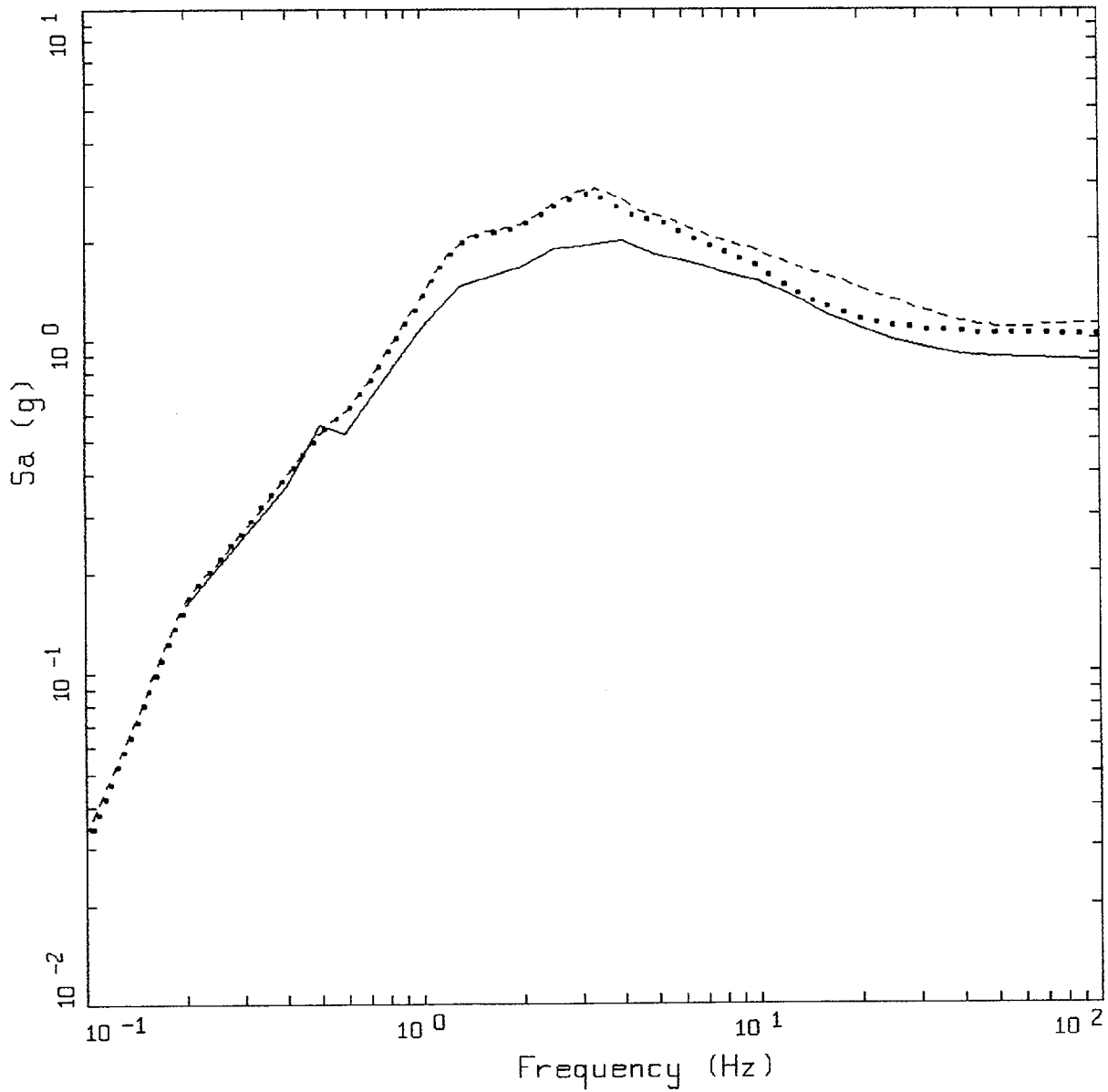
Figure 6-84. Comparison of soil spectra for Approach 2B with base case profile and deterministic profile variations (\pm factor of 2 on shear modulus); soil profile Rinaldi, CEUS conditions.



CEUS 1DE-4 APPROACH COMPARISON, RI

- LEGEND
- APPROACH 2, 1 HZ AND 10 HZ DEAGGREGATION EQKS, MEAN PGA = 0.487 G
 - APPROACH 1, 10-4 ROCK CONTROL MOTION, BASE CASE, 68TH PERCENTILE, PGA = 0.534 G
 - APPROACH 1, 10-4 ROCK CONTROL MOTION, BASE CASE, MEAN, PGA = 0.433 G
 - APPROACH 1, 10-4 ROCK CONTROL MOTION, BASE CASE, 32ND PERCENTILE, PGA = 0.331 G

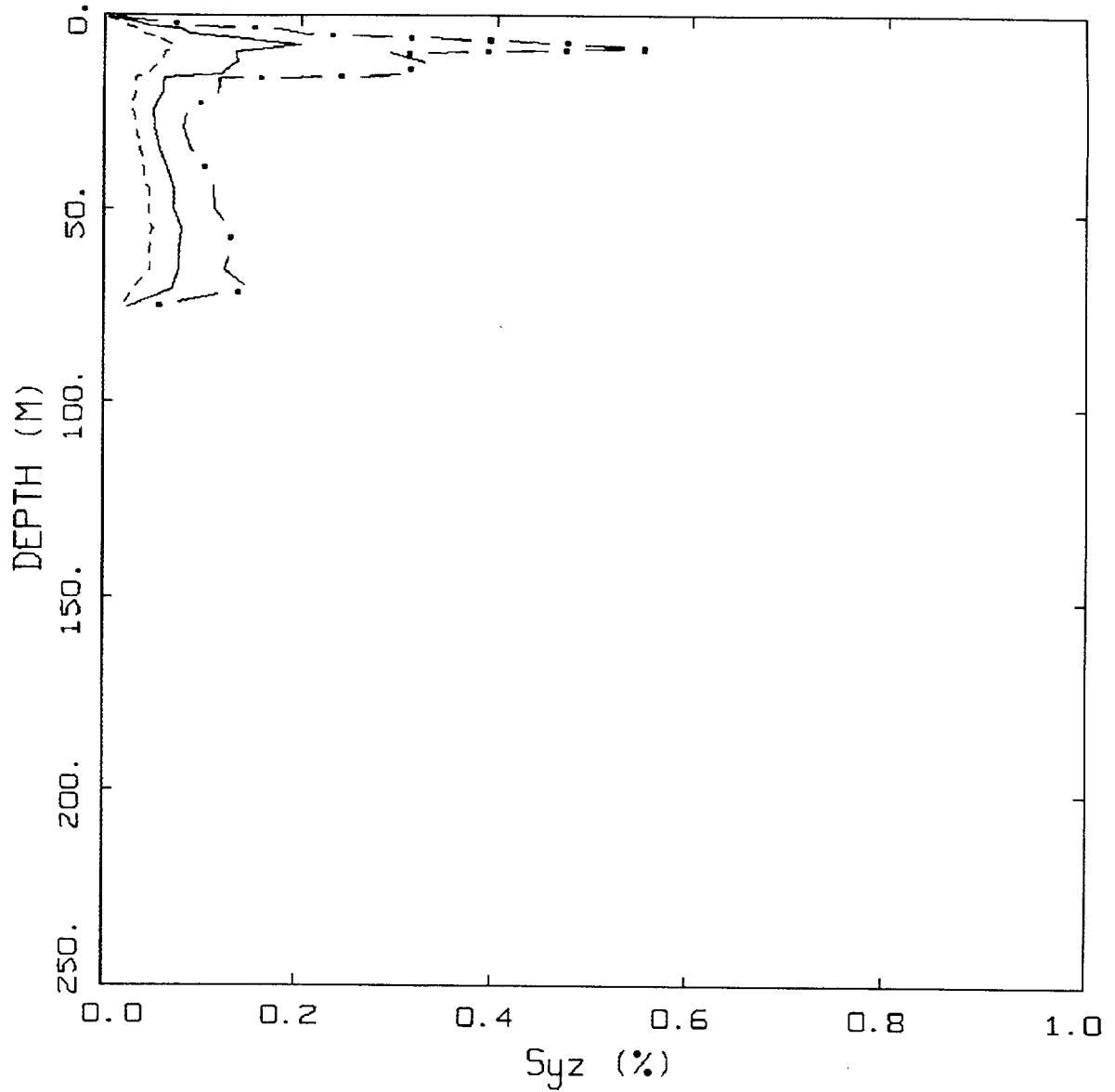
Figure 6-85. Comparison of soil spectra for Approach 2B with mean and $\pm 1\sigma$ variations of base case (\pm factor of 2 on shear modulus), soil profile Rinaldi, CEUS conditions.



WUS 10E-4 APPROACH COMPARISON, RI

- LEGEND
- APPROACH 4, 10⁻⁴ SOIL UNIFORM HAZARD SPECTRUM, PGA = 0.861 G
 - APPROACH 1, 10⁻⁴ ROCK CONTROL MOTION, MEAN PGA = 1.027 G
 - APPROACH 2, 1 HZ AND 10 HZ DEAGGREGATION EQKS, MEAN PGA = 1.114 G

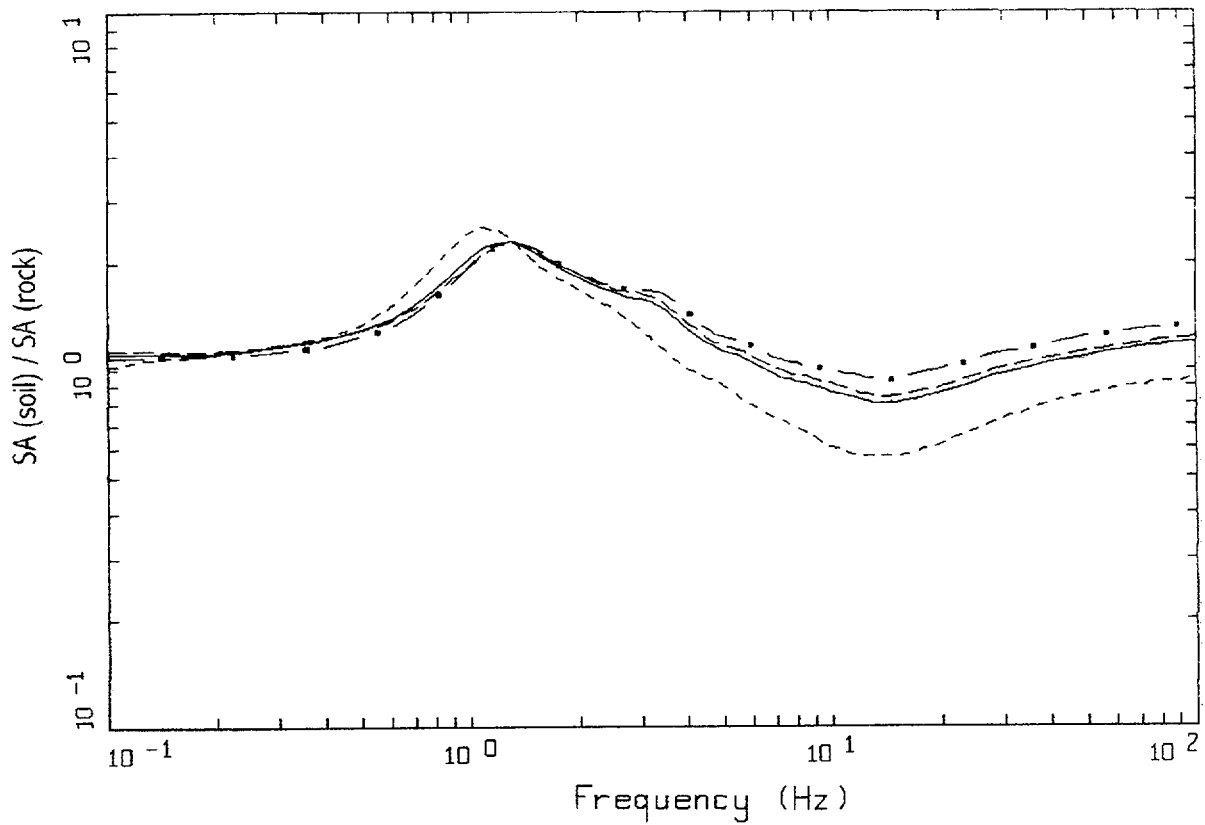
Figure 6-86. Comparison of Approaches 1, 2B, and 4 10⁻⁴ UHS on soil for profile Rinaldi: WUS conditions.



WUS, 10-4, RI
EFFECTIVE STRAINS (SYZ)

LEGEND
 - . - 84TH PERCENTILE
 ——— 50TH PERCENTILE
 - - - - 16TH PERCENTILE

Figure 6-87. Median and $\pm 1 \sigma$ effective strains for soil profile Rinaldi using Approach 1: WUS conditions.

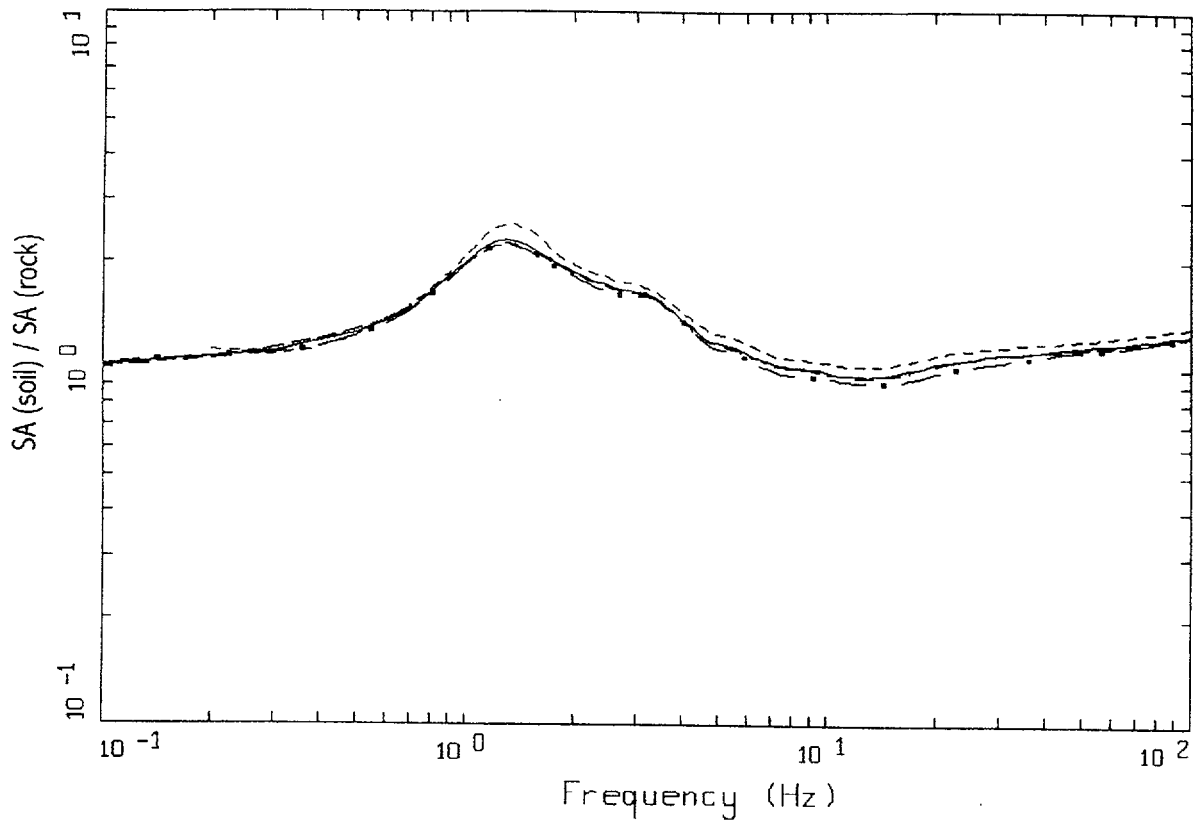


WUS, 10E-4, 1HZ DESIGN, RI
 SURFACE MOTION, 1HZ TRANSFER FUNCTION
 WEIGHTS: ML=0.24, MM=0.47, MH=0.29

LEGEND

- ML = 5.8, D = 10 KM MEAN RATIO
- . - . MM = 6.9, D = 14 KM, DESIGN MEAN RATIO
- • — MH = 7.8, D = 40 KM MEAN RATIO
- WEIGHTED MEAN RATIO

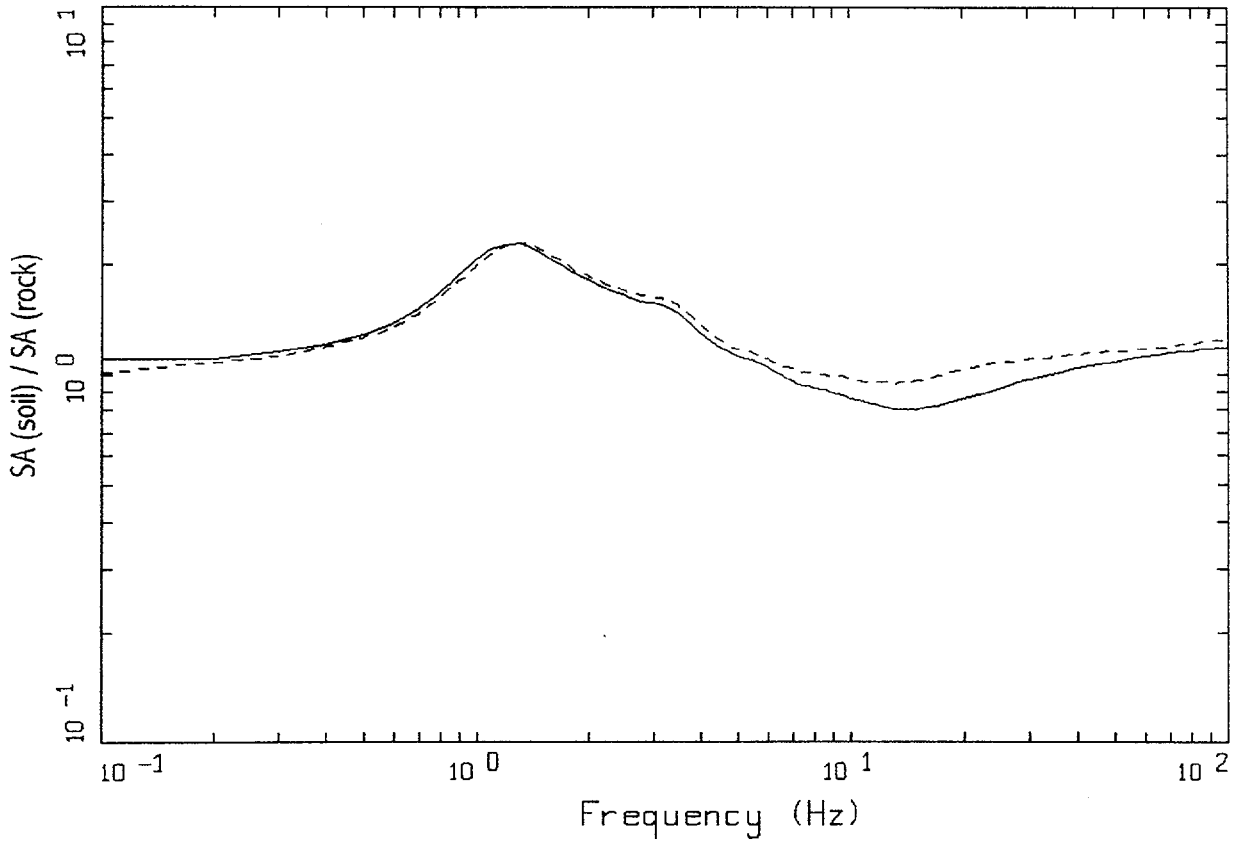
Figure 6-88. Comparison of transfer functions computed for the scaled 1 Hz design earthquake; soil profile Rinaldi, WUS conditions.



WUS, 10E-4, 10HZ DESIGN, RI
 SURFACE MOTION, 10HZ TRANSFER FUNCTION
 WEIGHTS: ML=0.20, MM=0.60, MH=0.20

LEGEND
 - - - - - ML = 5.1, D = 10 KM MEAN RATIO
 - · - · - MM = 6.1, D = 14 KM, DESIGN MEAN RATIO
 — · — MH = 7.8, D = 30 KM MEAN RATIO
 ——— WEIGHTED MEAN RATIO

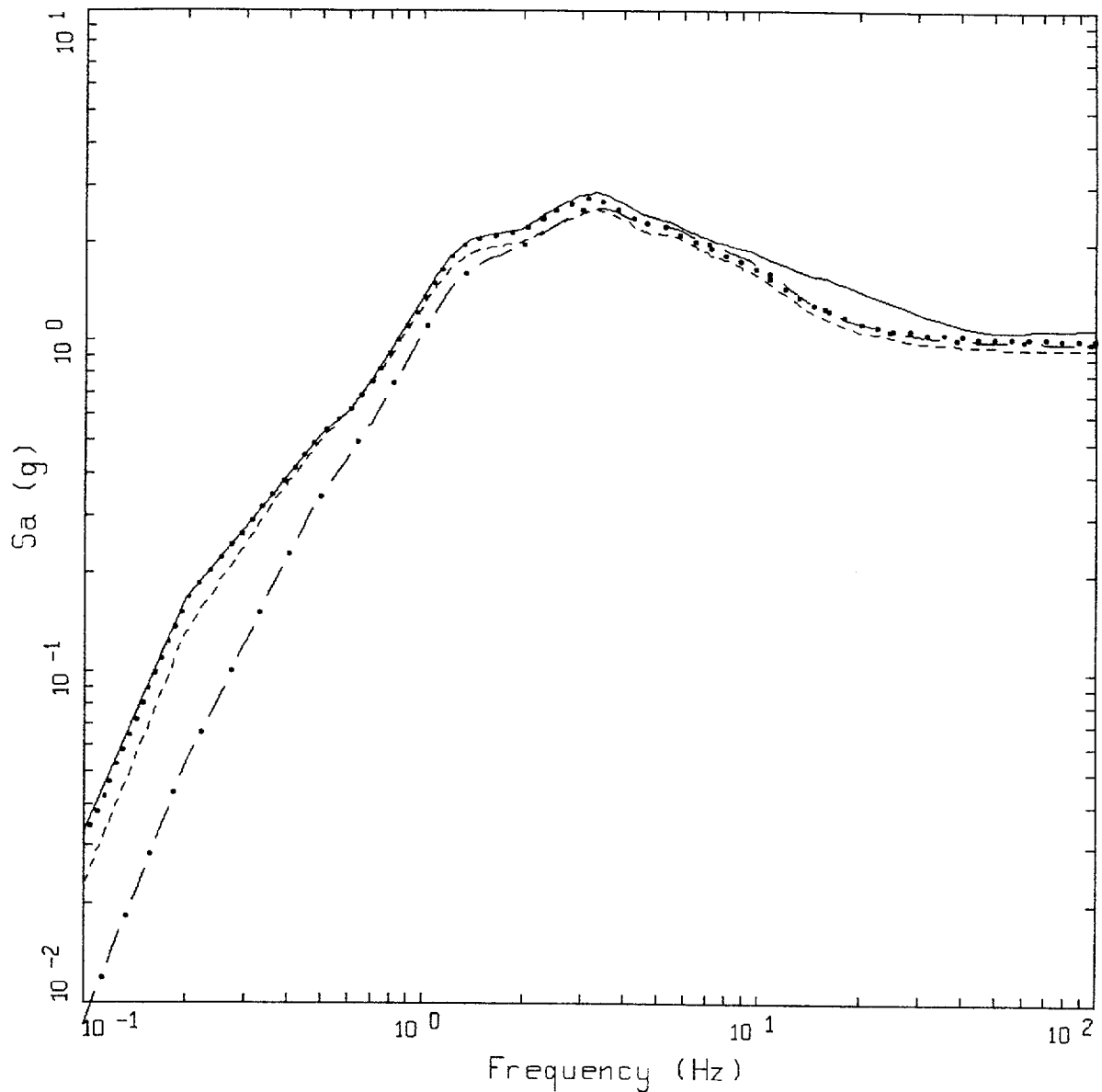
Figure 6-89. Comparison of transfer functions computed for the scaled 10 Hz design earthquake; soil profile Rinaldi, WUS conditions.



WUS, 10E-4, RI
AMPLIFICATION

LEGEND
 ——— 1 HZ WEIGHTED MEAN RATIO; WEIGHTS:ML=0.20,MM=0.60,MH=0.20
 - - - - 10 HZ WEIGHTED MEAN RATIO; WEIGHTS:ML=0.20,MM=0.60,MH=0.20

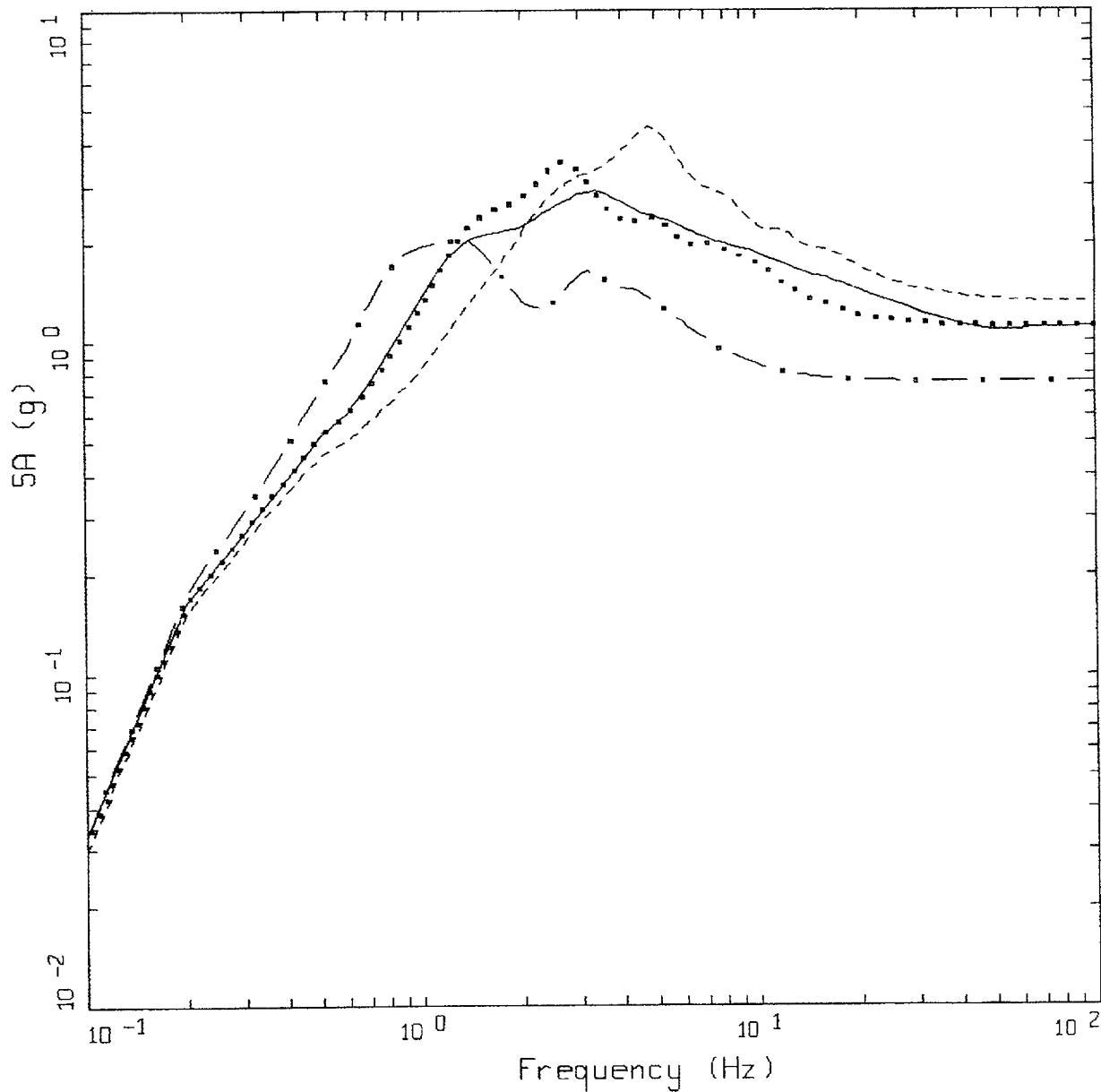
Figure 6-90. Comparison of mean transfer functions computed for the scaled 1 Hz and 10 Hz design earthquakes; soil profile Rinaldi, WUS conditions.



WUS, 10E-4 DESIGN SPECTRA, RI

- LEGEND
- APPROACH 2, 1 HZ AND 10 HZ DEAGGREGATION EQKS, MEAN PGA = 1.114 G
 - APPROACH 1, 10⁻⁴ ROCK CONTROL MOTION, MEAN PGA = 1.028 G
 - 1 HZ MEAN; PGA = 0.964 G
 - · - · 10 HZ MEAN; PGA = 1.003 G

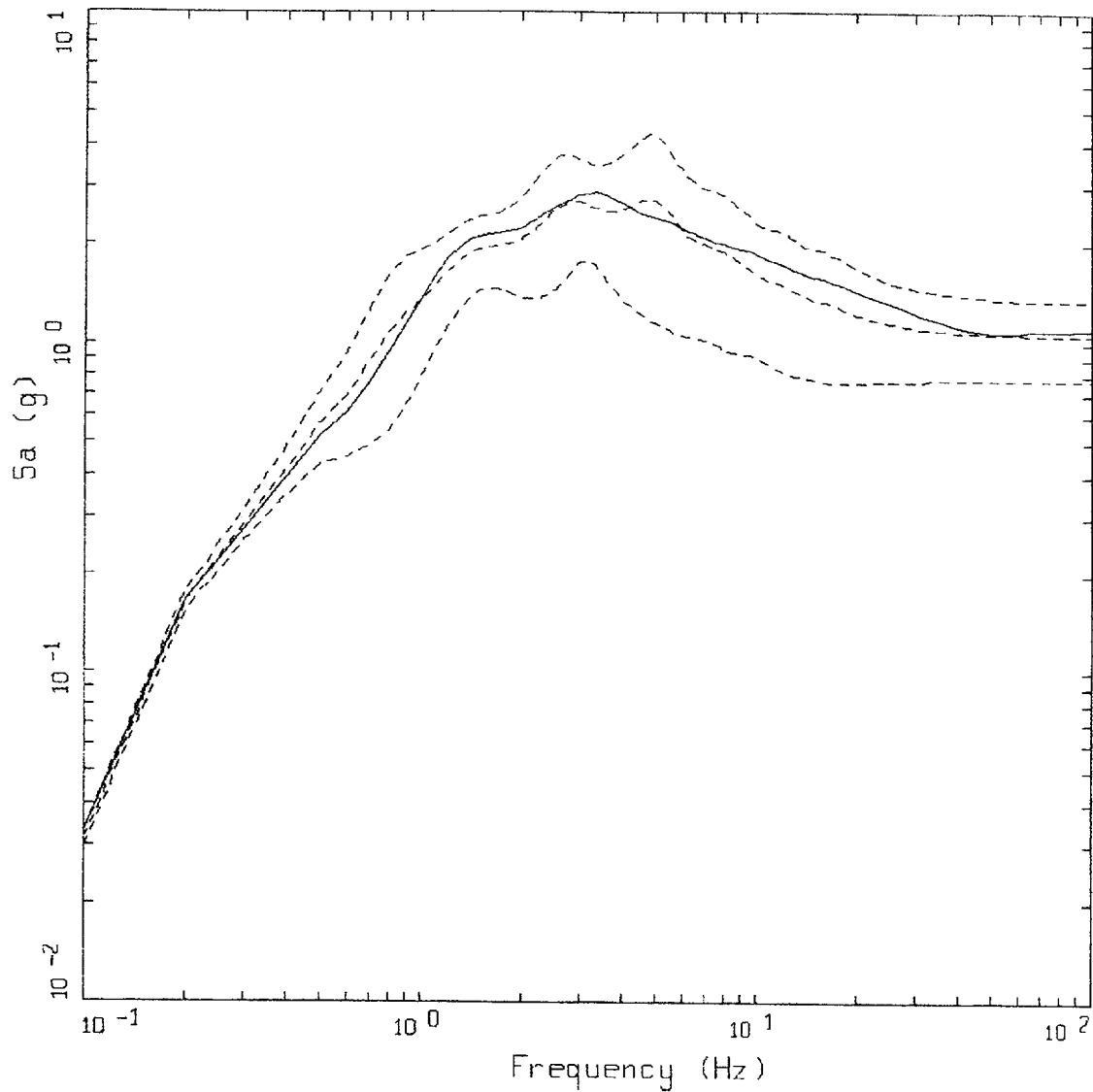
Figure 6-91. Comparison of soil spectra for Approaches 1, 2A, and 2B; soil profile Rinaldi, WUS conditions.



WUS 10E-4 APPROACH COMPARISON, RI

- LEGEND
- APPROACH 2, 1 HZ AND 10 HZ DEAGGREGATION EQKS, MEAN PGA = 1.114 G
 - APPROACH 1, 10-4 ROCK CONTROL MOTION, BASE CASE PGA = 1.132 G
 - APPROACH 1, 10-4 ROCK CONTROL MOTION, BASE CASE (UPPER) PGA = 1.101 G
 - . - . - APPROACH 1, 10-4 ROCK CONTROL MOTION, BASE CASE (LOWER) PGA = 0.756 G

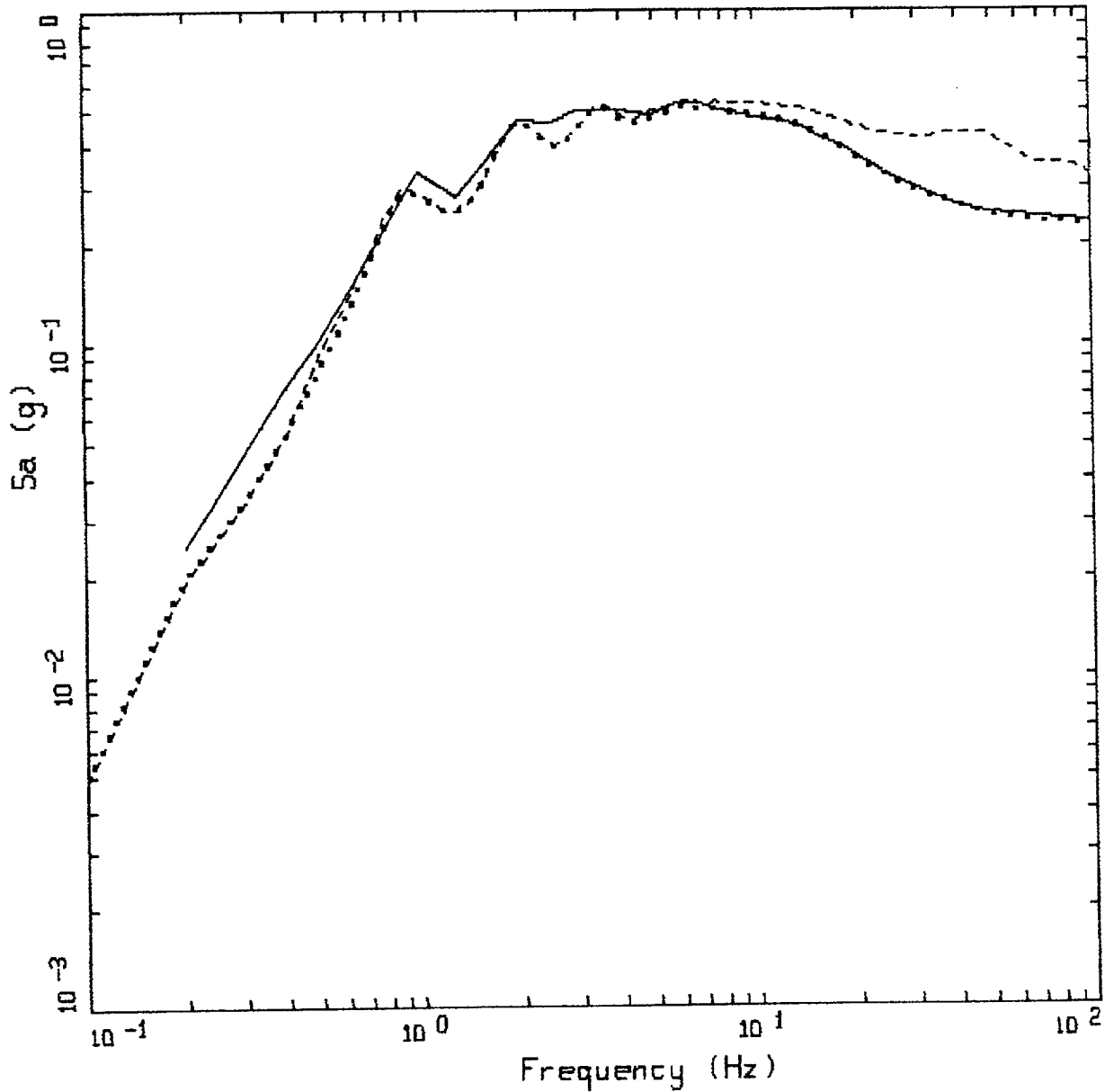
Figure 6-92. Comparison of soil spectra for Approach 2B with base case profile and deterministic profile variations (\pm factor of 2 on shear modulus); soil profile Rinaldi, WUS conditions.



WUS 10E-4 APPROACH COMPARISON, RI

- LEGEND
- APPROACH 2, 1 HZ AND 10 HZ DISAGGREGATION EQKS, MEAN PGA = 1.114 G
 - APPROACH 1, 10-4 ROCK CONTROL MOTION, BASE CASE, 84TH PERCENTILE, PGA = 1.342 G
 - - - - - APPROACH 1, 10-4 ROCK CONTROL MOTION, BASE CASE, MEAN, PGA = 1.060 G
 - · - · - APPROACH 1, 10-4 ROCK CONTROL MOTION, BASE CASE, 16TH PERCENTILE, PGA = 0.777 G

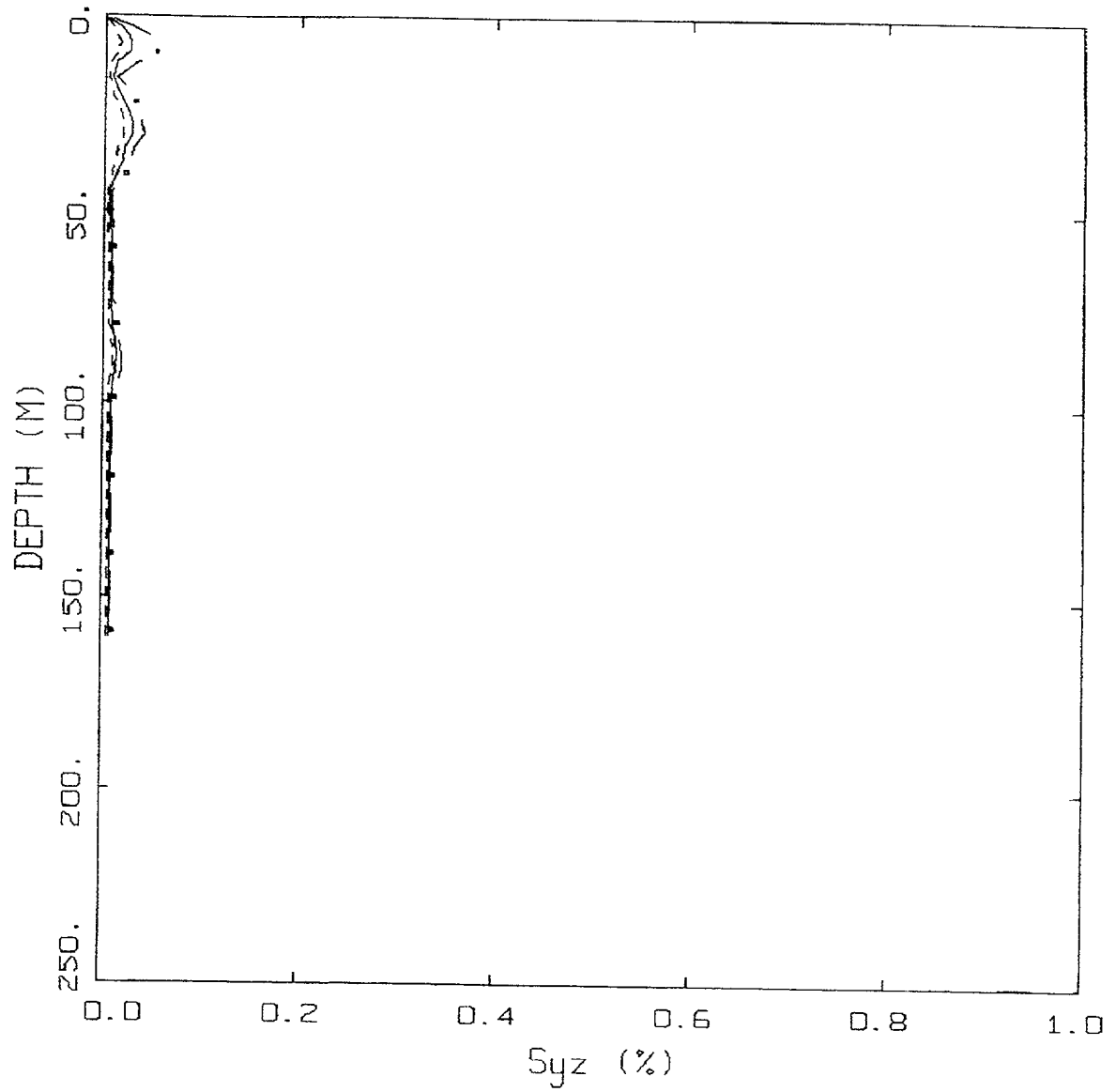
Figure 6-93. Comparison of soil spectra for Approach 2B with mean and $\pm 1\sigma$ variations of base case (\pm factor of 2 on shear modulus), soil profile Rinaldi, WUS conditions.



CEUS 10E-4 APPROACH COMPARISON, G2

- LEGEND
- APPROACH 4, 10⁻⁴ SOIL UNIFORM HAZARD SPECTRUM; PGA = 0.232 G
 - APPROACH 1, 10⁻⁴ ROCK CONTROL MOTION, MEAN PGA = 0.230 G
 - - - - APPROACH 2, 1 HZ AND 10 HZ DEAGGREGATION EQS, MEAN PGA = 0.325 G

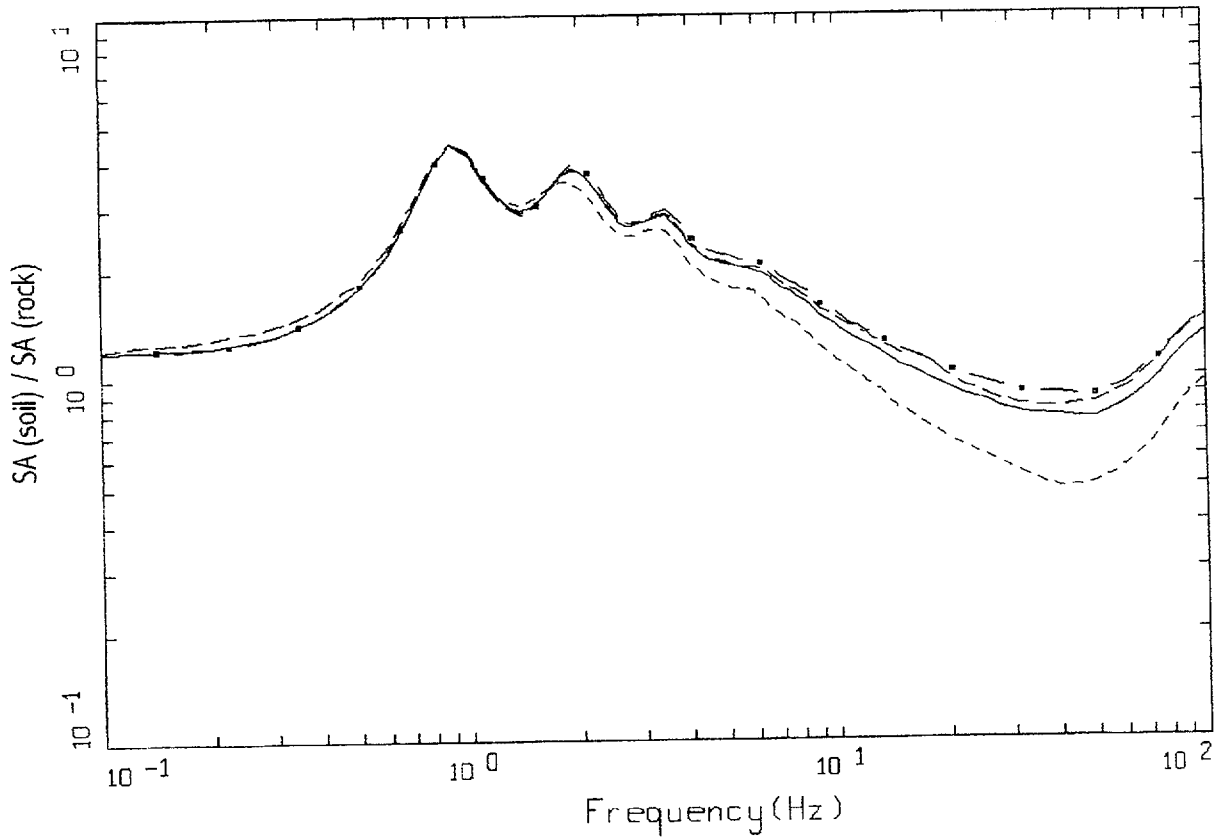
Figure 6-94. Comparison of Approaches 1, 2B, and 4 10⁻⁴ UHS on soil for profile Gilroy 2: CEUS conditions.



CEUS, 10-4, G2
 EFFECTIVE STRAINS (SYZ)

- LEGEND
- · — 84TH PERCENTILE
 - 50TH PERCENTILE
 - - - 16TH PERCENTILE

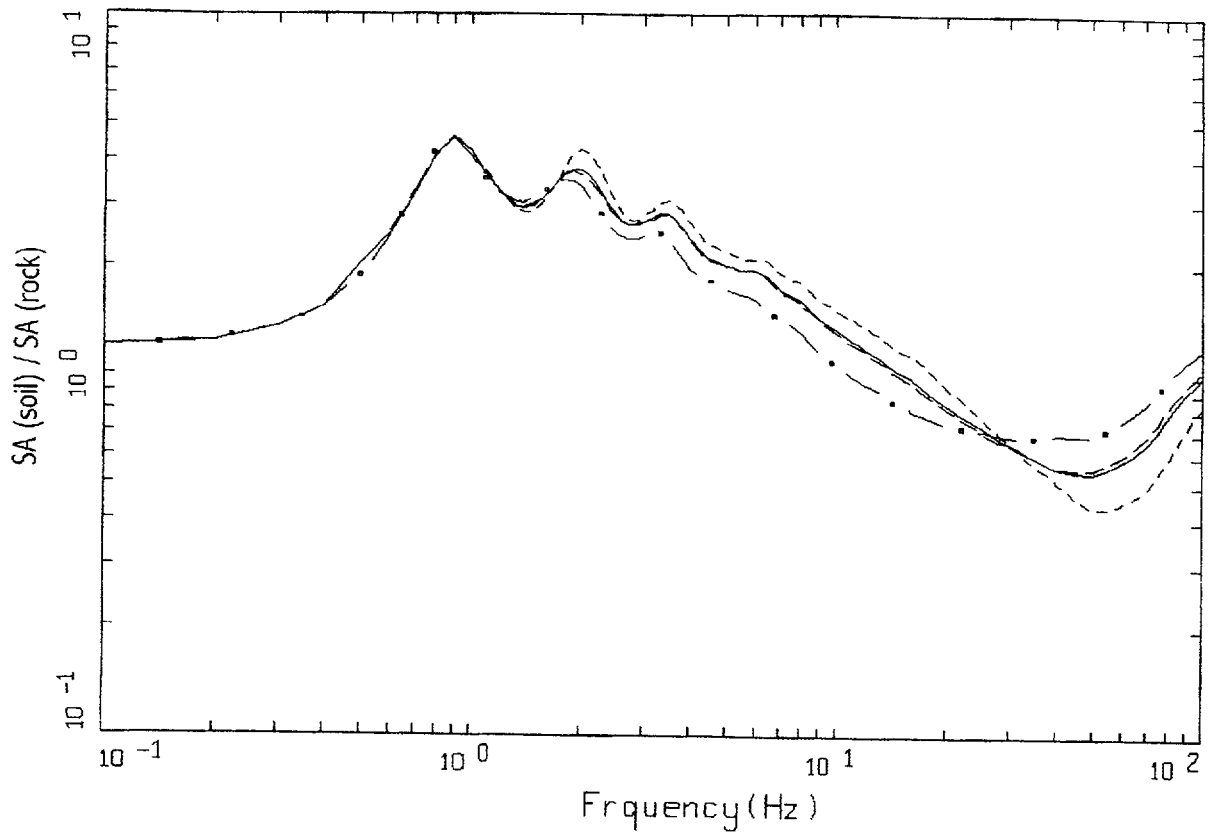
Figure 6-95. Median and $\pm 1 \sigma$ effective strains for soil profile Gilroy 2 using Approach 1: CEUS conditions.



CEUS, 10E-4, 1HZ DESIGN, G2
 SURFACE MOTION, 1HZ TRANSFER FUNCTION
 WEIGHTS: ML=0.30, MM=0.00, MH=0.70

- LEGEND
- ML = 5.7, D = 20 KM MEAN RATIO
 - · - · - MM = 7.0, D = 100 KM MEAN RATIO
 - · — MH = 7.7, D = 130 KM, DESIGN MEAN RATIO
 - WEIGHTED MEAN RATIO

Figure 6-96. Comparison of transfer functions computed for the scaled 1 Hz design earthquake, soil profile Gilroy 2, CEUS conditions.

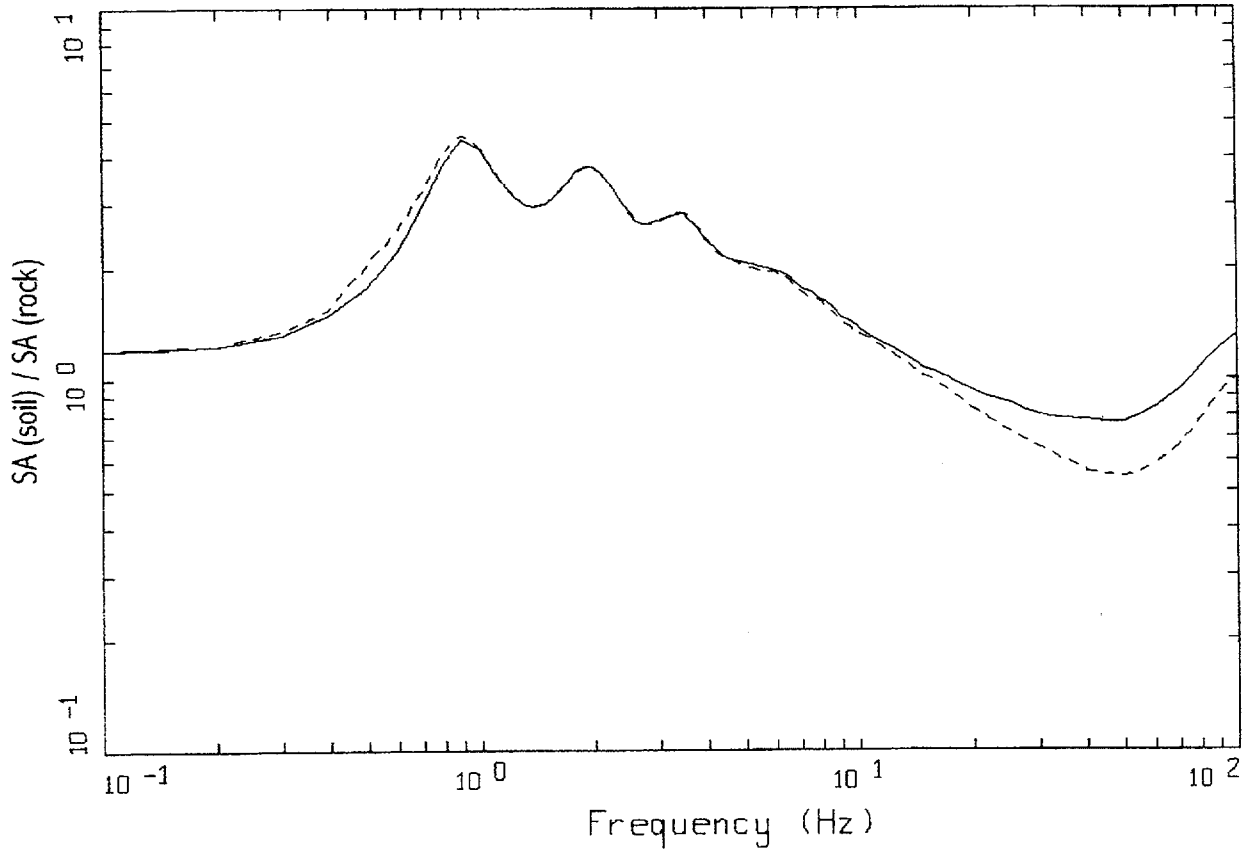


CEUS, 10E-4, 10HZ DESIGN, G2
 SURFACE MOTION, 10HZ TRANSFER FUNCTION
 WEIGHTS: ML=0.25, MM=0.63, MH=0.12

LEGEND

- ML = 4.6, D = 8 KM MEAN RATIO
- · - · - MM = 5.6, D = 8 KM, DESIGN MEAN RATIO
- · — MH = 7.7, D = 130 KM MEAN RATIO
- WEIGHTED MEAN RATIO

Figure 6-97. Comparison of transfer functions computed for the scaled 10 Hz design earthquake: soil profile Gilroy 2, CEUS conditions.

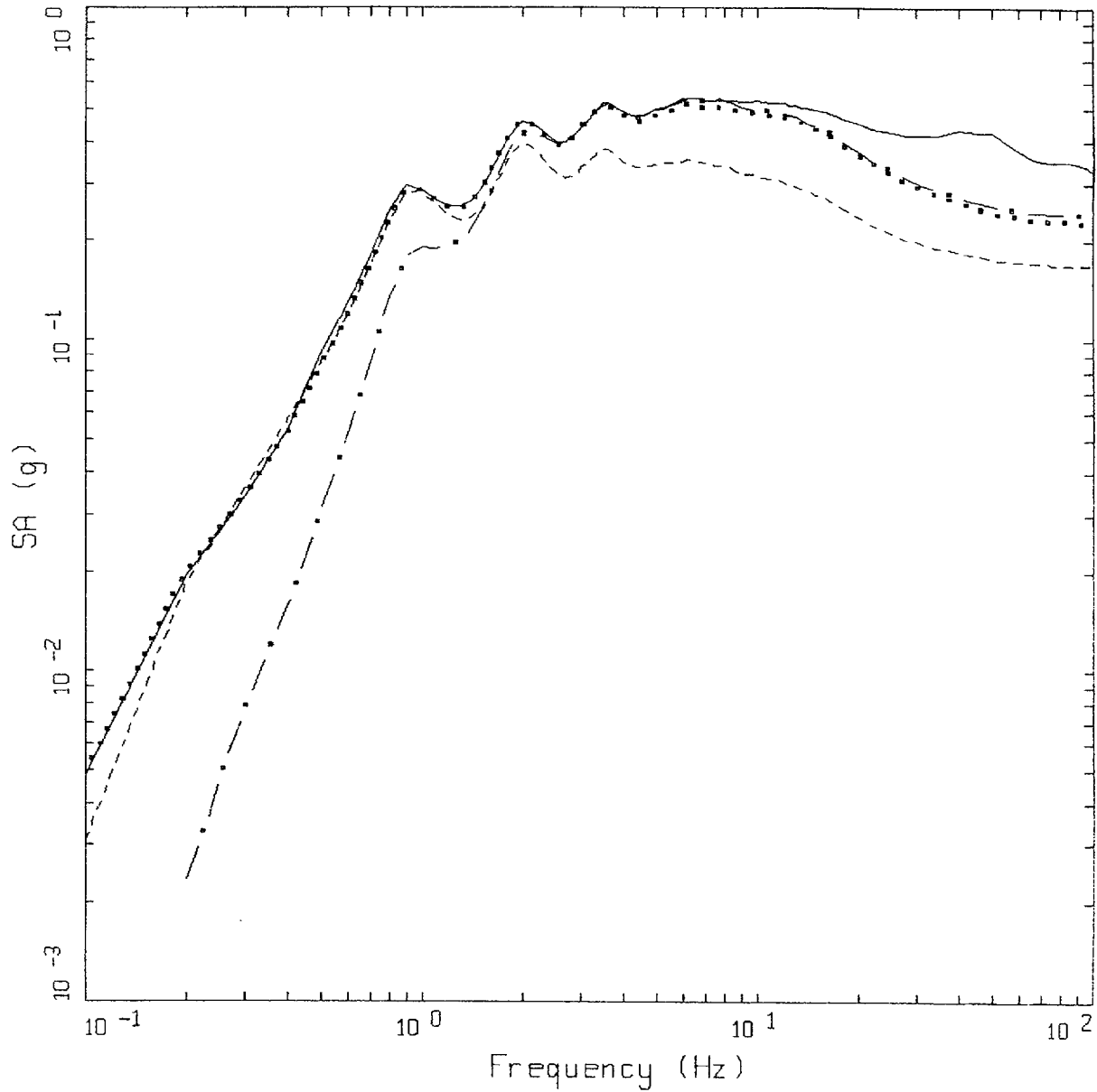


CEUS, 10E-4, G2
TRANSFER FUNCTION

LEGEND

- 1 HZ WEIGHTED MEAN RATIO; WEIGHTS:ML=0.30,MM=0.00,MH=0.70
- 10 HZ WEIGHTED MEAN RATIO; WEIGHTS:ML=0.25,MM=0.63,MH=0.12

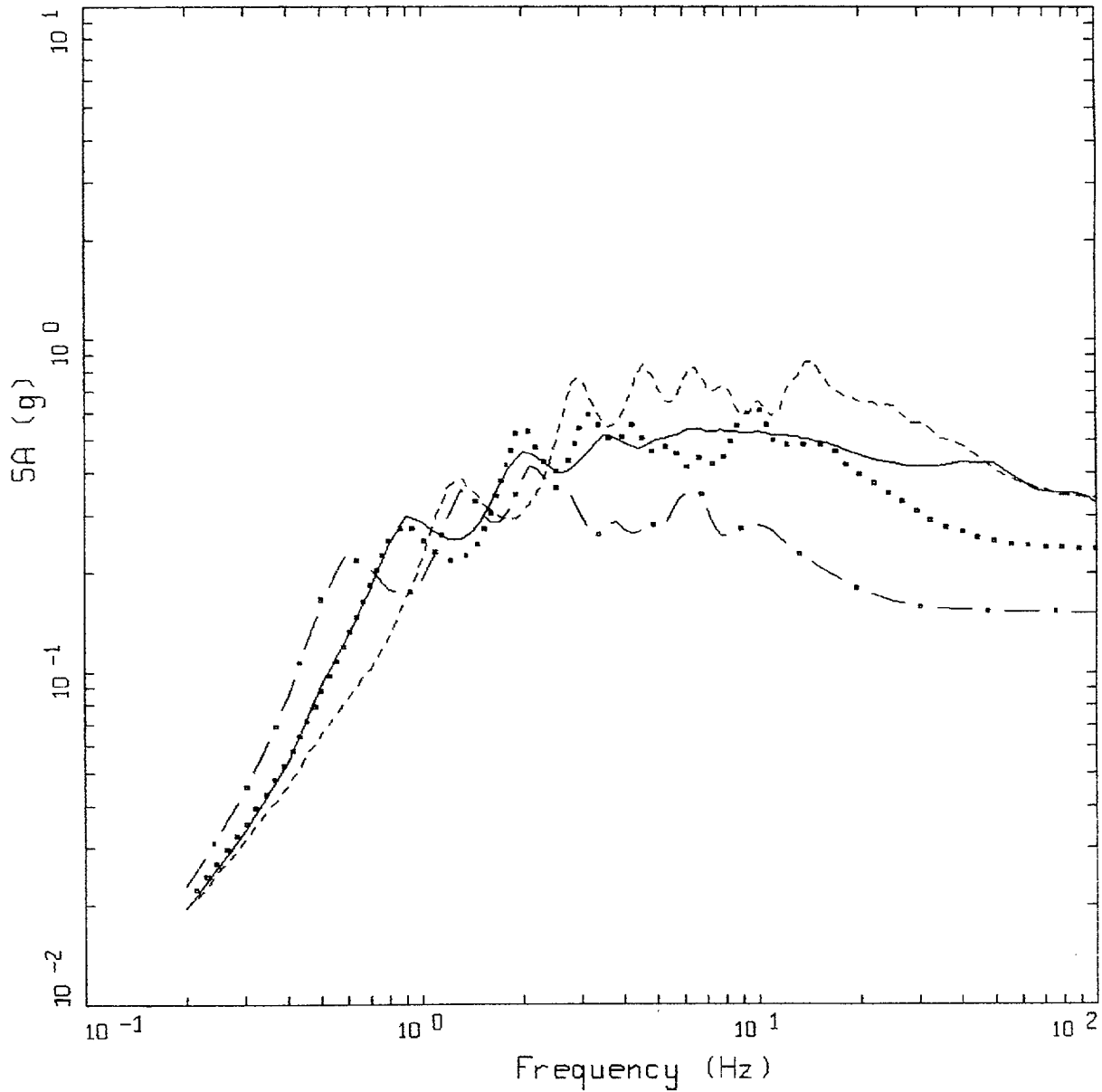
Figure 6-98. Comparison of mean transfer functions computed for the scaled 1 Hz and 10 Hz design earthquakes; soil profile Gilroy 2, CEUS conditions.



CEUS, 10E-4 DESIGN SPECTRA, GZ

- LEGEND
- APPROACH 2, 1 HZ AND 10 HZ DEAGGREGATION EQKS, MEAN PGA = 0.325 G
 - APPROACH 1, 10-4 ROCK CONTROL MOTION, MEAN PGA = 0.169 G
 - 1 HZ MEAN; PGA = 0.168 G
 - . - . 10 HZ MEAN; PGA = 0.241 G

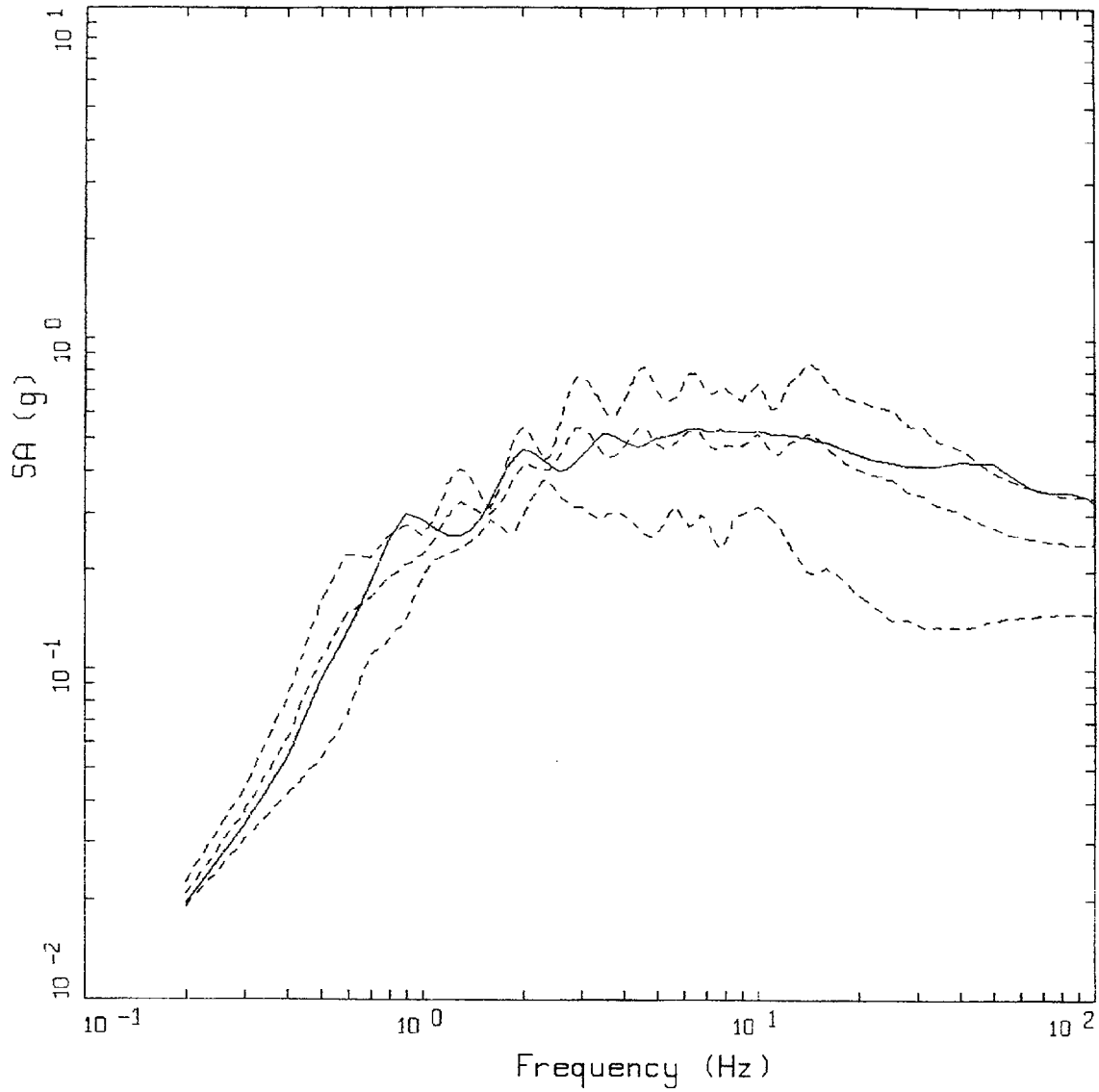
Figure 6-99. Comparison of soil spectra for Approaches 1, 2A, and 2B; soil profile Gilroy 2, CEUS conditions.



CEUS 1DE-4 APPROACH COMPARISON, G2

- LEGEND
- APPROACH 2, 1 HZ AND 10 HZ DEAGGREGATION EQKS, MEAN PGA = 0.325 G
 - APPROACH 1, 10-4 ROCK CONTROL MOTION, BASE CASE PGA = 0.237 G
 - APPROACH 1, 10-4 ROCK CONTROL MOTION, BASE CASE (UPPER) PGA = 0.335 G
 - . - . APPROACH 1, 10-4 ROCK CONTROL MOTION, BASE CASE (LOWER) PGA = 0.152 G

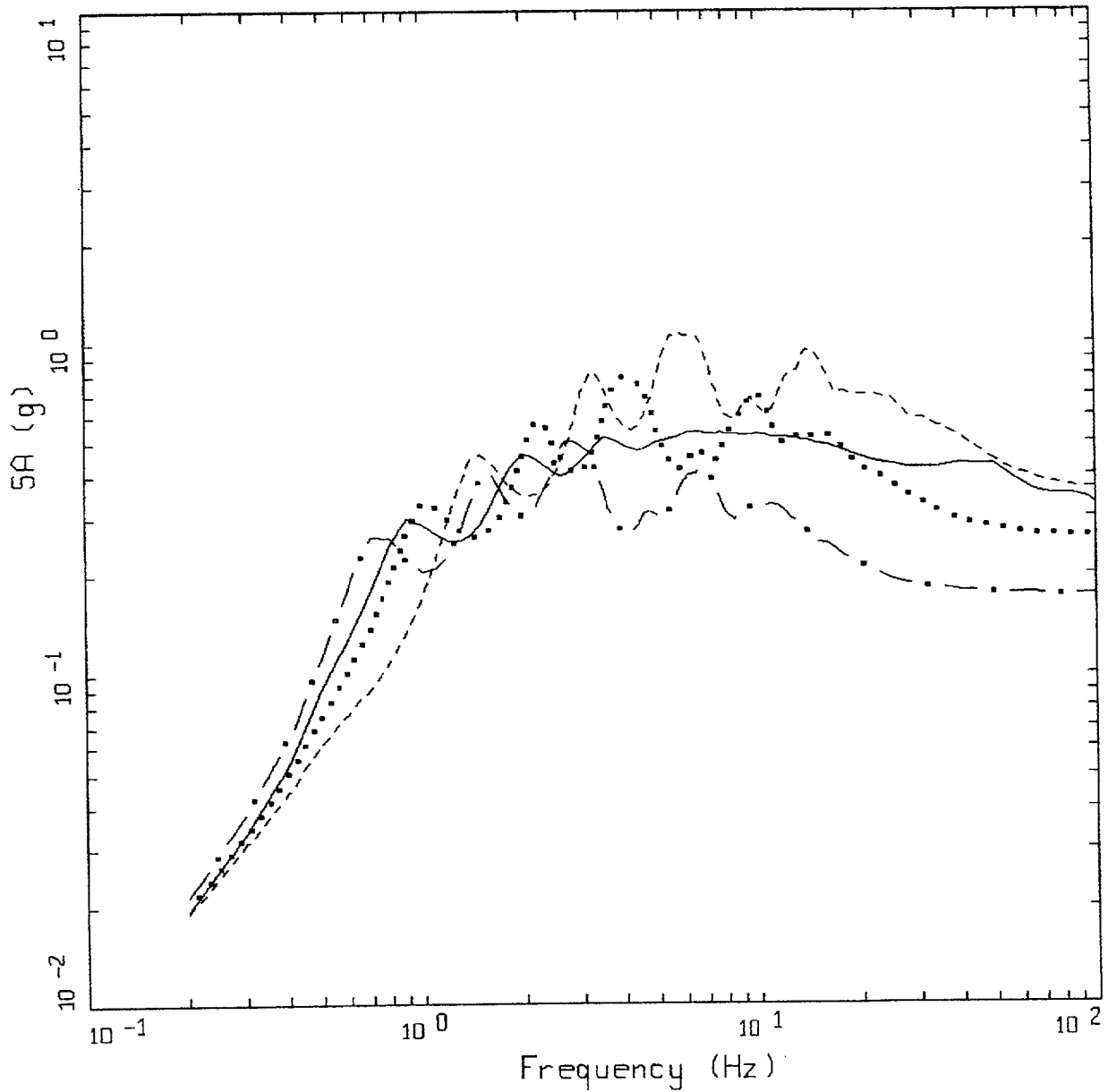
Figure 6-100. Comparison of soil spectra for Approach 2B with base case profile and deterministic profile variations (\pm factor of 2 on shear modulus); soil profile Gilroy 2, CEUS conditions.



CEUS 10E-4 APPROACH COMPARISON, G2

- LEGEND
- APPROACH 2, 1 HZ AND 10 HZ DEAGGREGATION EQKS, MEAN PGA = 0.325 G
 - APPROACH 1, 10-4 ROCK CONTROL MOTION, BASE CASE, 68TH PERCENTILE, PGA = 0.333 G
 - APPROACH 1, 10-4 ROCK CONTROL MOTION, BASE CASE, MEAN, PGA = 0.241 G
 - APPROACH 1, 10-4 ROCK CONTROL MOTION, BASE CASE, 32ND PERCENTILE, PGA = 0.150 G

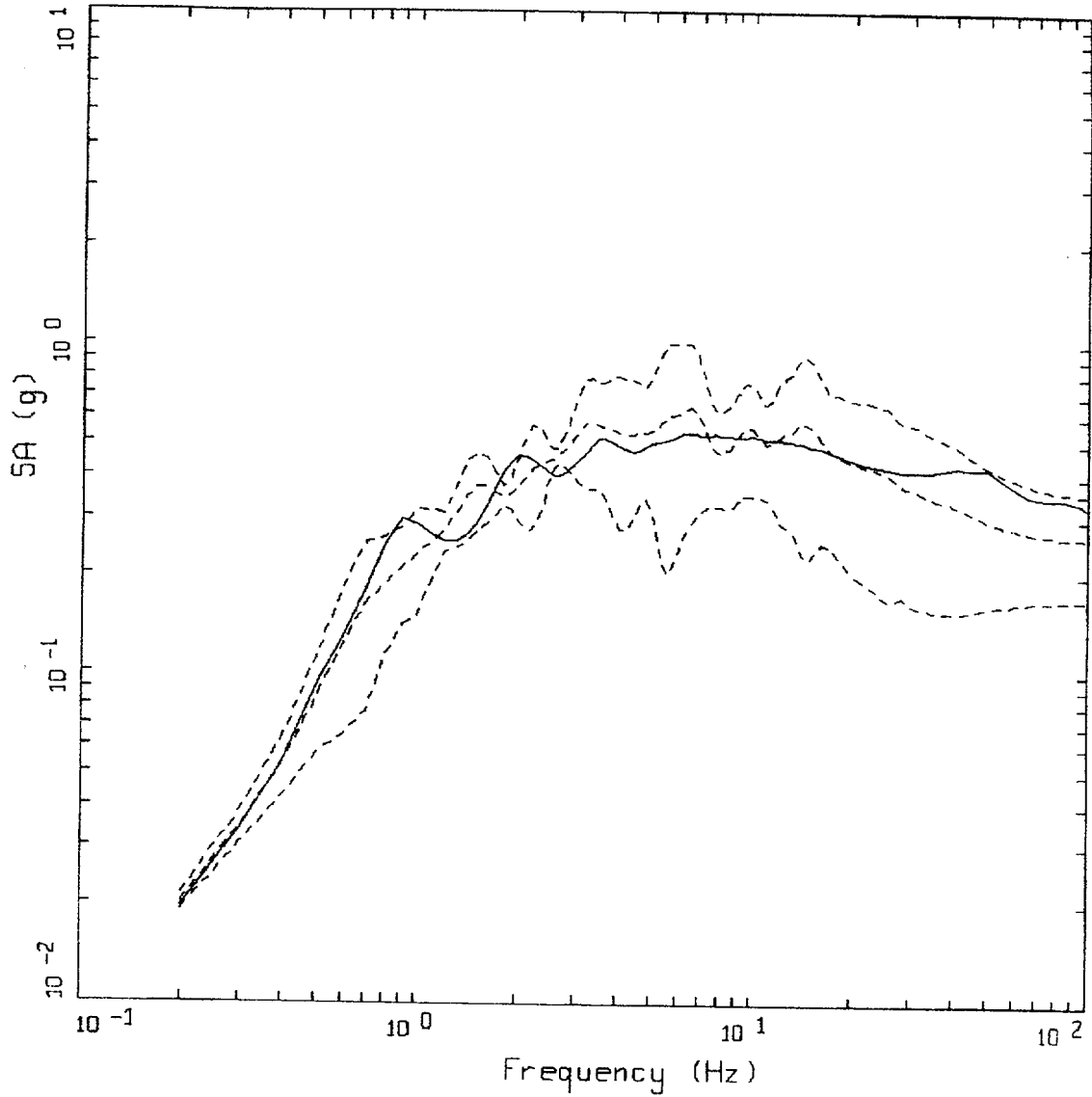
Figure 6-101. Comparison of soil spectra for Approach 2B with mean and $\pm 1\sigma$ variations of base case (\pm factor of 2 on shear modulus), soil profile Gilroy 2, CEUS conditions.



CEUS 10E-4 APPROACH COMPARISON, G2
 SOIL PROFILE TO 150 M (500 FT)

- LEGEND
- APPROACH 2, 1 HZ AND 10 HZ DEAGGREGATION EQKS, MEAN PGA = 0.325 G
 - APPROACH 1, 10-4 ROCK CONTROL MOTION, BASE CASE PGA = 0.259 G
 - APPROACH 1, 10-4 ROCK CONTROL MOTION, BASE CASE (UPPER) PGA = 0.361 G
 - . - APPROACH 1, 10-4 ROCK CONTROL MOTION, BASE CASE (LOWER) PGA = 0.172 G

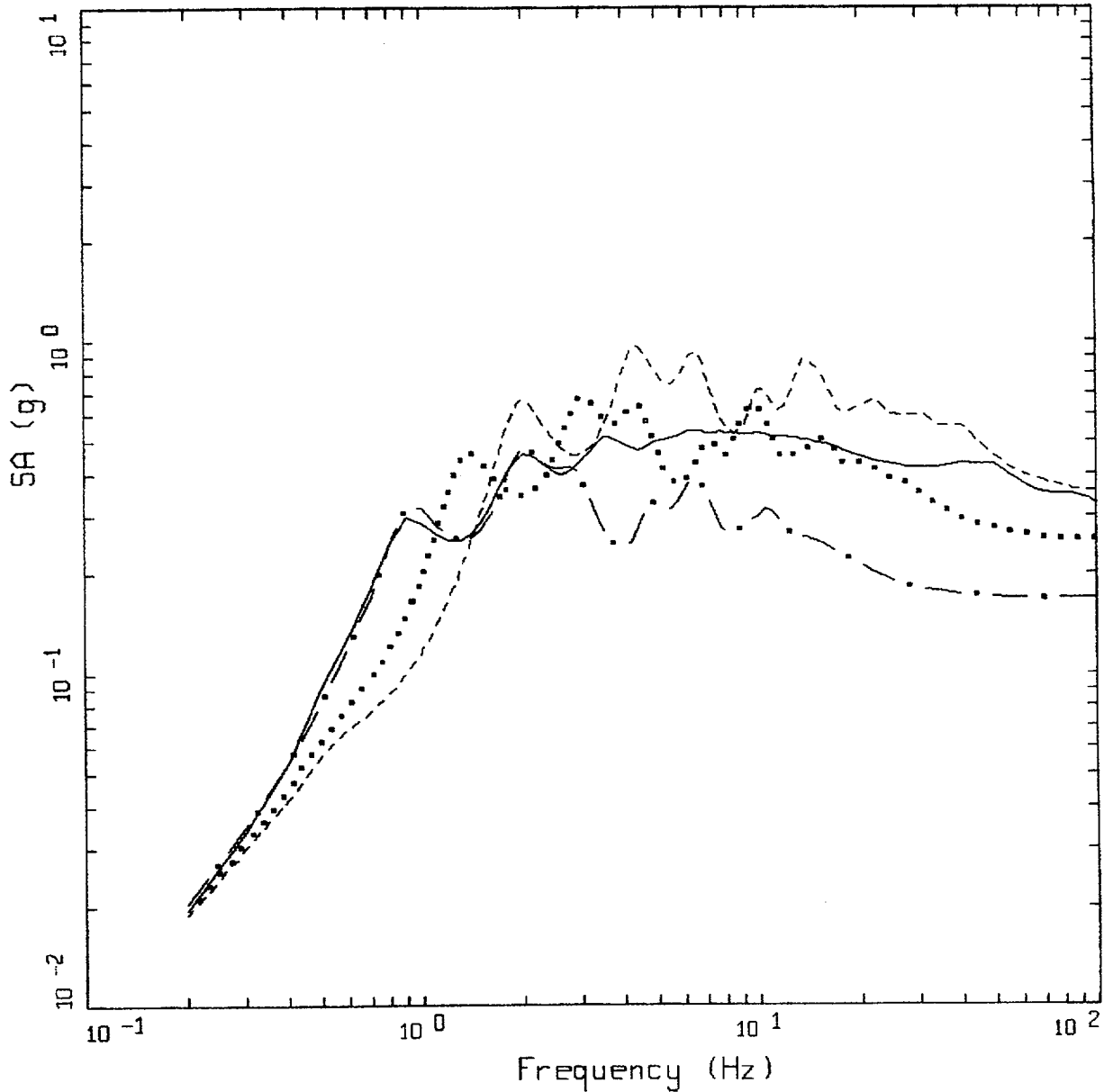
Figure 6-102. Comparison of soil spectra for Approach 2B (full profile) with base case profile and deterministic profile variations (\pm factor of 2 on shear modulus) with profile truncated at 150m; soil profile Gilroy 2, CEUS conditions.



CEUS 10E-4 APPROACH COMPARISON, G2
 SOIL PROFILE TO 150 M (500 FT)

- LEGEND
- APPROACH 2, 1 HZ AND 10 HZ DEAGGREGATION EQKS, MEAN PGA = 0.325 G
 - APPROACH 1, 10-4 ROCK CONTROL MOTION, BASE CASE, 68TH PERCENTILE, PGA = 0.358 G
 - APPROACH 1, 10-4 ROCK CONTROL MOTION, BASE CASE, MEAN, PGA = 0.264 G
 - APPROACH 1, 10-4 ROCK CONTROL MOTION, BASE CASE, 32ND PERCENTILE, PGA = 0.170 G

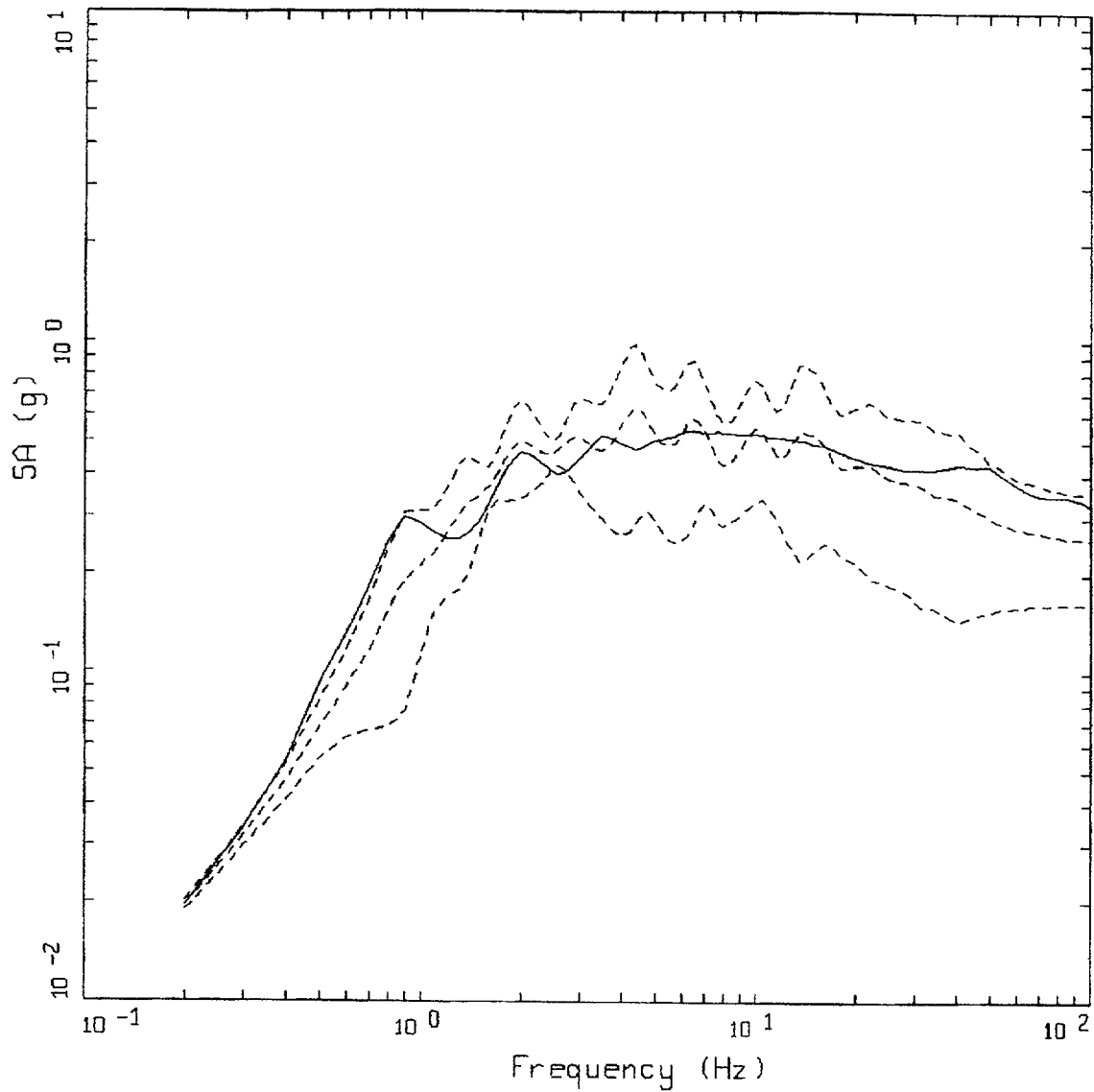
Figure 6-103. Comparison of soil spectra for Approach 2B (full profile) with mean and $\pm 1\sigma$ profile variations with profile truncated at 150m. Soil profile Gilroy 2, CEUS conditions.



CEUS 10E-4 APPROACH COMPARISON, G2
 SOIL PROFILE TO 90 M (300 FT)

- LEGEND
- APPROACH 2, 1 HZ AND 10 HZ DEAGGREGATION EQKS, MEAN PGA = 0.325 G
 - APPROACH 1, 10-4 ROCK CONTROL MOTION, BASE CASE PGA = 0.253 G
 - APPROACH 1, 10-4 ROCK CONTROL MOTION, BASE CASE (UPPER) PGA = 0.354 G
 - . - . APPROACH 1, 10-4 ROCK CONTROL MOTION, BASE CASE (LOWER) PGA = 0.167 G

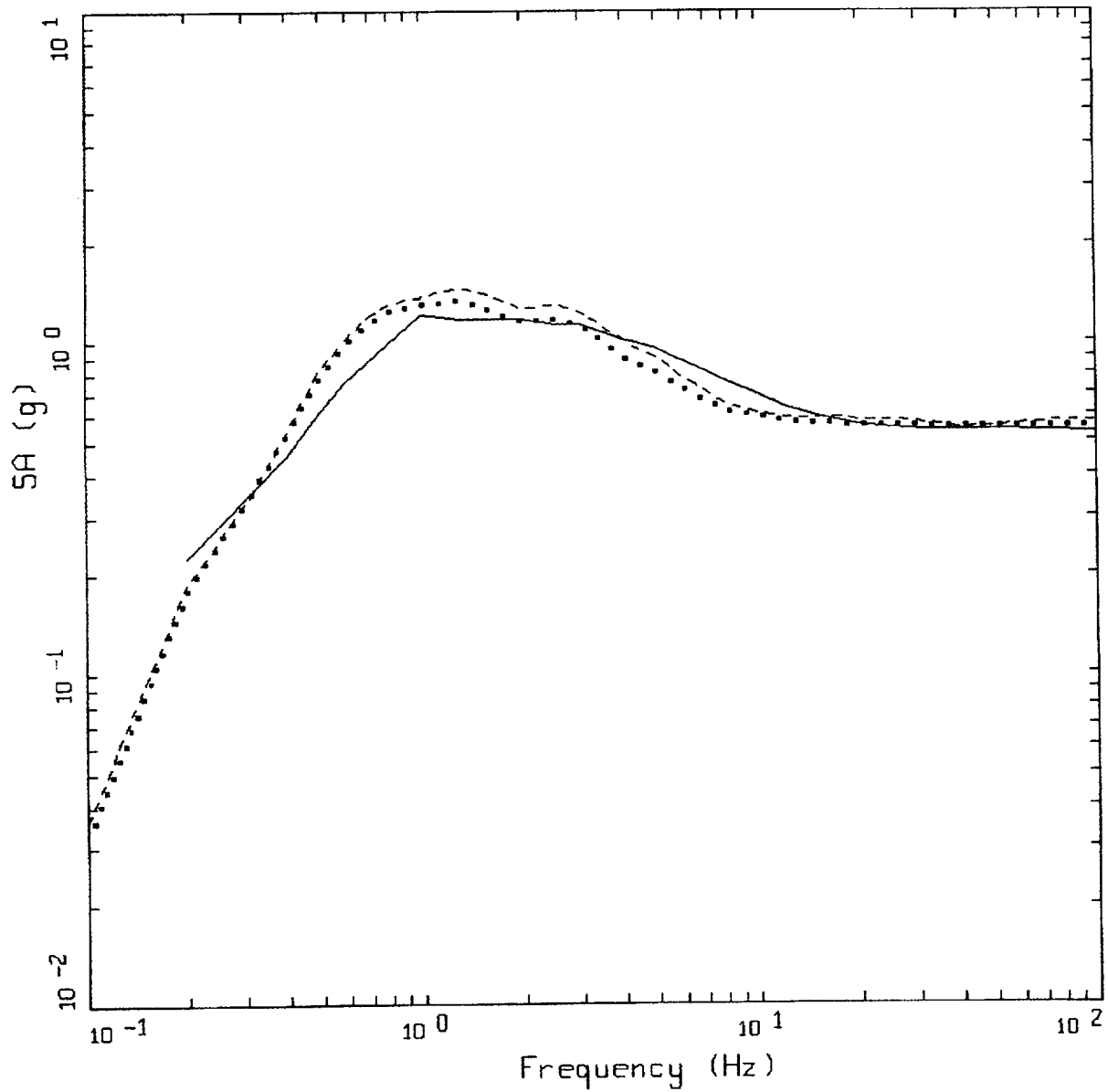
Figure 6-104. Comparison of soil spectra for Approach 2B (full profile) with base case profile and deterministic profile variations (\pm factor of 2 on shear modulus) with profile truncated at 90m; soil profile Gilroy 2, CEUS conditions.



CEUS 10E-4 APPROACH COMPARISON, GZ
 SOIL PROFILE TO 90 M (300 FT)

- LEGEND
- APPROACH 2, 1 HZ AND 10 HZ DEAGGREGATION EQKS, MEAN PGA = 0.325 G
 - - - - - APPROACH 1, 10-4 ROCK CONTROL MOTION, BASE CASE, 68TH PERCENTILE, PGA = 0.351 G
 - · - · - APPROACH 1, 10-4 ROCK CONTROL MOTION, BASE CASE, MEAN, PGA = 0.258 G
 - · · · · APPROACH 1, 10-4 ROCK CONTROL MOTION, BASE CASE, 32ND PERCENTILE, PGA = 0.165 G

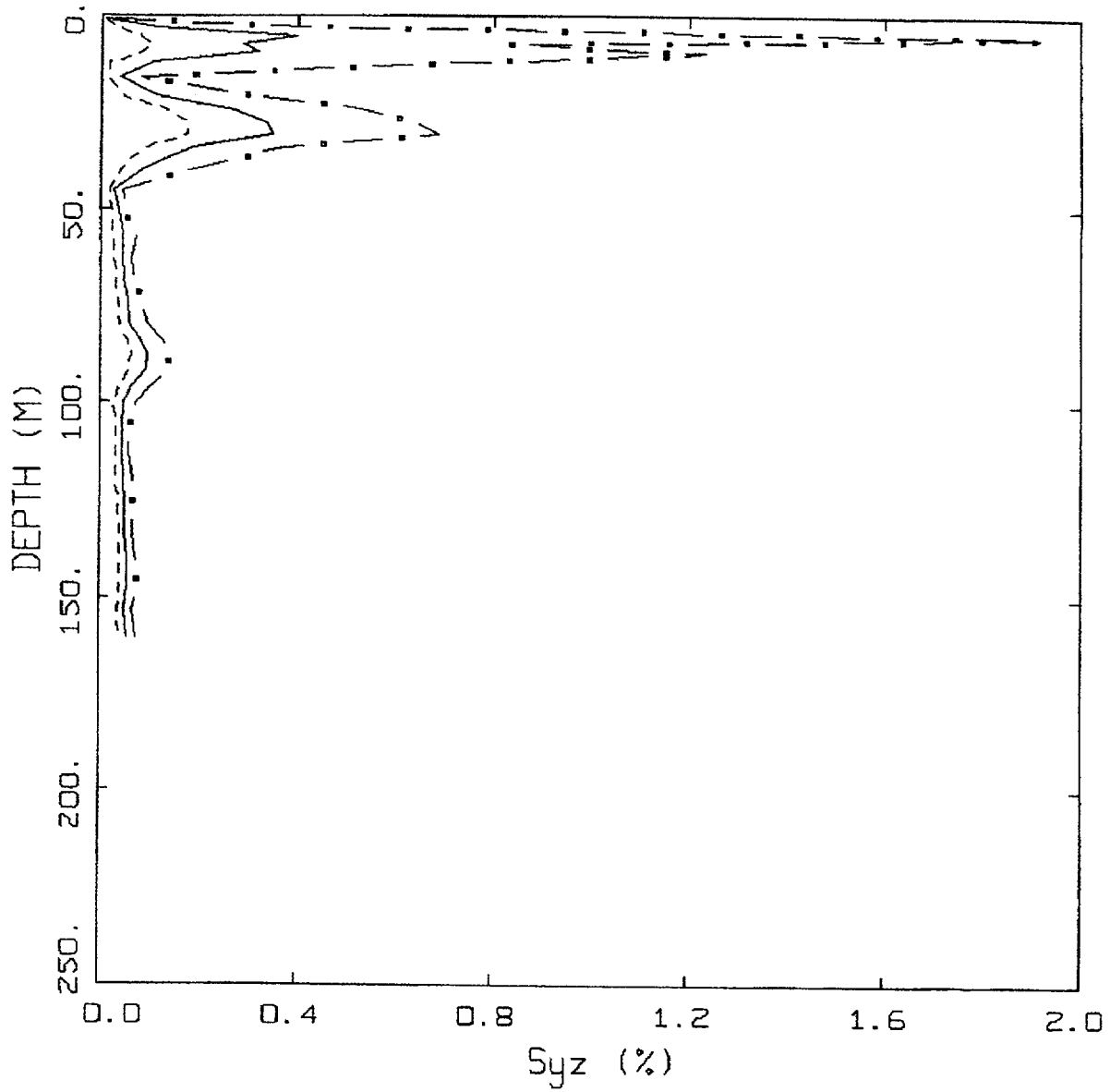
Figure 6-105. Comparison of soil spectra for Approach 2B (full profile) with mean and $\pm 1\sigma$ profile variations with profile truncated at 90m. Soil profile Gilroy 2, CEUS conditions.



WUS $10E-4$ APPROACH COMPARISON, G2

- LEGEND
- APPROACH 4, 10^{-4} SOIL UNIFORM HAZARD SPECTRUM, PGA = 0.532 G
 - APPROACH 1, 10^{-4} ROCK CONTROL MOTION, MEAN PGA = 0.550 G
 - APPROACH 2, 1 HZ AND 10 HZ DEAGGREGATION EQKS, MEAN PGA = 0.567 G

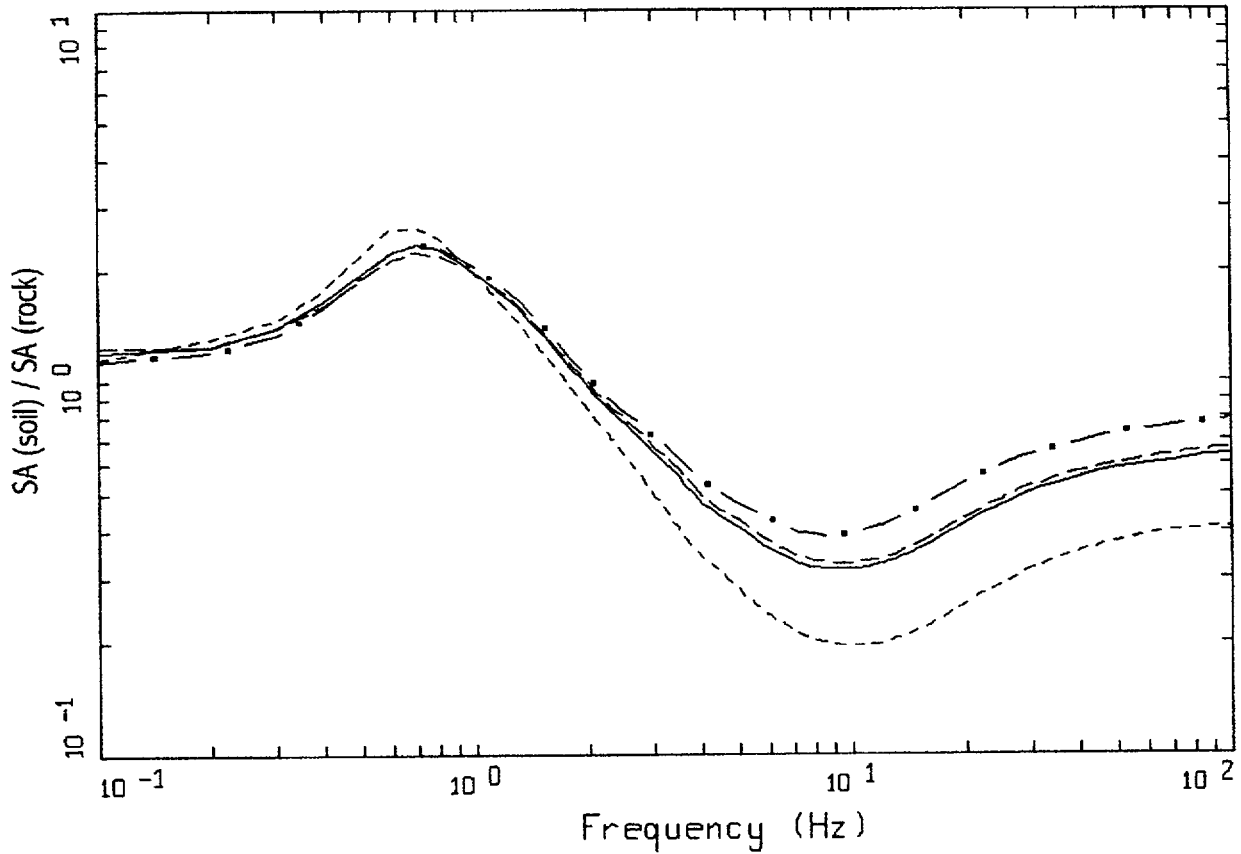
Figure 6-106. Comparison of Approaches 1, 2B, and 4 10^{-4} UHS on soil for profile Gilroy 2: WUS conditions.



WUS, 10-4, G2
 EFFECTIVE STRAINS (SYZ)

LEGEND
 - . - 84TH PERCENTILE
 ——— 50TH PERCENTILE
 - - - - 16TH PERCENTILE

Figure 6-107. Median and $\pm 1\sigma$ effective strain for soil profile Gilroy 2 using Approach 1: WUS conditions.

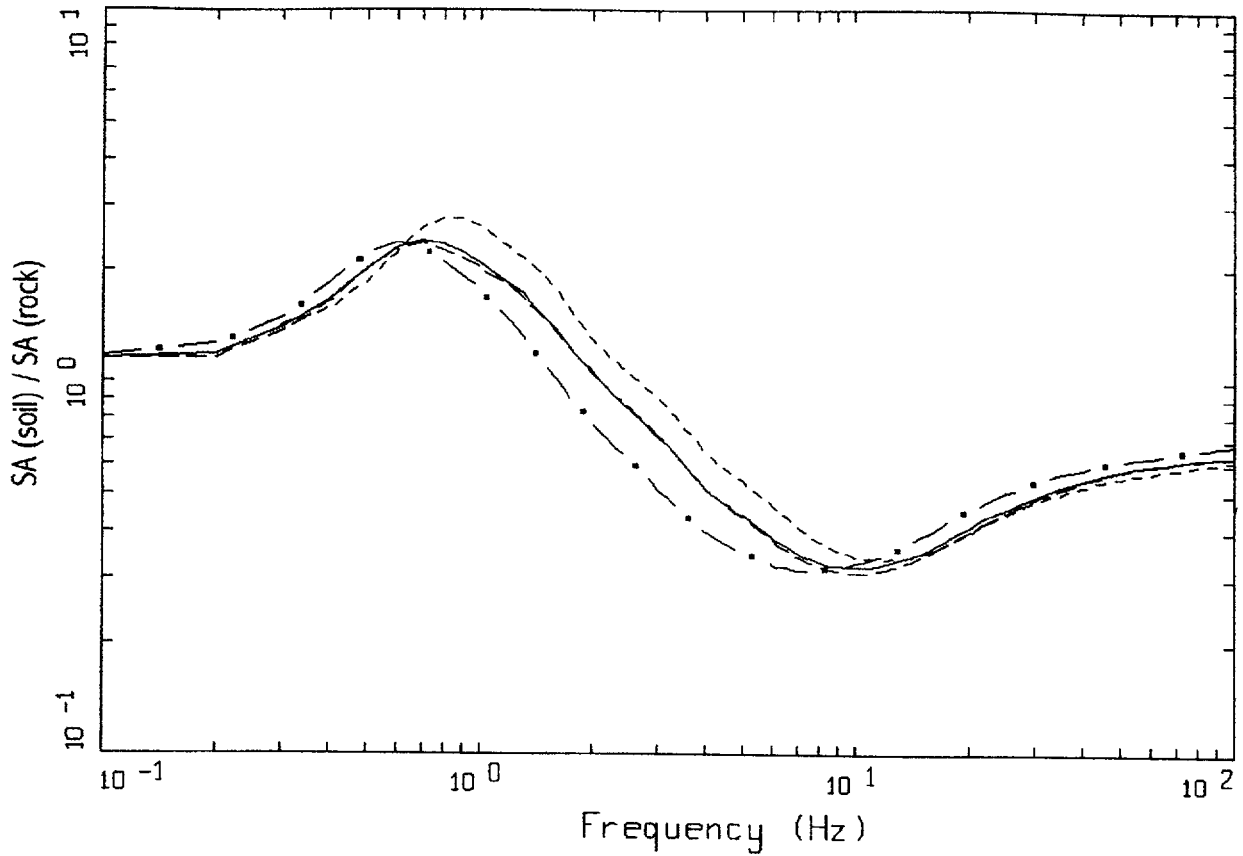


WUS, 1DE-4, 1HZ DESIGN, G2
 SURFACE MOTION, 1HZ TRANSFER FUNCTION
 WEIGHTS: ML=0.20, MM=0.60, MH=0.20

LEGEND

- ML = 5.4, D = 10 KM MEAN RATIO
- . - . - MM = 6.7, D = 18 KM, DESIGN MEAN RATIO
- MH = 7.8, D = 30 KM MEAN RATIO
- WEIGHTED MEAN RATIO

Figure 6-108. Comparison of transfer functions computed for the scaled 1 Hz design earthquake: soil profile Gilroy 2, WUS conditions.

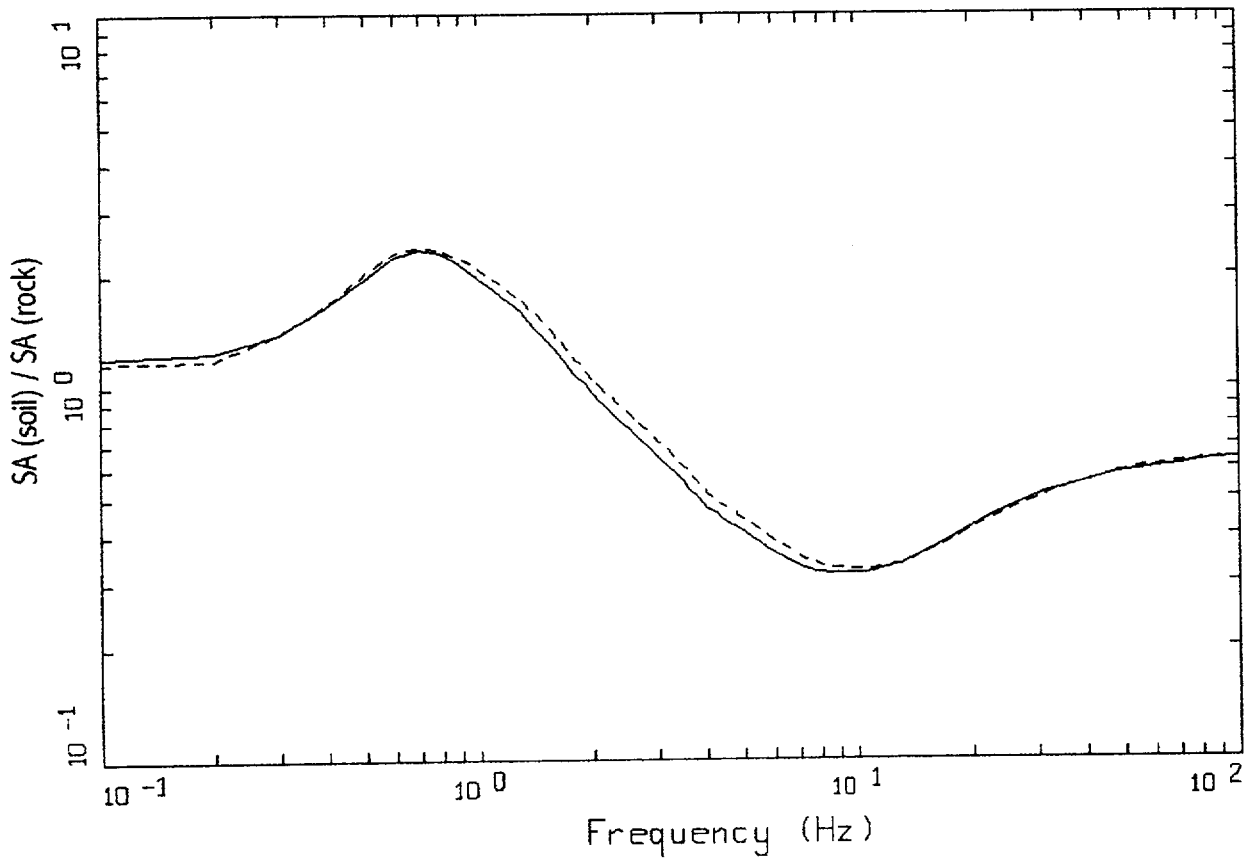


WUS, 10E-4, 10HZ DESIGN, G2
 SURFACE MOTION, 10HZ TRANSFER FUNCTION
 WEIGHTS: ML=0.20, MM=0.60, MH=0.20

LEGEND

- ML = 5.1, D = 10 KM MEAN RATIO
- · - · - MM = 6.1, D = 14 KM, DESIGN MEAN RATIO
- · — MH = 7.8, D = 30 KM MEAN RATIO
- WEIGHTED MEAN RATIO

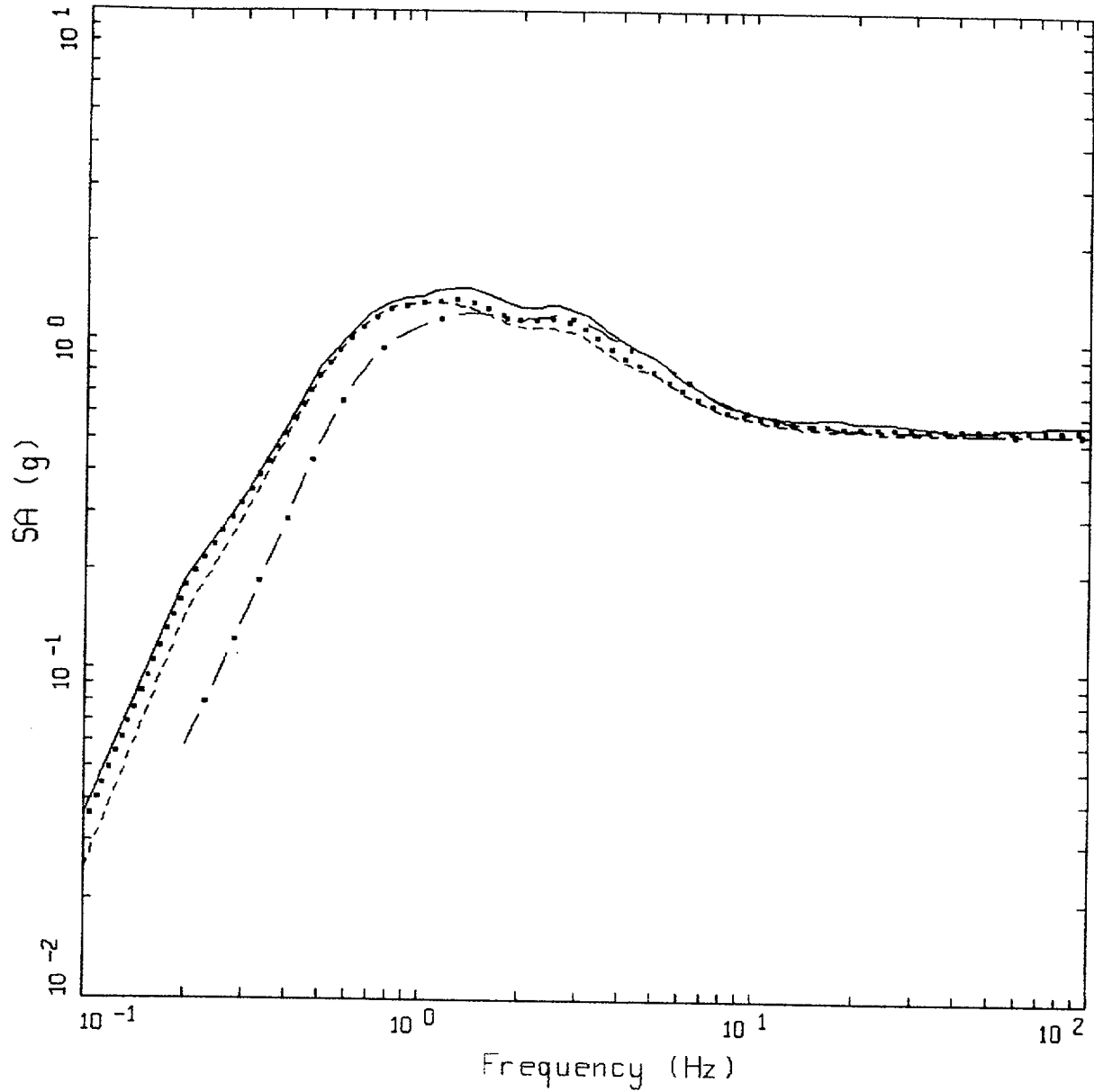
Figure 6-109. Comparison of transfer functions computed for the scaled 10 Hz design earthquake; soil profile Gilroy 2, WUS conditions.



WUS, $10E-4$, G2
AMPLIFICATION

LEGEND
 ——— 1 HZ WEIGHTED MEAN RATIO; WEIGHTS:ML=0.20,MM=0.60,MH=0.20
 - - - - 10 HZ WEIGHTED MEAN RATIO; WEIGHTS:ML=0.20,MM=0.60,MH=0.20

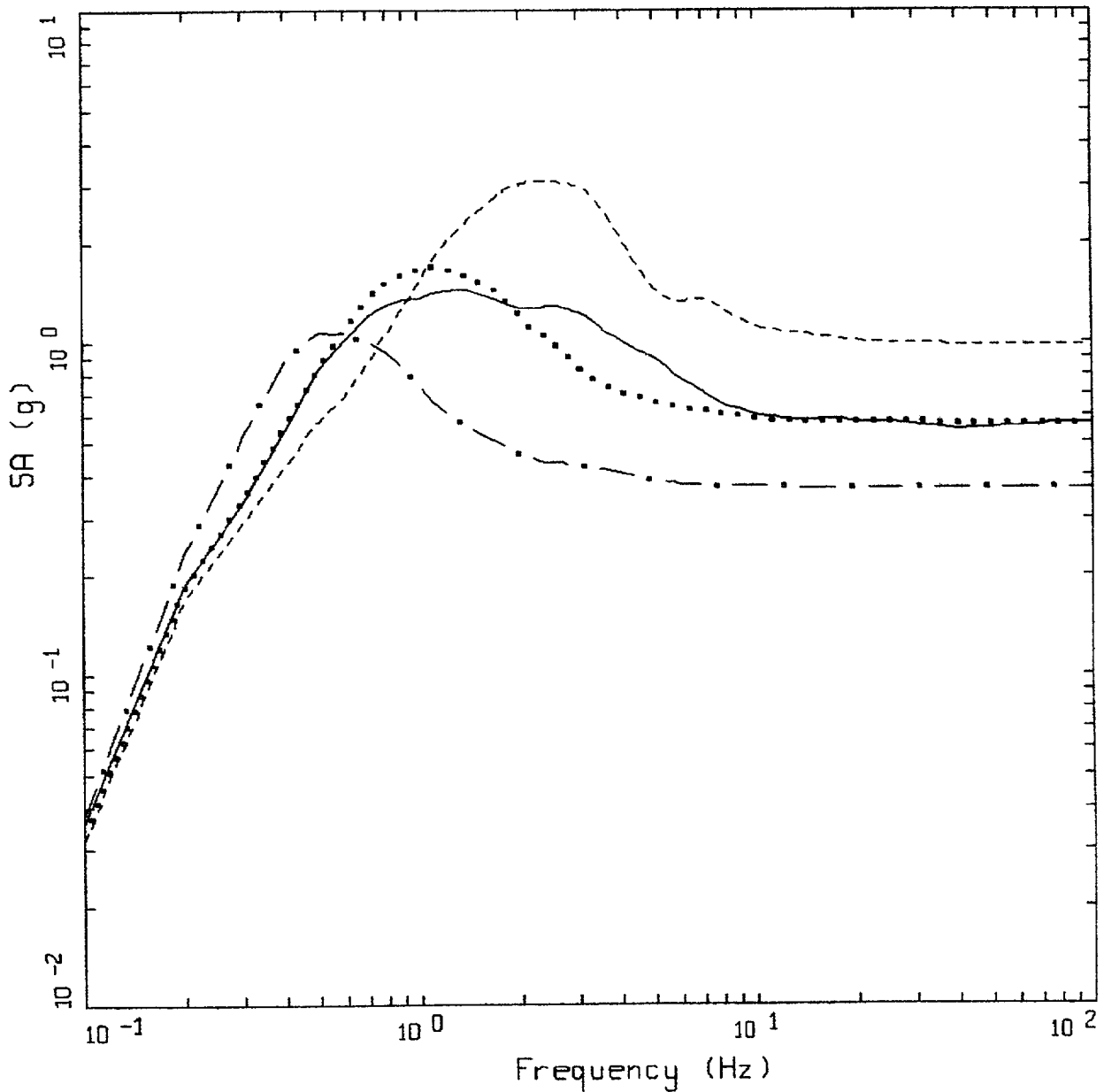
Figure 6-110. Comparison of mean transfer functions computed for the scaled 1 Hz and 10 Hz design earthquakes; soil profile Gilroy 2, WUS conditions.



WUS, 10E-4 DESIGN SPECTRA, GZ

- LEGEND
- APPROACH 2, 1 HZ AND 10 HZ DEAGGREGATION EQKS, MEAN PGA = 0.567 G
 - APPROACH 1, 10-4 ROCK CONTROL MOTION, MEAN PGA = 0.550 G
 - 1 HZ MEAN; PGA = 0.535 G
 - . - . 10 HZ MEAN; PGA = 0.539 G

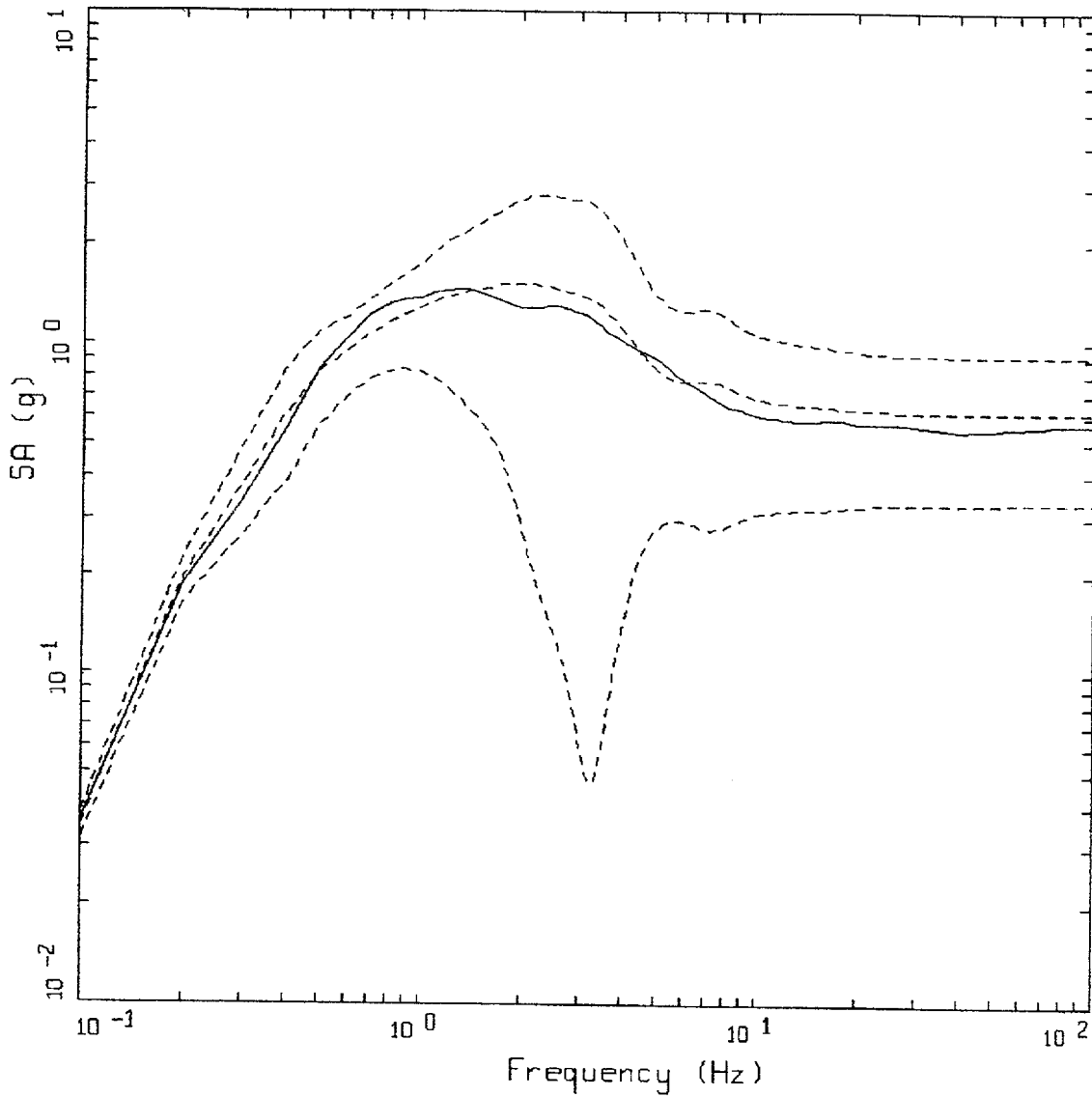
Figure 6-111. Comparison of soil spectra for Approaches 1, 2A, and 2B; soil profile Gilroy 2, WUS conditions.



WUS 10E-4 APPROACH COMPARISON, GZ

- LEGEND
- APPROACH 2, 1 HZ AND 10 HZ DEAGGREGATION EQKS, MEAN PGA = 0.567 G
 - APPROACH 1, 10⁻⁴ ROCK CONTROL MOTION, BASE CASE PGA = 0.571 G
 - APPROACH 1, 10⁻⁴ ROCK CONTROL MOTION, BASE CASE (UPPER) PGA = 0.978 G
 - · - APPROACH 1, 10⁻⁴ ROCK CONTROL MOTION, BASE CASE (LOWER) PGA = 0.368 G

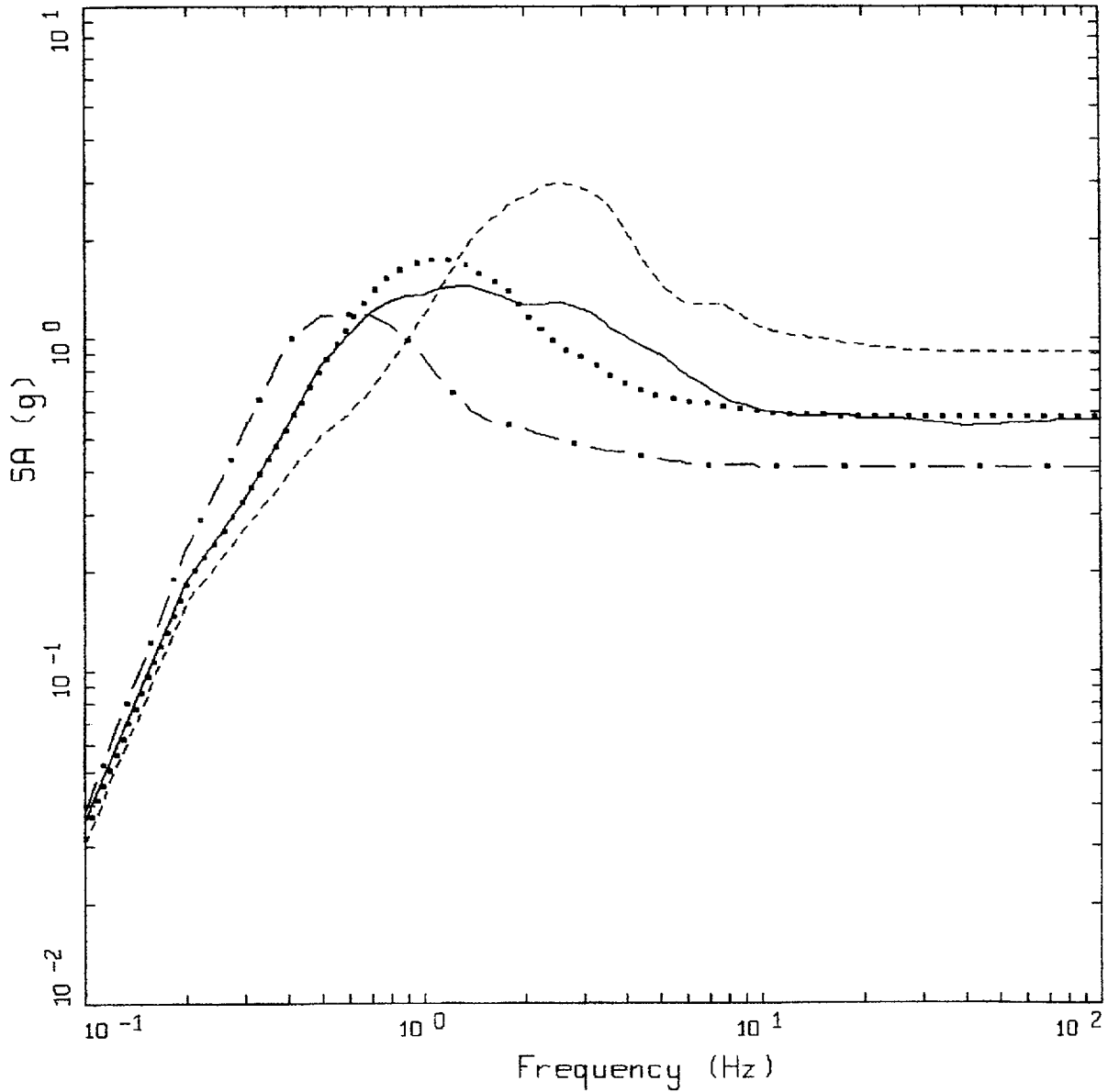
Figure 6-112. Comparison of soil spectra for Approach 2B with base case profile and deterministic profile variations (\pm factor of 2 on shear modulus); soil profile Gilroy 2, WUS conditions.



WUS 10E-4 APPROACH COMPARISON, GZ

- LEGEND
- APPROACH 2, 1 HZ AND 10 HZ DEAGGREGATION EQKS, MEAN PGA = 0.567 G
 - APPROACH 1, 10-4 ROCK CONTROL MOTION, BASE CASE, 84TH PERCENTILE, PGA = 0.912 G
 - APPROACH 1, 10-4 ROCK CONTROL MOTION, BASE CASE, MEAN, PGA = 0.621 G
 - APPROACH 1, 10-4 ROCK CONTROL MOTION, BASE CASE, 16TH PERCENTILE, PGA = 0.330 G

Figure 6-113. Comparison of soil spectra for Approach 2B with mean and $\pm 1\sigma$ variations of base case (\pm factor of 2 on shear modulus), soil profile Gilroy 2, WUS conditions.

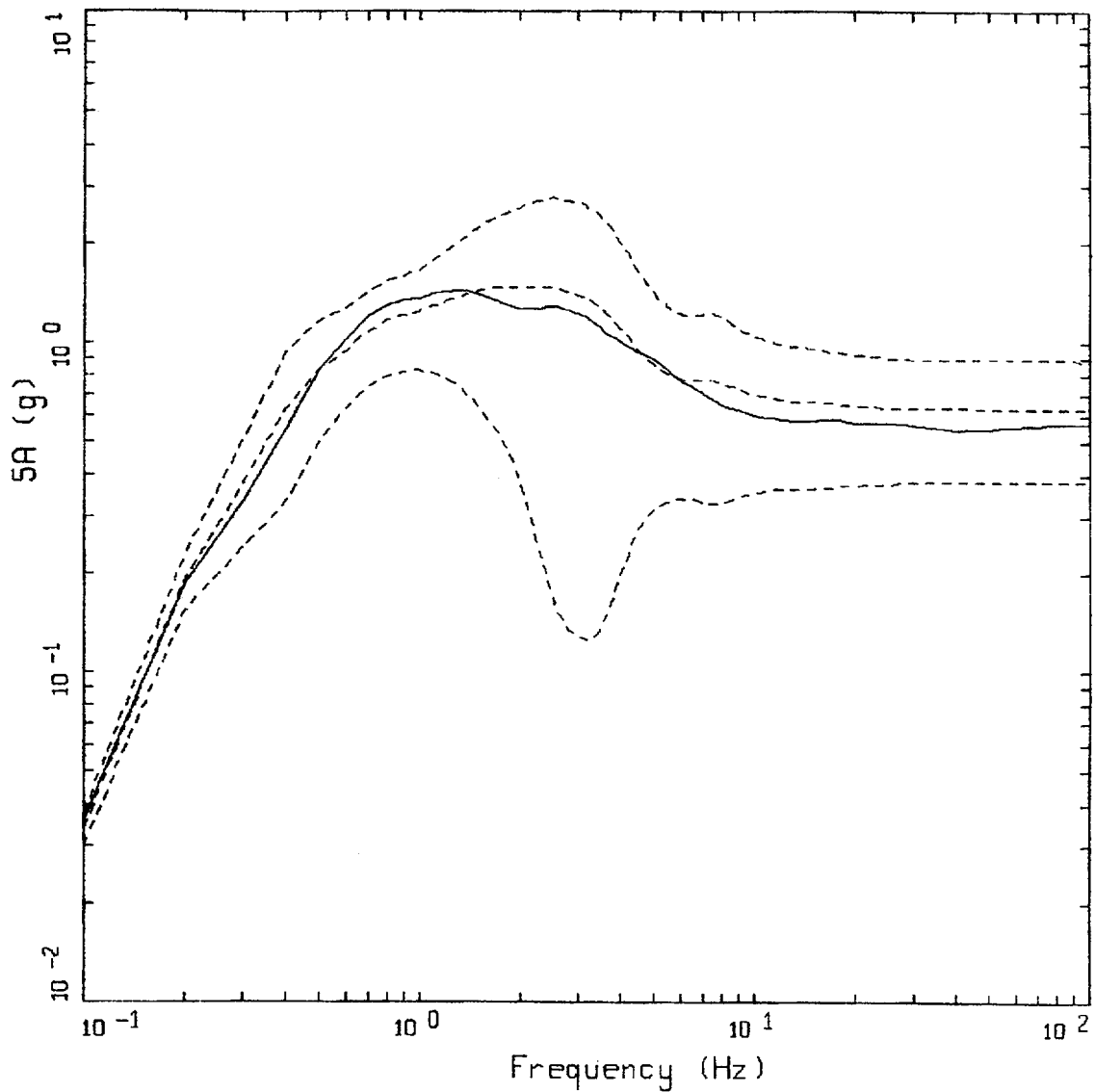


WUS 10E-4 APPROACH COMPARISON, G2
 SOIL PROFILE TO 150 M (500 FT)

LEGEND

- APPROACH 2, 1 HZ AND 10 HZ DEAGGREGATION EQKS, MEAN PGA = 0.567 G
- APPROACH 1, 10-4 ROCK CONTROL MOTION, BASE CASE PGA = 0.580 G
- APPROACH 1, 10-4 ROCK CONTROL MOTION, BASE CASE (UPPER) PGA = 0.908 G
- · - APPROACH 1, 10-4 ROCK CONTROL MOTION, BASE CASE (LOWER) PGA = 0.411 G

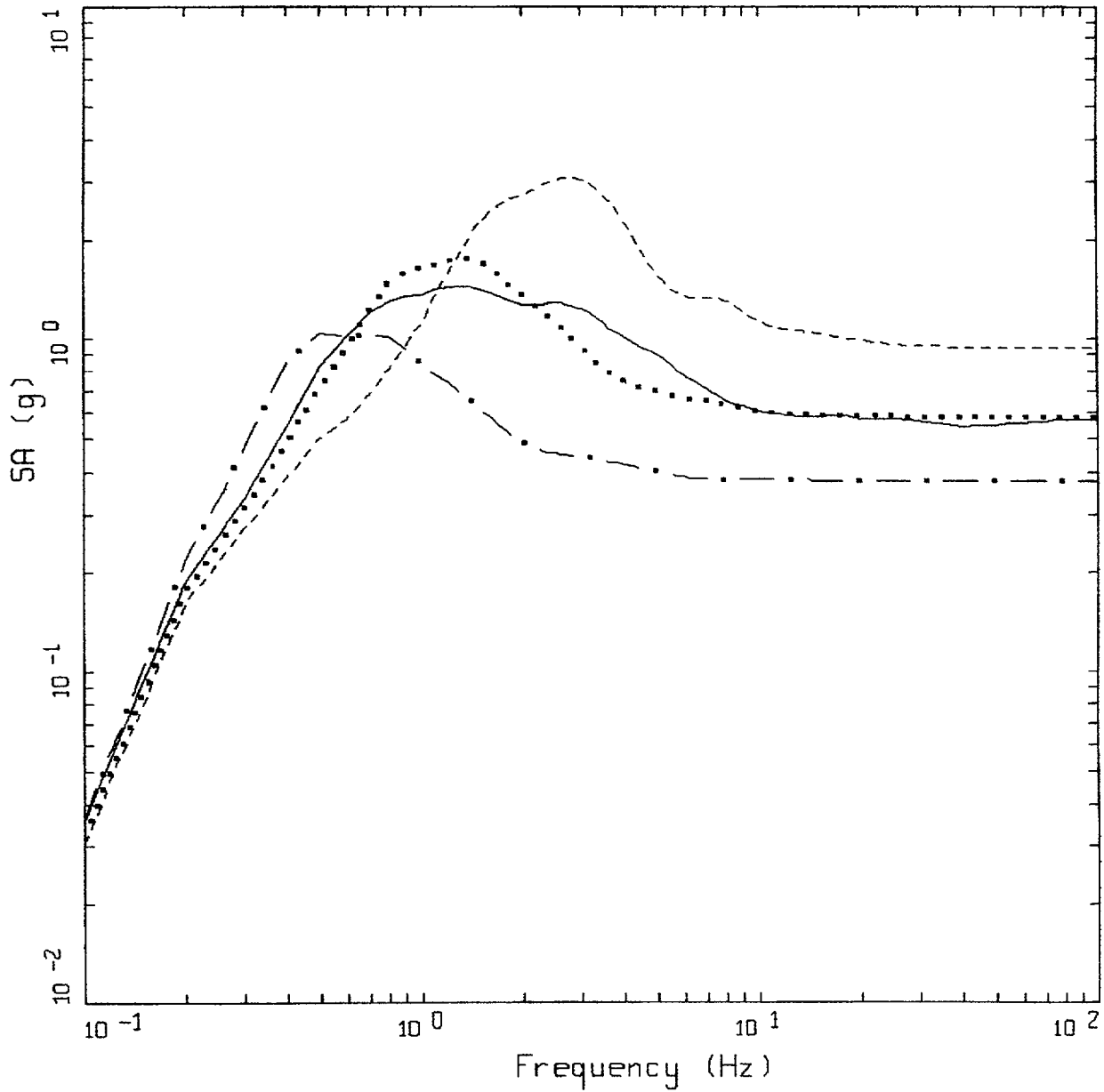
Figure 6-114. Comparison of soil spectra for Approach 2B (full profile) with base case profile and deterministic profile variations (\pm factor of 2 on shear modulus) with profile truncated at 150m; soil profile Gilroy 2, WUS conditions.



WUS 10E-4 APPROACH COMPARISON, GZ
 SOIL PROFILE TO 150 M (500 FT)

- LEGEND
- APPROACH 2, 1 HZ AND 10 HZ DEAGGREGATION EQKS, MEAN PGA = 0.567 G
 - APPROACH 1, 10-4 ROCK CONTROL MOTION, BASE CASE, 84TH PERCENTILE, PGA = 0.886 G
 - APPROACH 1, 10-4 ROCK CONTROL MOTION, BASE CASE, MEAN, PGA = 0.633 G
 - APPROACH 1, 10-4 ROCK CONTROL MOTION, BASE CASE, 16TH PERCENTILE, PGA = 0.380 G

Figure 6-115. Comparison of soil spectra for Approach 2B (full profile) with mean and $+1\sigma$ profile variations with profile truncated at 150m; soil profile Gilroy 2, WUS conditions.

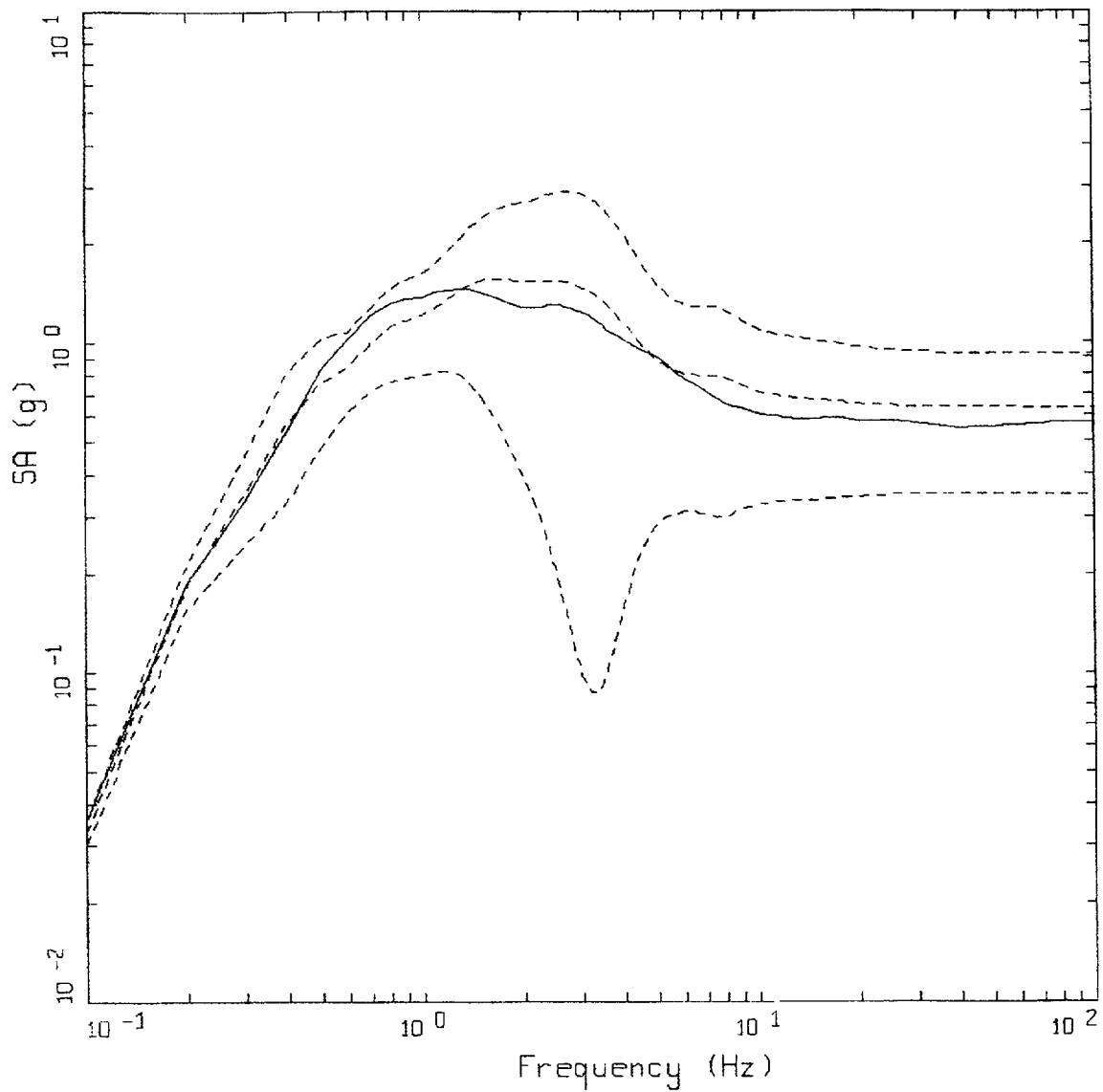


WUS 10E-4 APPROACH COMPARISON, GZ
 SOIL PROFILE TO 90 M (300 FT)

LEGEND

- APPROACH 2, 1 HZ AND 10 HZ DEAGGREGATION EQKS, MEAN PGA = 0.567 G
- APPROACH 1, 10-4 ROCK CONTROL MOTION, BASE CASE PGA = 0.583 G
- APPROACH 1, 10-4 ROCK CONTROL MOTION, BASE CASE (UPPER) PGA = 0.942 G
- . - . APPROACH 1, 10-4 ROCK CONTROL MOTION, BASE CASE (LOWER) PGA = 0.377 G

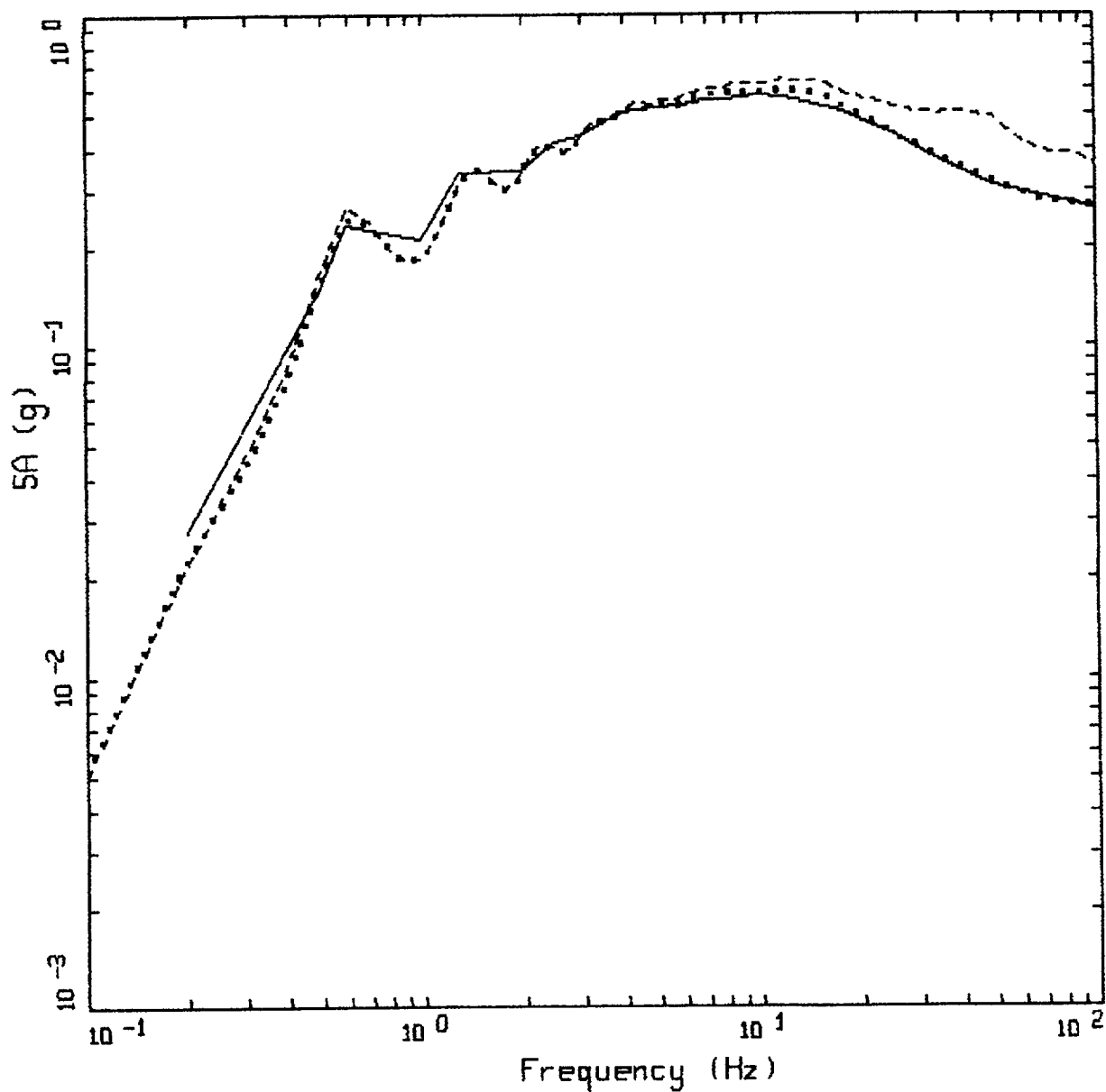
Figure 6-116. Comparison of soil spectra for Approach 2B (full profile) with base case profile and deterministic profile variations (\pm factor of 2 on shear modulus) with profile truncated at 90m; soil profile Gilroy 2, WUS conditions.



WUS 10E-4 APPROACH COMPARISON, GZ
 SOIL PROFILE TO 90M (300 FT)

- LEGEND
- APPROACH 2, 1 HZ AND 10 HZ DEAGGREGATION EQKS, MEAN PGA = 0.567 G
 - APPROACH 1, 10-4 ROCK CONTROL MOTION, BASE CASE, 84TH PERCENTILE, PGA = 0.920 G
 - APPROACH 1, 10-4 ROCK CONTROL MOTION, BASE CASE, MEAN, PGA = 0.634 G
 - APPROACH 1, 10-4 ROCK CONTROL MOTION, BASE CASE, 16TH PERCENTILE, PGA = 0.348 G

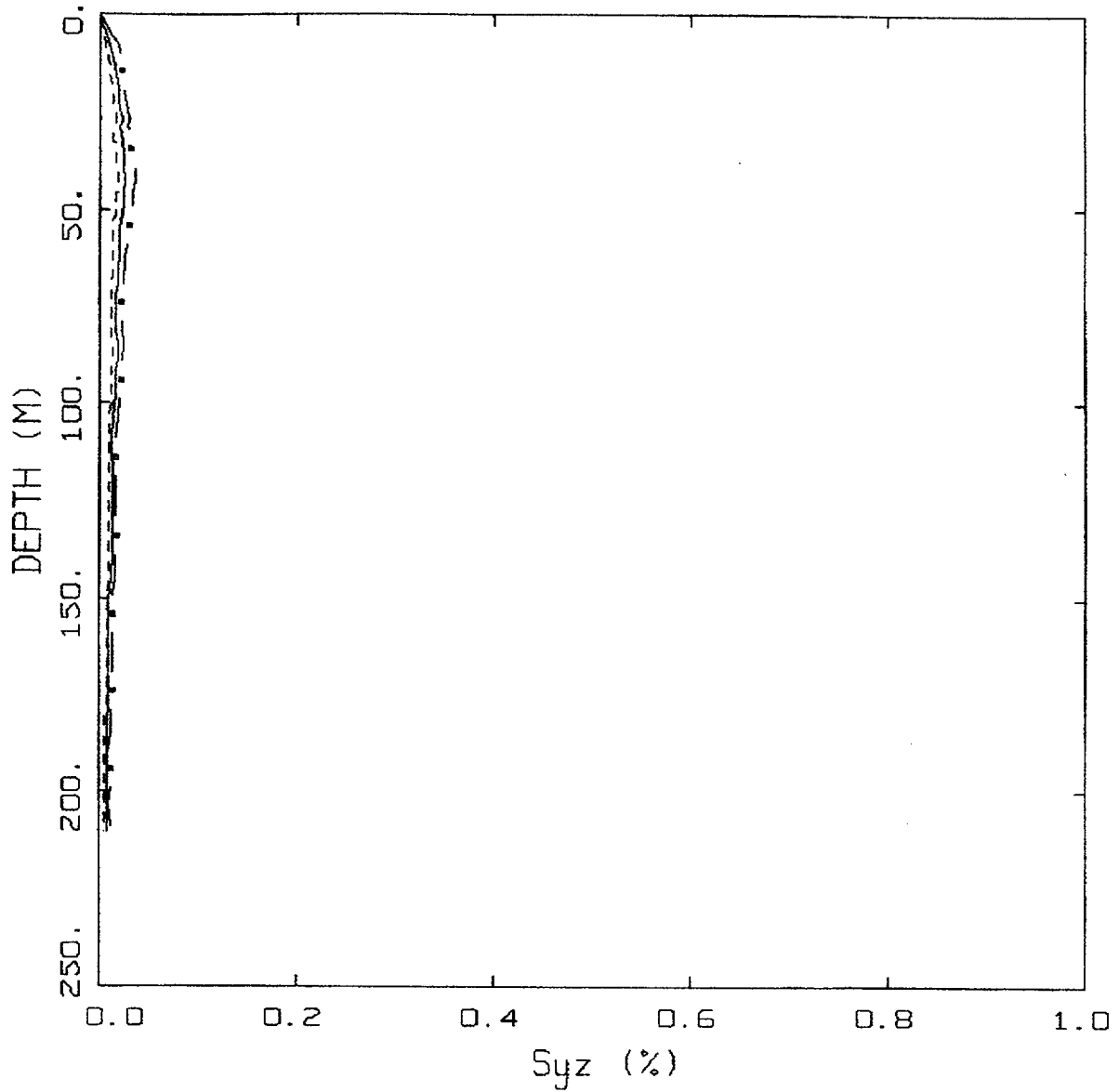
Figure 6-117. Comparison of soil spectra for Approach 2B (full profile) with mean and $\pm 1\sigma$ profile variations with profile truncated at 90m. Soil profile Gilroy 2, WUS conditions.



CEUS 10E-4 APPROACH COMPARISON, SR

- LEGEND
- APPROACH 4, 10⁻⁴ SOIL UNIFORM HAZARD SPECTRUM, PGA = 0.259 G
 - APPROACH 1, 10⁻⁴ ROCK CONTROL MOTION, MEAN PGA = 0.265 G
 - - - - APPROACH 2, 1 HZ AND 10 HZ DEAGGREGATION EQKS, MEAN PGA = 0.355 G

Figure 6-118. Comparison of Approaches 1, 2B, and 4, 10⁻⁴ UHS on soil for profile Savannah River Generic: CEUS conditions.

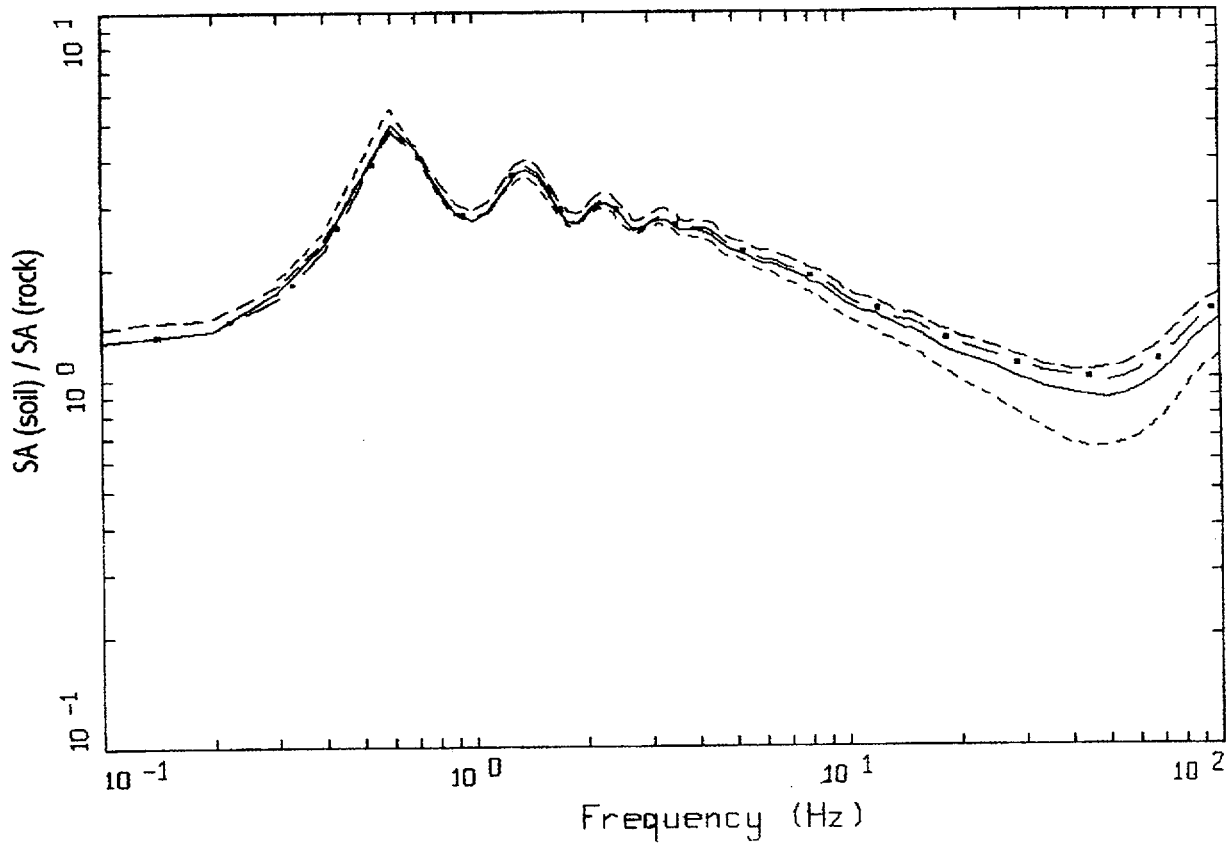


CEUS, 10-4, SR
EFFECTIVE STRAINS (SYZ)

LEGEND

- · — 84TH PERCENTILE
- 50TH PERCENTILE
- 16TH PERCENTILE

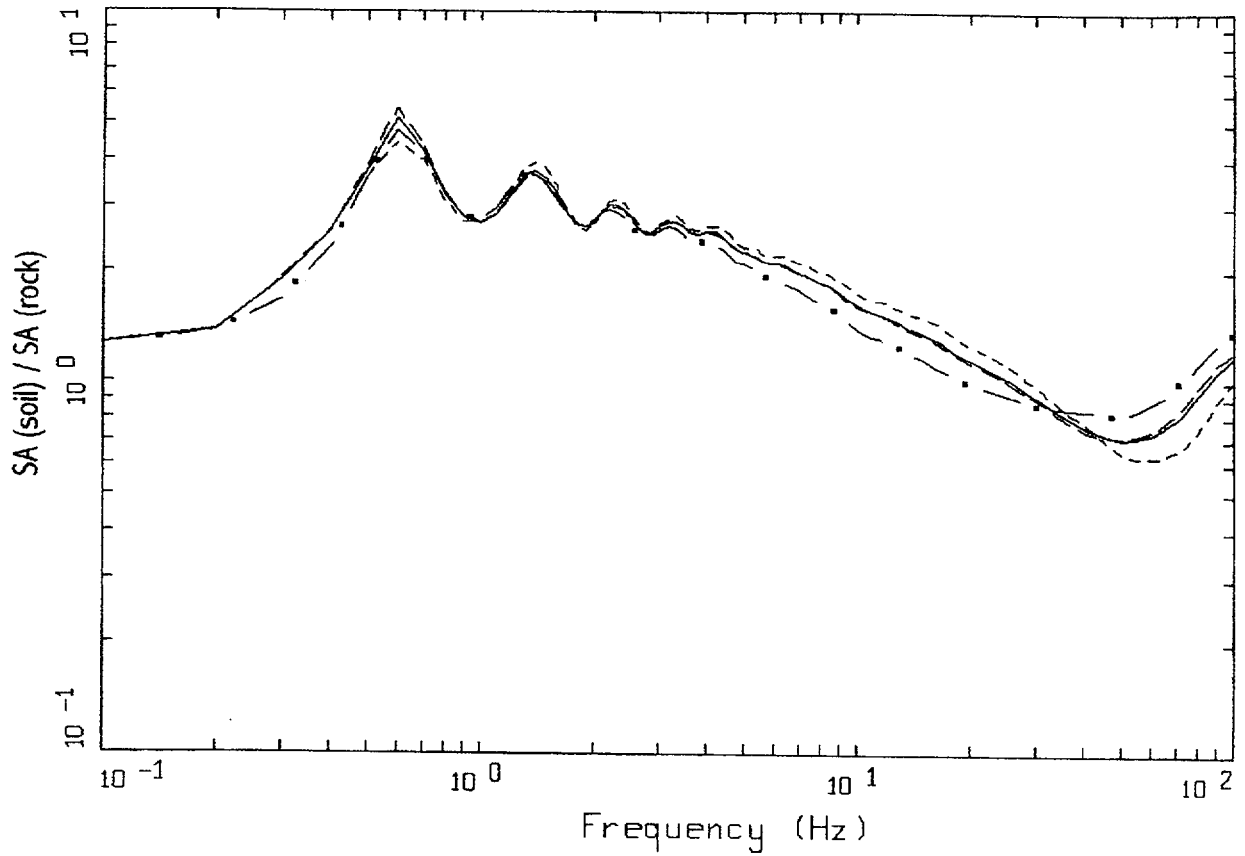
Figure 6-119. Median and $\pm 1\sigma$ effective strains for soil profile Savannah River Generic using Approach 1: CEUS conditions.



CEUS, 10E-4, 1HZ DESIGN, SR
 SURFACE MOTION, 1HZ TRANSFER FUNCTION
 WEIGHTS: ML=0.30, MM=0.00, MH=0.70

LEGEND
 - - - - ML = 5.7, D = 20 KM MEAN RATIO
 - · - · MM = 7.0, D = 100 KM, DESIGN MEAN RATIO
 — · — MH = 7.6, D = 130 KM MEAN RATIO
 ——— WEIGHTED MEAN RATIO

Figure 6-120. Comparison of transfer functions computed for the scaled 1 Hz design earthquake; soil profile Savannah River Generic, CEUS conditions.

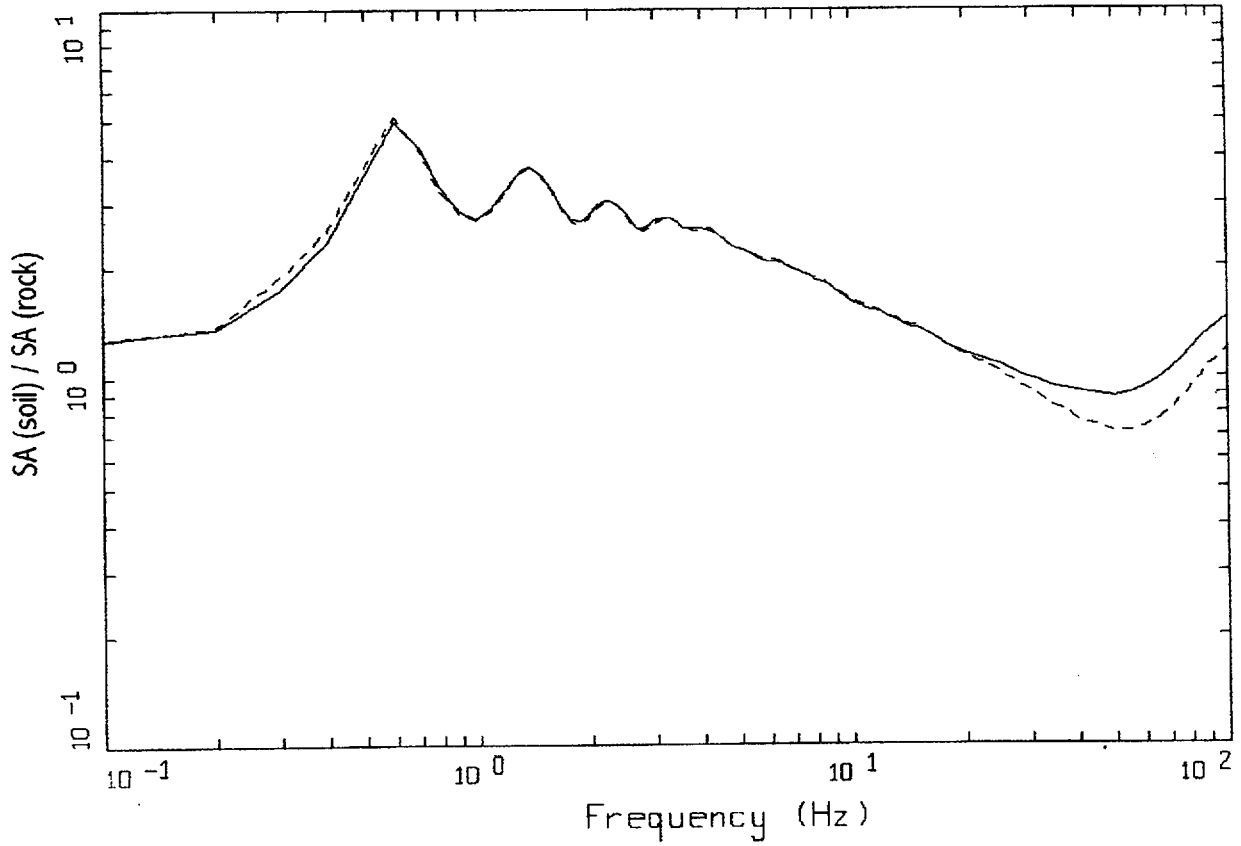


CEUS, 10E-4, 10HZ DESIGN, SR
 SURFACE MOTION, 10HZ TRANSFER FUNCTION
 WEIGHTS: ML=0.25, MM=0.63, MH=0.12

LEGEND

- ML = 4.6, D = 8 KM MEAN RATIO
- · - · - MM = 5.6, D = 8 KM, DESIGN MEAN RATIO
- · — MH = 7.7, D = 130 KM MEAN RATIO
- WEIGHTED MEAN RATIO

Figure 6-121. Comparison of transfer functions computed for the scaled 10 Hz design earthquake; soil profile Savannah River Generic, CEUS conditions.

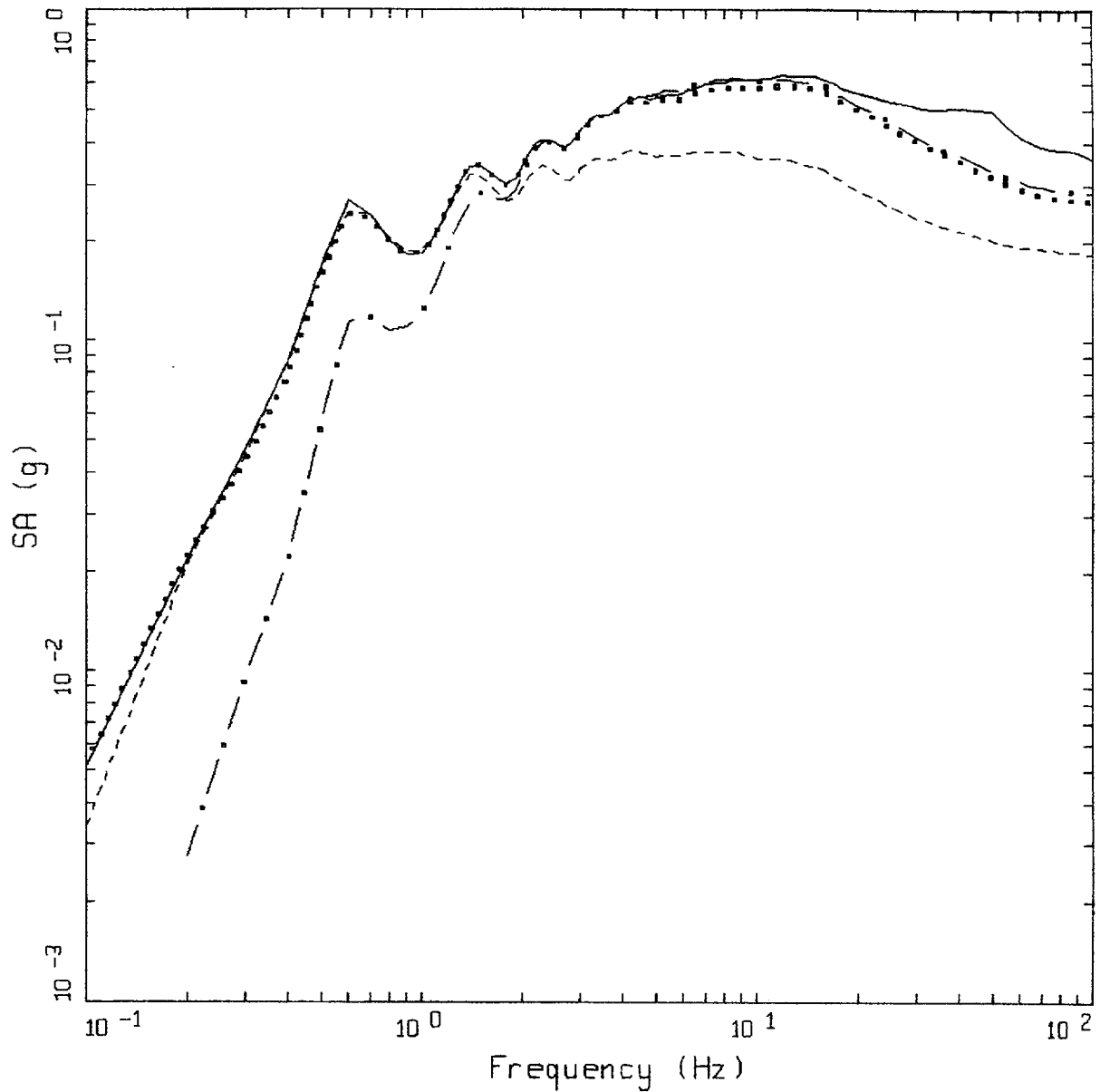


CEUS, 10E-4, SR
TRANSFER FUNCTION

LEGEND

- 1 HZ WEIGHTED MEAN RATIO; WEIGHTS: ML=0.30, MM=0.00, MH=0.70
- 10 HZ WEIGHTED MEAN RATIO; WEIGHTS: ML=0.25, MM=0.63, MH=0.12

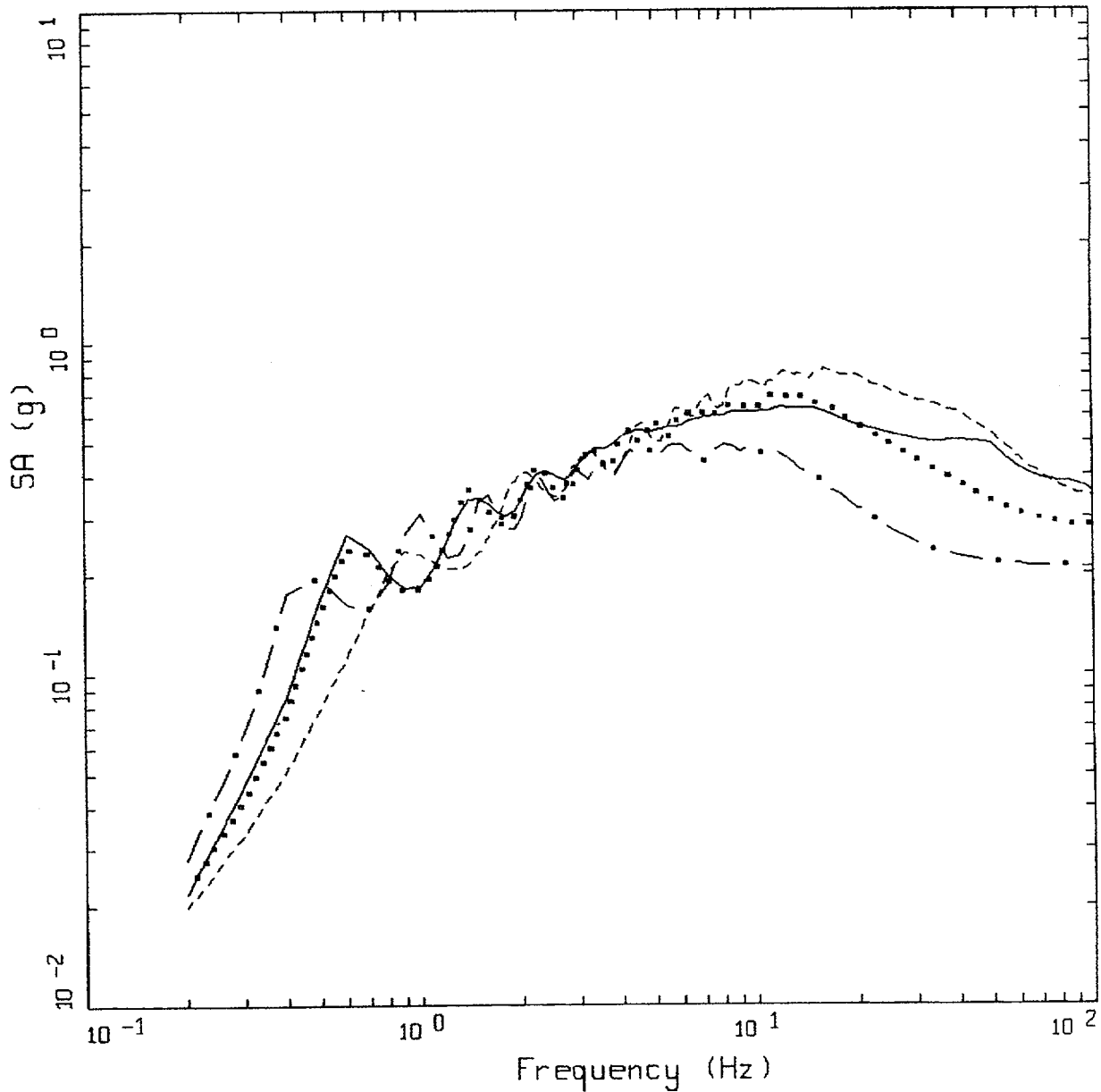
Figure 6-122. Comparison of mean transfer functions computed for the scaled 1 Hz and 10 Hz design earthquakes; soil profile Savannah River Generic, CEUS conditions.



CEUS, 10E-4 DESIGN SPECTRA, SR

- LEGEND
- APPROACH 2, 1 HZ AND 10 HZ DEAGGREGATION EQKS, MEAN PGA = 0.355 G
 - APPROACH 1, 10-4 ROCK CONTROL MOTION, MEAN PGA = 0.265 G
 - - - - 1 HZ MEAN; PGA = 0.185 G
 - . - . 10 HZ MEAN; PGA = 0.280 G

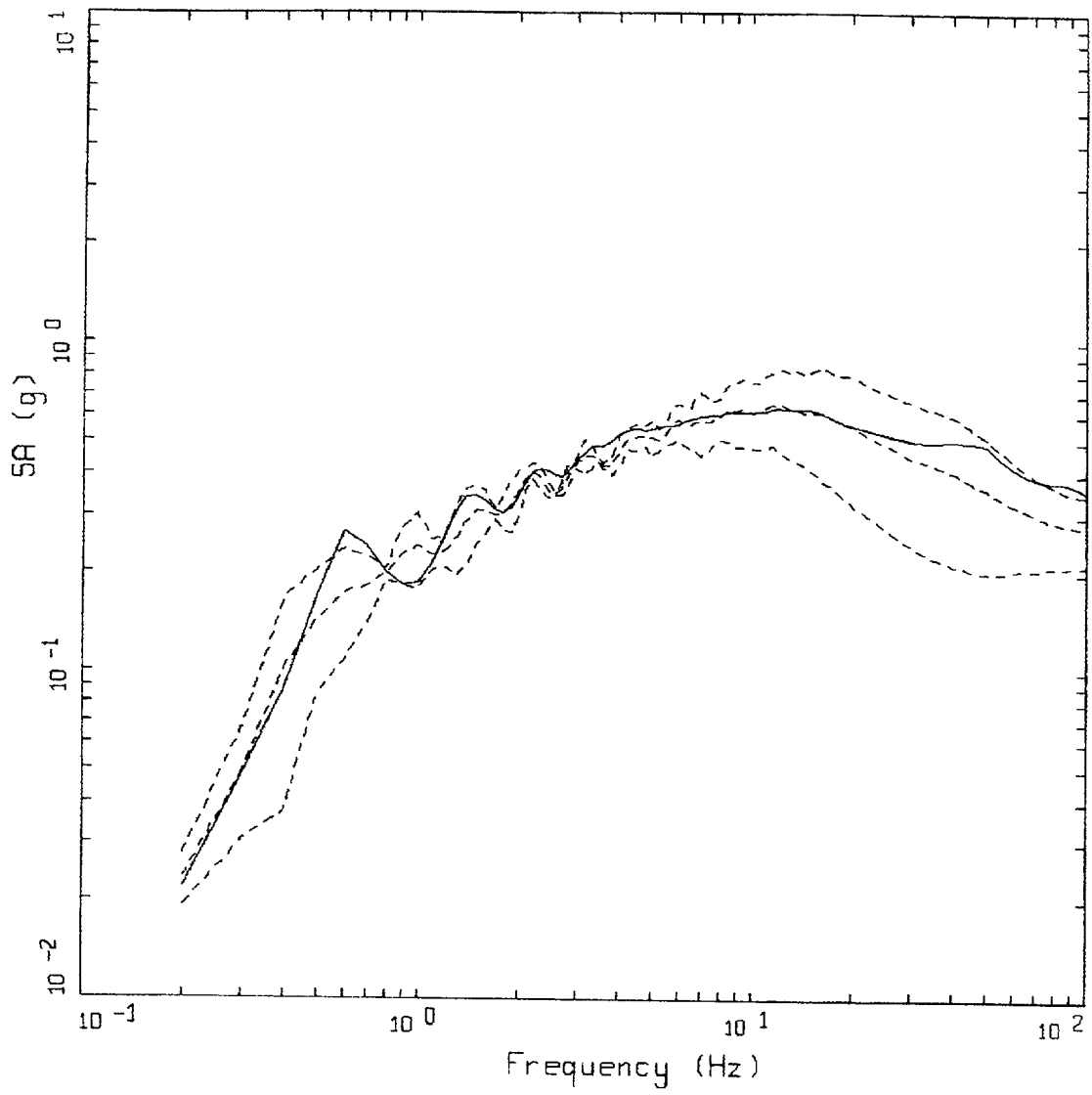
Figure 6-123. Comparison of soil spectra for Approaches 1, 2A, and 2B; soil profile Savannah River Generic, CEUS conditions.



CEUS 10E-4 APPROACH COMPARISON, SR

- LEGEND
- APPROACH 2, 1 HZ AND 10 HZ DEAGGREGATION EQKS, MEAN PGA = 0.355 G
 - APPROACH 1, 10-4 ROCK CONTROL MOTION, BASE CASE PGA = 0.280 G
 - APPROACH 1, 10-4 ROCK CONTROL MOTION, BASE CASE (UPPER) PGA = 0.344 G
 - . - . - APPROACH 1, 10-4 ROCK CONTROL MOTION, BASE CASE (LOWER) PGA = 0.210 G

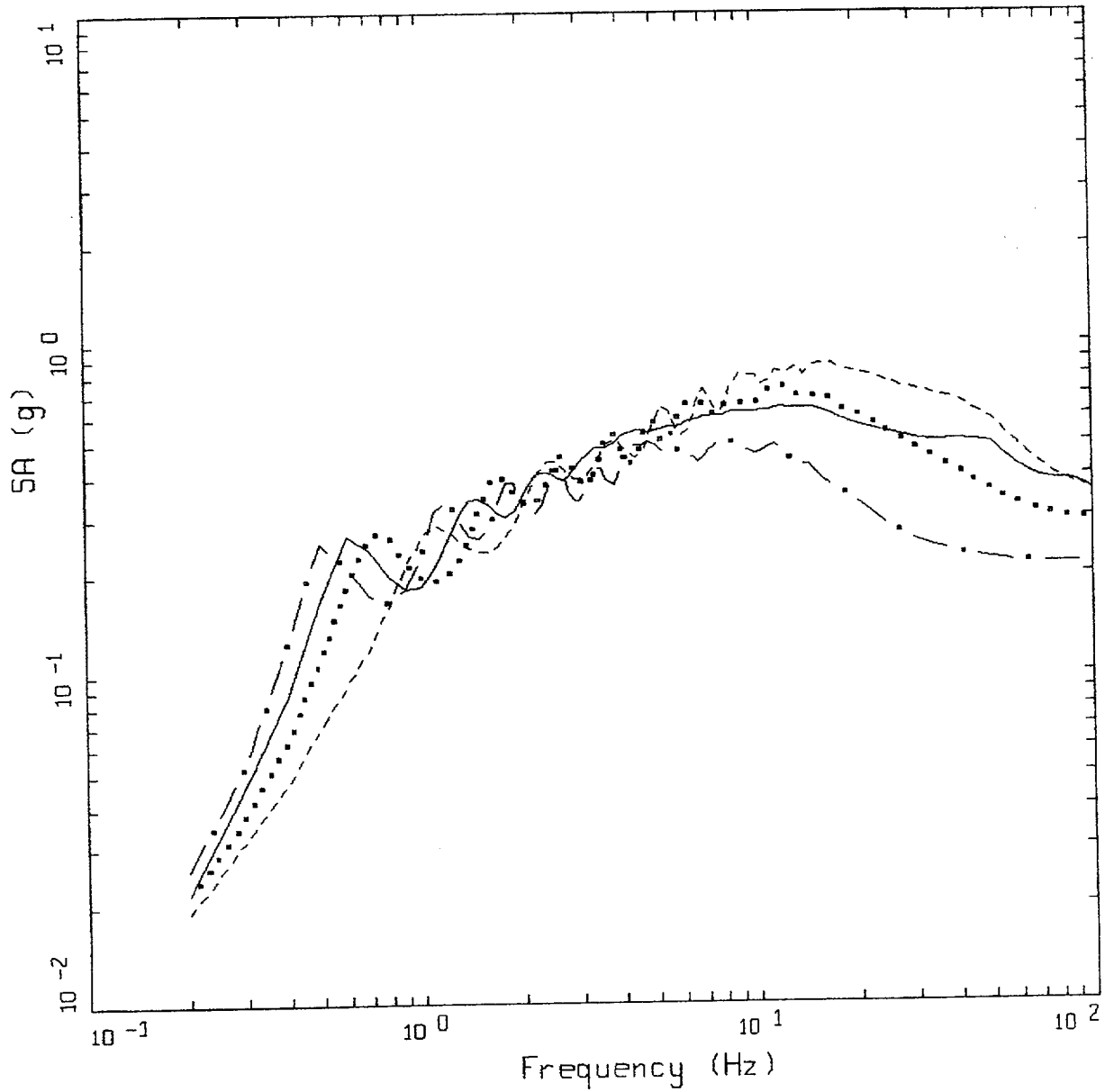
Figure 6-124. Comparison of soil spectra for Approach 2B with base case profile and deterministic profile variations (\pm factor of 2 on shear modulus); soil profile Savannah River Generic, CEUS conditions.



CEUS 10E-4 APPROACH COMPARISON, SR

- LEGEND
- APPROACH 2, 1 HZ AND 10 HZ DEAGGREGATION EQKS, MEAN PGA = 0.355 G
 - - - - - APPROACH 1, 10-4 ROCK CONTROL MOTION, BASE CASE, 68TH PERCENTILE, PGA = 0.346 G
 - · - · - APPROACH 1, 10-4 ROCK CONTROL MOTION, BASE CASE, MEAN, PGA = 0.278 G
 - · · · · APPROACH 1, 10-4 ROCK CONTROL MOTION, BASE CASE, 32ND PERCENTILE, PGA = 0.211 G

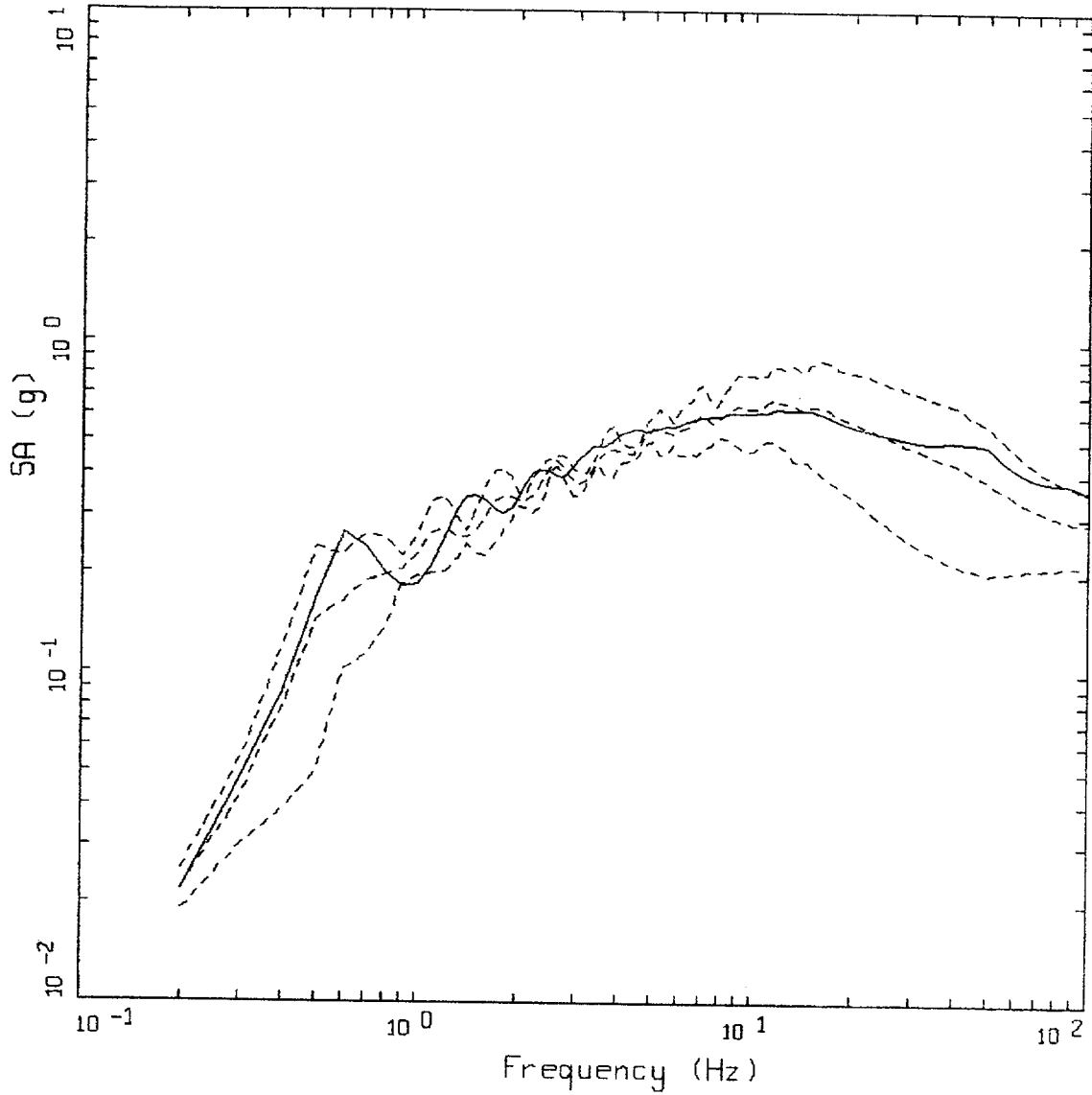
Figure 6-125. Comparison of soil spectra for Approach 2B with mean and $\pm 1\sigma$ variations of base case (\pm factor of 2 on shear modulus), soil profile Savannah River Generic, CEUS conditions.



CEUS 1DE-4 APPROACH COMPARISON, SR
SOIL PROFILE TO 150 M (500 FT)

- LEGEND
- APPROACH 2, 1 HZ AND 10 HZ DEAGGREGATION EQKS, MEAN PGA = 0.355 G
 - APPROACH 1, 10-4 ROCK CONTROL MOTION, BASE CASE PGA = 0.290 G
 - APPROACH 1, 10-4 ROCK CONTROL MOTION, BASE CASE (UPPER) PGA = 0.360 G
 - . - . APPROACH 1, 10-4 ROCK CONTROL MOTION, BASE CASE (LOWER) PGA = 0.213 G

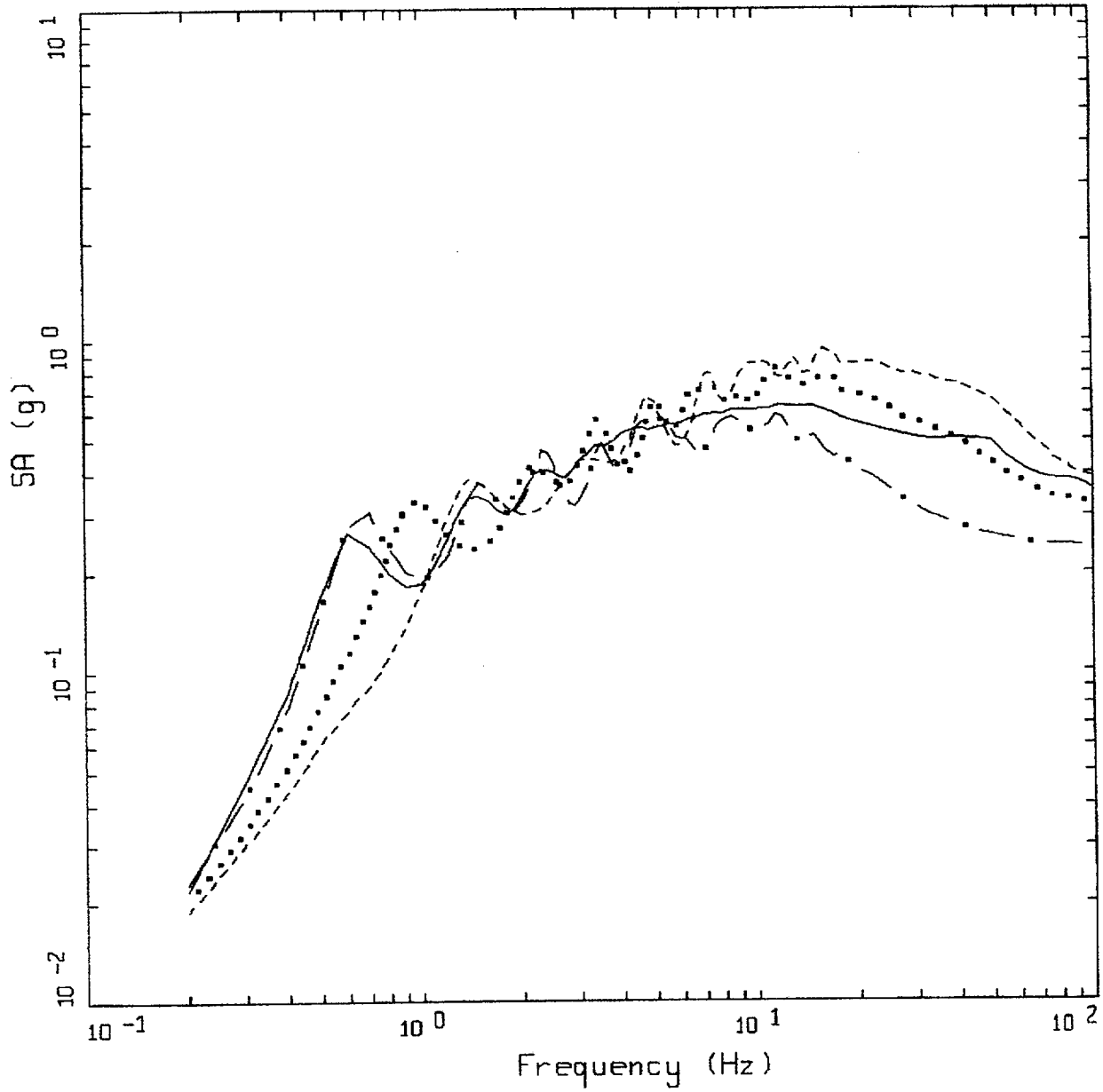
Figure 6-126. Comparison of soil spectra for Approach 2B (full profile) with base case profile and deterministic profile variations (\pm factor of 2 on shear modulus) with profile truncated at 150m; soil profile Savannah River Generic, CEUS conditions.



CEUS 10E-4 APPROACH COMPARISON, SR
SOIL PROFILE TO 150 M (500 FT)

- LEGEND
- APPROACH 2, 1 HZ AND 10 HZ DEAGGREGATION EQKS, MEAN PGA = 0.355 G
 - - - APPROACH 1, 10-4 ROCK CONTROL MOTION, BASE CASE, 68TH PERCENTILE, PGA = 0.361 G
 - · - APPROACH 1, 10-4 ROCK CONTROL MOTION, BASE CASE, MEAN, PGA = 0.288 G
 - · - APPROACH 1, 10-4 ROCK CONTROL MOTION, BASE CASE, 32ND PERCENTILE, PGA = 0.214 G

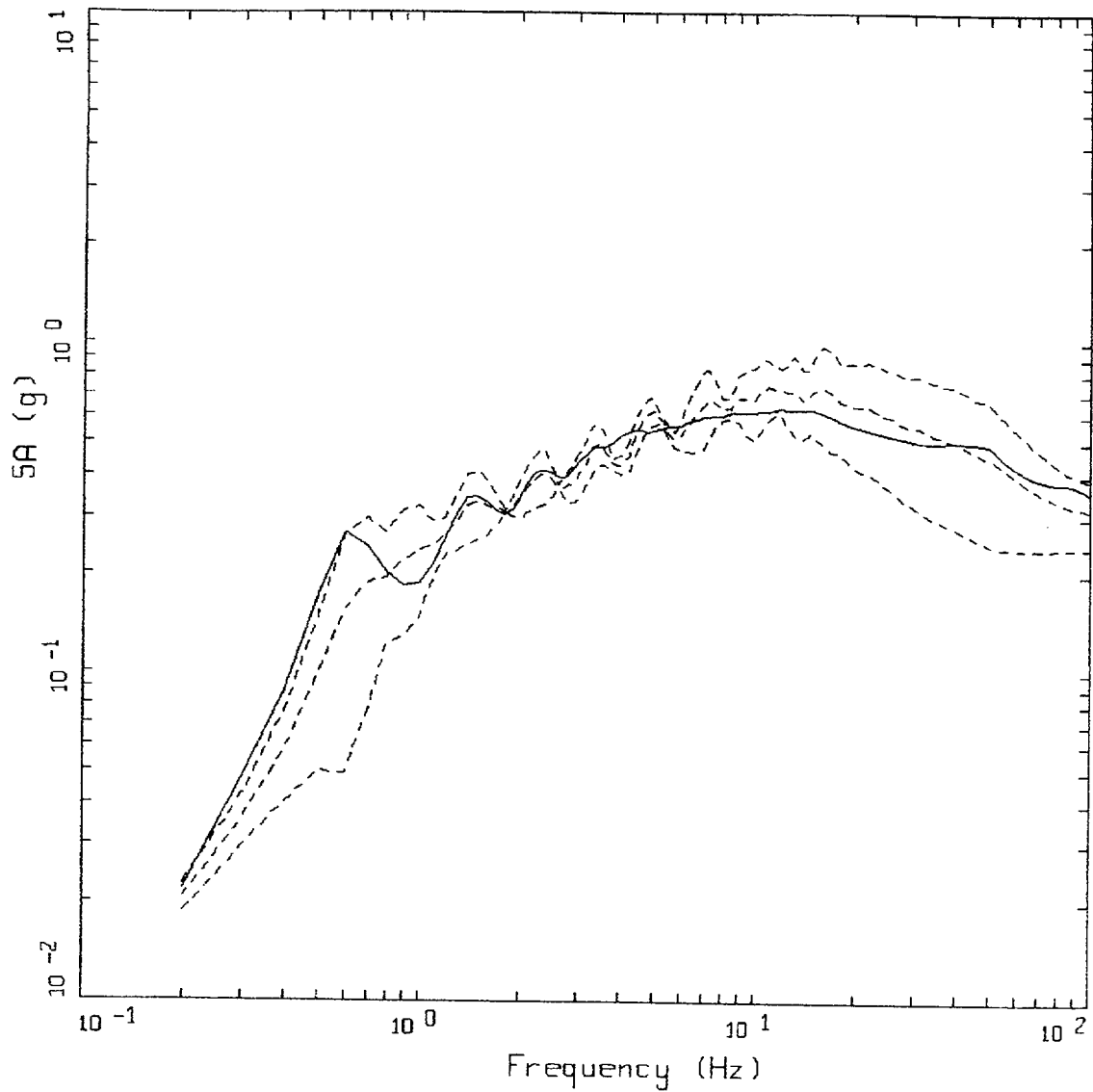
Figure 6-127. Comparison of soil spectra for Approach 2B (full profile) with mean and $\pm 1\sigma$ profile variations with profile truncated at 150m. Soil profile Savannah River Generic; CEUS conditions.



CEUS 10E-4 APPROACH COMPARISON, SR
SOIL PROFILE TO 90 M (300 FT)

- LEGEND
- APPROACH 2, 1 HZ AND 10 HZ DEAGGREGATION EQKS, MEAN PGA = 0.355 G
 - APPROACH 1, 10-4 ROCK CONTROL MOTION, BASE CASE PGA = 0.321 G
 - APPROACH 1, 10-4 ROCK CONTROL MOTION, BASE CASE (UPPER) PGA = 0.388 G
 - . - . - APPROACH 1, 10-4 ROCK CONTROL MOTION, BASE CASE (LOWER) PGA = 0.240 G

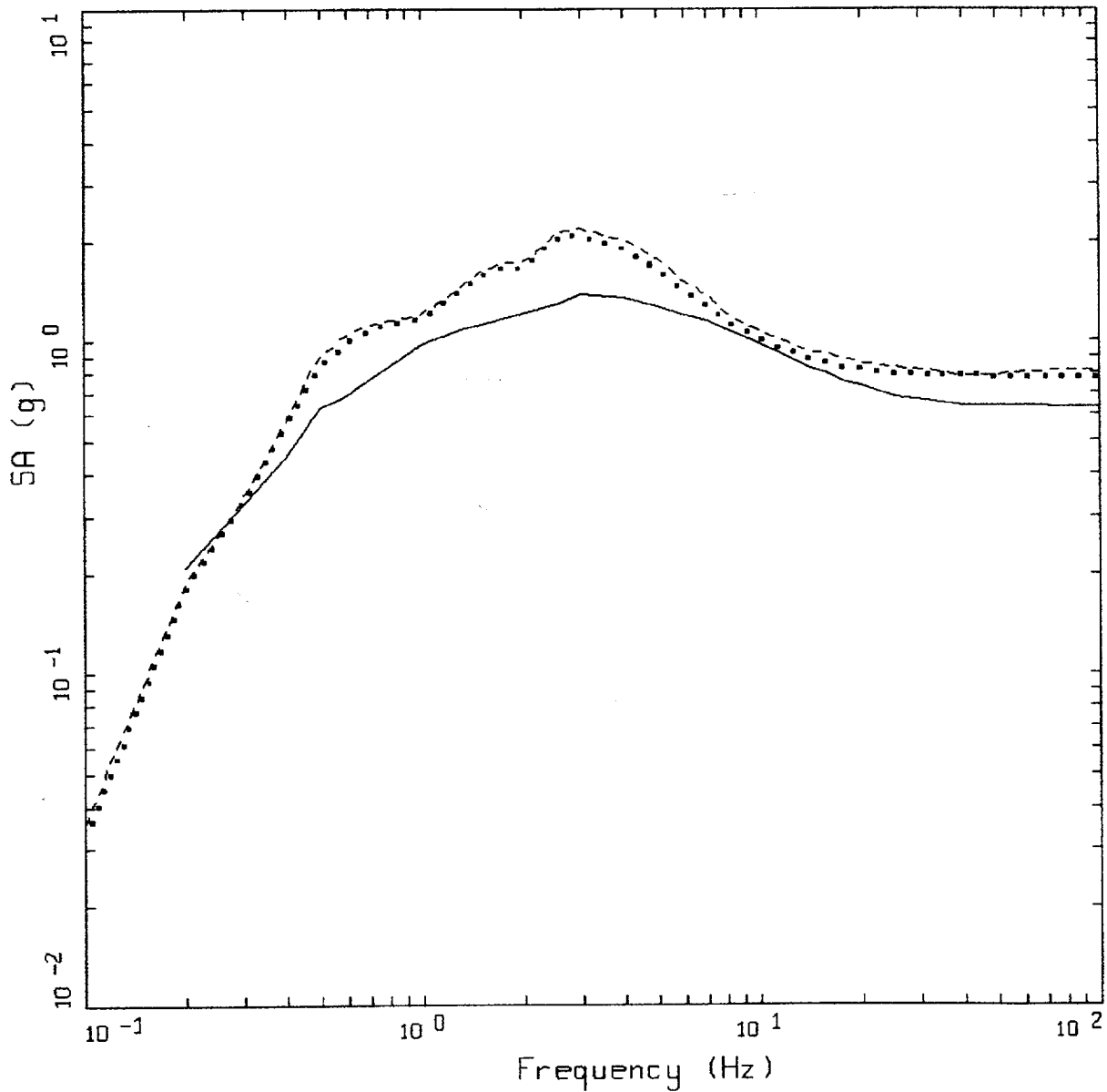
Figure 6-128. Comparison of soil spectra for Approach 2B (full profile) with base case profile and deterministic profile variations (\pm factor of 2 on shear modulus) with profile truncated at 90m; soil profile Savannah River Generic, CEUS conditions.



CEUS 10E-4 APPROACH COMPARISON, SR
SOIL PROFILE TO 90 M (300 FT)

- LEGEND
- APPROACH 2, 1 HZ AND 10 HZ DEAGGREGATION EQKS, MEAN PGA = 0.355 G
 - APPROACH 1, 10-4 ROCK CONTROL MOTION, BASE CASE, 68TH PERCENTILE, PGA = 0.390 G
 - APPROACH 1, 10-4 ROCK CONTROL MOTION, BASE CASE, MEAN, PGA = 0.316 G
 - · - · - APPROACH 1, 10-4 ROCK CONTROL MOTION, BASE CASE, 32ND PERCENTILE, PGA = 0.242 G

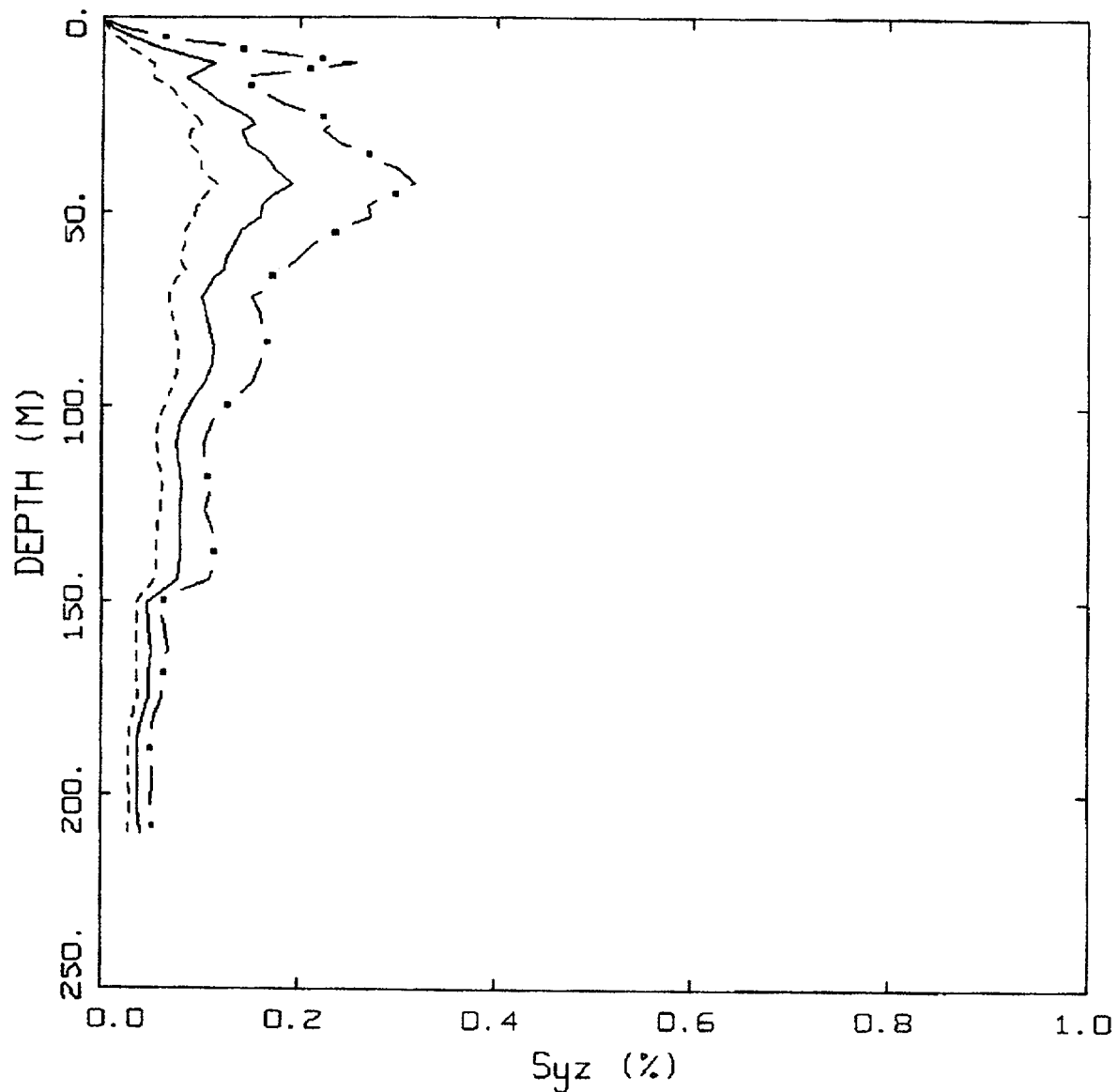
Figure 6-129. Comparison of soil spectra for Approach 2B (full profile) with mean and $\pm 1\sigma$ profile variations with profile truncated at 90m. Soil profile Savannah River Generic, CEUS conditions.



WUS $10E-4$ APPROACH COMPARISON, SR

- LEGEND
- APPROACH 4, 10^{-4} SOIL UNIFORM HAZARD SPECTRUM, PGA = 0.811 G
 - APPROACH 1, 10^{-4} ROCK CONTROL MOTION, MEAN PGA = 0.777 G
 - - - APPROACH 2, 1 HZ AND 10 HZ DEAGGREGATION EQKS, MEAN PGA = 0.560 G

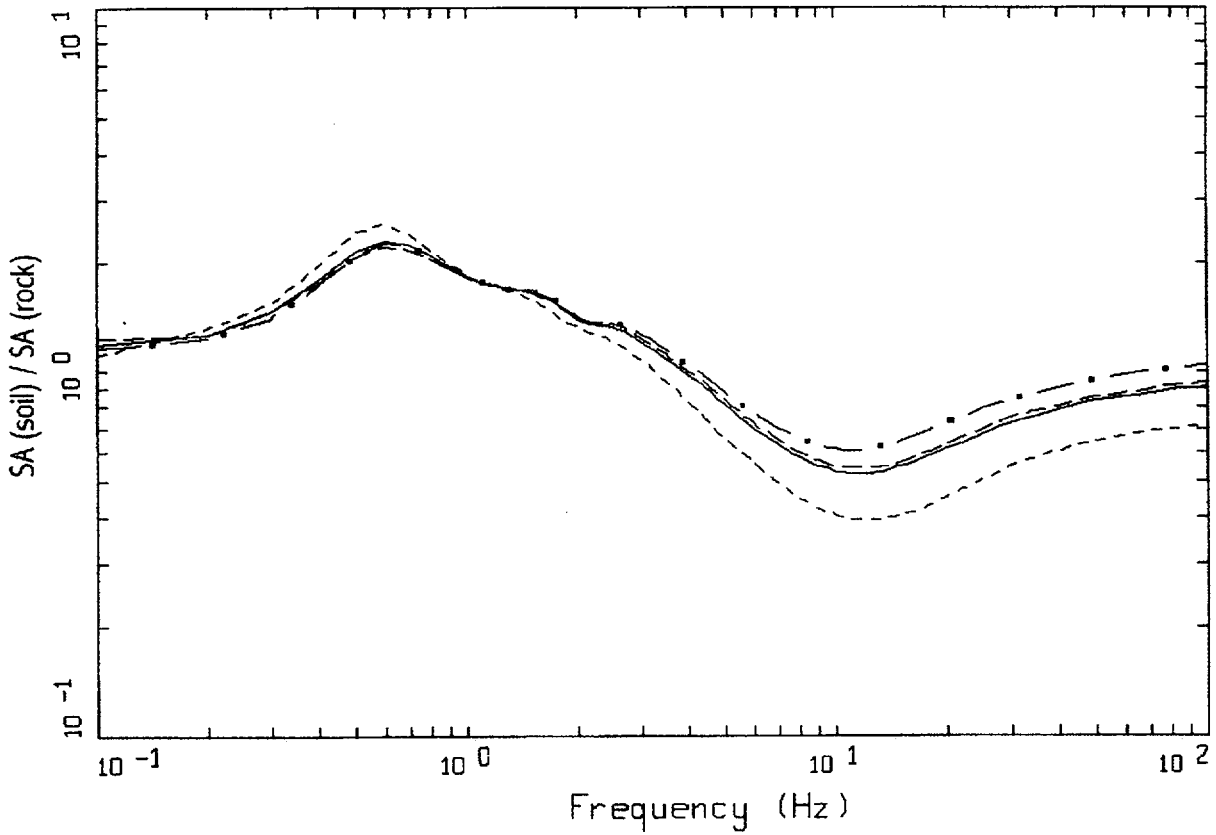
Figure 6-130. Comparison of Approaches 1, 2B, and 4 soil spectra for profile Savannah River Generic: WUS conditions.



WUS, 10⁻⁴, SR
 EFFECTIVE STRAINS (SYZ)

- LEGEND
- · — 84TH PERCENTILE
 - 50TH PERCENTILE
 - 16TH PERCENTILE

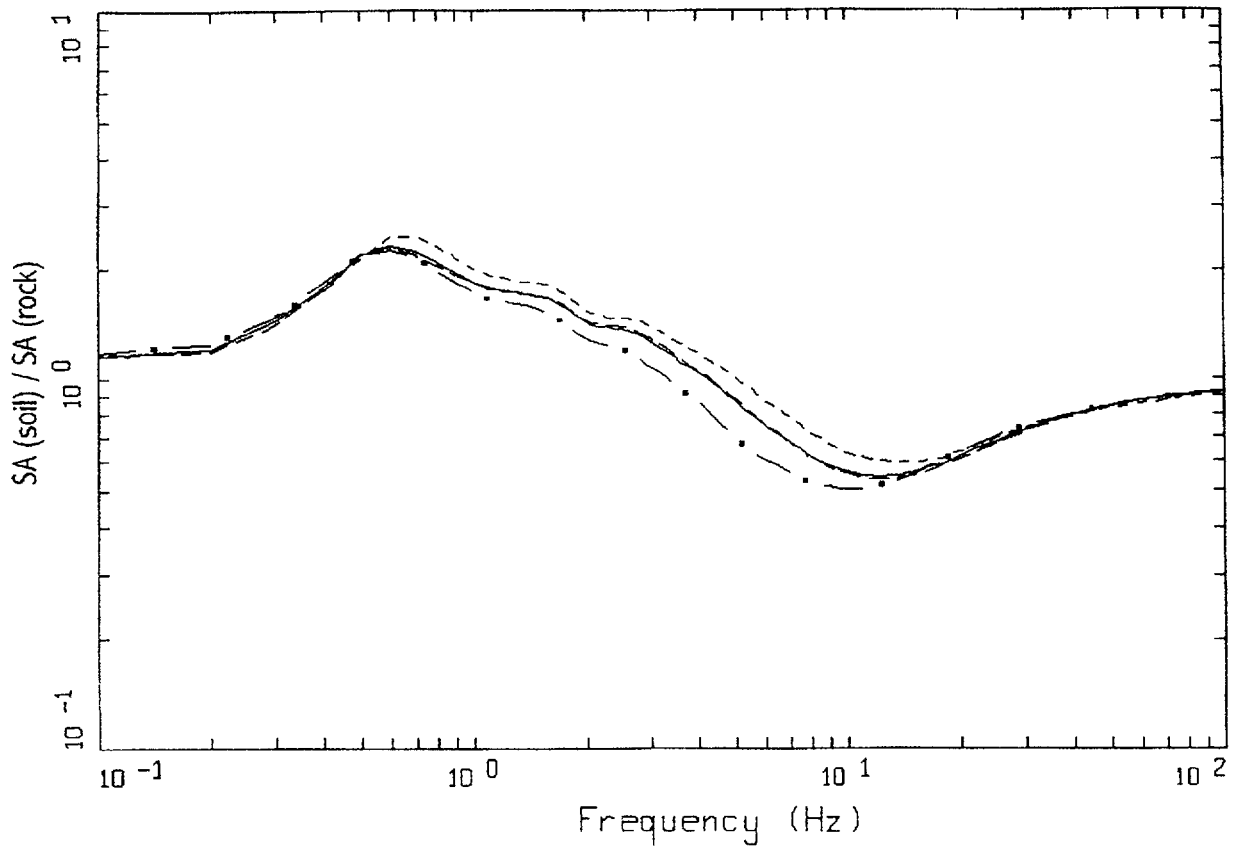
Figure 6-131. Median and $\pm 1\sigma$ effective strains for soil profile Savannah River Generic using Approach 1: WUS conditions.



WUS, 10E-4, 1HZ DESIGN, SR
 SURFACE MOTION, 1HZ TRANSFER FUNCTION
 WEIGHTS: ML=0.20, MM=0.60, MH=0.20

- LEGEND
- ML = 5.4, D = 10 KM MEAN RATIO
 - . - . - MM = 6.7, D = 18 KM, DESIGN MEAN RATIO
 - • — MH = 7.8, D = 30 KM MEAN RATIO
 - WEIGHTED MEAN RATIO

Figure 6-132. Comparison of transfer functions computed for the scaled 1 Hz design earthquake; soil profile Savannah River Generic, WUS conditions.

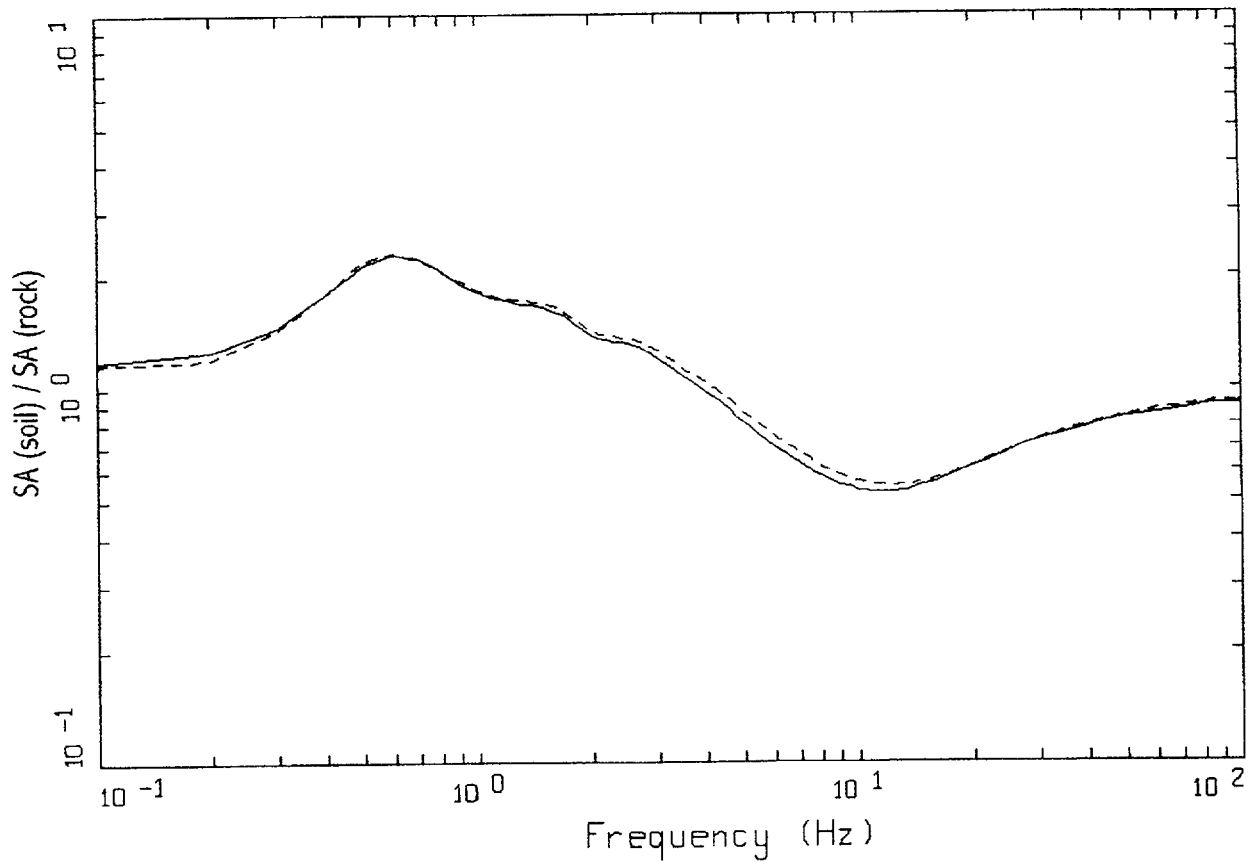


WUS, 10E-4, 10HZ DESIGN, SR
 SURFACE MOTION, 10HZ TRANSFER FUNCTION
 WEIGHTS: ML=0.20, MM=0.60, MH=0.20

LEGEND

- ML = 5.1, D = 10 KM MEAN RATIO
- . - . - . MM = 6.1, D = 14 KM, DESIGN MEAN RATIO
- • — MH = 7.8, D = 30 KM MEAN RATIO
- WEIGHTED MEAN RATIO

Figure 6-133. Comparison of transfer functions computed for the scaled 10 Hz design earthquake; soil profile Savannah River Generic, WUS conditions.

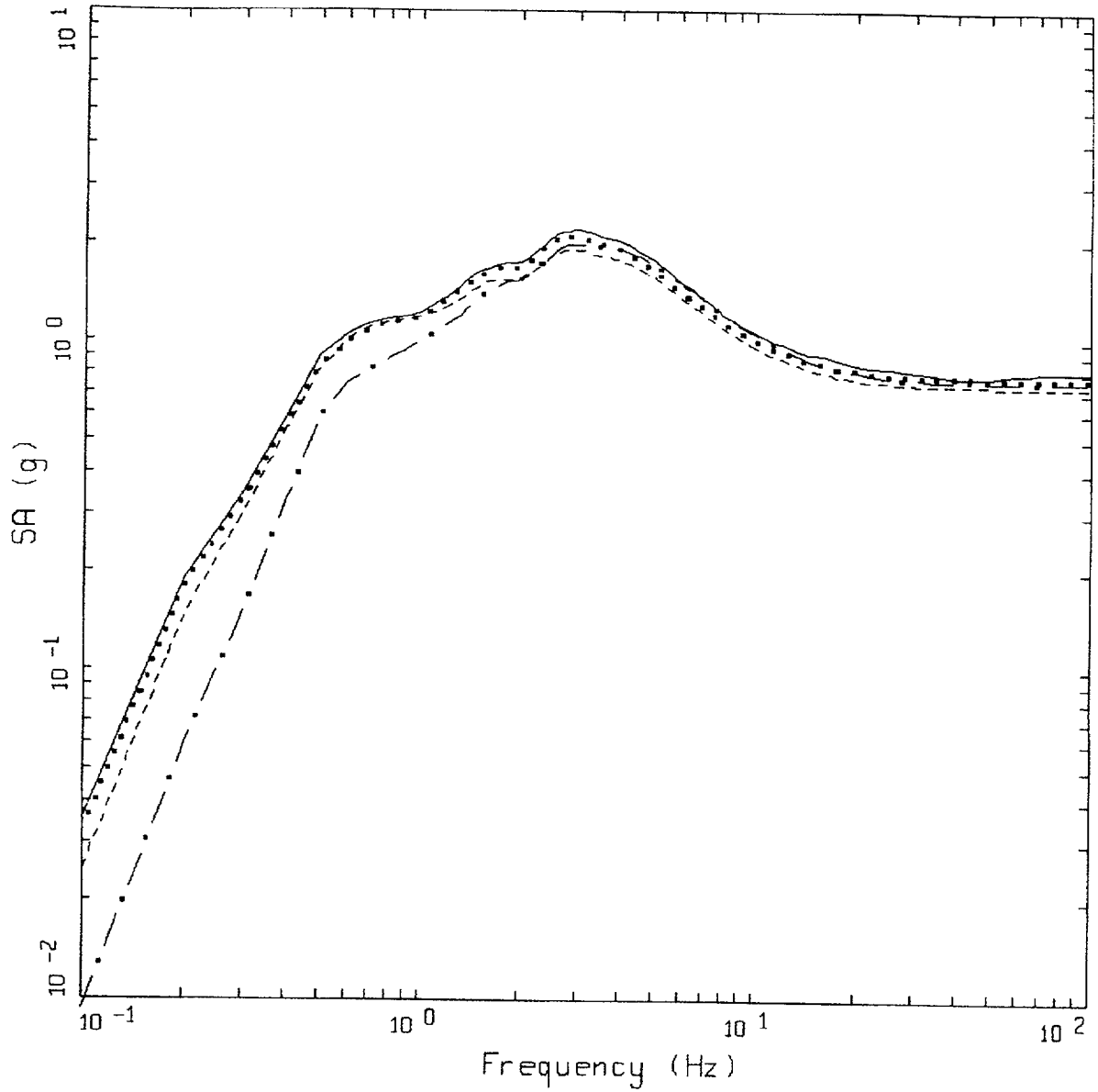


WUS, $10E-4$, SR
AMPLIFICATION

LEGEND

- 1 HZ WEIGHTED MEAN RATIO; WEIGHTS:ML=0.20,MM=0.60,MH=0.20
- 10 HZ WEIGHTED MEAN RATIO; WEIGHTS:ML=0.20,MM=0.60,MH=0.20

Figure 6-134. Comparison of mean transfer functions computed for the scaled 1 Hz and 10 Hz design earthquakes; soil profile Savannah River Generic, WUS conditions.

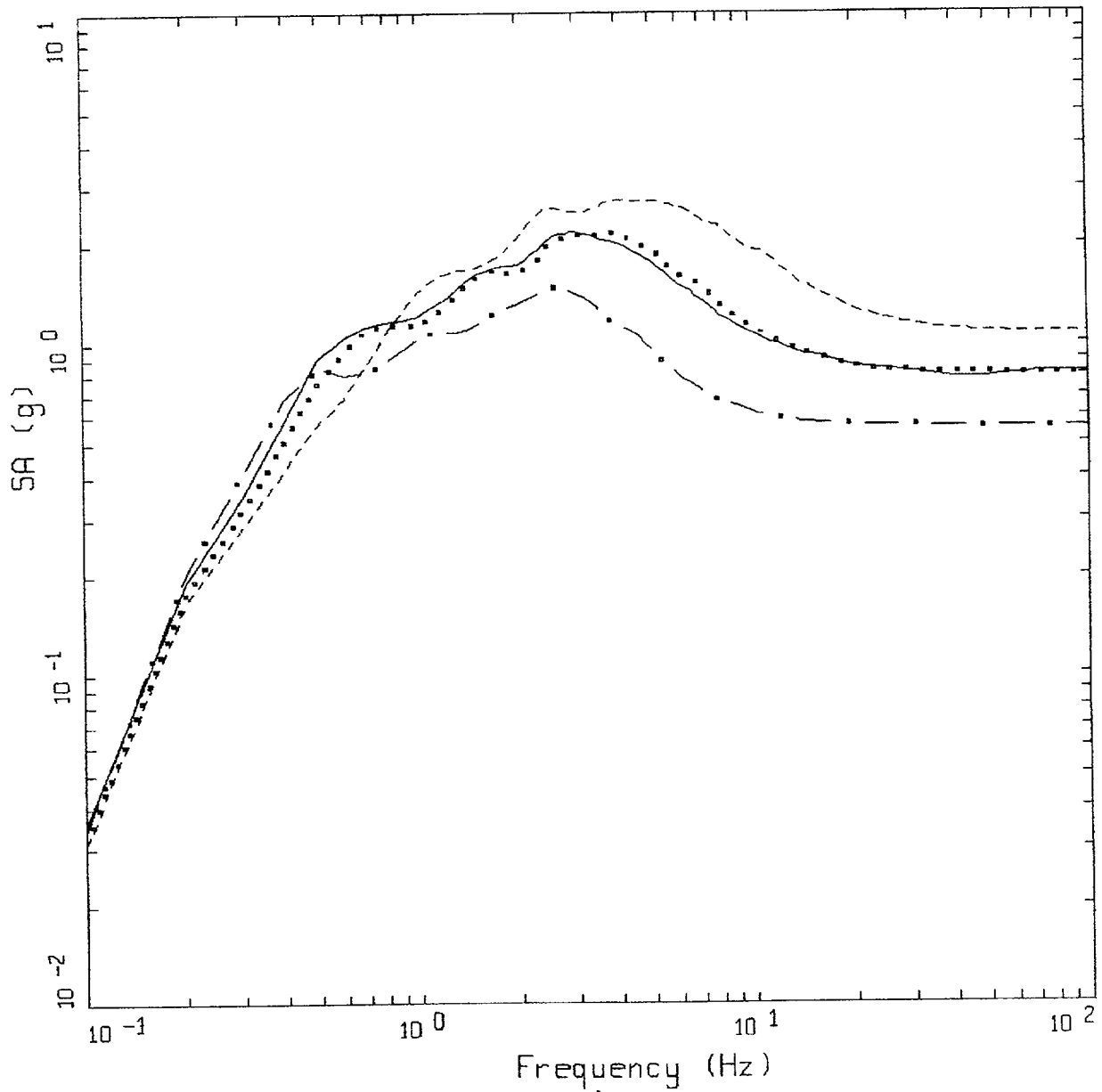


WUS, 10E-4 DESIGN SPECTRA, SR

LEGEND

- APPROACH 2, 1 HZ AND 10 HZ DEAGGREGATION EQKS, MEAN PGA = 0.811 G
- APPROACH 1, 10-4 ROCK CONTROL MOTION, MEAN PGA = 0.777 G
- - - - 1 HZ MEAN; PGA = 0.734 G
- . - . 10 HZ MEAN; PGA = 0.759 G

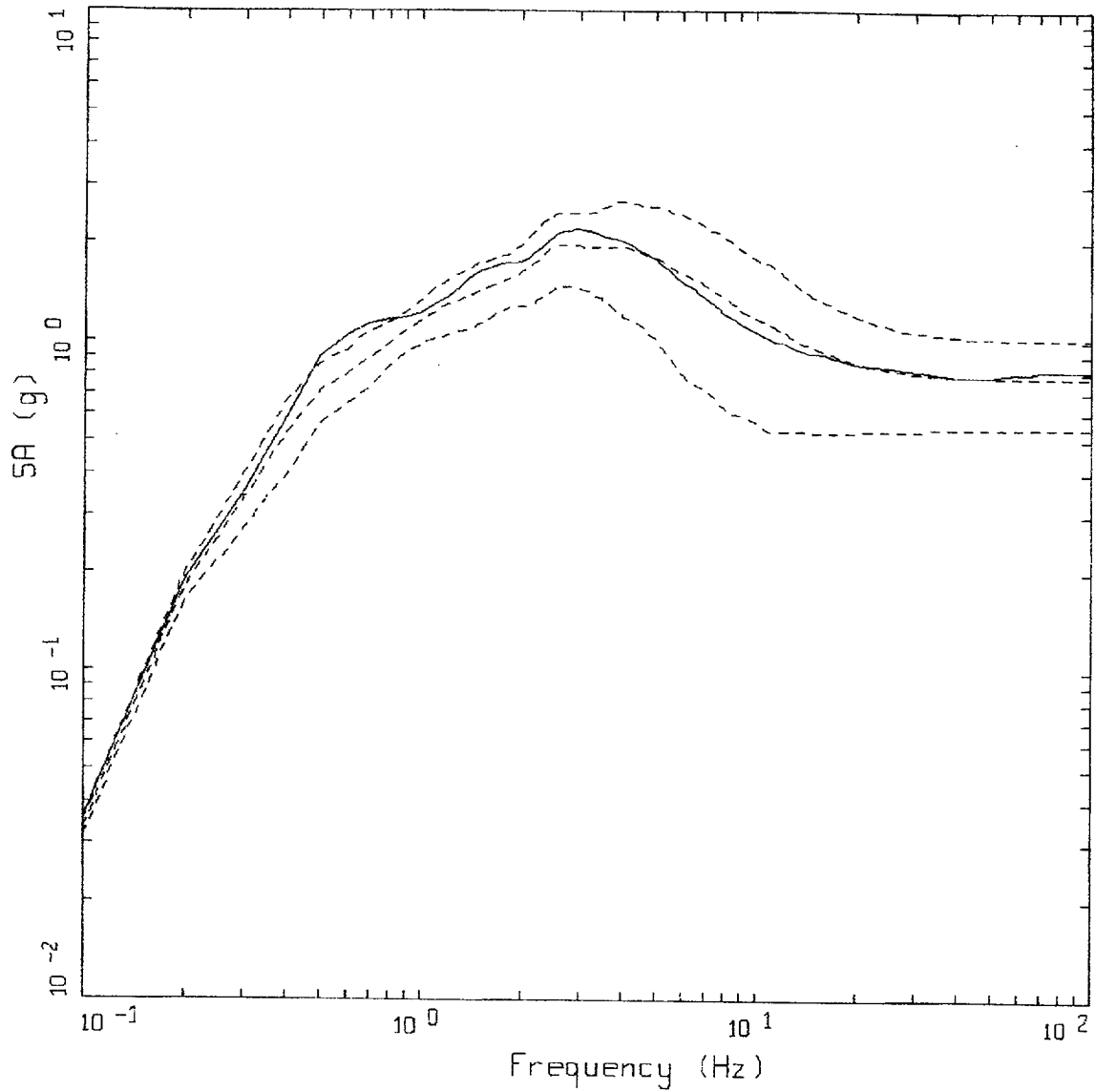
Figure 6-135. Comparison of soil spectra for Approaches 1, 2A, and 2B; soil profile Savannah River Generic, WUS conditions.



WUS 10E-4 APPROACH COMPARISON, SR

- LEGEND
- APPROACH 2, 1 HZ AND 10 HZ DEAGGREGATION EQKS, MEAN PGA = 0.811 G
 - APPROACH 1, 10-4 ROCK CONTROL MOTION, BASE CASE PGA = 0.805 G
 - APPROACH 1, 10-4 ROCK CONTROL MOTION, BASE CASE (UPPER) PGA = 1.070 G
 - . - . APPROACH 1, 10-4 ROCK CONTROL MOTION, BASE CASE (LOWER) PGA = 0.556 G

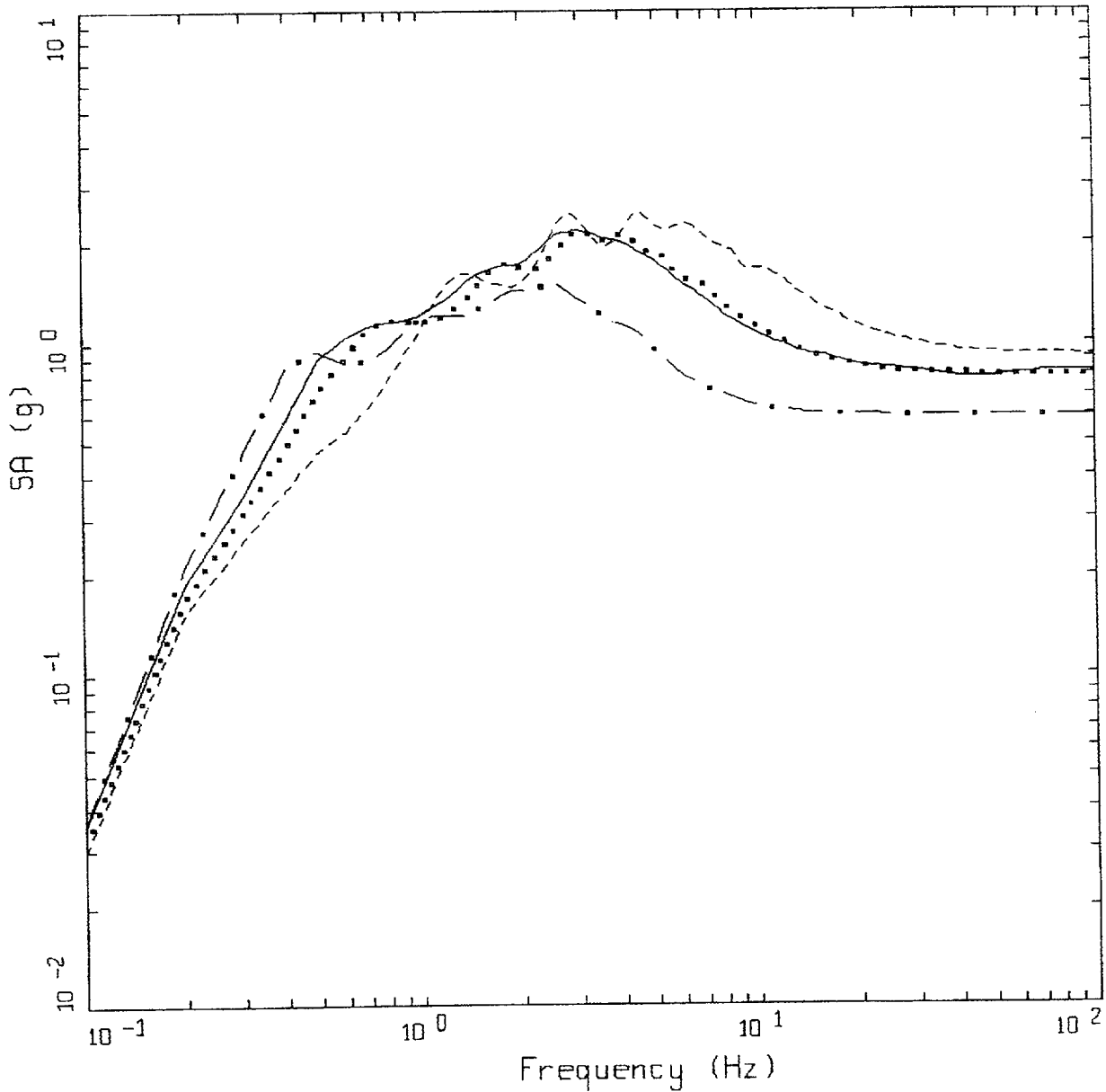
Figure 6-136. Comparison of soil spectra for Approach 2B with base case profile and deterministic profile variations (\pm factor of 2 on shear modulus); soil profile Savannah River Generic, WUS conditions.



WUS 10E-4 APPROACH COMPARISON, SR

- LEGEND
- APPROACH 2, 1 HZ AND 10 HZ DEAGGREGATION EQKS, MEAN PGA = 0.811 G
 - APPROACH 1, 10-4 ROCK CONTROL MOTION, BASE CASE, 84TH PERCENTILE, PGA = 1.006 G
 - APPROACH 1, 10-4 ROCK CONTROL MOTION, BASE CASE, MEAN, PGA = 0.774 G
 - APPROACH 1, 10-4 ROCK CONTROL MOTION, BASE CASE, 16TH PERCENTILE, PGA = 0.542 G

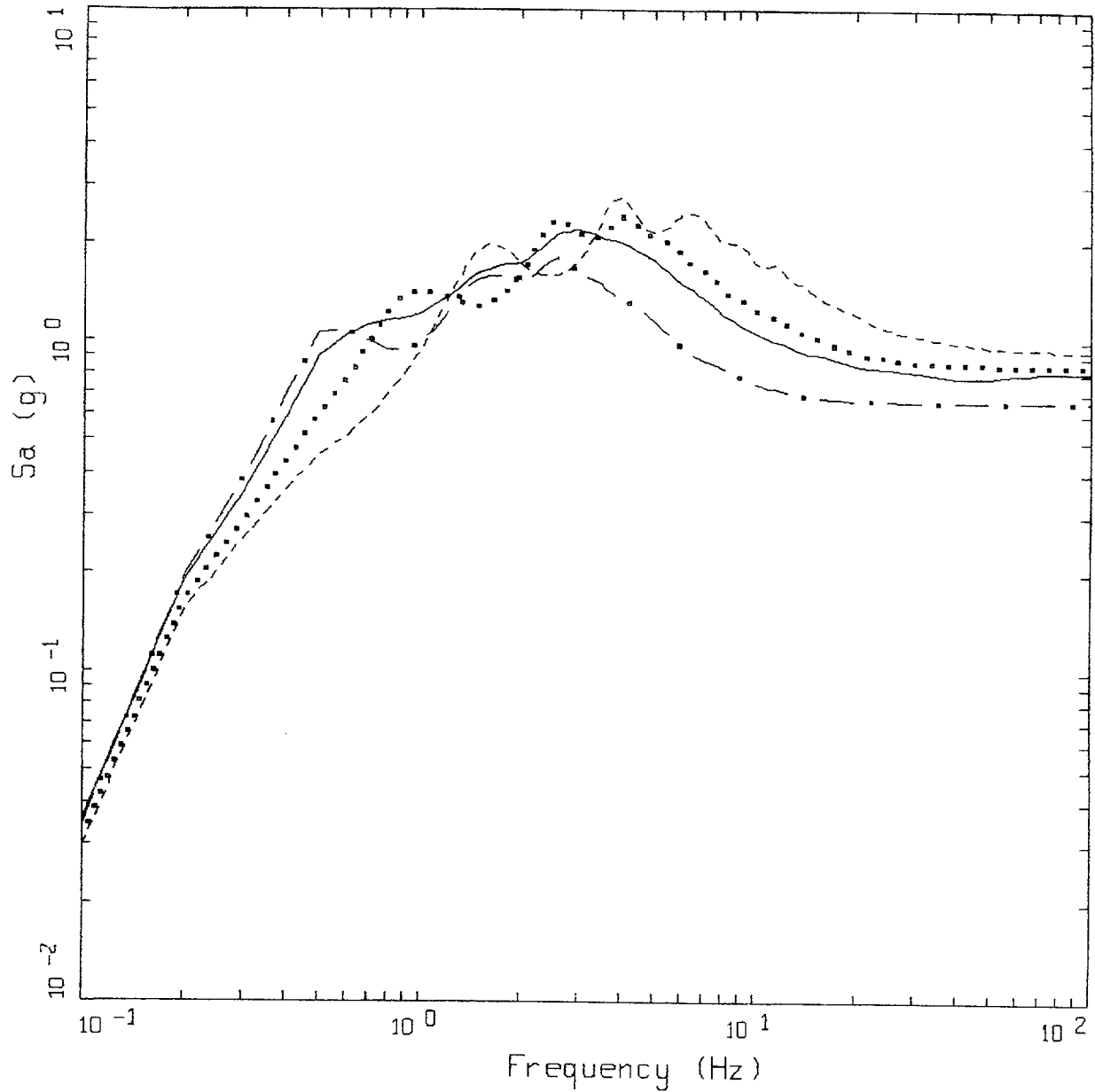
Figure 6-137. Comparison of soil spectra for Approach 2B with mean and $\pm 1\sigma$ variations of base case (\pm factor of 2 on shear modulus), soil profile Savannah River Generic, WUS conditions.



WUS 10E-4 APPROACH COMPARISON, SR
SOIL PROFILE TO 150 M (500 FT)

- LEGEND
- APPROACH 2, 1 HZ AND 10 HZ DEAGGREGATION EQKS, MEAN PGA = 0.811 G
 - APPROACH 1, 10-4 ROCK CONTROL MOTION, BASE CASE PGA = 0.793 G
 - APPROACH 1, 10-4 ROCK CONTROL MOTION, BASE CASE (UPPER) PGA = 0.916 G
 - . - . APPROACH 1, 10-4 ROCK CONTROL MOTION, BASE CASE (LOWER) PGA = 0.595 G

Figure 6-138. Comparison of soil spectra for Approach 2b (full profile) with base case profile and deterministic profile variations (\pm factor of 2 on shear modulus) with profile truncated at 150m; soil profile Savannah River Generic, WUS conditions.

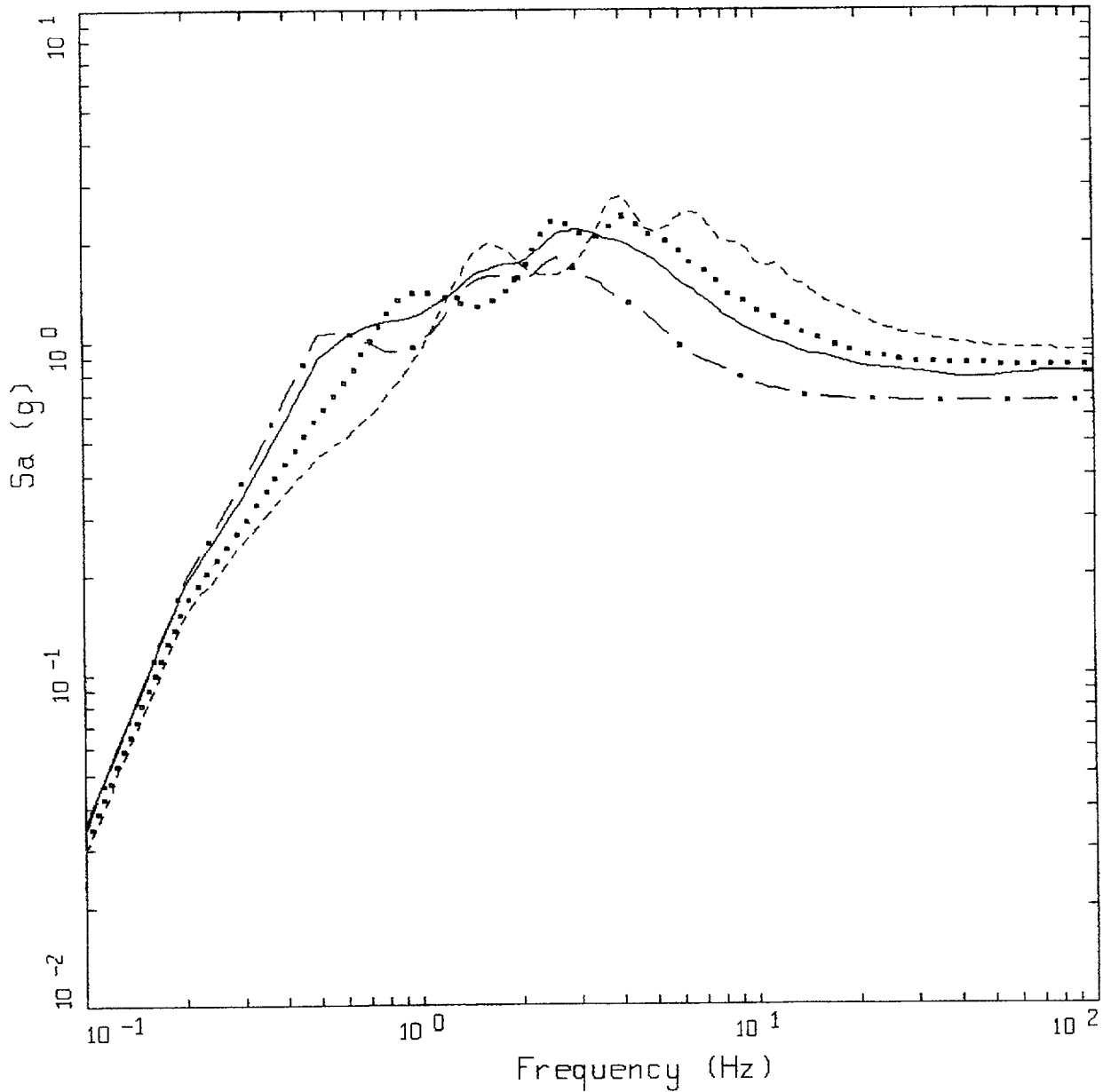


WUS 10E-4 APPROACH COMPARISON, SR
SOIL PROFILE TO 90 M (300 FT)

LEGEND

- APPROACH 2, 1 HZ AND 10 HZ DEAGGREGATION EQKS, MEAN PGA = 0.811 G
- APPROACH 1, 10-4 ROCK CONTROL MOTION, BASE CASE PGA = 0.851 G
- APPROACH 1, 10-4 ROCK CONTROL MOTION, BASE CASE (UPPER) PGA = 0.946 G
- . - APPROACH 1, 10-4 ROCK CONTROL MOTION, BASE CASE (LOWER) PGA = 0.659 G

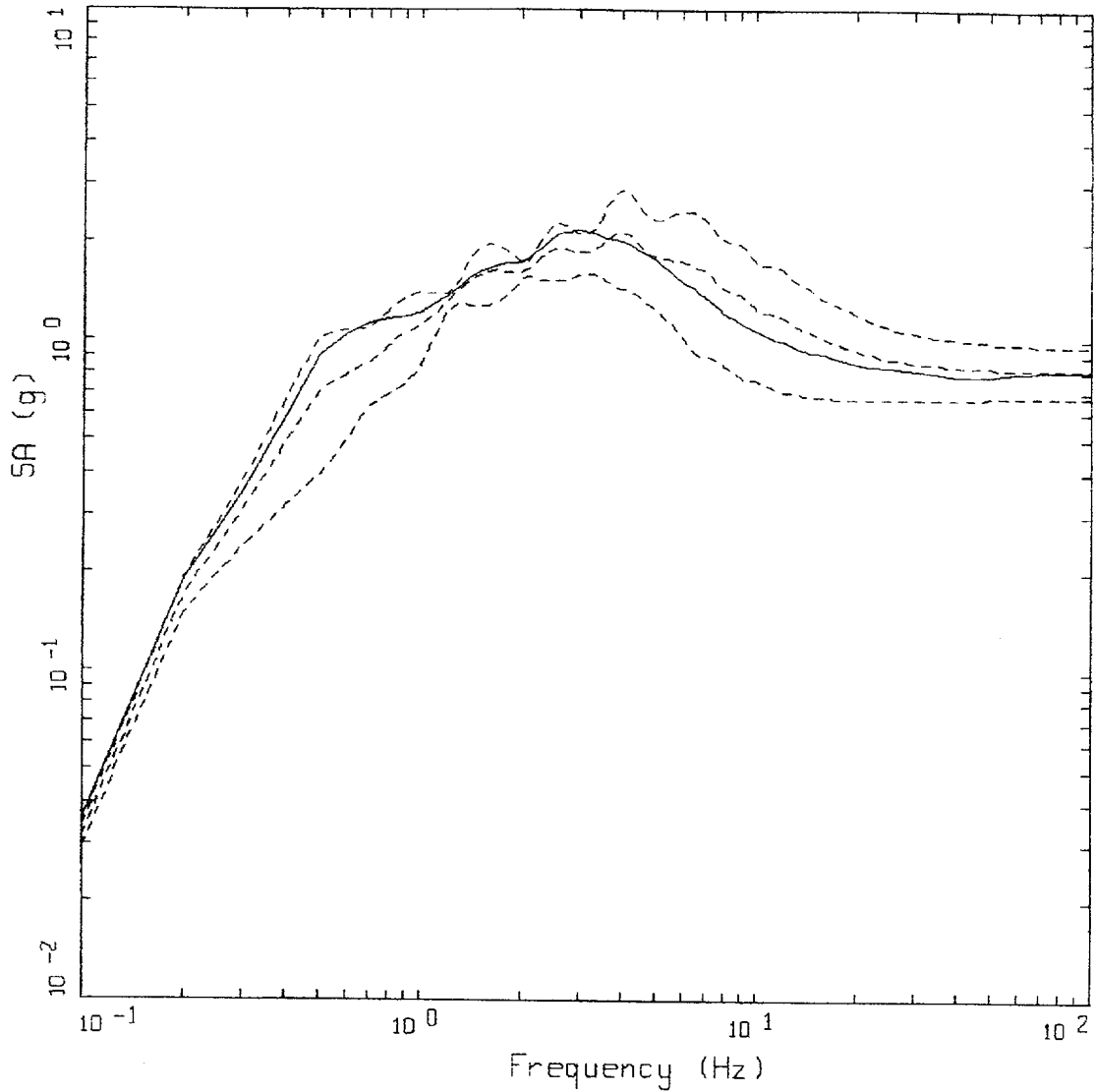
Figure 6-139. Comparison of soil spectra for Approach 2B (full profile) with mean and $\pm 1\sigma$ profile variation with profile truncated at 150m. Soil profile Savannah River Generic, WUS conditions.



WUS 10E-4 APPROACH COMPARISON, SR
SOIL PROFILE TO 90 M (300 FT)

- LEGEND
- APPROACH 2, 1 HZ AND 10 HZ DISAGGREGATION EQKS, MEAN PGA = 0.811 G
 - APPROACH 1, 10-4 ROCK CONTROL MOTION, BASE CASE PGA = 0.851 G
 - APPROACH 1, 10-4 ROCK CONTROL MOTION, BASE CASE (UPPER) PGA = 0.946 G
 - . - . APPROACH 1, 10-4 ROCK CONTROL MOTION, BASE CASE (LOWER) PGA = 0.659 G

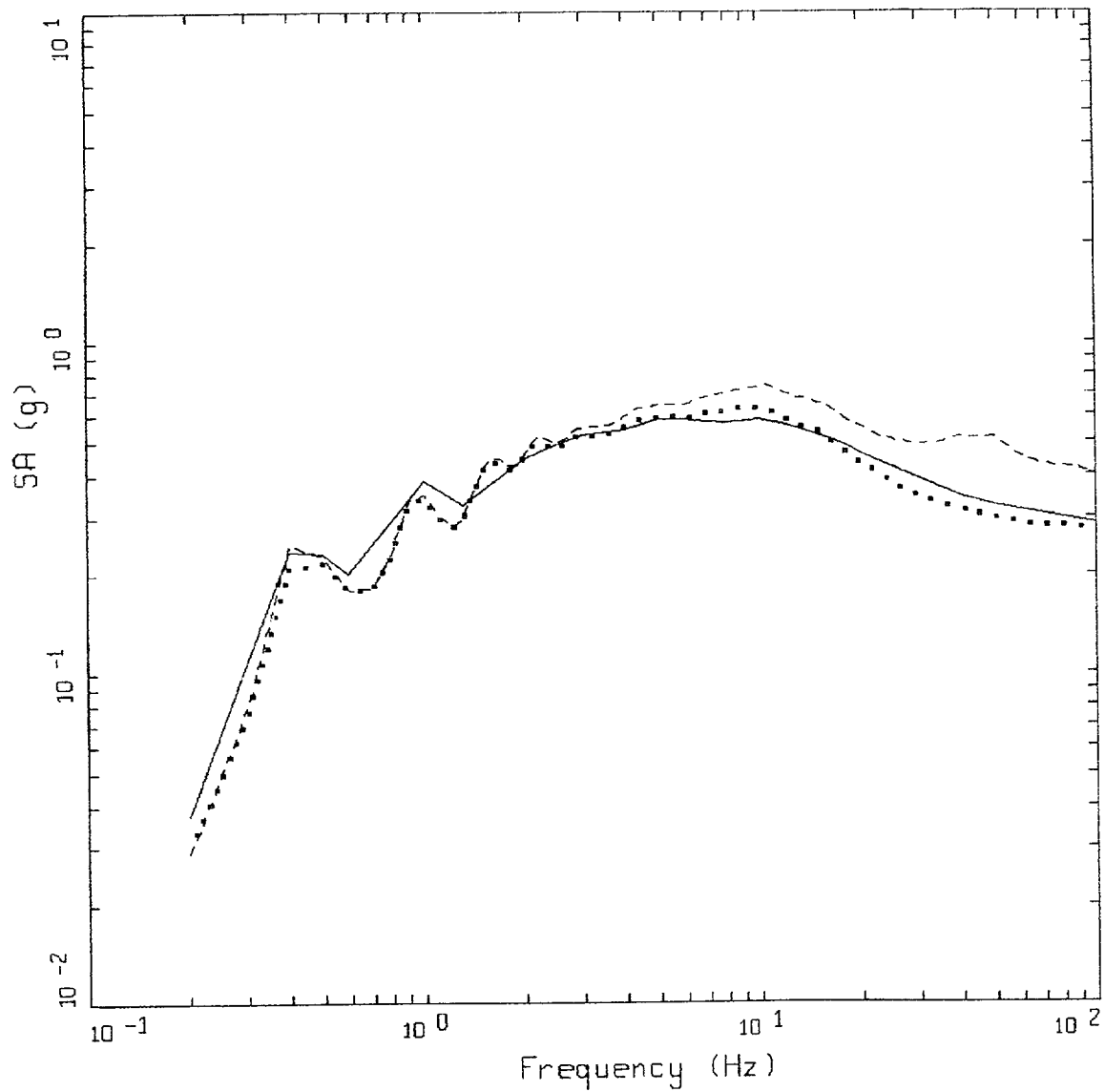
Figure 6-140. Comparison of soil spectra for Approach 2B (full profile) with base case profile and deterministic profile variations (\pm factor of 2 on shear modulus) with profile truncated at 90m; soil profile Savannah River Generic, WUS conditions.



WUS 10E-4 APPROACH COMPARISON, SR
SOIL PROFILE TO 90 M (300 FT)

- LEGEND
- APPROACH 2, 1 HZ AND 10 HZ DEAGGREGATION EQKS, MEAN PGA = 0.811 G
 - - - - APPROACH 1, 10-4 ROCK CONTROL MOTION, BASE CASE, 84TH PERCENTILE, PGA = 0.965 G
 - - - - APPROACH 1, 10-4 ROCK CONTROL MOTION, BASE CASE, MEAN, PGA = 0.819 G
 - - - - APPROACH 1, 10-4 ROCK CONTROL MOTION, BASE CASE, 16TH PERCENTILE, PGA = 0.672 G

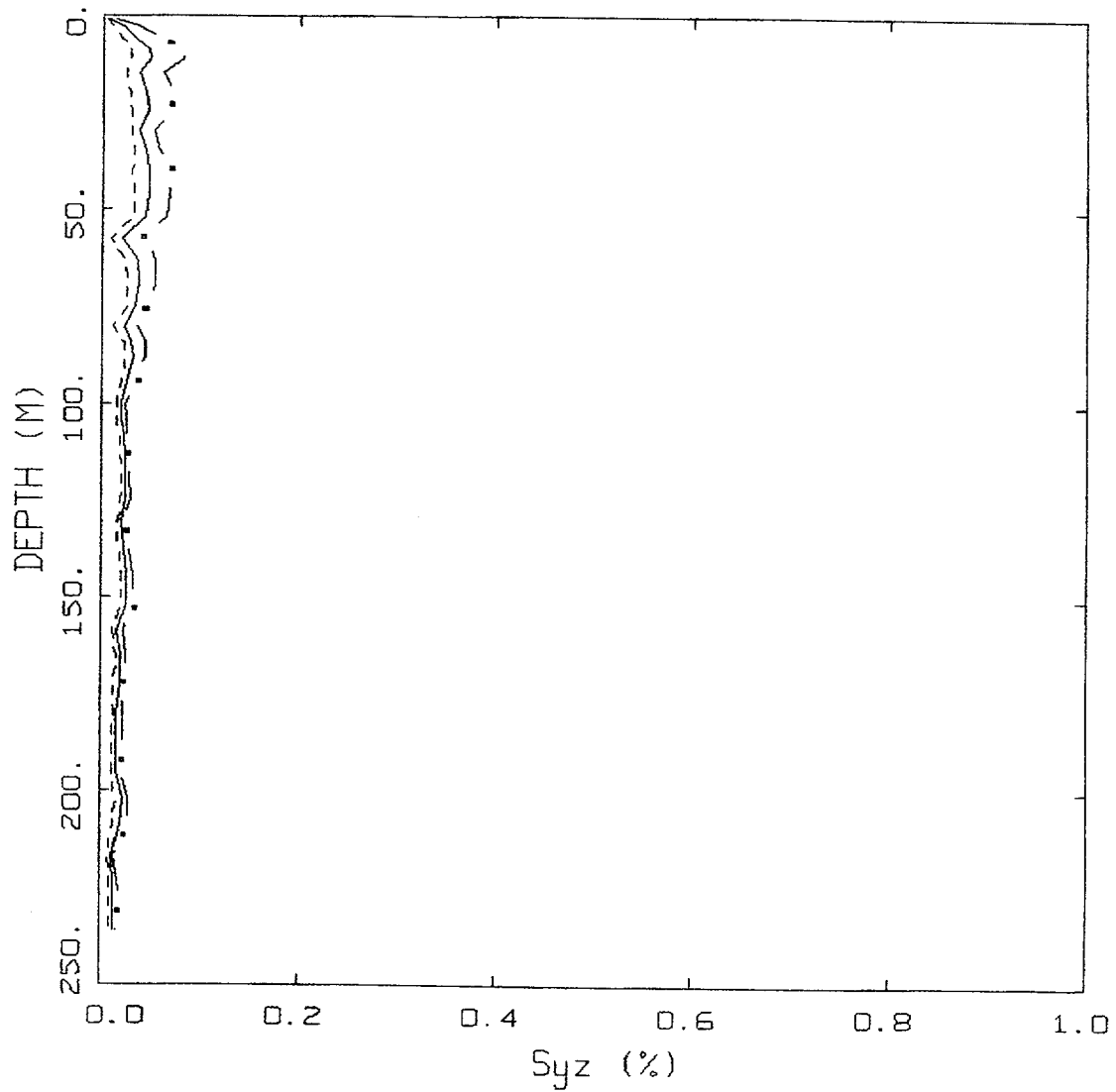
Figure 6-141. Comparison of soil spectra for Approach 2B (full profile) with mean and $\pm 1\sigma$ profile variations with profile truncated at 90m. Soil profile Savannah River Generic, WUS conditions.



CEUS $10E-4$ APPROACH COMPARISON, IV

- LEGEND
- APPROACH 4, 10^{-4} SOIL UNIFORM HAZARD SPECTRUM; PGA = 0.284 G
 - APPROACH 1, 10^{-4} ROCK CONTROL MOTION, MEAN PGA = 0.276 G
 - APPROACH 2, 1 HZ AND 10 HZ DEAGGREGATION EQKS, MEAN PGA = 0.395 G

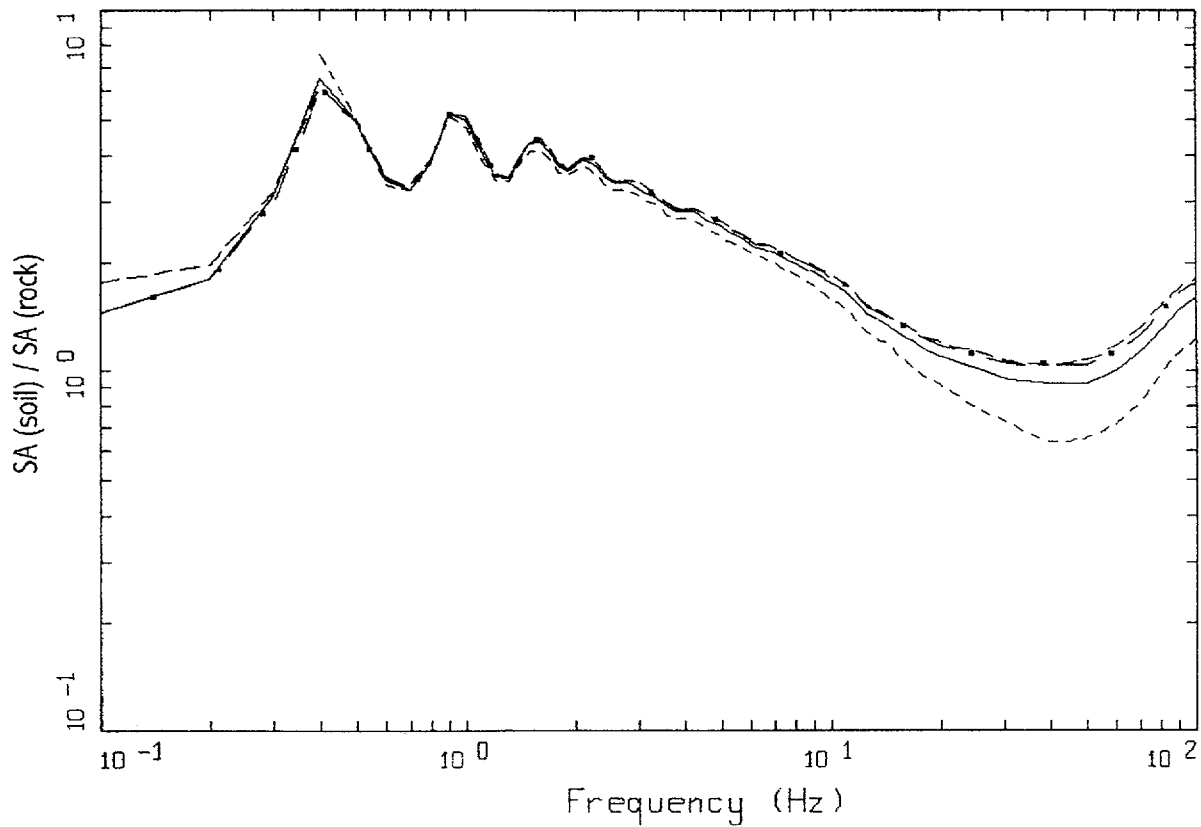
Figure 6-142. Comparison of Approaches 1, 2B, and 4 soil spectra for profile Meloland; CEUS conditions.



CEUS, 10-4, IV
 EFFECTIVE STRAINS (SYZ)

LEGEND
 - . - 84TH PERCENTILE
 ——— 50TH PERCENTILE
 - - - 16TH PERCENTILE

Figure 6-143. Median and $\pm 1\sigma$ effective strains for soil profile Meloland using Approach 1: CEUS conditions.

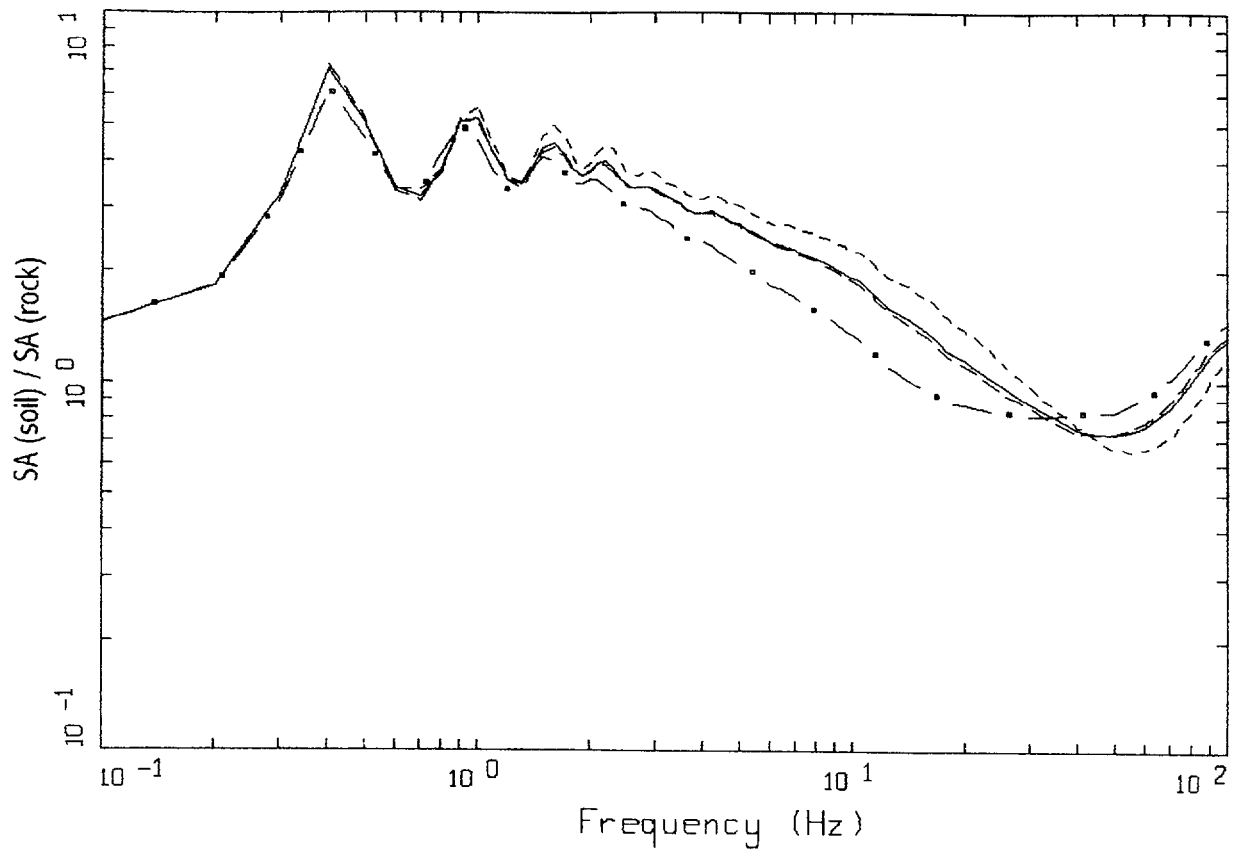


CEUS, 10E-4, 1HZ DESIGN, IV
 SURFACE MOTION, 1HZ TRANSFER FUNCTION
 WEIGHTS: ML=0.30, MM=0.00, MH=0.70

LEGEND

- ML = 5.7, D = 20 KM MEAN RATIO
- · - · - MM = 7.0, D = 100 KM, DESIGN MEAN RATIO
- · — MH = 7.6, D = 130 KM MEAN RATIO
- WEIGHTED MEAN RATIO

Figure 6-144. Comparison of transfer functions computed for the scaled 1 Hz design earthquake; soil profile Meloland, CEUS conditions.

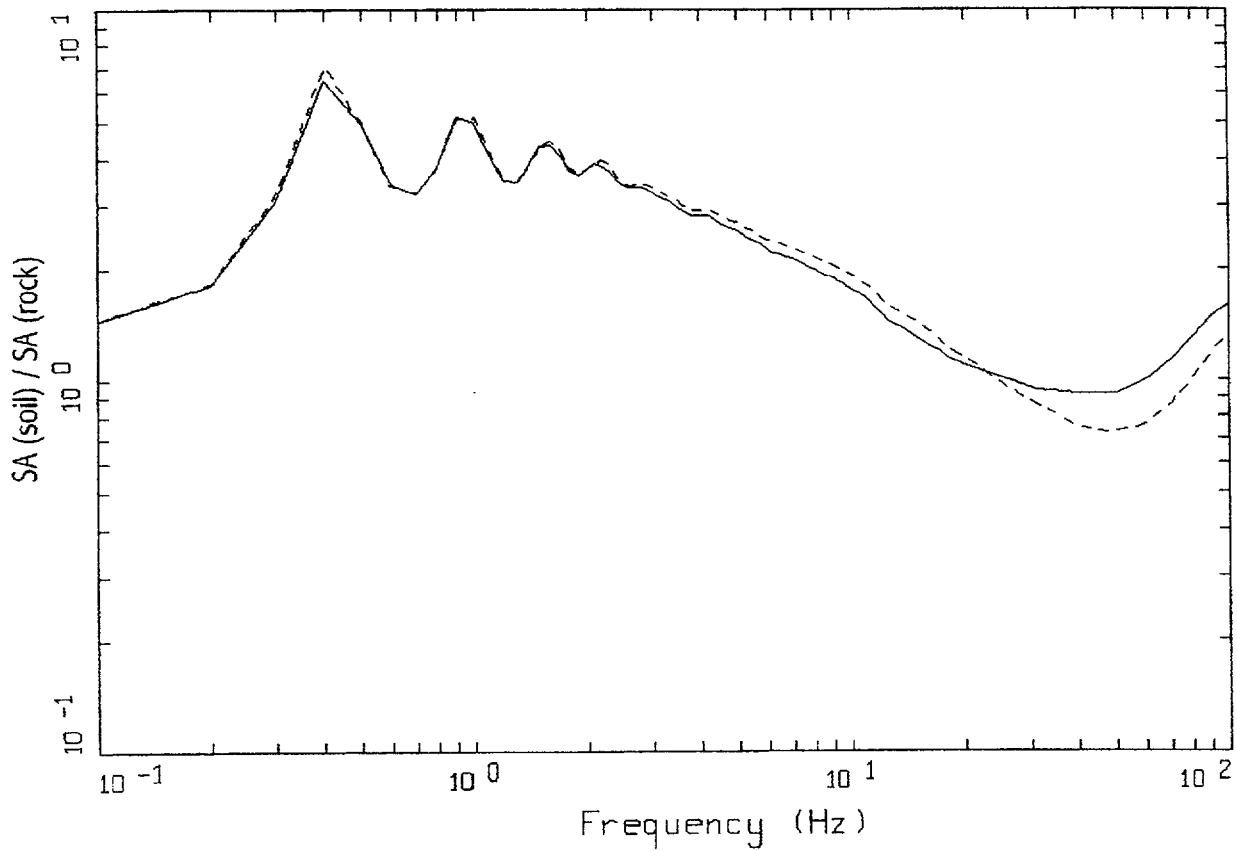


CEUS, 10E-4, 10HZ DESIGN, IV
 SURFACE MOTION, 10HZ TRANSFER FUNCTION
 WEIGHTS: ML=0.25, MM=0.63, MH=0.12

LEGEND

- ML = 4.6, D = 8 KM MEAN RATIO
- · - · - MM = 5.6, D = 8 KM, DESIGN MEAN RATIO
- · — MH = 7.7, D = 130 KM MEAN RATIO
- WEIGHTED MEAN RATIO

Figure 6-145. Comparison of transfer functions computed for the scaled 10 Hz design earthquake; soil profile Meloland, CEUS conditions.

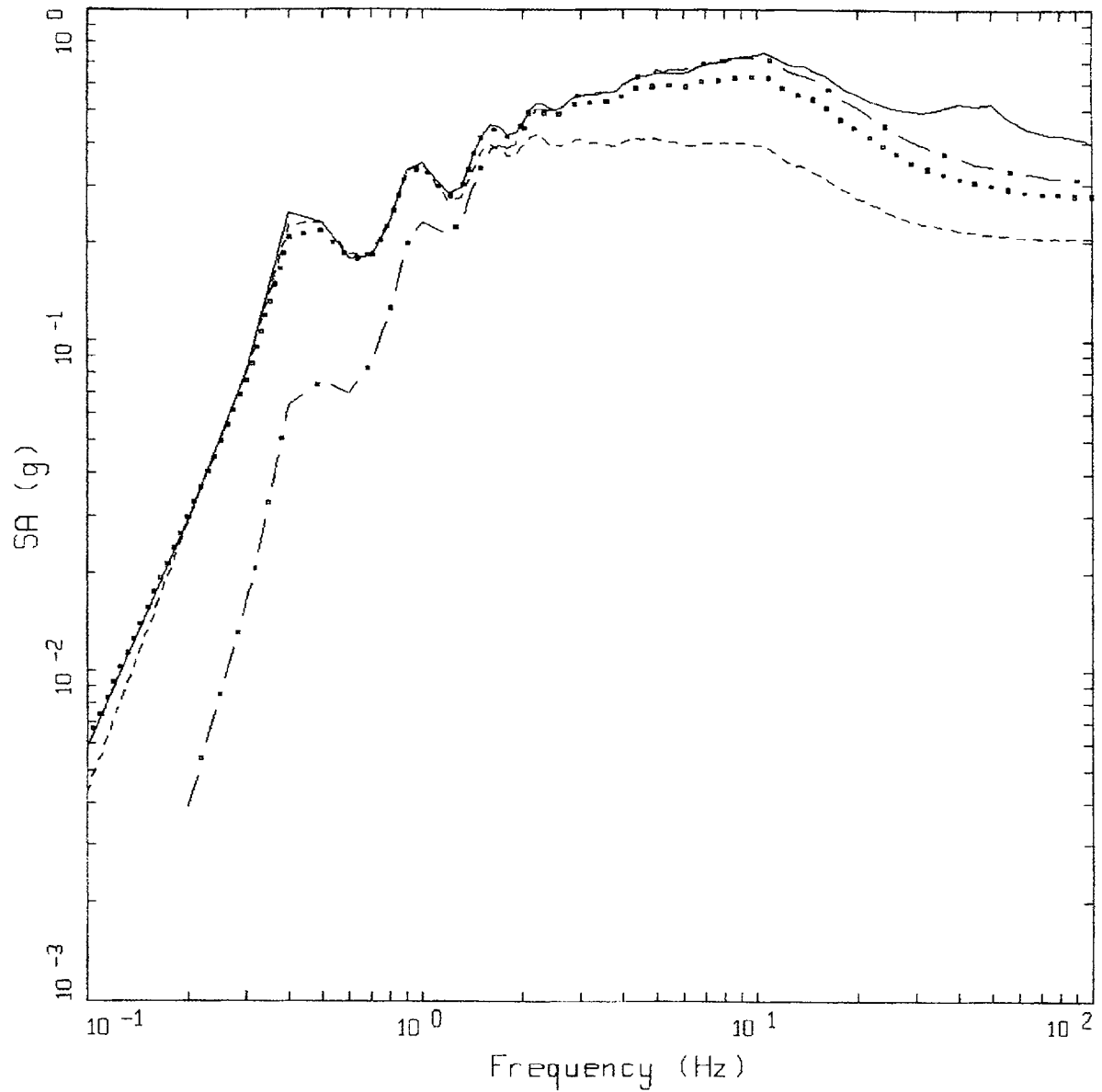


CEUS, 10E-4, IV
TRANSFER FUNCTION

LEGEND

- 1 HZ WEIGHTED MEAN RATIO; WEIGHTS:ML=0.30,MM=0.00,MH=0.70
- 10 HZ WEIGHTED MEAN RATIO; WEIGHTS:ML=0.25,MM=0.63,MH=0.12

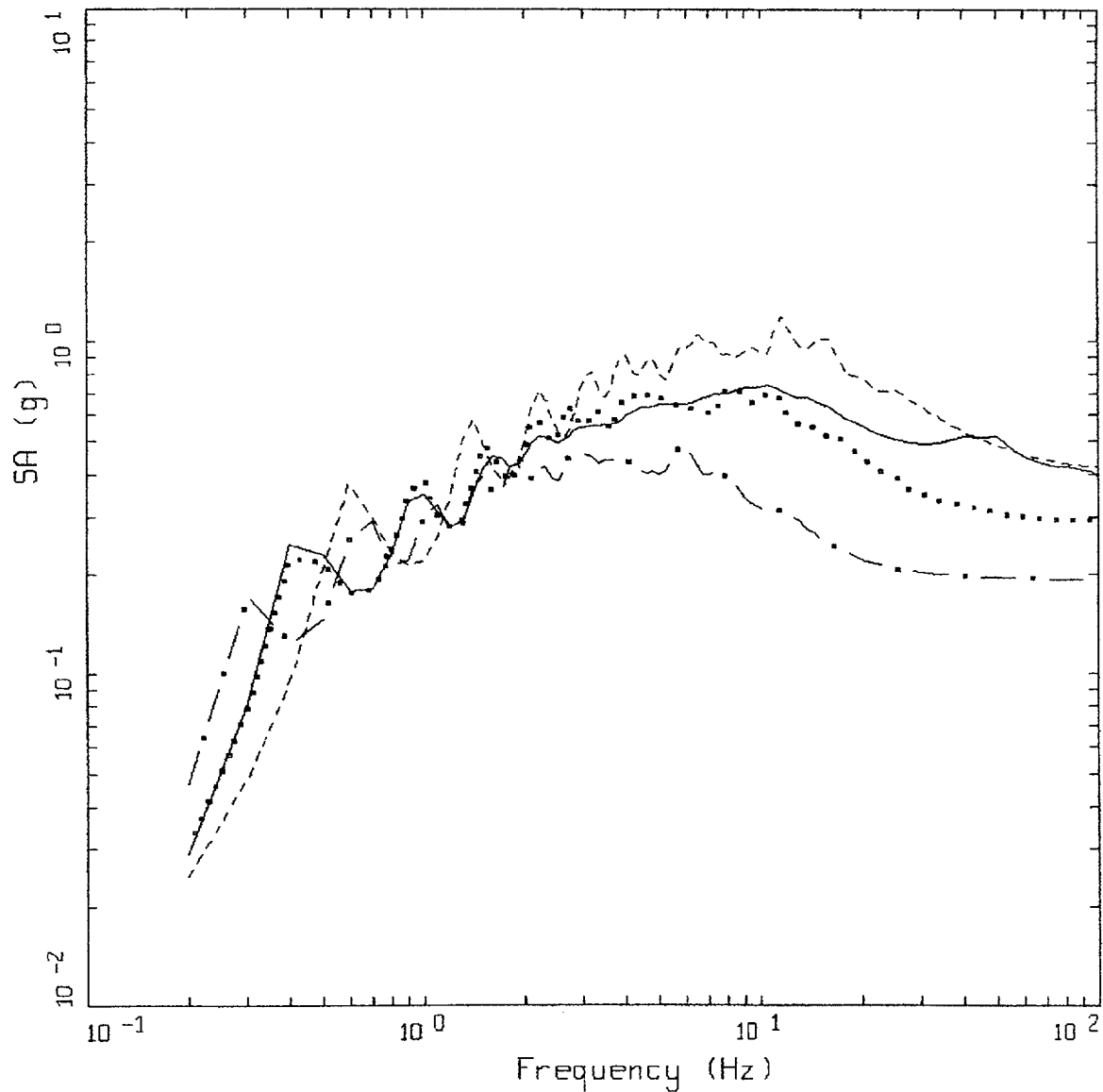
Figure 6-146. Comparison of mean transfer functions computed for the scaled 1 Hz and 10 Hz design earthquakes; soil profile Meloland, CEUS conditions.



CEUS, 10E-4 DESIGN SPECTRA, IV

- LEGEND
- APPROACH 2, 1 HZ AND 10 HZ DEAGGREGATION EQKS, MEAN PGA = 0.395 G
 - APPROACH 1, 10-4 ROCK CONTROL MOTION, MEAN PGA = 0.276 G
 - 1 HZ MEAN; PGA = 0.203 G
 - . - . 10 HZ MEAN; PGA = 0.309 G

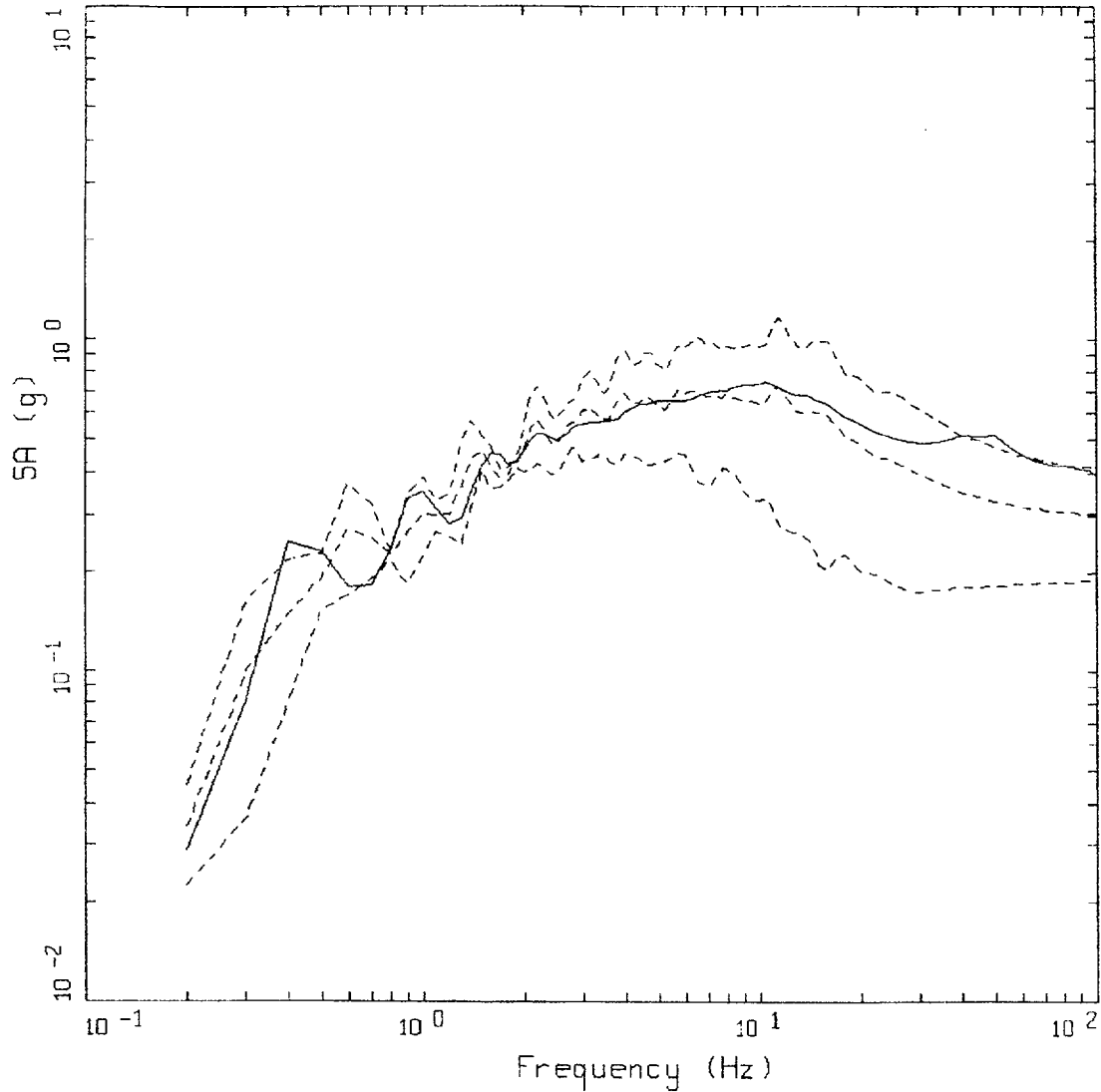
Figure 6-147. Comparison of soil spectra for Approaches 1, 2A, and 2B; soil profile Meloland, CEUS conditions.



CEUS 10E-4 APPROACH COMPARISON, IV

- LEGEND
- APPROACH 2, 1 HZ AND 10 HZ DEAGGREGATION EQKS, MEAN PGA = 0.395 G
 - APPROACH 1, 10-4 ROCK CONTROL MOTION, BASE CASE PGA = 0.291 G
 - - - - APPROACH 1, 10-4 ROCK CONTROL MOTION, BASE CASE (UPPER) PGA = 0.421 G
 - . - . APPROACH 1, 10-4 ROCK CONTROL MOTION, BASE CASE (LOWER) PGA = 0.193 G

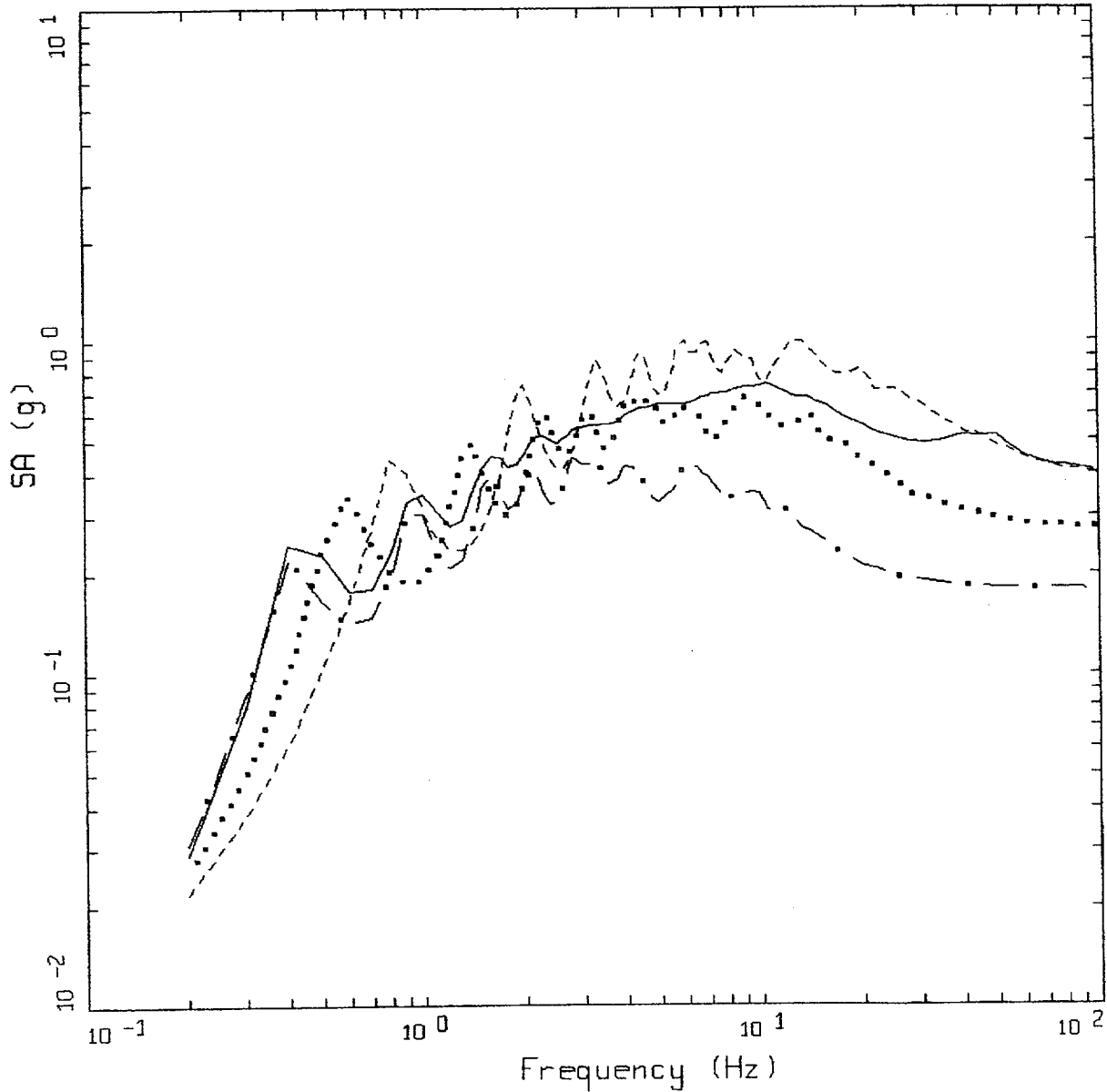
Figure 6-148. Comparison of soil spectra for Approach 2B with base case profile and deterministic profile variations (\pm factor of 2 on shear modulus); soil profile Meloland, CEUS conditions.



CEUS 10E-4 APPROACH COMPARISON, IV

- LEGEND
- APPROACH 2, 1 HZ AND 10 HZ DEAGGREGATION EQKS, MEAN PGA = 0.395 G
 - APPROACH 1, 10-4 ROCK CONTROL MOTION, BASE CASE, 84TH PERCENTILE, PGA = 0.416 G
 - APPROACH 1, 10-4 ROCK CONTROL MOTION, BASE CASE, MEAN, PGA = 0.301 G
 - APPROACH 1, 10-4 ROCK CONTROL MOTION, BASE CASE, 16TH PERCENTILE, PGA = 0.188 G

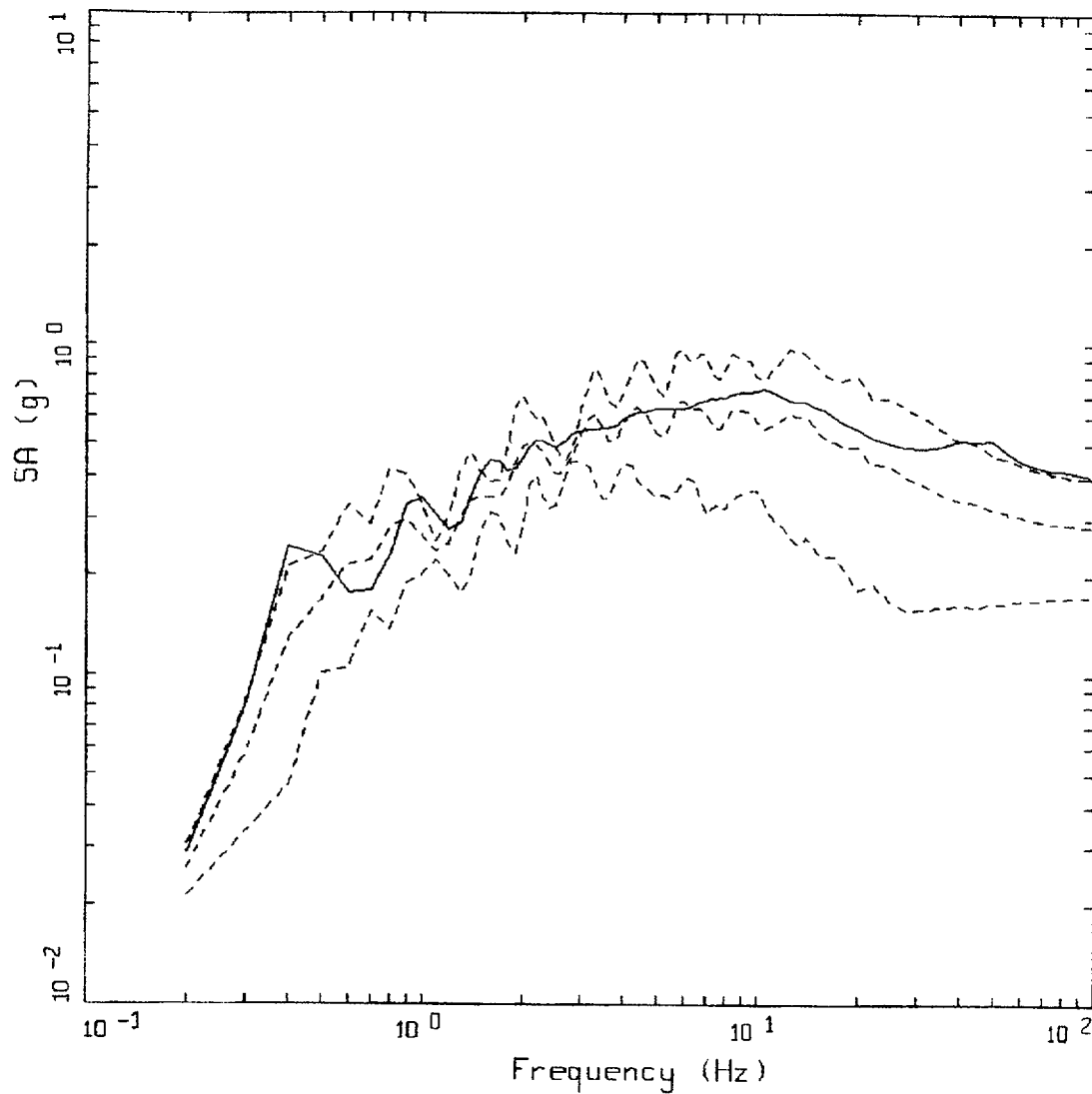
Figure 6-149. Comparison of soil spectra for Approach 2B with mean and $\pm 1\sigma$ variations of base case (\pm factor of 2 on shear modulus); soil profile Meloland, CEUS conditions.



CEUS 10E-4 APPROACH COMPARISON, IV
SOIL PROFILE TO 150 M (500 FT)

- LEGEND
- APPROACH 2, 1 HZ AND 10 HZ DEAGGREGATION EQKS, MEAN PGA = 0.395 G
 - APPROACH 1, 10-4 ROCK CONTROL MOTION, BASE CASE PGA = 0.275 G
 - APPROACH 1, 10-4 ROCK CONTROL MOTION, BASE CASE (UPPER) PGA = 0.400 G
 - . - . APPROACH 1, 10-4 ROCK CONTROL MOTION, BASE CASE (LOWER) PGA = 0.193 G

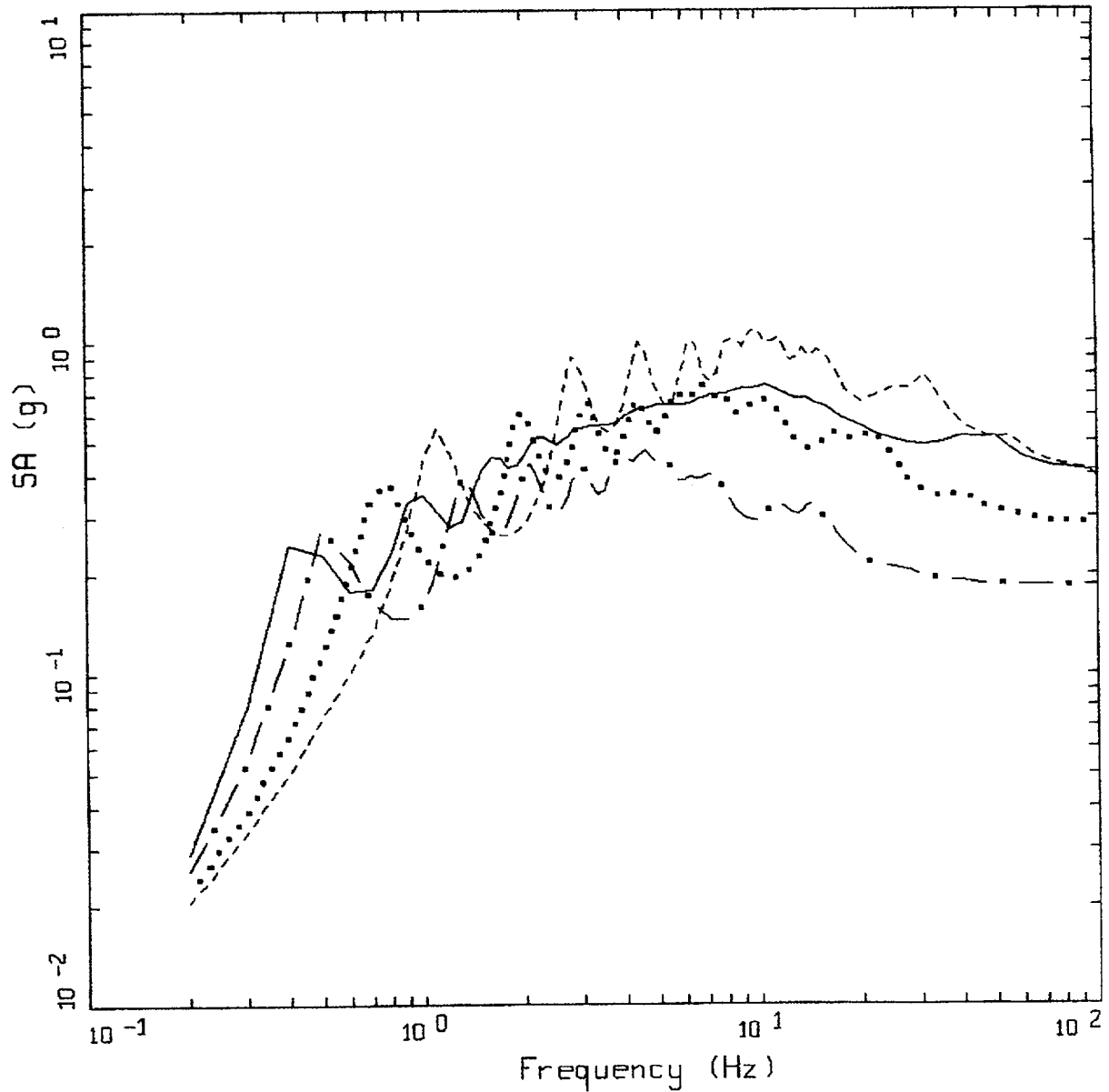
Figure 6-150. Comparison of soil spectra for Approach 2B (full profile) with base case profile and deterministic profile variations (\pm factor of 2 on shear modulus) with profile truncated at 150m; soil profile Meloland, CEUS conditions.



CEUS 1DE-4 APPROACH COMPARISON, IV
 SOIL PROFILE TO 150 M (500 FT)

- LEGEND
- APPROACH 2, 1 HZ AND 10 HZ DEAGGREGATION EQKS, MEAN PGA = 0.395 G
 - APPROACH 1, 10-4 ROCK CONTROL MOTION, BASE CASE, 84TH PERCENTILE, PGA = 0.395 G
 - APPROACH 1, 10-4 ROCK CONTROL MOTION, BASE CASE, MEAN, PGA = 0.285 G
 - APPROACH 1, 10-4 ROCK CONTROL MOTION, BASE CASE, 16TH PERCENTILE, PGA = 0.174 G

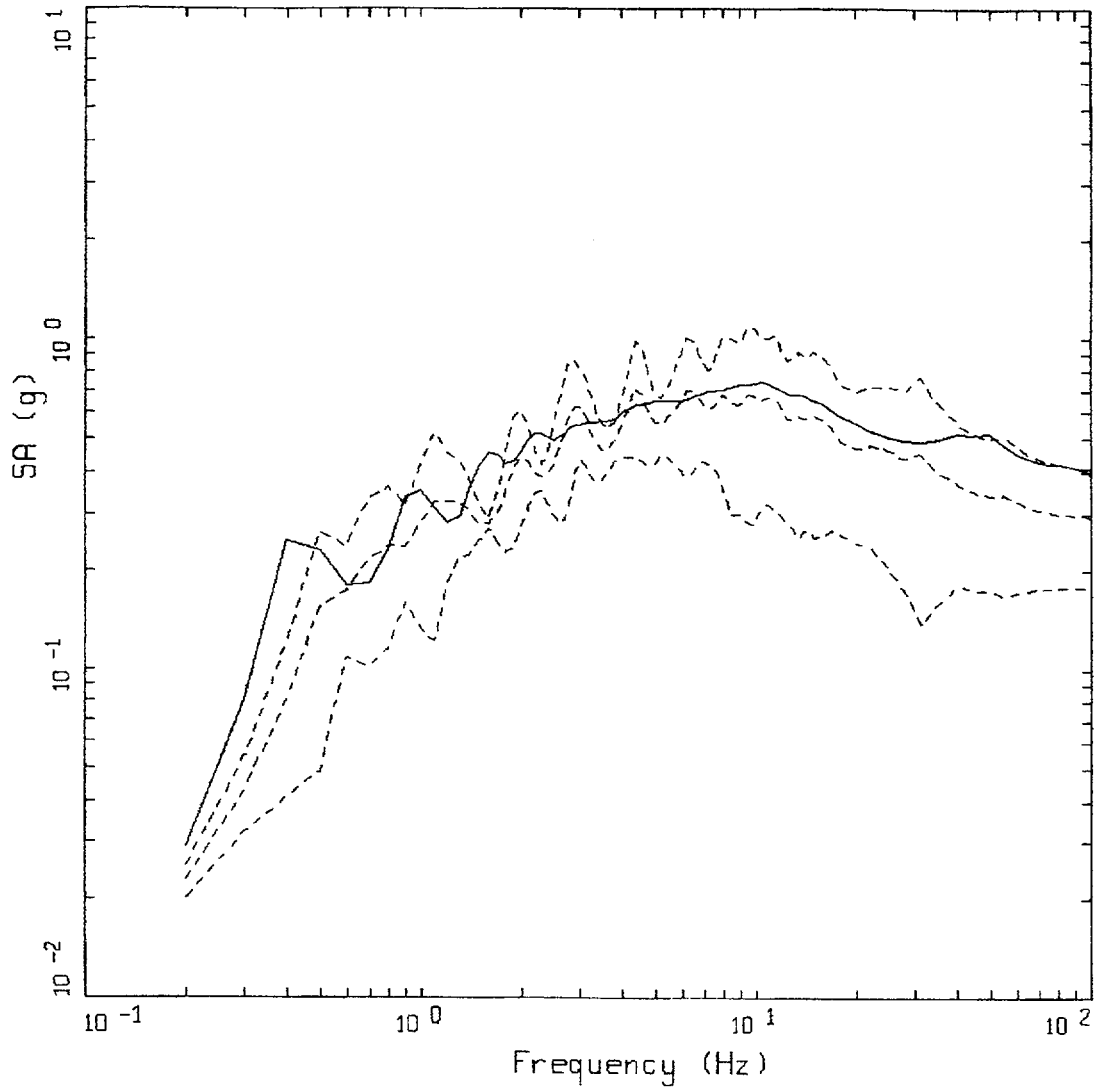
Figure 6-151. Comparison of soil spectra for Approach 2B (full profile) with mean and $\pm 1\sigma$ profile variations with profile truncated at 150m. Soil profile Meloland, CEUS conditions.



CEUS 10E-4 APPROACH COMPARISON, IV
SOIL PROFILE TO 90 M (300 FT)

- LEGEND
- APPROACH 2, 1 HZ AND 10 HZ DEAGGREGATION EQKS, MEAN PGA = 0.395 G
 - APPROACH 1, 10-4 ROCK CONTROL MOTION, BASE CASE PGA = 0.411 G
 - APPROACH 1, 10-4 ROCK CONTROL MOTION, BASE CASE (UPPER) PGA = 0.298 G
 - . - . - APPROACH 1, 10-4 ROCK CONTROL MOTION, BASE CASE (LOWER) PGA = 0.183 G

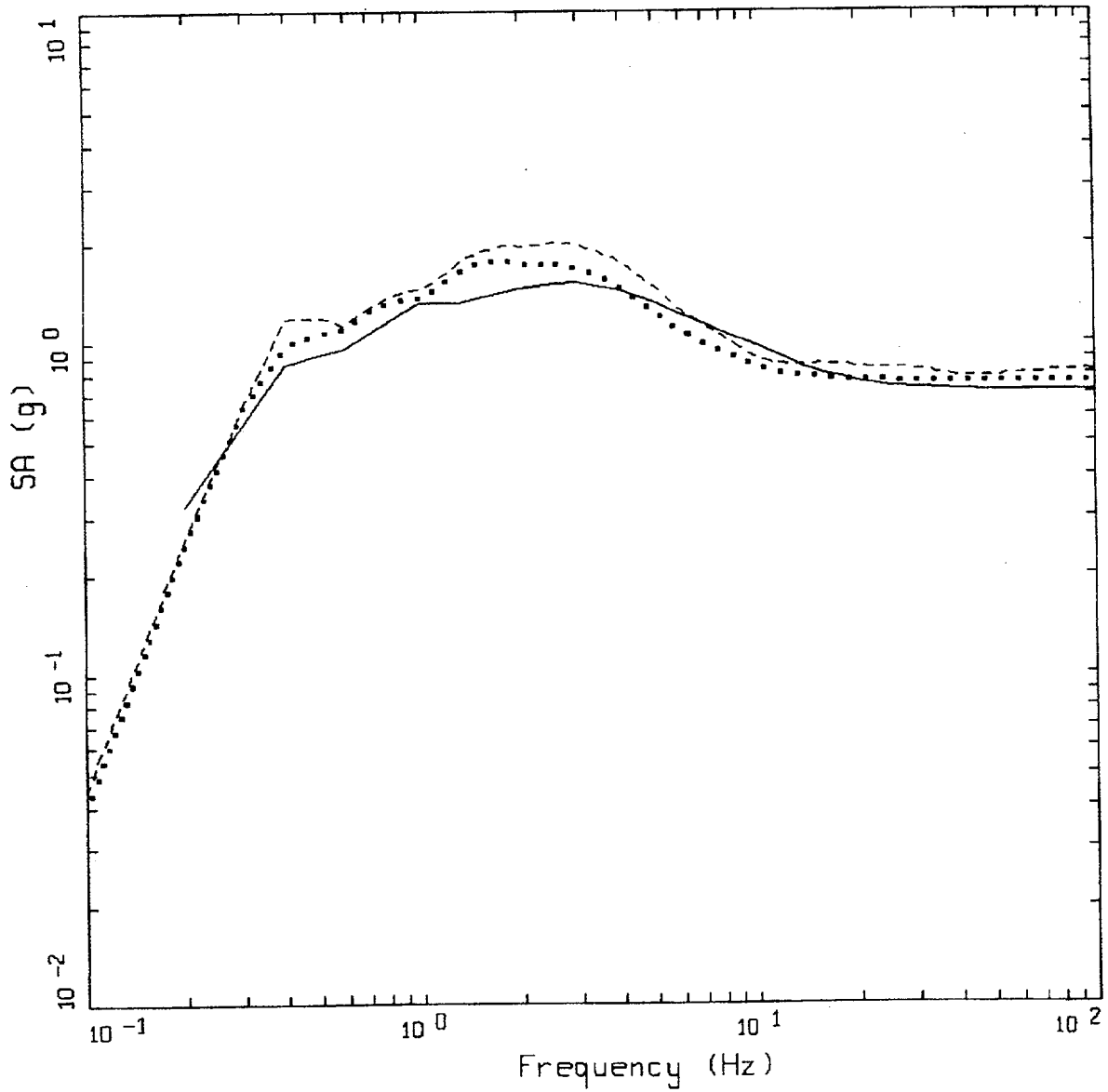
Figure 6-152. Comparison of soil spectra for Approach 2B (full profile) with base case profile and deterministic profile variations (\pm factor of 2 on shear modulus) with profile truncated at 90m; soil profile Meloland; CEUS conditions.



CEUS 10E-4 APPROACH COMPARISON, IV
 SOIL PROFILE TO 90 M (300 FT)

- LEGEND
- APPROACH 2, 1 HZ AND 10 HZ DEAGGREGATION EQKS, MEAN PGA = 0.395 G
 - APPROACH 1, 10-4 ROCK CONTROL MOTION, BASE CASE, 84TH PERCENTILE, PGA = 0.407 G
 - · - · - APPROACH 1, 10-4 ROCK CONTROL MOTION, BASE CASE, MEAN, PGA = 0.293 G
 - APPROACH 1, 10-4 ROCK CONTROL MOTION, BASE CASE, 16TH PERCENTILE, PGA = 0.179 G

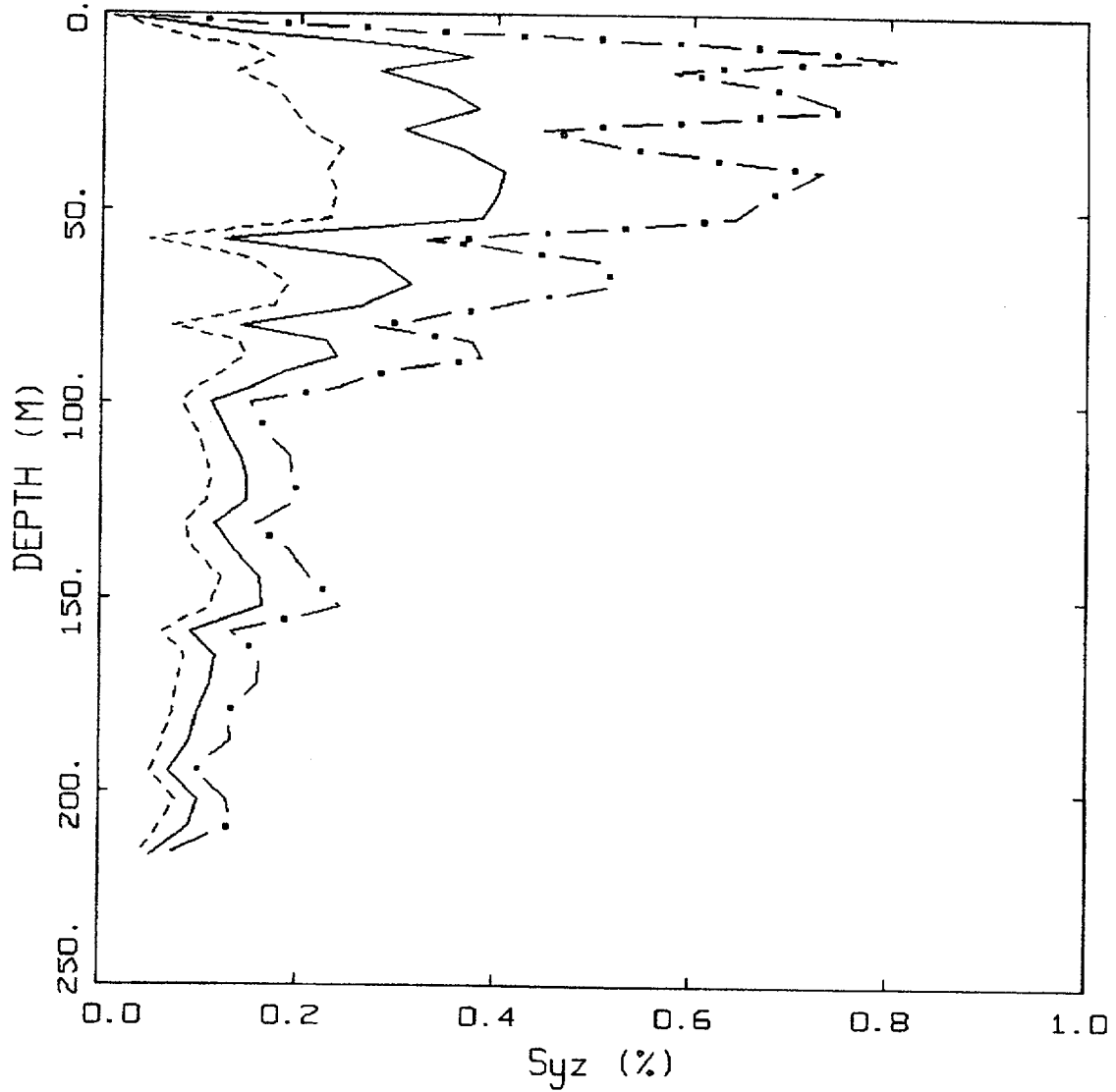
Figure 6-153. Comparison of soil spectra for Approach 2B (full profile) with mean and $\pm 1\sigma$ profile variations with profile truncated at 90m. Soil profile Meloland, CEUS conditions.



WUS 10E-4 APPROACH COMPARISON, IV

- LEGEND
- APPROACH 4, 10-4 SOIL UNIFORM HAZARD SPECTRUM, PGA = 0.704 G
 - APPROACH 1, 10-4 ROCK CONTROL MOTION, MEAN PGA = 0.755 G
 - - - - APPROACH 2, 1 HZ AND 10 HZ DEAGGREGATION EQKS, MEAN PGA = 0.817 G

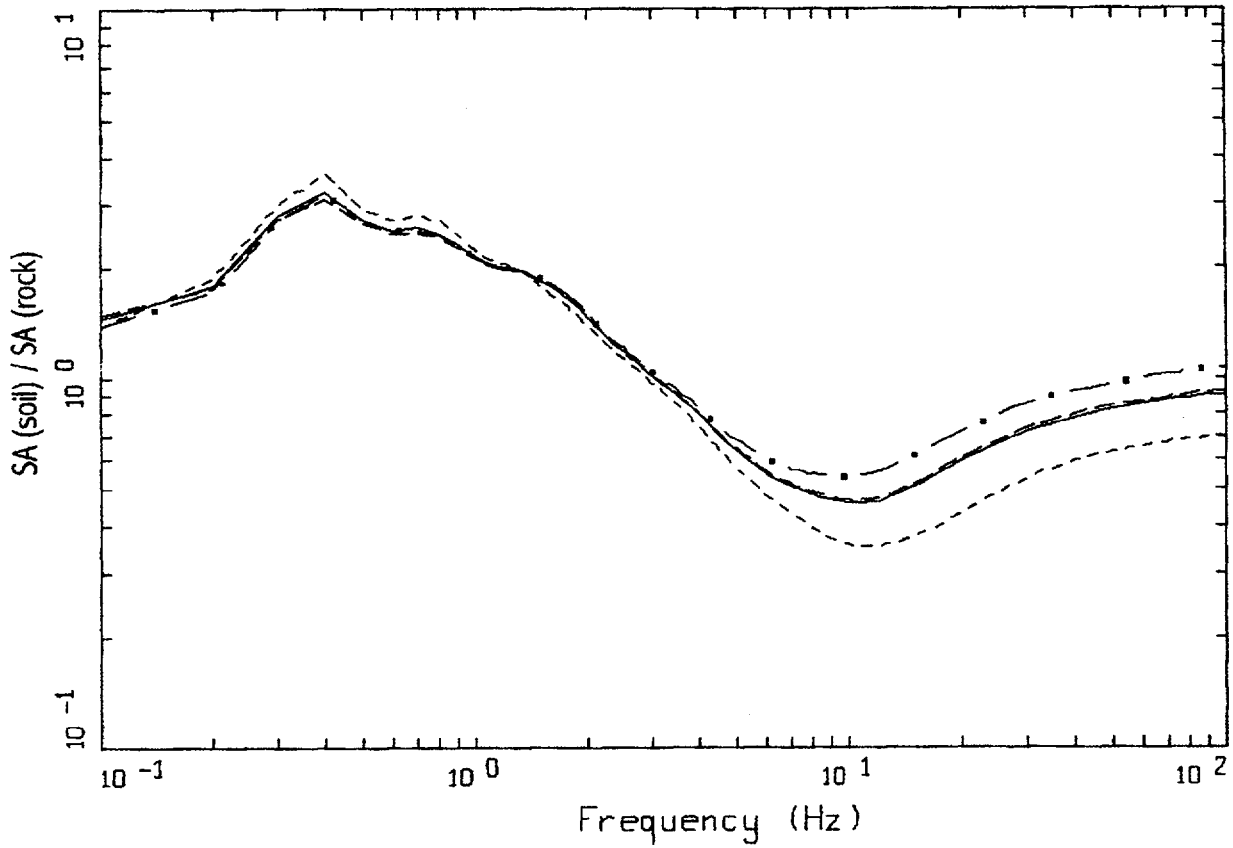
Figure 6-154. Comparison of Approaches 1, 2B, and 4 soil spectra for profile Meloland: WUS conditions.



WUS, 10-4, IV
EFFECTIVE STRAINS (SYZ)

LEGEND
 - . - 84TH PERCENTILE
 — 50TH PERCENTILE
 - - - 16TH PERCENTILE

Figure 6-155. Median and $\pm 1\sigma$ effective strains for soil profile Meloland using Approach 1 WUS conditions.

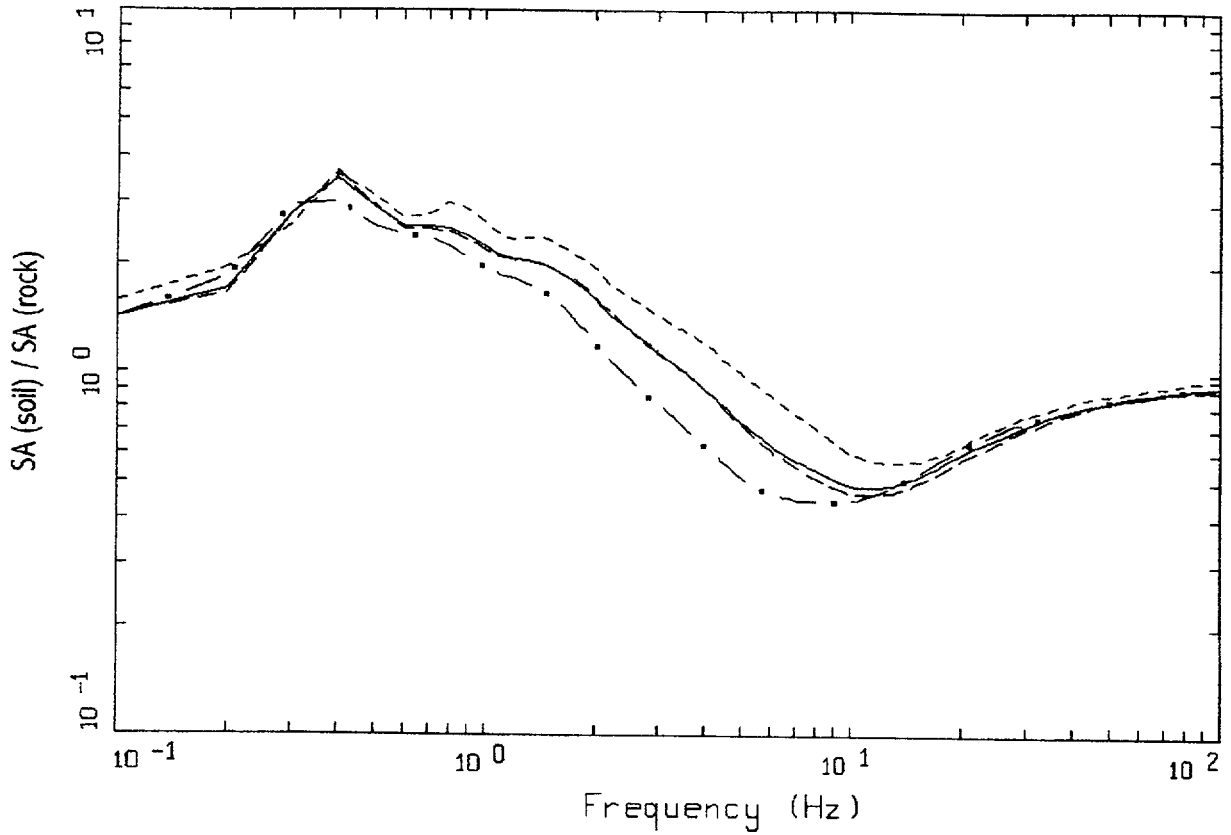


WUS, 10E-4, 1HZ DESIGN, IV PROFILE
 SURFACE MOTION, 1HZ TRANSFER FUNCTION
 WEIGHTS: ML=0.20, MM=0.60, MH=0.20

LEGEND

- ML = 5.4, D = 10 KM MEAN RATIO
- . - . - MM = 6.7, D = 18 KM, DESIGN MEAN RATIO
- • — MH = 7.8, D = 30 KM MEAN RATIO
- WEIGHTED MEAN RATIO

Figure 6-156. Comparison of transfer functions computed for the scaled 1 Hz design earthquake; soil profile Meloland, WUS conditions.

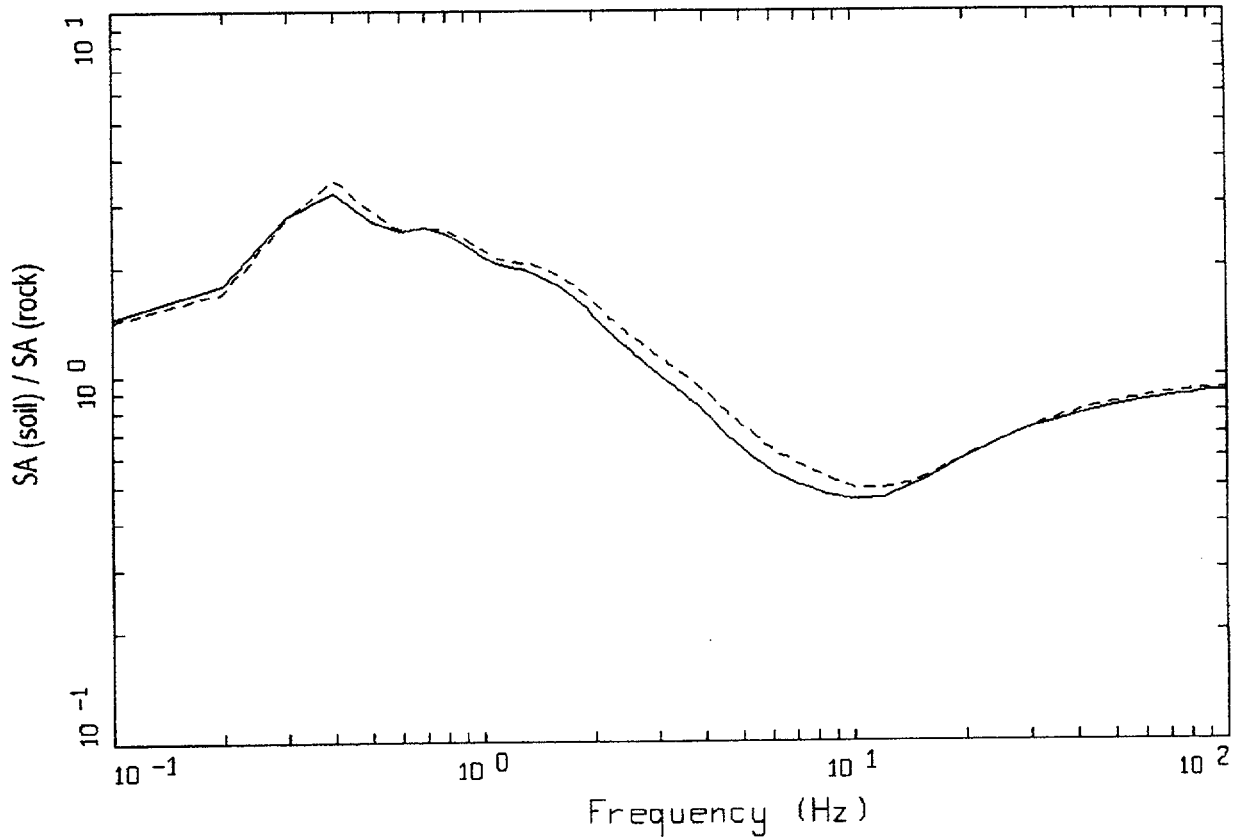


WUS, 10E-4, 10HZ DESIGN, IV PROFILE
 SURFACE MOTION, 10HZ TRANSFER FUNCTION
 WEIGHTS: ML=0.20, MM=0.60, MH=0.20

LEGEND

- ML = 5.1, D = 10 KM MEAN RATIO
- · - · - MM = 6.1, D = 14 KM, DESIGN MEAN RATIO
- · — MH = 7.8, D = 30 KM MEAN RATIO
- WEIGHTED MEAN RATIO

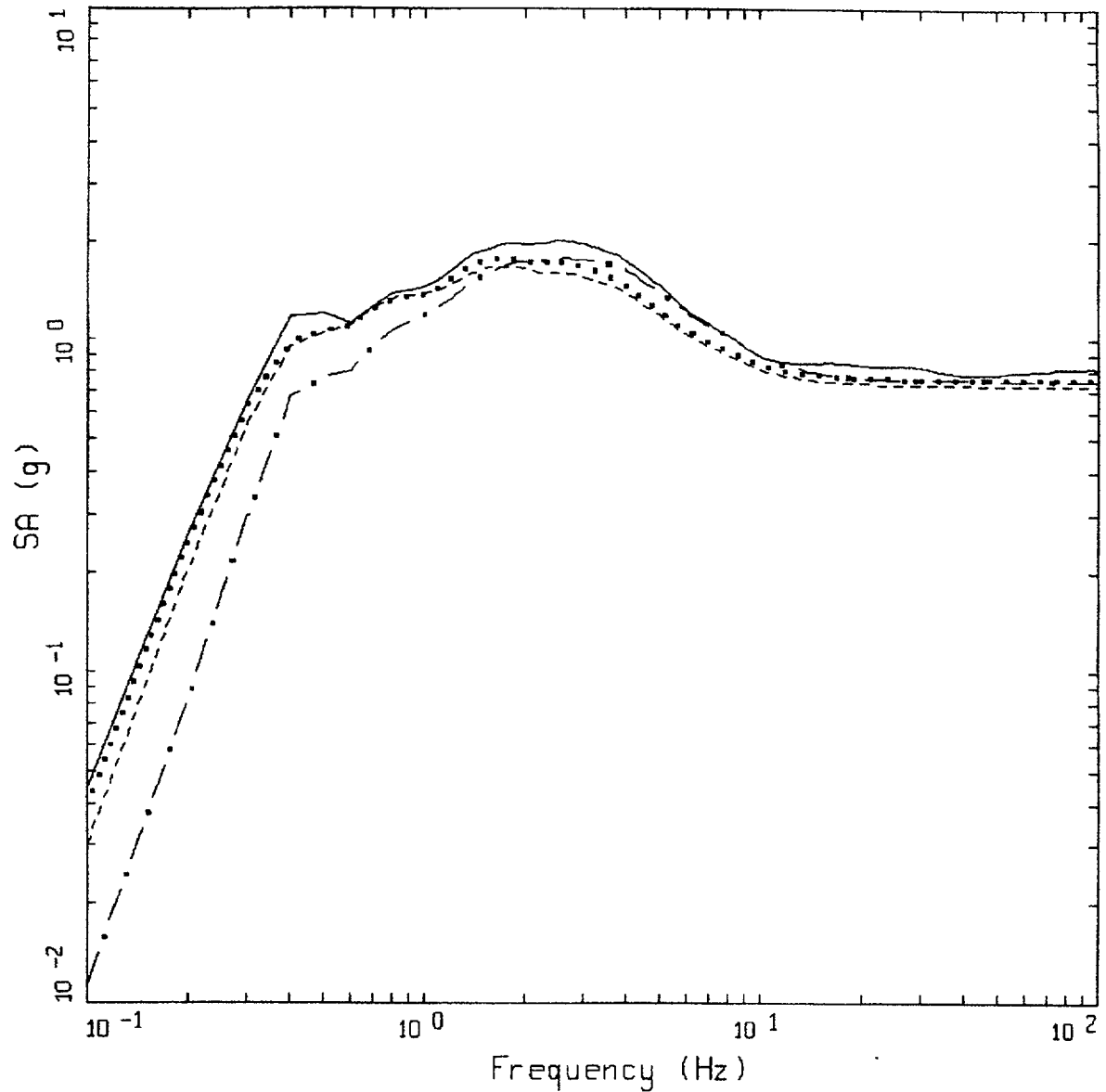
Figure 6-157. Comparison of transfer functions computed for the scaled 10 Hz design earthquake; soil profile Meloland, WUS conditions.



WUS, 10E-4, IV PROFILE
AMPLIFICATION

LEGEND
 ——— 1 HZ WEIGHTED MEAN RATIO; WEIGHTS:ML=0.20,MM=0.60,MH=0.20
 - - - - 10 HZ WEIGHTED MEAN RATIO; WEIGHTS:ML=0.20,MM=0.60,MH=0.20

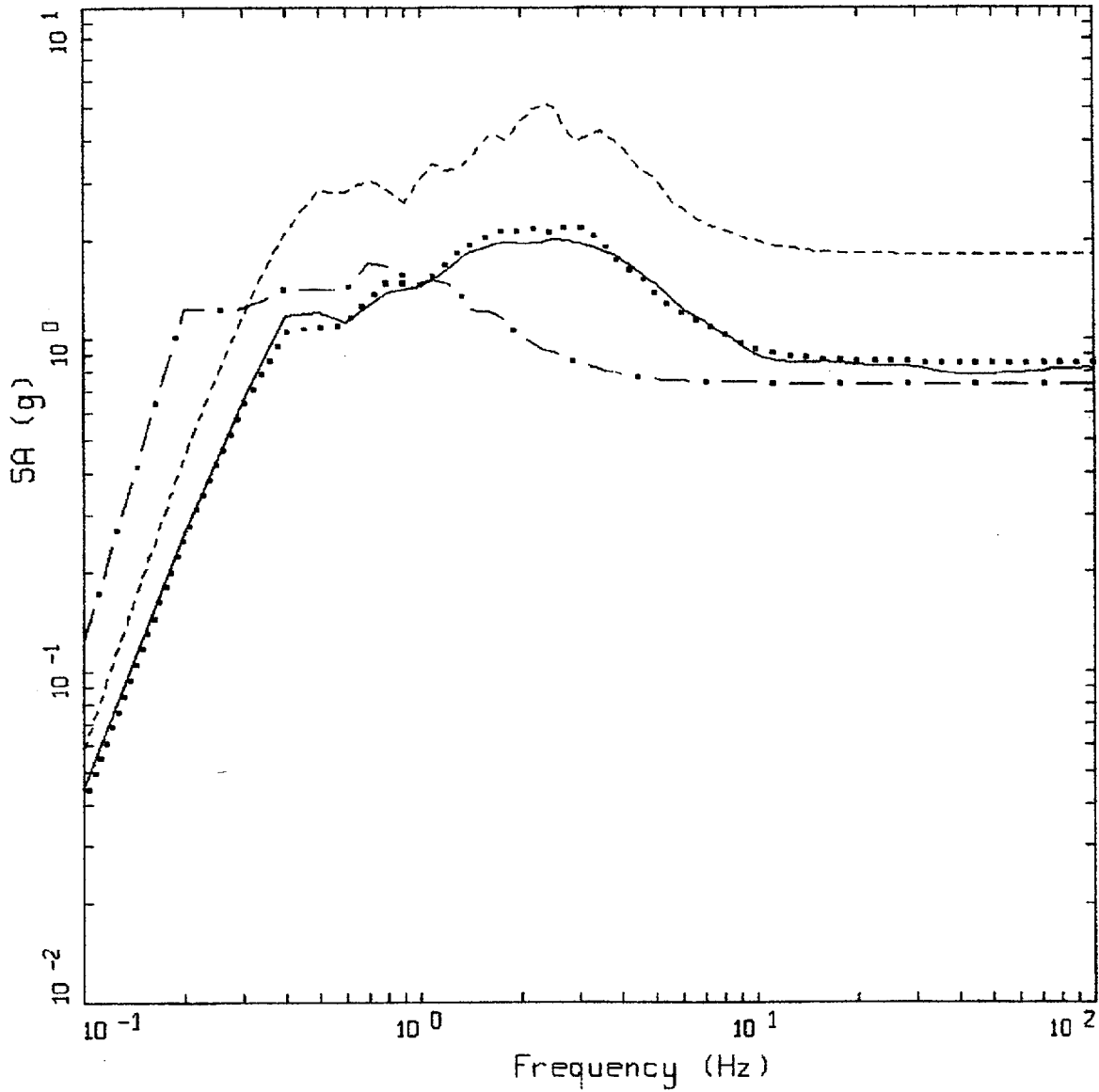
Figure 6-158. Comparison of mean transfer functions computed for the scaled 1 Hz and 10 Hz design earthquakes; soil profile Meloland, WUS conditions.



WUS, 10E-4 DESIGN SPECTRA, IV

- LEGEND
- APPROACH 2, 1 HZ AND 10 HZ DEAGGREGATION EQKS, MEAN PGA = 0.563 G
 - APPROACH 1, 10-4 ROCK CONTROL MOTION, MEAN PGA = 0.755 G
 - 1 HZ MEAN; PGA = 0.727 G
 - . - . 10 HZ MEAN; PGA = 0.752 G

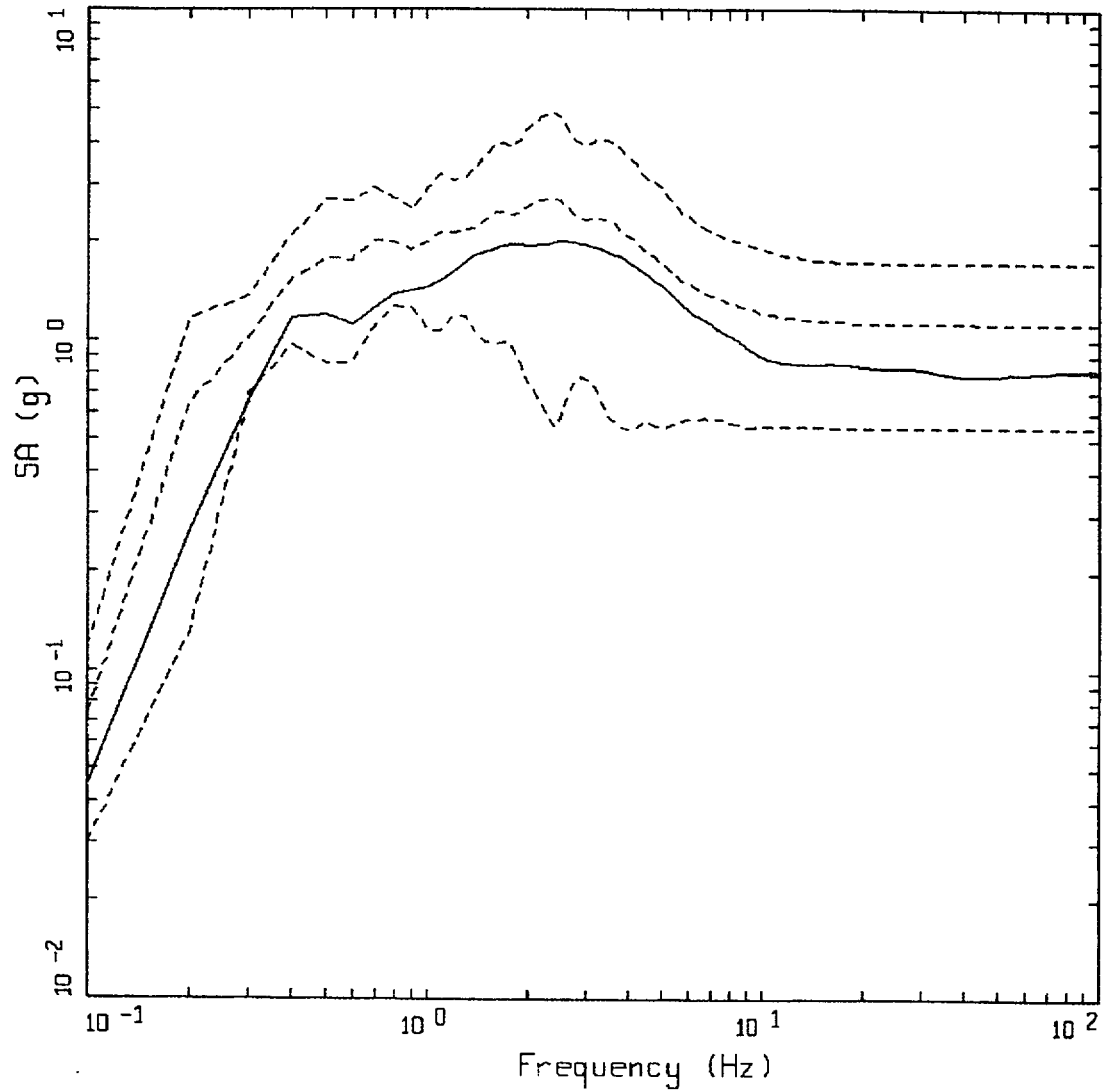
Figure 6-159. Comparison of soil spectra for Approaches 1, 2A, and 2B; soil profile Meloland, WUS conditions.



WUS 10E-4 APPROACH COMPARISON, IV

- LEGEND
- APPROACH 2, 1 HZ AND 10 HZ DEAGGREGATION EQKS, MEAN PGA = 0.817 G
 - APPROACH 1, 10-4 ROCK CONTROL MOTION, BASE CASE PGA = 0.851 G
 - APPROACH 1, 10-4 ROCK CONTROL MOTION, BASE CASE (UPPER) PGA = 2.804 G
 - . - . - . APPROACH 1, 10-4 ROCK CONTROL MOTION, BASE CASE (LOWER) PGA = 0.733 G

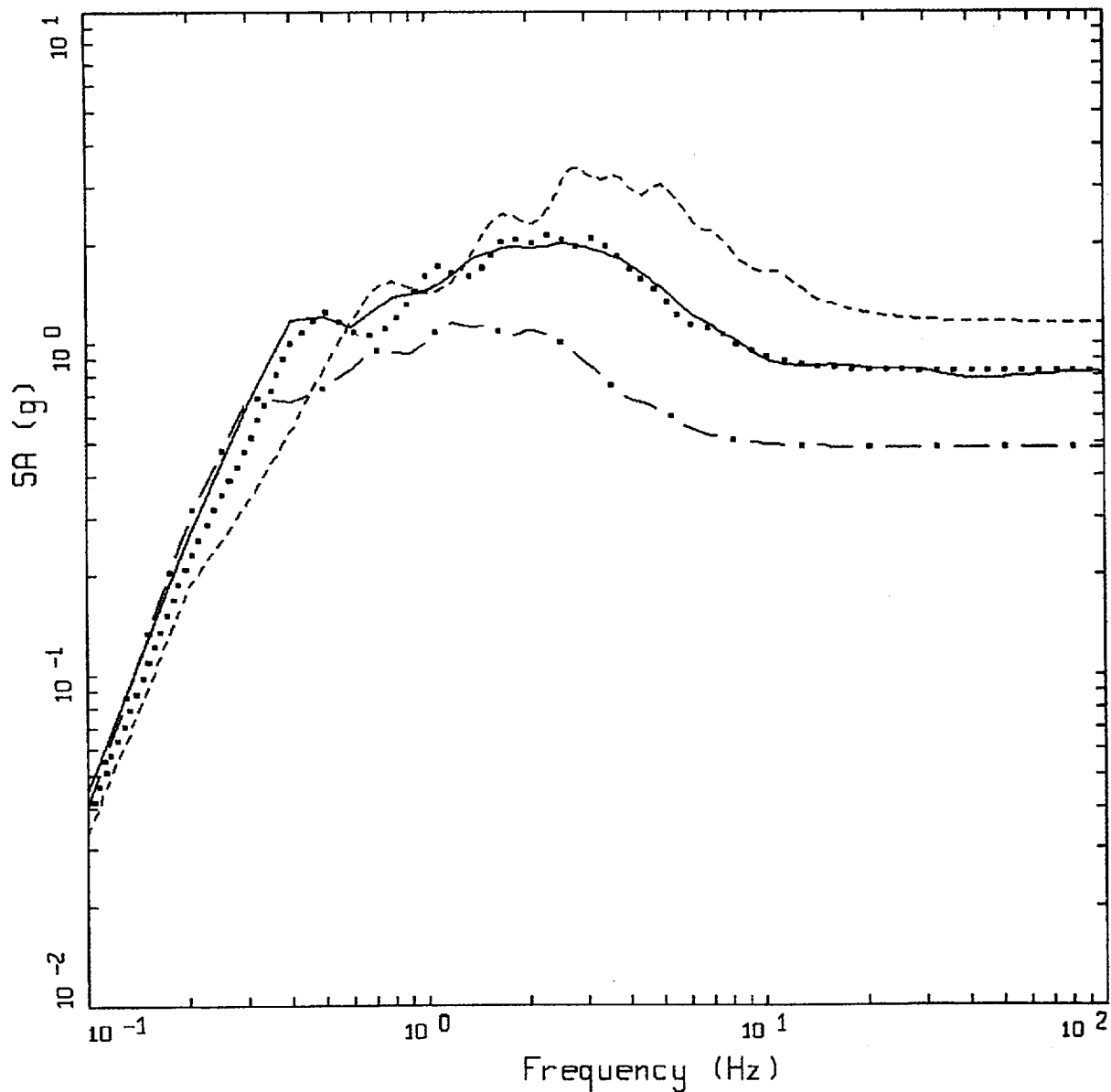
Figure 6-160. Comparison of soil spectra for Approach 2B with base case profile and deterministic profile variations (\pm factor of 2 on shear modulus); soil profile Meloland, WUS conditions.



WUS 10E-4 APPROACH COMPARISON, IV

- LEGEND
- APPROACH 2, 1 HZ AND 10 HZ DEAGGREGATION EQKS, MEAN PGA = 0.817 G
 - - - - APPROACH 1, 10-4 ROCK CONTROL MOTION, BASE CASE, 84TH PERCENTILE, PGA = 1.708 G
 - - - - APPROACH 1, 10-4 ROCK CONTROL MOTION, BASE CASE, MEAN, PGA = 1.126 G
 - - - - APPROACH 1, 10-4 ROCK CONTROL MOTION, BASE CASE, 16TH PERCENTILE, PGA = 0.544 G

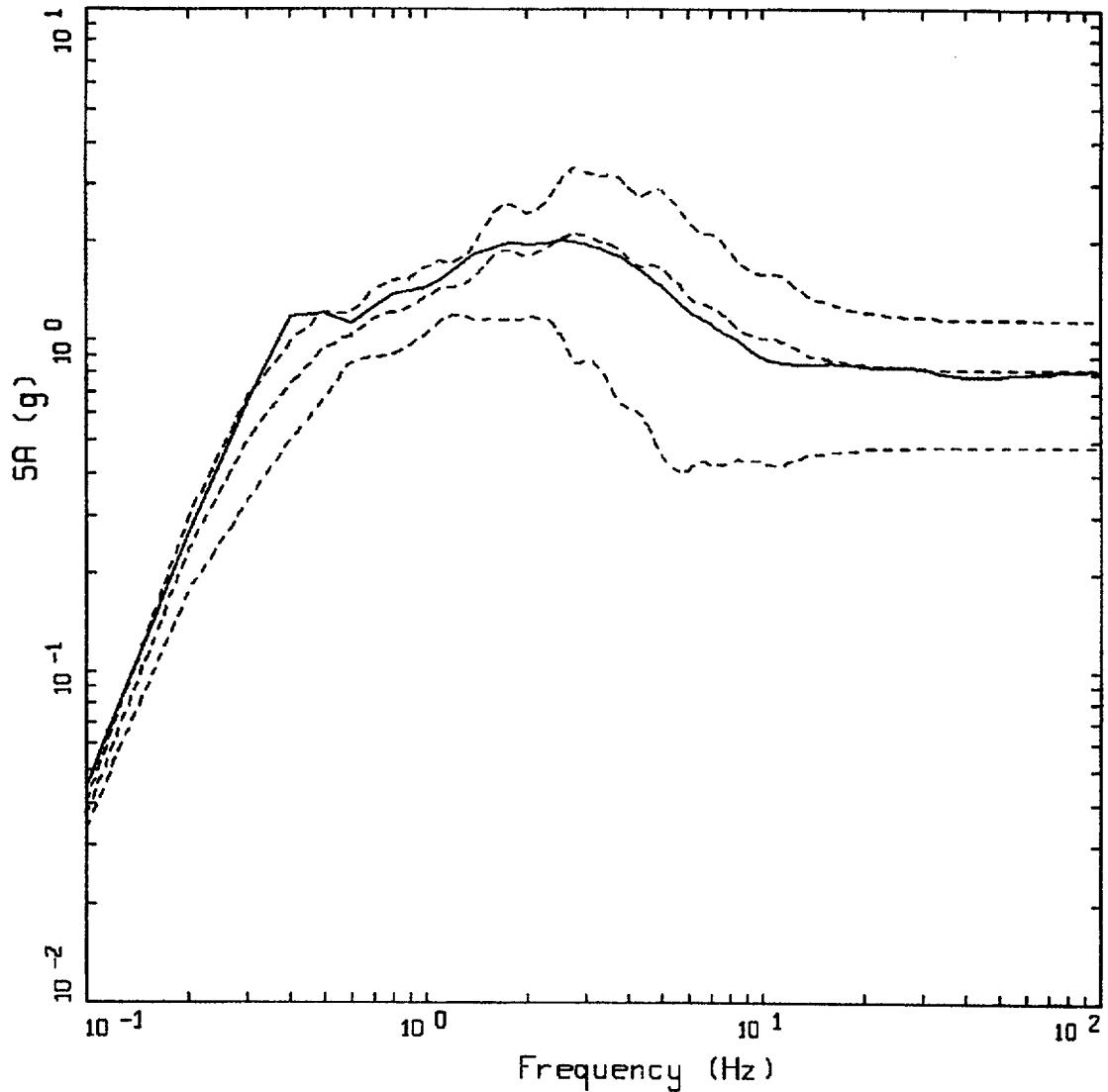
Figure 6-161. Comparison of soil spectra for Approach 2B with mean and $\pm 1\sigma$ variations of base case (\pm factor of 2 on shear modulus), soil profile Meloland, WUS conditions.



WUS 10E-4 APPROACH COMPARISON, IV
 SOIL PROFILE TO 150 M (500 FT)

- LEGEND
- APPROACH 2, 1 HZ AND 10 HZ DEAGGREGATION EQKS, MEAN PGA = 0.817 G
 - APPROACH 1, 10-4 ROCK CONTROL MOTION, BASE CASE PGA = 0.708 G
 - - - - APPROACH 1, 10-4 ROCK CONTROL MOTION, BASE CASE (UPPER) PGA = 1.150 G
 - . - . APPROACH 1, 10-4 ROCK CONTROL MOTION, BASE CASE (LOWER) PGA = 0.733 G

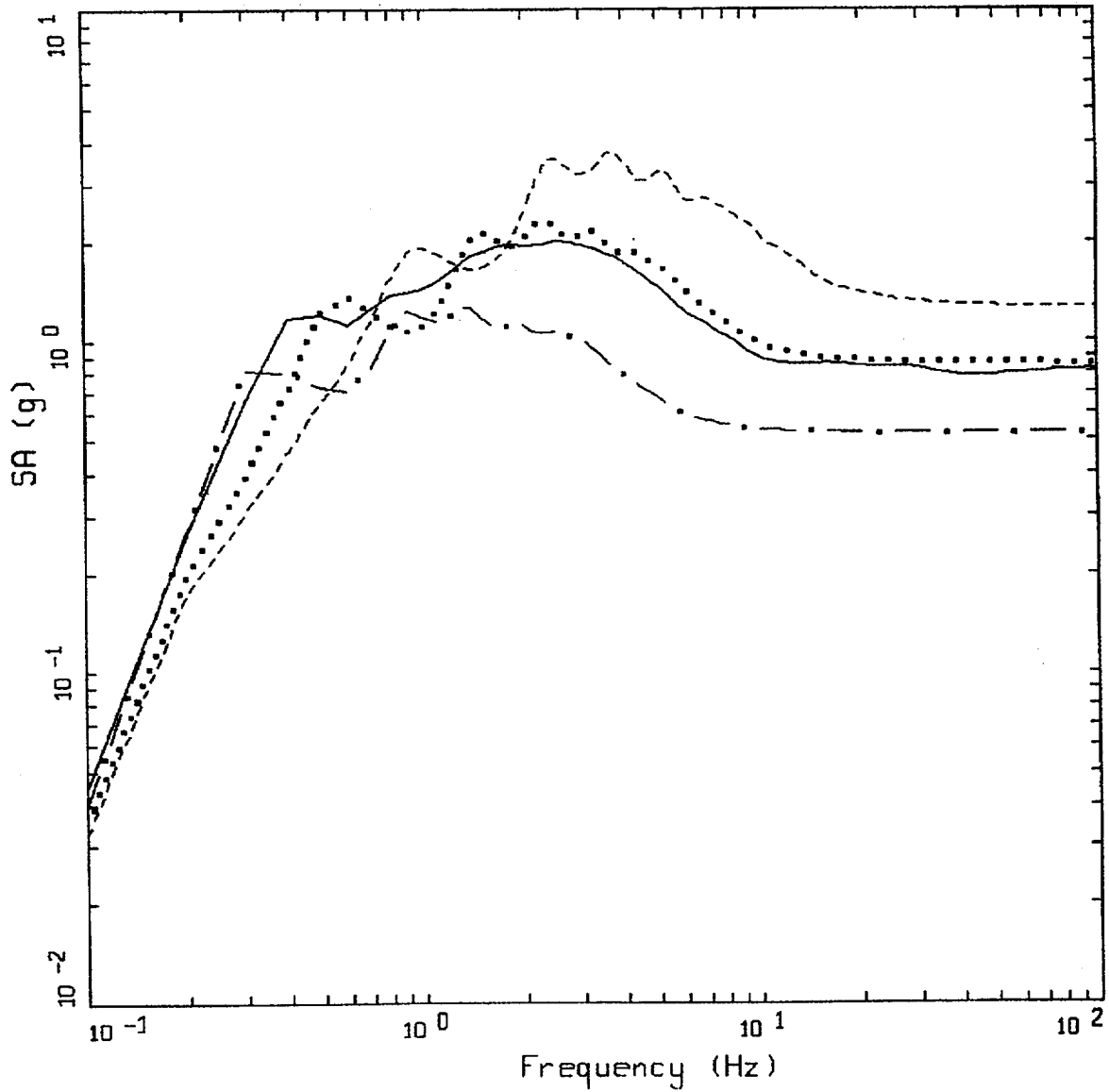
Figure 6-162. Comparison of soil spectra for Approach 2B (full profile) with base case profile and deterministic profile variations (\pm factor of 2 on shear modulus) with profile truncated at 150m; soil profile Meloland, WUS conditions.



WUS 10E-4 APPROACH COMPARISON, IV
 SOIL PROFILE TO 150 M (500 FT)

- LEGEND
- APPROACH 2, 1 HZ AND 10 HZ DEAGGREGATION EQS, MEAN PGA = 0.817 G
 - - - APPROACH 1, 10-4 ROCK CONTROL MOTION, BASE CASE, 84TH PERCENTILE, PGA = 1.152 G
 - - - APPROACH 1, 10-4 ROCK CONTROL MOTION, BASE CASE, MEAN, PGA = 0.818 G
 - - - APPROACH 1, 10-4 ROCK CONTROL MOTION, BASE CASE, 16TH PERCENTILE, PGA = 0.483 G

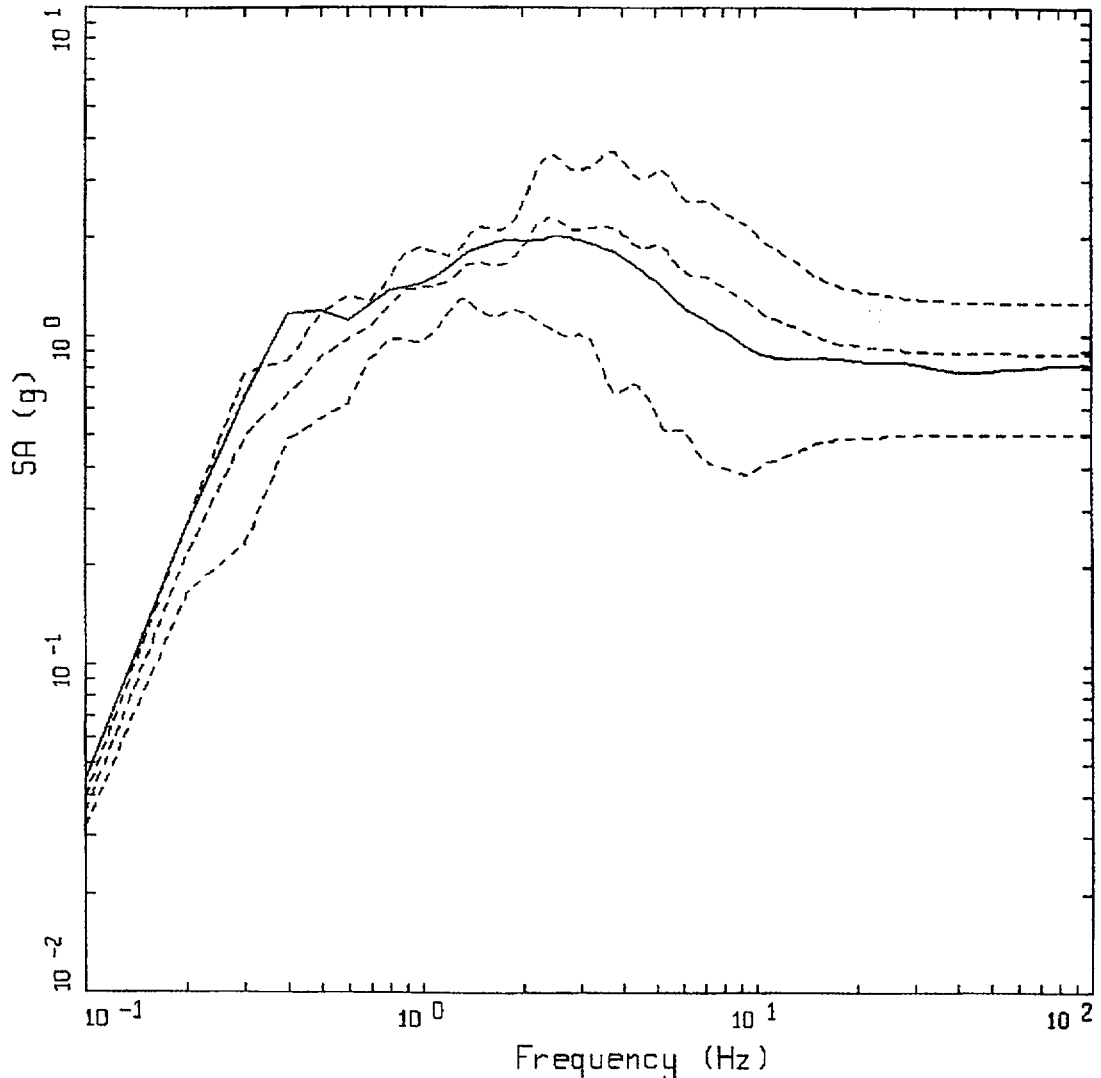
Figure 6-163. Comparison of soil spectra for Approach 2B (full profile) with mean and $\pm 1\sigma$ deterministic profile variations with profile truncated at 150m. Soil profile Meloland, WUS conditions.



WUS 10E-4 APPROACH COMPARISON, IV
 SOIL PROFILE TO 90 M (300 FT)

- LEGEND
- APPROACH 2, 1 HZ AND 10 HZ DEAGGREGATION EQKS, MEAN PGA = 0.817 G
 - APPROACH 1, 10-4 ROCK CONTROL MOTION, BASE CASE PGA = 0.855 G
 - APPROACH 1, 10-4 ROCK CONTROL MOTION, BASE CASE (UPPER) PGA = 1.150 G
 - . - - APPROACH 1, 10-4 ROCK CONTROL MOTION, BASE CASE (LOWER) PGA = 0.733 G

Figure 6-164. Comparison of soil spectra for Approach 2B (full profile) with base case profile and deterministic profile variations (\pm factor of 2 on shear modulus) with profile truncated at 90m; soil profile Meloland, WUS conditions.



WUS 10E-4 APPROACH COMPARISON, IV
 SOIL PROFILE TO 90 M (300 FT)

- LEGEND
- APPROACH 2, 1 HZ AND 10 HZ DEAGGREGATION EQKS, MEAN PGA = 0.817 G
 - APPROACH 1, 10-4 ROCK CONTROL MOTION, BASE CASE, 84TH PERCENTILE, PGA = 1.259 G
 - · - · - APPROACH 1, 10-4 ROCK CONTROL MOTION, BASE CASE, MEAN, PGA = 0.884 G
 - APPROACH 1, 10-4 ROCK CONTROL MOTION, BASE CASE, 16TH PERCENTILE, PGA = 0.508 G

Figure 6-165. Comparison of soil spectra for Approach 2B (full profile) with mean and $\pm 1\sigma$ profile variations with profile truncated at 90m. Soil profile Meloland, WUS conditions.

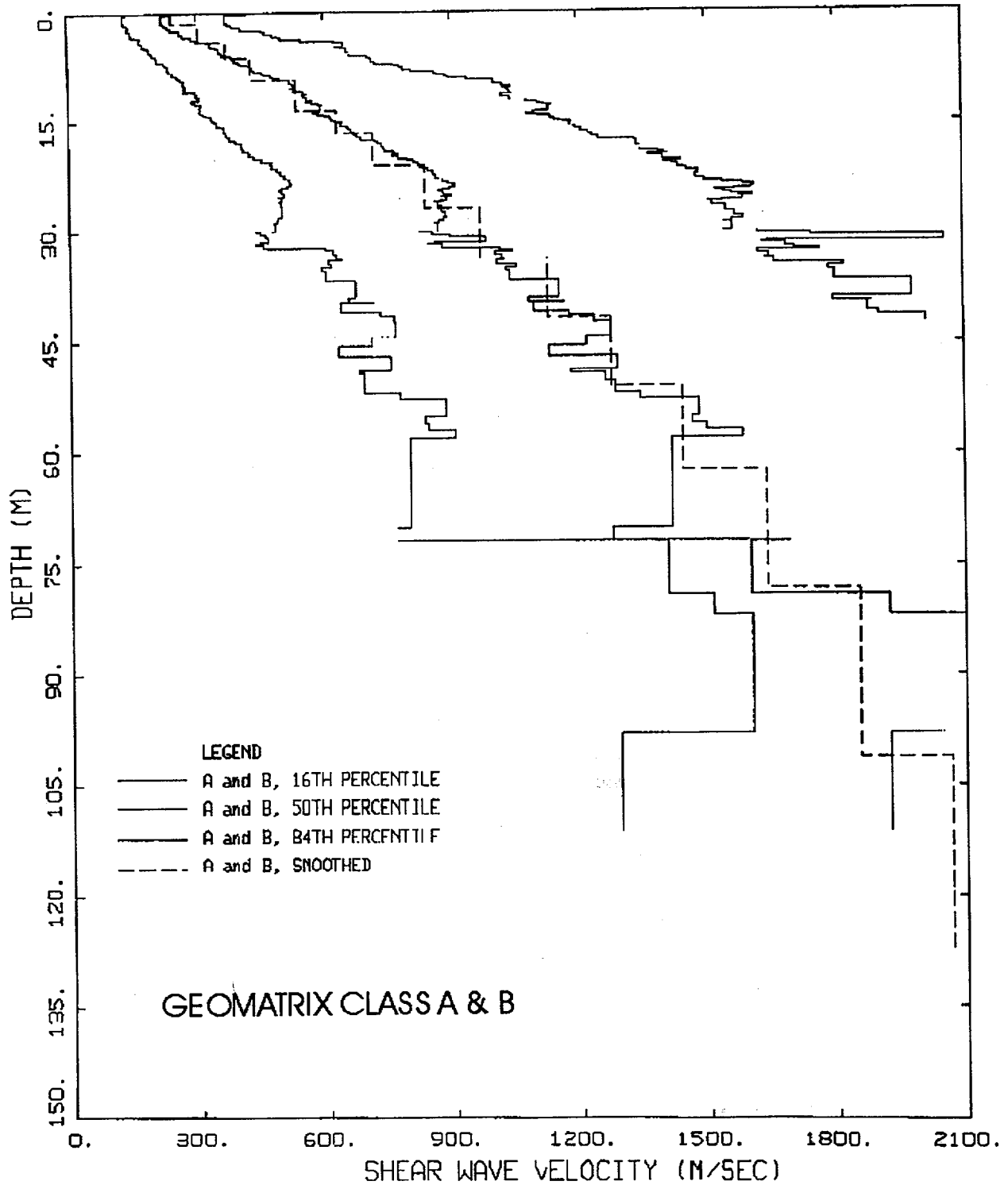
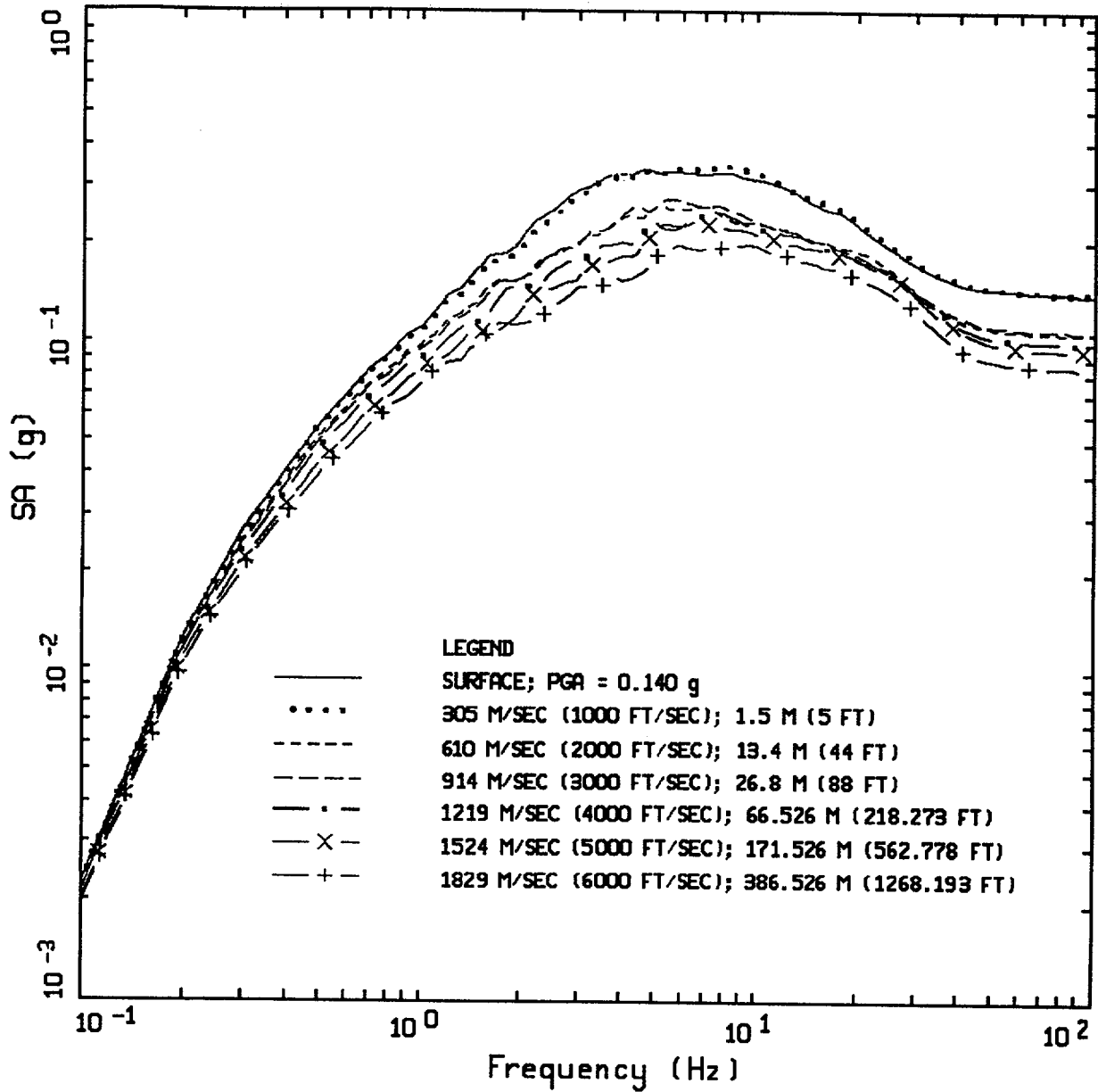
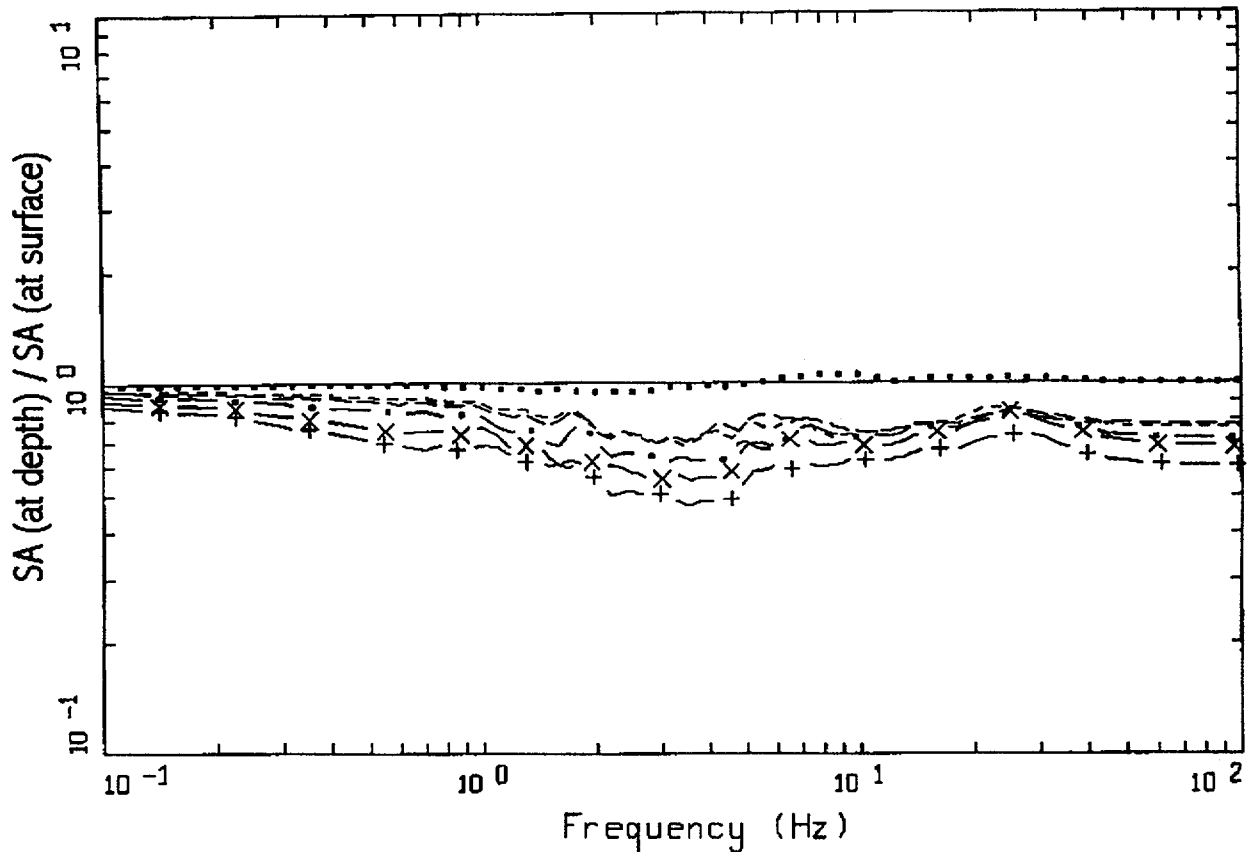


Figure 6-166. Median and $\pm 1\sigma$ shear-wave velocities based on measurements at WUS rock strong motion sites. Geomatrix categories A and B (Appendix A) assumed to reflect rock site conditions. Dashed line is smooth model used in analyses.



NRC, AVERAGE HORIZONTAL SPECTRA
M=6.5, D=25 KM, STRESS DROP = 55 BARS

Figure 6-167. Median WUS rock response spectra (5% damping) computed for $M = 6.5$ at a distance of 25 km using the soft rock profile (Figure 6-166) and the point source model (Appendix D). Suite of depths (shear-wave velocities) reflect depth to which overlying materials are removed.

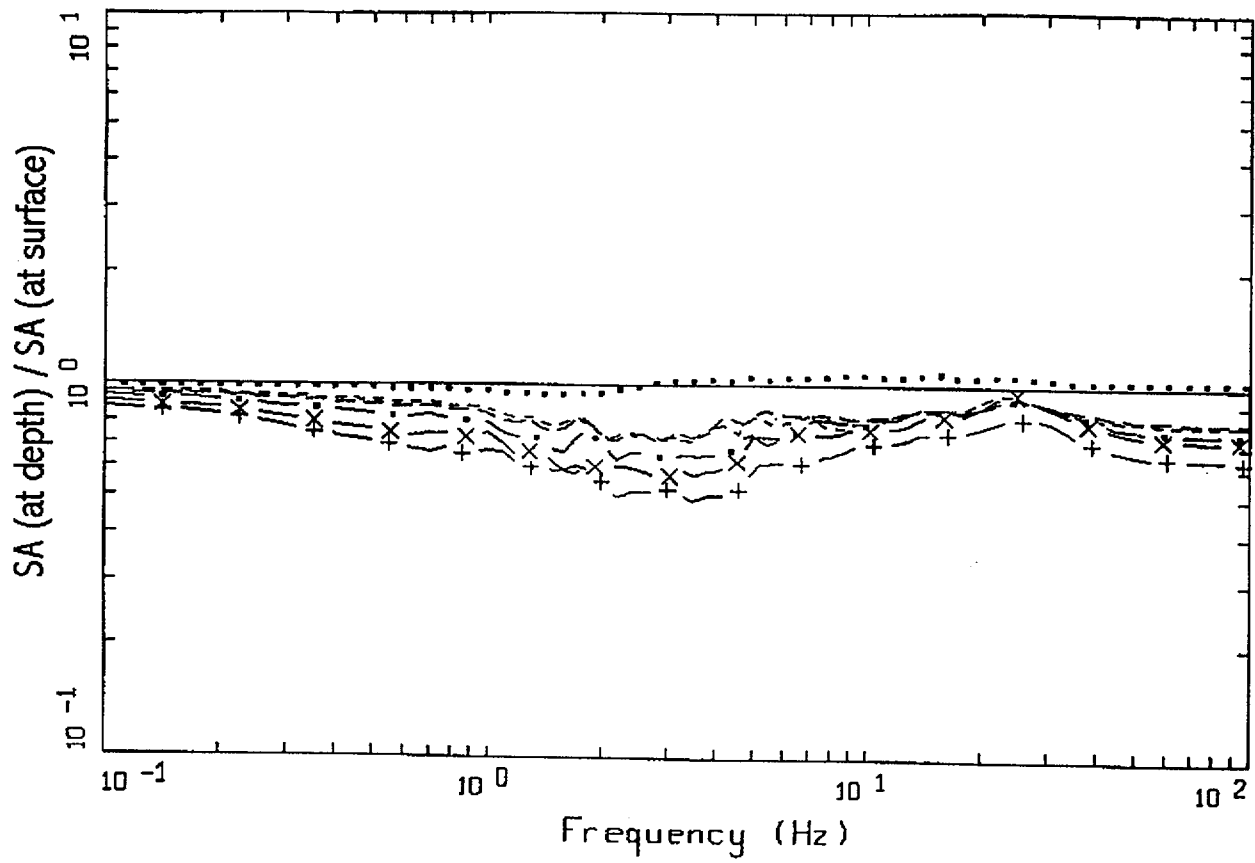


NRC, M=6.5, D=25 KM

LEGEND

- SURFACE RATIO OVER SURFACE; 0 M; PGA = 0.140 g
- 305 M/SEC (1000 FT/SEC) RATIO OVER SURFACE; 1.5 M (5 FT)
- 610 M/SEC (2000 FT/SEC) RATIO OVER SURFACE; 13.4 M (44 FT)
- 914 M/SEC (3000 FT/SEC) RATIO OVER SURFACE; 26.8 M (88 FT)
- . - 1219 M/SEC (4000 FT/SEC) RATIO OVER SURFACE; 66.526 M (218.273 FT)
- X - 1524 M/SEC (5000 FT/SEC) RATIO OVER SURFACE; 171.526 M (562.778 FT)
- + - 1829 M/SEC (6000 FT/SEC) RATIO OVER SURFACE; 386.526 M (1268.193 FT)

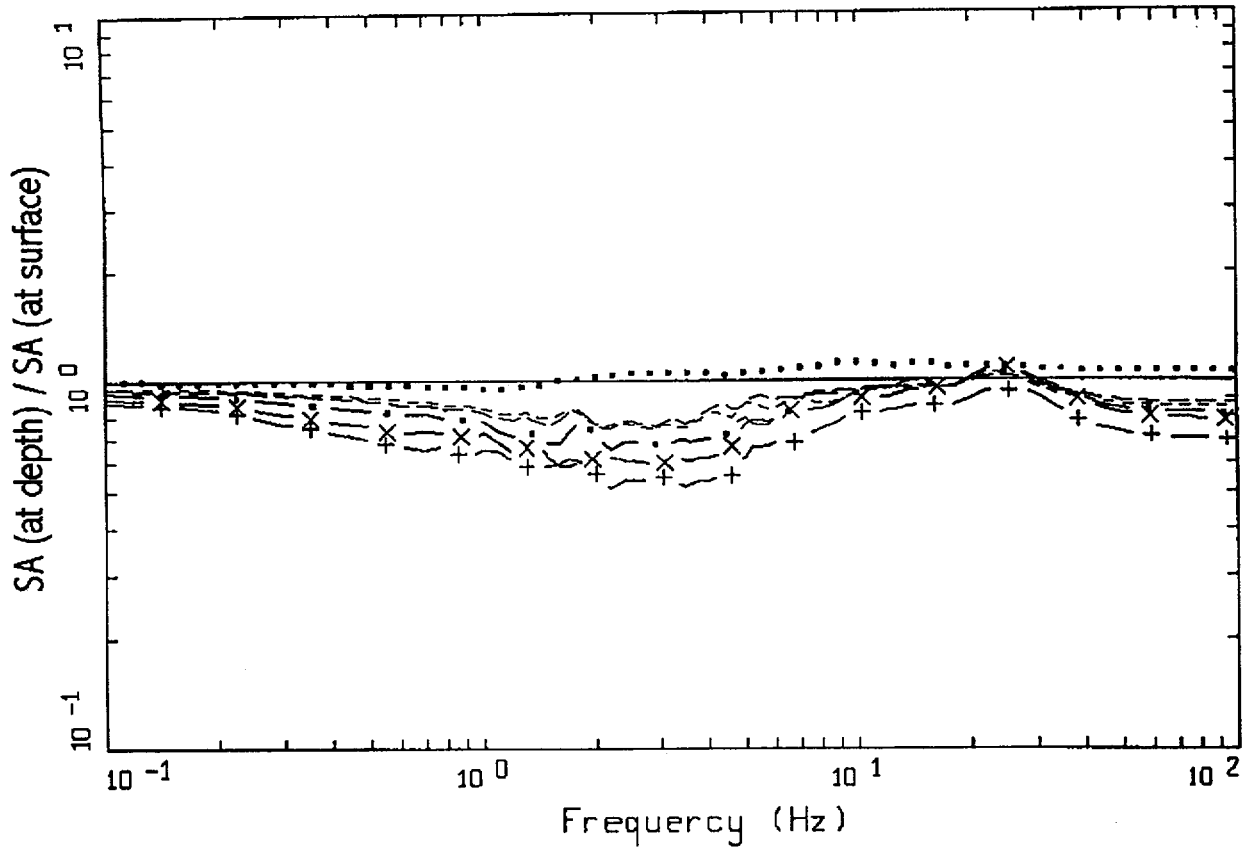
Figure 6-168. Depth-to-surface response spectral ratios (median estimates) computed for the suite of spectra shown on Figure 6-167.



NRC, M=6.5, D=10 KM

- LEGEND
- SURFACE RATIO OVER SURFACE; 0 FT; PGA = 0.306 g
 - 305 M/SEC (1000 FT/SEC) RATIO OVER SURFACE; 1.5 M (5 FT)
 - 610 M/SEC (2000 FT/SEC) RATIO OVER SURFACE; 13.4 M (44 FT)
 - 914 M/SEC (3000 FT/SEC) RATIO OVER SURFACE; 26.8 M (88 FT)
 - · - 1219 M/SEC (4000 FT/SEC) RATIO OVER SURFACE; 66.526 M (218.273 FT)
 - X - 1524 M/SEC (5000 FT/SEC) RATIO OVER SURFACE; 171.526 M (562.778 FT)
 - + - 1829 M/SEC (6000 FT/SEC) RATIO OVER SURFACE; 386.526 M (1268.193 FT)

Figure 6-169. Depth-to-surface response spectral ratios (median estimates) computed for M=6.5 at a distance of 10 km.

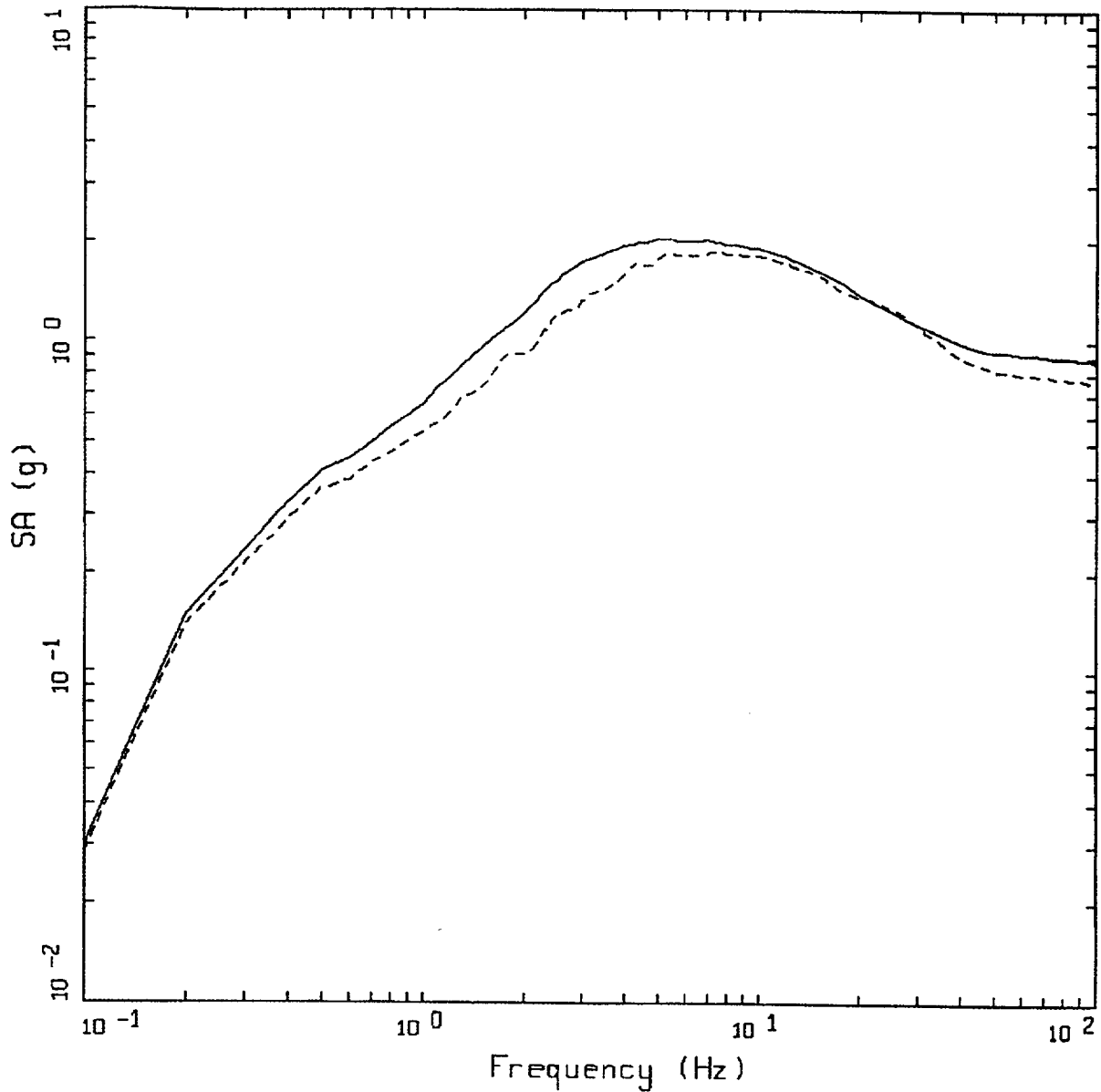


NRC, M=6.5, D=1 KM

LEGEND

- SURFACE RATIO OVER SURFACE; 0 M; PGA = 0.483 g
- 305 M/SEC (1000 FT/SEC) RATIO OVER SURFACE; 1.5 M (5 FT)
- 610 M/SEC (2000 FT/SEC) RATIO OVER SURFACE; 13.4 M (44 FT)
- 914 M/SEC (3000 FT/SEC) RATIO OVER SURFACE; 26.8 M (88 FT)
- · — 1219 M/SEC (4000 FT/SEC) RATIO OVER SURFACE; 66.526 M (218.273 FT)
- × — 1524 M/SEC (5000 FT/SEC) RATIO OVER SURFACE; 171.526 M (562.778 FT)
- + — 1829 M/SEC (6000 FT/SEC) RATIO OVER SURFACE; 386.526 M (1268.193 FT)

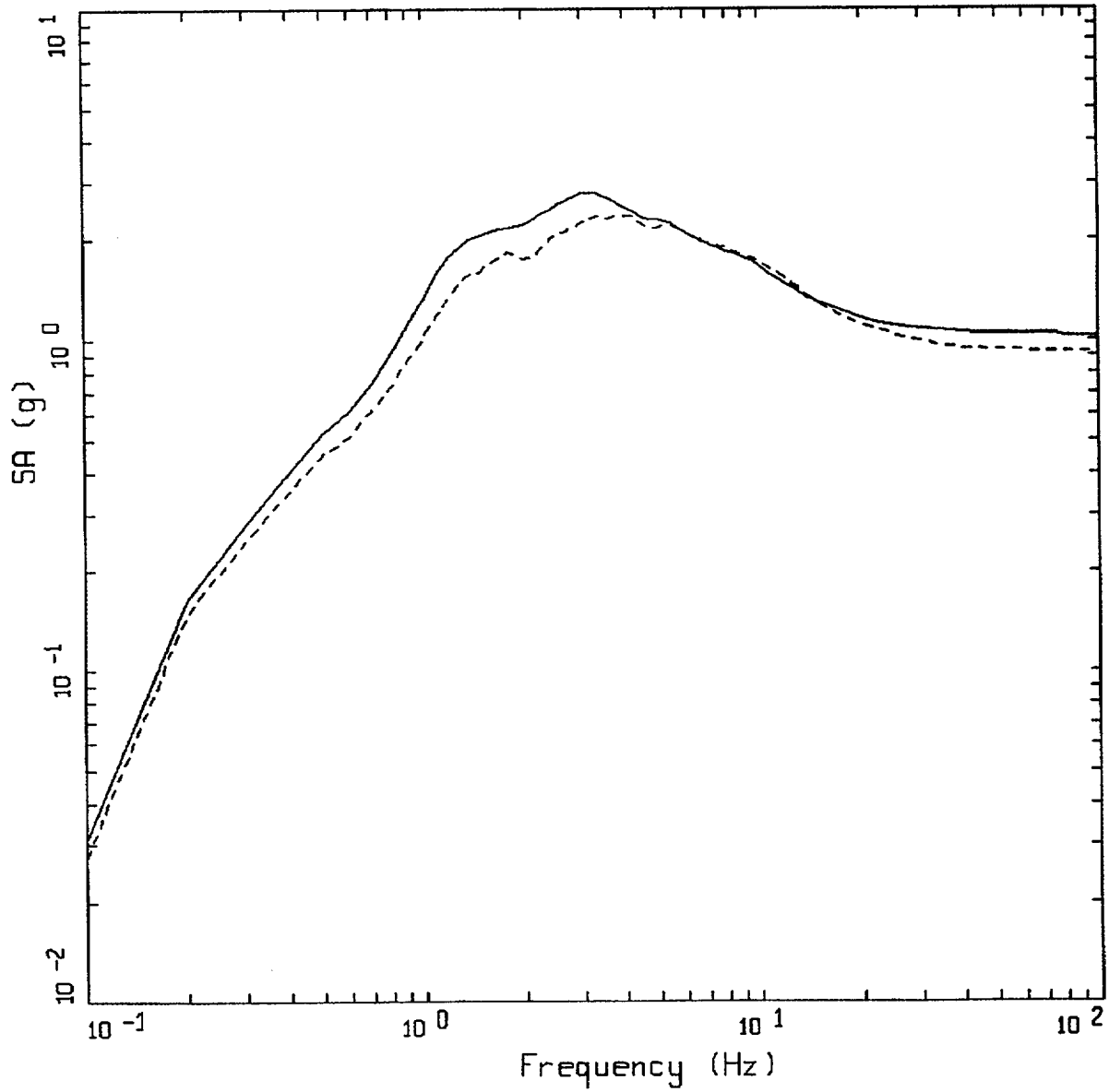
Figure 6-170. Depth-to-surface response spectral ratios (median estimates) computed for M=6.5 at a distance of 1 km.



ROCK OUTCROP SPECTRA

LEGEND
 — WUS ROCK UNIFORM HAZARD SPECTRA, PGA=0.884 g
 - - - MODIFIED ROCK UNIFORM HAZARD SPECTRA, PGA=0.767 g

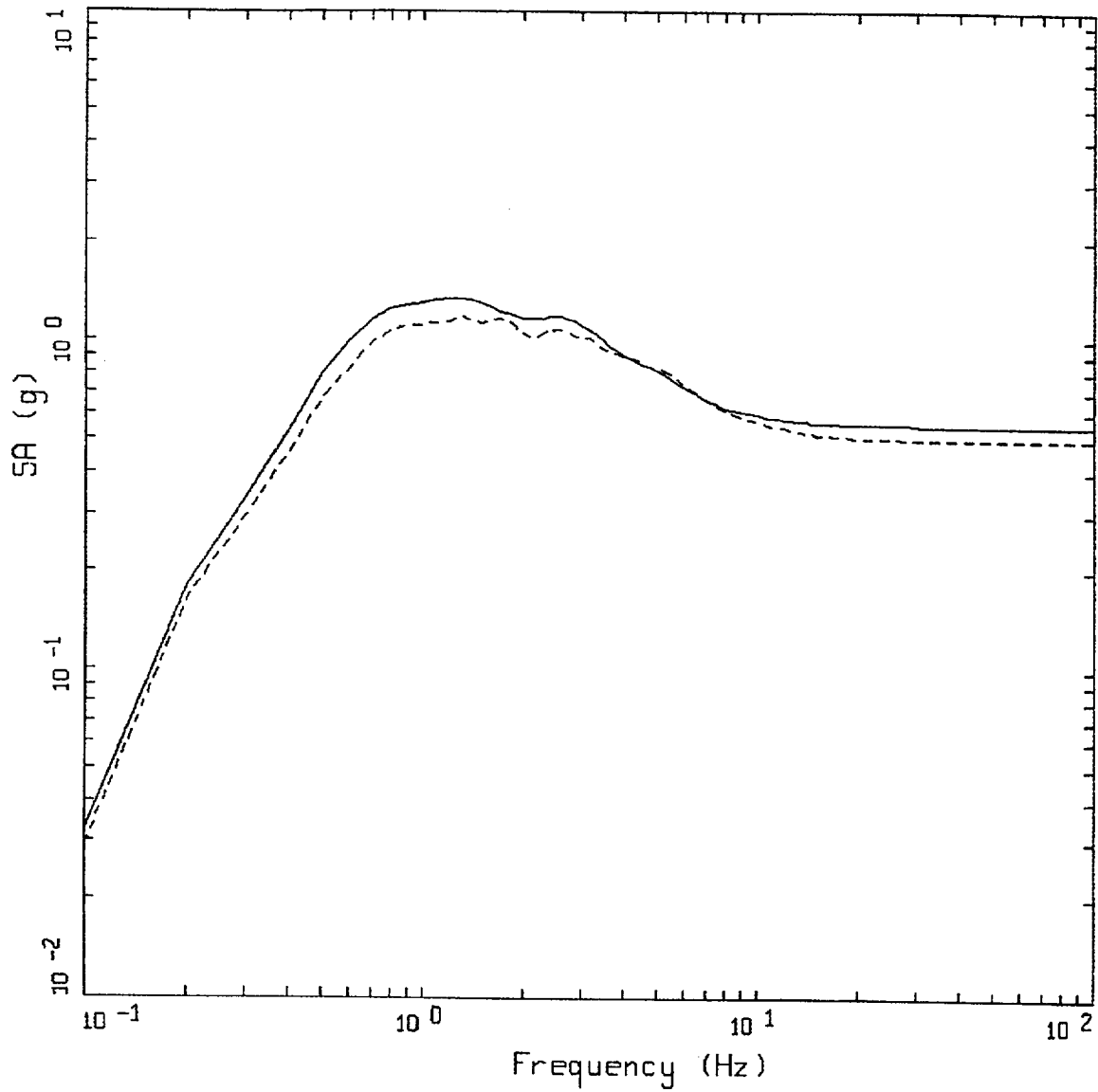
Figure 6-171. Comparison of WUS UHS at surface of rock site (solid line) and UHS at free surface with a shear-wave velocity of 914m/sec (3,000 ft/sec) using transfer function corresponding to surface acceleration of 0.483g (Figure 6-170). Modified spectrum represents modification of surface soft rock motions to base-of-soil motions.



CONTROL MOTION COMPARISON, RI

- LEGEND
- APPROACH 1, 10-4 ROCK CONTROL MOTION, MEAN PGA = 1.027 G
 - - - APPROACH 1, MODIFIED 10-4 ROCK CONTROL MOTION, MEAN PGA = 0.922 G

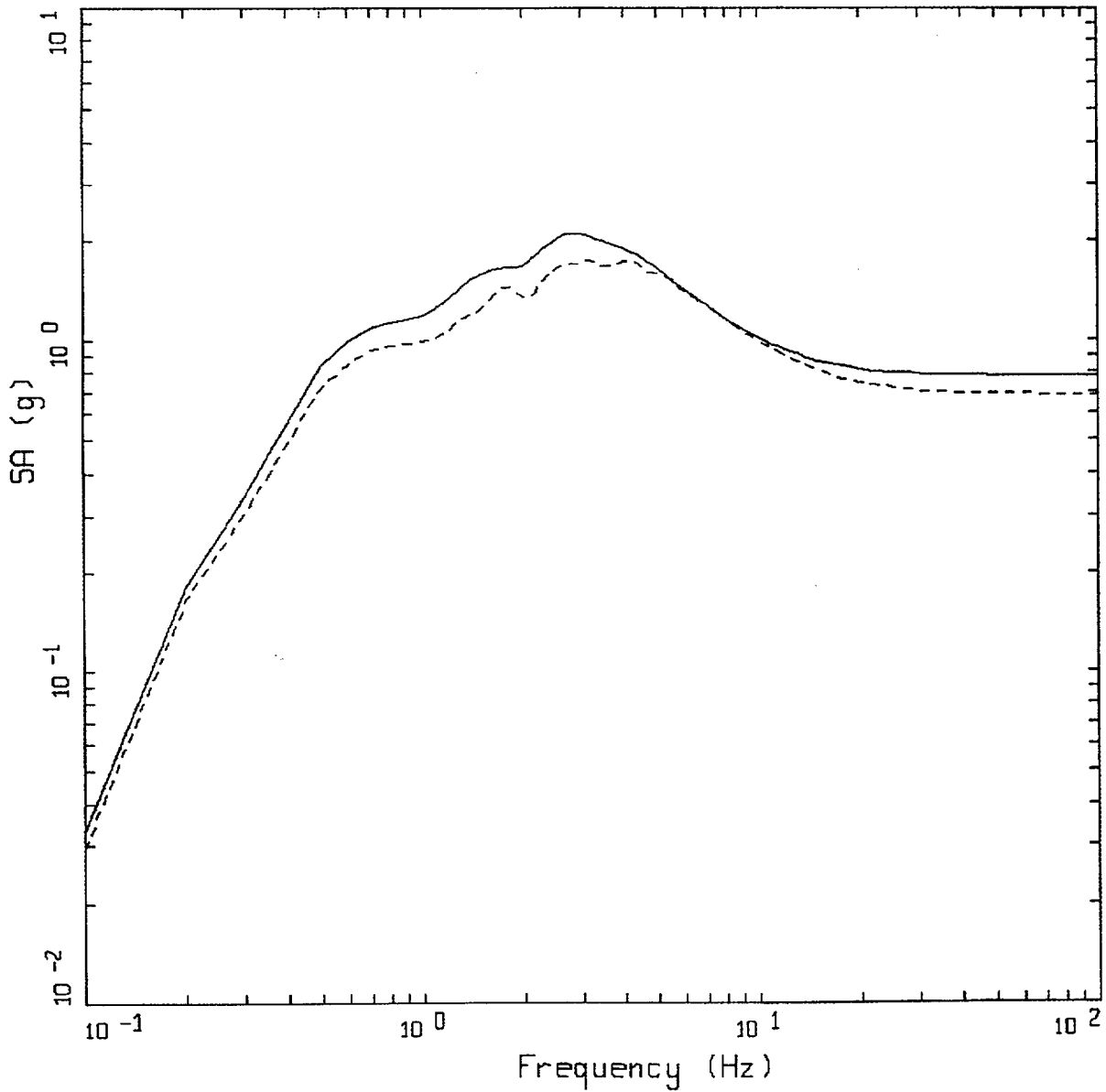
Figure 6-172. Comparison of WUS soil motions using rock UHS and modified rock (base-of-soil) UHS soil profile Rinaldi.



CONTROL MOTION COMPARISON, GZ

- LEGEND
- APPROACH 1, 10-4 ROCK CONTROL MOTION, MEAN PGA = 0.550 G
 - - - APPROACH 1, MODIFIED 10-4 ROCK CONTROL MOTION, MEAN PGA = 0.500 G

Figure 6-173. Comparison of WUS soil motions using rock UHS and modified rock (base-of-soil) UHS soil profile Gilroy 2.

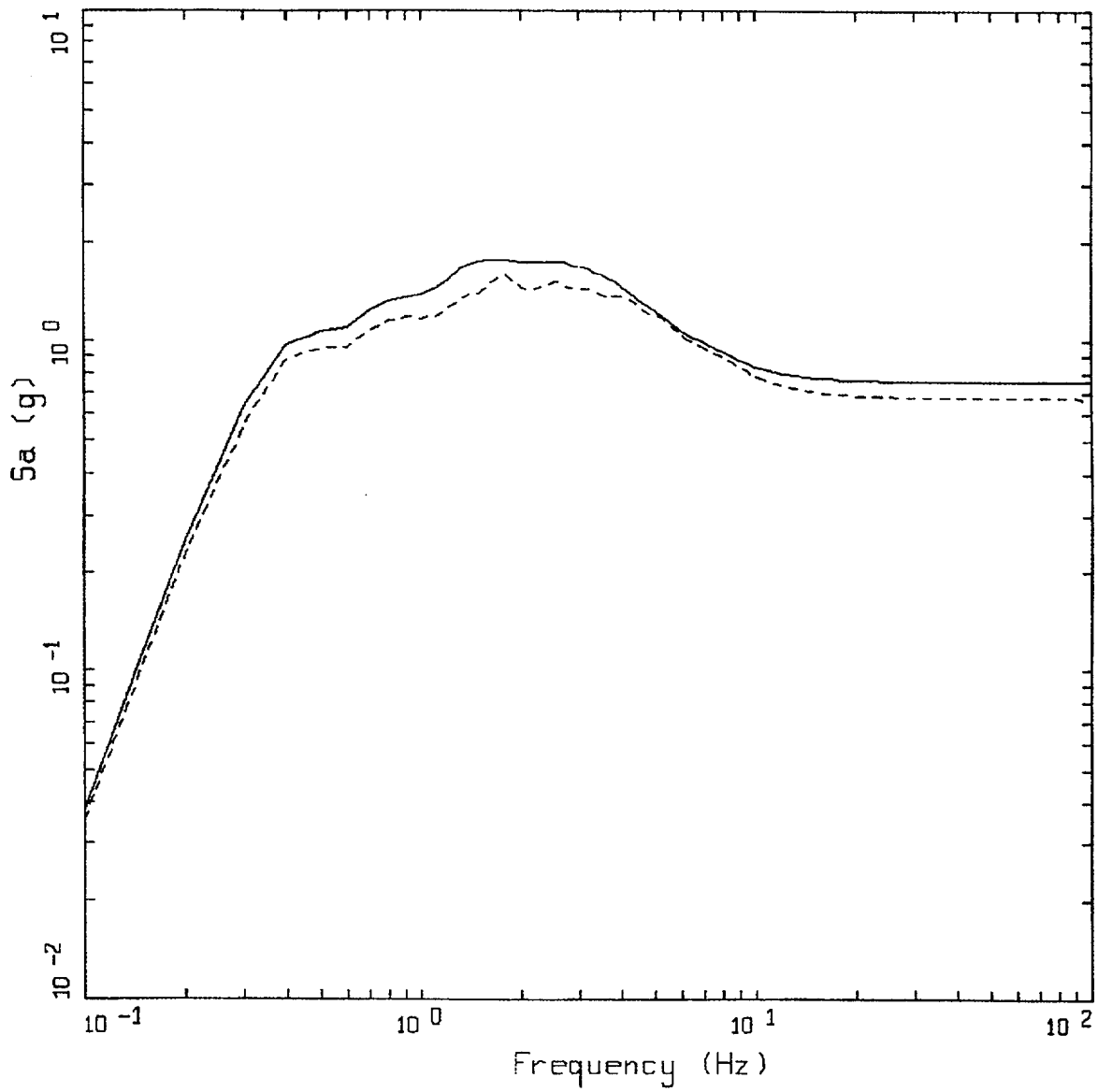


CONTROL MOTION COMPARISON, SR

LEGEND

- APPROACH 1, 10⁻⁴ ROCK CONTROL MOTION, MEAN PGA = 0.777 G
- APPROACH 1, MODIFIED 10⁻⁴ ROCK CONTROL MOTION, MEAN PGA = 0.686 G

Figure 6-174. Comparison of WUS soil motions using rock UHS and modified rock (base-of-soil) UHS soil profile Savannah River Generic.



CONTROL MOTION COMPARISON, IV

- LEGEND
- APPROACH 1, 10-4 ROCK CONTROL MOTION, MEAN PGA = 0.755 G
 - - - APPROACH 1, MODIFIED 10-4 ROCK CONTROL MOTION, MEAN PGA = 0.672 G

Figure 6-175. Comparison of WUS soil motions using rock UHS and modified rock (base-of-soil) UHS soil profile Meloland.